Trinity College Dublin

The University of Dublin

Pre-clinical evaluation of targeting autophagy for the treatment of Oral Squamous Cell Carcinoma

Thesis submitted to the University of Dublin, Trinity College

for the Degree of Doctor of Philosophy

by

Stefania Magnano, MSc

School of Biochemistry and Immunology,

Trinity College Dublin

February 2021

Supervised by

Prof Daniela M. Zisterer

Co-supervised by

Dr Jeffrey O'Sullivan

Declaration

I declare that this thesis has not been submitted as an exercise for a degree at this or any other university and it is entirely my own work. Figure 3.6 and Figure 3.8 were carried out with Ronan Duffy. I agree to deposit this thesis in the University's open access institutional repository or allow the library to do so on my behalf, subject to Irish Copyright Legislation and Trinity College Library conditions of use and acknowledgement.

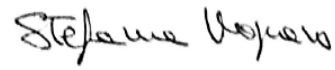

Stefania Magnano

Acknowledgement

First and foremost, I would like to thank my supervisor Danny, for her guidance and support over the past three years. Thanks for being such a great mentor and thanks for your incredible patience and kindness that really helped me to go throughout this project. Thanks to my co-supervisor Jeff, for his constant help and for being always available every time I needed. Also, thanks for all the opportunities to go to conferences.

I would also like to thank our collaborators: Jose Bagan and Eloisa Jantus Lewintre at the General University Hospital of Valencia (Spain) and Mary Toner, Esther O' Regan and Lisa Ryan at the St. James's Hospital (Ireland), without whom the patient study would not have been possible. Also, thanks to Giuseppe Campiani and Stefania Butini at the University of Siena (Italy) for the successful publications achieved.

Thanks to all TRACT PhD students: Valentina, Éilis, Sara, Niamh, Ewelina, Prasanth, Magda, Tuhina, Enis and Marilena. I really loved being part of this incredible programme and I couldn't have shared this experience with a better group of people. Also, thanks to all PIs involved in the TRACT programme and to Catherine, for her incredible job as project manager. A special thanks to Marilena and Ewelina, my long-term work partners. Thanks for your help and support in the lab, and most important thanks for having been my second family over the past years. I can't explain how much your friendship meant to me, I wouldn't have made it through without you.

Thanks also to all present and past members of the sixth floor reading room: Claire, Sinéad, Rachel, Patricia, Rebecca, Emma, Magda, Jill, Louie, Callum, Catriona, Brian, Nick, Mary, Tania, Gillian and Ciara. Thanks for all the cakes, drinks and laughs over the past years. I had so much fun with you guys! I would especially like to thank the DZ lab members: Rachel, Rebecca and Patricia, for all the advice, support and friendship. I really enjoyed every day in the lab and every lab meeting with you. Big thanks also to everyone in the Biochemistry and Immunology department, and in particular to Barry, Gavin and Liam for their incredible expertise and for their kind help.

A huge thanks to Giulio, for his kindness, optimism and support. I couldn't thank you enough for all your patience during the last months.

To my parents and my brother, who have always believed in me. You were a great source of encouragement and love and I will be forever grateful for it. Finally, I would like to dedicate this thesis to my nephew, we are all waiting for you.

Thanks to Horizon 2020 Marie Sklodowska-Curie Actions (ITN Project No. 721906 – TRACT) for funding this project.

Summary

Oral Squamous Cell Carcinoma (OSCC) is the sixth most common form of cancer worldwide. It is typically aggressive and closely correlated with disease recurrence and poor survival. Chemoresistance is a critical problem associated with OSCC leading to therapeutic failure, tumour recurrence and progression. Autophagy, a physiological catabolic process that allows the degradation and recycling of unnecessary or dysfunctional cellular components, has acquired an emerging interest in cancer as it has been shown to be frequently activated in tumour cells treated with chemotherapeutics. Whether drug-induced autophagy represents a mechanism that allows cancer cells to survive or a pro-death mechanism associated with apoptosis remains controversial. Additionally, a role for autophagy during cancer development has also been proposed, but its role in OSCC remains poorly understood.

The aim of this study was to determine whether autophagy is involved in the cellular response to cisplatin in OSCC and in the development of chemoresistance and whether targeting autophagy represents a valuable treatment strategy to sensitise cells to chemotherapy. Moreover, this preclinical study investigated the expression of key autophagic regulatory proteins in oral cancer patient samples in order to elucidate the role of autophagy in OSCC development.

Cisplatin, a representative OSCC chemotherapeutic agent, was shown to concurrently induce both apoptosis and autophagy in two OSCC cell lines, SCC4 and SCC9. To evaluate the role of cisplatin-induced autophagy in OSCC and to investigate the relationship between autophagy and apoptosis, the effect of targeting autophagy on cisplatin-induced apoptosis was examined. Autophagy inhibition using two early stage autophagy inhibitors, 3-methyladenine and SAR405, did not sensitise OSCC cells to cisplatin treatment. This finding was supported by data showing that knockdown of the key autophagy protein ATG5, necessary during the early stage of the autophagic process, did not significantly modulate sensitivity to cisplatin. In contrast, treatment of cells with two late stage autophagy inhibitors, chloroquine and bafilomycin-A1, was shown to significantly enhance cisplatin-induced apoptosis in OSCC cells. However, off-target, autophagic-independent effects of these inhibitors could not be ruled out. Interestingly, inhibition of cisplatin-induced apoptosis with the general caspase inhibitor Z-VAD-fmk

abrogated cisplatin-induced autophagy in OSCC cells further indicating a complex interplay between autophagy and apoptosis.

The crosstalk between cisplatin-induced autophagy and apoptosis was further investigated by examining the signalling pathway(s) involved in the cellular response to cisplatin. Cisplatin was shown to induce oxidative stress by increasing the generation of Reactive Oxygen Species (ROS). Moreover, pre-treatment of cells with the antioxidant N-acetyl cysteine was shown to protect cells from cisplatin-induced apoptosis and autophagy and to suppress cisplatin-induced JNK activation. Additionally, the JNK inhibitor SP600125 was shown to partially reduce both autophagy and caspase 3 activation, suggesting a coordinated activation of cisplatin-induced autophagy and apoptosis in OSCC through the ROS/JNK signalling pathway.

Analysis of chemoresistance in OSCC was carried out through the generation of a cisplatin-resistant OSSC cell line (SCC4cisR) obtained by pulsed stepwise exposure of SCC4 cells to cisplatin. The SCC4cisR cell line was shown to be approximately 14 times more resistant to cisplatin than the parental SCC4 cell line and displayed a reduced apoptotic ability following cisplatin treatment. Autophagy did not appear to play a role in acquired resistance to cisplatin in this cell model. In contrast, cellular adaptation to ROS-induced oxidative stress was identified as a mechanism implicated in cisplatin resistance. In fact, enhanced ROS generation and concurrent activation of the antioxidant Nrf2/HO-1 pathway were demonstrated in the SCC4cisR cells. Furthermore, targeting the antioxidant systems glutathione and Nrf2 with inhibitors was shown to partially restore the cisplatin-sensitive phenotype in the SCC4cisR cells, indicating that this may prove a valuable strategy to improve chemotherapy in OSCC patients.

Finally, evaluation of the expression of key autophagic proteins LC3, p62 and Beclin-1 in OSCC tissue samples from two independent patient cohorts (Spanish and Irish) was performed by western blotting and immunohistochemistry, respectively. An increase in the expression of LC3 and Beclin-1 along with a decrease in p62 in cancerous samples compared to non-cancerous samples was demonstrated, suggesting autophagy activation during OSCC progression. Moreover, preliminary results showed a potential application of LC3 and Beclin-1 as biomarkers for OSCC detection, thus further analysis with a bigger sample size may be warranted.

Table of Contents

List of Figures

Chapter 1

Chapter 2

Chapter 3

Chapter 4

Chapter 5

Chapter 6

Appendix

List of Tables

Chapter 1

Chapter 2

Chapter 3

Chapter 5

Chapter 6

Abbreviations

μM	Micromolar
$^{1}O2$	Singlet oxygen
3-MA	3-methyladenine
4-PBA	4-phenylbutyric acid
ABC	ATP binding cassette
AIF	Apoptosis inducinf factor
AKT	Protein kinase B
ALDH	Aldehyde dehydrogenase
AMBRA1	Activating molecule in Beclin-1-regulated autophagy
AMPK	AMP-activated protein kinase
ANOVA	Analysis of variance
Apaf-1	Apoptotic protease factor 1
Apo3L	Apo3 ligand
Ara-C	Arabinoside
ARE	Antioxidant responsive element
ATG	Autophagy-related protein
ATM	Ataxia telangiectasia mutated
ATO	Arsenic trioxide
ATP	Adenosine triphosphate
ATR	ATM and Rad3-related
AUC	Area under the curve
Bad	Bcl-2 associated agonist of cell death
BAF	Bafilomycin-A1
Bak	Bcl-2 antagonist/killer
BARA	β-α-repeated-autophagy-related domain
Bax	Bcl-2-associated X protein
Bcl-2	B cell lymphoma-2
Bcl-xL	B-cell lymphoma-extra large
BCNU	3-bis (2-chloroethyl)-1-nitrosourea
BCRP	Breast cancer resistance protein
BECN1	Beclin-1
BH	Bcl-2 homology
Bid	BH3 interacting domain death antagonist
BIM_L	BIM-long
BIM_S	BIM-short
BIM_{XL}	BIM-extra long
BIP	Immunoglobulin heavy chain-binding protein
BNIP3	Bcl-2/adenovirus E1B 19 kDa-interacting protein 3
BSO	Buthionine sulfoximine

Caspase	Cysteine-aspartic proteases
CC1	Cell conditioner 1
CCD	Central coiled-coil domain
CDC25A	Cell division cycle 25A
CDDP	Cis-diamminedichloroplatinum II (cisplatin)
CFA	Colony forming assay
Chk1	Checkpoint kinase 1
CHOP	C/EBP homologous protein
CML	Chronic myeloid leukaemia
CPT	Camptothecin
CRC	Colorectal cancer
CSC	Cancer stem cells
CSF-1	Colony stimulating factor-1
CTR1-2	Copper transporters
CYP1A1	Cytochrome P450 family 1 member A1
DAPK	Death-associated protein kinase
DCF	2′,7′-dichlorofluorescein
DDR	DNA damage response
DED	Death effector domains
DHA	Docosahexaenoic acid
Diablo	Direct inhibitor of apoptosis-binding protein with low pI
DISC	Death-inducing signalling complex
DMEM	Dulbecco’s Modified Eagle Medium
DMEM-F12	Dulbecco's Modified Eagle Medium/Nutrient Mixture F-12
DMSO	Dimethyl sulfoxide
DNA	Deoxyribonucleic acid
DR	Death receptor
DRAM	Damage-regulated modulator of autophagy
DTT	Dithiothreitol
EBSS	Earle's Balanced Salt Solution
ECAR	Extracellular acidification rate
ECD	Evolutionarily conserved domain
ECL	Electrochemiluminescence
ECM	Extracellular matrix
EDTA	Ethylene-diamine-tetra-acetic acid
EGFR	Epidermal growth factor receptor
EIF2AK2	Eukaryotic translation initiation factor 2-α kinase 2
EL	Erythroleukoplakia
EMT	Epithelial-mesenchymal transition
EndoG	Endonuclease G
EPG5	Ectopic P-granules autophagy protein 5 homolog

ER	Endoplasmic reticulum
ErbB-2	Erb-B2 receptor tyrosine kinase 2
ERCC1	Excision repair cross-complementing protein
ERK	Extracellular signal-related kinases
FADD	Fas-associated protein with death domain
FasL	Fas ligand
FasR	Fas receptor
FBS	Fetal bovine serum
FDA	Food and Drug Administration
FdUMP	Fluorodeoxuridine monophosphate
FITC	Flurescein isothiocyanate
FLIP	FADD-like IL-1β-converting enzyme-inhibitory protein
FOXO	Forkhead box O
FSC	Forward scatter
FUTP	Fluorouracil triphosphate
G6PD	Glucose-6-phosphate dehydrogenase
GAPDH	Glyceraldehyde 3-phosphate dehydrogenase
g-GCS	Glutamylcysteine synthetase
GPX	Glutathione peroxidase
GSH	Reduced glutathione
GSSG	Oxidazed glutathione
GST	Glutathione-S-transferase
GSTM1	Glutathione S-transferase M1
h	Hours
H&E	Haematoxylin & Eosin
H_2DCFDA	2',7'-Dichlorodihydrofluorescein-diacetate
H_2O_2	Hydrogen peroxide
HCQ	Hydroxychloroquine
HDM2	Human double minute 2 homolog
HEPES	4-(2-hydroxyethyl)-1-piperazineethanesulfonic acid
HIF-1α	Hypoxia-inducible factor 1-alpha
HL	Homogeneous leukoplakia
HMGB1	High mobility group box 1 protein
hMSH2	DNA mutS homolog 2
HNC	Head and neck cancer
HNC	Head and neck cancer
HO-1	Heme oxygenase-1
HPV	Human papillomavirus
HRP	Horseradish peroxidise
IAP	Inhibitor of apoptosis protein
IARC	International Agency and Research on Cancer

IC_{25}	25% inhibitory concentration
IC_{50}	50% inhibitory concentration
IFN-	Interferon-
Ig	Immunoglobulin
IL-	Interleukin-
IRE1	Inositol-requiring enzyme 1
JAK	Janus kinase
JNK	c-Jun N-terminal kinases
kDa	KiloDalton
Keap1	Kelch-like ECH-associated protein 1
LAMP	Lysosomal-associated membrane protein 1
LIR	LC3 interacting region
MAP1LC3	Microtubule-associated protein1 light chain 3
MAPK	Mitogen-activated protein kinase
MAPK	Mitogen-activated protein kinase
Mcl-1	Myeloid cell leukaemia-1
MDR	Multidrug resistance
MDR1	Multidrug resistance protein 1
MEF	Mouse embryonic fibroblasts
MEK	Mitogen-activated protein kinase kinase
MFI	Median fluorescence intensity
mg	Milligrams
MGMT	O6-methylguanine DNA methyltransferase
min	Minutes
miRNA	MicroRNA
mL	Millilitre
MLSMR	Molecular Libraries Small Molecule Repository
mm	Millimiters
mM	Millimolar
mRNA	Messenger RNA
MRP	Multidrug resistance proteins
MRP1	Multidrug associated-associated protein 1
MT	Metallothionein
MTA	Microtubule targeting agent
mTOR	Mammalian target of rapamycin
mTORC1/2	mTOR complex 1/2
NAC	N-acetyl cysteine
NAF-1	Nutrient-deprivation autophagy factor-1
NF-κB	Nuclear factor-κB
nM	Nanomolar
nm	Nanometer

Noxa	Phorbol-12-myristate-13-acetate-induced protein 1
NQO1	NAD(P)H-quinone oxidoreductase 1
Nrf2	Nuclear factor erythroid 2–related factor 2
NT siRNA	Non-targeting siRNA
$O_2^{\bullet-}$	Superoxide anion
OCR	Oxygen consumption rate
OCT1-3	Organic cation transporters 1-3
OH•	Hydroxyl radical
OSCC	Oral squamous cell carcinoma
PBS	Phosphate buffered saline
PCD	Programmed cell death
PE	Phosphoethanolamine
PE	Plating efficiency
PERK	Protein kinase R (PKR)-like endoplasmic reticulum kinase
PI	Propidium iodide
PI3K	Phosphatidylinositol-3-kinase
pRb	Retinoblastoma protein
PS	Phospatidyl serine
PtdIns3 complex	Phosphatidylinositol-3-kinase complex
PVDF	Polyvinylidene difluoride
qHTS	Quantitative high-throughput screen
Raf	Rapidly accelerated fibrosarcoma
RAP	Rapamycin
Ras	Rat sarcoma
RCS	Reactive chloride species
Rheb	Ras homolog enriched in brain
RI	Resistance index
RIPA	Radioimmunoprecipitation
RNA	Ribonucleic acid
RNS	Reactive nitrogen species
RO•	Alkoxyl radicals
ROC	Receiver operating characteristic
ROO•	Peroxyl radicals
ROS	Reactive oxygen species
RS	Reactive species
RSS	Reactive sulphur species
S.E.M.	Standard error of the mean
SCC	Squamous cell carcinoma
SCC4cisR	Cisplatin-resistant SCC4 cells
SDS	Sodium dodecyl sulfate
SDS-PAGE	Sodium dodecyl sulphate polyacrylamide gel electrophoresis

SF	Survival fraction
shRNA	Short hairpin RNA
siRNA	Small interfering RNA
Smac	Second mitochondria-derived activator of caspase
SNARES	SNAP receptors
SOD	Superoxide dismutase
SQTM1	Sequestosome1
SSC	Side scatter
Stat3	Signal transducer and activator of transcription 3
TBS	Tris buffered saline
TBST	Tris buffered saline tween
TEMED	Tetramethylethylenediamine
TGF-β	Transforming growth factor beta
TME	Tumour microenvironment
TNFR1	Tumor necrosis factor receptor 1
TNFα	Tumour necrosis factor-alpha
TNM	Tumour, node and metastasis
TRADD	TNFR1-associated death domain protein
TS	Thymidylate synthetase
TSC	Tuberous sclerosis complex
TTP	Thymidine triphosphate
UBL	Ubiquitin-like
ULK	Unc-51 like autophagy activating kinase
UV	Ultraviolet
UVRAG	UV radiation resistance-associated gene protein
VL	Verrucous leukoplakia
x g	Times gravity
XIAP	X-linked inhibitor of apoptosis protein

Thesis outputs: Publications, Presentations and Awards

Publications

Brindisi M, Ulivieri C, Alfano G, Gemma S, de Asís Balaguer F, Khan T, Grillo A, Chemi G, Menchon G, Prota AE, Olieric N, Lucena-Agell D, Barasoain I, Diaz JF, Nebbioso A, Conte M, Lopresti L, **Magnano S**, Amet R, Kinsella P, Zisterer DM, Ibrahim O, O'Sullivan J, Morbidelli L, Spaccapelo R, Baldari C, Butini S, Novellino E, Campiani G, Altucci L, Steinmetz MO, Brogi S (2018) Structure-activity relationships, biological evaluation and structural studies of novel pyrrolonaphthoxazepines as antitumor agents. Eur J Med Chem 162:290–320. doi: 10.1016/j.ejmech.2018.11.004

Khan T, Relitti N, Brindisi M, **Magnano S**, Zisterer D, Gemma S, Butini S, Campiani G (2019) Autophagy modulators for the treatment of oral and esophageal squamous cell carcinomas. Med Res Rev 40(3):1002-1060. doi: 10.1002/med.21646

Conference Presentations

Oral Presentations

- 96th General Session & Exhibition of the IADR. IADR Pan European Regional Congress. London, England, 2018

Poster Presentations

- Irish Division of International Association of Dental Research (IADR) annual meeting. Belfast, Ireland, 2017
- "A Matter of Life or Death: From Basic Cell Death Mechanisms to Novel Cancer Treatments". EACR conference. Amsterdam, The Netherlands, 2018.
- "Molecular targets and therapeutics"-ENA2018, the 30th EORTC–NCI–AACR Symposium. Dublin, Ireland 2018.

Awards

- International Association of Dental Research (IADR) – first place in the President's Poster Competition. Belfast, Ireland, 2017.
- Trinity Trust Travel Grant 2017 to attend the EACR Conference - "A Matter of Life or Death: From Basic Cell Death Mechanisms to Novel Cancer Treatments".

Amsterdam, The Netherlands, 2018.

- Trinity Trust Travel Grant 2018 to attend the IADR Pan European Regional Congress. 96th General Session & Exhibition of the IADR. London, England, 2018.

1. Introduction

1.1. Oral Squamous Cell Carcinoma

Oral Squamous Cell Carcinoma (OSCC) is a malignant neoplasm of the oral cavity. Squamous cells are flat, thin epithelial cells that form the outer layer of the skin and the mucous membrane of body cavities. OSCC affects squamous cells that line the surface of the oral cavity and it can occur in any region of the mouth including lips, tongue, floor of the mouth, hard and soft palate, gums and cheeks [1]. OSCC belongs to a larger group of cancers known collectively as head and neck cancers (HNC) that can be further categorised by the area in which the tumour originates: nasopharyngeal cancers, salivary gland cancers, hypopharyngeal and laryngeal cancers, paranasal sinus and nasal cavity cancers and oropharyngeal and oral cancers [2]. OSCC has been studied separately from the other forms of HNC because it shows risk factors and pathological features specific to the oral cavity [3]. Although OSCC is a subtype of oral cancer, the two terms are frequently used interchangeably since OSCC represents 95% of all oral neoplasms [4]. Other malignant tumours of the oral cavity are uncommon and include: minor salivary gland carcinoma, mucoepidermoid carcinoma, adenocarcinoma, adenoid cystic carcinoma, sarcomas, lymphomas, mucosal melanomas, odontogenic tumours and osteosarcomas of the mandible or maxilla [1].

1.1.1. Epidemiology

Worldwide, OSCC accounts for 5 % of all cancers and approximately 220,000 new cases of oral cancer are reported every year [5]. The incidence of this malignancy differs by age, sex, geographical location and ethnic-racial groups. It has been observed that OSCC affects mainly people above 45 years old and more often men than women, with a ratio of 1.5:1 respectively [6, 7]. The highest incidence and prevalence of oral cancer has been found in developing countries with a peak in India, followed by Taiwan, Pakistan and Hungary. This is chiefly due to high-risk habits of tobacco, betel quid and areca-nut chewing typical of these regions [3, 8]. It has been estimated that in developing countries, OSCC is the 6th commonest cancer in males (after lung, prostate, colorectal, stomach and bladder cancer) with an incidence rate of 6.6/100,000 and a mortality rate of 3.1/100,000. On the other hand, OSCC represents the 10th commonest cancer in females (after breast, colorectal, lung, stomach, uterus, cervix, ovary, bladder and liver cancer) with an incidence rate of 2.9/100,000 and a

mortality rate of 1.4/100,000 [9]. In the last number of years, an increase in OSCC morbidity has been reported from an overall average of 3-4 cases per 100,000 per year at all ages, to 100 cases per 100,000 per annum in people over 75 years of age. Moreover, alarming data have reported a rise of incidence among younger people due to early exposure to tobacco by teenagers [7].

The 5-year survival rate of patients with OSCC is less than 50% with no gender difference. This poor survival rate has not improved in the last 30 years and it is mainly attributable to late diagnosis. In fact, it has been observed that about 2/3 of people already have an advanced stage of malignancy at the time of diagnosis, either due to inaccessibility of medical care, initial misdiagnosis or ignorance of the patients [6, 9]. Additionally, in the U.S., it has been observed that black people have a lower 5-year survival rate than people of other ethnicity and significantly more advanced stage of OSCC at the time of diagnosis [10]. The racial disparity can be correlated to pathobiological factors or cultural and socio-economic reasons that can influence indirectly the morbidity rate [7].

1.1.2. Risk factors

OSCC is a multi-factorial disease due to both individual predisposition and exposure to carcinogens. The main risk factors are usually related to lifestyle behaviour and include tobacco and alcohol consumption, betel quid and areca nut chewing, alongside infections by high risk genotypes of Human Papillomavirus (HPV).

1.1.2.1. Tobacco

Tobacco is the main risk factor associated with OSCC. Nitrosamines, benzopyrenes and aromatic amines are the main groups of pre-carcinogens found in cigarettes, which can promote cancer by damaging the genome or interacting with cellular metabolic processes. It has been estimated that 75% of all cases of oral cancer are attributable to tobacco smoking, with smokers having a 3-fold higher risk of developing oral cancer compared with non-smokers [4, 11]. Additionally, it has been suggested that all forms of tobacco are carcinogens. In fact, snuff and chewing tobacco are also associated with an increased risk of developing oral cancer at the site of tobacco placement, even though the risk is lower when compared to smoking tobacco [12]. Second-hand smoke is also considered a risk factor; indeed, it has been reported that the risk of developing

oral cancer is 87% higher in non-smokers exposed to cigarette smoke compared to non-smokers that have not been exposed [13].

1.1.2.2. Alcohol

Heavy alcohol drinking increases the risk of developing oral cancer by enhancing the penetration of pre-carcinogens (usually contained in alcoholic beverages) into tissues, which can cause epithelial atrophy and genome disruption [13]. N-nitrosodiethylamine and polycyclic aromatic hydrocarbons are the main carcinogenic substances contained in alcoholic beverages, and in addition, acetaldehyde, the first ethanol metabolite, has been identified recently as an oral cancer promoter [3]. Overall, it has been estimated that 7-19% of OSCC cases are attributable to regular alcohol consumption and this correlation is dose-dependent [14]. Additionally, the risk of developing oral cancer is further increased (14-fold) when alcohol is consumed in combination with tobacco, suggesting a synergistic effect [15, 16].

1.1.2.3. Betel quid

Betel quid (or paan) is a preparation containing areca nut wrapped in a betel leaf, widely consumed by Indian and Taiwanese populations for its intoxicant properties and for its stimulant and psychoactive effects. Recently, the International Agency for Research on Cancer (IARC) has classified betel quid as an oral carcinogen in humans [14]. In fact, it has been reported that betel quid chewing produces reactive oxygen species (ROS) that can induce gene mutations and structural changes in the oral mucosa, resulting in the permeabilisation of the mucosa to other betel quid ingredients and environmental toxicants [9]. Betel quid chewing often results in a pre-malignant condition known as oral submucous fibrosis, which can potentially develop into oral cancer [14]. Various studies have shown that the risk of OSCC is 1-4 times higher when betel quid is consumed without tobacco, however the combination with tobacco creates a synergistic effect that increases the risk between 8 and 15 times [17].

1.1.2.4. HPV

Among the 150 subtypes of HPV isolated so far, there are a few which have been recognised as oncogenic [11, 18]. These “high-risk” HPVs have been strongly correlated with oral lesions, and in particular HPV-16 and HPV-18 are the most common subtypes detected in OSCC (22% and 14% of oral cancers, respectively) [14].

It has been reported that the viral proteins E6 and E7 are both involved in carcinogenesis through the regulation of the onco-suppressive key proteins p53 and pRb [13]. However, it is believed that HPV infection alone is not sufficient to induce malignant transformation, thus it requires the presence of other risk factors to cause oral cancer [14].

1.1.2.5. Other risk factors

In several epidemiological studies the importance of diet and nutrition in oral cancer has been reported. In fact, it is believed that deficiency of vitamin A, E or C can be linked to a higher risk of developing oral neoplasia [9]. Additionally, a family history of head and neck cancer and individual predisposition to cancer must be considered risk factors for OSCC. Individual predisposition to cancer is usually associated with immune defects and with an impaired ability to metabolise carcinogens or to repair DNA damaged by mutagens [4]. Finally, for lip cancers only, overexposure to UV radiation has been indicated as a risk factor [19].

1.1.3. Genetic alterations

Genetic alterations, caused by intrinsic and extrinsic factors, define the molecular basis of oral carcinogenesis. Genetic damage can affect single genes or chromosome portions and include point mutations, amplifications, rearrangements, deletions and epigenetic modifications such as the methylation of DNA and acetylation or methylation of histones [20, 21]. The genome regions frequently found deleted in OSCC include 3p, 4q, 5q21-22, 8p21-23, 9p21-22, 11q13, 11q23, 13q, 14q, 17p, 18q, and 22q [3]. In particular, it has been reported that the risk of progression from premalignant lesion to cancer increases when there is a genetic loss in the region 3p and 9p alongside 4p, 8p, 11q, 13q and 17p [9]. Oncogene activation and tumour suppressor inactivation are the main consequences of the disruption of regulatory pathways involved in basic cellular functions including cell division, differentiation, and cell death. The epidermal growth factor receptor (EGFR), c-Myc, ErbB-2, Stat-3, Bcl-2 and Cyclin D are some of the oncogenes implicated in oral carcinogenesis, whereas p53, RB1 and p16 are the main tumour suppressor genes [22]. p53 is the most commonly mutated gene in oral cancer (50 % of OSCC patients) and it has been indicated that the normal p53 pathway is down regulated in 80% of OSCC [23, 24]

Additionally, some gene mutations such as the polymorphisms in glutathione S-transferase M1 (GSTM1), the cytochrome P450 family 1 member A1 (CYP1A1) and aldehyde dehydrogenase (ALDH1B and ALDH2) have been strongly correlated to OSCC [25].

1.1.4. Clinical features

From a clinical point of view, OSCC lesions can arise *de novo* in the normal mucosa or can be preceded by premalignant lesions. Premalignant lesions usually occur after repeated insults of carcinogens and can be displayed as white (leukoplakia) or red (erythroplakia) patches, which may potentially develop into a primary tumour (Figure 1.1) [3]. It has been suggested that OSCC has a better prognosis when it evolves from a premalignant lesion, even though there is not a significant difference compared to *de novo* OSCC [26]. Several factors are important at the time of the diagnosis of OSCC: the size and the depth of the lesion, the site affected, the presence of regional lymph node metastases and the histopathological grade of the carcinoma. All these factors can influence the prognosis of OSCC [7]. The size of OSCC lesions varies from a few millimetres to several centimetres and it is usually correlated to the stage of the cancer. The initial lesions can arise in the form of erythro-leukoplakia lesions and are usually small and asymptomatic [27]. On the other hand, advanced lesions are usually big and painful, and they can arise as necrotic looking ulcers or with a broad based exophytic mass [7]. The prognosis for early stage OSCC is relatively favourable compared to late stage OSCC and it has been estimated that the 5-year survival rate varies from 90% down to 40% between early and advanced lesions [12, 13]. Regarding the localisation of the tumour, several reviews report that even though OSCC can affect any region of the mouth, there are some sites more affected than others. In fact, about 50% of all cases of oral cancers concern the tongue (20-40%) and the floor of the mouth (15-20%), mainly because of the fact that carcinogens can easily penetrate through the thin non-keratinised epithelium that line these surfaces [11, 12]. Squamous Cell Carcinoma (SCC) of the tongue and of the floor of the mouth are considered more aggressive and they are associated with a poor prognosis compared to SCC of other regions of the mouth (e.g. lips or gums) because they can likely metastasise to regional lymph nodes [7]. Likewise, poorly differentiated (high-grade) OSCC are considered more aggressive compared to well-differentiated (low-grade) OSCC because they tend to

metastasise to regional lymph nodes early during the disease [28]. Overall, the TNM staging system (T-tumour size, N-lymphnode metastasis M-distant metastasis) is used to predict the course of primary tumours and the survival rate. This system aims to assess the extension of the disease before treatment in order to assign the clinical stage of the malignancy. In fact, it is important to differentiate between localised disease (stage I and II) and advanced disease (stage III and IV). However, although TNM staging is routinely used, the course of OSCC and the response to the treatment are often unpredictable [13]. Due to these reasons, research into identification of biomarkers for OSCC early diagnosis and prognosis prediction is emerging in recent times.

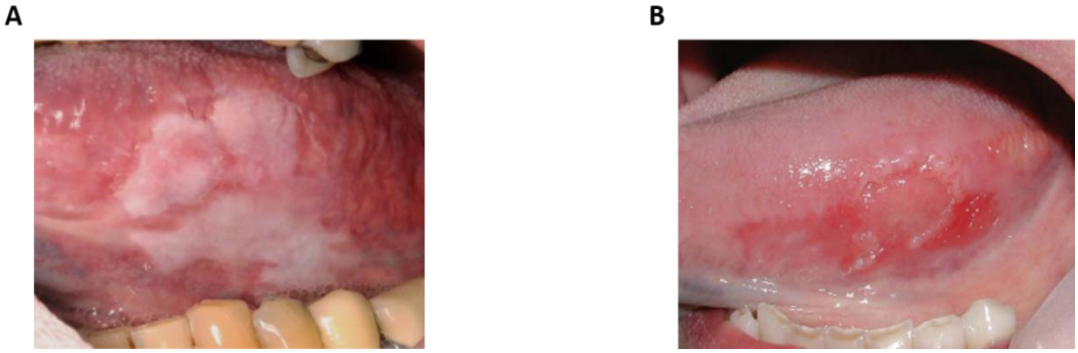

Figure 1.1 Leukoplakia and erythroplakia on the lateral border of the tongue.
Leukoplakia (**A**) and erythroplakia (**B**). Images taken from [27, 29] .

Primary tumour (T)	
TX	Cannot be assessed
T0	No evidence of primary tumour
Tis	Carcinoma in situ (CIS)
T1	Tumour 2 cm or less in greatest dimension
T2	Tumour more than 2 cm but not more than 4 cm in greatest dimension
T3	Tumour more than 4 cm in greatest dimension
T4a	Moderately advanced local disease. Lip: Tumour invades through cortical bone, inferior alveolar nerve, floor of mouth, or skin (chin or nose). Oral cavity: Tumour invades through cortical bone, into deep/extrinsic muscle of tongue (genioglossus, hyoglossus, palatoglossus, and styloglossus), maxillary sinus, or skin of face.
T4b	Very advanced local disease. Lip and oral cavity: Tumour invades masticator space, pterygoid plates, or skull base; or encases internal carotid artery

Regional lymph nodes (N)	
NX	Cannot be assessed
N0	No regional lymph node metastasis
N1	Metastasis in a single ipsilateral lymph node, 3 cm or less in greatest dimension
N2	Metastasis as specified in N2a, 2b, 2c (see below)
N2a	Metastasis in a single ipsilateral lymph node, more than 3 cm but not more than 6 cm in greatest dimension
N2b	Metastasis in multiple ipsilateral lymph nodes, none more than 6 cm in greatest dimension
N2c	Metastasis in bilateral or contralateral lymph nodes, none more than 6 cm in greatest dimension
N3	Metastasis in a lymph node more than 6 cm in greatest dimension

Distant metastasis (M)	
MX	Distant metastasis cannot be assessed
M0	No distant metastasis

Clinical stages (T+N+M)			
0	Tis	N0	M0
I	T1	N0	M0
II	T2	N0	M0
III	T3 (enough alone), T2 or T1	N1	M0
IV A	T4a	N0 or N1	M0
	T1, T2 or T3	N2	M0
IV B	any T	N3	M0
	T4b	any N	M0
IV C	any T	any N	M1

Table 1.1 TNM definition of oral cancer.

Table modified from [13]**.**

1.1.5. Treatment

The treatment of OSCC generally requires a team of multidisciplinary specialists including dentists, maxillofacial surgeons, medical oncologists, radiation oncologists, radiologists and speech/swallowing pathologists [30]. The main therapeutic strategies against oral cancer are surgery, radiotherapy and chemotherapy. The choice of the treatment depends on the stage of the malignancy, the site affected and the general condition of the patient [7]. Surgical removal of the tumour represents the preferred treatment strategy for OSCC, even though it can have a significant impact on the quality of life of the patients. In fact, surgery commonly results in orofacial disfigurement and speech impediments which can have a psychosocial effect on patients [31]. Radiotherapy and chemotherapy are usually used before surgery to shrink the tumour (neoadjuvant therapy) or after surgery to prevent recurrences (adjuvant therapy), alternatively they can be used alone or in combination as a primary treatment when surgery is not realisable (induction therapy) [32–34]. Overall, early stage OSCC is usually treated with surgery and/or radiotherapy, whereas advanced stage OSCC is often treated with a combination of surgery, radiotherapy and chemotherapy [4]. In fact, chemotherapy is highly recommended in OSCC cases with distant metastasis since it acts systemically allowing access to metastatic cells, unlike radiation and surgery which have effects on localised areas only [33]. The standard OSCC chemotherapeutics include platinum-based agents (cisplatin and carboplatin), taxanes (docetaxel and paclitaxel) and antimetabolites (5-fluorouracil) [30]. All these chemotherapeutic drugs can be used alone or in combination with each other to enhance to effect of the treatment, although this can increase the side effects. A commonly used combination is cisplatin with 5-fluorouracil or cisplatin and 5-fluorouracil combined with docetaxel.

1.1.5.1. Platinum-based agents

Platinum-based drugs are currently used in the treatment of various cancer types. These compounds are characterised by a platinum core which assists in the interaction with DNA to form inter- and intra-strand DNA adducts that cause cytostatic and cytotoxic effects. Cis-diamminedichloroplatinum II or cisplatin (CDDP) was the first platinum-based drug synthesised and it is currently the most commonly used antineoplastic agent in the treatment of OSCC [35]. Cisplatin is usually inert, and it is

activated intracellularly through spontaneous aquation reactions that lead to form more chemically reactive mono- and bi-acquated cisplatin products [36]. This results in the activation of several signalling pathways, such as ATM (ataxia telangiectasia mutated) and ATR (ATM and Rad3-related), MAPK (mitogen-activated protein kinase), p53, and 73, leading subsequently to cell death via apoptosis [37].

1.1.5.2. Antimetabolite agents

Antimetabolite agents are compounds very similar to normal metabolites involved in nucleic acid synthesis within the cells. For this reason, these molecules can be incorporated into either DNA or RNA and interfere with normal cellular functions. The most commonly used antimetabolite agent in OSCC treatment is 5-flurouracil. It is similar in structure to uracil but contains a fluoride atom at the 5-carbon position on the pyrimidine ring. In mammalian cells, 5-fluorouracil is converted to two active metabolites (fluorodeoxuridine monophosphate (FdUMP) and fluorouracil triphosphate (FUTP)), which are incorporated into DNA causing a disruption of its functions and cytotoxicity. Additionally, FdUMP acts by forming a stable complex with thymidylate synthetase (TS), resulting in its inhibition and depletion of thymidine triphosphate (TTP), while FUTP is incorporated into RNA leading to faulty translation of RNA [38, 39].

1.1.5.3. Taxanes

Taxanes are a class of compounds belonging to microtubule targeting agents (MTAs) which are commonly used as chemotherapeutics because of their ability to decrease cell proliferation and to trigger apoptosis by inhibition of mitosis. For this reason, they are often called anti-mitotic drugs. Taxanes contain a binding site on β-tubulin and act by preventing normal microtubule dynamic instability, which is necessary for cell cycle progression. Paclitaxel and docetaxel are the most commonly used taxanes employed for the treatment of OSCC. They both promote microtubule polymerisation and inhibit depolymerisation, which results in cell cycle arrest in G2 and M phases and subsequent cell death [40]. It has been reported that, although both paclitaxel and docetaxel share a similar mechanism of action, they show some differences in their molecular pharmacology, pharmacokinetics and pharmacodynamic profiles that can influence their clinical activity and toxicity [41].

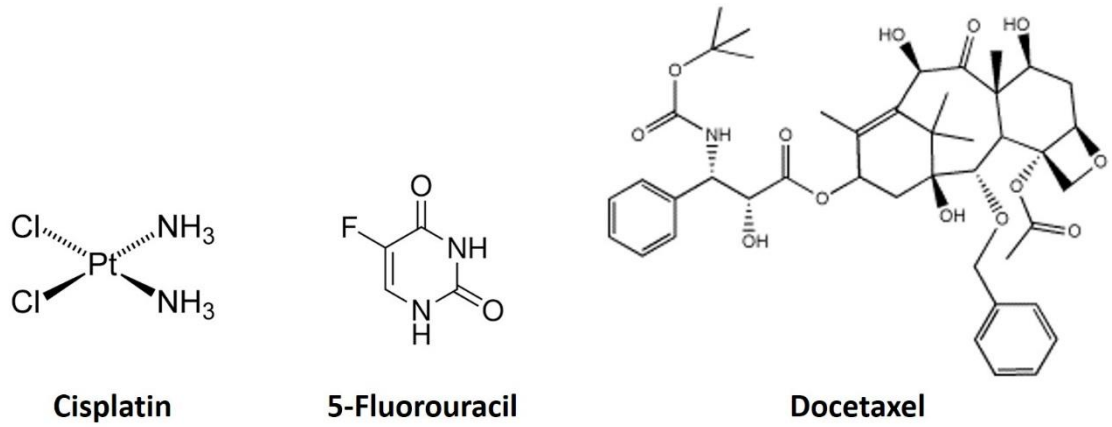

Figure 1.2 The chemical structures of cisplatin, 5-flurouracil and docetaxel.

1.2. Chemoresistance

Chemoresistance is considered as the lack of response of cells to a specific drug. This phenomenon was first observed in bacteria resistant to antibiotics, but a similar mechanism was then found in other diseases, including cancer [42]. In a cancer setting, chemoresistance results in the failure of tumour growth inhibition and in tumour dissemination.

Chemoresistance can be classified as primary drug resistance, which exists prior to any given cancer treatment, or acquired drug resistance, which occurs after the initial therapy [43]. Primary and acquired resistance can occur separately or co-exist together during chemotherapy, resulting in the failure of the treatment [44]. Primary or intrinsic resistance is characterised by an innate tolerance of patients to drugs and it may be due to inherited mutations of genes usually involved in cancer cell growth and/or cell death. Also, it can be attributed to a pre-existing subpopulation of drug-insensitive cells within tumours. In fact, tumours are characterised by a heterogeneous population of cells, including sub-clonal mutated cells and cancer stem cells, which cannot respond to apoptotic stimuli. In this case, primary resistance can be confused with acquired resistance, as patients will initially respond to the therapy because of the effect of the drug on the sensitive cells; however, a relapse can occur after the treatment due to the resistant sub-population [45–48]. On the other hand, acquired resistance is characterised by a gradual reduction of drug efficiency after chemotherapy. Acquired resistance can occur in about a ratio of 1 in 10^6-10^7 cancer cells for an average

detectable tumour of 10^9 cells. It has been proposed that in a typical tumour the presence of 10-1000 resistant cells is enough to determine the recurrence of the tumour after the destruction of the sensitive cells induced by chemotherapy [49]. Acquired resistance may be due to the acquisition of new mutations after the exposition of cells to the drug. Indeed, genotoxic stresses may increase the probability of developing new mutations in oncogenes, tumour suppressor genes and drug targets, resulting in tumour relapse. Additionally, it has also been associated with changes in the tumour microenvironment (TME) during chemotherapy, due to the release of exosomes and microRNAs by cancer cells [44].

Currently, drug resistance represents one of the major impediments in medical oncology. The mechanisms involved in chemoresistance are widely investigated and further discussed below. However, several questions about the development of a resistance phenotype are still unsolved. The huge variability observed among patients in response to different drugs is one of the main issues related to chemoresistance. This is exacerbated by the fact that, during a standard clinical trial, a drug can be considered approved when it has effect on at least the 20% of patients within a selected group, which means that the remaining 80% of patients is susceptible to a different response [49]. Therefore, it is important to perform genomic and biochemical analyses to determine the best treatment per each patient, in order to avoid the possibility of encountering pre-existing drug resistance [44]. Furthermore, the most common approach to overcome drug resistance is the treatment of the tumour by using more than one drug at the same time. Although this method offers good benefits at the beginning of the therapy, it may result in the phenomenon of multidrug resistance (MDR), which is defined as the insensitivity of various cancers to a broad range of antineoplastic drugs. Currently, MDR is becoming a common issue among patients. Based on these considerations, a better understanding of the mechanisms involved in drug resistance including in OSCC is necessary in order to improve therapeutic strategies aimed at long term remission and hopefully cures.

1.2.1. Mechanisms of drug resistance

Several mechanisms underlying drug resistance have been identified thus far. They include: drug inactivation, drug target modification, membrane transport alterations,

tumour-related signalling pathway dysregulations, DNA damage repair, adaptation to drug-induced stress, microRNAs, tumour microenvironment and epithelial-mesenchymal transition (Figure 1.3). All these mechanisms can act independently or in combination, and they can occur through various signalling pathways [42].

1.2.1.1. Drug inactivation

Many chemotherapeutic agents require metabolic activation in order to acquire clinical efficacy. Failed drug activation or inactivation has been associated with drug resistance and this has been correlated with the dysregulation of drug-metabolising enzymes. Thus, resistance to arabinoside (ara-C), the antineoplastic drug used for the treatment of acute myeloid leukaemia, has been linked to the under-expression of deoxycytidine kinase, the enzyme responsible of its activation [49, 50]. Moreover, resistance to platinum agents can occur through the over-expression of glutathione, which contributes to the inactivation of the drug by forming conjugates that are expelled from cells [51, 52]. Likewise, the direct binding of platinum drugs to metallothionein (MT), a small cysteine-rich protein, represents another mechanism of drug inactivation occurring in platinum resistance [53, 54].

1.2.1.2. Drug target modification

Drug resistance can also result from mutations that modify the activity or reduce the expression of drug target molecules. Examples of this mechanism have been observed in the acquired resistance to taxanes, associated with mutations of its target β-tubulin, and in the acquired resistance to 5-fluorouracil associated with a dysregulation of its enzyme target thymidylate synthase [42]. Another example of drug resistance due to target modification is given by the T315I mutation in the BCR-ABL tyrosine kinase, which can occur in the 20-30% of patients affected by chronic myelogenous leukaemia [55]. Substitution of threonine with isoleucine at the residue 315 of the BCR-ABL kinase domain results in the reduced efficacy of the anti-cancer drug imatinib, a tyrosine kinase inhibitor, by reducing the hydrogen bonds necessary for the binding of imatinib to the ATP-binding site of BCR-ABL [55, 56].

1.2.1.3. Membrane transport alterations

Alterations in cell surface receptors and transporters can influence drug uptake and efflux, resulting in drug resistance development. In this context, a crucial role is played

by the ATP binding cassette (ABC) proteins, belonging to a transport system superfamily and involved in the translocation across the membrane of various substrates, such as ions, amino acid, lipids and xenobiotics. All the ABC proteins contain 2 transmembrane domains necessary for the binding and the transport of the substrates, and 2 nucleotide-binding domains which promote conformational changes of the transporter through the binding and hydrolysis of adenosine triphosphate (ATP), which facilitates the pumping of the substrates across the membrane [42, 43]. It has been shown that the ABC transporters mediate the efflux of drugs during chemotherapeutic treatments and increased expression of these proteins has been linked to decreased intracellular drug accumulation and reduced drug potency, suggesting their role in chemotherapy resistance [44].

The most studied ATP transporters include: the multidrug resistance protein 1 (MDR1), the multidrug resistance-associated protein 1 (MRP1) and the breast cancer resistance protein (BCRP). All these transporters are naturally able to promote the efflux of many compounds from cells and their overexpression has been implicated in many drug resistant cancers [42]. The MDR1 protein, also called P-glycoprotein (P-gp) or ABCB1, mediates the efflux of hydrophobic, uncharged or positively charged compounds, including doxorubicin, paclitaxel and vinblastine [49]. In acute lymphocytic and myelocytic leukaemia and in lung cancer, a substantial increase of this protein has been found after chemotherapy [57–60]. Additionally, high levels of MDR1 has also been observed in several cancers (e.g. kidney, lung, liver, colon and rectum) before and after chemotherapy, suggesting its involvement in both intrinsic and acquired resistance [61]. The MRP1 transporter, or ABCC1 protein, mediates the transport of several compounds (including alkaloids, anthracyclines and methotrexate) and organic anionic substances as compounds conjugated to glutathione or sulphate [44, 62]. Overexpression of MRP1 has been associated with chemoresistance in lung and oesophageal cancer, leukaemia and neuroblastoma [63–66]. Similarly, high levels of BCRP (or ABCG2), which mediates the efflux of both positively or negatively charged drugs such as mitoxantrone, flavopiridol and anthracyclines, has been linked to drug resistance in breast cancer, as well as in lung cancer and leukaemia [67–69]. Inhibition of BCRP by gefitinib, a tyrosine kinase inhibitor, has been shown to reverse drug resistance in breast cancer [70].

1.2.1.4. Dysregulation of tumour-related signalling pathways

Chemoresistance has been associated with dysregulation of signalling pathways correlated to tumour initiation and progression. The nuclear factor-κB (NF-κB), the phosphatidylinositol-3-kinase (PI3K)/protein kinase B (Akt), the janus kinase/signal transducers and activators of transcription (JAK/Stat3), and the Ras/extracellular-signal-regulated kinase (ERK) pathways are examples of signalling pathways involved in differentiation, proliferation and survival. Dysregulation of these pathways by intrinsic or acquired oncogene and tumour suppressor gene mutations are strongly implicated in drug resistance. For example, overexpression of EGFR may lead to resistance to cisplatin by triggering the NF-κB and PI3K/Akt signalling pathway in lung cancer cells [71]. Down-regulation of p53 may also contribute to cisplatin resistance in lung cancer cells through the activation of the JAK/Stat3 signalling pathway [72]. Also, H-Ras mutations may mediate cisplatin resistance through the Raf/ERK signalling pathway in ovarian cancer cells [73]. Similarly, K-Ras mutations have been linked to resistance to chemotherapy in various cancers [88][89]. A greater activation of the Ras/ERK pathway has also been associated with the development of acquired drug resistance in leukaemia [87]. Furthermore, inhibition or dysregulation of cell death pathways might also represent a determinant mechanism of therapy resistance. In this regard, the overexpression of survivin (an inhibitor of apoptosis protein) was positively linked to cisplatin resistance in prostate cancer cells, while overexpression of the anti-apoptotic proteins Bcl-2 and Bcl-xL was correlated to chemoresistance in mesothelioma and laryngeal cancer [43].

1.2.1.5. DNA damage repair

The anticancer activity of many drugs depends on their capacity to induce DNA damage. It has been observed that enhanced ability of cells to repair DNA damage may represent another mechanism that allows cells to become resistant. Therefore, exposure of cells to these drugs may lead to acquired resistance due to the overexpression of proteins involved in the DNA Damage Response (DDR) pathway. For example, the ability of cisplatin to induce DNA adducts is usually counteracted by the DNA repair protein ERCC1 (excision repair cross-complementing protein), which activates the nucleotide excision repair and the inter-strand crosslink repair pathways [74]. Interestingly, high levels of ERCC1 have been observed in cisplatin-resistant

cells compared with cisplatin-sensitive cells, suggesting its role in cisplatin resistance [49, 75]. Likewise, guanine O6 alkylation induced by alkylated agents is usually counteracted by the O6-methylguanine DNA methyltransferase (MGMT). Overexpression of this protein has been linked to nitrosourea and temozolomide resistance in melanoma cells [76]. In addition, it has also been reported that an up-regulation of genes involved in the DDR pathway (e.g. FEN1, FANCG, RAD23B), were found in 5-fluorouracil-resistant cells of colon cancer [77, 78]. Given this, it has been proposed that targeting the DDR pathway may represent a good strategy to bypass drug resistance. However, the potential risk of developing new mutations because of the dysregulation of DDR makes this strategy still controversial [44].

1.2.1.6. Adaptation to drug-induced stress

Treatment of cells with chemotherapeutics results in cellular stress and induction of a cellular stress response [79]. Various types of stress have been linked to the effect of drugs, including genotoxic stress, endoplasmic reticulum (ER) stress and oxidative stress. Genotoxic stress results as a consequence of the ability of many drugs to induce DNA damage [80]. The ER plays an important role in calcium homeostasis, lipid biosynthesis and protein folding and trafficking. Accumulation of unfolded or incompletely folded proteins in the ER after treatment with various chemotherapeutics results in ER stress [81]. Moreover, enhanced generation of ROS following treatment with various chemotherapeutics has been linked to a marked cellular oxidative environment resulting in oxidative stress [82]. Cellular adaptation to stress induced by drugs has been proposed as a mechanism implicated in acquired resistance to chemotherapeutics [79, 83]. In particular, an emerging role for autophagy as an adaptive response to limit drug-induced cellular stress by reducing ROS and accumulated misfolded proteins from the ER lumen has been suggested [80, 84, 85]. Moreover, enhancement of intracellular antioxidant systems to escape from drug-induced oxidative stress has also been implicated in chemoresistance [86]. The role of autophagy and antioxidant systems in cancer and in chemoresistance will be further discussed below.

1.2.1.7. MicroRNAs

MicroRNAs or miRNA are small non-coding RNAs formed by 19–22 nucleotides [87]. This class of molecules is involved in the post-transcriptional regulation of many

genes and it is therefore implicated in various biological processes such as survival, apoptosis and the cell cycle. Interestingly, disruption of the microRNA biogenesis pathway has been associated with both tumour promoter and tumour suppressor activity [88]. Moreover, emerging evidence has shown a correlation between microRNAs and chemoresistance. In fact, since miRNAs can regulate the expression of proteins related to chemoresistance, selective expression of microRNAs has been linked to chemotherapy resistance in various tumours. For example, the regulatory activity of miRNA-21 and miRNA-200 on DNA MutS homolog 2 (hMSH2) protein (involved in DNA Damage Repair) has been correlated to chemoresistance to 5-fluorouracil and docetaxel in colorectal and lung cancer [89, 90]. Also, miR-15b and miR-16 have been shown to modulate multidrug resistance by targeting the anti-apoptotic protein Bcl-2 in human gastric cancer cells [91]. Additionally, miRNA-24 has been shown to reduce apoptosis resulting in drug resistance in non-small cell lung carcinoma [92]. All these examples highlight the relationship between microRNAs and chemoresistance.

1.2.1.8. Tumour microenvironment (TME)

The structure of solid tumours is very complex. It usually includes a heterogeneous population of cancer cells surrounded by a tumour microenvironment, which is composed of the extracellular matrix (ECM), blood vessels, signalling molecules and different kind of cells, such as fibroblasts, immune cells and mesenchymal stem cells. TME plays a crucial role in tumour initiation and progression, and it has also been associated with both intrinsic and acquired chemoresistance. A TME factor which has been linked to intrinsic resistance is the pH. In a normal setting, the intracellular pH of cells is slightly higher than the extracellular pH, whereas an opposite condition has been found in cancer cells. The “reverse pH gradient” observed in cancer cells results in a low extracellular pH, which can form a physiological drug barrier through a phenomenon called “ion trapping” [83, 93]. Additionally, intrinsic resistance has been also linked to the dynamic nature of vasculature in tumours, which results in oxidative stress induced by fluctuating hypoxia conditions. Oxidative stress conditions may determine a cellular genetic instability, which can lead to the development of a subpopulation characterised by a resistant phenotype [94]. Moreover, the inter-cellular communication mechanisms occurring among different cell types within the tumour may also contribute to chemoresistance; in fact, the releasing of signalling molecules

from a donor cell may determine drastic changes in a recipient cell. In this regard, secretion of high levels of colony stimulating factor-1 (CSF-1) by macrophages has been associated with proliferation and survival in glioma cells [95, 96]. Additionally, it has been observed that acquired resistance to paclitaxel may be mediated by survivin-containing exosomes in breast cancer cells and exosomal microRNAs may activate survival pathways in chemoresistant prostate and breast cancer cells [97–99].

1.2.1.9. Epithelial-mesenchymal transition (EMT)

EMT is an important process during development that consists of the loss in polarity and adhesion of epithelial cells, leading to their conversion to mesenchymal stem cells, characterised by migratory and invasive properties [43]. It has been demonstrated that EMT cells show a similar stem-like phenotype to cancer stem cells (CSCs), which are defined as multipotent and highly tumorigenic cells capable of self-renewal [100, 101]. Also, it has been suggested that the emergence of CSCs in tumours may occur in part as a result of EMT. Recently, a link between CSCs and EMT and drug resistance have been proposed. In this regard, it has been reported that treatment of CSC and non-CSC cells with chemotherapeutics results in the elimination of non-CSCs cells and in the survival of the CSC cells, suggesting the ability of the CSC cells to resist the effect of the drugs [102]. Consistently, a CSC-enriched subpopulation of chronic myeloid leukaemia (CML) cells treated with imatinib was shown to be more resistant to the drug compared to the CSC-deprived subpopulation of the CML cells from the same patients [103]. Moreover, knockdown of EMT transcription factors, such as Twist1 or Snail1, resulted in an enhancement of sensitivity to gemcitabine in pancreatic adenocarcinoma mice [104]. Also, overexpression of Twist1 and Snail1 has been correlated to enhanced activity of ABCB1, suggesting that some ABC transporter genes may be controlled by EMT transcription factors [105]. Interestingly, it has been proposed that EMT induction may be controlled by several stimuli, including cytokines, growth factors, microRNAs and hypoxia [43]. For example, EMT-mediated doxorubicin chemoresistance has been linked to high levels of transforming growth factor beta (TGF-β) in colon cancer cells, while EMT-mediated doxorubicin chemosensitivity has been linked to miR-760 in breast cancer [106, 107].

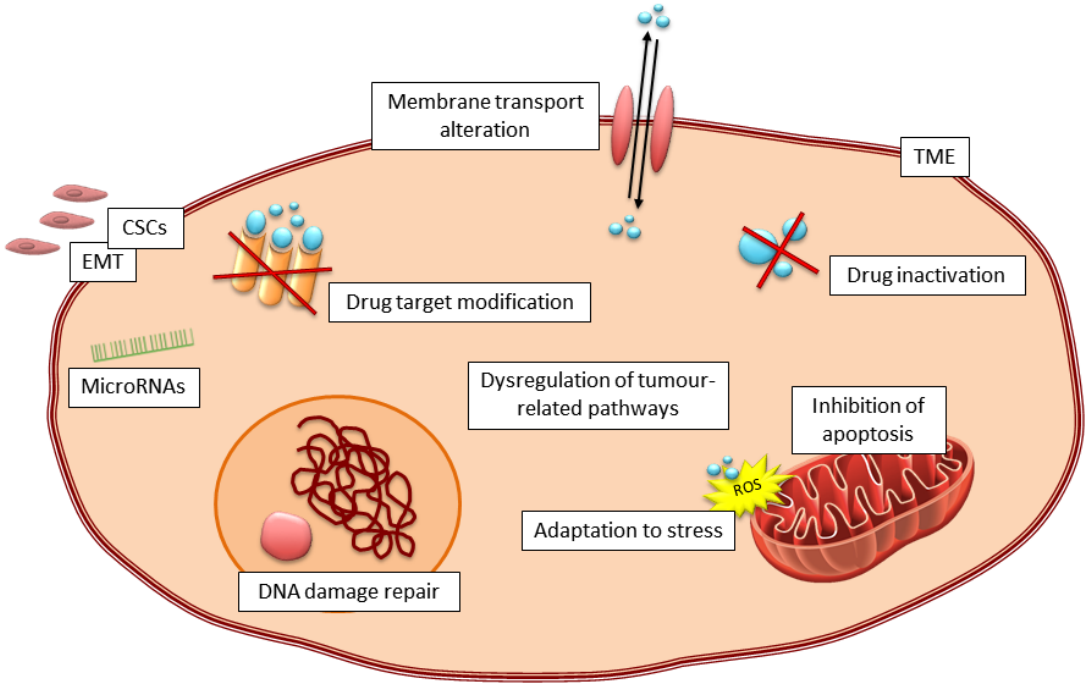

Figure 1.3 Graphical overview of the mechanisms underlying drug resistance.
Chemoresistance can result as a consequence of drug inactivation, drug target mutations, decreased intake or increased efflux of the drug. Dysregulation of tumour-related or stress-related signalling pathways can also reduce the cellular response to drugs. MicroRNAs regulate numerous signalling pathways implicated in chemoresistance. Tumour microenvironment (TME) and inter-cellular communication influences the ability of cells to respond to drugs. Cancer stem cells (CSCs) or CSC-like cells originated from the EMT contributes to chemoresistance through their stemness-like properties.

1.2.2. Chemoresistance in oral cancer

Drug resistance represents one of the main issues encountered during the treatment of OSCC. The mechanisms underlying chemoresistance in oral cancer are still not fully understood, however several studies have attempted to elucidate its molecular basis. Based on the current findings, a variety of factors may contribute to innate and acquired resistance in oral cancer, suggesting that more than one mechanism among the ones reported above can lead to the development of a resistant phenotype [108]. Mutations in the drug molecular targets, such as MDR1, MRP1 and BCRP, have been widely reported in oral cancer [63]. MDR1 overexpression has been observed in cisplatin-resistant OSCC cells, while MRP1 overexpression has been reported in both cisplatin- and vincristine-resistant OSCC cells [109, 110]. Also, high levels of BCRP

in oral cancer were found in a cancer stem-like side population of cells characterised by multidrug resistance properties [111–113]. Enhanced DNA Damage Repair has also been linked to chemoresistance in oral cancer. In this regard, an increased expression of ERCC1 in a carboplatin-resistant tongue carcinoma cell line compared to the corresponding sensitive cell line has been demonstrated [114]. In addition, recent papers have reported that 5-fluorouracil and cisplatin-resistant OSCC cells displayed epithelial to mesenchymal transition changes, suggesting an involvement of EMT in the development of chemotherapy resistance in oral cancer [115, 116]. Accordingly, it has been observed that Snail1 induced EMT in erlotinib-resistant cells and promoted a EMT-mediated cancer stem-like phenotype in head and neck cancer [117, 118]. Recently, a role for microRNAs in OSCC chemoresistance has also acquired more importance. A differential microRNA expression profile has been found in cisplatin-sensitive and resistant tongue carcinoma cell lines. From the analysis, miR-214 and miR-23 were denoted as chemoresistant microRNAs, while miR-21 was shown to sensitise cells to cisplatin [119]. Also, miR-200b and miR-15b may be involved in chemoresistance by inducing EMT in tongue cancer [116]. Finally, an impairment of apoptotic and autophagic pathways has recently been linked to OSCC chemoresistance, as this will be further discussed below.

1.3. Apoptosis

Apoptosis or programmed cell death (PCD) is a highly regulated and energy-dependent process, which involves the genetically determined suicide of cells [120]. Apoptosis is a physiological mechanism that occurs normally to maintain cell homeostasis and it has a critical role during development and ageing. It can also occur as an immunological and anti-tumour defence mechanism when it is induced by external factors [121]. Dysregulation of apoptosis has been linked to many human conditions such as, neurodegenerative diseases, ischemic damage, autoimmune disorders and cancer [120]. Cells that are undergoing apoptosis display distinctive morphological changes, including nuclear and cytoplasmic condensation, DNA fragmentation, cytoskeletal collapse, cell shrinkage and membrane blebbing. It results in a process called “budding” resulting in the separation of cell fragments into apoptotic bodies, which are subsequently phagocytosed by macrophages, thereby preventing an inflammatory response.

1.3.1. Apoptotic signalling pathways

The induction of the apoptotic pathway is usually mediated by a class of enzymes called caspases (cysteine aspartate-directed proteases). Caspases are usually present in the cytosol as inactive pro-enzyme forms containing an N-terminal pro-domain, followed by a large subunit (P20) and a small subunit (P10) (Figure 1.4). Caspase activation results in the cleavage of the pro-enzyme form at the aspartic acid cleavage sites existing between each of the subunits and the pro-domain [122]. Thus, cleaved caspase forms represent the active forms of the enzyme whose function is to activate other caspases, allowing the initiation of a protease cascade and the amplification of the apoptotic signalling pathway, resulting in cell death [120]. So far, the main caspases involved in apoptosis can be categorised into two classes: the initiator caspases (caspases 2, 8, 9 and 10) and the effector caspases (caspases 3, 6, and 7) depending on their function. Initiator caspases are responsible for intercepting pro-apoptotic signals and initiating caspase cascades, while effector caspases are activated by the initiator caspases and are responsible for the cleavage of targeted cellular proteins that ultimately result in the demise of the cell [122].

Apoptosis can be activated intracellularly or extracellularly resulting in two different pathways: the intrinsic or mitochondrial pathway and the extrinsic or death receptor pathway. However, it has been reported that the two pathways are linked and that molecules in one pathway can influence the other [123].

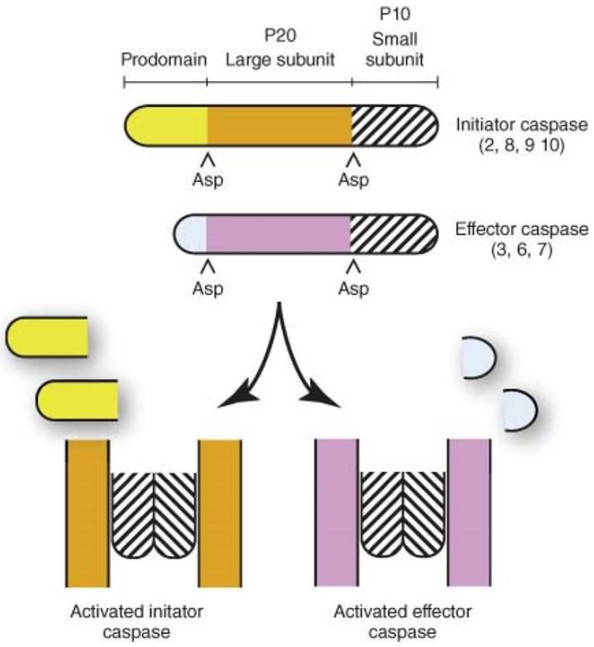

Figure 1.4 Structure and activation of apoptotic caspases.

The catalytically inactive pro-enzyme form of caspases contains an N-terminal pro-domain, a large (P20) and a small subunit (P10). The pro-domain of the initiator caspases (2, 8, 9 and 10) is much longer than that of effector caspases 3, 6 and 7. Caspase maturation occurs with cleavage of the pro-domain. Cleavage at the aspartic acid cleavage sites between the large and small subunits results in caspase activation. Rearrangement of the large and small subunits results in a catalytically active heterodimer. Image taken from [124].

1.3.1.1. The intrinsic pathway

The intrinsic signalling pathways or mitochondrial pathway is initiated by different non-receptor-mediated intracellular stimuli that produce a response within the cell. The main stimuli that initiate this pathway are the loss of cell survival factors, hypoxia, free radicals, viral infections, toxins and genotoxic agents such as radiation and chemotherapeutics [120]. All these apoptotic signals cause loss of the mitochondrial transmembrane potential and release of pro-apoptotic proteins (normally sequestered by mitochondria) into the cytosol [125]. Cytochrome c, Smac/Diablo and the serine protease HtrA2/Omi represent a class of pro-apoptotic proteins that once released into the cytosol can activate the caspase-dependent mitochondrial pathway (Figure 1.5). Smac/Diablo and HtrA2/Omi promote apoptosis by inhibiting XIAP (an inhibitor of apoptosis protein), while cytochrome c binds and activates Apaf-1 (apoptotic protease factor 1) and pro-caspase 9 forming the apoptosome [123, 125]. The activation of caspase 9 within the apoptosome induces the cleavage of pro-caspase 3 to form cleaved

caspase 3 resulting in cell death. The release of cytochrome c from the mitochondria is believed to be under the control of the Bcl-2 family of proteins which are regulated by the tumour suppressor protein p53. Bcl-2 family proteins contain both pro-apoptotic (e.g. Bad, Bax, Bak) and anti-apoptotic proteins (e.g. Bcl-2, Bcl-xL, Mcl-1). Additionally, it has been indicated that the mitochondrial pathway can also be activated in a caspase-independent mechanism through the release of two other apoptotic proteins: apoptosis inducing factor (AIF) and endonuclease G (EndoG). These proteins are usually released from the mitochondria into the cytosol as a late event, after cells have committed to die and they act through translocation to the nucleus and causing DNA fragmentation [120]. Caspase-dependent and caspase-independent pathways are not mutually exclusive, thus activation of one pathway may lead to the eventual activation of the other.

1.3.1.2. The extrinsic pathway

The extrinsic pathway or death receptor pathway involves transmembrane receptor-mediated interactions. Apoptosis is initiated by the binding of cell death ligands to their corresponding death receptors on the cell surface. To date, the best characterised ligand-receptors include Fas ligand (FasL)/Fas receptor (FasR), tumour necrosis factor-alpha (TNFα)/ tumour necrosis factor receptor 1 (TNFR1), Apo3 ligand (Apo3L)/ death receptor3 (DR3), Apo2L/DR4 and Apo2L/DR5 [120]. Death receptors are all members of the TNFR superfamily and are all characterised by similar cysteine-rich extracellular domains and a cytoplasmic domain called the "death domain", which has a critical role in transmitting the signal from the cell surface to inside the cell [126]. Upon ligand binding, death receptors trimerise and cytoplasmic adapter proteins are recruited. For example, FasL/FasR binding results in the interaction with the adapter protein Fas-associated protein with death domain (FADD), while TNF-α/TNFR1 binding results in the recruitment of TNFR1-associated death domain protein (TRADD). All these adaptor proteins contain N-terminal death effector domains (DED) that interact with the DED on pro-caspase 8 forming the death-inducing signalling complex (DISC). Under these conditions, pro-caspase 8 is auto-cleaved into its active form which can activate pro-caspase 3 and 7, triggering the proteolytic cascade and apoptosis. Moreover, caspase 8 can also trigger the intrinsic pathway by the activation of Bid (BH3 interacting domain death antagonist) resulting in the release of cytochrome c, Smac/Diablo and HtrA2/Omi [127].

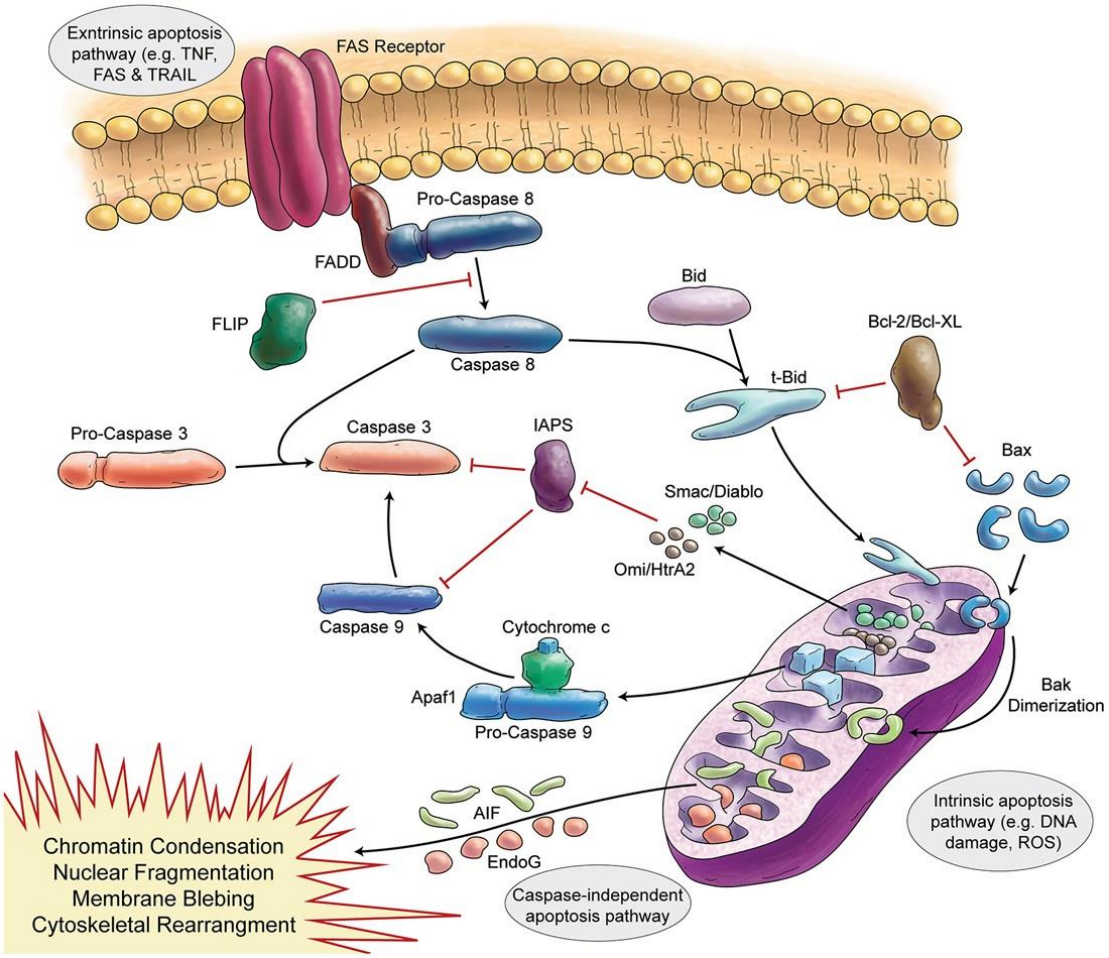

Figure 1.5 The extrinsic and intrinsic pathways of apoptosis.

In the extrinsic pathway, extracellular death receptor ligands bind their cognate death receptors, resulting in the activation of caspase 8. This either goes on to activate caspase 3, which triggers the proteolytic cascade, or Bid, which triggers the intrinsic pathway. The intrinsic pathways divided into caspase-dependent or caspase-independent pathways. The caspase-dependent pathway results in the release of pro-apoptotic proteins from the mitochondria. Cytochrome c binds and activates Apaf-1 and pro-caspase 9, Smac/Diablo and HtrA2/Omi inhibit XIAP. The caspase-independent apoptosis pathway results in the release of AIF and EndoG which translocate into the nucleus causing DNA fragmentation and chromatin condensation. Image modified from [128].

1.3.2. Apoptosis in cancer and chemoresistance

Evasion of apoptosis plays an important role in carcinogenesis allowing tumour cells to divide and grow uncontrollably [129]. This is usually due to defects in the apoptotic pathway and it results in a reduction of apoptosis or apoptosis resistance. It has been indicated that the over- or under-expression of genes encoding pro- or anti-apoptotic

proteins can be linked to a decrease of apoptosis and subsequent carcinogenesis [130]. In this regard, overexpression and deregulation of Bcl-2, Bax, Bcl-xL and IAPs have been reported in many cancers, and defects in p53 have been correlated to more than 50% of human neoplasia [131]. It has been reported that expression of mutant p53 protein alongside an increase in Bcl-2 and a decrease in Bax proteins were observed in OSCC [132]. Low levels of caspases or impairment of their function can also be associated with a reduction in apoptosis and it has been found that a downregulation of caspase 9 is frequent in stage II colorectal cancer patients [133]. Moreover, another important mechanism which contributes to the evasion of apoptosis can be the downregulation of the death receptors or an impairment of their function [130]. In addition, impairment in the apoptotic pathway has been shown to play a crucial role in chemoresistance. Not surprisingly, high levels of the anti-apoptotic Bcl-2 and Bcl-xL proteins were found in a drug-resistant OSCC cell line, and inhibition of these proteins was associated with an increase in carboplatin and cisplatin toxicity in oral and ovarian cancer, respectively [134, 135]. Similarly, overexpression of the IAP family member survivin was observed in several chemoresistant cancer cells and inhibition of survivin using sepantronium bromide (YM155) was shown to reverse cisplatin resistance in head and neck cancer both *in vitro* and *in vivo* [136–138].

Induction of apoptosis is one of the main strategies to treat cancer. Targeting the apoptotic pathway in order to stop the uncontrollable growth of cancer cells represents a key goal of many anticancer therapies. Moreover, combining standard chemotherapeutic agents with IAP and anti-apoptotic Bcl-2 family inhibitors may also represent a valuable strategy to bypass drug-resistance [139].

1.4. Autophagy

The term autophagy derives from the Greek words *auto*, meaning “self” and *phagein*, “to eat”. Autophagy is a basic catabolic process that takes place in all eukaryotic cells [140] and allows the degradation and the recycling of unnecessary or dysfunctional cellular components in order to maintain cell homeostasis. It occurs via a lysosome-dependent mechanism, in contrast to the ubiquitin-proteasome system which allows the direct degradation of intracytoplasmic proteins [141]. Under physiological conditions, autophagy operates as an intracellular quality control system, ensuring the

continual removal and turnover of potentially dangerous entities including organelles, proteins and/or portions thereof [142]. Thus, autophagy plays an essential role in tissue homeostasis, development, ageing, differentiation of many cell types and immune responses [143].

Beyond the constitutive role of autophagy, it has been observed that many conditions such as nutrient starvation and metabolic stress can lead to autophagy activation. In this regard, induced autophagy represents a stress responsive mechanism essential to sustain cell integrity and survival by the degradation and recycling of damaged proteins and organelles in order to generate ATP and new 'building blocks' for anabolic processes. Therefore, given the importance of autophagy, it is not surprising that its dysregulation can have severe consequences. In fact, it has been demonstrated that autophagy is implicated in the pathogenesis of several diseases such as cardiac and neurodegenerative diseases, diabetes, obesity and cancer [143]. Three different types of autophagy, differing in their mechanisms and functions, have been identified: macroautophagy, microautophagy and chaperone mediated autophagy. All of these pathways converge in lysosomes to ensure intracellular degradation and they differ in the mechanisms related to the recognition and embedding of cellular components. In macroautophagy, the engulfment of cytoplasmic materials is mediated by double-membrane vesicles that fuse with lysosomes; whereas in microautophagy, cytoplasmic material becomes trapped in the lysosome by a random process of membrane invagination. In contrast, in chaperone mediated autophagy, heat shock proteins (such as Hsp70) are employed by the cell for the recognition and the translocation of proteins into the lysosome [144]. To date, macroautophagy is the most well characterised mechanism and, for this reason, the terms "macroautophagy" and "autophagy" are frequently used interchangeably.

1.4.1. Autophagy process

Autophagy is a multi-step process involving autophagosome formation (consisting of nucleation, expansion and closure), fusion, degradation and recycling (Figure 1.6). The nucleation phase results in the progressive segregation of proteins and organelles by double membrane structures known as phagophores or isolation membranes [142]. The origin of the phagophore is still unclear but it is believed that they are lipid bilayers

derived by the ER or the trans-Golgi and the endosomes [140]. The extension and the sealing of phagophores leads to the engulfment of cytoplasmic material into intact double membrane vesicles named autophagosomes (size range 300-900 nm), which then fuse with the lysosomes in order to form the autolysosomes [143]. Autolysosome formation is mediated by a microtubule network which controls the vesicle motility, two lysosome-associated proteins (LAMP-1 and LAMP-2) necessary for the integrity of lysosomes membranes, and a set of proteins that controls the attachment and fusion of the vesicles, such as SNAP receptors (SNARES) and the EPG5 (ectopic P-granules autophagy protein 5 homolog) [145]. In the autolysosomes, cytoplasmic materials are degraded by lysosomal hydrolases, and the metabolites generated are then exported by lysosomal permeases out to the cytoplasm in order to be reused as a source of energy or building blocks for the synthesis of new macromolecules [141].

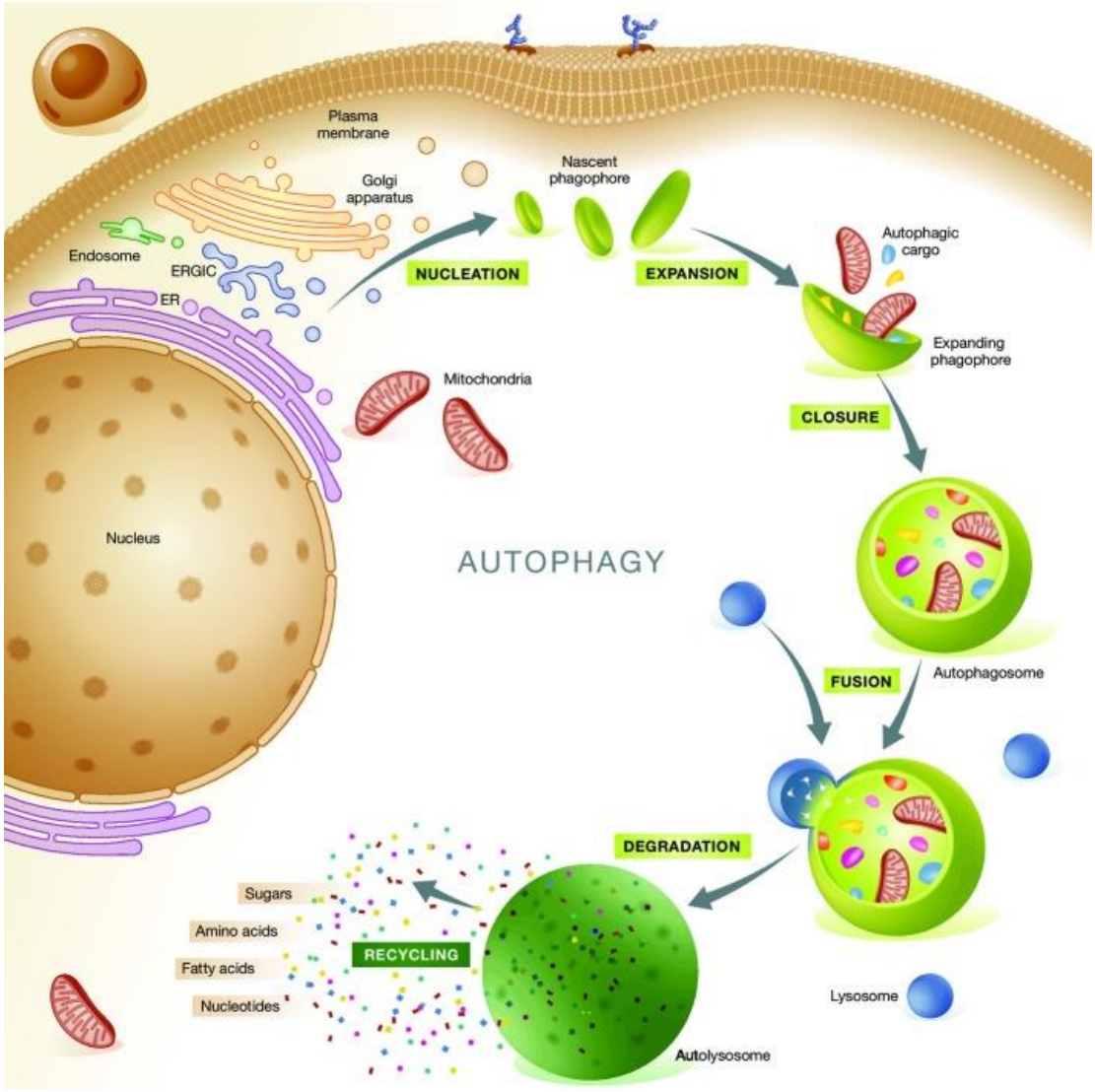

Figure 1.6 The process of autophagy.

Autophagy initiates with the progressive segregation of proteins and organelles into doubled membrane structures known as phagophores. Completely sealed phagophores, known as autophagosomes, fuse with lysosomes to form autolysosomes. In the autolysosomes, the autophagosomal cargo is degraded and the products reach the cytosol via transporters of the lysosomal membrane and are recycled by anabolic or bioenergetic processes. Image taken from [142].

1.4.2. Molecular machinery of autophagy

Formation of the autophagosome involves the recruitment of various proteins, including the autophagy-related (ATG) proteins, which are usually referred to as the molecular core machinery. Thus far, more than 36 ATG proteins have been identified in yeast and the orthologs of most of these proteins have been found in mammals, suggesting that autophagy is an evolutionarily conserved mechanism [146]. In

mammals, the core machinery proteins can be divided into different functional subgroups: the ULK (unc-51 like autophagy activating kinase) complex, the PtdIns 3-kinase (PtdIns3K) complexes, the ATG9 system and two ubiquitin-like (ubl) conjugation systems [147] (Figure 1.7).

The ULK complex is involved in the induction of autophagosome formation and it can be activated via mTOR (mammalian target of rapamycin)-dependent or -independent pathways, as further discussed in the next paragraph. The ULK complex includes various proteins: ULK1/2, ATG13, RB1CC1/FIP200 and C12orf44/ATG101 and its activation results in the phosphorylation of ATG13 and RB1CC1/FIP200 by ULK1/2 [147].

The PtdIns3K complex is crucial during the autophagosome formation and it is produced by the binding of Vps34 (PIK3C3) to its core partners Vps15 (PIK3R4) and Beclin-1. Beclin-1, a BH3 domain-only protein, is activated and phosphorylated by ULK1 and regulates both autophagosome nucleation and expansion. Autophagosome nucleation is mediated by the interaction of Beclin-1 with the ATG14 complex (containing AMBRA1 (activating molecule in Beclin-1-regulated autophagy) and Bcl-2), whereas autophagosome maturation occurs via the interaction of Beclin-1 with two other complexes: the UVRAG (UV radiation resistance-associated gene protein) complex where ATG14 and AMBRA1 are replaced with UVRAG and its positive regulator SH3GLB1, and a second complex where SH3GLB1 is replaced with Rubicon, which inhibits UVRAG [147]. Therefore, the Beclin-1/Vps34/UVRAG complex positively regulates autophagosome maturation, while Beclin-1/Vps34/UVRAG/Rubicon complex negatively regulates the process [143]. The interaction of Beclin-1 with Vps34 and UVRAG depends on the detachment of Beclin-1 from the anti-apoptotic proteins Bcl-2 and Bcl-xL, which can be consequentially considered negative autophagy regulators.

The ATG9 protein is also important during the nucleation phase and it acts by delivering membranes to the expanding phagophore or directing this process. It has been observed that it is the only transmembrane protein in the core machinery and its activation is dependent on the activity of ULK1 and Vps34 [146].

Finally, two ubl-conjugation systems take part during the last stages of autophagosome formation: the ATG12 system and the microtubule-associated protein1 light chain 3

(MAP1LC3) system. ATG12 is activated by ATG7 (E1 step), transferred to ATG10 (E2 step) and then conjugated with ATG5 in order to form a complex with ATG16 [148]. On the other hand, MAP1LC3 protein, also known as LC3, is cleaved by ATG4 to form LC3-I and subsequently conjugated to the phospholipid phosphoethanolamine (PE) at the C-terminal glycine residue, through ATG7 (E1 step), ATG3 (E2 step) and ATG12/ATG5/ATG16 (E3 step) [149]. The PE-conjugated form of LC3-I is known as LC3-II and it is anchored to the phagophore and the autophagosome membranes through the PE-group that promotes the integration of the protein into the lipid bilayers. Moreover, LC3-II plays an important role in selecting cargo for degradation by its interaction with sequestosome1 (SQTM1), also known as p62 [146]. In fact, p62/SQTM1 is a cargo receptor for selective autophagy and it is involved in the delivery of ubiquitinated proteins to the autophagosome for degradation. It has been observed that p62/SQTM1 binds specific cargo proteins, through an ubiquitin-binding domain, and simultaneously anchors them to LC3-II proteins present on the autophagosome interior membrane, through an LC3 interacting region (LIR) [150, 151]. LC3 and p62/SQTM1 are two well-characterised autophagic proteins and for this reason are commonly used as markers for autophagy. Indeed, the conversion of LC3-I to LC3-II with the consequential increase of LC3-II, alongside the decrease of p62/SQTM1, due to its degradation inside the autolysosomes, are widely used methods to monitor autophagic flux [151].

A canonical autophagy pathway involves all the ATG proteins, as mentioned above. However, it has been found that under certain circumstances autophagy may also be activated through non-canonical pathways which require only a subset of ATGs [144]. These alternative forms of autophagy can occur independently of some proteins involved in the molecular machinery, including Beclin-1, ULK, ATG5, ATG7 and LC3. For example, it has been observed that Beclin-1 independent autophagy bypasses Beclin-1 activation during autophagosome formation, while it requires both ubl-conjugation systems. This non-canonical pathway has been found commonly induced following the exposure of cells to pro-apoptotic compounds, but also during differentiation and bacterial toxin uptake [152].

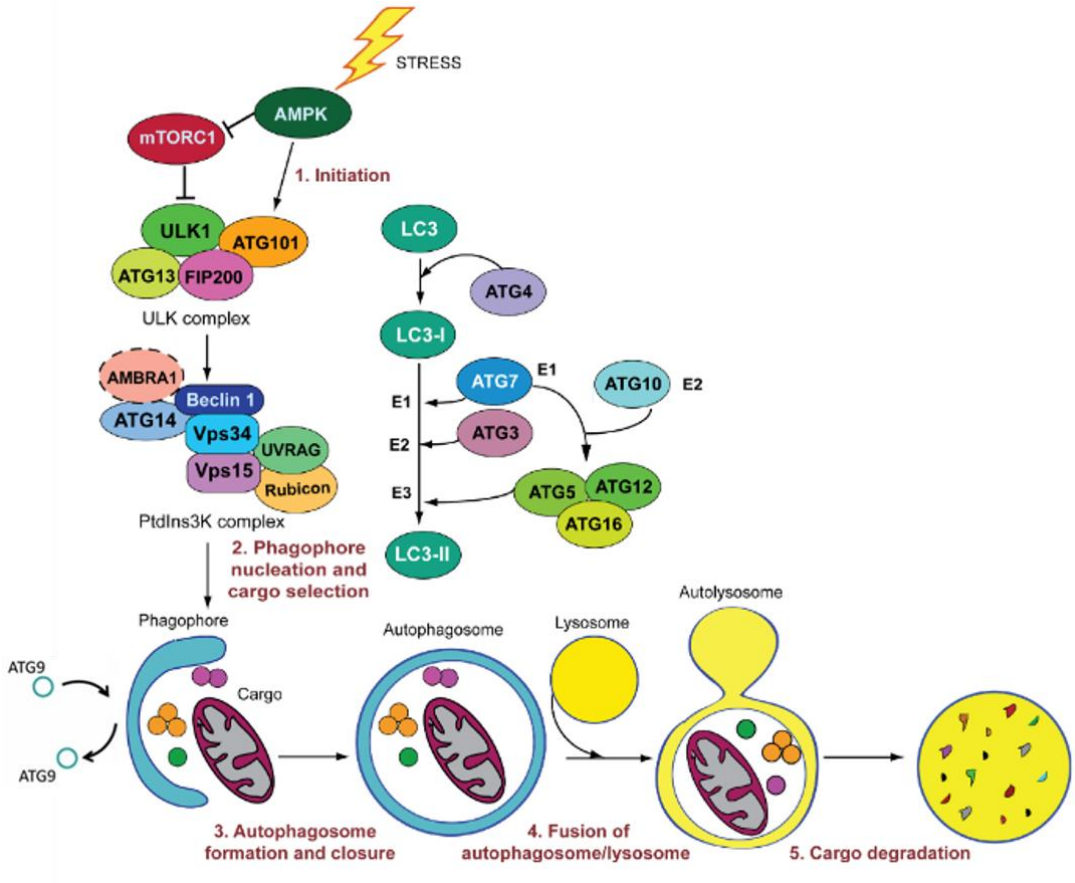

Figure 1.7 Molecular machinery of autophagy in mammals.

In the canonical pathway, autophagosome formation occurs through the activation of the ULK complex, the PtdIns3K complex and ATG9 protein. Two ubiquitin-like modification systems take also part during the autophagosome formation and maturation. ATG12 is activated by ATG7 (E1 step), transferred to ATG10 (E2 step), conjugated to ATG5 and subsequently forms a complex with ATG16. LC3 is cleaved by ATG4 to LC3-I, activated by ATG7 (E1 step), transferred to ATG3 (E2 step), and conjugated to the ATG12/ATG5/ATG16 complex (E3 step) forming LC3-II. Image modified from [149].

1.4.3. Autophagy regulation

Autophagy is a highly regulated process, which is controlled by various signalling pathways upstream of the autophagy machinery. The main autophagy regulators are also involved in tumour progression and they include: mTOR, AMPK, Ras, p53, Stat3 and the Bcl-2 protein family [148].

To date, the best characterised regulator of autophagy is mTOR, a serine/threonine kinase existing in two forms: mTOR complex 1 (mTORC1), strongly involved in autophagy regulation, and mTOR complex 2 (mTORC2) which is not a direct autophagy regulator [141]. In general, mTORC1 is an important regulator of cell

homeostasis involved in several cellular processes (e.g. lipid biogenesis, protein synthesis, and cell cycle progression), and it can respond to multiple stimuli such as the presence of growth factors, nutrients, energy levels and stress conditions [153]. mTORC1 is directly activated by Rheb (Ras homolog enriched in brain), which in turn is under negative control of the GTPase-activating protein complex TSC1/TSC2 (TSC, tuberous sclerosis complex) [153]. mTORC1 negatively controls the autophagic process, indeed, its activation leads to the phosphorylation and inhibition of ULK1/2 and Vps34, necessary for autophagosome formation as described above [154]. Thus, under physiological conditions, the activation of mTORC1 results in the maintenance of autophagy at basal levels, whereas cell starvation or stressful conditions lead to mTORC1 inhibition and consequential upregulation of autophagy. mTORC1 activation is regulated by several signalling pathways, including the PI3K/Akt/mTOR pathway, the AMPK/mTOR pathway, Ras/Raf/MEK/ERK pathway, and the p53 pathway [155]. The PI3K/Akt/mTOR pathway is considered one of the main autophagy regulating mechanisms. It is usually triggered by growth factors, amino acids, nutrients, and cytokines (e.g. IL-3) which lead to PI3K activation and subsequent phosphorylation of Akt at serine residue 475 (Ser^{475}). This signalling results in the activation of mTORC1 by its direct interaction with Akt or by TSC1/2 inactivation and Rheb activation [154].

AMPK (AMP-activated protein kinase) is also an important autophagy regulator. AMPK is a stress sensor protein which is activated in response to energy stress by sensing increases in AMP:ATP and ADP:ATP ratios [156]. AMPK activation under nutrient and energy depletion conditions leads to TSC1/2 activation and subsequently to mTORC1 inactivation and autophagy induction. Therefore, AMPK is a positive regulator of autophagy and controls the pathway by regulating mTORC1 [148]. Moreover, AMPK can also directly control autophagy in an mTOR-independent mechanism, through ULK1 phosphorylation.

Another important autophagy sensor is Ras which is usually activated by growth factors and it can control autophagy by triggering other downstream signalling pathways. It has been reported that the role Ras plays in autophagy regulation is context-dependent. In fact, it can act as negative autophagy regulator by activating mTORC1, but also as positive autophagy regulator through an mTORC1-independent mechanism that involves the activation of ERK and JNK [157–159].

Autophagy regulation can also be mediated by the p53 tumour suppressor. It has been reported that p53 can positively and negatively regulate autophagy, depending on its cellular localisation [160]. Under genotoxic stress, the nuclear p53 pool promotes autophagy through the activation of AMPK and through the transcriptional regulation of other autophagy modulators such as DAPK (death-associated protein kinase), DRAM (damage-regulated modulator of autophagy) and Sestrin1/2. Sestrin1/2 was shown to activate autophagy by activating AMPK and inhibiting mTORC1, whilst DAPK and DRAM were showed to induce autophagy by directly or indirectly regulating autophagosome formation [161, 162]. On the other hand, cytoplasmic p53 can inhibit autophagy in the absence of cellular stresses by inhibiting of TSC1/2, which subsequently results in mTORC1 activation. Moreover, several stimuli (e.g. ER stress) induce autophagy through the degradation of the cytoplasmic form of p53 by HDM2 (the p53-specific E3 ubiquitin ligase). In this regard, it has been shown that inhibition of HDM2 prevents autophagy activation by blocking p53 degradation [163].

Stat3 is a signalling molecule which can be transcriptionally activated through tyrosine phosphorylation by JAK in response to various stimuli such as cytokines and growth factors [164]. Similar to p53, Stat3 is also involved in autophagy regulation and its function depends on its subcellular localisation. It has been proposed that the unphosphorylated form of Stat3 localises in the cytoplasm, while the phosphorylated form can dimerise and translocate to the nucleus or the mitochondria [144]. Under normal conditions, cytoplasmic Stat3 has been shown to negatively control autophagy by sequestering the eukaryotic translation initiation factor 2-α kinase 2 (EIF2AK2) and forkhead box O (FOXO) 1 and 3 [165]. EIF2AK2 acts as an autophagy promoter by phosphorylating EIF2A (eukaryotic translation initiation factor), which in turn upregulates ATF4. FOXO1 and FOXO3 also act as autophagy promoters by transcriptionally activating various autophagy-related genes (e.g. ULK, Beclin-1, ATG12 and LC3). Once activated, STAT3 can translocate to the mitochondria, where it negatively regulates autophagy by suppressing ROS production, or into the nucleus, where it can both activate or suppress autophagy-related genes (e.g. Bcl-2, Beclin-1, Vps34) resulting in either autophagy induction or abrogation in a context-dependent manner [165].

Finally, several studies implicate the Bcl-2 family of proteins as further autophagy regulators. Under physiological conditions, the anti-apoptotic Bcl-2 proteins inhibit

the autophagic pathway by binding Beclin-1 and disrupting its association with the PtdIns3 kinase complex, whereas under starvation conditions, the release of Beclin-1 from Bcl-2 proteins induces the activation of the autophagic pathway. Moreover, the implication of the Bcl-2 family of proteins in both apoptosis and autophagy suggest that there is highly regulated crosstalk between these two pathways that will be further described below [166].

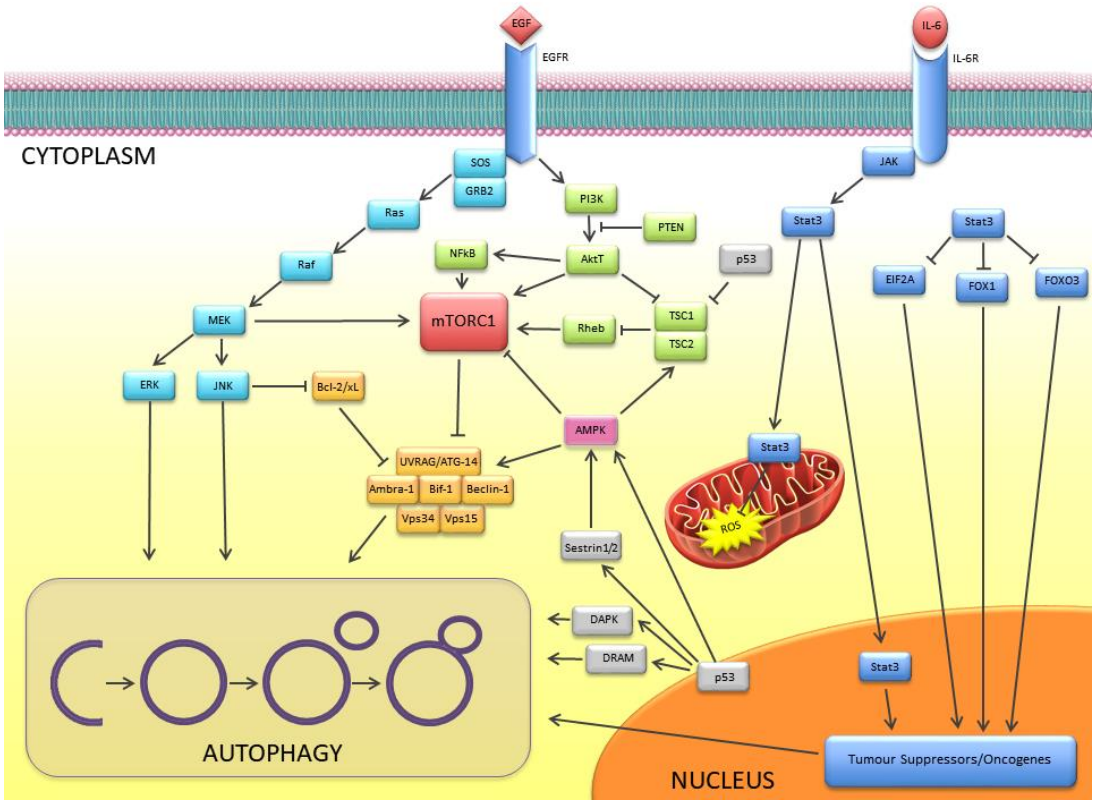

Figure 1.8 Schematic representation of the signalling pathways that regulate autophagy.
Autophagy is regulated by several signalling pathways. The PI3K/Akt/mTOR pathway plays a central role and positively regulates autophagy. Ras controls the Ras/Raf/MEK pathway resulting in mTORC1 activation (authophagy inhibition) or ERK/JNK activation (authophagy induction). The JAK/Stat3 pathway positively or negatively regulates autophagy through mTORC1-independent mechanisms. DNA damage and energy depletion can trigger autophagy by the AMPK and p53 pathways. The Bcl-2 family of proteins negatively regulates autophagy through an interplay with the PtdIns3 kinase complex.

1.4.4. Role of autophagy in cancer

Dysregulation of autophagy may have implications for the pathogenesis of several diseases including cancer. So far, the involvement of autophagy has been implicated

in different kinds of cancers such as pancreatic, breast, hepatocellular, colorectal and lung cancer [167]. However, the role of autophagy in cancer is complex and controversial, in fact, it has been observed that during tumorigenesis autophagy can act as a pro-tumour or anti-tumour mechanism.

It is known that autophagy is a survival mechanism important in maintaining cellular homeostasis under nutrient deprivation and hypoxia. During tumorigenesis autophagy confers to cancer cells a high-grade tolerance against stress, which results in reduction in tumour cell damage, increase in viability and maintenance of dormancy. Additionally, it has been reported that this pro-tumour effect of autophagy represents a prominent mechanism to escape not only from hypoxic and metabolic stress but also detachment-induced and therapeutic stress, thus it can be correlated to metastasis development and resistant phenotype to chemo- and radio-therapy [168]. By contrast, it has been suggested that autophagy driven anti-tumour activity can be exerted by the suppression of chromosomal instability and oxidative stress (which represent oncogenic stimuli), the induction of senescence phenotype and the reduction of local inflammation [168]. This paradoxical dual role of autophagy in cancer has resulted in autophagy being considered as a double-edged sword during tumorigenesis (Figure 1.9) [143].

It has been proposed that autophagy function depends on the kind of cancer and the stage of the malignancy, resulting in finely tuned regulation of the autophagic pathway and of its effect on the course of tumorigenesis [169]. During tumour initiation, decreased levels of autophagy are associated with an increase in metabolic stress and DNA damage, resulting in autophagy tumour suppressor activity by reducing cell proliferation and chromosome instability and by inducing senescence [143]. Later, during tumour progression, under conditions of starvation, hypoxia and metabolic stress (due to the poor vascularisation), high levels of autophagy have been shown to induce increased cancer cell survival, thus eliciting an autophagic pro-tumour effect [170]. Additionally, high levels of autophagy allow for tumour cell adaptation to the tumour microenvironment and consequential cell growth resulting in cancer maintenance [143]. The role of autophagy in OSCC is still not completely understood, although it has been implicated in oral tumorigenesis [140].

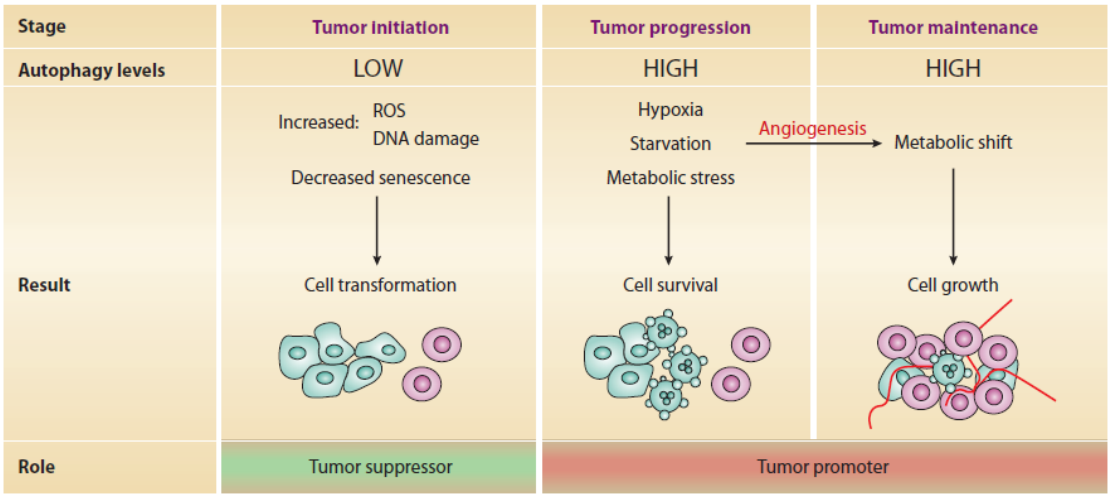

Figure 1.9 The role of autophagy in cancer.

The role of autophagy in cancer is context-dependent. During tumour initiation, autophagy acts as tumour suppressor mechanism, thus low autophagy levels result in an increase of ROS and DNA damage, and a decrease in senescence, leading to cell transformation. Later, during tumour progression, hypoxia, starvation and metabolic stress results in an enhancement of autophagy which in turn promotes cell survival. Cancer cells subsequently become dependent on autophagy to sustain cell growth, resulting in cancer maintenance. During these two later stages of tumour cell biology, autophagy acts as a tumour promoter mechanism. Image taken from [143].

1.4.5. Dysregulation of autophagy in cancer

As mentioned above, dysregulation of autophagy has been associated with tumorigenesis and cell survival. Dysregulation of autophagy may be determined by an abnormal expression of key autophagic proteins due to mutations occurring in the corresponding genes. In this regard, monoallelic Beclin-1 deletions and mutations of UVRAG and ATG genes represent the most common examples of mutated autophagic genes. They have been found in several human cancers, including breast, ovarian, prostate, gastric and colorectal cancer [171–173]. In addition, it has been observed that impairment of the signalling pathways controlling autophagy may also result in autophagy dysregulation. In this context, both tumour suppressors and oncogenes play a crucial role in autophagy regulation, leading to autophagy activation or inhibition. Given the dual role of autophagy as pro-tumour and anti-tumour mechanisms, it is not surprising that both inhibition and activation of autophagy can occur during cancer development. Generally, tumour suppressor genes are considered pro-autophagic factors, whereas oncogenes are considered anti-autophagic factors [155]. For example,

loss in PTEN, a PI3K inhibitor, in prostate cancer results in a constitutive activation of the PI3K/Akt/mTOR pathway and in autophagy inhibition [174]. Similarly, loss in p53 and downregulation of autophagy has been linked to tumorigenesis in an *in vitro* model of colon cancer cells [175]. Inhibition or downregulation of autophagy in these cancers may suggest its role as a cell survival mechanism. On the other hand, high levels of autophagy have been observed in K-Ras and B-Raf-mutated pancreatic cancers and in pediatric brain tumours [176–179]. Also, AMPK-dependent autophagy activation may be linked to cell survival in triple breast cancer cells [180]. Activation of autophagy in these cancers has been correlated to the development of an autophagy-dependent phenotype of cancer cells, which suggests an involvement of autophagy as pro-tumour mechanism. It has been proposed that screening of specific markers, such as Ras, B-Raf or p53 may represent a valuable strategy to predict whether autophagy may be activated or inhibited in cancer [177]. Understanding the autophagy dysregulation mechanisms implicated in a certain tumour may also clarify the role of autophagy in cancer. This will be crucial to develop specific therapeutic treatments targeting autophagy.

Dysregulation of autophagy has also been reported in oral cancer. Indeed, some somatic aberrations commonly associated with head and neck cancer such as mutations in PI3K have been linked with autophagy dysregulation [181]. Moreover, an increase of LC3 expression levels has been observed in OSCC samples compared to normal oral mucosa samples by immunohistochemistry, and it has been associated with poor clinical outcomes [182]. Several studies have also shown low levels of Beclin-1 and aberrant ATG genes in both OSCC tissue and cell lines [183–187]. Additionally, overexpression of ATG9 in the cytoplasm of tumour cells has been proposed as a potential biomarker for the recurrence and survival of OSCC [188]. A further investigation of autophagy dysregulation will be necessary to determine the role of autophagy in oral tumorigenesis.

1.4.6. Autophagy and chemotherapy

Recent studies have demonstrated that autophagy is frequently activated in tumour cells treated with chemotherapy. Similar to its dual role in cancer, a paradoxical role of autophagy has been observed following anticancer treatments. [189]. On the one

hand, autophagy induction has been considered as a cell death mechanism following the exposure of cells to chemotherapeutics. In fact, the exposure of cells to persistent stress, leads to an ultimate cellular response for limiting the proliferation of abnormal cells resulting in programmed type I cell death or apoptosis. In many cases, it has been observed that autophagic vesicles are present in dying cells, suggesting that an alternative mechanism of cell death known as autophagic cell death or type II cell death may occur [190]. On the other hand, autophagy induction may represent a protective mechanism to mediate the acquired resistance phenotype of some cancer cells during anticancer therapy. Indeed, it can be activated as a stress response mechanism to maintain cell homeostasis following the genotoxic effects of chemotherapy (see Figure 1.10). It has been suggested that this dual role of drug-induced autophagy, resulting in the enhancement or inhibition of anticancer treatments, is highly dependent on the tumour type and treatment characteristic. Nevertheless, several studies *in vitro* and *in vivo* seem to more strongly support the pro-survival role of autophagy, thus its ability to facilitate drug resistance during anticancer treatment. In this regard, autophagy inhibitors may represent a new therapeutic strategy to re-sensitise cancer cells to chemotherapy [189].

In OSCC, it has been shown that numerous chemotherapeutics activate the autophagic pathway, but the role of autophagy following chemotherapeutic treatment remains poorly understood. In fact, activation of autophagy has been observed following treatment with cisplatin in oral and oesophageal cancer [191, 192]. In these studies, inhibition of autophagy was correlated to an enhancement in cisplatin sensitivity, suggesting a potential role of autophagy in chemoresistance. Similar findings were also observed in hypopharyngeal and salivary adenoid cystic carcinoma cells, where inhibition of autophagy using both genetic and pharmacological approaches was shown to induce cisplatin toxicity [193, 194]. Additionally, high levels of Beclin-1, ATG5-ATG12 and LC3-II have been observed in a methotrexate-resistant tongue carcinoma cell line compared to the sensitive cell line [195]. By contrast, several studies have also proposed that drug-induced autophagy may also play an anticancer effect in oral cancer. For example, treatment of cells with sulfasalazine, thymoquinone and tetrandrine has been linked to autophagic cell death in oral cancer [196–198]. Given this, further studies on the role of autophagy in response to chemotherapy and its implication in chemoresistance are required.

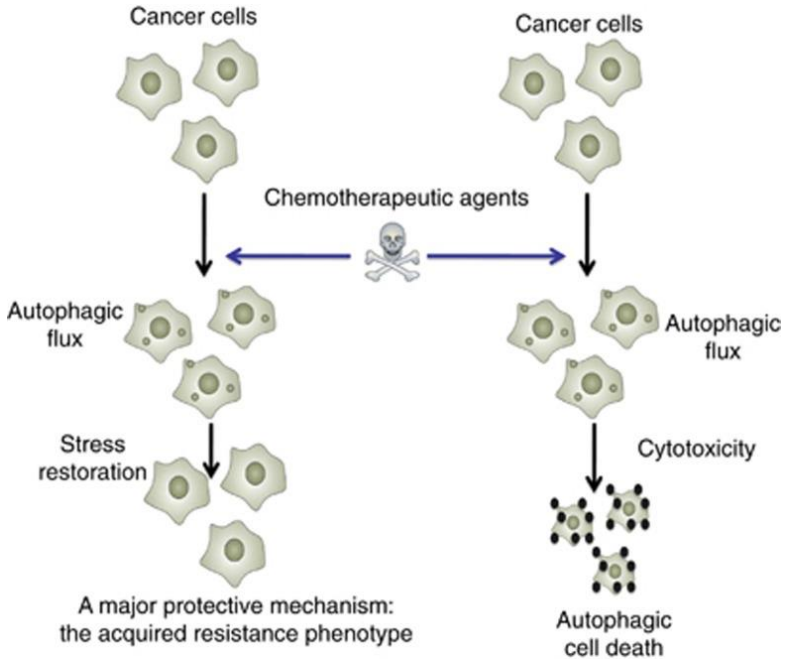

Figure 1.10 Dual role of autophagy during chemotherapy.

On one hand, autophagy is activated as a cell survival mechanism that may lead to the acquisition of a resistance phenotype of some cancer cells. On the other hand, autophagy is activated as a cell death mechanism, resulting in the autophagic cell death. Image taken from [189].

1.4.7. Autophagy inhibitors

In the last decade, the importance of autophagy in cell homeostasis and its implication in many diseases has drawn the attention of the scientific community. In particular, the potential role of autophagy as a cell survival mechanism for cancer cells has led to the hypothesis that targeting autophagy may represent a new strategy in cancer therapy. Thus far, different compounds have been described in the literature as potential inhibitors of the autophagy process, however most of them show somewhat poor selectivity. Overall, there are two classes of autophagy inhibitors: the early stages autophagy inhibitors and the late stages autophagy inhibitors.

The early stage autophagy inhibitors act through targeting proteins or complexes involved in the initial steps of the core autophagy machinery. They include: the pan-PI3K inhibitors (e.g. 3-methyladenine, wortmannin, LY294002) the Vps34 inhibitors (e.g. spautin-1, SAR405) and the ULK inhibitors (e.g. compound 6). The pan-PI3K inhibitors are widely used autophagy inhibitors, although they have shown limited

potency (except wortmannin) and selectivity [141]. An example is 3-methyladenine (3-MA) that requires use at about 10 mM to inhibit the activity of Vps34, but at such a high concentration, it can also target other kinases such as the class I PI3K, p38MAPK or JNK. By contrast, the higher selectivity of Vps34 inhibitors and ULK inhibitors make them a more reliable group of autophagy regulators. Among them, it is worth mentioning spautin-1, which acts by promoting the ubiquitination of Beclin-1 leading to its proteasomal degradation, and SAR405, which affects the catalytic activity of both ATG14 and UVRAG complexes.

On the other hand, the late autophagy inhibitors target the final steps of the autophagy process and include: the acid protease inhibitors (e.g. pepstatin A and E64d), the vacuolar-type H1-ATPase inhibitors (e.g. bafilomycin-A1) and the lysosomotropic agents (e.g. chloroquine and hydroxychloroquine). Pepstatin A and E64d directly target the lysosome hydrolases cathepsins D, E and B, H, L respectively, whereas bafilomycin-A1 (BAF) and chloroquine indirectly inhibit the lysosomal hydrolases. In fact, bafilomycin-A1 exerts its function by blocking the lysosomal proton transporter necessary to maintain the acidic pH microenvironment of the vacuole, whereas chloroquine (CQ) and its analogue hydroxychloroquine (HCQ) accumulates in lysosomes causing an increase in the lysosomal pH [141]. These mechanisms lead to the deacidification of the lysosomes resulting in blocking their fusion with autophagosomes, thus inhibiting autophagy. So far, chloroquine and hydroxychloroquine are the only clinically available autophagy inhibitors, as they have already been approved for use as treatments for malaria and arthritis [177].

Currently, much research in this area aims to evaluate the effects of targeting autophagy as an adjuvant therapy to standard cancer treatments. As mentioned above, many chemotherapeutic agents induce autophagy as a cell survival mechanism, hence it would be expected that combining them with autophagy inhibitors would enhance their cytotoxicity [168]. In this regard, several studies *in vitro* have demonstrated an enhancement of apoptosis in various cancer cells (such as glioma, gastric cancer and colorectal cancer cells) treated with chemotherapeutic drugs in combination with autophagy inhibitors [199–201]. However, it is still important to understand whether blocking the early or later stages of autophagy is more effective. Moreover, recent preclinical trials have shown that HCQ alone and in combination therapy leads to

enhancement of tumour shrinkage in non-small cell lung cancer and pancreatic cancer [202–204].

1.5. Crosstalk between apoptosis and autophagy

The autophagic and the apoptotic processes are tightly correlated. Under stress conditions, cells can trigger the autophagic pathway as a survival mechanism to overcome the stress; however, prolonged stresses beyond repair can lead to the activation of the apoptotic pathway, resulting in cellular suicide to prevent further damage [205]. Moreover, an autophagic mechanism of cell death has been observed in dying cells as an alternative to apoptosis or in collaboration with it [206]. The interplay between autophagy and apoptosis has been studied over the last decade and it can be summarised by three types of relationships: antagonism, partnership and enablement [206]. In the first relationship, autophagy antagonises apoptosis by promoting cell integrity and survival, thus inhibition of autophagy can enhance apoptosis. In the second relationship, autophagy can enable apoptosis without inducing cell death itself, resulting in autophagy-dependent apoptosis. Finally, both autophagy and apoptosis can cooperate to promote cell death. In this setting, autophagy can occur together with apoptosis or it can be activated as a back-up mechanism in case of failure of apoptosis (Figure 1.11). Therefore, depending on the cellular stresses, activation of autophagy and/or apoptosis is crucial to establish the cellular fate, which is controlled by the ability of cells to switch on and off the two signalling pathways. The balance between life and death is regulated by a complex mechanism of crosstalk between autophagy and apoptosis which is still not well understood. It has been proposed that even though autophagy and apoptosis represent two distinct biological processes, they can be mutually influenced at several levels [205].

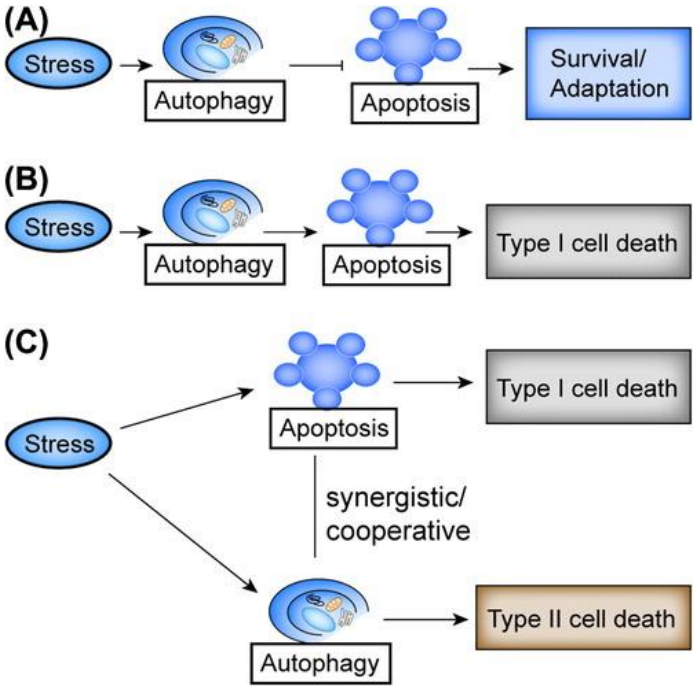

Figure 1.11 Interplay between autophagy and apoptosis.

The relationship between autophagy and apoptosis is context-dependent and it can be summarised by three models. **A**. Antagonism: autophagy antagonises apoptosis by promoting cell integrity and survival. **B**. Partnership: autophagy can enable apoptosis resulting in autophagy-dependent apoptosis. **C**. Enablement: autophagy and apoptosis can cooperate to promote cell death. Image taken from [207].

1.5.1. Molecular mediators in the apoptosis-autophagy interplay

The main factors connecting autophagy and apoptosis include: Beclin-1/Bcl-2 interaction, caspases, ATG proteins, p53, FLIP, UVRAG and BIM.

1.5.1.1. Beclin-1/Bcl-2

The Beclin-1/Bcl-2 interaction represents an essential link between autophagy and apoptosis. As mentioned above, association of Bcl-2 proteins (including Bcl-2 and Bcl-xL) to Beclin-1 negatively regulates autophagy by preventing the assembly of the autophagosomes. Conversely, dissociation of Bcl-2 proteins from Beclin-1 determines the activation of the latter which consequently leads to autophagy activation [205]. The ability of Beclin-1 to interact with the Bcl-2 family of proteins is due to its structure. Indeed, Beclin-1 is a multi-domain protein formed by a C-terminal ECD-BARA domain constituted by a β-α-repeated-autophagy-related (BARA) domain and evolutionarily conserved domain (ECD), a central coiled-coil domain (CCD) and a N-terminal Bcl-2 homology (BH-3) domain [208] (Figure 1.12). The interaction of

Beclin-1 to Bcl-2 proteins, through the BH-3 domain, results in the stabilisation of inactive CCD-mediated Beclin-1 dimers. The antiparallel orientation of Beclin-1 homodimers do not allow the binding of Beclin-1 to the Vps34 complex, necessary for the autophagosome formation [209]. In line with that, it has been suggested that Bcl-2 and Bcl-xL play a dual role as anti-apoptotic proteins but also as anti-autophagic proteins, essential to maintain autophagy at basal levels in order to promote cell homeostasis [210]. Under autophagy-inducing stimuli, the dissociation of Bcl-2 from Beclin-1 is controlled by several mechanisms. An important role is played by the competitive binding proteins such as the pro-apoptotic BH3-only proteins (e.g. Bad and Noxa), which compete with Beclin-1 to bind Bcl-2 and Bcl-xL, and are thus positive regulators of autophagy [205, 211, 212]. Likewise, induction of autophagy is also mediated by HMGB1 (high mobility group box 1 protein) and BNIP3 (Bcl-2/adenovirus E1B 19 kDa-interacting protein 3). The former competes with Beclin-1 to bind Bcl-2, the latter competes with Bcl-2 to interact with Beclin-1 [213, 214]. Moreover, the dissociation of the Beclin-1/Bcl-2 complex is also mediated by the phosphorylation of the two proteins. In this regard, phosphorylation of the Bcl-2 proteins by JNK is considered one of the main nodes in the crosstalk between autophagy and apoptosis and it can lead to the activation of both pathways [215]. On the one hand, the JNK-mediated Bcl-2 phosphorylation determines the release of Beclin-1, which leads to the activation of autophagy. On the other hand, it can convert Bcl-2 into a pro-apoptotic protein, causing a drop in the mitochondrial membrane potential, the release of the cytochrome c and activation of the caspase cascade [215]. Additionally, numerous kinases have been demonstrated to activate or inhibit Beclin-1 through phosphorylation of various phospho-sites, including ULK1 (S15, S30), AMPK (S93, S96, T388) and AKT1 (S234, S295). Interestingly, Beclin-1 phosphorylation at the N-terminal region has been linked to autophagy activation and/or inhibition through the regulation of the Beclin-1/Bcl-2 interaction. In this context, it has been found that DAPK1, DAPK2 and ROCK1 (Rho -associated coiled-coil containing protein kinase-1) can promote autophagy through the disruption of the Beclin-1/Bcl-2 complex by phosphorylating Beclin-1 at the residue T119 in the BH3 domain [216–218]. Conversely, it has been demonstrated that the pro-apoptotic kinase SKT (serine/threonine Kinase-4)/Mst1 (mammalian STE20-like protein Kinase 1) can stabilise the Beclin-1/Bcl-2 complex by phosphorylating Beclin-1 at the residue T108, resulting eventually in autophagy inhibition in cardiomyocytes [219]. Another factor

important in the regulation of the Beclin-1/Bcl-2 complex involves the cellular localisation of the proteins. In fact, it has been reported that the interplay between Bcl-2 and Beclin-1 can occur at the ER and mitochondria [209]. The ER pool of Bcl-2 is mainly regulated by NAF-1 (nutrient-deprivation autophagy factor-1) and JNK resulting in autophagy activation under starvation or stress conditions, whereas the mitochondrial Bcl-2 pool interacts with Bak and Bax, resulting in apoptotic regulation [220–223]. The apoptotic-autophagic switch can be also regulated by the Bcl-2 and Beclin-1 expression levels. In this regard, it is not surprising that in breast cancer 60% of patients are characterised by an overexpression of Bcl-2, while there is a loss of Beclin-1 in 40-70% of cases [210].

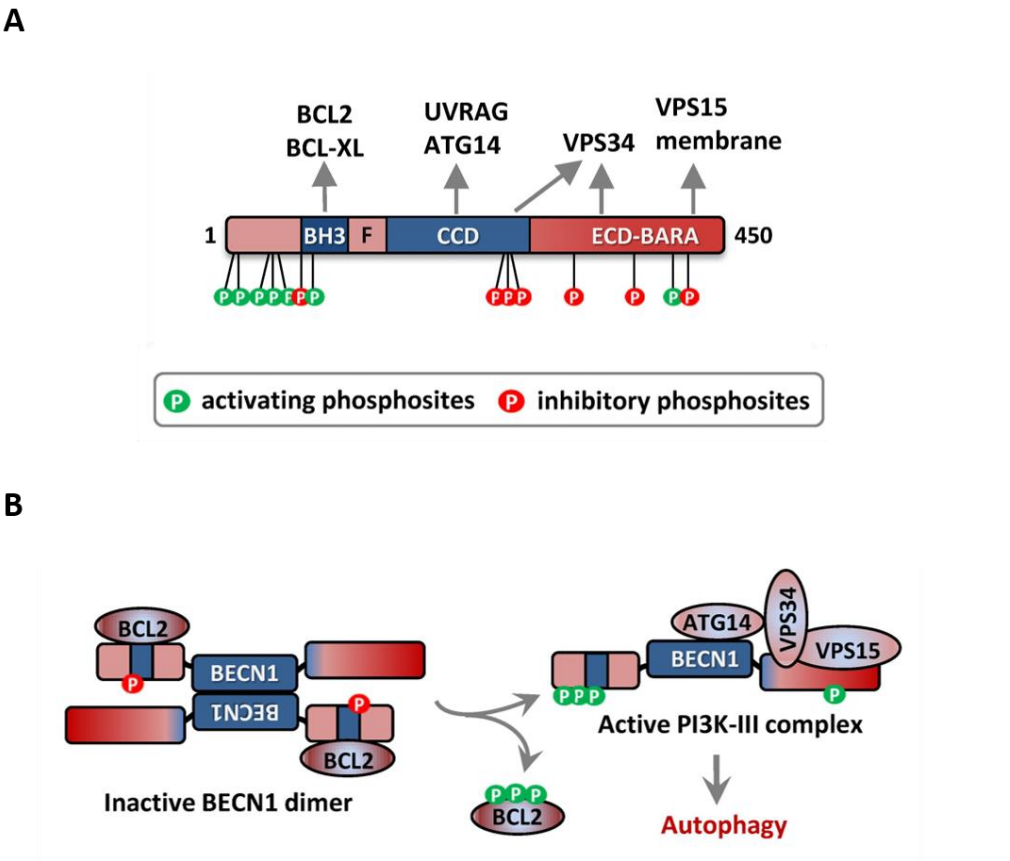

Figure 1.12 Beclin-1 phosphorylation-dependent activation.

A. Primary structure of Beclin-1 (BECN1) showing its phosphorylation and binding sites. **B**. Beclin-1 interacts with Bcl-2 forming an inactive homodimer. Phosphorylation of Beclin-1 and Bcl-2 results in the release of Bcl-2 and in the activation of the PtdIns3 (PI3K-III) complex, which leads to autophagy activation. Image modified from [208].

1.5.1.2. Caspases

Caspases are well-known proteins involved in the apoptotic pathway. Recently, an emerging role of caspases in the interplay between autophagy and apoptosis has been proposed [224]. It has been suggested that caspases control autophagy activation by interacting directly with key autophagic proteins and leading to their cleavage. Caspase-mediated degradation of these proteins may result in the inhibition of autophagy, but also in the enhancement of the apoptotic pathway through their conversion from pro-autophagic proteins to pro-apoptotic proteins [166, 224]. Moreover, recent findings demonstrate that the amount and the activity of caspases can be regulated by the autophagic pathway [225]. Caspase 3 represents a good example of the caspase-mediated crosstalk between autophagy and apoptosis, since it is one of the main effector caspases involved in apoptosis and it has shown also a predominant role in the autophagic process [226]. In fact, it has been reported that caspase 3 can cleave Beclin-1 at positions 124 and 149 during staurosporine-induced apoptosis in HeLa cells [227]. Cleaved Beclin-1 results in autophagy suppression, as autophagy activation is regulated only by full-length Beclin-1, and in apoptosis enhancement, through the release of Bcl-2 from the Beclin-1/Bcl-2 complex [224, 228]. Also, the Beclin-1 c-terminal fragment localises at the mitochondria, triggering the apoptotic pathway [229]. Likewise, caspase 3 can mediate the cleavage of ATG4, which results in the failure of LC3 delipidation and in the migration of the cleaved ATG4 fragment at the mitochondria to induce cell death [230]. Additionally, other caspases are also implicated in the autophagy-apoptosis crosstalk. For example, caspase 6 activation has been linked to the cleavage of p62, ATG3, ATG5 and also Beclin-1, whereas caspase 7 and caspase 8 has been shown to mediate ATG3 degradation [231–233]. It has been observed that caspase 8 also plays an important role in apoptosis regulation by autophagy. In fact, the association of FADD with the ATG12-ATG5 complex promotes the recruitment of caspase 8 to the autophagosome membrane, where it is then activated to initiate the apoptotic caspase cascade [233]. Moreover, the interaction of caspase 9 with ATG7 facilitates autophagy activation and concurrently interferes with caspase 9 activation and apoptosis [234].

1.5.1.3. ATG proteins

The ATG proteins constitute the molecular machinery of autophagy, but their emerging role in apoptosis regulation has also been demonstrated [235]. Notably, ATG3 takes part in autophagosome formation and it plays a crucial role in the autophagy process. However, when ATG3 covalently binds ATG12, it leads to the formation of the ATG3-ATG12 complex, which is transferred to the mitochondrial outer membrane inducing apoptotic cell death [236]. Moreover, it has been observed that conjugation of ATG5 to ATG12 is necessary to determine autophagy activation, but the non-conjugated ATG5 and ATG12 proteins have also shown a non-canonical autophagic function by regulating apoptosis in response to several stresses. During apoptosis, the non-conjugated ATG5 protein can be cleaved by calpains, inducing the formation of a truncated ATG5 fragment, which can localise at the mitochondria leading to cytochrome C release and caspase activation [237]. Additionally, the non-conjugated form of ATG12 can bind Mcl-1 and Bcl-2 resulting in apoptosis induction [238]. Recent studies on the expression levels of ATG5 and ATG12 have also revealed their importance in apoptosis regulation. In fact, inhibition of ATG5 using siRNA has been shown to reduce chemotherapy-induced cell death, resulting in the acquisition of a resistant phenotype [237]. Also, knock down of ATG12 has been linked to Bax inhibition and apoptosis suppression [238].

1.5.1.4. p53

p53 is another important factor in the crosstalk between autophagy and apoptosis. Under genotoxic stresses, p53 takes part in apoptosis regulation by controlling both the extrinsic and the intrinsic pathways, depending on its cellular localisation. The nuclear p53 pool regulates the activation of the pro-apoptotic proteins (e.g. Bax and Noxa) and the inhibition of the anti-apoptotic Bcl-2 proteins, leading to the mitochondrial apoptotic pathway; whereas the cytoplasmic p53 pool promotes the apoptotic death receptor pathway by stimulating the Fas receptor. It has been demonstrated that p53 also plays an important role in autophagy regulation and its ability of promoting or suppressing autophagy depends again on its cellular localisation. Under genotoxic stresses, activation of autophagy by nuclear p53 can be mediated by mTOR inhibition and by the transcriptional activation of DRAM. Interestingly, DRAM-mediated autophagy has been also linked to apoptotic cell death

[239]. By contrast, it has been proposed that cytoplasmic p53 may negatively regulate autophagy, thus loss of p53 results in the activation of autophagy, which is not correlated to apoptosis.

1.5.1.5. FLIP

FADD-like IL-1β-converting enzyme-inhibitory protein (FLIP) represents another example of the interplay between autophagy and apoptosis. FLIP is an anti-apoptotic protein which acts by suppressing the extrinsic apoptotic pathway through the inhibition of caspase 8 cleavage [228]. Interestingly, knockdown of FLIP has shown to enhance rapamycin-induced autophagy [240]. The anti-autophagic activity of FLIP has been linked to its ability to compete with LC3 for the binding of ATG3, resulting in the suppression of LC3 lipidation. Moreover, it has been found that pro-autophagic stimuli can reverse this interaction, suggesting a context-dependent role of FLIP [240].

1.5.1.6. UVRAG

A dual role of UVRAG in both autophagy and apoptotic regulation has been recently suggested. Suppression of UVRAG in tumour cells has been shown to lead to an increase of apoptosis and a decrease of autophagy. Accordingly, an anti-apoptotic activity of UVRAG has been linked to its interaction with Bax, by preventing the translocation of Bax to the mitochondria [241]. Moreover, it has been observed that knockdown of UVRAG in $atg5^{-/-}$ autophagy deficient MEFs sensitises cells to doxorubicin-induced apoptosis, suggesting that UVRAG-mediated apoptosis regulation may occur independently from its role as autophagy regulator [242]. Additionally, interaction of UVRAG with Bif-1, a member of the endophilin B protein family involved in the pro-apoptotic activation of Bax and Bad, has also been correlated to enhanced autophagy [243].

1.5.1.7. BIM

B-cell lymphoma 2-interacting mediator of cell death (BIM) is a pro-apoptotic protein which exists in 3 isoforms: BIM-short (BIM_S), BIM-long (BIM_L), and BIM-extra long (BIM_{EL}). It has been proposed that BIM_S and BIM_{EL} are mainly involved in apoptosis activation, while BIM_L is mainly correlated to autophagy [244]. BIM-mediated apoptosis regulation occurs through the binding of BIM to the BH3 domain of Bcl-2, which prevents its interaction with Bax and Bak [245]. Additionally, regulation of

autophagy by BIM may occur through its binding to Beclin-1 at a different site from the Bcl-2 binding region, resulting in autophagy inhibition. It has also been observed that BIM-mediated autophagy inhibition can be reversed under starvation conditions [246].

1.6. Oxidative stress

Aerobic metabolism is essential to provide energy within cells. It consists of a series of redox reactions occurring in the mitochondria which lead to ATP generation. Several compounds are produced as result of this process, but a small amount of them (less than 5%) are considered dangerous for cells due to their ability of chemically reacting with other cellular components. It has been reported that a low concentration of these reactive species is normally maintained in cells and it may be necessary for some cellular events including signal transduction, enzyme activation, gene expression, protein folding and caspase activation [247]. Reactive Species (RS) can be divided in four groups based on their structure and origin: Reactive Oxygen Species (ROS), Reactive Nitrogen Species (RNS), Reactive Sulphur Species (RSS) and Reactive Chloride Species (RCS) [247]. Under certain circumstances, increase in RS levels may affect cellular homeostasis, thus antioxidant systems able to scavenge RS have been evolutionary developed by cells as a defensive mechanism [247]. When the prooxidant/antioxidant equilibrium is disrupted in cells, oxidative stress is generated. Therefore, oxidative stress can be defined as the imbalance between RS generation and the antioxidant capacity of cells [248]. Oxidative stress has been implicated in a variety of human diseases, including Alzheimer's, Parkinson's, diabetes, immune system dysfunctions as well as in cancer [247].

1.6.1. Reactive Oxygen Species

ROS are considered the most abundant reactive species within cells. They can be classified based on their structure into two main groups: (1) oxygen centered radicals and (2) oxygen centered non-radicals. The former includes ROS with one or more unpaired electron(s) in the external orbitals, such as the superoxide anion ($O_2^{\bullet -}$), the hydroxyl radicals ($OH^{\bullet}$), the alkoxyl radicals ($RO^{\bullet}$) and the peroxyl radicals ($ROO^{\bullet}$). The latter includes ROS like hydrogen peroxide (H_2O_2) and singlet oxygen ($^1O_2$),

which do not have unpaired electrons, but they can be converted to radical species [249]. Endogenous ROS production has been linked to mitochondria, cytosol, peroxisomes, endosomes, exosomes as well as to biological fluids like plasma [250]. Endogenous ROS generation may be the product of enzymatic reactions, like β-oxidation reaction in peroxisomes and NAPDH-mediated reaction in the phagocytes, or non-enzymatic reactions, like the electron transport chain in the mitochondria [249]. Generally, mitochondria are considered the main source of ROS [251]. Within the electron transport chain, a molecule of oxygen is reduced to water and a superoxide radical ($O_2^{\bullet-}$) is produced (Figure 1.13). The $O_2^{\bullet-}$ is then converted to hydrogen peroxide (H_2O_2) by superoxide dismutase (SOD), which is further converted to H_2O and $^1O_2$ by the detoxifying enzyme catalase, or to $OH^{\bullet}$ by the mitochondrial aconitase via the Fenton reaction [251, 252]. In addition, external sources of ROS including UV irradiation, environmental pollutants, smoking, alcohol, exercise and chemotherapeutic drugs may also contribute to ROS generation and cellular accumulation [247].

It has been suggested that ROS play an important role in cellular homeostasis. As aforementioned, low levels of ROS are crucial in several cellular processes as they are implicated in cellular proliferation, differentiation and migration. However, an aberrant redox homeostasis due to an abnormal metabolism or mitochondrial dysfunction may trigger ROS production, leading to their intracellular accumulation. High ROS levels in cells have been linked to cell damage and cell death [253].

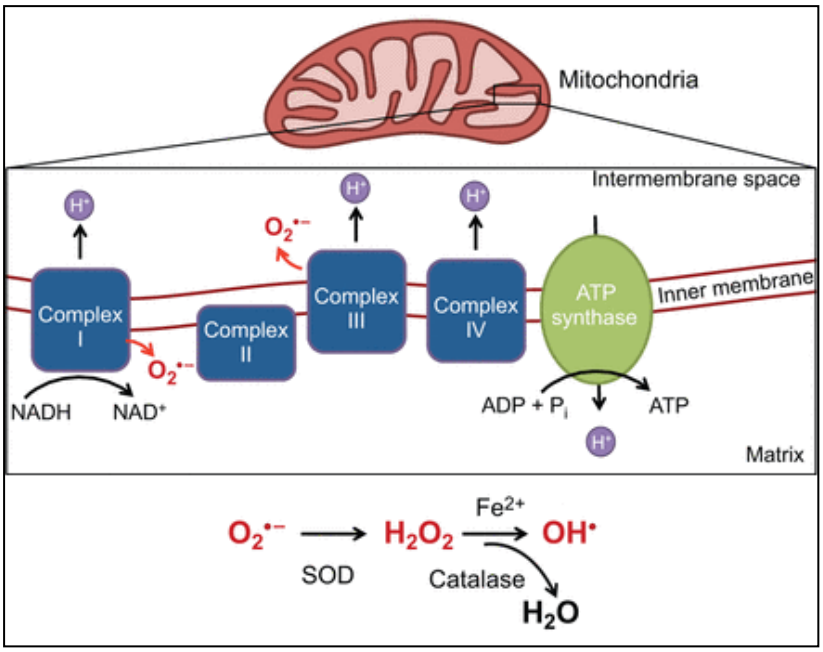

Figure 1.13 ROS generation in mitochondria.

Within the electron transport chain, the superoxide radical ($O_2^{\bullet-}$) can be generated from complexes I and III. The $O_2^{\bullet-}$ is then converted to hydrogen peroxide (H_2O_2) by the superoxide dismutase (SOD), which is further converted to H_2O by the detoxifying enzyme catalase, or to OH • via the Fenton reaction. Image modified from [254].

1.6.2. Antioxidant systems

Antioxidant systems play a crucial role in cellular homeostasis by counteracting ROS accumulation. They can be divided in two main groups: enzymatic antioxidants, including SOD, catalase, glutathione peroxidase (GPX), glutathione reductase, peroxiredoxins and heme oxygenase 1 (HO-1), and non-enzymatic antioxidants, such as glutathione and vitamin A, C and E [255]. As mentioned before, SOD is of primary importance for its dismutation of the superoxide anion, while catalase is essential in the cellular detoxification of hydrogen peroxide. A crucial role in the detoxification of peroxide is also played by glutathione, which is considered indispensable for cellular redox homeostasis [256]. Glutathione is a small protein consisting of three amino acid (glutamine, cysteine, and glycine) which can exist in a reduced (GSH) or oxidised (GSSG) form. It has been reported that 90% of total glutathione within cells exists as GSH and less than 10% as GSSG [257]. However, under oxidising conditions, GSH can donate its electron to H_2O_2 in order to convert it to H_2O and O_2. This reaction is mediated by glutathione peroxidase and it results in the formation of a disulphide bond

between two GSH molecules, which are converted to one molecule of GSSG. By contrast, under reducing conditions, glutathione transferase can reduce GSSG to again form GSH. The conversion of GSH to GSSG is generally considered a good marker of oxidative stress [255]. Finally, it is worth mentioning another of the main antioxidant defence systems, the nuclear factor erythroid 2–related factor 2 (Nrf2), a transcription factor involved in the regulation of antioxidant pathways. Under normal conditions, the binding of kelch-like ECH-associated protein 1 (Keap1) to Nrf2 determines its inhibition and degradation through the proteasomal pathway. However, in the presence of ROS, the release of Nrf2 from Keap1 leads to its translocation to the nucleus and its binding to the antioxidant responsive element (ARE) of antioxidant genes. Activation of Nrf2 results in the regulation of several genes, including superoxide dismutase, glutathione peroxidase (GPX), glutathione-*S*-transferase (GST), NAD(P)H-quinone oxidoreductase 1 (NQO1) and heme oxygenase-1 (HO-1) [258].

1.6.3. Oxidative stress and cancer

Several studies have focused their attention on the correlation between oxidative stress and cancer. It has been demonstrated that changes in the redox balance and dysregulation of redox signalling pathways are hallmarks of cancer cells [256]. Interestingly, elevated levels of ROS have been detected in tumour cells compared to normal cells [259]. In a cancer setting, an increase in ROS might be due to mitochondrial dysfunction, high metabolic rate, activation of oncogenes, peroxisomal activity and increased enzymatic activity of oxidase, cyclooxygenase and lipoxygenase enzymes [256]. Moreover, it has been observed that high levels of ROS within cells can chemically react with other cellular components causing damage to DNA, proteins and lipids. This may lead to altered gene regulation, loss of DNA repair activity, signal transduction dysregulation and mutations, resulting ultimately in altered cell growth, differentiation and apoptosis [250]. In this context, a crucial role for ROS in cancer tumour initiation and development has been proposed [260]. Accordingly, excessive ROS levels have been associated with mutations in oncogenes and tumour suppressor genes (e.g. PTEN, Ras, BCR-ABL and c-Myc) and activation of oncogenic signalling pathways. In this regard, it has been demonstrated that high H_2O_2 levels can lead to PTEN inactivation and concurrently Ras activation, which in turn activates survival pathways as the PI3K/Akt/mTOR and the MAPK/ERK

pathway, both involved in tumorigenesis [260]. High levels of ROS can also activate JNK, Nrf2 and NF-κB, all of which has been shown to translocate to the nucleus and promote tumour cell growth, angiogenesis and metastasis [260–262]. Moreover, ROS-induced mitochondrial DNA mutations have also been associated with metastasis development [263]. In addition to the pro-tumour role of ROS, it has been reported that permanent elevated ROS levels can also induce cell death by triggering the apoptotic pathway. Indeed, ROS can disrupt the mitochondrial membrane, promoting the release of cytochrome c resulting in apoptosome formation [264, 265]. Thus, similar to autophagy, ROS can be considered a double-edge sword in cancer biology [253] (Figure 1.14).

Nevertheless, it is worth noting that high levels of ROS in cancer cells are not deleterious as much as they would be in normal cells. In fact, it has been suggested that persistent high levels of ROS do not correlate with a proportional increase in oxidative stress in cancer cells. In fact, several studies have proposed that cancer cells have developed new redox balances in order to cope with ROS [247]. Therefore, it is not surprising that a high dependency on antioxidant systems has been observed in cancer cells as detoxification mechanisms from the high ROS microenvironment [256]. For example, higher levels of cellular GSH were found in human fibroblast tumour cell lines compared to normal fibroblasts [266–268]. Also, a constitutive upregulation of Nrf2 has been reported in pancreatic cancer cells and it has been linked to tumour maintenance [269]. Additionally, apart from an increase in the antioxidant systems, other cellular adaptations allow cancer cells to increase their metabolic and proliferation rate without inducing oxidative stress. An example of this is given by the metabolic reprogramming occurring in cancer cells, also known as the Warburg effect. The Warburg effect refers to the observation that cancer cells display a high glycolytic rate even when there are high levels of O_2 [270, 271]. In fact, Otto Warburg showed for the first time that normal cells usually produce ATP via aerobic respiration in mitochondria, whereas cancer cells prefer to produce ATP via anaerobic glycolysis. It has been proposed that even though anaerobic glycolysis leads to reduced ATP production, it is faster than oxidative phosphorylation, thus it can support better the high proliferative rate of cancer cells. Moreover, since reduced levels of ROS are produced during anaerobic glycolysis, this may represent an adaptive mechanism that allows cancer cells to escape from the oxidative stress [247].

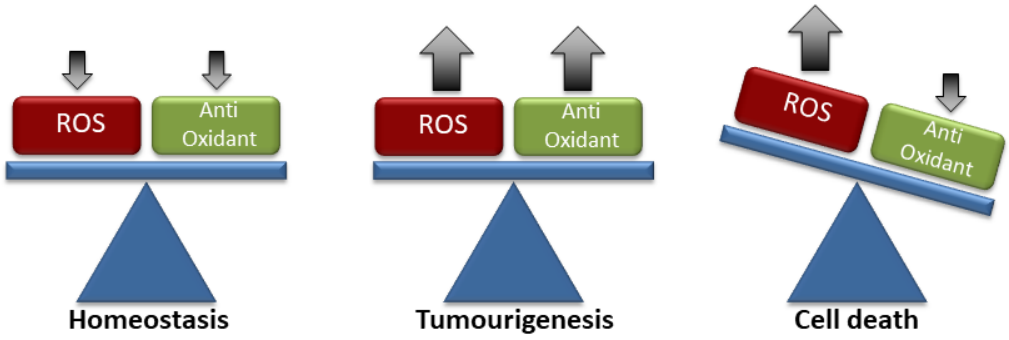

Figure 1.14 Cellular redox state during homeostasis, tumorigenesis and cell death.
Under normal conditions, cells maintain homeostasis by producing enough antioxidants to balance ROS production. During tumorigenesis, mitochondrial dysfunction and a high metabolic rate results in increased levels of ROS which are counteracted by enhanced antioxidant responses. However, excessive and toxic ROS production can lead to a disruption of the cellular redox balance, resulting eventually in oxidative stress and cell death.

The role of oxidative stress in oral cancer is not well understood. It has been proposed that ROS may play an important role in oral tumorigenesis, since the main risk factors associated with this type of cancer are generally considered external ROS sources. In fact, the exposure of the oral mucosa to tobacco and alcohol may lead to high levels of intracellular ROS, resulting in ROS-induced mutations and ultimately tumorigenesis. Additionally, high incidence of a single nucleotide polymorphism in the superoxide dismutase enzyme has been observed in OSCC patients who smoke compared to non-smokers [272]. Moreover, i*n vivo* studies have shown that betel quid chewing is linked to oxidative stress in oral cancer [273]. Likewise, HPV may be associated with oral cancer through ROS-based mechanisms [274]. Given this, further studies are required to elucidate the role of ROS in OSCC.

1.6.4. Oxidative stress and chemotherapy

It has been demonstrated that many chemotherapeutic agents can induce ROS production within cells. As mentioned above, excessive ROS production may result in oxidative stress, due to the inability of the antioxidant systems to counteract ROS generation, leading eventually to cell death (Figure 1.14). Accordingly, intracellular accumulation of drug-induced ROS has been associated with activation of the

apoptotic pathway, suggesting that the cytotoxic effect of many drugs may be mediated by oxidative stress. Paclitaxel, 5-fluorouracil and cisplatin are examples of chemotherapeutic drugs correlated to an increase in ROS formation. For example, it has been found that cisplatin may form adducts with GSH, leading to its depletion and consequently ROS accumulation; this mechanism has been linked to cisplatin cytotoxicity through ROS-induced apoptosis [275, 276]. Accordingly, targeting ROS with the ROS scavenger N-acetyl cysteine (NAC) has been shown to prevent drug-induced chemotoxicity [277, 278]. Interestingly, enhanced antioxidant systems, such as glutathione and Nrf2, have been found in several chemoresistant cell lines, suggesting that cancer cells can overcome the cytotoxic effect of drugs by counteracting drug-induced ROS [279, 280]. Accordingly, high levels of Nrf2 were found in doxorubicin-resistant breast cancer cells compared to the respective sensitive cells and were associated with an enhancement of the antioxidant response [281]. Also, overexpression of the GST enzyme, along with high GSH levels, have been reported to increase the rate of detoxification of ROS-induced chemotherapy agents, resulting in a decrease of their effectiveness [282]. Based on these findings, a potential role for the redox-signalling pathway in chemoresistance has been suggested. Therefore, targeting the antioxidant systems has been proposed as a valuable strategy to apply in the clinic to reduce chemoresistance [283]. In this context, several studies are currently investigating the beneficial effects of inhibiting glutathione and Nrf2 to increase the sensitivity of cells to chemotherapy [284–287].

1.7. Drug-induced autophagy and oxidative stress modulation: state of the art in OSCC treatment

As previously discussed, the implication of autophagy and oxidative stress in chemotherapy and chemoresistance has been widely investigated over the past decades. Currently, several studies are investigating whether targeting these pathways can be exploited in the clinic to improve cancer therapy. In the present study, the role of autophagy and oxidative stress during chemotherapy and their potential modulation for the treatment of OSCC was examined. A summary of the current state of the art in this field in OSCC has been reported in Table 1.2. Interestingly, a potential correlation between drug-induced autophagy and oxidative stress, along with an interesting interplay of these two pathways with various tumour-related processes (such as

apoptosis, angiogenesis, cell migration and EMT) may be suggested in OSCC. However, since the role of autophagy and oxidative stress seems to vary depending on the type of drug used, further studies are warranted to determine the beneficial effect of targeting these two pathways to improve the outcome of OSCC patients.

Treatments	Induced pathways	Role of induced pathways	Combined modulators	Effect of modulators	Ref
ANE	Autophagy	Pro-tumour	3-MA (autophagy inhib.)	Increased apoptosis	[288]
	Oxidative stress	Pro-tumour	NAC, (ROS inhib.)	Increased apoptosis	[288]
Beicalein	Autophagy	Pro-tumour	BAF (autophagy inhib.)	Increased caspase 3 activity	[289]
	Oxidative stress	Pro-tumour	NAC (ROS inhib.)	Increased caspase 3 activity	[289]
Cisplatin	Autophagy	Pro-tumour	3-MA, CQ (autophagy inhib.)	Increased apoptosis Reduced migration	[191, 290, 291]
		Cell death	Rapamycin (autophagy activ.)	Reduced tumour growth	[292]
	Oxidative stress	Cell death	BSO (GSH inhib.)	Slightly increased cell death	[293]
		Cell death	NAC (ROS inhib.)	Reduced apoptosis and autophagy	[294]
Curcumin	Autophagy	Cell death	3-MA (autophagy inhib.)	Protection from increased cell death	[295]
	Oxidative stress	Anti-tumour	NAC (ROS inhib.)	Reduced autophagic cell death	[295]
Erianin	Autophagy	Anti-tumour	N/A	N/A	[296]
Fisetin	Autophagy	Pro-tumour	3-MA (autophagy inhib.)	Increased apoptosis	[297]
HCD	Autophagy	Cell death	N/A	N/A	[298]
Methotrexate	Autophagy	Pro-tumour	N/A	N/A	[195]
Obtaclax	Autophagy	Anti-tumour	N/A	N/A	[299]
	Oxidative stress	Anti-tumour	N/A	N/A	[299]
Plumbagin	Oxidative stress	Cell death	GSH, NAC (ROS inhib.)	Protection from increased cell death	[300]
Resveratrol	Autophagy	Pro-tumour	3-MA, Cudaxantrone (autophagy inhib.)	Reduced EMT and cell migration	[301]
Safingol	Autophagy	Pro-tumour	3-MA, BAF (autophagy inhib.)	Increased apoptosis	[302]
	Oxidative stress	Cell death	NAC (ROS inhib.)	Prevention of cell death	[302]
Sandensolide	Oxidative stress	Cell death	NAC (ROS inhib.)	Reduced cytotoxicity	[303]
Sulfasalazine	Autophagy	Cell death	3-MA (autophagy inhib.)	Protection from reduced cell viability	[196]
Tetrandrine	Autophagy	Cell death	3-MA, BAF, CQ (autophagy inhib.)	Protection from reduced cell viability	[198]
Thymoquinone	Autophagy	Cell death	BAF (autophagy inhib.)	Protection from increased apoptosis	[197]
YM155	Autophagy	Cell death	Rapamycin (autophagy activ.)	Reduced tumour growth and angiogenesis	[304, 305]

Table 1.2 The effect of autophagy and oxidative stress modulation in OSCC.

1.8. Project aims

The overall aim of this project is to identify the role of autophagy in OSCC and determine whether autophagy may be implicated in oral carcinogenesis and chemoresistance. Moreover, the present study aims to evaluate whether a combination of chemotherapy and autophagy inhibition may represent a novel treatment strategy against OSCC.

More specifically the objectives are:

1. To investigate cell death mechanisms induced in oral cancer cells in response to standard OSCC chemotherapeutics and to evaluate the role of autophagy in response to chemotherapy;
2. To examine the signalling pathway(s) underlying drug-induced apoptosis and autophagy in OSCC;
3. To evaluate the mechanism(s) implicated in chemoresistance in OSCC;
4. To investigate the expression of autophagic proteins in oral cancer tissue samples during OSCC progression and to determine their relationship with clinical-pathological factors.

This project will determine the mechanisms implicated in the OSCC response to chemotherapeutics and whether their modulation may be considered in the design of new therapeutics for this malignancy.

2. Material and Methods

2.1. Materials and suppliers

Materials	Suppliers
2',7'-dichlorodihydrofluorescein-diacetate (H_2DCFDA)	Sigma-Aldrich
3-methyladenine (3-MA)	Sigma-Aldrich
5-fluorouracil	Sigma-Aldrich
Acrylamide	Ultra Pure
Alamar Blue	Life Technologies
Ammonium Persulfate	Sigma-Aldrich
Annexin V-FITC	iQ Products
Anti-CD24-APC (SN3 A5-2H10)	Invitrogen
Anti-CD44-FITC (IM7)	Invitrogen
Anti-ATG5 (2630)	Cell Signalling
Anti-Bcl-xL (2764)	Cell Signalling
Anti-Beclin-1 (NB500-249)	Novus Biological
Anti-Caspase 3 (9662S)	Cell Signalling
Anti-Cleaved Caspase 3 (9664S)	Cell Signalling
Anti-GAPDH (6C5)	Calbiochem
Anti-LC3-I/II (2775S, 3868)	Cell Signalling
Anti-LC3 5F10 (0231-100)	NanoTools
Anti-HO-1 (5853)	Cell Signalling
Anti-Mouse (A9044)	Sigma-Aldrich
Anti-Mouse (W402B)	Promega
Anti-Nrf2 (12721)	Cell Signalling
Anti-p44/42 MAPK (Erk1/2) (9102)	Cell Signalling
Anti-p62 (ab56416)	Abcam
Anti-phospho-p44/42 MAPK (Erk1/2) (Thr202/Tyr204) (9101)	Cell Signalling
Anti-phospho-SAP/JNK (Thr183/Tyr185) (4668)	Cell Signalling
Anti-Rabbit (A16035)	Invitrogen
Anti-Rabbit (W4011)	Promega
Anti-Ras (3965)	Cell Signalling
Anti-SAPK/JNK (9251)	Cell Signalling
Anti-α-tubulin (CP06)	Calbiochem
Anti-β-Actin (4967)	Cell Signalling

Bafilomycin-A1	Sigma-Aldrich
BCA protein reagents A and B	Pierce
Bond Primary Antibody Diluent	Ventana
Bradford	Sigma-Aldrich
Bromophenol blue	Sigma-Aldrich
Bovine Serum Albumin (BSA)	Sigma-Aldrich
BSA protein standards	Pierce
Buthionine sulfoximine (BSO)	Tocris
Calcium chloride	Sigma-Aldrich
Carboplatin	Sigma-Aldrich
Chloroquine	Enzo Life Sciences
Cis-diammine platinium (II) dichloride	Sigma-Aldrich
Complete Ultra Protease Inhibitor Tablets	Roche
Cryogenic tubes	Nalene
Crystal violet	Sigma-Aldrich
Cyto-ID® Autophagy Detection Kit	Enzo Life Sciences
Dimethyl sulfoxide (DMSO)	Sigma-Aldrich
Dulbecco's Modified Eagle Medium (DMEM)	Gibco
Dulbecco's Modified Eagle Medium/Nutrient Mixture F-12 (DMEM-F12)	Sigma-Aldrich
Docetaxel	Accord
Dithiothreitol (DTT)	Sigma-Aldrich
Earle's Balanced Salt Solution (EBSS)	Sigma-Aldrich
ECL detection kit	Pierce
Ethanol	Lennox
Fetal bovine serum (FBS)	Sigma-Aldrich
Filter paper	Whatman
Glycerol	Sigma-Aldrich
Glycine	Sigma-Aldrich
GSH/GSSG-Glo Kit	Promega
Hepes	Sigma-Aldrich
Hydrocortisol	Sigma-Aldrich
Iso-propanol	Sigma-Aldrich
L-glutamine	Sigma-Aldrich
Lipoafectamine 2000	Invitrogen

Menadione	Fluorochem
Methanol	Lennox
ML385	Sigma-Aldrich
N-acetyl cystein (NAC)	Sigma-Aldrich
Non-fat dried milk	Marvel
ON-target plus non-targeting pool siRNA	Dharmacon
ON-target plus SMART-pool ATG5 siRNA	Dharmacon
Opti-MEM	Bioscience
OptiView DAB IHC Detection Kit	Ventana
PageRuler™ Plus Prestained Protein Ladder	Thermo Scientific
Sterile PBS	Gibco
PBS tablets	Sigma-Aldrich
Penicillin-streptomycin	Sigma-Aldrich
Phosphatase Inhibitor Cocktails 2 and 3	Sigma-Aldrich
Propidium iodide (PI)	Sigma-Aldrich
Polyvinylidene difluoride (PVDF)	Millipore
Rapamycin	Enzo Life Sciences
RIPA lysis buffer	Sigma-Aldrich
RNAse A	Sigma-Aldrich
SAR405	APExBIO
Sodium chloride	Sigma-Aldrich
Sodium dodecyl sulfate (SDS)	Sigma-Aldrich
Sodium orthovanadate	Sigma-Aldrich
Sodium pyruvate	Sigma-Aldrich
Sorafenib	LC laboratories
SP600125	Fluorochem
Sterile H_2O	Sigma-Aldrich
TEMED	Sigma-Aldrich
Tissue-Tek Prisma H&E Stain Kit	Sakura
Trizma base	Sigma-Aldrich
TrypLe Express	Gibco
Tween-20	Sigma-Aldrich
Ultraview/iView Amplification Kit	Ventana
X-ray Film	Fisher Scientific
Z-VAD-fmk	Calbiochem

All sterile tissue culture flasks, pipettes, plates, pipette tips and universal tubes were from Greiner Bio-one Ld. Eppendorf® Refrigerated Microcentrifuge model 5417R was used to centrifuge 1.5 mL Eppendorf tubes and Sorvall T436 centrifuge was used for falcon tubes.

2.2. Contact details of distributors

Abcam: 330 Cambridge Science Park, Cambridge, CB4 OFL, U.K.
orders@abcam.com
APExBIO: 7505 Fannin street, Suite 410, TX 77054, Houston, U.S.A
info@apexbt.com
Bioscience: 3 Charlemont Terrace, Crofton Road, Dun Laoghaire, Co Dublin, A96 K7H7, Ireland
orders@biosciences.ie
Brennan Co: Stillorgan Industrial Park, Dublin, Ireland
enquiries@brennanco.ie
Calbiochem: La Jolla, California 92-39-2087, U.S.A.
CUSTOMER.SERVICE@MERCKBIOSCIENCES.CO.UK
Cell Signalling Technology: 3 Trask Lane, Denvers, Massachusetts 09123, U.S.A.
enquiries@brennanco.ie
Cruinn Diagnostics Ltd: 5b/6b Hume Centre, Park West Industrial Estate, Dublin 12, Ireland
info@cruinn.ie
Dharmacon: cs.dharmacon.eu@horizondyscovery.com
Enzo Life Sciences: 1 Colleton Crescent, Exeter, EX2 4DG, U.K.
info-uk@enzolifesciences.com
Fisher Scientific: Fisher Scientific Ireland, Suite3, Plaza212, Blanchardstown Corporate Park 2 Ballycoolin, Dublin 15
Fluorochem Ltd: Unit 14, Graphite Way, Hadfield, Derbyshire, SK13 1QH, U.K.
enquires@fluorochem.co.uk
GraphPad Software Inc: 2236 Avendia de la Playa, La Jolla, California 90237, U.S.A.
sales@graphpad.com
Greiner Bio-One-Ltd: Brunel Way, Stroudwater Business Park, Stonehouse, Gloustershire L10 3SX, U.K.

orders@cruinn.ie

Invitrogen Ltd: 3 Fountain Drive, Inchinnan Business Park, Paisley PA4 9RF, U.K.

Millipore: Tullagreen, carrigtwohill, Co. Cork, Ireland

eiorders@europe.sial.com

MyBio: Kilkenny Research and Innovation Centre, Kilkenny, Ireland

info@mybio.ie

NanoTools Antikörpertechnik GmbH&Co. KG: Tscheulinstr. 21, D-79331 Teningen, Germany

info@nanotools.de

Pierce Biotechnology Ltd.: P.O. Box 117, Rockford, Illinois 61105, U.S.A.

info@medical-supply.ie

Promega: MyBio Ltd. Kilkenny Research & Innovation Centre, St. Kieran's College, Kilkenny, Ireland

info@mybio.ie

R&D Systems: 19 Barton Lane, Abingdon Science Park, OX14 3NB, U.K.

info@RnDSystems.co.uk

Roche Diagnostics Ltd.: Burgess Hill, West Sussex, RH159RY, U.K.

burgesshill.ras@roche.com

Sigma-Aldrich Ireland Ltd: Vale Road, Arklow, Wicklow, Ireland

EIRCustsupport@sial.com

Tocris: Tocris House, IO Centre, Moorend Farm Avenue, Bristol BS11 0QL, U.K.

info@tocris.ie

VWR: Northwest Business Park, Dublin 15, Ireland

sales@ie.vwr.com

2.3. Cell culture

All cell culture procedures were carried out at room temperature in a class II tissue culture hood using aseptic technique. SCC4 and SCC9 cells were purchased from Sigma-Aldrich and supplied by European Collection of Authenticated Cell Cultures (ECACC). Both SCC4 and SCC9 cell lines are epithelial-like cells of human squamous carcinoma isolated from the tongue of a 51 and 25 years old males, respectively [306]. SCC4 are poorly differentiated cells which have shown overexpression of mutant p53 protein and

functional H-Ras protein, whilst SCC9 are moderately differentiated which have shown no expression of p53 protein and a non-synonymous mutation in H-Ras gene [21][307]. SCC4 cells were grown in Dulbecco's Modified Eagles (DMEM) GlutaMAX^{TM} supplemented with 10% (v/v) Foetal Bovine Serum (FBS) and 1% (v/v) penicillin-streptomycin. SCC9 were cultured in DMEM-F12 medium supplemented with 10% (v/v) FBS, 1% (v/v) penicillin-streptomycin, 400 ng/mL hydrocortisone, 0.5 mM sodium pyruvate and 2.5 mM L-glutamine.

2.3.1. Cell maintenance

Cells were routinely maintained in 75 cm^2 tissue culture flasks in a 5% CO_2 atmosphere at 37°C and were passaged when 70-80% confluent, approximately twice a week. For sub-culturing, media was removed from the flask and cells were washed with 3 mL Phosphate Buffered Saline (PBS). Following the removal of PBS, cells were incubated with 3 mL of TrpLE Express at 37°C until they had detached from the flask. TrpLE Express was then neutralised with 3 mL of fresh media, and cells were collected into a 50 mL falcon tube and centrifuged at 300 x g for 5 min. The pellet was resuspended in fresh media and diluted in a new cell culture flask with fresh growth media (10 mL).

2.3.2. Cell freezing and recovery

Cells were routinely stored in liquid nitrogen at -196°C. For freezing, cells were grown in a 75 cm^2 flask to a maximum confluence of 70%-80%. Cells were detached and centrifuged at 300 x g for 5 min at room temperature. The pellet was resuspended in 3 mL of freezing solution containing 90% (v/v) FBS and 10% (v/v) Dimethyl Sulfoxide (DMSO) and aliquoted into cryotubes (1 mL per tube). Then, cells were placed into a Mr. Frosty freezing container filled with isopropanol and stored at -80°C for approximately 24 h before transferring to liquid nitrogen. For thawing, cells were removed from liquid nitrogen and defrosted rapidly in a 37°C water bath for approximately 1-2 min. Cells were transferred into a 50 mL falcon tube with 10 mL fresh media and centrifuged at 300 x g for 5 min to remove any trace of DMSO. The supernatant was removed, and the pellet was resuspended in fresh media and diluted for growth in a 25 cm^2 flask. The following day the media was changed, and cells were passaged once confluent.

2.3.3. Cell counting

Prior to each experiment cells were counted. From a 70-80% confluent flask, cells were detached and centrifuged as described above. The pellet was resuspended in 5-8 mL of fresh media and 10 µL of a 1:2 dilution of cells was pipetted onto a Neubauer hemocytometer for cell counting. The haemocytometer had nine 1 x 1 mm squares engraved in it and the chamber between the grid and the coverslip was 0.1 mm thickness. Cells were counted in the four large corner squares of the hemocytometer and the average per small square was acquired and multiplied by the dilution factor and by 10^4 to determine the number of cells per mL.

2.4. Drug preparation

2.4.1. Cisplatin

Cisplatin (cis-diammine platinium (II) dichloride) was dissolved in sterile 0.9% NaCl to make a stock solution of 2 mM. The stock solution was filtered using syringe filters 0.2 µm pore size, aliquoted and stored protected from the light at -20°C for a long period or at 4°C for a short period (2-3 months). From the stock solution, the desired concentrations of cisplatin for each experiment were made up by further dilution in 0.9% NaCl.

2.4.2. 5-Fluorouracil

5-fluorouracil was dissolved in DMSO to make a stock solution of 400 mM. The stock solution was stored protected from the light at 4°C for 5 months. Working dilutions were prepared fresh on the day in sterile PBS with the final DMSO concentration applied to the cells at 0.1% (v/v).

2.4.3. Docetaxel

Docetaxel Accord contains 20 mg of docetaxel per 1 mL (dissolved in ethanol). Desired dilutions were prepared in 100% ethanol with the final ethanol concentration applied to the cells at 1% (v/v). The principal stock and working solutions were stored at 4°C protected from the light.

2.4.4. Carboplatin

Carboplatin was dissolved in sterile H_2O to make a stock solution of 25 mM. The stock solution was stored protected from the light at room temperature. Working dilutions were made up with H_2O to the concentration required.

2.4.5. Sorafenib

Sorafenib was dissolved in 100% ethanol to make a 10 mM stock. The stock solution was stored at 4°C. From the stock solution, the desired concentrations of sorafenib for each experiment were made up by further dilution in PBS with the final ethanol concentration applied to the cells at 1% (v/v).

2.4.6. Autophagy modulators

Bafilomycin-A1 and SAR405 were dissolved in DMSO to make stock solutions of 100 µM and 10 mM respectively. Chloroquine and rapamycin were supplied lyophilised in the Cyto-ID® Autophagy Detection kit. Chloroquine (7.5 µmoles) was reconstituted in 125 µL deionised H_2O and rapamycin (25 nmoles) in 50 µL DMSO, resulting in 60 mM and 500 µM stock solutions respectively. Stock solutions of bafilomycin-A1, SAR405, chloroquine and rapamycin were stored at -20°C and working solutions were prepared fresh on the day of the experiment in sterile PBS. Bafilomycin-A1, SAR405 and rapamycin were applied to the cells at a final concentration of 0.1% (v/v) DMSO. Finally, 3-methyladenine (3-MA) working solutions were made up fresh for each experiment by dissolving the required amount of 3-MA in cell culture media up to a concentration of 5 mM. Before applying to cells, working solutions were heated in a water bath to facilitate the dissolution of the compound and filtered using sterile syringe filters with 0.2 µm pore size to avoid bacterial contamination.

2.4.7. Z-VAD-fmk

1 mg of Z-VAD-fmk (caspase inhibitor I) was dissolved in 42.7 µL DMSO to give a 50 mM stock (stored at -20°C). Dilutions were prepared fresh on the day in sterile PBS with the DMSO concentration applied to the cells at a final concentration of 0.1% (v/v).

2.4.8. N-acetyl cysteine

NAC was prepared as a 100 mM stock solution in H_2O. Since the pH of the stock solution was low (~1.5), it was adjusted to 7.0-7.5 using NaOH. The stock solution was filtered

using sterile syringe filters with 0.2 μm pore size to avoid bacterial contamination and then stored for maximum 3 months at 4°C. Working dilutions were made up with H_2O to the concentration required.

2.4.9. SP600125

SP600125 was dissolved in DMSO to make a stock solution of 20 mM. The stock solution was stored protected from the light at 4°C. Working dilutions were prepared fresh on the day in sterile PBS with the final DMSO concentration applied to the cells at 0.1% (v/v).

2.4.10. Buthionine sulfoximine

Buthionine sulfoximine (BSO) was prepared as a 20 mM stock solution in H_2O. From the stock solution, the desired concentrations of BSO for each experiment were made up by further dilution in H_2O. The principal stock and working solutions were stored at -20°C.

2.4.11. ML385

5 mg of ML385 were diluted in 200 μL DMSO to give a 50 mM stock (stored at -20°C). Dilutions were prepared fresh on the day in sterile PBS with the DMSO concentration applied to the cells at a final concentration of 0.1% (v/v).

2.5. Induction of cisplatin resistance in OSCC cells

A cisplatin-resistant population of cells was generated from the SCC4 cell line by pulsed stepwise exposure to cisplatin over a period of 12 months (Figure 2.1). An untreated control set of parental SCC4 cells was grown alongside cisplatin treated cells in order to compare age-matched cell populations. Cells were seeded in 25 cm^2 flasks at a density of 300×10^3 cells/flask in complete media and allowed to attach overnight. The following day, cells were treated with 0.6 μM cisplatin (IC_{25}) diluted in fresh media for 72 h. Cisplatin-free fresh media was supplied to control cells and flasks were incubated for 72 h to mimic the treatment time. After incubation, the media was discarded in both sets of cells and replaced with cisplatin-free media in order to allow viable cells to recover. Fresh media was supplied every two days, and after 7-10 days resistant clones were obtained in the cisplatin-treated set of cells. Cells were passaged a couple of times before repeating the whole procedure again using stepwise increasing concentrations of cisplatin (0.7, 0.8, 0.9 μM). Every generation of 'cisplatin-resistant' cells, along with the age-matched

parental cells, was frozen in liquid nitrogen. Following cell thawing and maintenance for a number of days in cisplatin-free growth medium, a cell viability assay was performed to evaluate any fold change in IC_{50} values compared to the parental cell line. Thus, the SCC4 parental cells and the SCC4 'cisplatin-resistant' cells (SCC4cisR) were treated with several concentrations of cisplatin (0-25 µM) for 72 h and viability was determined through the alamar blue viability assay as detailed below.

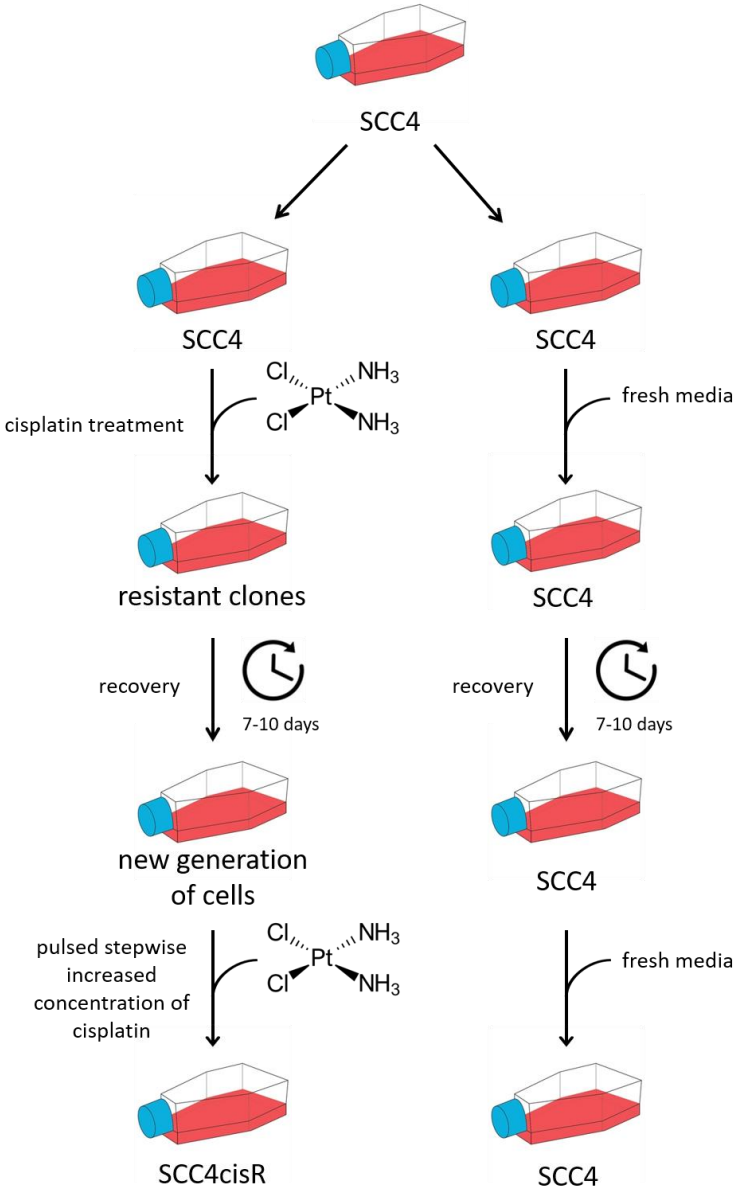

Figure 2.1 Generation of cisplatin-resistant SCC4cisR cells and age-matched parental SCC4 cells.

2.6. Cell viability assay

An alamar blue assay was performed to study cell viability in OSCC cells. The active constituent in alamar blue is resazurin, a blue non-fluorescent cell dye that is reduced to resorufin in healthy viable cells because of their naturally reductive environment (Figure 2.2). As the resorufin is pink and highly fluorescent, the viability of the cells can be quantitatively detected using a UV spectrophotometer at an emission and extinction wavelength of 544 nm and 590 nm respectively.

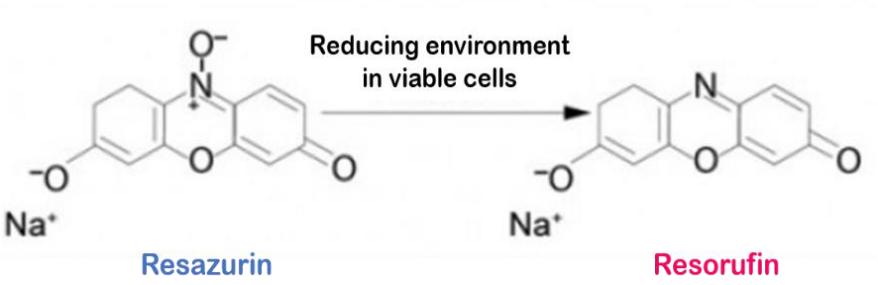

Figure 2.2 The principle of alamar blue assay.

2.6.1. Determination of the linear range of the assay

The linear range of the assay was determined in order to optimise the protocol. SCC4 and SCC9 cells were seeded in triplicate in complete media in 96 well flat bottom plates (200 µL/well) at varying cell densities (1-30 x 10^3 cells/well). Cells were allowed to grow at 37°C for 48 and 72 h before adding 20 µL of alamar blue. Plates were incubated at 37°C for 6 h wrapped in the tinfoil. The fluorescence was measured at an excitation wavelength of 544 nm and an emission wavelength of 590 nm on a SpectraMax Gemini EM Microplate Reader using SOFTmax Pro version 4.9. The values obtained were normalised by the blank and the mean of each triplicate was calculated. Data were graphed using GraphPad Prism version 5.0 (GraphPad software Inc., San Diego, CA, USA).

2.6.2. Determination of IC_{50} values of chemotherapeutic agents

Cells were seeded in 96 well flat bottom plates in triplicate at a density of 5 × 10^3 cells/well in complete media (~30-40% confluence) and allowed to attach overnight at

37°C. The following day, the media was replaced with varying concentrations of the relevant drug diluted in complete media (200 µL/well). Cells were incubated at 37°C for 24, 48 and 72 h and cell viability was determined by the addition of 10% (v/v) alamar blue to each well. Plates were incubated in the dark for up to 6 h until a colour change was observed. The fluorescence was measured at an excitation wavelength of 544 nm and an emission wavelength of 590 nm on a SpectraMax Gemini EM Microplate Reader using SOFTmax Pro version 4.9. The values obtained were normalised by the blank. Vehicle treated cells were taken as 100% viability and wells treated with drugs were calculated as a percentage of the vehicle control. The mean of each triplicate was calculated. Dose response curves were plotted and IC_{50} values were determined using GraphPad Prism version 5.0.

2.7. Colony forming assay

The colony forming assay (CFA) was employed to evaluate the survival potential of SCC4 and SCC4cisR cells treated with cisplatin. The CFA is an *in vitro* assay that allows one to determine the ability of cells to survive and reproduce after treatment with cytotoxic agents, such as drugs or radiation. The CFA is based on the capacity of single cells to grow into colonies [308]. Colonies are defined as a cluster of cells >50. Assuming that each colony derives from a single cell, detection and quantification of the number of colonies formed following cytotoxic treatments is indicative of the number of surviving cells.

2.7.1. Determination of the optimal seeding density for the CFA

Optimisation of seeding density was determined by plating increasing concentrations of cells in 6 well plates. Cells were seeded at a cell density range of 250-1500 cells/well in 2 mL of complete media and incubated at 37°C for 72 h to mimic the treatment times. The media was then replaced with 2 mL of fresh new media and cells were left to grow into colonies for 9 days. After the incubation, supernatants were discarded and colonies were washed with 1 mL of PBS. To fix and stain the colonies, each well was covered with 1 mL of 0.5% crystal violet solution diluted in 25% methanol and the plates were incubated for 1 h at room temperature. Colonies were then washed several times with distilled H_2O to remove any residue of the staining solution from the well surface, and

plates were left drying upside down on the bench. Images were acquired with the GelCount image scanner.

2.7.2. Determination of the survival fractions following treatment with cisplatin

Cells were seeded in 6 well plates at a density of 500 cells/well in complete media. After 24 h, cells were treated with increasing concentrations of cisplatin (0-2 µM) for 48 h. After the treatment, surviving cells were incubated at 37°C in drug-free media for 9 days to allow cell recovery. Then, supernatants were discarded and colonies obtained were washed with PBS before being fixed and stained with 0.5% crystal violet solution diluted in 25% methanol. After 1 h, plates were washed with distilled H_2O and left to dry at room temperature. Colonies were counted manually and images were acquired with the GelCount image scanner. The values obtained were used to calculate the plating efficiency (PE) and the survival fractions (SF) through the following formulas:

$$PE = \frac{no.\ of\ colonies\ formed\ for\ untreated\ cells}{no.\ of\ cells\ seeded}\ x\ 100\%$$

$$SF = \frac{no.\ of\ colonies\ formed\ after\ treatment}{no.\ of\ cells\ seeded\ x\ PE}$$

Data obtained were then used to determine the cell survival curves which are representative of the relationship between treatment doses and survival fractions. Survival curves were plotted using GraphPad Prism version 5.0. A summary of the entire procedure is showing Figure 2.3.

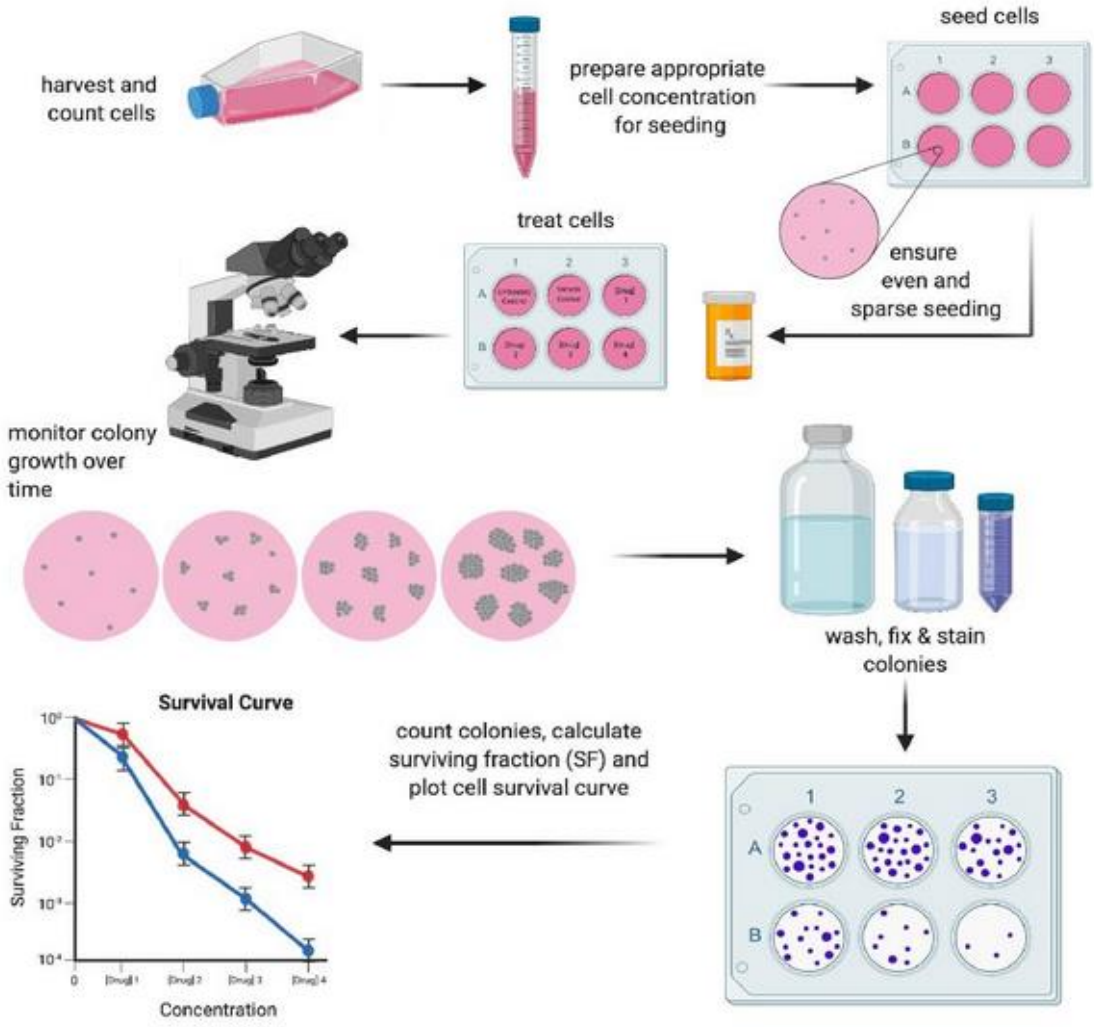

Figure 2.3 Summary of colony forming assay (CFA) protocol.

Image modified from [309].

2.8. Flow cytometry analysis

Flow cytometric analysis was carried out to study the cell cycle, apoptosis, autophagy, oxidative stress and the stem cell population in OSCC cell lines. This technique represents a quantitative approach to count and profile cells in a heterogeneous population. Depending on the analysis of interest, cells were stained with one or two fluorescent dyes and then analysed using a BD Accuri C6 flow cytometer. 10,000 cells were appropriately gated on vehicle treated cells and cell debris and aggregates were excluded. Data were acquired and graphed using GraphPad Prism version 5.0 or FlowJo v10.

2.8.1. Cell cycle analysis

Propidium iodide (PI) staining was used to measure the percentage of cells in G0/G1, S, G2/M and subG0/G1 peaks. PI is a fluorescent dye which binds stoichiometrically to DNA (excitation 488 nm and emission 600 nm). Thus, quantitative detection of PI fluorescence gives information about the amount of DNA in cells which correlates with the cell cycle phase of the cells as follows: G0/G1 (2n), S (2n-4n) and G2/M (4n). Furthermore, cells which have undergone apoptosis have fragmented DNA (<2n) resulting in low PI fluorescence. Apoptotic cells are represented as a subG0/G1 population.

Cells were seeded in 6 well plates at a density of 150×10^3 cells/well in complete media (~30-40% confluence). After 24 h, cells were treated with either vehicle (0.009% (v/v) NaCl) or varying concentrations of cisplatin at different time points. Cells were detached with 1 mL of TrpLE Express, harvested into a 50 mL falcon tube and centrifuged at 300 x g for 5 min. Pellets were washed with 1 mL PBS and then resuspended in 100 µL PBS before fixing with 1 mL of 70% ice cold ethanol added dropwise whilst vortexing. Samples were stored immediately at -20°C for at least 16 h before the analysis. To remove the ethanol, 1 mL PBS was added to each sample and cells were centrifuged at 1000 x g with the brake set at 1. Pellets were resuspended in 200 µL PBS and transferred to 1.5 mL Eppendorf tubes. Next, 10 µg/mL of RNase A and 100 µg/mL of PI were added to each tube and samples were incubated for 30 min at 37°C covered with tin foil before flow cytometric analysis. PI was detected using 585/40 bandpass filter and the percentage of cells in each peak was acquired using BD Accuri C6 software (Figure 2.4).

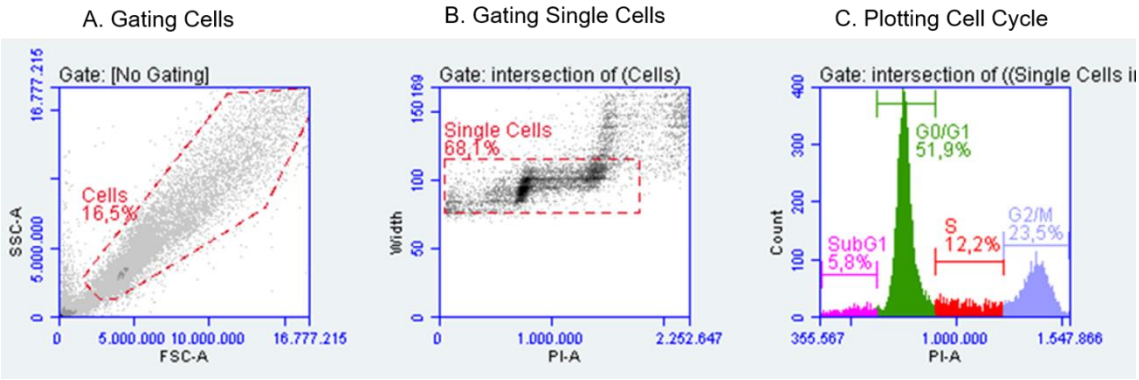

Figure 2.4 Gating strategy for cell cycle analysis.

SCC4 cells were stained with propidium iodide (PI) and then analysed using a BD Accuri flow cytometer. Forward (FSC-A) vs side (SSC-A) scatter area was plotted to identify cell population and to exclude debris **(A)**. Width vs PI (488 nm, FL-2 channel: 585/40 bandpass filter) area (PI-A) was then plotted to exclude clumped and doublet cells **(B)**. This gate was further analysed on a PI-A histogram. Cell cycle stages were gated on the basis of the level of PI intensity **(C)**.

2.8.2. Apoptosis analysis

Annexin V-Fluorescein Isothiocyanate (FITC) and PI staining was performed to study apoptosis in OSCC cells. This assay allows differentiation between early and late stage apoptosis based on cell positivity to annexin V and/or PI staining. Annexin V is a phospholipid binding protein with high affinity for phospholipid phospatidyl serine (PS). In this assay, annexin V is labelled with the fluorochrome FITC. Annexin V-FITC can bind PS only during the apoptotic process when PS translocates from the inner to the outer leaflet of plasma membrane [310]. PI is a red fluorescent dye which binds DNA and it can only enter cells which have lost membrane integrity (late apoptotic/necrotic stages). Thus, based on their annexin V-affinity, apoptotic cells can be distinguished from annexin V-negative living cells and the combination with PI allows a further distinction of late apoptotic (annexin V+/PI+) and early apoptotic (annexin V+/PI-) cells.

Cells were plated as described above and treated with the relevant drugs. After incubation, cells were detached with TripLE Express and centrifuged at 300 x g for 5 min. The supernatant was discarded, and pellets were washed with 500 µL 1X annexin V Binding Buffer, diluted from the 20X solution in PBS (0.1 M HEPES, 1.4 M NaCl, 25 mM $CaCl_2$, pH 7.4). Cells were then centrifuged and resuspended in 50 µL annexin V-FITC antibody (diluted 1:33.3 in 1X annexin V Binding Buffer) and incubated on ice in the dark. After 20 min, cells were pelleted (600 x g, 5 min, 4°C) and resuspended in approximately 300

µL PI (diluted 1:2000 in 1X annexin V Binding Buffer) before flow cytometric analysis. annexin V-FITC (455 nm) was detected using 530/30 bandpass filter while PI (488 nm) with a 585/40 bandpass filter and the percentage of cells positive to annexin V and/or PI was acquired using BD Accuri C6 software (Figure 2.5). Single stained vehicles were used as compensation controls.

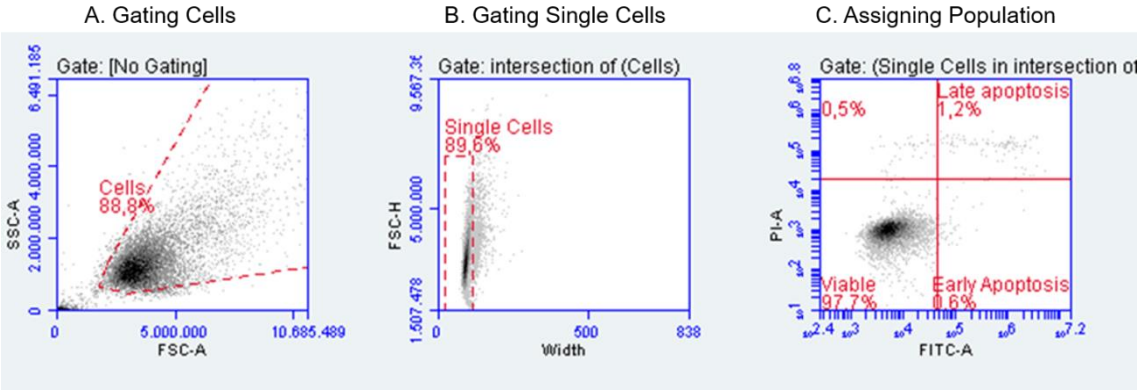

Figure 2.5 Gating strategy for annexin V/PI analysis.

SCC4 cells were stained with annexin V-FITC and PI and then analysed using a BD Accuri flow cytometer. Forward (FSC-A) vs side (SSC-A) scatter area was plotted to identify cell population and to exclude debris **(A)**. Width vs forward scatter height (FSC-H) was plotted to exclude clump and doublet cells **(B)**. This gate was further analysed on a FITC area (FITC-A) vs PI area (PI-A) dot plot. Viable cells: annexin V-/PI-; early apoptotic cells: annexin V+/PI-; late apoptotic cells: annexin V+/PI+ **(C)**.

2.8.3. Autophagy analysis

The Cyto-ID Autophagy Detection Kit was used to analyse autophagy induction in SCC4 and SCC9 cells. This assay represents a specific and quantitative approach for monitoring autophagy induction in live cells [311]. The green fluorescent dye supplied in the kit becomes brightly fluorescent in vesicles produced during autophagy and it can be detected through flow cytometric analysis at an extinction wavelength of 488 nm. The intensity of the signal is proportional to the number of autophagic vesicles, thus is indicative of autophagy activation.

Cells were seeded in 6 well plates at a density of 150 × 10^3 cells/well (~30-40% confluence) and allowed to adhere overnight prior to the treatment. Cells were left untreated or treated with the relevant drugs. A combination of the autophagy inducer rapamycin (RAP) and the autophagy inhibitor chloroquine (CQ) was used as a positive

control and added to the cells 48 h before analysis. Cells were detached with 1 mL of TrpLE Express, harvested into a 50 mL falcon tube and centrifuged at 300 x g for 5 min. Pellets were then washed with 200 µL 1X Assay Buffer (diluted from the 10X solution in H_2O) and transferred into 1.5 mL Eppendorf tubes. After centrifugation, cells were resuspended in 200 µL 1X Assay Buffer and 200 µL Cyto-ID® Green dye solution (diluted 1:1000 in 1X Assay Buffer) was added in each tube. Samples were incubated for 30 min at 37°C covered with tinfoil. Cells were centrifuged (600 x g, 5 min) and resuspended in 300 µL 1X Assay Buffer before flow cytometric analysis. Cyto-ID® Green dye (463/534 nm) was detected using 530/30 bandpass filter and Median Fluorescence Intensity (MFI) was acquired using BD Accuri C6 software (Figure 2.6).

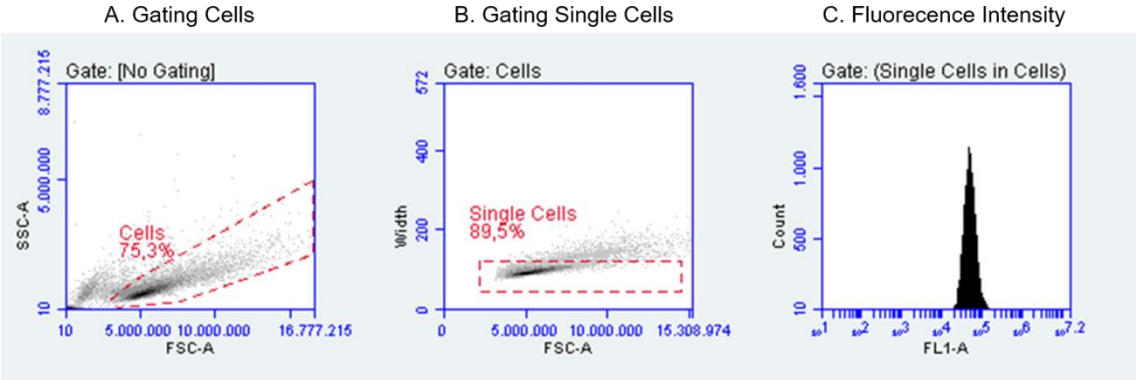

Figure 2.6 Gating strategy for Cyto-ID analysis.

SCC4 cells were stained with Cyto-ID® Green dye and then analysed using a BD Accuri flow cytometer. Forward (FSC-A) vs side (SSC-A) scatter area was plotted to identify cell population and to exclude debris **(A)**. Width vs forward scatter height (FSC-H) was plotted to exclude clumped and doublet cells **(B)**. This gate was further analysed on a FL1-A histogram to acquire MFI values **(C)**.

2.8.4. Measurement of intracellular Reactive Oxygen Species

Intracellular levels of ROS were measured in OSCC cells using 2',7'-dichlorodihydrofluorescein-diacetate (H_2DCFDA) staining. H_2DCFDA is a cell permeant dye which can freely diffuse across cell membranes. In the cytoplasm, this compound is hydrolysed by intracellular esterases and it is converted to H_2DCF through cleavage of the two acetate groups. Even though H_2DCF is a non-fluorescent compound, it can be oxidised by ROS into the highly fluorescent molecule DCF (Figure 2.7). Thus, fluorescence depends on the presence of ROS within cells and fluorescence intensity

correlates with their accumulation. Accordingly, acquisition of fluorescence intensity through flow cytometry can be used as a quantitative method to measure ROS levels in cells.

Cells were seeded in 6 well plates at a density of 150 × 10^3 cells/well (~30-40% confluence) and allowed to adhere overnight prior to the treatment. Cells were left untreated or treated with the relevant drugs for the required time. After incubation, 10 µM H_2DCFDA was added to each well and plates were left for 30 min at 37°C covered with tinfoil. Then, supernatants were discarded, and 1 mL PBS was used to wash the cells. Following the detachment with 1 mL of TrpLE Express, cells were harvested into a 50 mL falcon tube and centrifuged at 600 x g for 5 min. Pellets were then washed with 200 µL PBS and transferred into 1.5 mL Eppendorf tubes. After centrifugation, cells were washed again with PBS and resuspended in 300 µL PBS prior to flow cytometric analysis. DCF dye (485/535) was detected using a 530/30 bandpass filter and MFI was acquired using Accuri C6 software through the same gating strategy as shown for the Cyto-ID analysis (Figure 2.6).

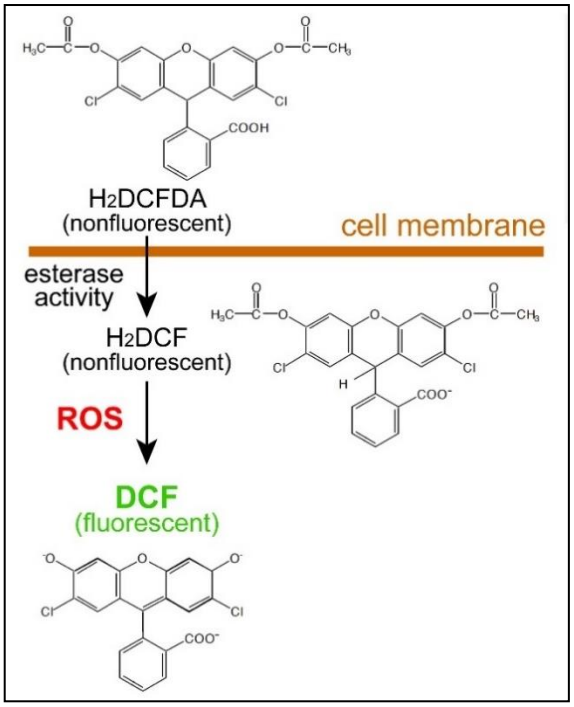

Figure 2.7 H_2DCFDA cellular staining for intracellular ROS detection.

Image modified from [312].

2.8.5. Analysis of $CD44^+/CD24^-$ cells

CD44 and CD24 are cell surface glycoproteins involved in tumor initiation and metastasis [313]. The presence of CD44 along with the lack of CD24 ($CD44^+/CD24^-$) on the cell surface has been proposed as a marker of CSC phenotype in various cancers, including breast cancer, colon cancer and as well OSCC [314]. Analysis of the $CD44^+/CD24^-$ cell population was performed to investigate the stem-like properties of the SCC4 and SCC4cisR cells. In this assay, an anti-CD44 antibody labelled with the fluorochrome FITC and an anti-CD24 antibody labelled with the fluorochrome APC were utilised.

Cells were seeded at a density of 150 x 10^3 cells/well on a 6-well plate (~30-40% confluence) and left to adhere to the plate overnight. The next day, the media was removed, and cells were detached with TripLE Express. After centrifugation at 300 x g for 5 min, the supernatant was discarded, and pellets were washed with 500 µL PBS and transferred into 1.5 mL Eppendorf tubes. Cells were centrifuged (600 x g, 5 min), resuspended in 100 µL CD44-FITC and CD24-APC antibodies (diluted 1:500 and 1:200 respectively in PBS) and incubated at 4°C for 30 min in the dark. After the incubation, cells were centrifuged and washed with 500 µL PBS before being resuspended in 300 µL PBS and analysed in the BD Accuri C6 flow cytometer. $CD44^+$ (488/520 nm) and $CD24^+$ (633/780) cells were detected using 530/30 and 675/25 bandpass filters respectively and MFI was acquired using BD Accuri C6 software.

2.9. Glutathione assay

The GSH/GSSG-Glo kit was employed to evaluate glutathione levels and the cellular redox state in OSCC cells. In cells, glutathione can exist in reduced state (GSH) or in oxidised state (GSSG). The GSH/GSSG-Glo kit is a luminescent-based system which allows the quantification of total glutathione (GSH+GSSG) and GSSG levels within cells. This assay results in the reduction of GSSG to GSH, which is used as substrate for a GSH-dependent conversion of Luciferin-NT to luciferin. This process is then coupled to a firefly luciferase reaction to generate a quantifiable luminescent signal. Thus, the light from luciferase depends on the amount of luciferin formed, which in turn depends on the amount of GSH present. As shown in Figure 2.8, reduction of GSSG to GSH allows the determination of total glutathione (GSH+GSSG) levels within cells, whilst conversion of

GSSG to GSH along with the block of endogenous GSH using N-Ethylmaleimide (NEM) allows the quantification of only GSSG.

The GSH/GSSG-Glo assay was performed according to the manufacturer's protocol and reagents were prepared as reported in Table 2.1 using the components provided in the kit. Two sets of cells (one for the total glutathione measurement and one for the oxidised glutathione measurement) were seeded in duplicate in sterile 96 well flat bottom plates at a density of 5 $\times 10^3$ cells/well in complete media (~30-40% confluence) and allowed to attach overnight at 37°C. The following day, the media was replaced with the relevant drugs diluted in fresh media (200 µL/well) and cells were incubated at 37°C for the required time of the treatment. After the incubation, the treatment was discarded and replaced with either 50 µl of Total Glutathione Lysis Reagent for the total glutathione cell set, or 50 µl of Oxidised Glutathione Lysis Reagent for the oxidised glutathione cell set, and plates were incubated for 5 min at room temperature on a plate shaker. The Total Glutathione Lysis Reagent was used to release from cells the reduced and the oxidized glutathione and to convert all glutathione to the reduced form. The Oxidised Glutathione Reagent was used as well to release both the reduced and the oxidised glutathione, but the reaction of NEM with GSH resulted in the formation of a non-luminescent compound and consequentially in the blockage of endogenous GSH. Following cell lysis, 50 µl of Luciferin Generation Reagent was added to generate luciferin from the GSH-probe, Luciferin-NT, in the presence of GSH and plates were incubated for 30 min at room temperature. Finally, the contents of each well (100 µl final volume) were transferred to non-sterile white opaque 96 well plates before adding 100 µl of Luciferin Detection Reagent containing the Ultra-Glo™ Luciferase, which concurrently stopped the luciferin generation reaction and initiated a luminescent signal directly proportional to the amount of GSH derived from total glutathione (GSH + GSSG) or GSSG alone. After 15 min incubation at room temperature, luminescence was measured on a SpectraMax Gemini EM Microplate Reader using SOFTmax Pro version 4.9. Values obtained from luminescence measurements (in relative light units, RLU) were normalised by the blank and the mean of the two replicas was calculated. GSH levels were computed by subtracting the GSSG values from the total glutathione measurements (GSH+GSSG) and data were graphed using GraphPad Prism version 5.0. The GSH/GSSG ratio was calculated to evaluate oxidative stress. In fact, in healthy cells, more than 90% of glutathione exists as GSH, while in oxidant conditions, intracellular accumulation of

GSSG results as a consequence of GSH oxidation by glutathione peroxidase [257]. Given this, the GSH/GSSG ratio is considered a good indicator of the cellular redox state. As per guideline recommendations, since in this assay two moles of GSH are generated from one mole of GSSG, a twofold adjustment was applied to the GSSG values in order to obtain an accurate measurement of the GSSG levels. Accordingly, the GSH/GSSG ratio was calculated using the formula reported below, and values obtained were then graphed using GraphPad Prism version 5.0.

$$GSH/GSSG\ ratio = \frac{Total\ glutathione - GSSG}{GSSG/2}$$

Total Glutathione Lysis Reagent	**Oxidized Glutathione Lysis Reagent**	**Luciferin Generation Reagent**
2% Luciferin-NT 20% Passive Lysis Buffer 5X H_2O	2% Luciferin-NT 1% NEM, 25mM 20% Passive Lysis Buffer 5X H_2O	2.5 % DTT, 100mM 3% Glutathione-S Transferase Glutathione Reaction Buffer

Table 2.1 Reagents for GSH/GSSG assay.

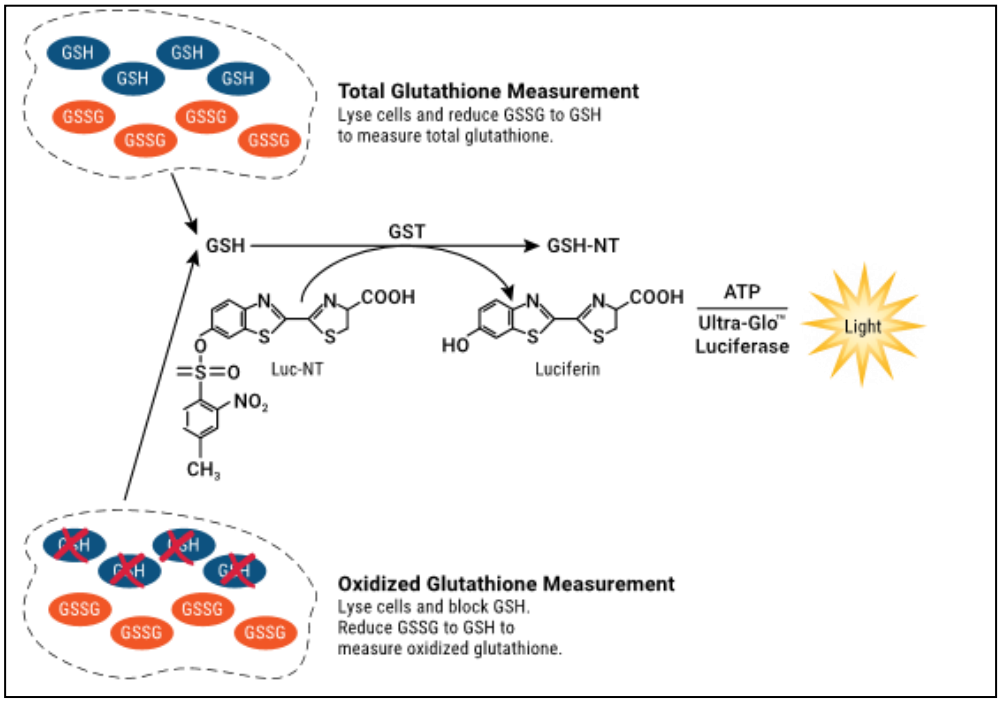

Figure 2.8 Principle of GSH/GSSG-Glo Assay.

Image taken from the GSH/GSSG-Glo™ Assay Technical Manual.

2.10. Western blot analysis of cultured cells

Western Blot analysis was performed to study protein expression of key apoptotic and autophagic markers in OSCC cells.

2.10.1.Protein extraction

Cells were seeded in 25 cm^2 flasks at a density of 300×10^3 cells/flask in complete media (~30-40% confluence). The following day, cells were treated with the relevant drugs and incubated at 37°C. After incubation, cells were harvested by scraping and centrifuged at 300 x g for 5 min. Pellets were washed with 500 µl PBS and lysed straightaway or stored dry at -80°C until further use. The lysis of the samples was performed using ice-cold radioimmunoprecipitation (RIPA) buffer (Table 2.4) supplemented with 10% (v/v) protease inhibitor and 1% (v/v) phosphatase inhibitor cocktail 2 and 3. Approximately 50-200 µL of complete lysis buffer was added to each tube and samples were incubated for 30 min on ice. After centrifugation (10,000 x g, 10 min, 4°C), the pellet was discarded, and the supernatant was transferred to a 1.5 mL Eppendorf tube and stored at -20°C.

2.10.2.Protein quantification

Quantification of protein concentration was carried out using the BCA assay. A stock solution of Bovine Serum Albumin (BSA) was serially diluted in H_2O to prepare the BSA protein standards (0.062, 0.125, 0.25, 0.5, 1, 2 mg/mL) to create a standard curve (Table 2.2). Standards and unknown samples (diluted 5-fold or 10-fold in H_2O) were pipetted into a 96 well flat bottom plate in duplicate (10 µL/well). According to the user guide of the Pierce BCA Protein Assay Kit, the working reagent was prepared by mixing 50 parts of BCA Reagent A (containing bicinchoninic acid) with 1 part of BCA reagent B (containing cupric sulphate). 200 µL of BCA working reagent was added to each well and the plate was incubated at 37°C for 30 min. The absorbance was measured at 562 nm on a SpectraMax 340 PC Microplate Reader (Molecular Devices, LLC, CA, USA) and unknown sample values were interpolated with the standard curve to calculate protein concentrations using SoftMax Pro 6.0 software (Figure 2.9).

Vial	Volume of Dilutent (µL)	Volume and source of BSA (µL)	Final Concentration of BSA (mg/mL)
A	0	Stock Solution	2
B	500	500 of A	1
C	500	500 of B	0.5
D	500	500 of C	0.25
E	500	500 of D	0.125
F	500	500 of E	0.0625
G	500	---	0

Table 2.2 Preparation of BSA standards.

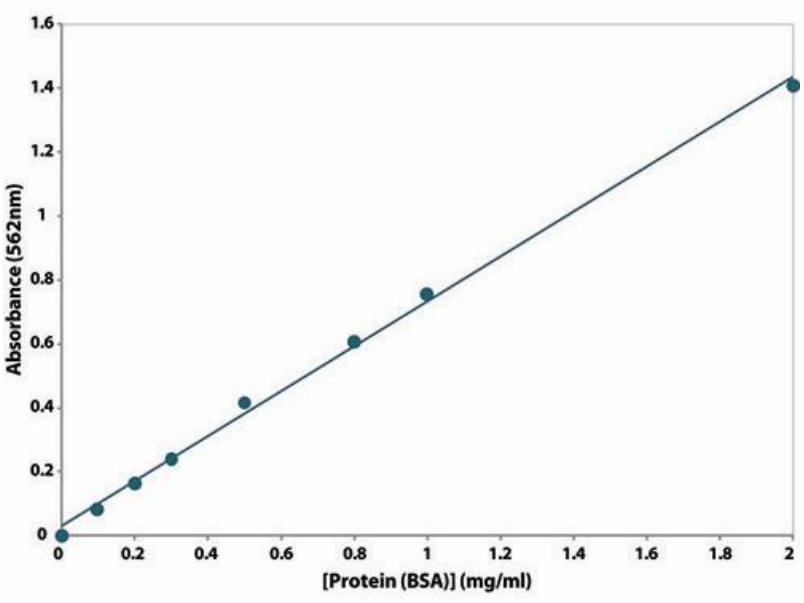

Figure 2.9 Standard curve for BCA assay.

2.10.3.Sample preparation

Samples were denatured prior to SDS-PAGE immunoblotting analysis. To denature, 5X Laemlli Sample Buffer (Table 2.4) was mixed in 1:5 ratio with the required amounts of protein lysate and the mixture was boiled at 70°C for 10 min before adding 50 mM Dithiothreitol (DTT). Samples were loaded straightaway onto a SDS gel or stored at -20°C until further use.

2.10.4.SDS-PAGE

Proteins were separated based on their molecular weight using Sodium Dodecyl Sulphate Polyacrylamide gel electrophoresis (SDS-PAGE) under denaturing conditions. For the analysis, 1.5 mm thickness gels (15 wells) were assembled using Mini-PROTEAN® Tetra Cell Casting stands. A 12% or 15% resolving gel was prepared and poured in between the two glass plates and 200 µL isopropanol were added on the surface of the gel to avoid bubbles. After polymerisation, the isopropanol was removed by washing with H_2O and a 5% stacking gel was poured on the top of the resolving gel. Resolving and stacking gels were made as described in the Table 2.3. The polymerised gel was then placed in the electrophoresis tank and 10-20 µg of proteins (no more than 30 µL) were loaded into each well alongside 5µL PageRuler Plus Prestained Protein Ladder. Samples were run in 1X Running Buffer diluted from a 10X solution (Table 2.4) in H_2O at 80V through the stacking gel (approximately 20 min) and then at 120V through the resolving gel until the samples reached the end of the gel (approximately 2 h). If the gel was not immediately required, it was wrapped in wet tissue and stored at 4°C.

Components	**Resolving gel 12 % (10 mL)**	**Resolving gel 15 % (10 mL)**	**Stacking gel 5 % (5mL)**
H_2O	3.3	2.3	3.4
30% Acrylamide Mix	4.0	5.0	0.83
Tris-Cl (1.5 M, pH 8.8)	2.5	2.5	-
Tris-Cl (1 M, pH 6.8)	-	-	0.63
10% SDS	0.1	0.1	0.05
10% Ammonium Persulphate (APS)	0.1	0.1	0.05
TEMED	0.004	0.004	0.005

Table 2.3 Components for preparation of gels for SDS-PAGE.

2.10.5.Immunoblotting

SDS gels were transferred to Polyvinylidene difluoride (PVDF) membranes. Prior to transfer, the membrane was activated with 100% methanol for 2 min, and sponges and filter paper were soaked in the 1X Transfer Buffer diluted from the 10X solution (Table 2.4) in H_2O and supplemented with 100 mL 100% methanol. The gel and the membrane were sandwiched between sponges and filter papers (sponge > 2 filter papers > gel > membrane > 2 filter papers > sponge) and were kept tight in a gel holder cassette avoiding bubble formation. The cassette was then placed into a transfer tank filled completely with 1X Transfer Buffer alongside an icepack to prevent overheating during transfer. The transfer was performed at 200 mA for 90 min and the pre-stained molecular weight protein ladder served as an indication of successful transfer.

RIPA Buffer	**Laemmli Sample Buffer**	**10X Running Buffer**
150 mM NaCl 50 mM Tris 1.0% IGEPAL® CA-630 0.5% (v/v) sodium deoxycholate 0.1% (v/v) SDS H_2O pH 8.0	62.5 mM Tris-HCl (pH 6.7) 10 % (v/v) Glycerol 2 % (v/v) SDS 0.002 % (w/v) bromophenol blue containing DTT 50 μM H_2O	25 mM Tris 192 mM Glycine 0.1 % (v/v) SDS H_2O
Blocking Buffer	**10X Transfer Buffer**	**10X TBS**
5% (w/v) Marvel milk 1X TBS-0.1% tween®20	25 mM Tris 192 mM Glycine H_2O	200 mM Tris 1.5 M NaCl H_2O pH 8

Table 2.4 Buffers used for western blot analysis.

2.10.6.Immunostaining

Prior to detecting the proteins of interest, the PVDF membrane was kept in fresh Blocking Buffer (Table 2.4) for 1 h at room temperature with constant agitation. The membrane was then incubated with the primary antibody diluted in Blocking Buffer and left on a rocker overnight at 4°C. The next day, the membrane was washed 3 times for 10 min with

1X TBS diluted from the 10X solution (Table 2.4) in H_2O and supplemented with 0.1% (v/v) Tween®20 before incubating for 1 h at room temperature with the secondary antibody conjugated to horseradish peroxidise (HRP) diluted in Blocking Buffer. The dilutions used for each antibody are reported in Table 2.5. The membrane was washed again 3 times for 10 min with 1X TBS-0.1% (v/v) Tween®20 and the bands were detected through enhanced chemiluminescence. After accurately washing with 1X TBS-0.1% (v/v) Tween®20, the same procedure was repeated with the loading controls (GAPDH, α-tubulin or β-actin).

Antibody	**Host**	**Dilution**
Anti-ATG5	Rabbit	1:1000
Anti- Cleaved caspase 3	Rabbit	1:500
Anti-Caspase 3	Rabbit	1:1000
Anti-GADPH	Mouse	1:5000
Anti-HO-1	Rabbit	1:1000
Anti-LC3-I/II	Rabbit	1:1000
Anti-Nrf2	Rabbit	1:1000
Anti-p42/44 (ERK1/2)	Rabbit	1:2000
Anti-p62	Mouse	1:1000
Anti-phospho-p42/44 (ERK1/2)	Rabbit	1:2000
Anti-phospho-SAP/JNK	Rabbit	1:1000
Anti-SAP/JNK	Rabbit	1:1000
Anti-Ras	Rabbit	1:1000
Anti-α-Tubulin	Mouse	1:5000
Anti-β-Actin	Mouse	1:2000
Anti-Rabbit (W4011)	Goat	1:2500
Anti-Mouse (W402B)	Goat	1:5000

Table 2.5 Antibodies used for western blot analysis of cultured cells.

2.10.7.Protein detection and data analysis

Protein bands were detected using electrochemiluminescence (ECL). Before the analysis, equal amount of Reagent 1 and Reagent 2 (Pierce ECL Western Blotting Substrate) were mixed and added to the membrane for 1 min. The blot was developed in a BioRad Gel DocTM XR+System and both chemiluminescent and colorimetric pictures were acquired using the Image Lab software to visualise the protein of interest and the protein marker. The images were then merged to provide an estimate of protein size. The relative amount of protein was calculated through densitometric analysis using Image Lab software. This programme automatically removes background noise and allows quantification of the density of the bands through the number of pixels. The relative density obtained for each protein of interest was normalised by the loading control and data were plotted on a bar chart using GraphPad Prism version 5.0.

2.11. SiRNA knockdown

Genetic inhibition of autophagy was performed in OSCC cells by using a small interfering RNA (siRNA) approach against ATG5 protein. SiRNAs are double-stranded RNA molecules formed by 21-28 nucleotides, which downregulate specific proteins by binding to their transcripts based on the sequence complementarity [315]. In the present study, a SMART-Pool technology (Dharmacon) combining four gene-specific siRNAs into a single reagent pool was employed to enhance the efficiency of the knockdown.

SCC4 cells were seeded at a density of 200 x 10^3 cells/well on a 6-well plate (~50% confluence) in complete media and left to adhere to the plate overnight. The next day, cells were washed three times in PBS and antibiotic/FBS-free media was added to cells for two hours before transfection. ON-target plus SMART-pool ATG5 siRNA was employed for ATG5 knockdown, while ON-target plus non-targeting pool siRNA served as negative control. Both ATG5 siRNA or non-targeting siRNA was diluted into opti-MEM reduced serum media to a concentration of 250 nM, while Lipofectamine 2000 was diluted 1 in 50 into opti-MEM reduced serum media. Following 5 min incubation, the two solutions were pooled together in a 1:1 ratio, and the new solution obtained was incubated for further 20 min at room temperature to allow the formation of siRNA-Lipofectamine complexes. The latter were then added to cells at a final concentration of 25 nM. Following 5 h incubation at 37°C, media was replaced with antibiotic free media

enriched with FBS, and cells were incubated for 48 h or for 24 h before being treated with cisplatin (10 uM) for a further 24 h. After incubation, western blot analysis was performed as described above to confirm ATG5 knockdown and to investigate autophagy and apoptosis levels in ATG5 knockdown cells.

2.12. Western blot analysis of patient tissue samples

Protein levels of key autophagy markers were studied in fresh tissue samples by western blot. The analysis was performed at the University of Valencia, in the Molecular Oncology Laboratory of the General University Hospital Research Foundation. 57 oral biopsy samples (Normal N=20, Precancerous N=19 and OSCC N=21) were collected from patients over a period of 12 months by Prof Jose Bagan at the Department of Stomatology and Maxillofacial Surgery at the General University Hospital of Valencia after informed consent, and immediately frozen and stored at -80°C. Samples were defrosted beforehand and 12-15 mg of tissue was dissected using sterile scalpels and washed twice with PBS before adding 75 μL of RIPA buffer supplemented with 10% (v/v) protease inhibitor and 1 mM sodium orthovanadate. Then, samples were homogenised using an electric homogeniser (for approximately 5 min) and incubated for 30 min on ice. After centrifugation (10,000 x g, 10 min, 4°C), supernatants were transferred into a new tube and stored at -20°C or used straight away. Protein quantification was performed using a Bradford assay. BSA standards were prepared (see Table 2.2) and pipetted into a 96 well flat bottom plate in triplicate (5 μL/well) alongside unknown samples diluted 1:10 or 1:20. 200 μL of Bradford reagent was added to each well and the plate was incubated in the dark for 5 min at room temperature. The absorbance was measured at 595 nm in a Victor 3 1420 Multilabel Counter. Samples were prepared and 60 μg of proteins were separated on a 15% SDS-PAGE gel, transferred to a PVDF membrane and blotted with the antibodies of interest as described above (Table 2.6). The membrane was incubated in the dark with ECL for 1 min and then placed into a developing cassette between two transparent sheet protectors. In the dark room, an X-ray film was placed on the top of the membrane and the cassette was closed. Films were exposed for 5-30 min before being submerged in the tray containing the developer solution (10 seconds), rinsed in the tray containing water and submerged in the tray containing fixer solution (15 seconds). Primary and secondary antibodies were then

removed by stripping the membrane with Stripping Solution (0.2 M glycine pH 2.5, 0.4 % (w/v) SDS) for 15 min at room temperature. Thus, the membrane was re-probed with anti-β-actin antibody (loading control) with the same procedure. The relative amount of proteins was calculated through densitometric analysis using ImageJ software and values were graphed using GraphPad Prism version 5.0.

Antibody	Host	Dilution
Anti-LC3-I/II	Rabbit	1:1000
Anti-p62	Mouse	1:1000
Anti-β-Actin	Mouse	1:2000
Anti-Rabbit (A16035)	Goat	1:2000
Anti-Mouse (A9044)	Goat	1:80000

Table 2.6 Antibodies used for western blot analysis of patient tissue samples.

2.13. Immunohistochemical analysis of tissue patient samples

Immunohistochemical staining of autophagy-related proteins was performed on paraffin-embedded tissue samples at the Central Pathology Laboratory situated at St. James' Hospital, Dublin. 29 oral biopsies were provided by Dr Mary Toner, lead pathologist of the Oral Maxillofacial & Pathology Unit in St. James's Hospital. Samples were retrieved and cut into 4 µm sections by using the Thermo Scientific HM 355S Automatic Microtome. Sections were then mounted on microscope glass slides in a water bath and slides were left drying for 1 h at 60°C. Control slides were stained with a Haematoxylin & Eosin (H&E) stain using the automated Tissue-Tek Prisma® Plus Automated Slide Stainer for histological assessment. H&E slides were reviewed by Dr Mary Toner and the presence of Normal, Dysplasia and OSCC tissues was assessed for each slide. Overall, N=20 Normal, N=23 Dysplasia and N=17 OSCC tissue samples were analysed in this study. Immunohistochemical slides were stained on a Ventana BenchMark Immunostainer, which is a fully automated instrument that allows one to stain 30 slides at the same time, using different protocols. For each protein of interest, a specific protocol was optimised depending on the primary antibody, as reported in Table 2.7. Lung carcinoma tissue was used as positive control tissue for the optimisation of LC3 antibody. Colon tissue and kidney tissue were used as positive control tissue for the optimisation of

Beclin-1 antibody. Prostate tissue and gastric cancer tissue were used as positive control tissue for the optimisation of Bcl-xL antibody. During the pre-treatment step, samples were deparaffinised and antigen retrieval was performed using the Cell Conditioner 1 (CC1), consisting of ethylene-diamine-tetra-acetic acid (EDTA)-based heat-induced antigen retrieval at pH=8. During the staining step, primary antibodies were manually added on the top of the slides at the dilution required (Table 2.8) and incubated at 36°C (an air vortex mixing ensured uniform reagent coverage across the surface of the slide). For the LC3 staining, an additional amplification step was also performed using the Ultraview/iView Amplification Kit. Upon antibody incubation, a counter-stain was performed with Hematoxylin and Bluing reagent. Primary antibodies were then detected and visualised using the OptiView DAB IHC Detection Kit, and slides were washed in water with a drop of dishwashing detergent before mounting the coverslip using a Tissue-Tek Film Automated Coverslipper. Slides were viewed and imaged using the Olympus BX51 upright microscope with representative pictures taken at 10, 20 and 40X magnification. Immunostaining was double scored blindly (Magnano S. & Flis E.) based on the staining intensity and three score were assigned to the samples: +1 (weak staining), +2 (medium staining), +3 (strong staining) and +4 (very strong staining). The IHC scores obtained were then averaged and plotted using GraphPad Prism 5.0.

	LC3	**Beclin-1**	**Bcl-xL**
Antigen retrieval	64 min	48 min	64 min
Primary antibody	16 min	32 min	32 min
Amplification	8 min	-	-
Counter staining	4 min	4 min	4 min
Bluing Reagent	4 min	4 min	4 min

Table 2.7 Immunohistochemistry (IHC) protocols for LC3, Beclin-1 and Bcl-xL staining.

Antibody	**Host**	**Dilution**
Anti-LC3 (monoclonal)	Rabbit	1:50
Anti-Beclin-1 (polyclonal)	Rabbit	1:400
Anti-Bcl-xL (monoclonal)	Rabbit	1:300

Table 2.8 Antibodies used for immunohistochemical analysis of patient tissue samples.

2.13.1.ROC analysis

ROC analysis was performed to evaluate the diagnostic power of Beclin-1 and LC3 in OSCC. This analysis allows to determine the performance of a diagnostic test through the evaluation of sensitivity (true positive rate) and specificity (false positive rate) as measures of accuracy of test in comparison with gold standard status (e.g. patient's disease status) [316]. The ROC curve consists of a graphical representation of sensitivity in function of 100-specificity of a certain parameter across all the possible threshold values [316]. The Area Under the Curve (AUC) represents a measure of the predictive power of test to discriminate between two groups (e.g. normal/disease) at the optimal cut off values [316]. AUC values close to 1 indicate that the test perfectly discriminates between the two groups, whilst AUC values close to 0.5 indicate that the test cannot distinguish between the two groups examined [317]. In the present study, the IHC scores obtained from the immunohistochemical analysis of Beclin-1 and LC3 were used to compute ROC curves. AUC, sensitivity and specificity at the optimal cut-off values were calculated using the MedCalc software.

2.14. Statistical analysis

Statistical analysis was carried out using GraphPad Prism version 5.0 and GraphPad Prism version 8.0. Results were expressed as mean ± the standard error of the mean (S.E.M.). For comparison of two treatment groups within the same cell line, a two-tailed unpaired t-test was performed. For comparison of more than two treatment groups within the same cell line, a one-way ANOVA followed by Dunnett's or Tukey's Multiple Comparison Tests was performed. For comparison of two independent cell lines in the presence/absence of the treatment, a two-way ANOVA followed by Multiple Comparison Tests was performed. For comparison of protein expression levels between groups of OSCC patients, a non-parametric Kruskal-Wallis H Test followed by Dunn's Multiple Comparison Test and Mann-Whitney Test were performed. Association analysis between protein expression and histological stage of OSCC progression was performed using the Pearson's chi squared test. Values of $*p<0.05$, $**p<0.01$ and $***p<0.001$ were considered to be significant.

3.Evaluation of targeting autophagy for the treatment of OSCC

3.1. Introduction

OSCC is a major health problem worldwide. It has been reported that nearly 5% of all cancers diagnosed in the world concern the oral cavity, and in 95% of cases they are classified as OSCC [4, 5]. The survival rate associated with OSCC is one of the lowest likely due to late diagnosis. In fact, it has been demonstrated that less than 50% of malignant lesions are detected and treated before development of the cancer [318]. The fast progression of OSCC results in the prevalent diagnosis of advanced stages of malignancy, which correlates with a poor prognosis and a low survival rate. Additionally, a high morbidity rate has been associated with OSCC due to reduced quality of life and residual deformity following therapeutic treatments.

Surgical removal of the tumour and radiation, in combination with chemotherapy, are the current treatment regimens against OSCC. The type of therapy carried out usually depends on the location and the stage of the tumour. Surgery and radiotherapy represent the main therapeutic strategies when the tumour is localised to an accessible region of the mouth, whereas chemotherapy has recently become an important adjuvant therapy for OSCC, which is used pre- and post-surgery or as a primary therapy when surgery is not possible [34]. Cisplatin, 5-fluouracil and docetaxel are standard chemotherapeutic agents commonly used in the treatment of OSCC. It has been reported that the sensitivity of tumours to anti-cancer drugs is highly variable, indicating that the choice of the drug for the treatment of OSCC should be personalised based on the type of tumour and the genetic mutations present [319].

Cisplatin represents a frontline therapy for many types of cancer including lung, ovarian, breast as well as OSCC. Cisplatin is a square planar compound containing two amine and two chloride groups coordinated to a central platinum atom in a *cis* configuration [320]. It is usually injected intravenously to patients and it can enter cells by simply diffusing through cell membranes or it can be actively transported into cells by copper transporters. Upon cisplatin influx into the cytoplasm, acquation reactions lead to the replacement of the chloride ions with two water or hydrogen groups, resulting in a positively charged molecule which becomes active by reacting with nucleophiles within cells [321]. Cisplatin mechanisms of action have been widely studied over the past 50 years. The ability of cisplatin to induce DNA damage has been considered the primary mechanism implicated in its cytotoxicity. In fact, cisplatin forms 1,2 or 1,3 intra- and inter-strand cross links with DNA by reacting with purines [321]. Formation of DNA adducts results

in DNA damage and consequentially in inhibition of DNA replication, cell cycle arrest and apoptosis [322].

Although cisplatin exhibits overall high efficacy for the treatment of OSCC, several challenges have been attributed to the use of this drug. First of all, numerous undesirable side effects have been experienced by cancer patients treated with cisplatin; particularly nephrotoxicity, neurotoxicity, gastrointestinal disorders and haemorrhage [322]. To overcome this problem, several analogues to cisplatin have been synthesised and tested to enhance the therapeutic efficacy of cisplatin. Amongst them, just one, carboplatin, has been clinically approved so far, but others are still in clinical trials [323]. Carboplatin is currently used for the treatment of ovarian, lung and head and neck cancers. The advantage of using carboplatin as an alternative to cisplatin is due to reduced side effects, particularly the nephrotoxicity. However, it has been demonstrated that carboplatin is less potent than cisplatin, in fact four times more carboplatin is needed to achieve the same efficacy as cisplatin [323]. Another crucial issue associated with cisplatin is that numerous people do not respond to the treatment due to an innate or acquired resistance to the drug.

Chemoresistance has been reported as one of the major problems arising during the treatment of OSCC. This results in the ability of cancer cells to reduce sensitivity to anti-cancer drugs, leading to tumour recurrence and progression. As described in the general introduction, drug resistance can be innate or acquired, depending on whether it occurs before or after the treatment and it can be linked to several mechanisms. Combining different anticancer drugs has been proposed as a potential mechanism to enhance cytotoxicity and bypass drug resistance in several cancers [324]. In this regard, multidrug regimens with cisplatin and 5-fluorouracil or cisplatin and docetaxel/paclitaxel have been shown to stabilise tumour progression in advanced forms of head and neck cancer and OSCC by enhancing the cytotoxic effects of chemotherapy [325, 326]. Nevertheless, this strategy may lead to strong side effects due to the high toxicity of the drugs and to the development of multidrug resistance. Therefore, a greater understanding the mechanisms involved in chemoresistance is required in order to develop new and more valuable strategies.

Autophagy is a catabolic process that allows the degradation and recycling of unnecessary or dysfunctional cellular components [327]. Autophagy occurs in cells at basal levels, playing a housekeeping role as it functions to remove redundant, damaged or

dysfunctional organelles. Even though it is considered a physiological process, autophagy is implicated in numerous pathologies as a mechanism to provide nutrients and supply energy under stressful conditions. In fact, an upregulation of autophagy has been observed during cellular stress, including nutrient depletion, hypoxia and exposure to cell toxins such as chemotherapeutics. Moreover, an interesting correlation between autophagy and cancer has been demonstrated in the last few years. A dual role of autophagy as a tumour suppressor and tumour promoter mechanism has been reported in various cancers [143], but the role of autophagy in OSCC remains poorly understood.

Autophagy activation in response to chemotherapeutics has been demonstrated in several cancers [189]. On the one hand, autophagy may represent a protective mechanism for cells to overcome stress induced by chemotherapy. On the other hand, extended stress might lead to autophagy activation as an anti-tumour mechanism, resulting in cell death. In support of the protective role of drug-induced autophagy, recent studies suggest that tumour resistance to therapy could be related to cell survival through autophagy [328]. Thus, heightened autophagy may be a mechanism of resistance for cancer cells faced with metabolic and therapeutic stress. Accordingly, targeting autophagy has been proposed as a novel strategy to bypass drug resistance and improve patient outcomes. Nevertheless, even though the efficacy of combining autophagy inhibitors and chemotherapeutics has been demonstrated in several studies, this strategy appears to be context-specific, depending on the type of cancer, the genetic composition of cells and the type of drug the cells are exposed to [329].

The role of autophagy in response to chemotherapeutics in OSCC and its implication in chemoresistance is still unclear. In this regard, the aim of this chapter was to investigate the cell death pathway(s) initiated by chemotherapeutic treatment in OSCC cell lines and to evaluate whether autophagy is indeed activated in response to chemotherapy. Furthermore, this chapter examined whether autophagy inhibition, through knockdown of key autophagic proteins and the use of pharmacological autophagy inhibitors, is effective in improving chemosensitivity. Combining chemotherapeutics with autophagy inhibition may represent a valuable treatment strategy to promote OSCC cytotoxicity and diminish resistance in OSCC patients.

3.2. Results

3.2.1. Optimisation of the seeding density for the alamar blue assay in OSCC cell lines

The alamar blue assay was employed to study cell viability in OSCC cell lines following treatment with standard chemotherapeutics. The active chemical resazurin is irreversibly reduced to resorufin in the presence of the naturally reductive environment of healthy viable cells, which results in a change of colour from blue to pink. Since resorufin is highly fluorescent, the acquisition of fluorescence values using an UV spectrophotometer allows quantification of cell viability [330]. Dead and damaged cells are less metabolically active and therefore present a lower rate of conversion. However, the validity of this assay is confirmed only when there is a linear correlation between fluorescence and cell density. In fact, a high seeding density may result in the saturation with resorufin, resulting in a fluorescence plateau, whereas a low seeding density may influence cell growth and viability due to lack of cell contact. Therefore, before commencing the experiments, optimisation of the assay was required by assessing the optimal seeding density in each cell line.

The two OSCC cell lines, SCC4 and SCC9, were seeded in a 96 well plate at various cell densities. A seeding density range of 1-30x10^3 cells/well was evaluated for both cell lines, and cell viability was determined after 48, 72 and 96 h to mimic the treatment times. 6 h prior to analysis, cells were stained with alamar blue (10% (v/v)) and incubated at 37°C in the dark. Fluorescence was measured on a SpectraMax Gemini EM Microplate Reader at an excitation wavelength of 544 nm and an emission wavelength of 590 nm using SOFTmax Pro version 4.9. An increase in fluorescence was observed at increasing cell densities and incubation times in the SCC4 cell line, with fluorescence reaching a plateau at seeding densities above 10x10^3 cells/well at 48 and 72 h incubation (Figure 3.1). Conversely, in the SCC9 cell line, a linear correlation between cell density and fluorescence was found at all cell densities and time points examined. A cell seeding density of 5x10^3 cells/well was used for subsequent experiments in both cell lines as it falls within the linear range.

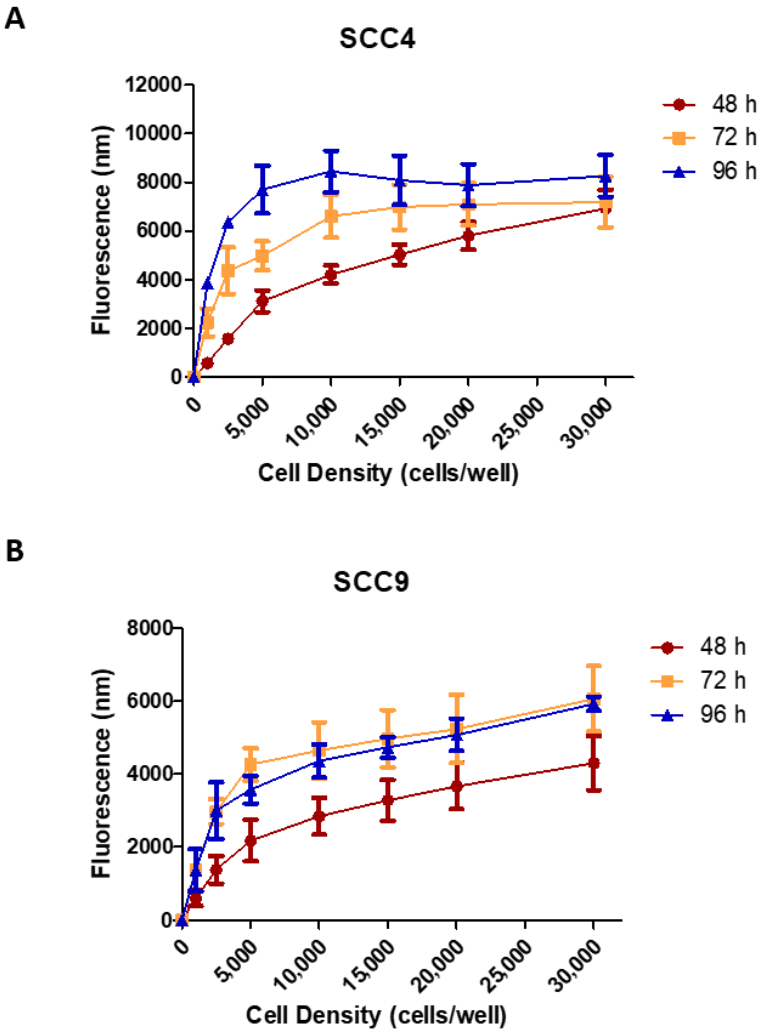

Figure 3.1 Optimisation of the seeding density for the alamar blue assay in SCC4 and SCC9 cell lines. SCC4 (**A**) and SCC9 (**B**) cell lines were seeded at various densities (1-30 x10^3 cells/well) in 96 well plates with a total volume of 200 µL in each well. Cells were incubated for 48, 72 or 96 h. 20 µl of alamar blue was added to each well and, after 6 h incubation, fluorescence was measured on the SpectraMax Gemini EM Microplate Reader at an excitation wavelength of 544nm and an emission wavelength of 590nm using SOFTmax Pro version 4.9. Results were plotted using Graphpad Prism 5. Values represent the mean ± S.E.M. of three independent experiments.

3.2.2. The effect of cisplatin, docetaxel and 5-fluorouracil on the viability of OSCC cell lines

The alamar blue assay was employed to evaluate the effect of various OSCC anti-neoplastic drugs on cell viability. Cisplatin, docetaxel and 5-fluorouracil were selected for this study as representative chemotherapeutic agents widely used for the treatment of oral cancer [331]. The effect of these drugs on cell viability was evaluated in two OSCC cell lines: SCC4 cells are generally considered poorly differentiated and SCC9 are generally considered moderately differentiated [21]. The SCC4 cell line was treated with several concentrations of cisplatin (0.75-100 µM), docetaxel (0.04-10 nM) and 5-fluorouracil (3.1-200 µM), while a higher range of drug concentrations were used for the SCC9 cell line: cisplatin (1.5-200 µM), docetaxel (0.13-90 nM) and 5-fluorouracil (1.5-400 µM). Cell viability was determined following a 24, 48 or 72 h treatment in both cell lines.

Cisplatin decreased the viability of both SCC4 and SCC9 cell lines in a dose- and time-dependent manner (Figure 3.2). Moreover, a higher sensitivity to cisplatin was observed in the SCC4 cell line compared to the SCC9 cell line, confirming the different susceptibility of the two cell lines to drug treatment. In order to estimate the variation in cell sensitivity to cisplatin, IC_{50} values were calculated. After a 24 h treatment, the concentration of cisplatin required to inhibit 50% of cell viability was 19.8±6.9 µM in SCC4 cell line, whereas even the highest concentration of 200 µM cisplatin did not reduce the viability below 50% in the SCC9 cell line. After a 48 h treatment, IC_{50} values of 2.9±0.3 µM and 42.0±2.7 µM were obtained for SSC4 and SCC9 cell lines respectively, whilst IC_{50} values of 1.1±0.4 µM and 22.1±0.4 µM were obtained for SSC4 and SCC9 cell lines respectively after a 72 h treatment. These results conclusively showed an effect of cisplatin in the micromolar range as early as 24 h, and a 12-15 fold difference in cisplatin sensitivity between the two OSCC cell lines.

Likewise, docetaxel reduced the viability of OSCC cell lines in a dose- and time-dependent manner (Figure 3.3). Although no significant effect was observed after the 24 h treatment, IC_{50} values of 2.6±1.0 nM and 1.5±1.3 nM were obtained after 48 and 72 h treatment respectively in the SCC4 cell line. In contrast, a substantial decrease in cell viability was observed only at 72 h treatment in the SCC9 cell line (IC_{50}= 0.2±0.4 nM).

Finally, a slight decrease only in cell viability was observed in OSCC cell lines treated with 5-fluorouracil (Figure 3.4) demonstrating a low sensitivity to this drug. An IC_{50} value could only be obtained after a 72 h treatment in the SCC4 cell line (IC_{50}= 25.6±2.7 μM).

From this preliminary screen, cisplatin was chosen as a representative OSCC chemotherapeutic drug for this study as both cell lines were sensitive to treatment with the drug at 48 h (Table 3.1 to 3.3).

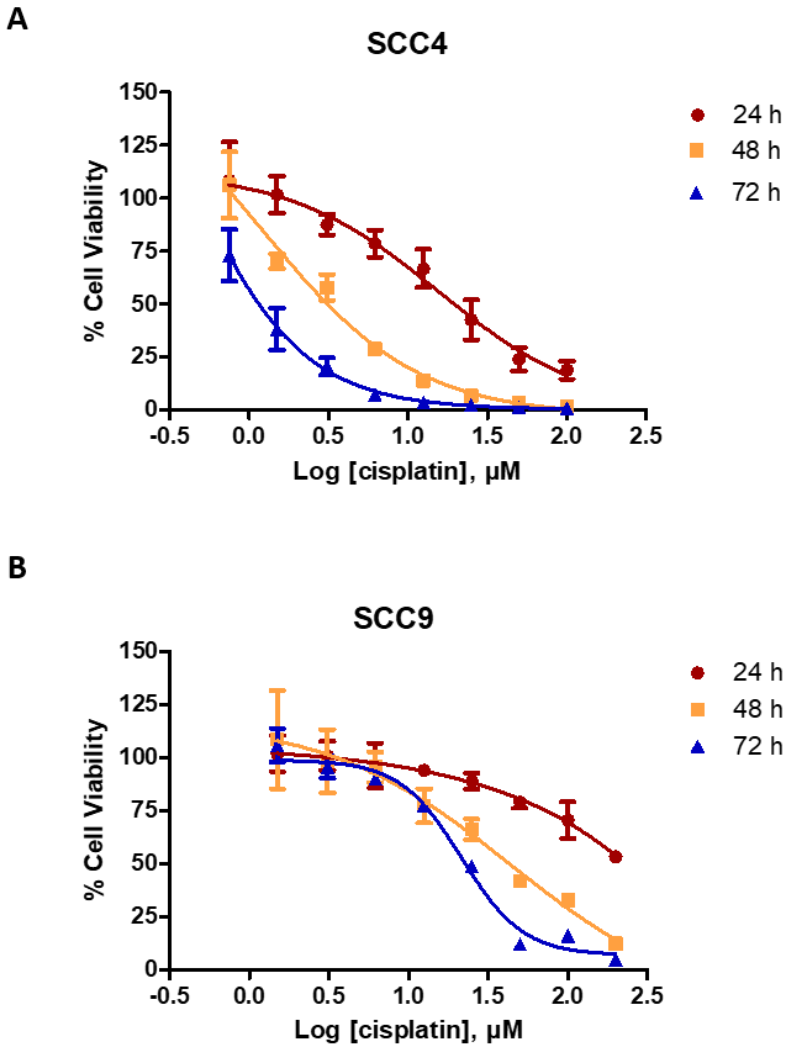

Figure 3.2 Cisplatin reduces the viability of OSCC cell lines.

OSCC cell lines were seeded at $5x10^3$ cells/well in 96 well plates. Cells were left for 24 h to adhere to the plate and then were treated with a vehicle (0.009% (v/v) NaCl) or a range of concentrations of cisplatin (0.75-100 µM and 1.5-200 µM for SCC4 (**A**) and SCC9 (**B**) cell lines, respectively) for 24, 48 or 72 h. Alamar blue (10% (v/v)) was added to each well 6 h before the end of the treatment and plates were kept in the dark at 37°C. Fluorescence was measured on the SpectraMax Gemini EM Microplate Reader at an excitation wavelength of 544 nm and an emission wavelength of 590 nm. Values obtained from cells treated with cisplatin were normalised against vehicle treated cells and results were plotted using Graphpad Prism 5. Values represent the mean ± S.E.M. of three independent experiments.

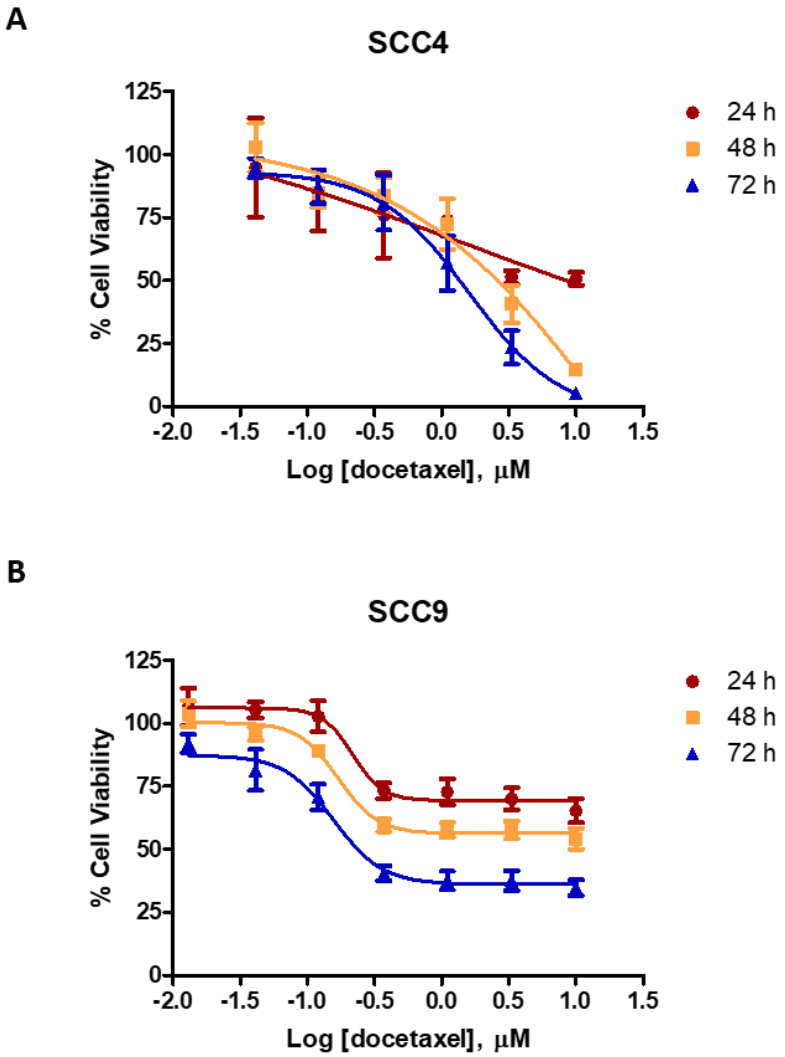

Figure 3.3 Docetaxel reduces the viability of OSCC cell lines.

OSCC cell lines were seeded at $5x10^3$ cells/well in 96 well plates. Cells were left for 24 h to adhere to the plate and then were treated with a vehicle (1% (v/v) ethanol) or a range of concentrations of docetaxel (0.04-10 nM and 0.13-90 nM for SCC4 (**A**) and SCC9 (**B**) cell lines, respectively) for 24, 48 and 72 h. Alamar blue (10% (v/v)) was added to each well 6 h before the end of the treatment and plates were kept in the dark at 37°C. Fluorescence was measured on the SpectraMax Gemini EM Microplate Reader at an excitation wavelength of 544 nm and an emission wavelength of 590 nm. Values obtained from cells treated with docetaxel were normalised against vehicle treated cells and results were plotted using Graphpad Prism 5. Values represent the mean ± S.E.M. of three independent experiments**.**

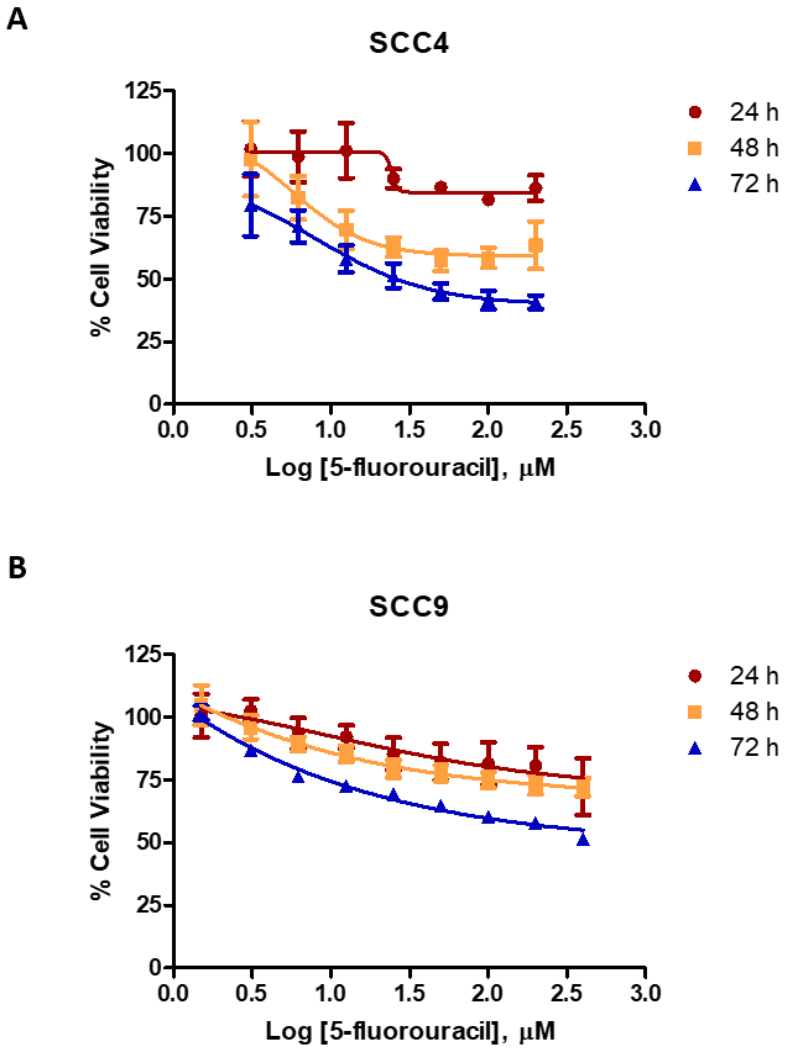

Figure 3.4 5-Fluorouracil reduces the viability of OSCC cell lines.

OSCC cell lines were seeded at $5x10^3$ cells/well in 96 well plates. Cells were left for 24 h to adhere to the plate and then were treated with a vehicle (0.1% (v/v) DMSO) or a range of concentrations of 5-fluorouracil (3.1-200 µM and 1.5-400 µM for SCC4 (**A**) and SCC9 (**B**) cell lines, respectively) for 24, 48 and 72 h. Alamar blue (10% (v/v)) was added to each well 6 h before the end of the treatment and plates were kept in the dark at 37°C. Fluorescence was measured on the SpectraMax Gemini EM Microplate Reader at an excitation wavelength of 544 nm and an emission wavelength of 590 nm. Values obtained from cells treated with 5-fluorouracil were normalised against vehicle treated cells and results were plotted using Graphpad Prism 5. Values represent the mean ± S.E.M. of three independent experiments.

Cisplatin			
	24 h	**48 h**	**72 h**
SCC4	19.8 ± 6.9 µM	2.9 ± 0.3 µM	1.1 ± 0.4 µM
SCC9	ND	42.0 ± 2.7 µM	22.1 ± 0.4 µM

Table 3.1 IC_{50} values for 24, 48 or 72 h treatment with cisplatin in OSCC cell lines.

ND = not determined.

Docetaxel			
	24 h	**48 h**	**72 h**
SCC4	ND	2.6 ± 1.0 nM	1.5 ± 1.3 nM
SCC9	ND	ND	0.2 ± 0.4 nM

Table 3.2 IC_{50} values for 24, 48 or 72 h treatment with docetaxel in OSCC cell lines.

ND = not determined.

5-Fluorouracil			
	24 h	**48 h**	**72 h**
SCC4	ND	ND	25.6 ± 2.7 µM
SCC9	ND	ND	ND

Table 3.3 IC_{50} values for 24, 48 or 72 h treatment with 5-fluorouracil in OSCC cell lines.

ND = not determined.

3.2.3. The effect of cisplatin treatment on the cell cycle of OSCC cell lines

The alamar blue assay showed a reduction in cell viability following treatment with cisplatin in OSCC cell lines. The decreased cell viability may be the result of cell cycle arrest, cell death or alternatively a combination of both. To investigate this, flow cytometric analysis of PI stained cells was carried out in order to determine the distribution of cells across each phase of the cell cycle and the presence of dead cells following cisplatin treatment.

SCC4 and SCC9 cell lines were treated with vehicle or with increasing concentrations of cisplatin (1-15 μM and 12.5-100 μM, respectively) for 48 h. Cells were then fixed and stained with PI and the subG0/G1, G0/G1, S, G2/M peaks were determined using the BD Accuri flow cytometer. Cisplatin treatment increased the subG0/G1 peak in a dose-responsive manner in SCC4 and SCC9 cell lines, suggesting an induction of cell death (Figure 3.5, Figure A.1, Table 3.4). In the SCC4 cell line, a statistically significant increase in the subG0/G1 peak was found in cells treated with 5 μM cisplatin (approximately 45% of cells) compared to vehicle treated cells (approximately 10% of cells) after 48 h of treatment. The percentage of cells in subG0/G1 peak increased with increasing concentrations, reaching a maximum of 66% of cells following treatment with 15 μM cisplatin. A similar trend was obtained in the SCC9 cell line, where a statistically significant increase in the subG0/G1 peak was first found in cells treated with 25 μM cisplatin (approximately 12%) compared to vehicle treated cells (approximately 2%). A progressive increase in the subG0/G1 peak was then observed after treatment with increasing concentrations of cisplatin, reaching a maximum of 33% of cells in subG0/G1 peak at the highest concentration tested (100 μM). Additionally, SCC9 cells treated with 12.5 μM cisplatin showed a significant increase of almost 3-fold of cells in the S-phase compared with vehicle treated cells, suggesting cell cycle arrest at low concentrations of cisplatin. Similarly, a slight although non significant increase of cells in the S-phase was also displayed in SCC4 cells treated with 1 μM cisplatin compared to vehicle treated cells. Finally, a decrease in the percentage of cells in the S phase was observed with increasing concentrations of cisplatin along with the concomitant decrease in the G0/G1 and G2/M peaks in both cell lines likely linked with increased cell death. Taken together, these results suggest that low concentrations of cisplatin may induce cell cycle arrest followed by cell death at higher concentrations of cisplatin in OSCC cell lines.

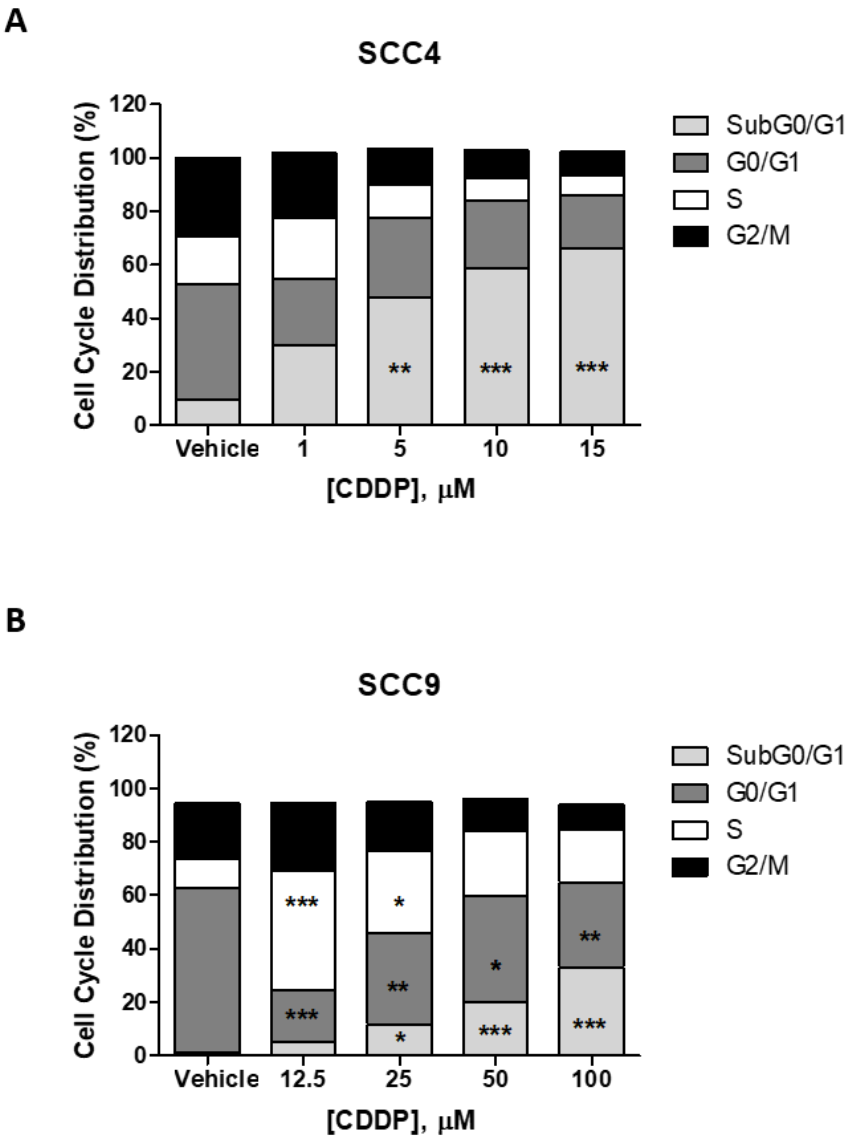

Figure 3.5 Cisplatin induces S-phase arrest and cell death in OSCC cell lines.

OSCC cell lines were seeded at 150 x 10^3 cells/well in 6 well plates. Cells were left for 24 h to adhere to the plate and then were treated with vehicle (0.009% (v/v) NaCl) or varying concentrations of cisplatin (CDDP): 1-15 μM and 12.5-100 μM for SCC4 (**A**) and SCC9 (**B**) cell lines, respectively. After 48 h, cells were harvested, fixed with 70% ice cold ethanol and stained with PI. Cells were analysed by flow cytometry using BD FACS Accuri software. 10,000 single cells were gated on vehicle treated cells and the percentage of cells in the subG0/G1 peak and the G0/G1, S and G2/M phases of the cell cycle was determined. Results are representative of three independent experiments. Statistical analysis was performed for the subG0/G1 and S peak using one-way ANOVA with Dunnett's Multiple Comparison Test to compare mean values between vehicle and treated cells (Graphpad Prism 5). *** $p<0.001$, ** $p<0.01$, * $p<0.05$.

SCC4				
CDDP (µM)	**SubG0/G1 %**	**G0/G1 %**	**S %**	**G2/M %**
Vehicle	9.3 ± 1.4	43.6 ± 26.2	17.6 ± 10.0	29.3 ± 17.4
1	29.7 ± 8.5	24.7 ± 11.0	23.7 ± 12.4	24.2 ± 7.7
5	47.6 ± 14.8	30.1 ± 14.8	12.1 ± 6.1	13.5 ± 16.4
10	58.4 ± 5.2	25.5 ± 10.6	8.5 ± 4.5	10.2 ± 12.4
15	66.3 ± 3.7	19.8 ± 7.03	7.4 ± 5.1	8.6 ± 10.7
SCC9				
CDDP (µM)	**SubG0/G1 %**	**G0/G1 %**	**S %**	**G2/M %**
Vehicle	1.4 ± 0.8	61.5 ± 5.0	10.4 ± 4.6	21.1 ± 1.9
12.5	5.1 ± 1.9	19.5 ± 9.6	44.4 ± 10.0	25.2 ± 3.8
25	11.6 ± 3.7	33.9 ± 10.1	30.9 ± 5.9	18.4 ± 1.4
50	20.0 ± 3.4	39.9 ± 8.2	24.2 ± 7.3	11.6 ± 7.8
100	33.0 ± 5.8	31.6 ± 1.8	19.7 ± 7.1	9.4 ± 10.1

Table 3.4 Analysis of cell cycle profile of SCC4 and SCC9 cells treated with cisplatin.

CDDP=cisplatin. Values represent the mean ± S.E.M of the percentage of cells in SubG0/G1, G0/G1, S and G2/M peaks. Data are the mean of three independent experiments.

3.2.4. Cisplatin induces apoptotic cell death in a dose- and time-responsive manner in OSCC cell lines

Results from the cell cycle analysis showed that cisplatin induced cell death in OSCC cell lines. Cisplatin-induced cell death was further analysed by flow cytometric analysis of annexin V/PI stained cells and by western blot analysis of caspase 3 activation, in order to establish whether apoptotic cell death was induced following treatment with cisplatin.

3.2.4.1. Flow cytometric analysis of cisplatin-induced apoptosis in OSCC cell lines

Apoptosis induction was evaluated in relation to dose- and time-dependency in OSCC cell lines. Firstly, cells were treated with vehicle or with increasing concentrations of cisplatin (1-15 μM and 12.5-100 μM in SCC4 and SCC9 cells respectively) for 48 h. Cells were then double stained with annexin V-FITC and PI, and the percentage of cells positive to one or both stains was determined using the BD Accuri flow cytometer. A dot plot showed the different cell populations: healthy cells (annexin V^-/ PI^-) in the lower left quadrant, early apoptosis (annexin V^+/ PI^-) in the lower right quadrant, and late apoptosis (annexin V^+/ PI^+) in the upper right quadrant. Cisplatin induced apoptosis in a dose-responsive manner in both SCC4 and SCC9 cell lines (Figure 3.6 and Figure 3.7). A substantial increase in the apoptotic rate (above 50%) was observed after 48 h of treatment when concentrations of cisplatin increased from 5 μM to 10 μM in SCC4 cells and from 25 μM to 50 μM in SCC9 cells. Additionally, no apoptotic increase was displayed at higher cisplatin concentrations (15 μM and 100 μM in SCC4 and SCC9 cell lines respectively), resulting in a plateau of the apoptotic rate possibly due to the fact that cells were too damaged to be recognised as apoptotic cells.

Moreover, time course analysis of annexin V/PI stained cells was performed to determine the effect of a single concentration of cisplatin at varying time points on OSCC cell lines. The SCC4 cell line was treated with 5 μM cisplatin for 4, 8, 16, 24 and 48 h, whilst the SCC9 cell line was treated with 25 μM cisplatin for 8, 16, 24, 48 and 72 h. Cisplatin induced apoptosis in a time-responsive manner in both SCC4 and SCC9 cell lines (Figures 3.8-9). In the SCC4 cell line, a statistically significant apoptotic rate was observed as early as 24 h, whilst a significant level of apoptosis was first observed at 48 h in the SCC9 cell line. These results are in agreement with the results from the alamar blue viability assay and confirm the enhanced sensitivity of SCC4 cells to cisplatin when compared with SCC9 cells.

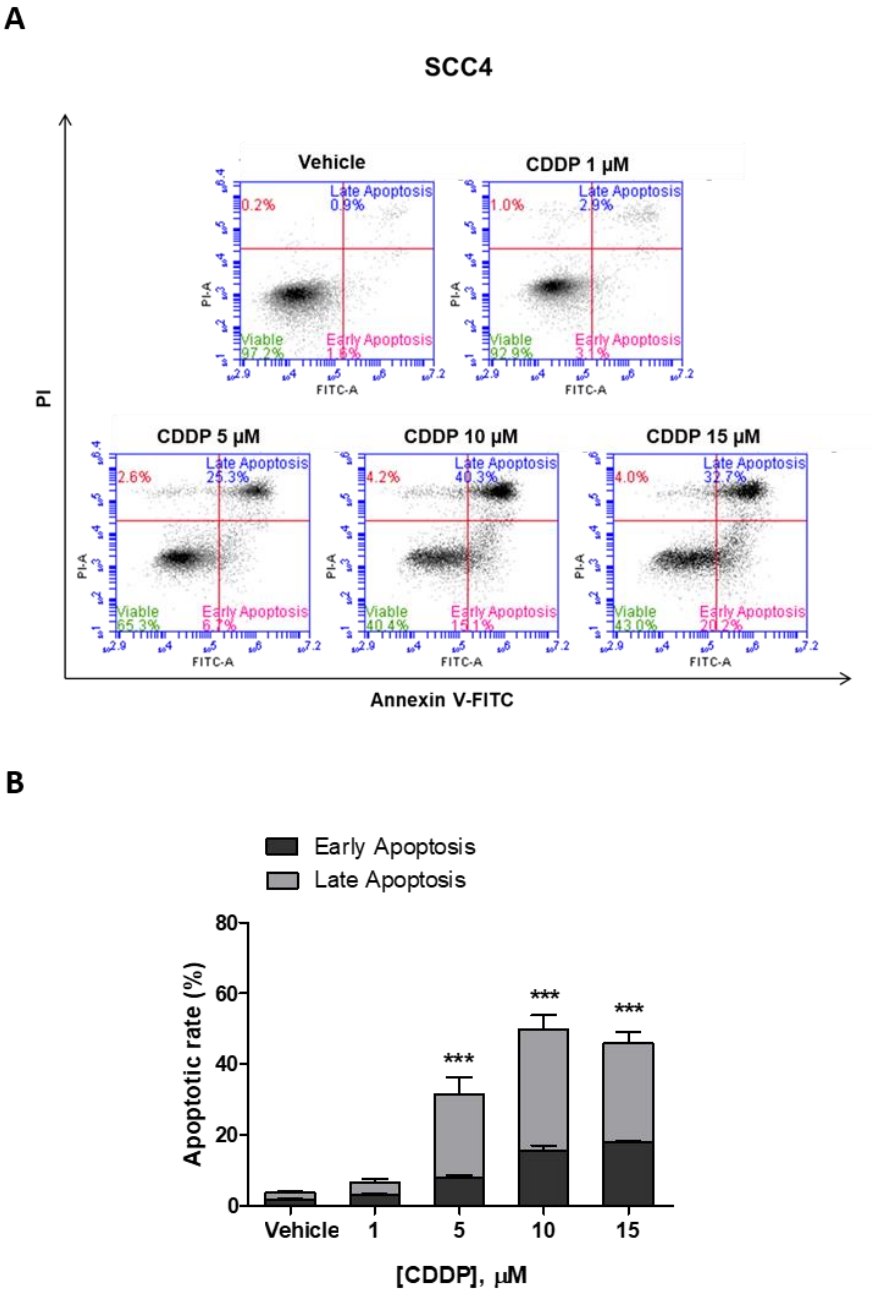

Figure 3.6 Cisplatin induces apoptosis in SCC4 cells in a dose-dependent manner.

The SCC4 cell line was seeded at 150 x10^3 cells/well in 6 well plates. Cells were left for 24 h to adhere to the plate and then were treated with vehicle (0.009% (v/v) NaCl) or varying concentrations of cisplatin (CDDP) (1-15 µM). After 48 h, cells were harvested, and double stained with annexin V/PI. Cells were then analysed by flow cytometry using BD FACS Accuri software. 10,000 single cells were gated on vehicle treated cells and the percentage of cells undergoing early and late apoptosis was determined. **A**. Representative dot plot of treated cells. **B**. Values represent the mean and S.E.M. of three independent experiments. Statistical analysis was performed using one-way ANOVA with Dunnett's Multiple Comparison Test to compare mean values between vehicle and treated cells (Graphpad Prism 5). *** $p<0.001$.

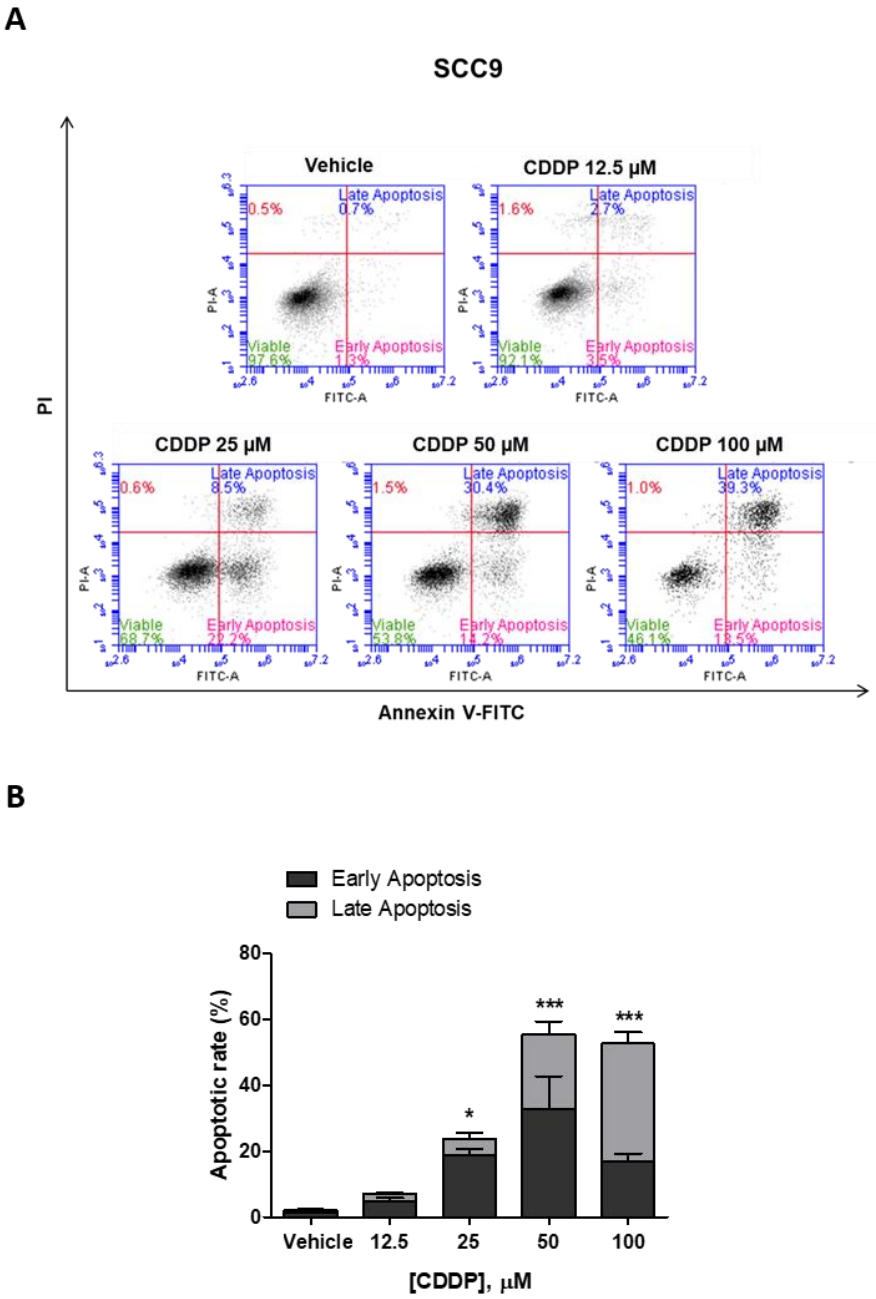

Figure 3.7 Cisplatin induces apoptosis in SCC9 cells in a dose-dependent manner.

The SCC9 cell line was seeded at 150 x10^3 cells/well in 6 well plates. Cells were left for 24 h to adhere to the plate and then were treated with vehicle (0.009% (v/v) NaCl) or varying concentrations of cisplatin (CDDP) (12.5-100 µM). After 48 h, cells were harvested, and double stained with annexin V/PI. Cells were then analysed by flow cytometry using BD FACS Accuri software. 10,000 single cells were gated on vehicle treated cells and the percentage of cells undergoing early and late apoptosis was determined. **A**. Representative dot plot of treated cells. **B**. Values represent the mean and S.E.M. of three independent experiments. Statistical analysis was performed using one-way ANOVA with Dunnett's Multiple Comparison Test to compare mean values between vehicle and treated cells (Graphpad Prism 5). *** $p<0.001$, * $p<0.05$.

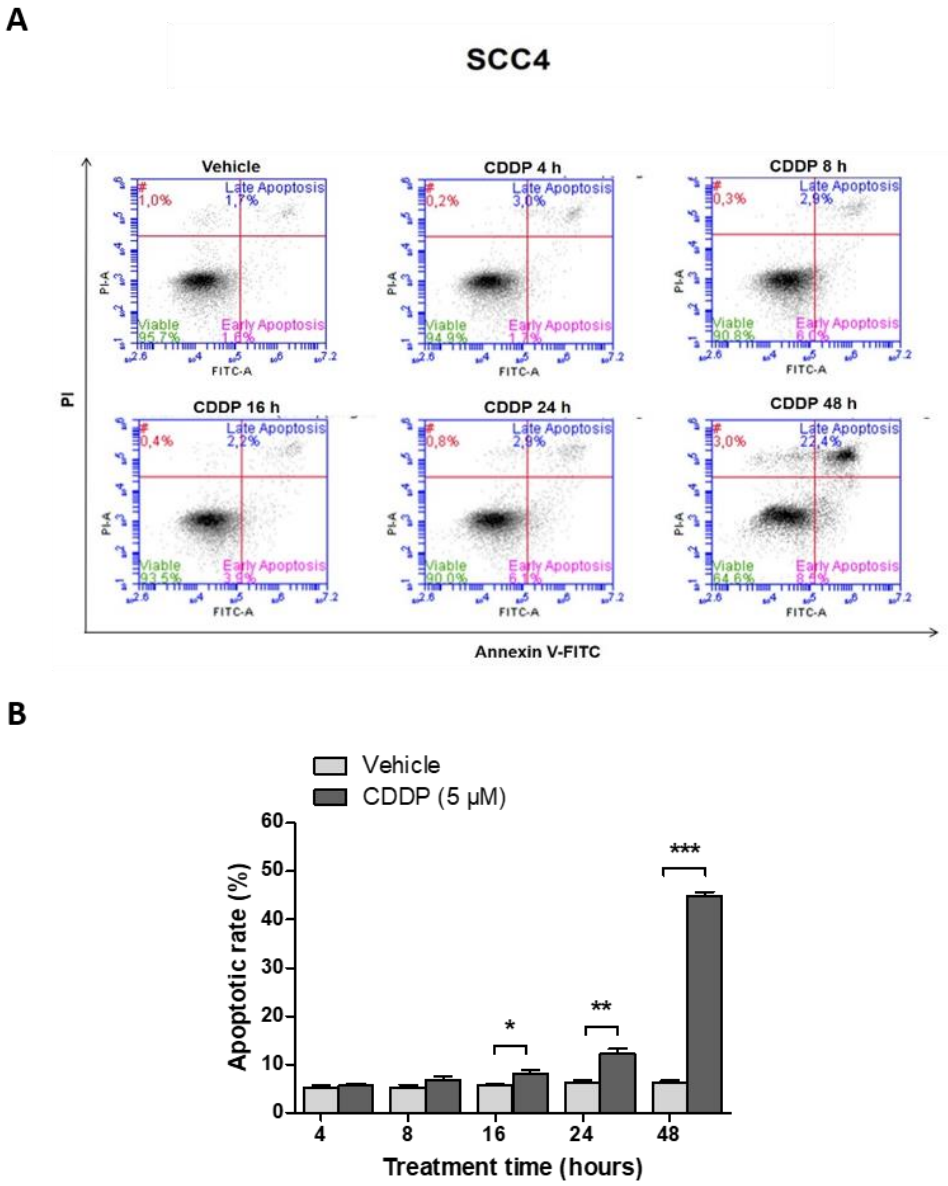

Figure 3.8 Cisplatin induces apoptosis in SCC4 cells in a time-dependent manner.

The SCC4 cell line was seeded at 150 x10^3 cells/well in 6 well plates. Cells were left for 24 h to adhere to the plate and then were treated with either vehicle (0.009% (v/v) NaCl) or with 5 µM cisplatin (CDDP). After the indicated times, cells were harvested, and double stained with annexin V/PI. Cells were then analysed by flow cytometry using BD FACS Accuri software. 10,000 single cells were gated on vehicle treated cells and the percentage of cells undergoing apoptosis was determined. **A**. Representative dot plot of treated cells. **B**. Values represent the mean and S.E.M. of three independent experiments. Statistical analysis was performed using unpaired two-tailed student t-test to compare mean values between vehicle and treated cells (Graphpad Prism 5). *** $p<0.001$, ** $p<0.01$, * $p<0.05$.

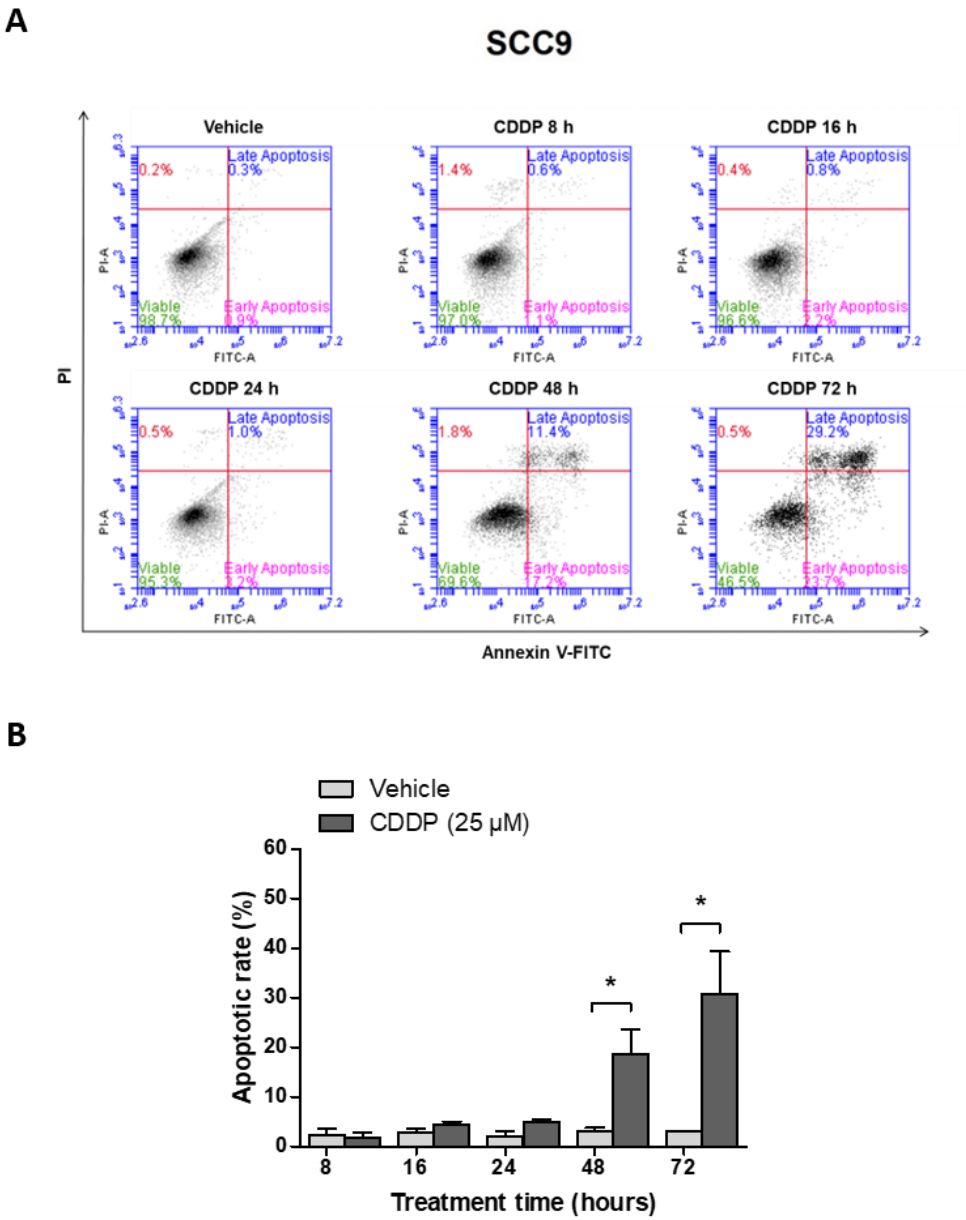

Figure 3.9 Cisplatin induces apoptosis in SCC9 cells in a time-dependent manner.

The SCC9 cell line was seeded at 150 x10^3 cells/well in 6 well plates. Cells were left for 24 h to adhere to the plate and then were treated with vehicle (0.009% (v/v) NaCl) or with 25 µM cisplatin (CDDP). After the indicated times, cells were harvested, and double stained with annexin V/PI. Cells were then analysed by flow cytometry using BD FACS Accuri software. 10,000 single cells were gated on vehicle treated cells and the percentage of cells undergoing apoptosis was determined. **A**. Representative dot plot of treated cells. **B**. Values represent the mean and S.E.M. of three independent experiments. Statistical analysis was performed using unpaired two-tailed student t-test to compare mean values between vehicle and treated cells (Graphpad Prism 5). * $p<0.05$.

3.2.4.2. Western blot analysis of cisplatin-induced caspase 3 activation in OSCC cell lines

The activation of the extrinsic or intrinsic apoptotic pathways leads to the cleavage of pro-caspase 3 resulting in the formation of cleaved caspase 3 (15-12 kDa), which is commonly considered a reliable marker of apoptosis [332]. To further investigate apoptotic cell death, the disappearance of the pro-enzyme form of caspase 3 along with the appearance of cleaved fragments was evaluated by western blot in the SCC4 cell lines.

Firstly, cells were treated with increasing concentrations of cisplatin (1-15 μM) for 48 h. Secondly, in order to evaluate time-dependent activation of caspase 3, cells were treated with 5 μM cisplatin for 16, 24 and 48 h. Lysates were prepared and run on a 12% SDS-PAGE gel before being probed for both the pro-form and cleaved caspase 3. Cisplatin induced caspase 3 cleavage in a dose- and time-dependent manner in the SCC4 cell line (Figures 3.10-11). The disappearance of pro-caspase 3 and the appearance of cleaved caspase 3 was displayed following treatment with 5 μM cisplatin in the SCC4 cell line and increased up to 10 μM. However, cells treated with 15 μM cisplatin showed a decrease in cleaved caspase 3 possibly due to the fact that cells were very damaged. Activation of caspase 3 was observed as early as 24 h after treatment, reaching a peak at 48 h.

These results correlate with the flow cytometric analysis results, suggesting that cisplatin induced apoptosis in a dose- and time-dependent manner.

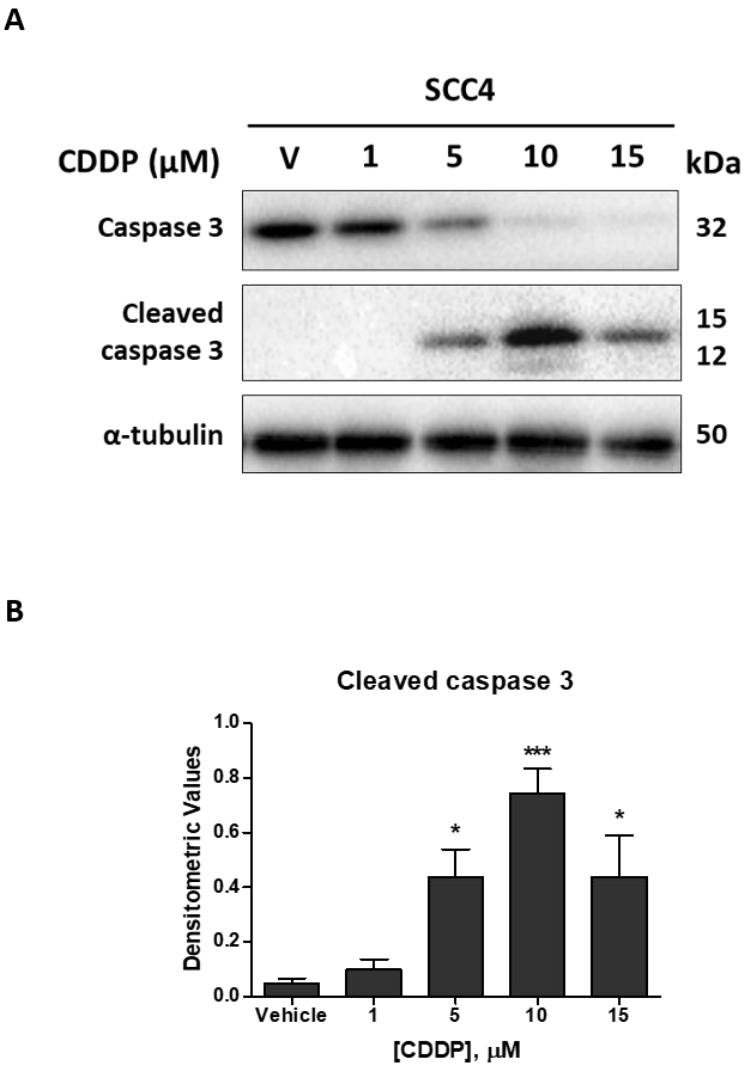

Figure 3.10 Cisplatin induces activation of caspase 3 in SCC4 cells in a dose-responsive manner. SCC4 cells were seeded at 300 x10^3 cells/flask in T25 flasks. Cells were left for 24 h to adhere to the flask and then were treated with vehicle (V) (0.009% (v/v) NaCl) or with varying concentrations of cisplatin (CDDP) (0-15 μM). After 48 h, cells were lysed and 20 μg of protein was loaded and separated on a 12% SDS-PAGE gel, transferred to a PVDF membrane and probed with the pro-form of caspase 3 and cleaved caspase 3 antibodies; α-tubulin served as loading control. **A**. Results are representative of three independent experiments. **B**. Densitometric analysis of cleaved caspase 3 bands was performed using ImageLab software and values were normalised by the loading control. Statistical analysis was performed using one-way ANOVA with Dunnett's Multiple Comparison Test to compare mean values between vehicle and treated cells (Graphpad Prism 5). *** $p<0.001$, * $p<0.05$.

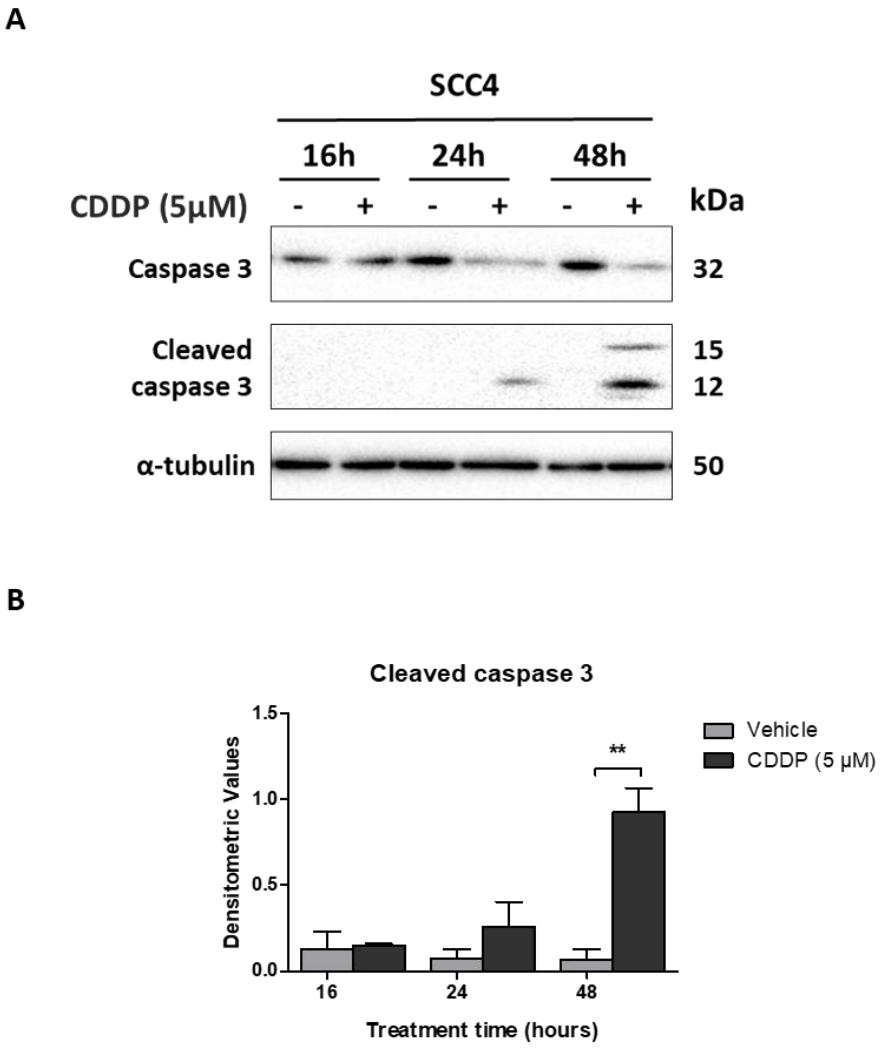

Figure 3.11 Cisplatin induces activation of caspase 3 in SCC4 cells in a time-responsive manner. SCC4 cells were seeded at 300 x10^3 cells/flask in T25 flasks. Cells were left for 24 h to adhere to the flask and then were treated with vehicle (0.009% (v/v) NaCl) or with 5 µM cisplatin (CDDP). After the indicated times, cells were lysed and 20 µg of protein was loaded and separated on a 12% SDS-PAGE gel, transferred to a PVDF membrane and probed with the pro-form of caspase 3 and cleaved caspase 3 antibodies. α-tubulin served as loading control. **A**. Results are representative of three independent experiments. **B**. Densitometric analysis of cleaved caspase 3 bands was performed using ImageLab software and values were normalised by the loading control. Statistical analysis was performed using unpaired two-tailed student t-test to compare mean values between vehicle and treated cells (Graphpad Prism 5). ** $p<0.05$.

3.2.5. Cisplatin triggers caspase-dependent apoptosis in OSCC cells

Apoptosis has previously been reported to be mediated through both caspase-dependent and -independent pathways [120]. The role of caspase activation in the cell death mediated by cisplatin in OSCC cell lines was further investigated using the pan-caspase inhibitor Z-VAD-fmk.

Cells were pre-treated with 50 μM Z-VAD-fmk for 1 h prior to the treatment with cisplatin (5 μM and 25 μM in SCC4 and SCC9 cell lines, respectively) for 48 h. Cells were then double stained with annexin V-FITC and PI, and the percentage of cells in early and late apoptosis was acquired using the BD Accuri flow software. Pre-treatment of OSCC cells with Z-VAD-fmk completely protected against apoptosis, suggesting that cisplatin-induced apoptosis occurs in a caspase-dependent manner (Figure 3.12-13)

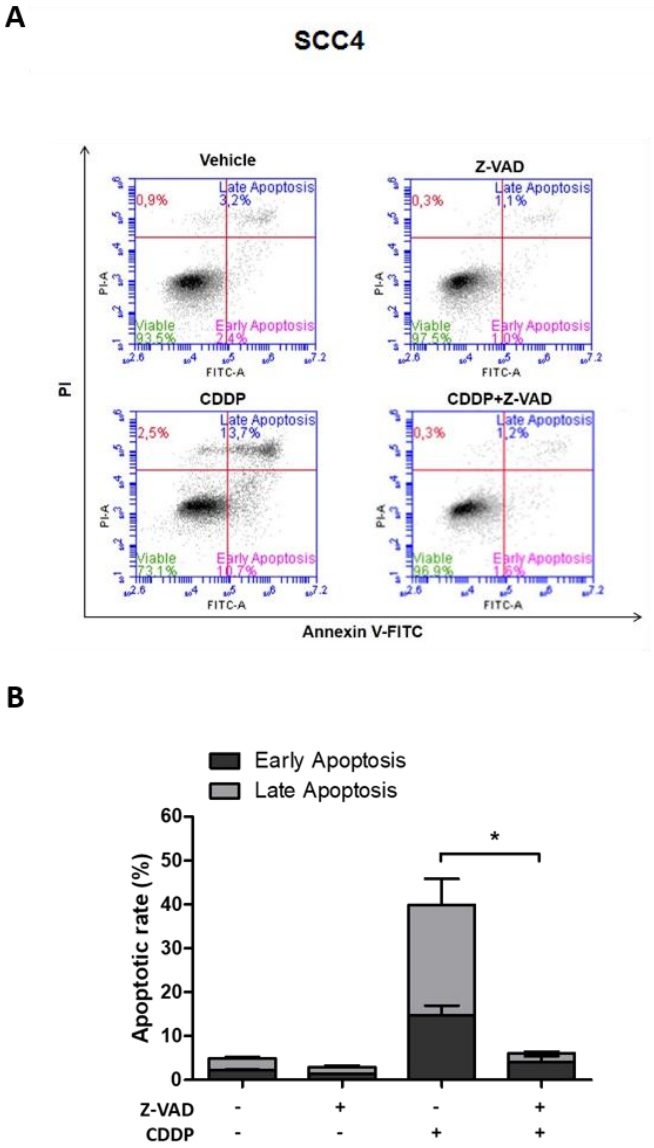

Figure 3.12 The pan-caspase inhibitor Z-VAD-fmk protects against cisplatin-induced apoptosis in the SCC4 cell line.

The SCC4 cell line was seeded at $150x10^3$ cells/well in 6 well plates and left for 24 h to adhere to the plate. Cells were treated either with vehicle (0.009% (v/v) NaCl), Z-VAD-fmk alone (50 µM), 5 µM cisplatin (CDDP) alone or with Z-VAD-fmk (50 µM) for 1 h before being treated with cisplatin (5 µM). After 48 h, cells were harvested, and double stained with annexin V/PI. Cells were then analysed by flow cytometry using BD FACS Accuri software. 10,000 single cells were gated on vehicle treated cells and the percentage of cells undergoing early and late apoptosis was acquired. **A**. Representative dot plot of treated cells. **B**. Values represent the mean and S.E.M. of three independent experiments. Statistical analysis was performed using unpaired two-tailed student t-test to compare mean values between cells treated with cisplatin and cells treated with cisplatin in combination with Z-VAD-fmk (Graphpad Prism 5). * $p<0.05$.

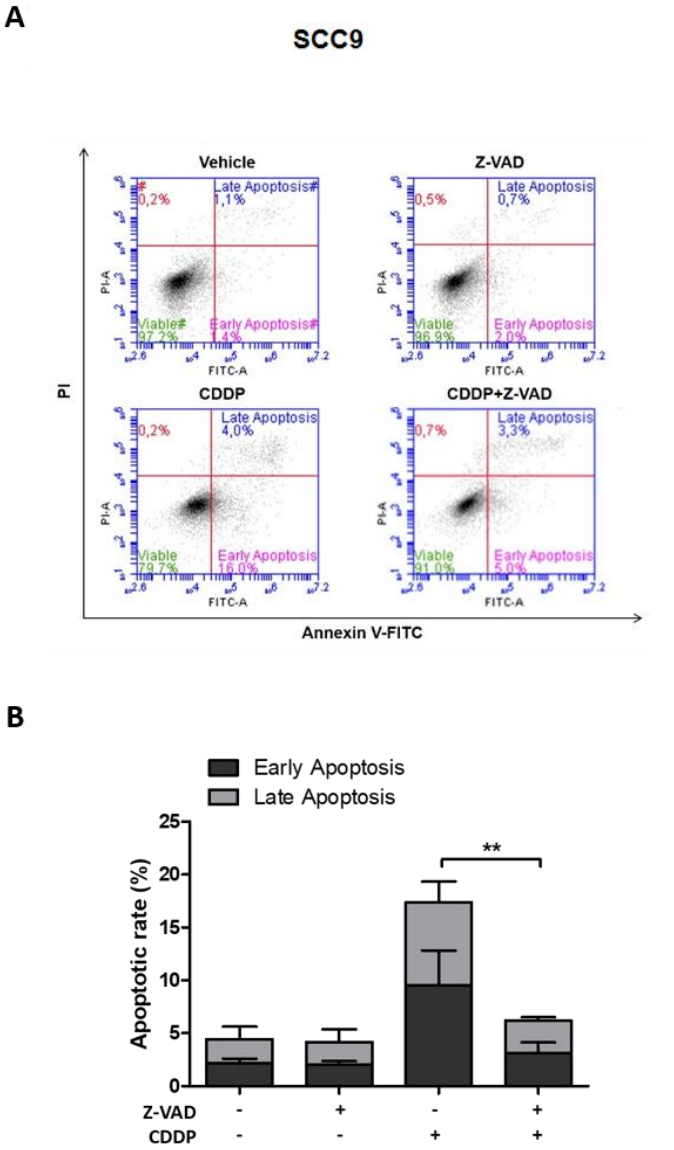

Figure 3.13 The pan-caspase inhibitor Z-VAD-fmk protects against cisplatin induced apoptosis in the SCC9 cell line.

The SCC9 cell line was seeded at 150 x10^3 cells/well in 6 well plates and left for 24 h to adhere to the plate. Cells were treated either with vehicle (0.009% (v/v) NaCl), Z-VAD-fmk alone (50 µM), 25 µM cisplatin (CDDP) alone or with Z-VAD-fmk (50 µM) for 1 h before being treated with cisplatin (25 µM). After 48 h, cells were harvested, and double stained with annexin V/PI. Cells were then analysed by flow cytometry using BD FACS Accuri software. 10,000 single cells were gated on vehicle treated cells and the percentage of cells undergoing early and late apoptosis was acquired. **A**. Representative dot plot of treated cells. **B**. Values represent the mean and S.E.M. of three independent experiments. Statistical analysis was performed using unpaired two-tailed student t-test to compare mean values between cells treated with cisplatin and cells treated with cisplatin in combination with Z-VAD-fmk (Graphpad Prism 5). ** $p<0.01$.

3.2.6. Evaluation of basal levels of autophagy in OSCC cell lines

Basal levels of autophagy and its activation in response to external stimuli were next evaluated in SCC4 and SCC9 cell lines. Autophagy was assessed under normal and starvation conditions by using western blot analysis of LC3-I/II and p62 protein levels.

Western blot analysis of LC3-I/II and p62 protein expression represents a reliable method for the indirect measurement of autophagy activity [151]. During the autophagic process, LC3 is cleaved by the cysteine protease ATG4 to a LC3-I fragment, which is then conjugated with phosphatidylethanolamine (PE) to form LC3-II. The lipidation of LC3 can be detected by western blot analysis because of the difference in the molecular weight of the two fragments, resulting in two distinct bands. In fact, LC3-I shows an apparent molecular weight of 16–18 kDa on SDS-PAGE gels, while LC3-II migrates around 14–16 kDa. The conversion of LC3-I to the LC3-II form is considered a reliable marker to study autophagy induction [333]. Moreover, the evaluation of p62 degradation by western blot is an alternative method widely used to monitor autophagic activity [151]. In fact, the interaction of p62 with LC3-II leads to the internalisation of p62 into the autophagosome. Thus, autophagy induction results in a decrease of p62 protein due to its degradation by lysosomal enzymes.

Autophagy activity was evaluated by monitoring autophagy flux, which is defined as the balance between autophagosome generation and clearance [333–336]. Inhibition of the flux by using lysosomal autophagy inhibitors (such as bafilomycin-A1 or chloroquine) represents the conventional way of monitoring the autophagic flux [151]. In fact, blocking autophagy at the late stages prevents autophagosome turnover, thus allowing the determination of autophagy activation over the period of the experiment [151].

OSCC cell lines were left untreated or treated with a starvation media (Earle's Balanced Salt Solution - EBSS) for 2 or 4 h in presence/absence of bafilomycin-A1 (100 μM) added 1 h before the end of the incubation period. LC3-I/II and p62 protein expression levels were then determined by western blot analysis. Results obtained showed an accumulation of LC3-II and p62 in cells treated with bafilomycin-A1 compared to control cells in both SCC4 and SCC9 cell lines, suggesting that basal levels of autophagy are constitutively activated in these cell lines under normal conditions (Figure 3.14). Additionally, conversion of LC3-I in LC3-II and degradation of p62 was observed in both SCC4 and

SCC9 cells treated with EBSS for 2 and 4 h, indicating activation of the autophagic flux under starvation conditions.

This result confirms the ability of these cell lines to undergo autophagy in response to external stimuli such as starvation. EBSS treated cells were used as positive control for autophagy in subsequent western blot experiments.

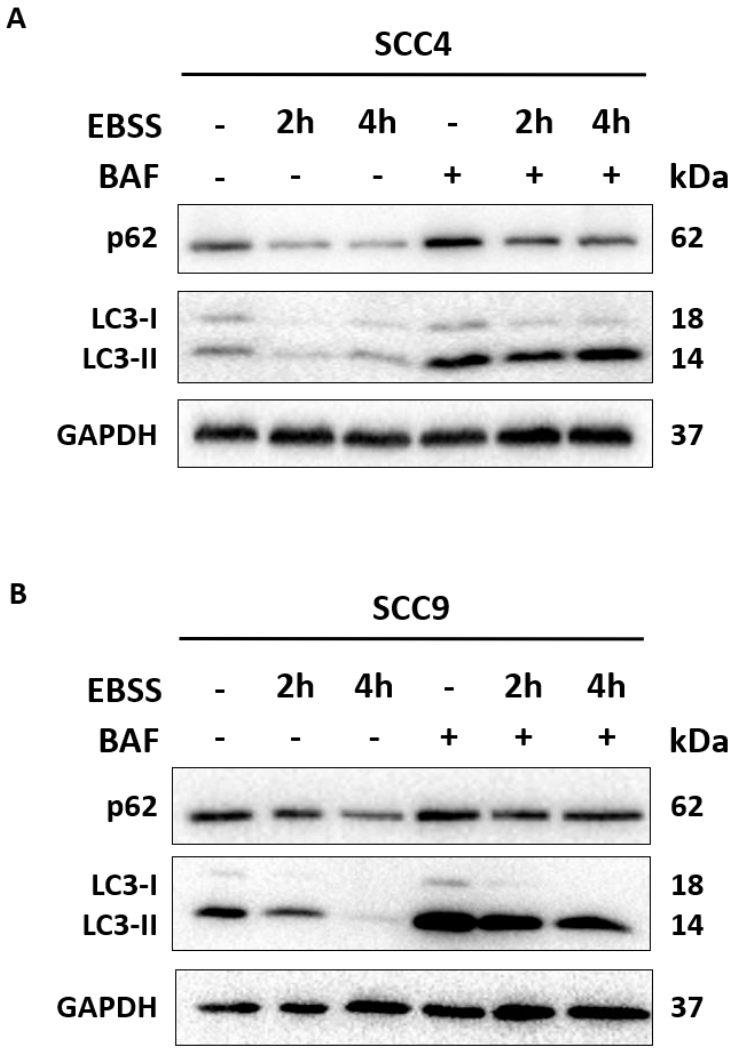

Figure 3.14 Evaluation of basal levels of autophagy in OSCC cell lines.

SCC4 (**A**) and SCC9 (**B**) cells were seeded at 300 x10^3 cells/well in 6 well plates. Cells were left for 24 h to adhere to the plate and then were treated with EBSS for 2 or 4 h in presence/absence of bafilomycin-A1 (100 µM) added 1 h before the end of the treatment. Cells were lysed and 20 µg of protein was loaded and separated on a 15% SDS-PAGE gel, transferred to a PVDF membrane and probed with anti-p62 and anti-LC3-I/II antibodies. GAPDH served as loading control. Blots are representative of three independent experiments.

3.2.7. Flow cytometric analysis of cisplatin-induced autophagy in OSCC cell lines

Several reports have indicated that cisplatin can simultaneously induce autophagy and apoptosis in cancerous cells such as ovarian cancer and oesophageal cancer [334, 337]. Basal levels of autophagy and autophagy activation in response to cisplatin in OSCC cell lines was next investigated by flow cytometric analysis of Cyto-ID stained cells. The Cyto-ID green autophagy dye (Enzo Life Sciences) is a fluorescent cationic amphiphilic tracer that diffuses into the autophagosomes [338]. The integration of the dye into autophagic vesicles results in a change in fluorescence which can be measured through flow cytometric analysis at an extinction wavelength of 488 nm. Since the amount of autophagic vesicles correlates with autophagy induction, the Cyto-ID Autophagy Detection Kit provides a rapid and quantitative approach for monitoring autophagic activity at the cellular level [311].

SCC4 and SCC9 cells were treated with 5 μM and 25 μM cisplatin respectively for 48 h. Cells were then stained with the Cyto-ID green autophagy dye and analysed on a BD Accuri flow cytometer. Rapamycin (autophagy inducer) in combination with chloroquine (lysosomal autophagy inhibitor) was used as positive control. In fact, the induction of autophagy followed by its inhibition at the end of the process leads to a build-up of autophagosome vesicles, which results in high levels of fluorescence. Both SCC4 and SCC9 cells treated with cisplatin showed a notable shift to the right of the fluorescence peak indicating a statistically significant increase in autophagic vesicles compared to vehicle treated cells after 48 h treatment (Figure 3.15).

In addition, autophagic flux was monitored in cisplatin-treated OSCC cells for a more accurate estimation of autophagic activity [335]. In fact, the number of autophagosomes is a function of the balance between the rate of their generation and the rate of their conversion into autolysosomes. Thus, a high amount of autophagosomes can represent a consequence of autophagy induction or, alternatively, suppression of autophagosome maturation [336]. On the other hand, a low amount of autophagosomes can be due to an impairment in the autophagy process or a high turnover rate of the autophagosome vesicles as result of autophagy induction [151]. Evaluation of cisplatin-induced autophagic flux was determined in the presence/absence of the lysosomal autophagy inhibitor chloroquine. OSCC cell lines were treated with cisplatin alone (5 and 25 μM in SCC4 and SCC9 respectively), chloroquine (10 μM) alone and cisplatin in combination

with chloroquine, for 48 h. Cells were then stained with the Cyto-ID green autophagy dye and analysed on the BD Accuri cytometer. Rapamycin in combination with chloroquine was again used as positive control. As expected, OSCC cells treated with chloroquine alone showed a slight increase in autophagic vesicles versus vehicle treated cells, likely due to the block of autophagosome turnover resulting in a build-up of autophagosomes (Figure 3.16, Figure A.2). Moreover, a significant increase in autophagic vesicles was observed in both OSCC cell lines treated with chloroquine in combination with cisplatin compared to cells treated with chloroquine alone or cisplatin alone. This increment reflects the number of autophagosomes induced by cisplatin that would have been degraded by autophagy during the treatment period.

Taken together, these results suggest that treatment with cisplatin promotes an increase in autophagic vesicles due to the activation of autophagic flux and excludes secondary accumulations due to autophagic degradation blockade.

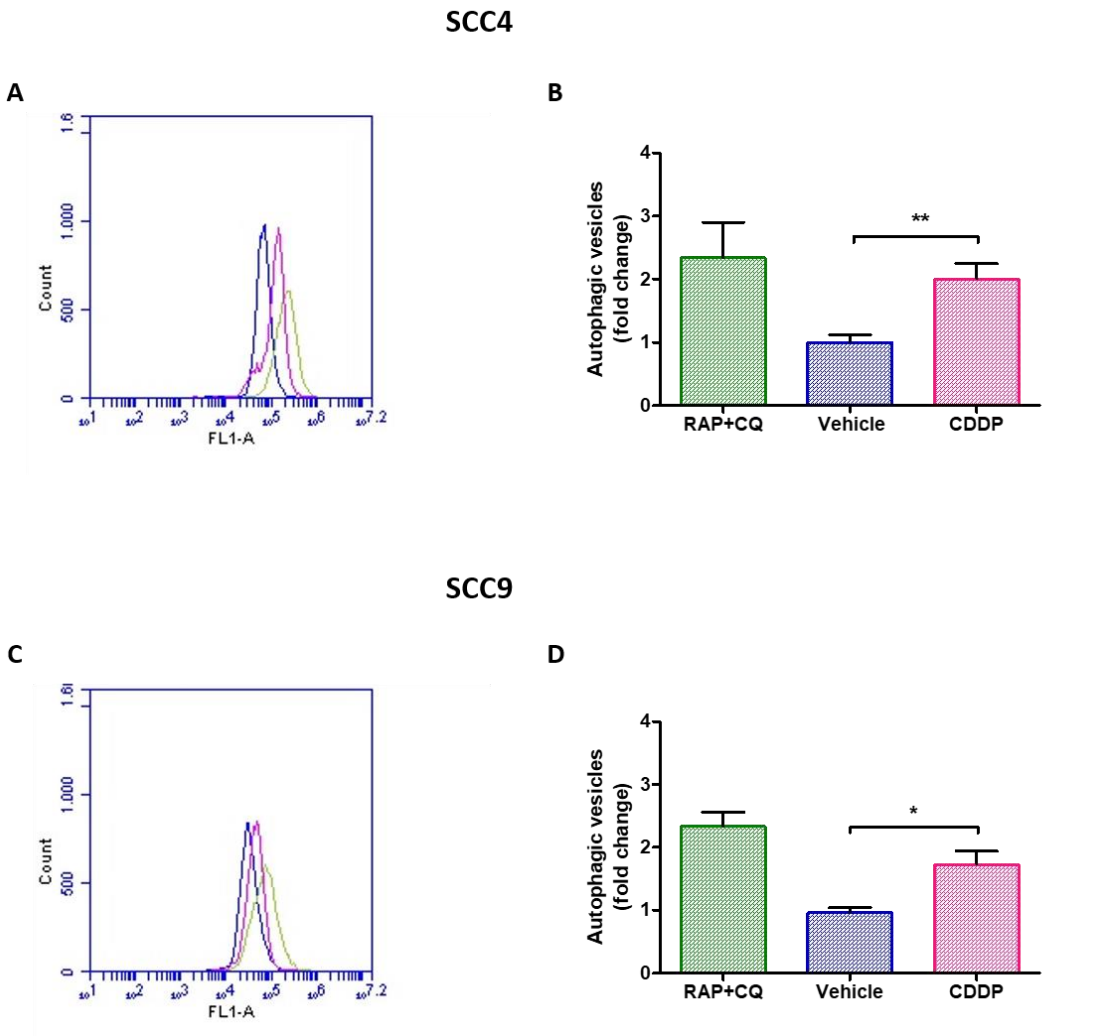

Figure 3.15 Treatment with cisplatin increases the number of autophagic vesicles in OSCC cell lines. OSCC cells were seeded at 150 x10^3 cells/well in 6 well plates. Cells were left for 24 h to adhere to the plate and then were treated with the vehicle (0.009% (v/v) NaCl) or with cisplatin (CDDP) 5 µM and 25 µM in SCC4 (**A-B**) and SCC9 (**C-D**) cells respectively. Rapamycin (RAP) 0.5 µM in combination with chloroquine (CQ) 10 µM was used as positive control. After 48 h, cells were harvested and stained with Cyto-ID green autophagy dye. Cells were then analysed on the flow BD FACS Accuri cytometer. 10,000 single cells were gated on vehicle treated cells and fluorescence values were acquired. **A-C**. Representative flow cytometric histogram of vehicle and cisplatin treated cells alongside the positive control. **B-D**. Values represent the mean ±S.E.M. of three independent experiments. Statistical analysis was performed using unpaired two-tailed student t-test to compare mean values between vehicle and treated cells (Graphpad Prism 5). ** $p<0.01$, * $p<0.05$.

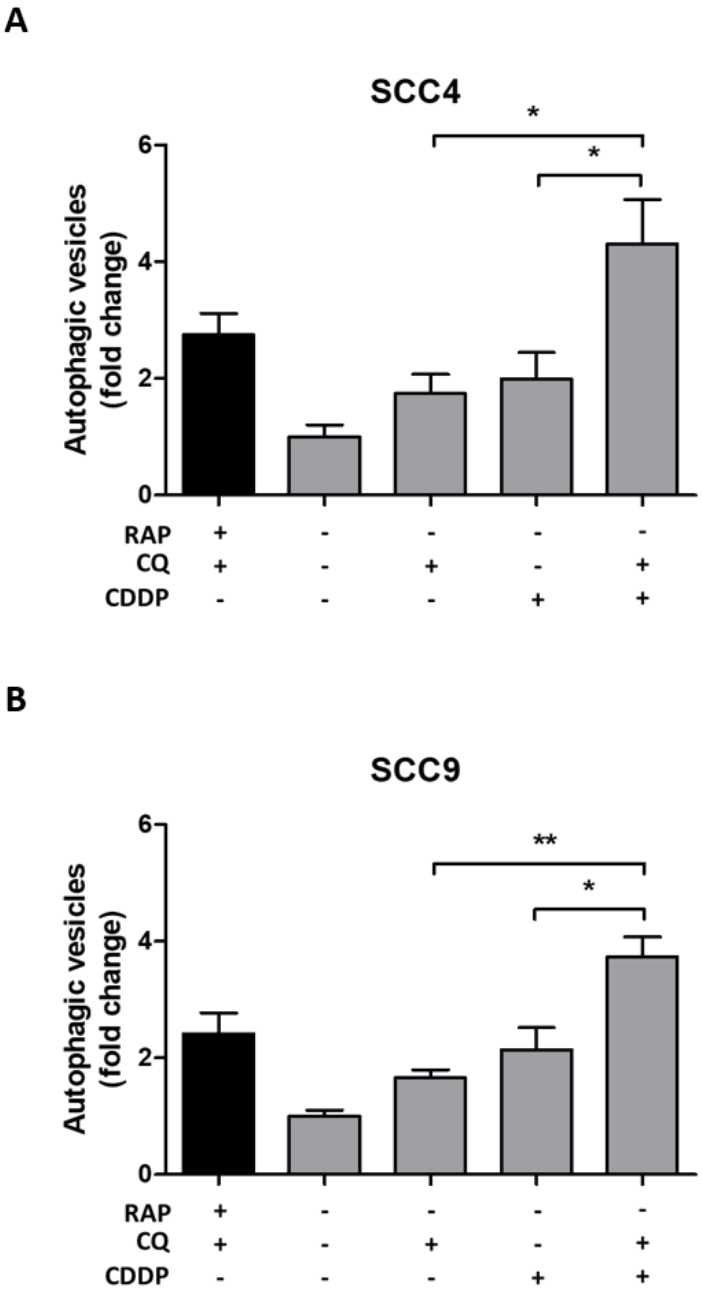

Figure 3.16 Cisplatin promotes autophagic flux activation in OSCC cell lines.

OSCC cells were seeded at 150 x10^3 cells/well in 6 well plates. Cells were left for 24 h to adhere to the plate and then were treated with the vehicle (0.009% (v/v) NaCl), chloroquine (CQ) 10 μM alone, cisplatin (CDDP) alone (5 μM and 25 μM in SCC4 (A) and SCC9 (B) cells respectively) or cisplatin in combination with chloroquine. Rapamycin (RAP) 0.5 μM in combination with chloroquine 10 μM was used as positive control. After 48 h, cells were harvested and stained with Cyto-ID green autophagy dye. Cells were then analysed on the flow BD FACS Accuri cytometer. 10,000 single cells were gated on vehicle treated cells and fluorescence values were acquired. Values represent the mean ±S.E.M. of three independent experiments. Statistical analysis was performed using one-way ANOVA with Tukey's Multiple Comparison Test (Graphpad Prism 5). ** $p<0.01$, * $p<0.05$.

3.2.8. Cisplatin induces autophagy in OSCC cell lines in a dose- and time-dependent manner

Time-dependency of cisplatin-induced autophagy was investigated in OSCC cell lines by flow cytometric analysis of Cyto-ID stained cells. SCC4 were treated with 5 μM cisplatin for 4, 8, 16, 24 and 48 h, while SCC9 cells were treated with 25 μM cisplatin for 4, 8, 16, 24, 48 and 72 h. Results obtained showed a progressive increase of autophagic vesicles in cisplatin treated cells in a time-dependent manner in both OSCC cell lines. A statistically significant increase of vesicles occurred as early as 48 h following cisplatin treatment in both SCC4 and SCC9 cells. This increment increased up to the 72 h time point in SCC9 cells (Figure 3.17, Figure A.3).

Dose-dependency of cisplatin-induced autophagy was next investigated in OSCC cell lines by western blot analysis of LC3-I/II and p62 protein expression. SCC4 cells were treated with increasing concentrations of cisplatin (1-15 μM). Samples were lysed and run on a 15% SDS-PAGE gel before being probed for p62 and LC3-I/II. Serum starved cells incubated for 4 h in EBSS were used as a positive control for autophagic induction. Densitometric analysis of p62, LC3-I and LC3-II bands was performed using ImageLab software. Autophagy induction was quantified through the acquisition of the LC3-II/LC3-I ratio. A statistically significant increase in the LC3-II/LC3-I ratio was observed in cells treated with increasing concentrations of cisplatin (with a peak at 10 and 15 μM) along with a progressive decrease in p62 protein expression (Figure 3.18). Taken together, these results suggest that in addition to apoptosis, autophagy is induced in a dose- and time-responsive manner in OSCC cell lines treated with cisplatin.

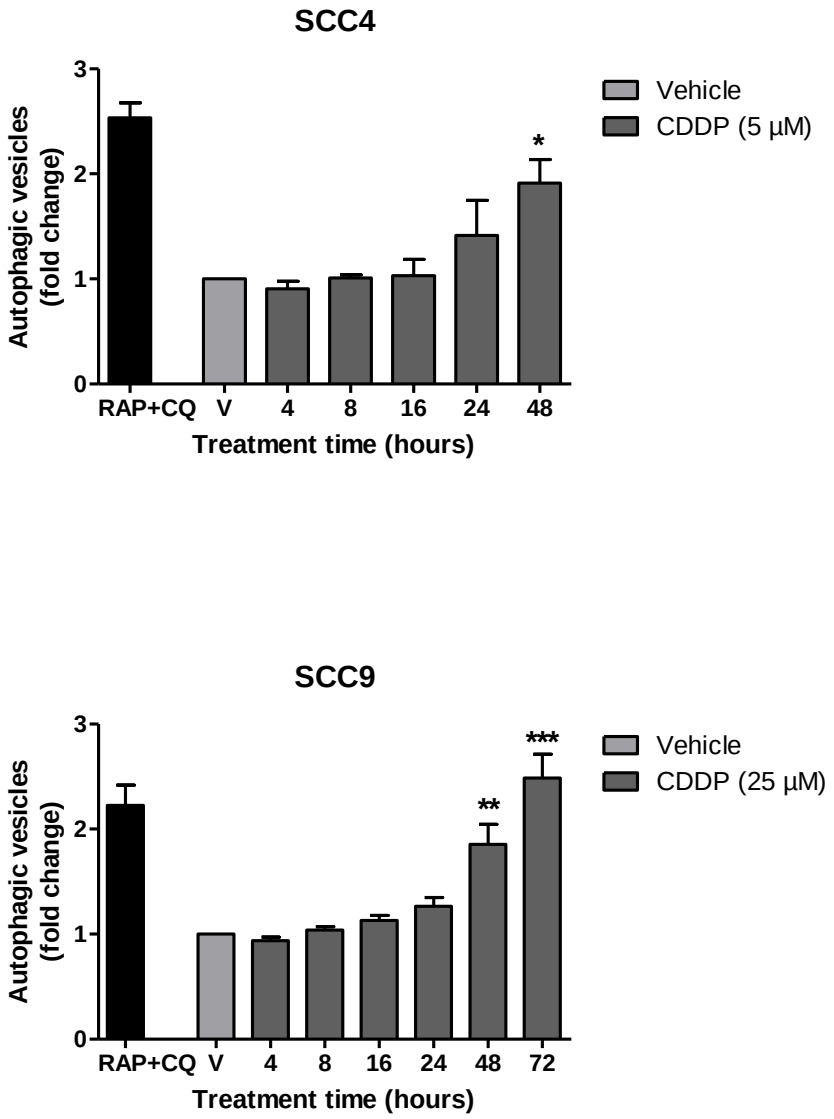

Figure 3.17 Cisplatin induces autophagy in OSCC cell lines in a time-responsive manner.

OSCC cells were seeded at 150 x10^3 cells/well in 6 well plates. Cells were left for 24 h to adhere to the plate and then were treated with the vehicle (V) (0.009% (v/v) NaCl) or with cisplatin (CDDP) 5 or 25 µM in SCC4 (**A**) and SCC9 (**B**) respectively for the indicated times. Rapamycin (RAP) 0.5 µM in combination with chloroquine (CQ) 10 µM was used as positive control. Cells were harvested and stained with Cyto-ID green autophagy dye. Cells were then analysed on the flow BD FACS Accuri cytometer. 10,000 single cells were gated on vehicle treated cells and fluorescence values were acquired. Values represent the mean ±S.E.M. of three independent experiments. Statistical analysis was performed using one-way ANOVA with Dunnett's Multiple Comparison Test to compare mean values between vehicle and treated cells (Graphpad Prism 5). *** $p<0.001$, ** $p<0.01$, * $p<0.05$.

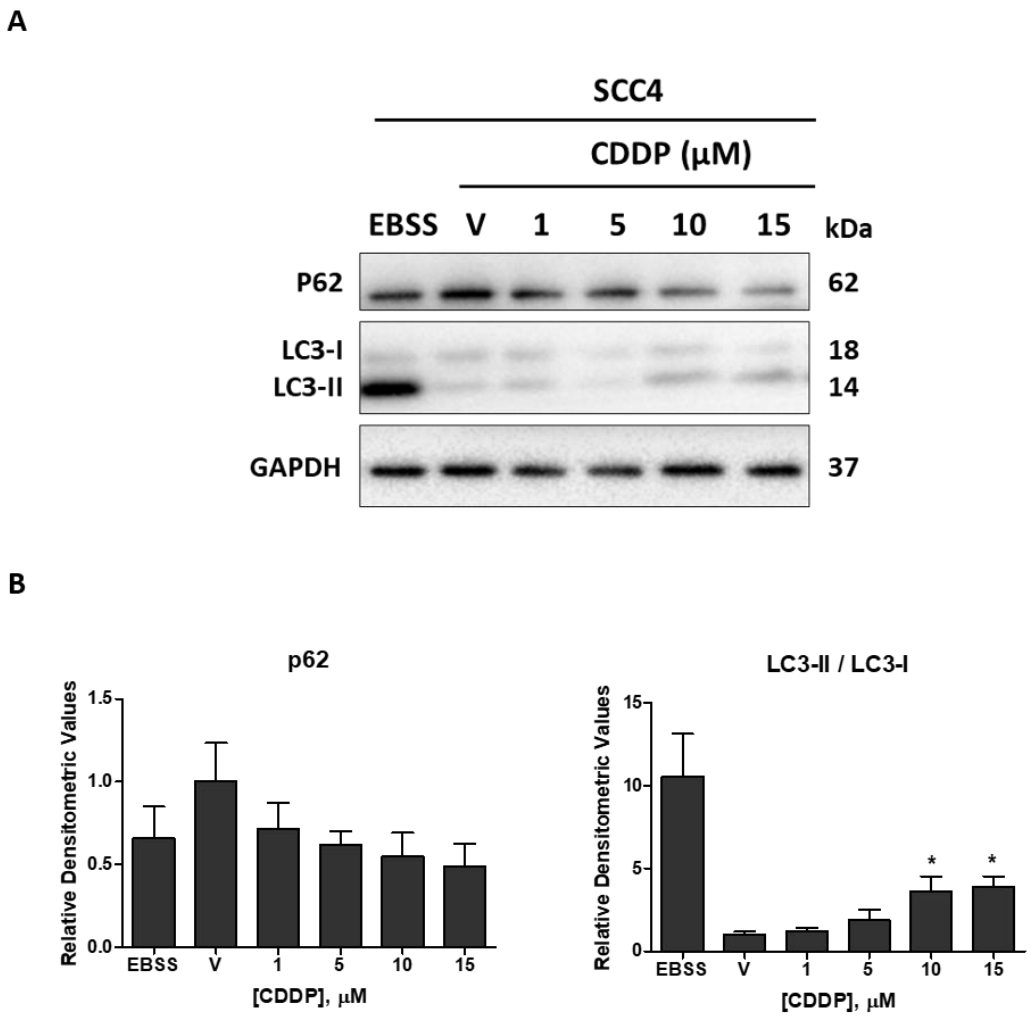

Figure 3.18 Cisplatin induces autophagy in the SCC4 cell line in a dose-responsive manner.

SCC4 cells were seeded at 300 x10^3 cells/mL in T25 flasks. Cells were left for 24 h to adhere to the flask and then were treated with the vehicle (V) (0.009% (v/v) NaCl) or with varying concentrations of cisplatin (CDDP) (1-15 μM) for 48 h. Cells treated with EBSS for 4 h were used as a positive control. After incubation, cells were lysed and 20 μg of protein was loaded and separated in a 15% SDS-PAGE gel, transferred to a PVDF membrane and probed with anti-p62 and anti-LC3-I/II antibodies. GAPDH served as loading control. **A**. Results are representative of three independent experiments. **B**. Densitometric analysis of p62, LC3-I and LC3-II bands was performed using ImageLab software and values were normalised to the loading control. Data represent the mean ±S.E.M. of three independent experiments. Statistical analysis was performed using one-way ANOVA with Dunnett's Multiple Comparison Test to compare mean values between vehicle and treated cells (Graphpad Prism 5). * $p<0.05$.

3.2.9. Evaluation of targeting autophagy for the treatment of OSCC

The effect of genetic and pharmacological autophagy inhibitors was evaluated in OSCC cell lines to determine whether autophagy plays a role in cisplatin resistance and whether targeting autophagy may be a valuable strategy to overcome chemoresistance in OSCC. Since autophagic flux can be blocked at different stages, several autophagy inhibitors were examined in this study. They were generically classified as early and late stage autophagy inhibitors. The inhibitory activity of the autophagy inhibitors was validated by flow cytometric analysis of Cyto-ID stained cells or by western blot analysis of LC3-I/II protein levels, whilst cisplatin-induced apoptosis was investigated by flow cytometric analysis of annexin V/PI stained cells and by western blot for the evaluation of caspase 3 activation.

3.2.9.1. Targeting autophagy with early stage pharmacological autophagy inhibitors does not sensitise OSCC cells to cisplatin-induced apoptosis

The effect of 3-methyladenine (3-MA) and SAR405 on cisplatin-induced autophagy and apoptosis was first investigated in OSCC cell lines. It has previously been reported that 3-MA is a pan-PI3kinase inhibitor, whereas SAR405 acts as selective ATP-competitive inhibitor of PtdIns3K complex. Both have been classified as early stage autophagy inhibitors [141, 339, 340].

Inhibition of autophagosome formation with 3-MA and SAR405 was evaluated through quantification of autophagic vesicles in the SCC4 cell line. Cells were pre-treated with 3-MA (5 mM) or SAR405 (1 μM) for 1 h before treatment with cisplatin 5 μM for 48 h. Cells were then stained with Cyto-ID green autophagy dye and analysed on BD Accuri flow cytometer. Rapamycin in combination with chloroquine was used as a positive control. As expected, cisplatin treated cells showed a significant increase in autophagic vesicles compared to vehicle treated cells, due to autophagy activation (Figure 3.19, Figure A.4). A statistically significant decrease in autophagic vesicles was observed when cells were treated with cisplatin in combination with SAR405 compared to cells treated with cisplatin alone. Furthermore, an observable (although non-significant) decrease was also found in cells treated with cisplatin in combination with 3-MA compared to cells treated with cisplatin alone. This result validates the activity of 3-MA and SAR405 as autophagy inhibitors and additionally suggests the higher efficacy of SAR405.

The effects of 3-MA and SAR405 on cisplatin-induced apoptosis were then investigated by flow cytometric analysis of annexin V/PI stained cells in SCC4 and SCC9 cell lines. Cells were treated as described above (5 μM and 25 μM cisplatin was used in SCC4 and SCC9 cell lines, respectively) and after 48 h cells were double stained with annexin V-FITC and PI. The percentage of cells in early and late apoptosis was acquired using the BD Accuri flow software. As shown in Figure 3.20 and Figure 3.21, treatment of cells with both 3-MA and SAR405 alone showed no substantial changes to the basal rate of apoptosis in both SCC4 and SCC9 cell lines. However, a small increase in the apoptotic rate was observed in SCC4 cells treated with 3-MA alone, suggesting a potential off-target activity of this autophagy inhibitor. Moreover, as expected, treatment of cells with cisplatin induced apoptosis in both cell lines. Inhibition of autophagosome formation with 3-MA slightly increased cisplatin-induced apoptosis in both cell lines although this increase was not significant, whilst a marked and significant drop in the apoptotic rate was displayed in OSCC cells treated with SAR405 in combination with cisplatin compared to cells treated with cisplatin alone.

Taken together, these results suggest that targeting autophagy with the early stage pharmacological autophagy inhibitors 3-MA and SAR405 does not appear to sensitise OSCC cells to cisplatin-induced apoptosis. However, no firm conclusions could be drawn at this stage regarding the role of autophagy in mediating cisplatin resistance. Therefore, further experiments using late stage autophagy inhibitors were next conducted.

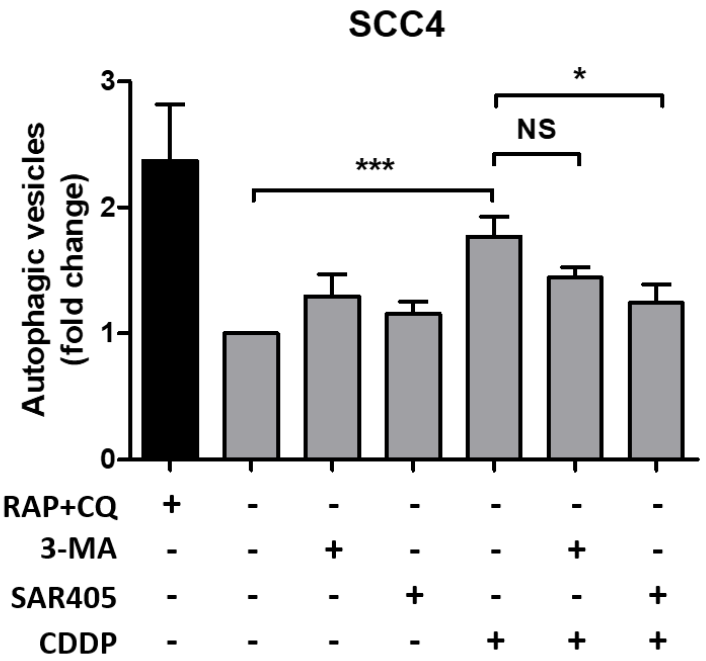

Figure 3.19 3-MA and SAR405 inhibits autophagosome formation in SCC4 cells.

SCC4 cells were seeded at 150 x10^3 cells/well in 6 well plates. Cells were pre-treated with either 3-MA (5 mM) or SAR405 (1 µM) for 1 h before adding cisplatin (5 µM) for a further 48 h. Rapamycin (RAP) 0.5 µM in combination with chloroquine 10 µM was used as positive control. After 48 h, cells were harvested and stained with Cyto-ID green autophagy dye. Cells were then analysed on the flow BD FACS Accuri cytometer. 10,000 single cells were gated on vehicle treated cells and fluorescence values were acquired. Values represent the mean ±S.E.M. of three independent experiments. Statistical analysis was performed using one-way ANOVA with Tukey's Multiple Comparison Test (Graphpad Prism 5). *** $p<0.001$, * $p<0.05$, NS: non-significant.

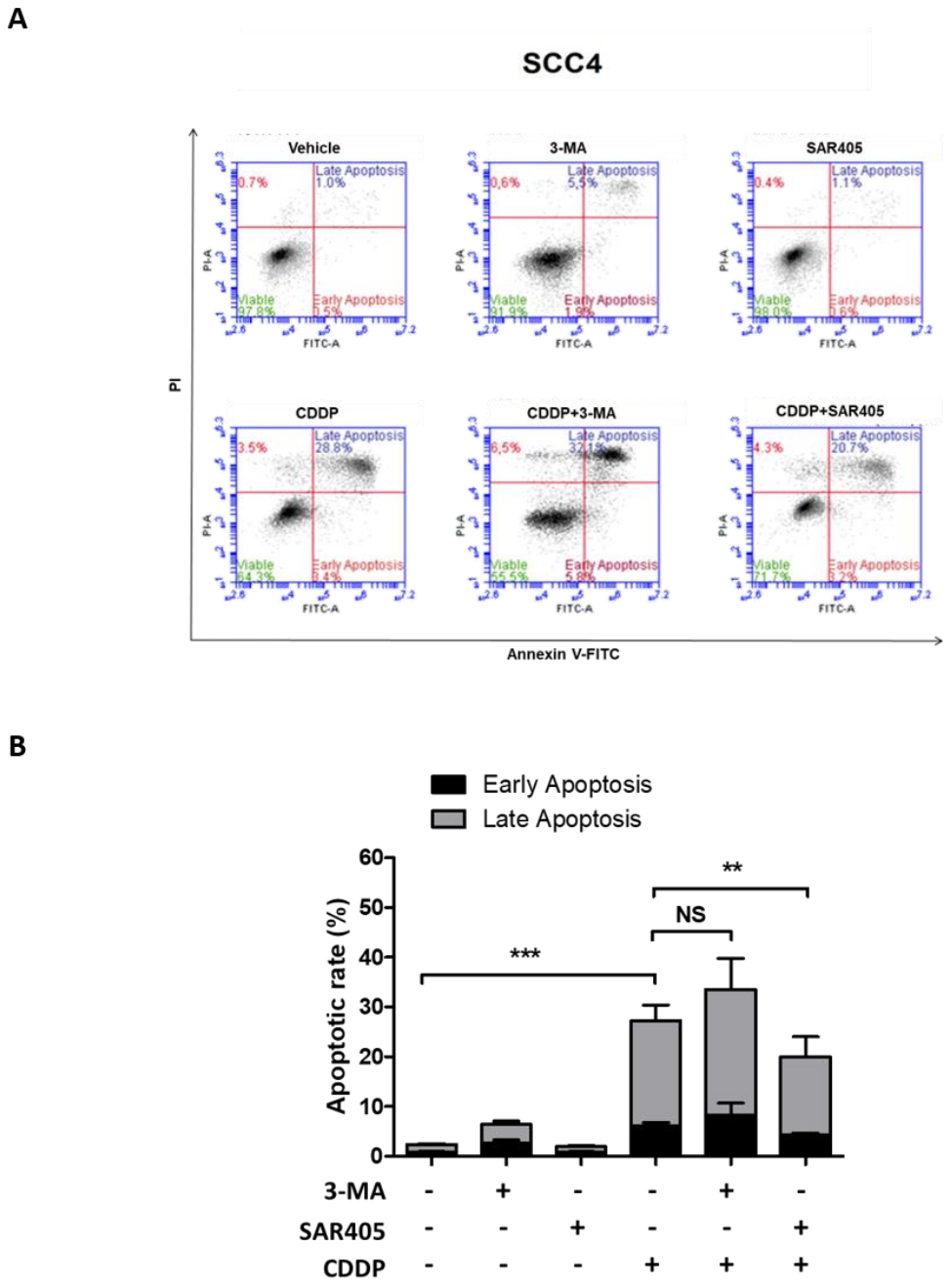

Figure 3.20 Effect of early stage autophagy inhibitors on cisplatin-induced apoptosis in SCC4 cells. SCC4 cells were seeded at 150 x10^3 cells/well in 6 well plates. Cells were pre-treated with either 3-MA (5 mM) or SAR405 (1 µM) for 1 h before adding cisplatin 5 µM for 48 h. Cells were then analysed by flow cytometry using BD FACS Accuri software. 10,000 single cells were gated on vehicle treated cells and the percentage of cells undergoing early and late apoptosis was acquired. **A**. Representative dot plot of treated cells. **B**. Values represent the mean and S.E.M. of three independent experiments. Statistical analysis was performed using one-way ANOVA with Tukey's Multiple Comparison Test (Graphpad Prism 5). *** $p<0.001$, ** $p<0.01$. NS: non-significant.

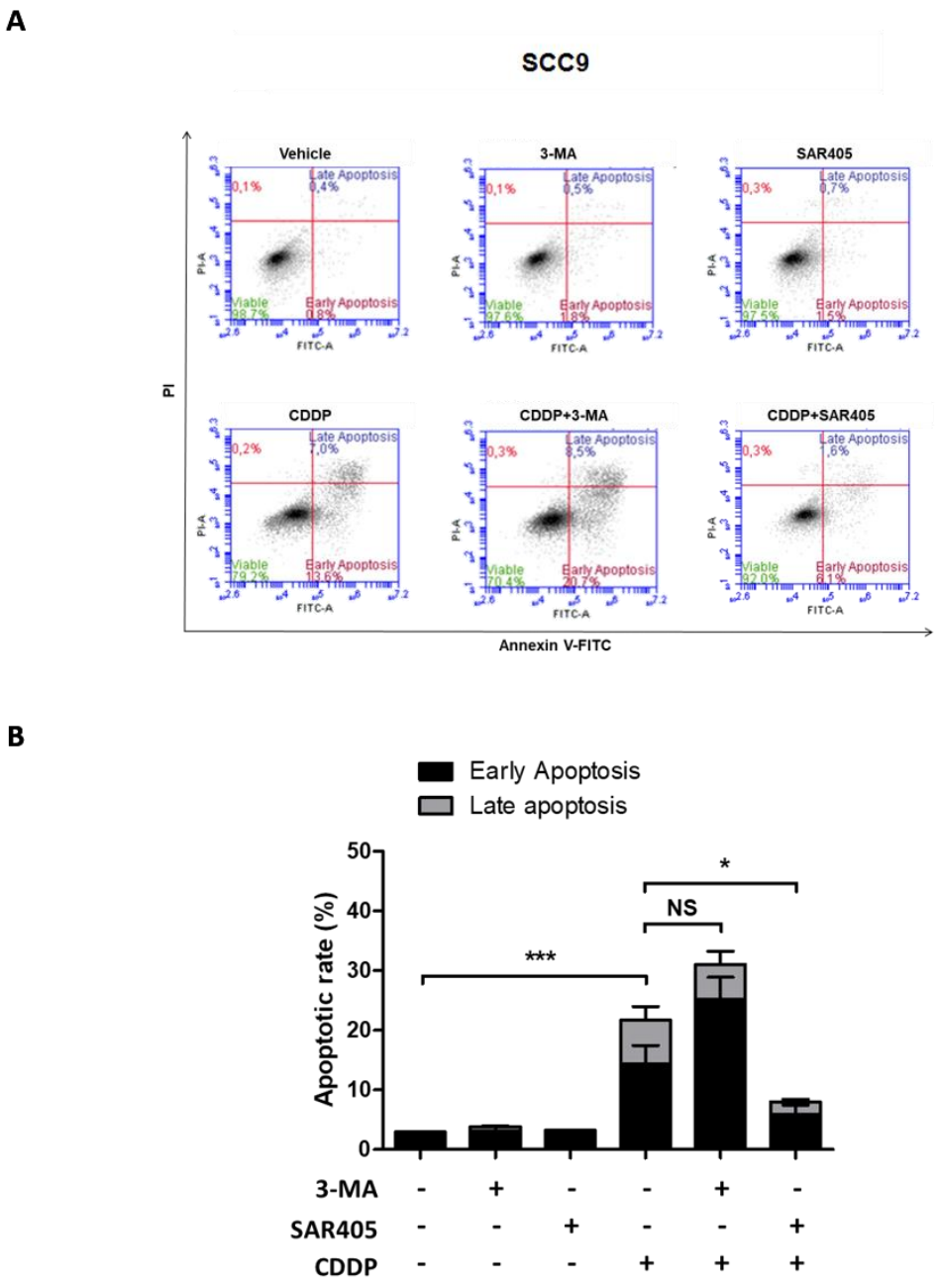

Figure 3.21 Effect of early stage autophagy inhibitors on cisplatin-induced apoptosis in SCC9 cells. SCC9 cells were seeded at 150 x10^3 cells/well in 6 well plates. Cells were pre-treated with 3-MA (5 mM) or SAR405 (1 µM) for 1 h before adding cisplatin 25 µM for 48 h. Cells were then analysed by flow cytometry using BD FACS Accuri software. 10,000 single cells were gated on vehicle treated cells and the percentage of cells undergoing early and late apoptosis was acquired. **A**. Representative dot plot of treated cells. **B**. Values represent the mean and S.E.M. of three independent experiments. Statistical analysis was performed using one-way ANOVA with Tukey's Multiple Comparison Test (Graphpad Prism 5). *** $p<0.001$, * $p<0.05$. NS: non-significant.

3.2.9.2. Targeting autophagy with late stage pharmacological autophagy inhibitors enhances cisplatin-induced apoptosis in OSCC cells

3.2.9.2.1. Chloroquine

Chloroquine is a late stage autophagy inhibitor that blocks autophagic flux by preventing the fusion of the lysosome with the autophagosome [341]. The effect of chloroquine on cisplatin-induced apoptosis was investigated by flow cytometric analysis of annexin V/PI stained cells in both SCC4 and SCC9 cell lines. Cells were treated with cisplatin (5 and 25 µM in SCC4 and SCC9 cells, respectively), chloroquine (10 µM) alone and cisplatin in combination with chloroquine, for 48 h. Cells were then double stained with annexin V-FITC and PI, and the percentage of cells in early and late apoptosis was acquired using the BD Accuri flow cytometer. As shown in Figure 3.22 and Figure 3.23, OSCC cells treated with chloroquine alone exhibited no increase in the apoptotic rate when compared to vehicle treated cells. On the other hand, both SCC4 and SCC9 cells treated with chloroquine in combination with cisplatin displayed a substantial and significant increase in the rate of apoptosis when compared to cells treated with cisplatin alone, suggesting that chloroquine sensitises cells to cisplatin-induced apoptosis in OSCC cell lines.

Additionally, this result was further confirmed by western blot analysis of SCC4 cells. In Figure 3.24, cells were treated as described above whilst serum starved cells were used as a positive control for autophagic induction. In agreement with the result presented in Figure 3.16, cisplatin induced an increase in LC3-II protein expression in the SCC4 cell line. Moreover, co-treatment with chloroquine led to a further LC3-II buildup due to the inhibition of the autophagic flux at the very late stages, resulting in the block of LC3-II turnover (Figure 3.24A). This result validates the inhibitory effect of chloroquine on autophagy and additionally confirmed autophagy activation in response to cisplatin by monitoring the autophagic flux, as previously shown in Figure 3.16.

Analysis of caspase 3 activation in SCC4 cells treated with cisplatin and cisplatin in combination with chloroquine was then performed. As expected, cisplatin induced caspase 3 cleavage in SCC4 cells, resulting in the appearance of cleaved caspase 3 fragments while chloroquine alone exhibited no effect (Figure 3.24A). From the densitometric analysis of cleaved caspase 3 fragment, a statistical increase in caspase 3 cleavage was observed in cells treated with cisplatin in combination with chloroquine

compared to cells treated with cisplatin alone, suggesting that chloroquine indeed enhances caspase 3 activation and thus apoptosis in SCC4 cells (Figure 3.24B).

Taken together, these results suggest that chloroquine enhances cisplatin-induced apoptosis and caspase 3 activation in OSCC cell lines. This is in marked contrast to the results obtained with the early stage autophagy inhibitor SAR405 which was shown to significantly inhibit cisplatin-induced apoptosis (Figures 3.20-21).

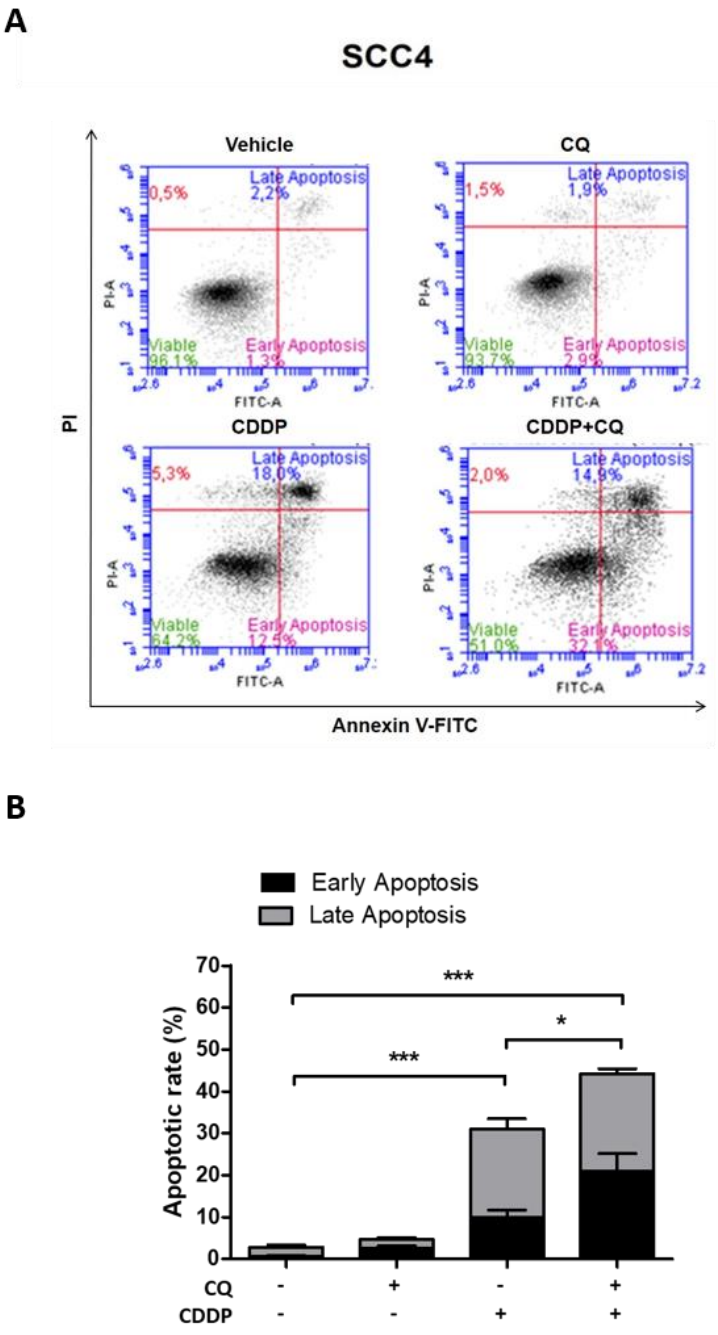

Figure 3.22 Chloroquine enhances cisplatin-induced apoptosis in the SCC4 cell line.

SCC4 cells were seeded at 150 x10^3 cells/well in 6 well plates. Cells were left for 24 h to adhere to the plate and then were treated with vehicle (0.009% (v/v) NaCl), 10 μM chloroquine (CQ) alone, 5 μM cisplatin (CDDP) alone, or cisplatin in combination with chloroquine for 48 h. Cells were then analysed by flow cytometry using BD FACS Accuri software. 10,000 single cells were gated on vehicle treated cells and the percentage of cells undergoing early and late apoptosis was acquired. **A**. Representative dot plot of treated cells. **B**. Values represent the mean and S.E.M. of three independent experiments. Statistical analysis was performed using one-way ANOVA with Tukey's Multiple Comparison Test (Graphpad Prism 5). *** $p<0.001$, * $p<0.05$.

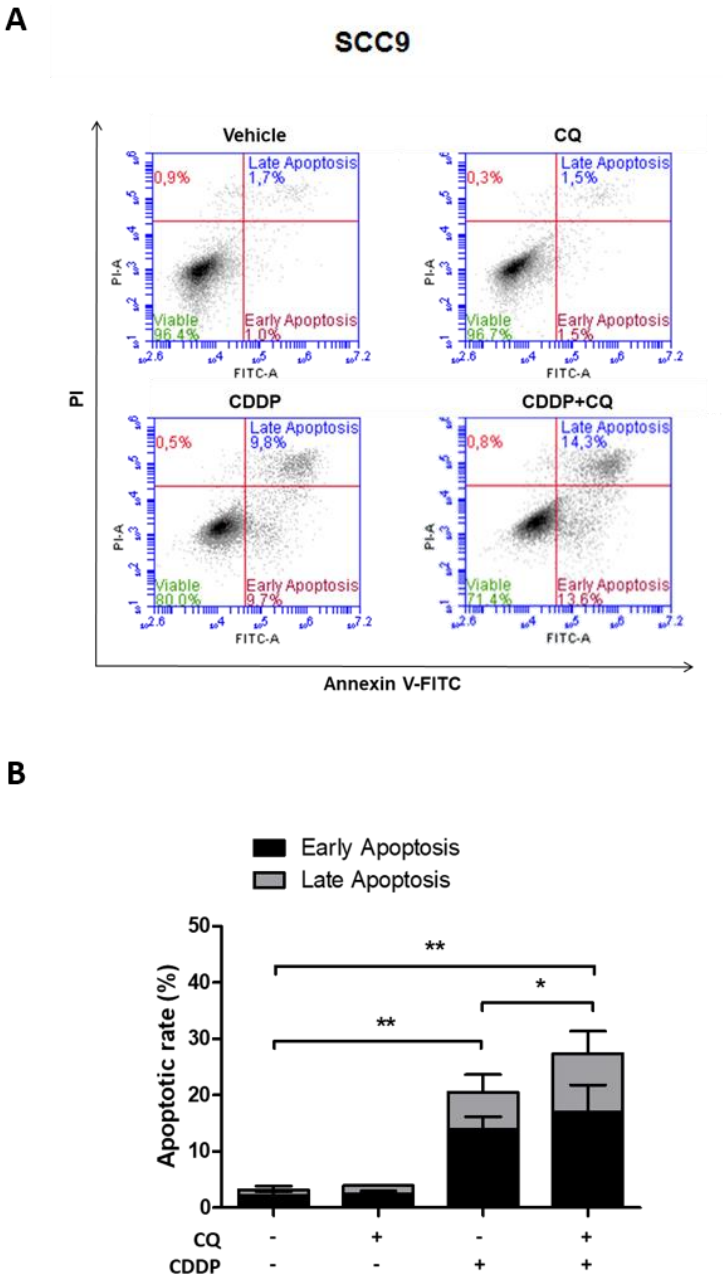

Figure 3.23 Chloroquine enhances cisplatin-induced apoptosis in the SCC9 cell line.

SCC9 cells were seeded at 150 x10^3 cells/well in 6 well plates. Cells were left for 24 h to adhere to the plate and then were treated with vehicle (0.009% (v/v) NaCl), 10 µM chloroquine (CQ) alone, 25 µM cisplatin (CDDP) alone, or cisplatin in combination with chloroquine for 48 h. Cells were then analysed by flow cytometry using BD FACS Accuri software. 10,000 single cells were gated on vehicle treated cells and the percentage of cells undergoing early and late apoptosis was acquired. **A**. Representative dot plot of treated cells. **B**. Values represent the mean and S.E.M. of three independent experiments. Statistical analysis was performed using one-way ANOVA with Tukey's Multiple Comparison Test (Graphpad Prism 5). ** $p<0.01$, * $p<0.05$.

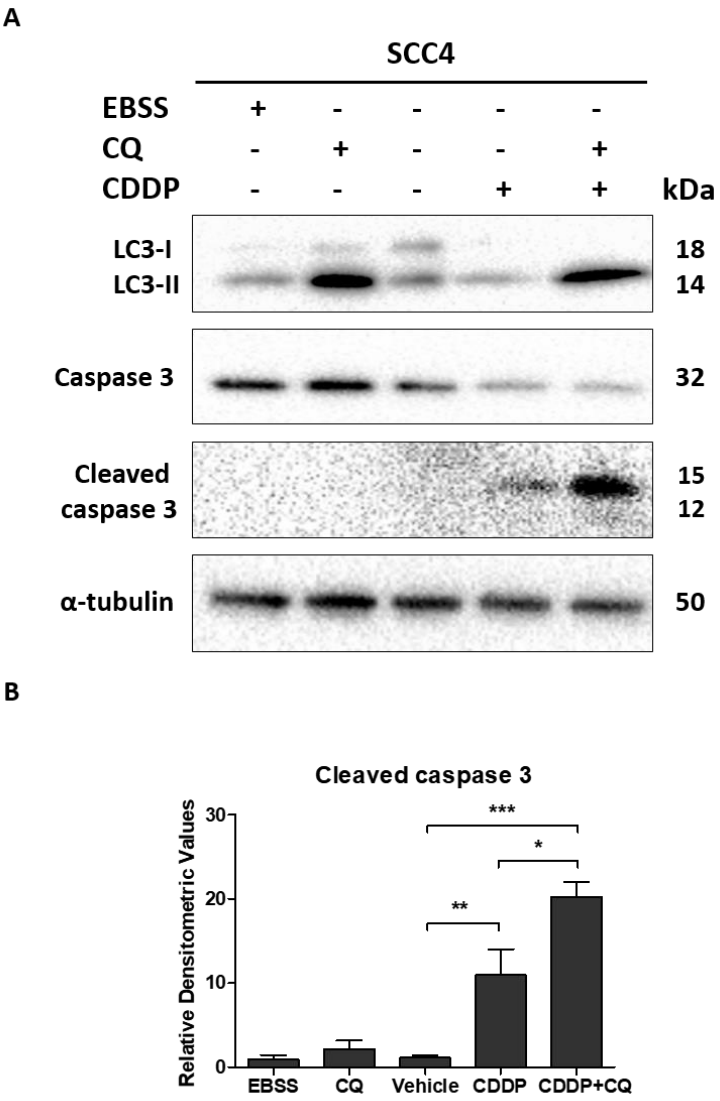

Figure 3.24 Chloroquine inhibits autophagic flux and enhances caspase 3 activation in SCC4 cells treated with cisplatin.

SCC4 cells were seeded at 300 x10^3 cells/flask in T25 flasks. Cells were left for 24 h to adhere to the flask and then were treated with the vehicle (0.009% (v/v) NaCl), chloroquine (CQ) 10 μM alone, cisplatin (CDDP) 5 μM alone or cisplatin in combination with chloroquine for 48 h. Cells treated with EBSS for 4 h were used as a positive control. After incubation, cells were lysed and 20 μg of protein was loaded and separated on a 12% SDS-PAGE gel, transferred to a PVDF membrane and probed with anti-LC3-I/II, anti-caspase 3 and anti-cleaved caspase 3 antibodies. α-tubulin served as loading control. **A**. Results are representative of three independent experiments. **B**. Densitometric analysis of cleaved caspase 3 bands was performed using ImageLab software and values were normalised by the loading control. Statistical analysis was performed using one-way ANOVA with Tukey's Multiple Comparison Test (Graphpad Prism 5). ***<0.001, ** p<0.01, * p<0.05.

3.2.9.2.2. Bafilomycin-A1

Bafilomycin-A1 is an inhibitor of vacuolar (V)-type ATPases, which prevents the fusion of lysosomes with autophagosomes, inhibiting the later stages of autophagy [342]. The effect therefore of a second late stage autophagy inhibitor, bafilomycin-A1, on cisplatin-induced apoptosis was next investigated by flow cytometric analysis of annexin V/PI stained cells. OSCC cells were treated with cisplatin (5 or 25 µM in SCC4 and SCC9 respectively) alone, bafilomycin-A1 (20 nM) alone or cisplatin in combination with bafilomycin-A1 for 48 h. Both SCC4 and SCC9 cell lines treated with bafilomycin-A1 alone exhibited no increase in the apoptotic rate when compared to vehicle treated cells (Figure 3.25-26). On the contrary, OSCC cells treated with bafilomycin-A1 in combination with cisplatin displayed a significant increase in the percentage of apoptosis when compared to cells treated with cisplatin alone, suggesting that bafilomycin-A1 enhances cisplatin-induced cytotoxicity in OSCC cell lines.

The statistically significant increase in apoptosis observed in cisplatin-treated SCC4 cells in the presence of bafilomycin-A1 was confirmed by western blot analysis. Cells were treated as described above and in addition serum starved cells incubated for 4 h in EBSS were used as a positive control for autophagic induction. Samples were lysed and run on a 12 and 15% SDS-PAGE gels before being probed for LC3-I/II, caspase 3 and cleaved caspase 3. As expected, conversion of LC3-I to LC3-II was observed in SCC4 cells treated with EBSS and with cisplatin compared to vehicle treated cells (Figure 3.27). Moreover, bafilomycin-A1 alone and in combination with cisplatin led to a further LC3-II accumulation due to a block in autophagic flux at the very late stages, validating the inhibitory effect on autophagy in SCC4 cells. Interestingly, analysis of caspase 3 activation showed a decrease in caspase 3 and a statistically significant increase in cleaved caspase 3 in cells treated with cisplatin in combination with bafilomycin-A1 compared to cells treated with cisplatin alone, suggesting that bafilomycin-A1 may enhance caspase 3 activation in cisplatin treated cells, and hence apoptotic cell death.

Taken together the results obtained implied that targeting autophagic flux with late stage autophagy inhibitors sensitises OSCC cells to cisplatin treatment. However, these results were in marked contrast with those obtained with the early stage inhibitors SAR-405 and 3-MA. SAR-405 was shown to significantly inhibit cisplatin-induced apoptosis whilst 3-MA elicited no significant effect. Since pharmacological inhibitors of autophagy have previously been shown to elicit off-target effects [343, 344], an RNA-interference

approach was required to further delineate the role of autophagy in mediating resistance to cisplatin-induced apoptosis.

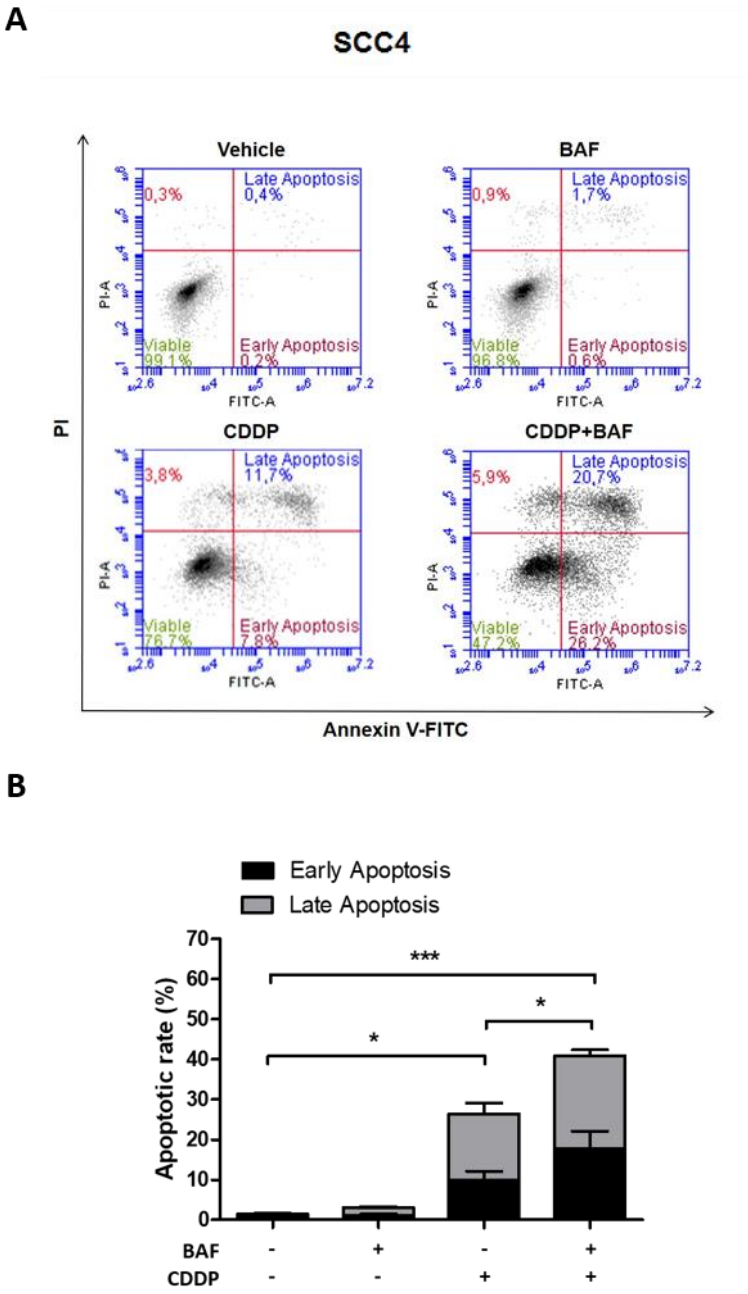

Figure 3.25 Bafilomycin-A1 enhances cisplatin-induced apoptosis in the SCC4 cell line.

SCC4 cells were seeded at $150x10^3$ cells/well in 6 well plates. Cells were left for 24 h to adhere to the plate and then were treated with vehicle (0.009% (v/v) NaCl), 20 nM bafilomycin-A1 (BAF) alone, 5 μM cisplatin (CDDP) alone or cisplatin in combination with bafilomycin-A1. After 48 h, cells were harvested and double stained with annexin V/PI. Cells were then analysed by flow cytometry using BD FACS Accuri software. 10,000 single cells were gated on vehicle treated cells and the percentage of cells undergoing early and late apoptosis was acquired. **A**. Representative dot plot of treated cells. **B.** Values represent the mean ±S.E.M of three independent experiments. Statistical analysis was performed using one-way ANOVA with Tukey's Multiple Comparison Test (Graphpad Prism 5). ** *p<0.001, * p<0.05.

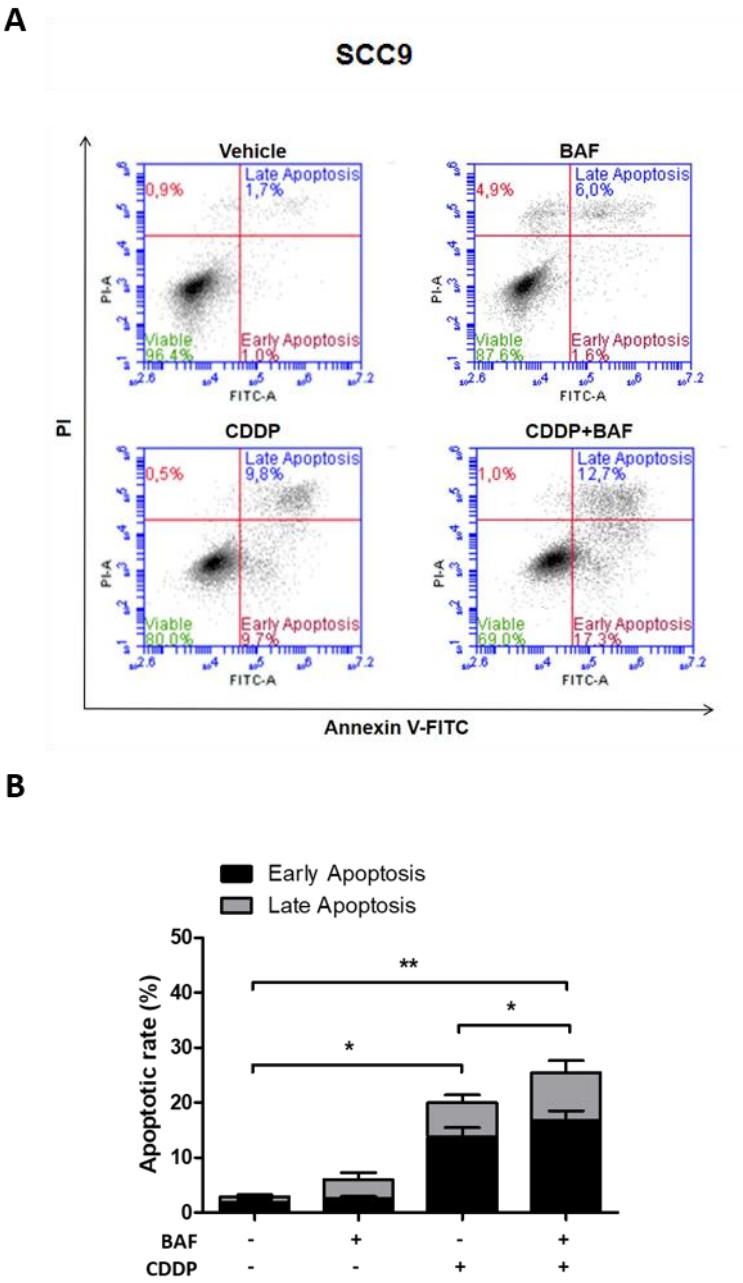

Figure 3.26 Bafilomycin-A1 enhances cisplatin-induced apoptosis in the SCC9 cell line.

SCC9 cells were seeded at $150x10^3$ cells/well in 6 well plates. Cells were left for 24 h to adhere to the plate and then were treated with vehicle (0.009% (v/v) NaCl), 20 nM bafilomycin-A1 (BAF) alone, 25 μM cisplatin (CDDP) alone or cisplatin in combination with bafilomycin-A1. After 48 h, cells were harvested and double stained with annexin V/PI. Cells were then analysed by flow cytometry using BD FACS Accuri software. 10,000 single cells were gated on vehicle treated cells and the percentage of cells undergoing early and late apoptosis was acquired. **A**. Representative dot plot of treated cells. **B**. Values represent the mean ±S.E.M of three independent experiments. Statistical analysis was performed using one-way ANOVA with Tukey's Multiple Comparison Test (Graphpad Prism 5). ** $p<0.01$, * $p<0.05$.

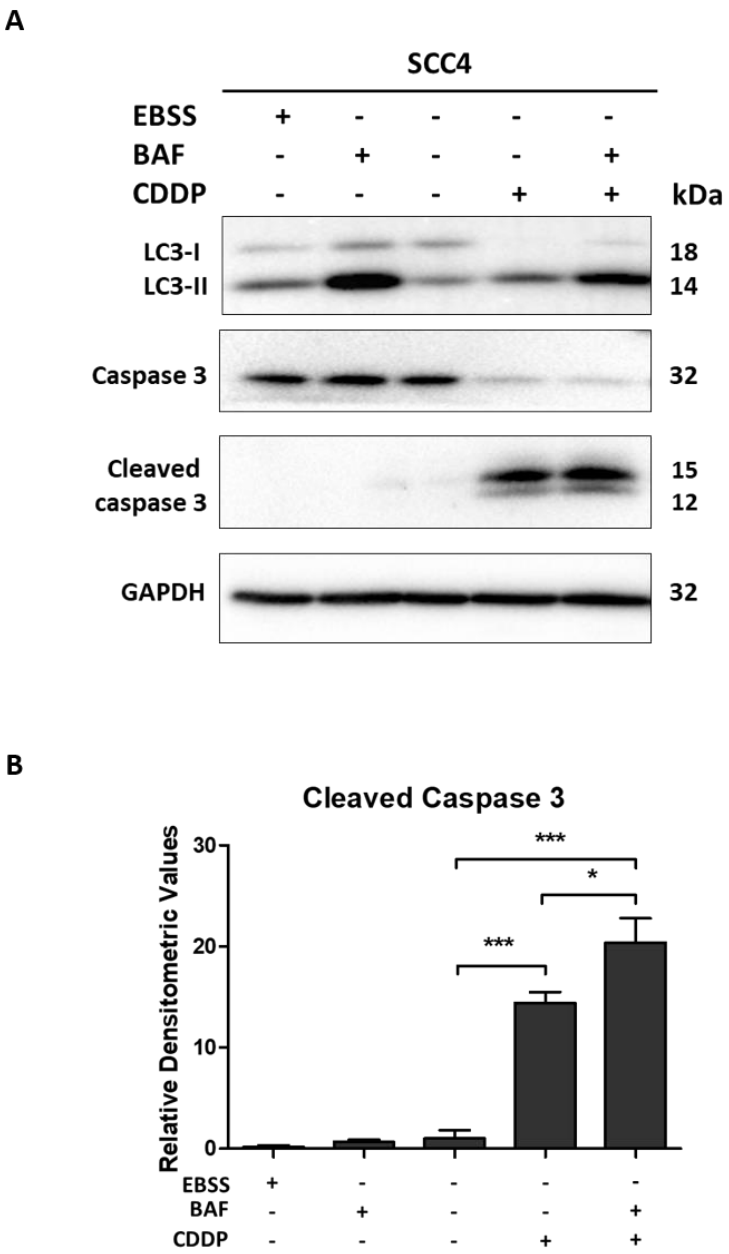

Figure 3.27 Bafilomycin-A1 inhibits autophagic flux and enhances caspase 3 activation in SCC4 cells treated with cisplatin.

SCC4 cells were seeded at $300x10^3$ cells/flask in T25 flasks. Cells were left for 24 h to adhere to the flask and then were treated with vehicle (0.009% (v/v) NaCl), bafilomycin-A1 (BAF) 20 nM alone, cisplatin (CDDP) 5 μM alone and cisplatin in combination with bafilomycin-A1 for 48 h. Cells treated with EBSS for 4 h were used as a positive control for autophagy induction. After incubation, cells were lysed and 20 μg of protein was loaded and separated in a 15% SDS-PAGE gel, transferred to a PVDF membrane and probed with anti-LC3-I/II, anti-caspase 3 and anti-cleaved caspase 3 antibodies. GAPDH served as loading control. **A**. Results are representative of three independent experiments. **B**. Densitometric analysis of cleaved caspase 3 bands was performed using ImageLab software and values were normalised by the loading control. Statistical analysis was performed using one-way ANOVA with Tukey's Multiple Comparison Test (Graphpad Prism 5). ***<0.001, * $p<0.05$.

3.2.9.3. Genetic inhibition of autophagosome formation does not enhance cisplatin-induced apoptosis in OSCC cells

An RNA-interference approach targeting autophagic proteins was next performed. This method represents a more accurate strategy to specifically target autophagy, avoiding the non-specific off-target effects of drug treatment. Autophagy-related 5 (ATG5) is a key autophagic protein involved in the extension of the phagophore membrane during autophagosome formation. In fact, association of ATG5 with ATG12 and subsequently with ATG16 results in the formation of the autophagy elongation complex (ATG5-12/16) which is necessary for LC3 lipidation and autophagosome generation [345]. Knockdown of ATG5 has been widely reported to block the autophagic flux in several studies [346–348]. The effect of ATG5 siRNA on cisplatin-induced apoptosis was therefore evaluated in the SCC4 cell line.

Firstly, the efficiency of the knockdown was examined by western blot analysis of ATG5 and LC3-I/II protein expression. SCC4 cells were transfected with Non-Targeting (NT) control siRNA or with ATG5 siRNA for 48 h using lipofectamine. Cells treated with lipofectamine alone served as negative control for this experiment. As shown in Figure 3.28, SCC4 cells transfected with ATG5 siRNA exhibited a substantial and significant decrease in ATG5-ATG12 protein expression compared to NT siRNA transfected cells and lipofectamine treated cells, suggesting that ATG5 siRNA specifically targets ATG5 mRNA resulting in its knockdown. Moreover, western blot analysis of LC3-I/II protein expression showed a slight although non-significant increase in the conversion of LC3-I to LC3-II in cells transfected with NT siRNA compared to lipofectamine treated cells, likely due to autophagy activation in response to siRNA reagents. However, a significant reduction in the conversion of LC3-I in LC3-II was observed when cells were transfected with ATG5 siRNA compared to NT siRNA transfected cells. This result indicates that knock down of ATG5 results in a failure of LC3 activation, necessary during the autophagosome formation, hence indicating an inhibition of the autophagic flux.

The effect of ATG5 knockdown on cisplatin-induced apoptosis was then investigated in order to determine whether genetic inhibition of autophagy may sensitise cells to cisplatin. SCC4 cells were transfected with NT control siRNA or with ATG5 siRNA for 24 h before adding cisplatin 10 µM for further 24 h. Lipofectamine treated cells and cells transfected with NT siRNA or with ATG5 siRNA alone for 48 h served as controls for this experiment. Cells were then double stained with annexin V-FITC and PI, and the

percentage of cells in early and late apoptosis was acquired using the BD Accuri flow cytometer. As shown in Figure 3.29, transfection of cells with both NT and ATG5 siRNA resulted in a slight but non-significant increase in the apoptotic rate compared to lipofectamine treated cells. Addition of cisplatin to NT and ATG5 transfected cells was shown to substantially increase the apoptotic rate. However, no significant differences were found between cells transfected with ATG5 siRNA in combination with cisplatin and cells transfected with NT siRNA in combination with cisplatin, indicating that ATG5 knockdown does not sensitise cells to cisplatin-induced apoptosis. Furthermore, these results correlate with the results obtained using the early stage pharmacological autophagy inhibitors, suggesting that targeting the autophagic flux at early stages does not sensitise OSCC cells to cisplatin.

Taken together, these results suggest that autophagy may not be implicated in chemoresistance in OSCC cells. On the contrary cisplatin-induced autophagy may be closely related to cisplatin-induced apoptosis through a crosstalk mechanism between the two pathways.

A

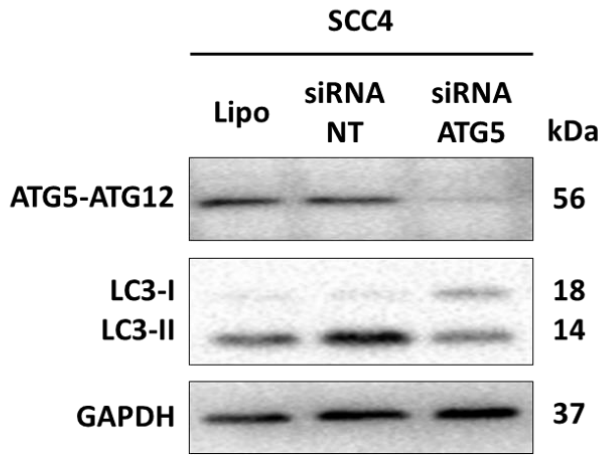

B

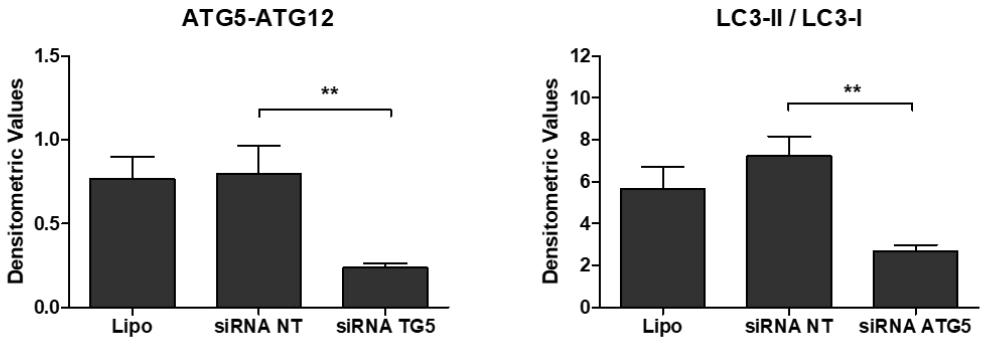

Figure 3.28 Knockdown of ATG5 protein inhibits autophagy in SCC4 cells.

SCC4 cells were seeded at 200 x10^3 cells/well in 6 well plates. Cells were transfected with Non-Targeting (NT) control siRNA or with ATG5 siRNA for 48 h by using lipofectamine. Cells treated with lipofectamine (Lipo) alone served as negative control. After incubation, cells were lysed and 20 µg of protein was loaded and separated in a 15% SDS-gel, transferred to a PVDF membrane and probed with anti-ATG5-ATG12 and anti-LC3-I/II antibodies. GAPDH served as loading control. **A**. Results are representative of three independent experiments. **B**. Densitometric analysis of ATG5-ATG12, LC3-I and LC3-II bands was performed using ImageLab software and values were normalised to the loading control. Data represent the mean ±S.E.M. of three independent experiments. Statistical analysis was performed using unpaired two-tailed student t-test to compare mean values between siRNA NT and siRNA ATG5 transfected cells (Graphpad Prism 5). ** $p<0.05$.

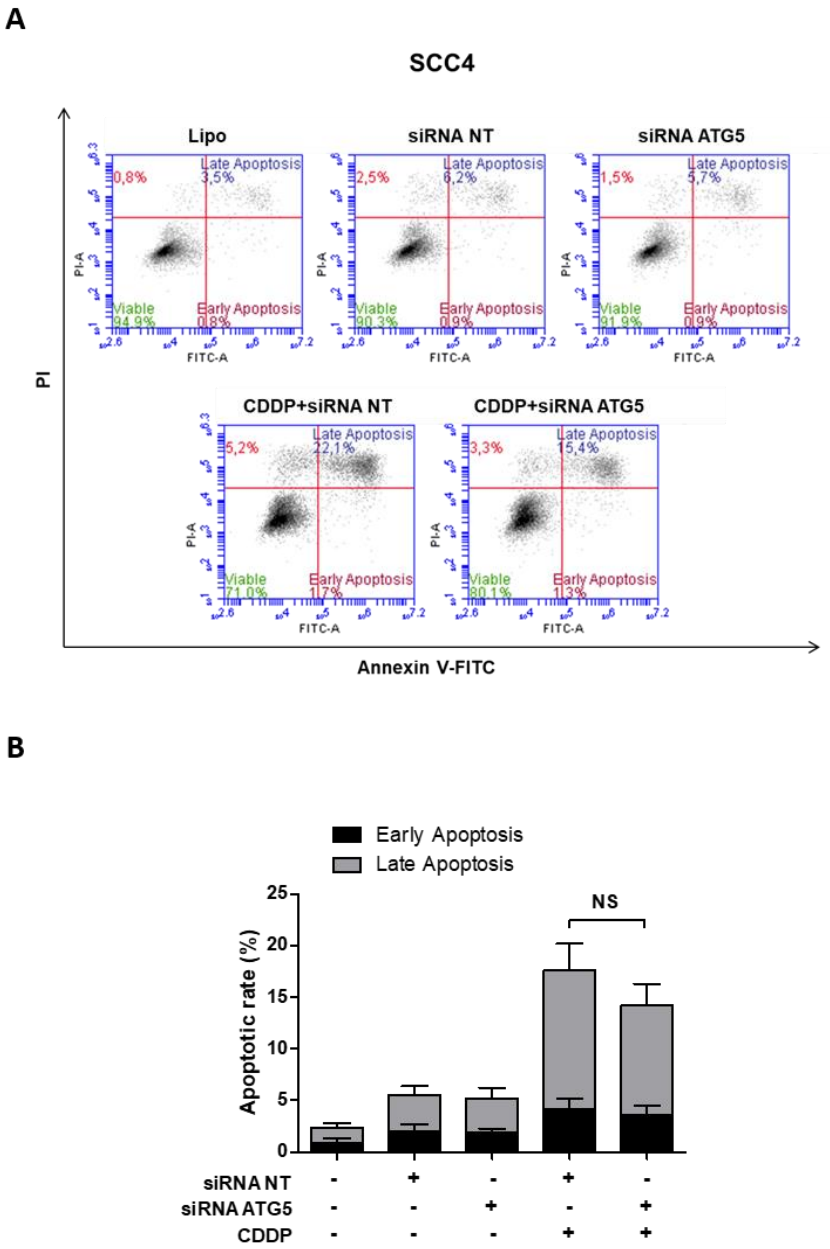

Figure 3.29 Knock down of ATG5 protein does not sensitise SCC4 cells to cisplatin.

SCC4 cells were seeded at 200 x10^3 cells/well in 6 well plates. Cells were transfected with NT control siRNA or with ATG5 siRNA for 24 h before the addition of cisplatin (10 µM) for a further 24 h. Lipofectamine treated cells and cells transfected with NT siRNA or with ATG5 siRNA alone for 48 h served as negative control. Cells were then analysed by flow cytometry using BD FACS Accuri software. 10,000 single cells were gated on vehicle treated cells and the percentage of cells undergoing early and late apoptosis was acquired. **A**. Representative dot plot of treated cells. **B**. Values represent the mean and S.E.M. of three independent experiments. Statistical analysis was performed using unpaired two-tailed student t-test to compare mean values between siRNA NT and siRNA ATG5 transfected cells treated with cisplatin **(**Graphpad Prism 5). NS: non-significant.

3.3. Discussion

OSCC is one of the most common cancers worldwide. Despite much scientific effort to improve therapies, the prognosis of OSCC patients is still poor and mortality rates have not reduced in recent years [4, 349]. Chemotherapy is an important adjuvant therapy for OSCC and it can be used pre- and post-surgery or as a primary treatment when surgery is not possible. However, resistance to chemotherapy is one of the major problems during the treatment of OSCC. Chemoresistance has been linked to the ability of cancer cells to survive under stressful conditions and to protect themselves from anti-cancer drugs. It may result not only in the failure of chemotherapeutic treatments, but also in tumour recurrence and progression. Thus, new treatment strategies are required to bypass chemoresistance in OSCC patients. Recent studies suggest that tumour resistance to therapy could be related to cell survival through autophagy [328]. Therefore, heightened autophagy may be a mechanism of resistance for cancer cells faced with metabolic and therapeutic stress. Targeting autophagy has thus been proposed as a new strategy to bypass drug resistance and improve patient outcomes. However, the role of autophagy in OSCC still remains unclear. In the present study it was hypothesised that autophagy may be activated in OSCC in response to chemotherapeutics and may lead to chemoresistance.

In this chapter cell death programmes initiated in OSCC cells in response to the chemotherapeutic agents were first investigated. Cisplatin, docetaxel and 5-fluorouracil are widely used chemotherapeutic agents for the treatment of OSCC [331]. In this chapter, the effect of cisplatin, docetaxel and 5-fluorouracil treatment was examined in two representative OSCC cell lines: the SCC4 and SCC9 cell lines. Both cell lines are derived from squamous cell carcinoma (SCC) of the tongue, which is considered the most aggressive form of OSCC [7]. SCC4 cells were isolated from a 55-year-old male who had received radiation and methotrexate treatment for the tumour for 16 months, while SCC9 cells were taken from a 25-year-old male who had received no treatment for the tumour [306]. Results presented herein demonstrated that cisplatin, docetaxel and 5-fluorouracil reduced the viability of both OSCC cells in a dose- and time-dependent manner. However, a higher sensitivity to these drugs was observed in SCC4 cells compared to SCC9 cells, likely due to the different degree of differentiation and the genetic asset of the two cell lines. In fact, SCC4 cells are commonly considered poorly differentiated cells, whilst SCC9 cells are commonly considered moderately differentiated cells [21]. Accordingly, in gastric cancer cells, it has been demonstrated that since the chemotherapeutic drugs act

on proliferating cells, they have a greater effect in poorly differentiated cells because of their ability to divide faster [350]. In addition, genomic data from Barretina *et al*. published in Nature in 2012 described the genetic profile of several head and neck squamous cell carcinoma cell lines [307]. From this analysis, different genetic mutations were reported for SCC4 and SCC9 cell lines. In particular, a different p53 expression pattern and H-Ras status was reported. In fact, SCC4 cells displayed overexpression of mutant p53 protein and functional H-Ras protein, whilst SCC9 cells displayed no expression of p53 protein and a non-synonymous mutation in H-Ras gene. Ras mutations have been associated with lack of response to anti-EGFR agents in colorectal cancer and accordingly, a recent study has proposed Ras mutation status as a predictor of chemotherapy response in colorectal cancer patients [351–354]. Additionally, studies carried out in ovarian and prostatic cancer have shown that the absence of p53 can be associated with cisplatin and docetaxel resistance [355–357]. Although no evidence has been reported so far, it cannot be excluded that p53 and Ras status may contribute to the different grade of sensitivity to chemotherapeutics observed in SCC4 and SCC9 cell lines. Results obtained in the present study showed that the IC_{50} values obtained after 72 h treatment with cisplatin were 1.1 ± 0.4 μM and 22.1 ± 0.4 μM in SCC4 and SCC9 respectively, whilst the IC_{50} values obtained with docetaxel were 1.5 ± 1.3 nM and 0.2 ± 0.4 nM. Overall, the low micromolar and nanomolar range obtained for the cell sensitivity to cisplatin and docetaxel respectively in both cell lines correlated with data reported in the GDSC (Genomics of Drug Sensitivity in Cancer). In contrast, results obtained for 5-fluorouracil in this study (IC_{50} value of 25.6 μM in SCC4 at 72 h) did not correlate particularly well with the GDSC database, wherein an IC_{50} values of 231 μM after 72 h of treatment was reported in the SCC4 cells. Any differences observed may be due to the differences in the techniques employed to assess viability [358]. Due to this discrepancy it was decided not to proceed with the use of 5-fluorouracil in subsequent experimentation.

Given the wide use of cisplatin as a first-line chemotherapeutic agent for the treatment of OSCC [359], it was selected as the representative anticancer drug for further analyses in the present study . In order to investigate whether cisplatin treated cells were undergoing a decrease in viability due to cell death or cell cycle arrest, flow cytometric analysis of PI stained cells was performed. Cell cycle arrest was observed at low concentrations of cisplatin, resulting in a significant increase of cells in S-phase at 12.5 μM cisplatin in

SCC9 cells. Moreover, a progressive increase in the subG0/G1 peak with increasing concentrations of cisplatin was shown in both OSCC cell lines, suggesting that cisplatin-induced cell death occurs in a dose-dependent manner. Taken together these results may suggest that low concentrations of cisplatin induce S-phase arrest in OSCC as an initial response to DNA damage, with higher concentrations of cisplatin resulting in extensive cell damage leading to cell death. According to Basu *et al*., cell cycle checkpoints are activated following cisplatin-induced DNA damage to provide time for DNA repair, resulting in a delay of cell cycle progression [357]. In this regard, the activation of ChK1 has been reported and linked to Cdc25A degradation and S-phase arrest in HeLa cells treated with cisplatin [360]. Furthermore, results in the present study correlate with recent findings on the cell cycle in human promyelocytic leukaemia cells showing that almost 40% of the cells in the G0/G1 peak were reduced after 48 h treatment with low concentrations of cisplatin with a corresponding accumulation of cells in S and subG0/G1 peaks [361]. This was followed by a progressive increase in the subG0/G1 after treatment of cells with increasing concentrations of cisplatin. Thus, treatment with high concentrations of cisplatin leads to a drastic cellular response resulting in the elimination of genetically unstable cells by cell death induction.

To establish whether apoptotic cell death occurs in OSCC cells following treatment with cisplatin, flow cytometric analysis of annexin V/PI stained cells was performed. Cisplatin-induced apoptosis was observed in a dose-dependent manner in both OSCC cell lines. After 48 h treatment, a noticeable increase in the apoptotic rate was first displayed at 5 μM and 25 μM cisplatin in SCC4 and SCC9 cells, respectively. The increase in the apoptotic rate obtained from the annexin V/PI assay correlated with the increase in the subG0/G1 peak obtained from cell cycle analysis, confirming that cisplatin-induced cell death in OSCC cells mainly occurs through apoptosis. Apoptotic cell death induced by cisplatin was further confirmed by western blotting through the evaluation of caspase 3 cleavage in SCC4 cells. Cisplatin-induced caspase 3 activation was first observed at 5 μM cisplatin and increased in a dose-dependent manner, providing a strong correlation with results obtained from the flow cytometric analysis of annexin V/PI stained cells. Additionally, the time dependency of cisplatin-induced apoptosis was also demonstrated in this study. From the flow cytometric analysis of annexin V/PI stained cells, a slight increase in the apoptotic rate of cisplatin treated cells compared to vehicle treated cells was first observed at the 16 h time point in both cell lines which progressively increased

with time, becoming significant at 24 h treatment in SCC4 cells and 48 h treatment in SCC9 cells. Moreover, from the western blot analysis a time-dependent activation of caspase 3 was observed in SCC4 cells treated with cisplatin, with a statistically significant increase in cleaved caspase 3 at 48 h treatment. Finally, various studies have demonstrated that cisplatin-induced apoptosis can occur either in a caspase-dependent or -independent manner [362, 363]. In the present study, it was shown that induction of apoptosis by cisplatin occurred as a caspase-dependent event in both SCC4 and SCC9 cell lines as pre-treatment with the pan-caspase inhibitor Z-VAD-fmk totally suppressed cisplatin-induced apoptosis.

Given that cisplatin induced apoptosis in OSCC cell lines, autophagy levels under normal conditions and in response to cisplatin treatment were then investigated. It has been reported that autophagy can be generally sub-classified as basal autophagy and induced autophagy [364, 365]. Basal autophagy is constitutively activated in order to allow the turnover of cytosolic components, whilst induced autophagy is activated in response to several stimuli such as starvation, oxidative stress or chemotherapeutic drugs. Mutation of autophagic genes or dysregulation of the autophagic pathway may lead to enhancement or repression of basal autophagy. Dysregulation of basal levels of autophagy have been observed in different cancer cell lines, suggesting a role for autophagy in tumorigenesis [167]. Whether autophagy acts as a tumour suppressive or tumour promoting mechanism is still poorly understood and is probably dependent on the type of tumour, the genetic asset of cells and the stage of malignancy. In the present study, basal levels of autophagy were assessed in SCC4 and SCC9 cell lines by western blot analysis of LC3-I/II and p62 protein expression. To date, the expression analysis of LC3-I/II and p62 proteins by western blot, alongside electron microscopy for autophagosome formation, are reported to be the best ways to detect autophagy activation [333, 366]. LC3 is a Ubl-conjugation system crucial during autophagosome formation and maturation. Autophagy activation results in the cleavage of LC3 by the cysteine protease ATG4 into a LC3-I fragment, which is then conjugated with phosphatidylethanolamine (PE) to form LC3-II [148]. p62/SQTM1 is a cargo receptor for selective autophagy and it is involved in the delivery of ubiquitinated proteins to the autophagosome for degradation [146]. The conversion of LC3-I to the LC3-II form alongside the degradation of p62 have been considered a reliable marker to study autophagy induction [151]. In order to evaluate basal levels of autophagy in OSCC cell lines, autophagic flux was investigated by using the lysosomal

inhibitor bafilomycin-A1. According to Mizushima *et al.*, determination of autophagic flux is important to estimate autophagic activity [335]. The term 'autophagic flux' denotes the dynamic process of the autophagosome formation, fusion with the lysosome and degradation of the autophagic substrates into the autophagolysosome [151]. The use of lysosomal inhibitors is considered the best way to monitor the autophagic flux, as preventing the completion of autophagy in the final steps leads to an accumulation of autophagic vesicles, which is evidence of efficient autophagic flux. On the other hand, the failure of autophagic vesicle accumulation in the presence of such inhibitors, may be indicative of a defect or a delay in vesicle trafficking, prior to degradation at the autophagolysosome [366]. Results obtained from western blot analysis herein showed that autophagic flux is constitutively activated at basal levels in both cell lines. Interestingly, a different expression pattern of LC3-II protein was found in the two cell lines, with higher levels of LC3-II in SCC9 cells compared to SCC4 cells under normal conditions. Since LC3-II expression positively correlates to basal levels of autophagy, this result may suggest higher basal levels of autophagy in the SCC9 cell line compared to the SCC4 cell line. A study conducted on 10 colorectal cancer (CRC) cell lines has proposed a correlation between basal levels of autophagy and sensitivity to drugs. According to this study, the CRC cell lines with lower basal levels of autophagy were shown to be more sensitive to the anti-cancer drug omega-3 fatty acid docosahexaenoic acid (DHA) compared to cells with high basal levels of autophagy [367]. A similar study has also reported a correlation between basal autophagic flux and sensitivity toward rLGALS9 treatment in CRC cells cell lines [368]. Moreover, oncogenic mutations of Ras have also been associated with high levels of basal autophagy in a panel of human cancer cell lines, implying a cell survival role of autophagy during tumorigenesis in Ras-driven cancers [178, 368, 369]. Taken together, these findings correlate with the results obtained in the present study, where the Ras-mutated SCC9 cell line exhibited less sensitivity to drugs and concurrently higher basal levels of autophagy. Additionally, starvation of cells with EBSS for 2 or 4 h was shown to induce LC3-I/II conversion in both SCC4 and SCC9 cell lines, confirming the ability of these cell lines to induce autophagy in response of external stimuli.

Autophagy has been shown to be induced in various cancers in response to chemotherapeutics [189, 370, 371]. Indeed, autophagy activation in response to cisplatin has been reported in ovarian cancer cells, human bladder cells, lung adenocarcinoma cells

and as well as in oral squamous carcinoma cells [290, 372–374]. In the present study, activation of autophagy in response to cisplatin in OSCC cells was demonstrated by flow cytometric analysis of Cyto-ID stained cells. This approach allows the quantification of autophagosomes through the detection of fluorescence [311]. The Cyto-ID Autophagy Detection Kit is reported to stain autophagic vesicles in a more specific manner than other lysosomotropic dyes such as acridine orange [333]. Results obtained herein demonstrated an increase of autophagic vesicles in both OSCC cell lines after 48 h treatment with cisplatin. Moreover, this result was further confirmed by evaluation of the autophagic flux. In fact, the static analysis of autophagic structures at certain time points may be difficult to interpret, as the appearance of more autophagosomes do not necessarily imply autophagy induction. Thus, the combinatorial evaluation of the samples in the presence/absence of lysosomal inhibitors permits an evaluation as to whether there has been an effective induction of autophagy or whether an accumulation of vesicles is occurring because of an inhibition of autophagic flux [151]. In this study, chloroquine was used as a late stage autophagy inhibitor to study cisplatin-induced autophagic flux. A significant increase in autophagosome levels was observed in both OSCC cell lines treated with chloroquine in combination with cisplatin compared to cells treated with chloroquine alone or cisplatin alone. This result suggests that treatment with cisplatin promotes autophagic flux activation and excludes secondary accumulations due to autophagic degradation blockade.

The time- and dose-dependent nature of autophagy induction in response to cisplatin was also examined in OSCC cell lines. Cyto-ID analysis showed a progressive increase in autophagic vesicles in a time-dependent manner in SCC4 and SCC9 cells, indicating that significant autophagy activation occurs at 48 h cisplatin treatment in both cell lines and increases up to 72 h treatment in SCC9 cells. Additionally, western blot analysis showed that cisplatin induced autophagy in a dose-dependent manner in OSCC cells lines, resulting in a progressive increase in LC3-II levels and a concomitant decrease in p62 levels. Taken together, these results suggest that autophagy is induced in a time- and dose-responsive manner in OSCC cell lines treated with cisplatin. Interestingly, these results highlight a parallel activation of cisplatin-induced autophagy and apoptosis in OSCC cells, suggesting the interplay of the two pathways in response to chemotherapeutics. In fact, treatment of SCC4 cells with a low concentration of cisplatin (1 µM) for 48 h did not elicit any effect on either the apoptotic or the autophagic pathway. On the other hand,

from 5 to 15 μM cisplatin, a strong enhancement of apoptosis and caspase 3 activation was associated with an increase in the LC3-II/I ratio and a decrease in p62 levels. Moreover, treatment of SCC4 cells with 5 μM cisplatin resulted in a noticeable autophagosome formation along with caspase 3 cleavage as early at 24 h, although a small increase in the apoptotic rate was observed by flow cytometric analysis already at 16 h. Both autophagy and apoptosis substantially and significantly increased at 48 h treatment with cisplatin.

Given that cisplatin induced both autophagy and apoptosis in OSCC cell lines, investigation into the role of cisplatin-induced autophagy was next undertaken. As previously discussed, the role of autophagy in cancer remains highly controversial. It can act as a pro-tumour mechanism that allows cells to adapt to stressful conditions, or as an anti-tumour mechanism leading to cell death [375]. Likewise, this dual role of autophagy has been reported in autophagy induced by treatment with chemotherapeutics in various types of cancer [189]. The pro-survival effect of autophagy has been demonstrated in colorectal cancer cells treated with 5-fluorouracil, in hepatocellular carcinoma cells treated with sorafenib and in breast cancer cells treated with epirubicin [201, 376, 377]. On the other hand, the pro-death effect of autophagy has been reported in oral squamous cell carcinoma cells following treatment with curcumin and in glioma cells treated with imatinib or cannabinoids [295, 378, 379]. It has been suggested that this paradoxical role of autophagy may be dependent on the anti-cancer drug employed and the cancer type [189].

Autophagy induced specifically by cisplatin has been shown to exert a pro-survival role in several types of cancer, such as oesophageal cancer, breast cancer and cervical cancer [192, 380, 381]. The pro-tumour effect of autophagy in response to cisplatin has been associated with the acquisition of a resistant phenotype, as it represents a cell mechanism to adapt to stress conditions induced by the drug. In human non-small lung carcinoma cells, the reduced expression of BIRC5 gene and the concomitant overexpression of Beclin-1 have been linked to cisplatin resistance [382]. In ovarian cancer cells, inhibition of ERK has resulted in a decrease in cisplatin-induced autophagy leading to an increase in cisplatin-induced apoptosis [372]. In bladder cancer cells, pharmacological autophagy inhibitors and ATG7/ATG12 shRNAs significantly enhanced cytotoxicity of cisplatin [373]. Overall, these studies support the idea that cisplatin-induced autophagy contributes to chemoresistance and acts as a survival pathway in a wide range of malignancies.

Accordingly, the potential role of autophagy in chemoresistance indicates that the manipulation of the autophagic pathway can be used to develop more effective anti-cancer therapies. Thus, targeting autophagy has been proposed as novel strategy to bypass cisplatin resistance in many cancers, such as osteosarcoma, ovarian and lung cancer [372, 383, 384].

However, the role of autophagy in OSCC remains controversial, and whether autophagy inhibition may represent a strategy to overcome cisplatin resistance in this type of cancer has been poorly reported. In this study, the relationship between apoptosis and autophagy in response to cisplatin in OSCC was investigated by targeting autophagy at early and late stages of autophagic flux. Two pharmacological early stage autophagy inhibitors were used to block cisplatin-induced autophagy in OSCC cells: 3-methyladenine (3-MA) and SAR405. 3-MA is a pan-PI3K inhibitor, which targets both the class I and class III PI3K indiscriminately, while SAR405 selectively inhibits the PtdIns3K complex [385–387]. Interestingly, following autophagy analysis, a small enhancement of autophagy was observed when cells were treated with 3-MA alone compared to vehicle treated cells. Conversely, a slight but non-significant decrease in autophagy was found when 3-MA was applied to cisplatin treated cells compared to cells treated with cisplatin alone. A similar inconsistency has been reported by Wu *et al.,* who showed that 3-MA can promote autophagy when applied to cells alone for a long period in complete media, whilst it can inhibit autophagy induced by starvation for a short period [385]. This dual role of 3-MA has been linked to its mechanism of action, since it can initiate a transient suppression of class III PI3K (negative autophagy regulator) and a permanent suppression of class I PI3K (positive autophagy regulator) [385]. Moreover, the ability of 3-MA to bind indiscriminately to both class I and III PI3K and possibly other survival-related enzymes has been reported in various studies in the literature and this has been associated with autophagy activation rather than inhibition [388, 389]. For example, O'Donovan *et al.* have shown that treatment of cells with 3-MA did not inhibit autophagy but led to enhanced vesicle formation and LC3 accumulation in oesophageal cancer [389]. In contrast, a stronger inhibitory activity has been reported in the literature for SAR405, which was shown to prevent autophagy induced by starvation or AZD8055 (mTOR inhibitor) treatment in Hela cells by selectively inhibiting the catalytic activity of Vp34 [390]. Consistently, in the present study, SAR405 significantly reduced cisplatin-induced autophagy in SCC4 cells.

Following apoptotic analysis of OSCC cells treated with cisplatin in combination with the two early stage autophagy inhibitors, a slight but non-significant increase in cisplatin-induced apoptosis was found in SCC4 and SCC9 cells pre-treated with 3-MA, whilst conversely significantly reduced levels of apoptosis were detected when SCC4 and SCC9 cells were pre-treated with SAR405. Overall, these results showed a non-consistent effect of the two inhibitors on cisplatin-induced apoptosis in OSCC cells. Studies in the literature have reported an enhancement of cisplatin-induced apoptosis following treatment of cells with 3-MA in several cancers, including OSCC. For example, Zaho *et al.* have found that pre-treatment of CAL-27 cells with 3-MA resulted in enhanced cisplatin-induced apoptosis and caspase 3 activation in OSCC [290]. Likewise, in the same cell line, Lin *et a.l* have reported a reduced cell viability following treatment of cells with 3-MA in combination with cisplatin compared with cells treated with cisplatin alone [291]. In both studies, the authors proposed a pro-survival role for cisplatin-induced autophagy in OSCC and an involvement of autophagy in chemoresistance. In contrast with these findings, non-specific activity of 3-MA has also been proposed and linked to some off-target effects, including activation of several biological pathways such as glycogen metabolism, lysosomal acidification and endocytosis [141]. As a result of these reported off-target effects of 3-MA and the positive inhibitory activity of SAR405 on cisplatin-induced autophagy demonstrated in the present study, results herein obtained with SAR405 may be considered the more robust. Nevertheless, the protective effect observed on cisplatin-induced apoptosis following treatment of SCC4 and SCC9 cells with SAR405 was in contrast with studies reported in the literature. For example, SAR405 was shown to increase apoptosis and caspase 3/7 activity in breast cancer cells treated with lapatinib [391]. Similarly, SAR405 was shown to reduce cell viability in a panel of urothelial carcinoma cells treated with cisplatin [392].

Due to the inconsistent results obtained with the two early stage autophagy inhibitors, evaluation of targeting the later stages of autophagic flux in OSCC cells was performed. Chloroquine and bafilomycin-A1 were used as late stage autophagy inhibitors, since they both prevent the fusion of the autophagosome with the lysosome [341, 342]. Analysis of annexin V/PI stained OSCC cells treated with cisplatin alone or cisplatin in combination with chloroquine or bafilomycin-A1 showed an increase in the apoptotic rate when the autophagic flux was inhibited, indicating that targeting the late stages of the autophagy may sensitise OSCC cells to cisplatin treatment. This result was further confirmed by

western blot analysis through the evaluation of caspase 3 activation. Accordingly, the use of chloroquine and bafilomycin-A1 *in vitro* has been widely reported to enhance the cytotoxic effect of many drugs. For instance, targeting autophagy with chloroquine and bafiloycin-A1 has been shown to promote 5-fluorouracil-induced apoptosis in gallbladder carcinoma cells and gastric cancer cells, respectively [200, 393]. Moreover, inhibition of autophagy with chloroquine and bafilomycin-A1 have also been shown to sensitise cells to radiotherapy in ovarian and in breast cancer [394, 395]. Nevertheless, in the present study, results obtained using late stage autophagy inhibitors were shown to be in direct contrast with results obtained using the early stage autophagy inhibitor SAR405, suggesting that targeting different phases of the autophagic flux may determine different effects on cisplatin-induced apoptosis. In this regard, a recent paper has reported the effect of autophagy inhibition at different stages in glioblastoma (GBM) cells [396]. Similar to what has been found in the present study, inhibition of early steps of autophagy through Beclin-1 knockdown decreased the cytotoxic effect of arsenic trioxide (ATO) in GBM cell lines, whilst inhibition of autophagy flux at late stage using chloroquine enhanced ATO cytotoxicity. According to the authors, the opposing effects observed can be linked to the complex mechanism of crosstalk between the autophagic and the apoptotic pathways. In fact, it has been proposed that autophagosomes may represent a platform for caspase activation, thus inhibition of autophagy at early stages can induce a decrease in autophagosome formation and consequently reduce caspase activation and apoptosis [205, 235, 396]. In this regard, Young *et al.* demonstrated that caspase 8 can be activated in an autophagy-dependent manner by a death-inducing signalling complex (DISC)-like complex which assembles on autophagosomal membranes [397]. Given that, depletion of key autophagic genes such as p62 and ATG5 resulted in the suppression of the caspase 8/3 cascade in mouse embryonic fibroblasts (MEF) cell lines treated with the pan-sphingosine kinase inhibitor SKI-I [397]. Interestingly, in the same study, inhibition of autophagy using lysosomal inhibitors such as chloroquine and bafilomycin-A1 in combination with SKI-I enhanced caspase 3 activation, likely because of the decreased autophagosome turnover.

Besides caspase activation, autophagosome accumulation in response to autophagy inducers and inhibitors has also been linked to enhanced apoptosis through increased ROS generation which resulted in mitochondrial permeabilisation and eventual cell death [398]. In addition, other studies have reported that both chloroquine and bafilomycin

may sensitise breast and tongue carcinoma cells to chemotherapy through autophagy-independent mechanism(s) [399, 400]. For example, in mouse breast cancer cell lines, 67NR and 4T1, autophagy was induced by cisplatin and chloroquine decreased the viability of cells treated with this chemotherapeutic drug. However, this effect could not be mimicked with bafilomycin-A1, the other late stage autophagy inhibitor or with ATG12 or Beclin-1 knockdown, which both inhibit early steps of the autophagy process [399]. These researchers therefore proposed that although chloroquine might be helpful in combination with chemotherapeutic drugs, its sensitising effects can occur independently of autophagy inhibition.

In the present study, both chloroquine and balfilomycin-A1 elicited similar effects and sensitised OSCC cells to cisplatin. However, whether the effect of these inhibitors on cisplatin cytotoxicity depends on accumulation of autophagic vesicles or other autophagy-independent mechanisms is still not clear. Nevertheless, regardless of their mechanism of action, treatment with these two compounds may represent a new strategy to enhance the chemotherapy in OSCC and improve the clinical outcome of patients. To date, the use of bafilomycin-A1 in combination with anticancer drugs has been tested *in vitro* and *in vivo* in several cancers, including colorectal cancer, gastric cancer cells and breast cancer, whilst chloroquine has been tested in various clinical trials as potential adjuvant therapy for the treatment of brain cancer and glioblastoma [371, 401–405]. However, clinical trials using chloroquine so far only showed moderate beneficial effects accompanied by many side effects [144]. Accordingly, hydroxychloroquine (HCQ), a less toxic metabolite of chloroquine, has been utilised over chloroquine in numerous clinical trials [202, 406].

As contrasting results were obtained between early and late stage pharmacological autophagy inhibitors with respect to improving sensitivity of OSCC cells to cisplatin, genetic inhibition of autophagosome formation through ATG5 knockdown was herein employed. As previously mentioned, ATG5 is a key autophagic protein which takes part in the autophagosome formation by forming an autophagosome elongation complex (ATG5-12/16) necessary for LC3 lipidation [345]. Knockdown of ATG5 has been shown to block LC3 lipidation and inhibit autophagic flux in several studies [346–348]. Consistently, in the present study, suppression of ATG5 using RNA interference was shown to reduce the LC3-II/LC3-I ratio in SCC4 cells, indicating autophagy inhibition. Interestingly, a notable but non-significant decrease in the apoptotic rate was observed in

ATG5 knockdown cells compared to ATG5 wild type cells, suggesting that genetic inhibition of autophagy does not result in enhanced cell death in OSCC cells. Similarly, reduced sensitivity toward staurosporine and doxorubicin has been reported in the literature in ATG5-deficient HeLa and breast cancer MDA-MA-231 cells respectively [237]. Also, suppression of IFN-γ-induced cell death was observed following ATG5 knockdown in Hela cells [407]. All these findings support the hypothesis that targeting autophagy through ATG5 knockdown may result in reduced chemotherapy-induced cell death. In contrast with these data, a body of evidence has instead shown enhanced cell death following ATG5 suppression. For example, inhibition of autophagy by ATG5 siRNA was shown to promote cisplatin-induced apoptosis in human lung cancer cells [408]. Likewise, ATG5 knockdown was shown to enhance bufalin-induced apoptosis in human gastric cancer cells [409]. Intriguingly, Hollomon *et al.* have reported that autophagy inhibition through shRNA-mediated knockdown of ATG5 had an opposing effect on two osteosarcoma cell lines treated with camptothecin (CPT), a natural anticancer drug [410]. In this study, ATG5-deficient DLM8 cells treated with CPT displayed increased viability compared to the corresponding ATG5 wild type cells, whilst ATG5-deficient K7M3 cells treated with CPT showed reduced viability when compared to the corresponding ATG5 wild type cells. According to the authors, such inconsistency between the two cell lines may be linked to the higher basal levels of autophagy observed in the K7M3 cell line, which may correlate with an increased dependence on autophagy. In fact, suppression of autophagy in the K7M3 cell line also resulted in reduced metabolic activity and cell growth. It is important to also take into consideration the autophagy-independent role of many ATG proteins and their potential implication in apoptosis regulation. In this regard, it has been demonstrated that ATG5 can negatively regulate the extrinsic apoptosis pathway by interrupting the interaction between FADD and DISC. On the other hand, ATG5 can also positively regulate the intrinsic apoptotic pathway through a calpain-mediated ATG5 cleaved product which can translocate to the mitochondria promoting cytochrome c release and eventually cell death [346]. Additionally, some studies have recently reported that the activation of an ATG5-independent form of autophagy may occur in ATG5-deficient cells. In this scenario, a double knockdown of ATG5 in combination with other key autophagic proteins such as Beclin-1 would be required to ensure actual autophagy inhibition.

In conclusion, this chapter demonstrated the novel finding that both apoptosis and autophagy are activated in response to cisplatin in SCC4 and SCC9 cells. However, the role of cisplatin-induced autophagy in these cells still remains controversial. Autophagy inhibition using a specific early stage autophagy inhibitor SAR405 was shown to reduce the cytotoxic effect of cisplatin, suggesting that cisplatin-induced autophagy may not represent a protective mechanism in these OSCC cell lines, thus autophagy may not be involved in chemoresistance. This conclusion was supported by data showing that knockdown of a key autophagy protein, ATG5, which resulted in a failure of LC3 activation necessary during the autophagosome formation, did not significantly modulate sensitivity to cisplatin. In contrast, treatment of cells with two late stage autophagy inhibitors, chloroquine and bafilomycin-A1 were shown to significantly sensitise OSCC cells to cisplatin treatment. However, off-target, autophagic-independent effects of these inhibitors could not be ruled out. Given this, no firm conclusions could be drawn at this stage in respect of the role of autophagy in mediating chemoresistance in OSCC. Moreover, it must be considered that one of the weakness of this study is the limited number of cell lines employed. In fact, it is well known that cancer cells can genetically differ among patients but also within the same tumour specimen [411]. This inter/intra-tumour heterogeneity usually occurs as consequence of genetic mutations and environmental changes, and it can result in poor prognosis and treatment failure due to inadequate clues to predict the overall treatment response in genetically different cells [412]. Therefore, the use of only two OSCC cell lines in this study can raise some doubts on whether these cell lines may be truly representative of primary oral cancers and whether they may represent a good model to predict human responses. Although similar results were obtained in the two OSCC cell lines employed in this study, it must be highlighted that a greater number of oral cancer cell lines from various regions of the mouth should be considered for future work to increase the reliability of this pre-clinical study. Also, further analysis is required through the generation and the evaluation of a cisplatin-resistant OSCC cell line. Additionally, results presented in this chapter warranted further study into the crosstalk between apoptotic and autophagic pathways in OSCC.

4. Investigation into the signalling pathway(s) underlying cisplatin-induced apoptosis and autophagy

4.1. Introduction

Cisplatin is considered one of the most effective drugs used in chemotherapy and it represents a first-line therapy for several cancers, including lung, breast, brain and head and neck cancers [323]. Over the past 50 years, the mechanism of action of cisplatin and the signalling pathways implicated in its cytotoxicity have been widely investigated. DNA has been identified as the main target of cisplatin [323]. In fact, it has been demonstrated that cisplatin can bind to the N7 reactive centre on purine residues, forming 1,2 or 1,3 intra- and inter-strand cross links with DNA [321]. Formation of DNA adducts results in DNA damage and consequentially in inhibition of DNA replication, cell cycle arrest and cell death [322]. The ability of cisplatin to induce DNA damage has been considered the primary mechanism implicated in its cytotoxicity [323]. This has been confirmed by several studies which demonstrated the high sensitivity to cisplatin of cells deficient in DNA repair [323, 413, 414]. Moreover, DNA damage in response to cisplatin has been associated with induction of apoptosis [415]. In fact, formation of DNA adducts leads to genotoxic stress and the consequential cellular response, consisting of the activation of DNA damage recognition proteins and in the transmission of DNA damage signals to downstream effectors, such as p53, mitogen-activated protein kinase (MAPK) and p73, which ultimately induce apoptosis through both the intrinsic and extrinsic pathways [415].

Apart from genotoxic stress, cisplatin cytotoxicity has also been associated with oxidative stress [416]. In fact, it has been proposed that exposure to cisplatin can also lead to the disruption of essential mitochondrial functions, including reduction of mitochondrial protein synthesis and impairment of the electron transport chain, resulting in the consequent enhancement of ROS generation [417]. Even though low levels of ROS are physiologically produced to maintain cell homeostasis, intracellular accumulation of ROS can result in oxidative stress and cytotoxicity. In this context, oxidative stress represents an imbalance in the cellular redox state caused by intracellular accumulation of ROS, likely due to the failure of antioxidant defence systems to counteract them [248]. Cisplatin-induced oxidative stress has been linked to the ability of cisplatin to enhance ROS formation, but also to its capacity of interacting with thiol proteins, such as glutathione [418, 419]. Glutathione is one of the major antioxidant systems within cells and it can exist in a reduced (GSH) or oxidised form (GSSG). Oxidation of glutathione is important for ROS reduction and neutralisation [420]. The ability of cisplatin to bind the

thiol group of GSH results in depletion of glutathione, which consequentially leads to intracellular ROS accumulation [323, 421, 422]. Once accumulated in cells, ROS can induce oxidative damage, which includes damage to several cellular components such as proteins, DNA and lipids resulting in cell death [423]. In this regard, several papers have reported activation of both the intrinsic and extrinsic apoptotic pathways in response to cisplatin-induced ROS [265].

The cisplatin mechanisms of action so far reported can result in apoptotic cell death through activation of multiple transduction pathways. Among them, it is worth mentioning the stress-induced MAPK pathway. MAPKs are a family of serine/threonine protein kinases which regulate fundamental cellular processes involved in cell growth, differentiation and survival. The MAPK protein family includes three major groups of enzymes: the extracellular signal-related kinases (ERKs), the c-Jun N-terminal kinases (JNKs), and the p38 kinases. Even though ERK (ERK1/2) has been generally recognised as a cell survival regulator, several studies have shown that cisplatin-induced ERK activation can lead to p53 phosphorylation, which in turn regulates the expression of apoptotic genes, such as the pro-apoptotic Bax, resulting in apoptotic cell death [424, 425]. Moreover, activation of JNK (JNK1/2) and p38 in response to cisplatin-induced stress has also been linked to apoptosis induction, through the activation of transcription factors and proteins involved in the apoptotic pathways, including ATF2, Elk1, p53, c-Jun, MEF-2C, p73 and p18 [425–428].

Interestingly, activation of the MAPK signalling pathway has also been implicated in autophagy induction. In this regard, a role for ERK and p38 in the regulation of autophagy at maturation stage has been proposed, whilst a role for JNK has been reported in ATG gene expression regulation [429, 430]. As mentioned above, autophagy can be activated as a stress response mechanism following exposure to chemotherapeutics. Autophagy activation in response to cisplatin has been extensively reported in several cancers, although its role still remains controversial. The potential implication of common regulatory pathways in both apoptosis and autophagy induction have suggested a tight correlation between these two processes. In this regard, a key role for JNK has been proposed. In fact, it has been reported that JNK can mediate both apoptosis and autophagy activation by regulating the interplay between Bcl-2 and Beclin-1 [430]. The Beclin-1/Bcl-2 complex represents a crucial node in the crosstalk between apoptosis and autophagy. Activation of JNK has been shown to promote Bcl-2 phosphorylation, leading

to its dissociation from Beclin-1. Release of Beclin-1 from the Beclin-1/Bcl-2 complex has been associated with autophagy induction, whilst JNK-induced phosphorylation of Bcl-2 has been correlated to apoptosis activation through the mitochondrial apoptotic pathway [215].

The last chapter demonstrated that both apoptosis and autophagy are activated concomitantly in response to cisplatin treatment in OSCC cells. A complex crosstalk between these two pathways has already been demonstrated in many cancerous cell types but further analysis is required in OSCC. Therefore, the aim of this chapter was to examine the relationship between cisplatin-induced apoptosis and autophagy in OSCC cells and to evaluate the molecular mechanisms underlying cisplatin-induced cytotoxicity in OSCC. In particular, the role of oxidative stress and the involvement of the JNK signalling pathway in apoptosis and autophagy in response to cisplatin were herein investigated.

4.2. Results

4.2.1. Cisplatin induces intracellular ROS generation in OSCC cell lines

Flow cytometric analysis of H_2DCFDA stained cells was employed to examine the levels of intracellular ROS generated in response to cisplatin treatment in OSCC cell lines. The H_2DCFDA or 2',7'-dichlorodihydrofluorescein-diacetate is a cell permeant dye widely used to detect ROS accumulation within cells [431]. After its diffusion into cells, cleavage of the two acetate groups by the intracellular esterase leads to the conversion of H_2DCFDA, a non-fluorescent compound, which can be then oxidised by ROS into 2',7'-dichlorofluorescein or DCF. Since DCF is highly florescent, the acquisition of fluorescence intensity through flow cytometry can be used as an indicator of ROS levels in cells.

The validity of this assay was first established using menadione, a well-known ROS inducer. Menadione, or vitamin K_3, is a redox cycling quinone recently used as chemotherapeutic agent for the treatment of several cancers [432]. The potent cytotoxic activity of menadione has been linked to its ability to induce ROS [433]. In fact, the naturally reductive environment of cells leads to the reduction of menadione to semiquinone radicals, which can induce the Fenton reaction resulting in ROS production [434]. Levels of ROS in response to menadione were assessed in OSCC cell lines through flow cytometric analysis of H_2DCFDA stained cells in order to demonstrate the specificity of the dye to ROS and the ability of cells to accumulate intracellular ROS. SCC4 cells were treated with vehicle (0.1% (v/v) DMSO) or with menadione 50 μM for 2 h. Cells were then stained with the H_2DCFDA dye and analysed on the BD Accuri cytometer. As shown in Figure 4.1, a notable shift to the right of the fluorescence peak was observed in menadione treated cells compared to vehicle cells, indicating a statistically significant increase in ROS levels after treatment with menadione. This result validates the specificity of the assay.

Levels of intracellular ROS were then examined in OSCC cells in response to cisplatin treatment. SCC4 and SCC9 cells were treated with 5 μM and 25 μM cisplatin respectively for 48 h. Cells were then stained with the H_2DCFDA dye and analysed on the BD Accuri flow cytometer. Both SCC4 and SCC9 cells treated with cisplatin showed a statistically significant increase in ROS production compared to vehicle treated cells (Figure 4.2,

Figure A.5). Moreover, a 2.7 fold difference in ROS generation between vehicle and cisplatin treated cells was found in the SCC4 cell line, while a 2.0 fold difference was detected in the SCC9 cell line. These results suggest that treatment with cisplatin promotes ROS accumulation in OSCC cells. Also, although a lower concentration of cisplatin was used in SCC4 cells, a marked increase in ROS levels was observed in this cell line compared to the SCC9 cell line, suggesting a potential correlation between ROS accumulation and sensitivity to cisplatin.

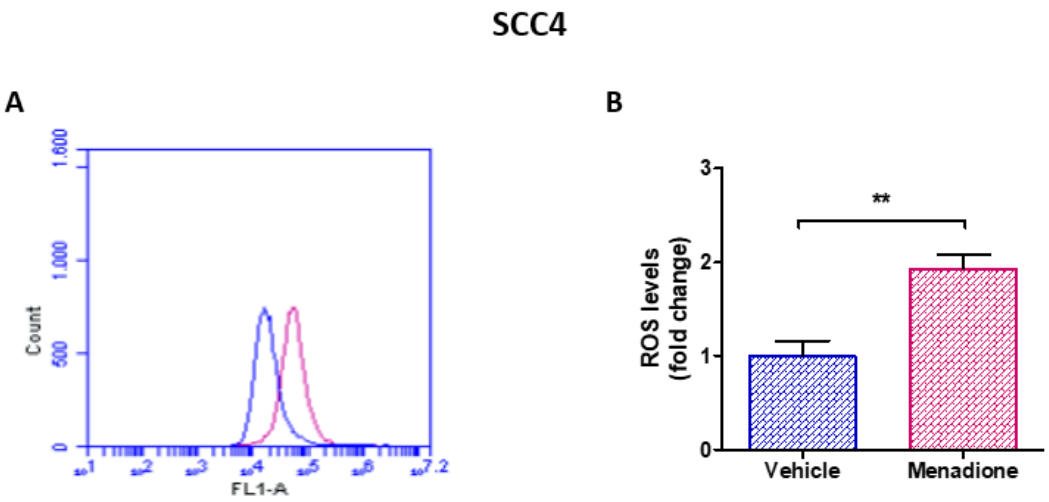

Figure 4.1 Validation of the H2DCFDA assay in SCC4 cells.

SCC4 cells were seeded at $150x10^3$ cells/well in 6 well plates. Cells were left for 24 h to adhere to the plate and then were treated with the vehicle (0.1% (v/v) DMSO) or with menadione 50 μM for 2 h. After incubation, 10 μM of H_2DCFDA dye was added to each well for 30 min. Cells were then harvested and analysed on the flow BD FACS Accuri cytometer. 10,000 single cells were gated on vehicle treated cells and the median fluorescence intensity (MFI) was acquired. **A**. Representative flow cytometric histogram of vehicle and menadione treated cells. **B**. Bar graph of the ROS levels in vehicle and menadione treated cells. MFI values of menadione treated cells were normalised by MFI values of vehicle treated cells to determine the fold change in ROS levels. Values represent the mean ±S.E.M. of three independent experiments. Statistical analysis was performed using an unpaired two-tailed student t-test to compare mean values between vehicle and treated cells (Graphpad Prism 5). ** $p<0.01$.

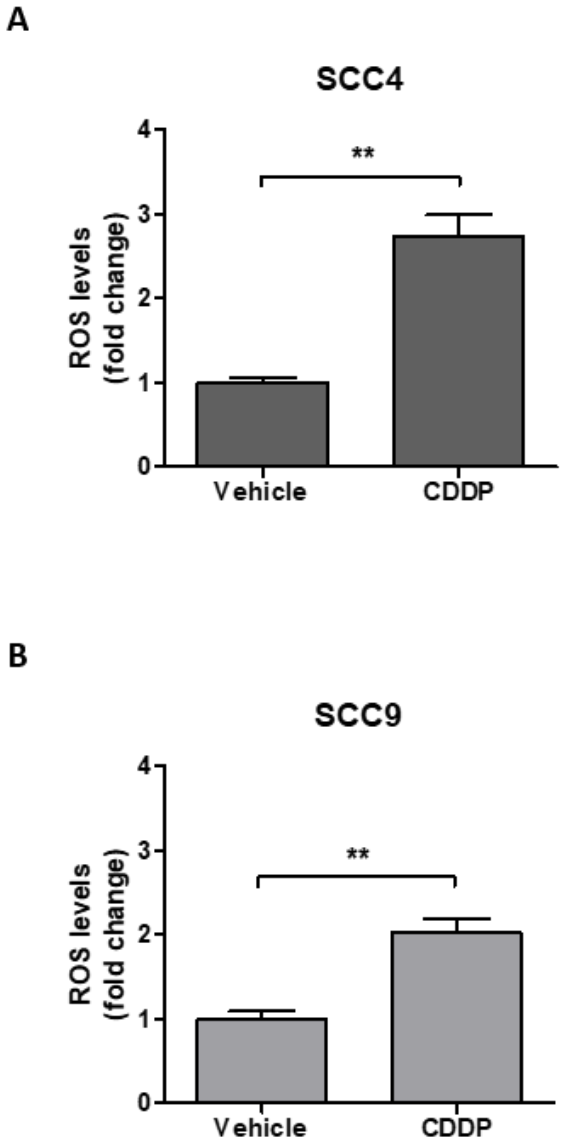

Figure 4.2 Cisplatin induces intracellular ROS generation in OSCC cell lines.

OSCC cells were seeded at $150x10^3$ cells/well in 6 well plates. Cells were left for 24 h to adhere to the plate and then were treated with the vehicle (0.009% (v/v) NaCl) or with cisplatin (CDDP) (5 μM and 25 μM in SCC4 (**A**) and SCC9 (**B**) cells respectively). After 48 h, 10 μM H_2DCFDA dye was added to each well for 30 min. Cells were then harvested and analysed on the flow BD FACS Accuri cytometer. 10,000 single cells were gated on vehicle treated cells and the median fluorescence intensity (MFI) was acquired. MFI values of cisplatin treated cells were normalised by MFI values of vehicle treated cells to determine the fold change in ROS levels. Values represent the mean ±S.E.M. of three independent experiments. Statistical analysis was performed using an unpaired two-tailed student t-test to compare mean values between vehicle and treated cells (Graphpad Prism 5). ** $p<0.01$.

4.2.2. Cisplatin induces oxidative stress in OSCC cell lines

Oxidative stress is defined as the imbalance between ROS generation and antioxidant capacity [248]. In order to determine whether ROS accumulation in response to cisplatin was associated with oxidative stress, the antioxidant capacity of OSCC cells treated with cisplatin was evaluated. It has been reported that glutathione is one of the main antioxidative systems within cells and it can exist in a reduced (GSH) or oxidised (GSSG) form [420]. In oxidant conditions, GSH is converted to GSSG by the glutathione peroxidase, whilst in reduced conditions, glutathione transferase can reduce GSSG to again form GSH. Thus, the conversion of GSH to GSSG is generally considered a good marker for oxidative stress [255].

The GSH/GSSG kit was employed to evaluate the levels of GSH and GSSG in OSCC cells following treatment with cisplatin. This assay utilises a luciferin-based reaction where a GSH probe, Luciferin-NT, is converted to luciferin by a glutathione transferase enzyme in the presence of GSH. Light from luciferase depends on the amount of luciferin formed, which in turn depends on the amount of GSH present. Thus, the luminescent signal is proportional to the amount of GSH. As shown in the Materials and Methods (Figure 2.8), conversion of GSSG to GSH allows the determination of total glutathione (GSH+GSSG) levels within cells, whilst conversion of GSSG to GSH along with a block in endogenous GSH allows the quantification of only GSSG. Determination of the GSH/GSSG ratio is indicative of the conversion of GSH to GSSG, thus is an indicator of oxidative stress [255, 435].

SCC4 and SCC9 cells were treated with 5 μM and 25 μM cisplatin respectively for 48 h. Cells were then analysed with the GSH/GSSG kit and luminescence intensity was detected using the SpectraMax Gemini EM Microplate Reader. A marked and statistically significant reduction of the GSH/GSSG ratio in response to cisplatin was observed in the SCC4 cell line, whilst a more modest reduction was found in the SCC9 cell line (Figure 4.3). Taken together, these results suggest a conversion of GSH to GSSG following treatment with cisplatin in both cell lines, with a marked conversion observed in the SCC4 cell line. This may imply that cisplatin induces oxidative stress in OSCC cells likely as a consequence of ROS accumulation.

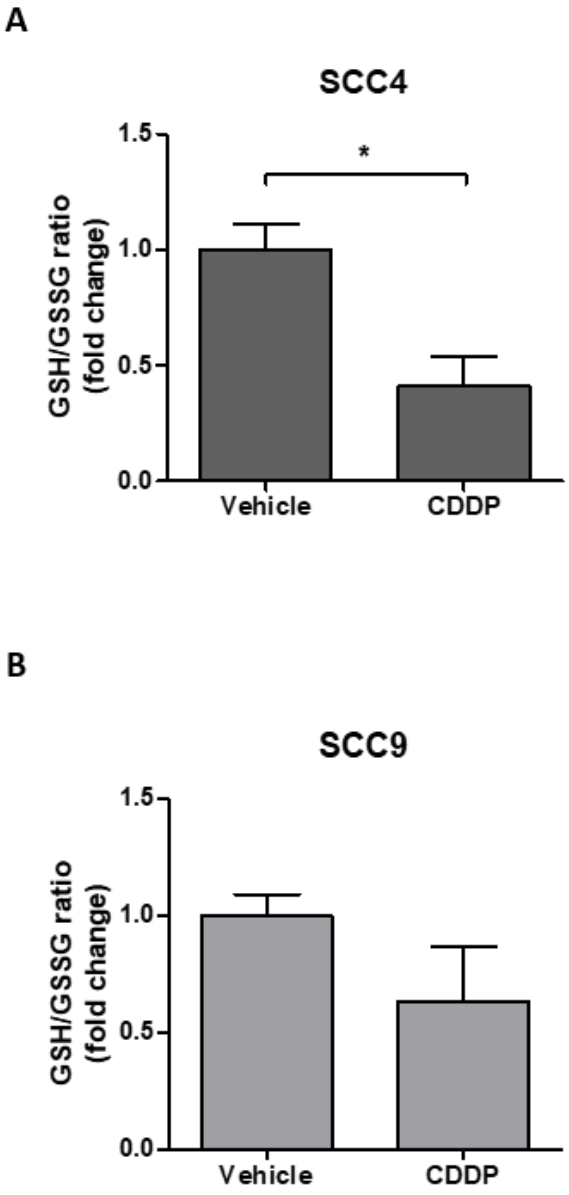

Figure 4.3 Treatment with cisplatin significantly decreases the GSH/GSSG ratio in SCC4 cells.
OSCC cells were seeded at $5x10^3$ cells/well in 96 well plates. Cells were left for 24 h to adhere to the plate and then were treated with the vehicle (0.009% (v/v) NaCl) or with cisplatin (CDDP) (5 μM and 25 μM in SCC4 (**A**) and SCC9 (**B**) cells respectively). After 48 h, cells were analysed using the GSH/GSSG kit and luminescence was measured on the SpectraMax Gemini EM Microplate Reader. GSH/GSSG ratio was calculated and values obtained from cisplatin treated cells were normalised by values obtained from vehicle cells to determine the fold difference in the GSH/GSSG ratio. Values represent the mean ± S.E.M. of three independent experiments. Statistical analysis was performed using an unpaired two-tailed student t-test to compare mean values between vehicle and treated cells (Graphpad Prism 5). * $p<0.05$.

4.2.3. The antioxidant N-acetyl cysteine abrogates cisplatin-induced oxidative stress by suppressing ROS in OSCC cell lines

In order to evaluate the role of cisplatin-induced oxidative stress in OSCC, the antioxidant N-acetyl cysteine (NAC) was employed. NAC is an aminothiol and synthetic precursor of intracellular cysteine and glutathione which can promote cell detoxification. It has been reported that the antioxidant activity of NAC can be correlated to its ROS scavenging property and as well to its ability of increasing intracellular GSH levels [436].

The antioxidant potential of NAC was firstly evaluated by assessing the GSH/GSSG ratio in SCC4 cells treated with NAC (5 mM) alone, cisplatin (5 μM) alone, or pre-treated with NAC for 1 h before adding cisplatin. After 48 h, cells were analysed with the GSH/GSSG kit and luminescence intensity was detected using the SpectraMax Gemini EM Microplate Reader. As expected, a decrease in the GSH/GSSG ratio was observed in SCC4 cells treated with cisplatin alone compared to control cells, whilst no difference in the GSH/GSSG ratio was found in SCC4 cells treated with NAC alone compared to control cells (Figure 4.4). Moreover, an increase in the GSH/GSSG ratio was displayed in SCC4 treated with cisplatin in combination with NAC compared to cells treated only with cisplatin. Although not significant, this result may suggest that NAC can reduce cisplatin-induced oxidative stress in OSCC cells.

Furthermore, to investigate the ROS scavenging property of NAC, ROS levels were examined by flow cytometric analysis of H_2DCFDA stained cells. OSCC cells were pre-treated with NAC (5 mM) for 1 h before adding cisplatin 5 μM or 25 μM in SCC4 or in SCC9 cells respectively. In Figure 4.5, Figure A.6, treatment with cisplatin increased ROS levels in both cell lines, as expected. Moreover, pre-treatment of cells with NAC significantly reduced cisplatin-induced ROS generation in both SCC4 and SCC9 cell lines, suggesting that NAC exerts its antioxidant activity by acting as a ROS scavenger.

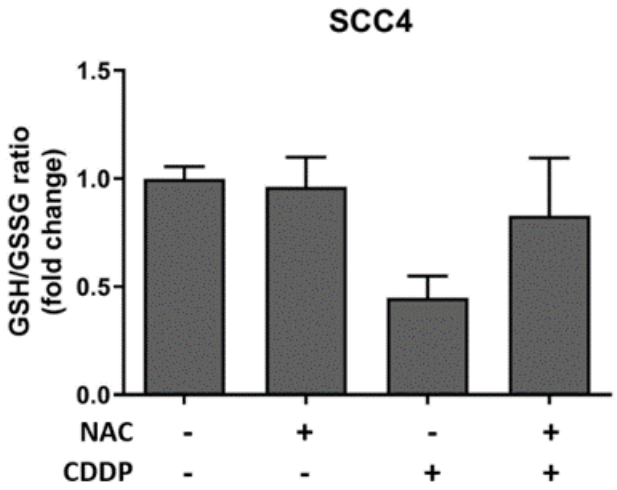

Figure 4.4 Pre-treatment with N-acetyl cysteine increases the GSH/GSSG ratio of SCC4 cells treated with cisplatin.

SCC4 cells were seeded at $5x10^3$ cells/well in 96 well plates. Cells were left for 24 h to adhere to the plate and then were treated with the vehicle (0.009% (v/v) NaCl), 5 mM NAC alone, 5 μM cisplatin (CDDP) alone or cisplatin in combination with NAC. After 48 h, cells were analysed using the GSH/GSSG kit and luminescence was measured on the SpectraMax Gemini EM Microplate Reader. GSH/GSSG ratio was calculated and values obtained from treated cells were normalised by values obtained from vehicle cells to determine the fold difference in the GSH/GSSG ratio. Values represent the mean ± S.E.M. of three independent experiments. Statistical analysis was performed using one-way ANOVA with Tukey's Multiple Comparison Test (Graphpad Prism 5).

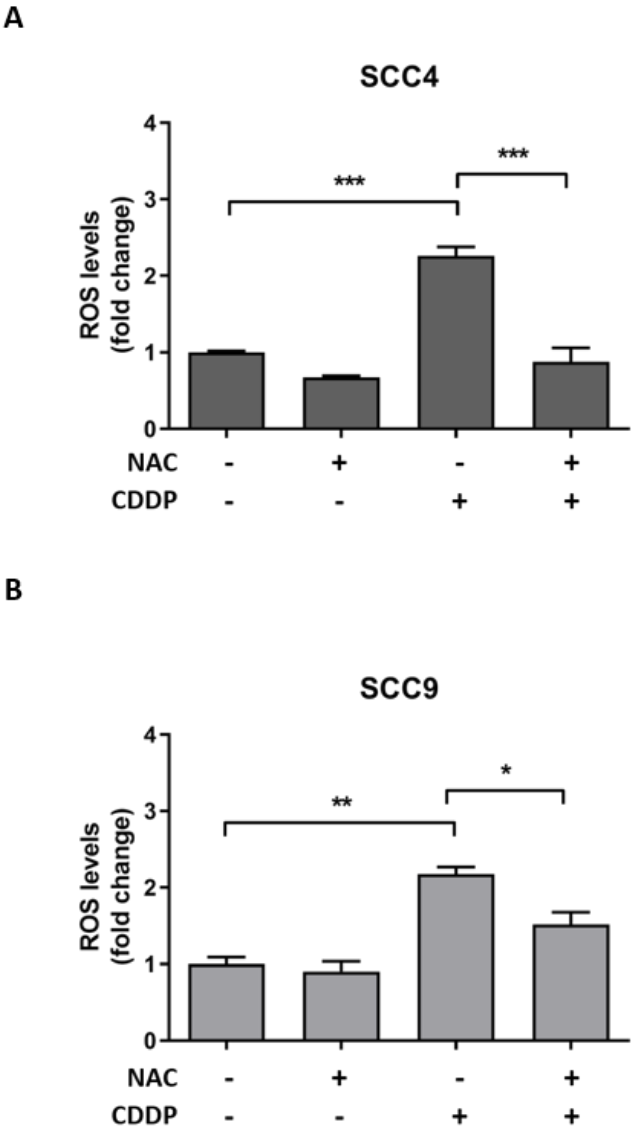

Figure 4.5 Pre-treatment with N-acetyl cysteine suppresses cisplatin-induced ROS in OSCC cell lines. OSCC cells were seeded at $150x10^3$ cells/well in 6 well plates. Cells were left for 24 h to adhere to the plate and then were treated with vehicle (0.009% (v/v) NaCl), NAC alone (5mM), cisplatin (CDDP) (5 μM or 25 μM in SCC4 (**A**) and SCC9 (**B**) cells respectively) or cisplatin in combination with NAC. After 48 h, 10 μM H_2DCFDA dye was added to each well for 30 min. Cells were then harvested and analysed on the flow BD FACS Accuri cytometer. 10,000 single cells were gated on vehicle treated cells and the median fluorescence intensity (MFI) was acquired. MFI values of treated cells were normalised by MFI values of vehicle cells to determine the fold change in ROS levels. Values represent the mean ± S.E.M. of three independent experiments. Statistical analysis was performed using one-way ANOVA with Tukey's Multiple Comparison Test (Graphpad Prism 5). *** $p<0.001$, ** $p<0.01$, * $p<0.05$.

4.2.4. Cisplatin-induced oxidative stress plays a role in cisplatin-induced cytotoxicity in OSCC

Results obtained in Figures 4.2 and 4.3 above showed a higher ROS generation and lower GSH/GSSG ratio in the SCC4 cell line treated with cisplatin compared to the SCC9 cell line. The differential sensitivity of the two cell lines to cisplatin suggested a potential implication of oxidative stress in cisplatin-induced cytotoxicity. The correlation between cisplatin-induced oxidative stress and cisplatin cytotoxicity was next investigated through evaluation of cell viability of OSCC cells treated with cisplatin alone or in combination with the antioxidant NAC.

SCC4 and SCC9 cells were treated with cisplatin (5 μM or 25 μM respectively) alone, NAC (5 mM) alone or cisplatin in combination with NAC for 48 h. Alamar blue assay was performed to determine cell viability. As expected, a decrease in cell viability was displayed in cisplatin treated cells compared to control treated cells in both cell lines (Figure 4.6). Moreover, cells treated with cisplatin in combination with NAC showed a statistically significant increase in cell viability compared to cisplatin treated cells, suggesting that pre-treatment with NAC somewhat protects OSCC cells against cisplatin-induced reduction of viability. This result suggests that oxidative stress may play a role in cisplatin-induced cytotoxicity in OSCC.

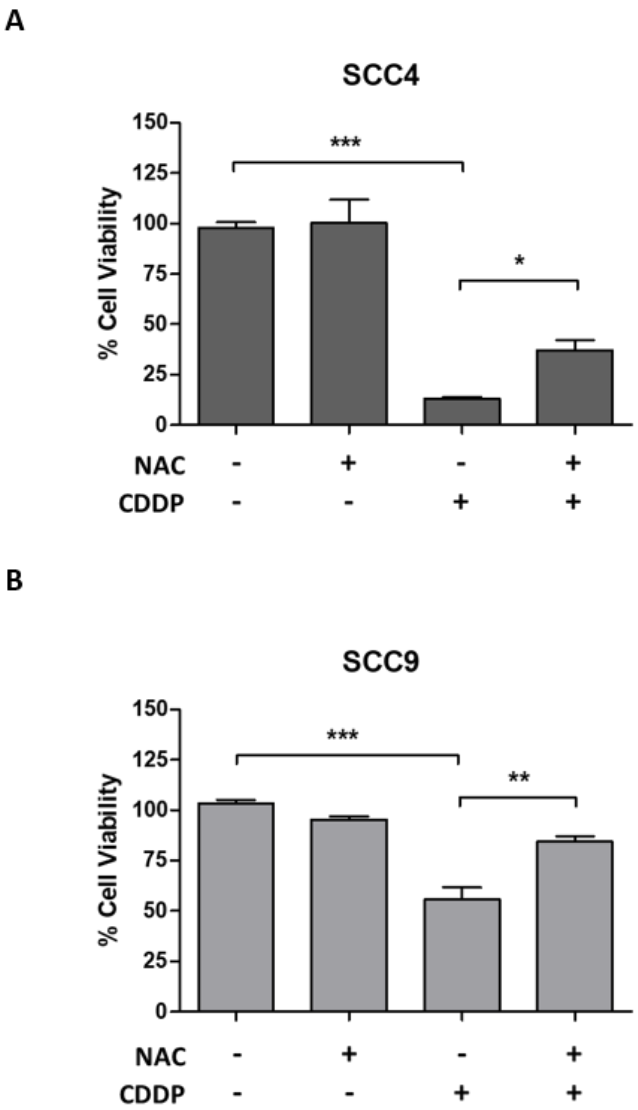

Figure 4.6 Pre-treatment with N-acetyl cysteine partially protects against cisplatin-induced reduction in OSCC cell viability.

OSCC cells were seeded at $150x10^3$ cells/well in 6 well plates. Cells were left for 24 h to adhere to the plate and then were treated with the vehicle (0.009% (v/v) NaCl), NAC alone (5mM), cisplatin (CDDP) (5 μM or 25 μM in SCC4 (**A**) and SCC9 (**B**) cells respectively) or cisplatin in combination with NAC. Alamar blue (10% (v/v)) was added to each well 6 h before the end of the treatment and plates were kept in the dark at 37°C. Fluorescence was measured on the SpectraMax Gemini EM Microplate Reader at an excitation wavelength of 544 nm and an emission wavelength of 590 nm. Values represent the mean ± S.E.M. of three independent experiments. Statistical analysis was performed using one-way ANOVA with Tukey's Multiple Comparison Test (Graphpad Prism 5). *** $p<0.001$, ** $p<0.01$, * $p<0.05$.

4.2.5. The antioxidant N-acetyl cysteine abrogates cisplatin-induced apoptosis and autophagy in OSCC cell lines

Several studies have implicated ROS in various signalling pathways regulating cell survival and cell death [437]. Thus, the role of oxidative stress in cisplatin-induced apoptosis and autophagy was next examined in OSCC cell lines.

Firstly, the role of oxidative stress was examined in cisplatin-induced apoptosis in SCC4 and SCC9 cell lines by flow cytometric analysis of annexin V/PI stained cells. OSCC cells were treated with cisplatin alone (5 μM or 25 μM in SCC4 and SCC9 cells, respectively), 5 mM NAC alone or cisplatin in combination with NAC. Cells were then double stained with annexin V-FITC and PI, and the percentage of cells in early and late apoptosis was acquired using the BD Accuri software. A substantial decrease in the apoptotic rate was observed in SCC4 and SCC9 cells treated with cisplatin in combination with NAC compared to cells treated with cisplatin alone, suggesting that NAC inhibits cisplatin-induced apoptosis in OSCC cell lines (Figures 4.7-8). This result was then confirmed through the evaluation of caspase 3 activation in the SCC4 cell line. Cells were treated as described above and the expression of caspase 3 and cleaved caspase 3 was determined by western blot analysis. As shown in Figure 4.9, pre-treatment with NAC reduced caspase 3 activation in SCC4 cells treated with cisplatin, resulting in an increase in the full-length caspase 3 form and a concurrent decrease in the cleaved caspase 3 form. This result correlates with the flow cytometric analysis, suggesting a role for ROS in cisplatin-induced apoptosis.

Secondly, the role of ROS in cisplatin-induced autophagy was also investigated in SCC4 cells. Cells were treated with cisplatin alone or pre-treated with NAC for 1 h before adding cisplatin and the expression of p62 and LC3-I/II was determined by western blot analysis. EBSS treated cells (4 h) were used as a positive control for autophagy induction. Results in Figure 4.10 showed that pre-treatment with NAC inhibited cisplatin-induced autophagy, resulting in a significant decrease in the LC3-II/LC3-I ratio and a marked increase in p62 protein expression in SCC4 cells treated with cisplatin in combination with NAC compared to cells treated with cisplatin alone.

In conclusion, these data suggest that ROS may mediate both cisplatin-induced apoptosis and autophagy in OSCC cell lines.

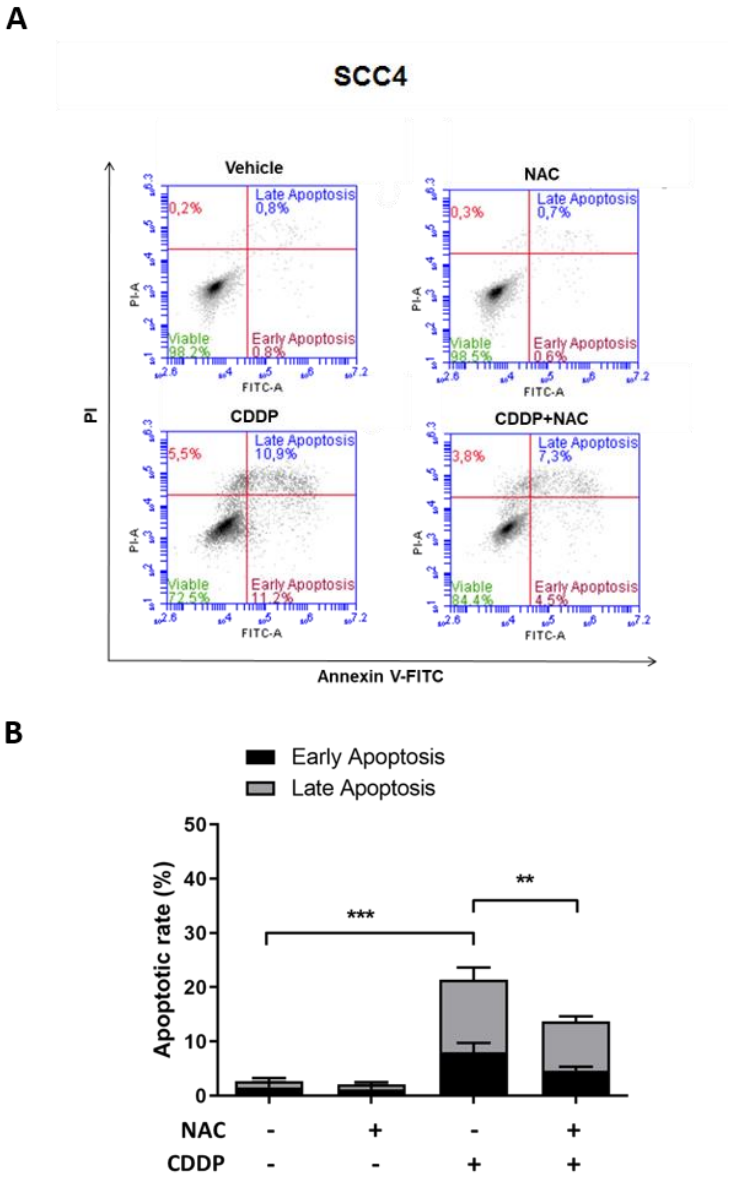

Figure 4.7 Pre-treatment with N-acetyl cysteine partially protects against cisplatin-induced apoptosis in SCC4 cells.

SCC4 cells were seeded at 150x10^3 cells/well in 6 well plates. Cells were left for 24 h to adhere to the plate and then were treated with vehicle (0.009% (v/v) NaCl), 5 mM NAC alone, 5 μM cisplatin (CDDP) alone or cisplatin in combination with NAC. After 48 h, cells were harvested, and double stained with annexin V/PI. Cells were then analysed by flow cytometry using BD FACS Accuri software. 10,000 single cells were gated on vehicle treated cells and the percentage of cells undergoing early and late apoptosis was acquired. **A**. Representative dot plot of treated cells. **B**. Values represent the mean ± S.E.M of three independent experiments. Statistical analysis was performed using one-way ANOVA with Tukey's Multiple Comparison Test (Graphpad Prism 5). *** $p<0.001$, ** $p<0.01$.

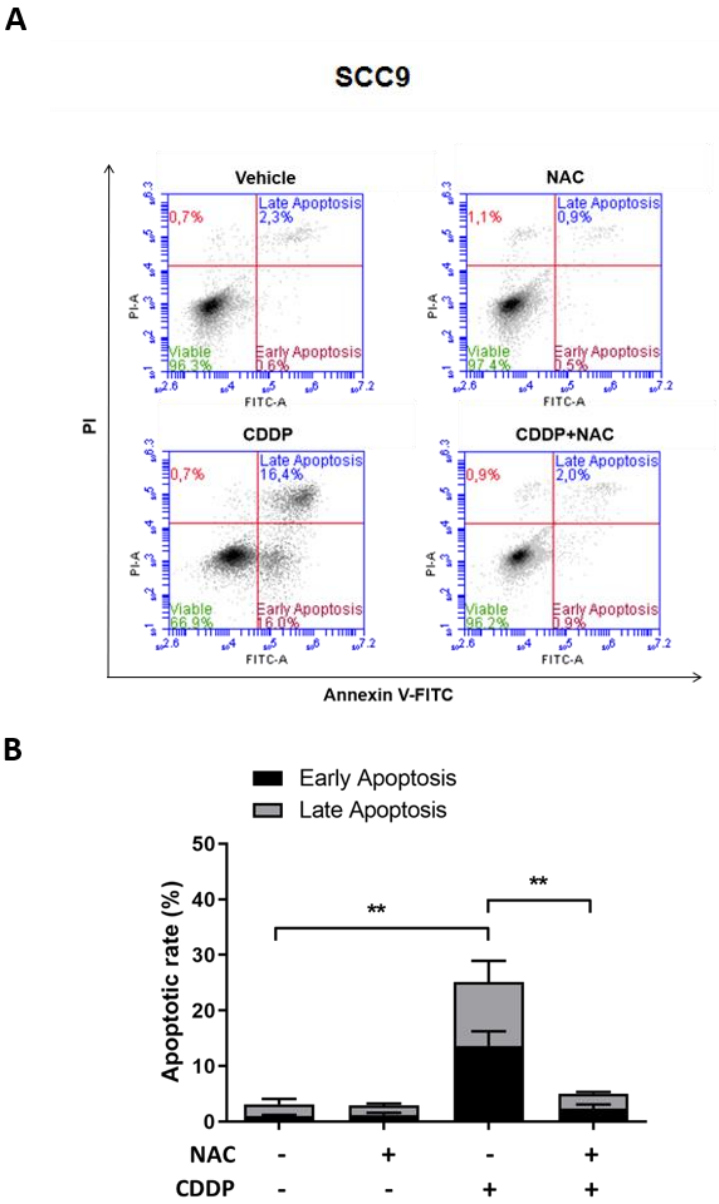

Figure 4.8 Re-treatment with N-acetyl cysteine protects against cisplatin-induced apoptosis in SCC9 cells.

SCC9 cells were seeded at $150x10^3$ cells/well in 6 well plates. Cells were left for 24 h to adhere to the plate and then were treated with vehicle (0.009% (v/v) NaCl), 5 mM NAC alone, 25 μM cisplatin (CDDP) alone or cisplatin in combination with NAC. After 48 h, cells were harvested, and double stained with annexin V/PI. Cells were then analysed by flow cytometry using BD FACS Accuri software. 10,000 single cells were gated on vehicle treated cells and the percentage of cells undergoing early and late apoptosis was acquired. **A**. Representative dot plot of treated cells. **B**. Values represent the mean ± S.E.M of three independent experiments. Statistical analysis was performed using one-way ANOVA with Tukey's Multiple Comparison Test (Graphpad Prism 5). ** $p<0.01$.

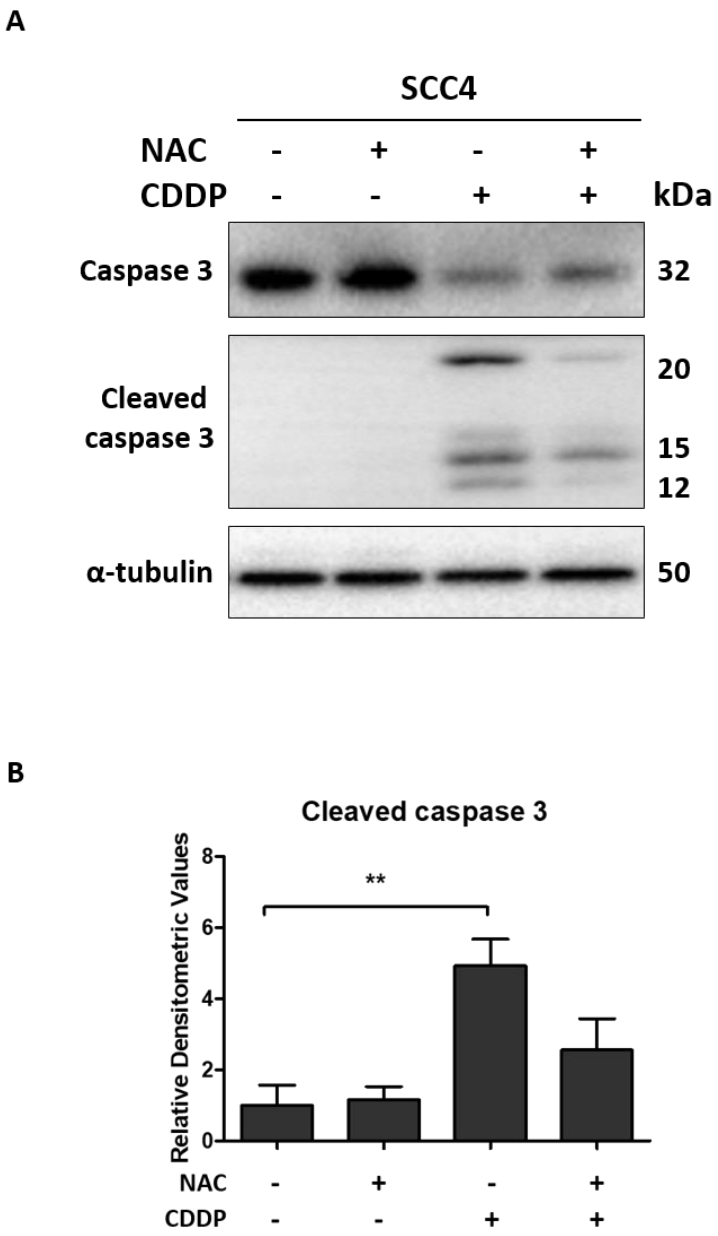

Figure 4.9 N-acetyl cysteine partially inhibits caspase 3 activation in the SCC4 cell line treated with cisplatin.

SCC4 cells were seeded at $300x10^3$ cells/flask. Cells were left for 24 h to adhere to the flask and then were treated with vehicle (0.009% (v/v) NaCl), 5mM NAC alone, 5 μM cisplatin (CDDP) alone or cisplatin in combination NAC for 48 h. After incubation, cells were lysed and 20 μg of protein was loaded and separated on a 12% SDS-PAGE gel and transferred to a PVDF membrane. **A**. Membranes were probed with anti-caspase 3 and anti-cleaved caspase 3. α-Tubulin served as loading control. **B**. Densitometric analysis of cleaved caspase 3 bands was performed using ImageLab software and values were normalised by the loading control and the vehicle. Values represent the mean ± S.E.M of three independent experiments Statistical analysis was performed using one-way ANOVA with Tukey's Multiple Comparison Test (Graphpad Prism 5). ** $p<0.01$.

A

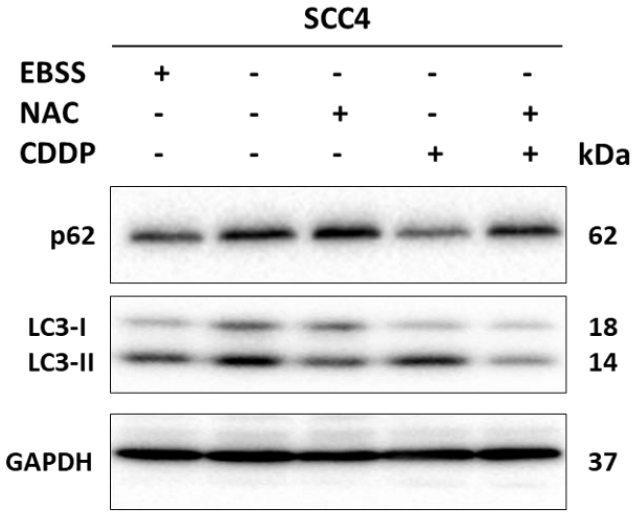

B

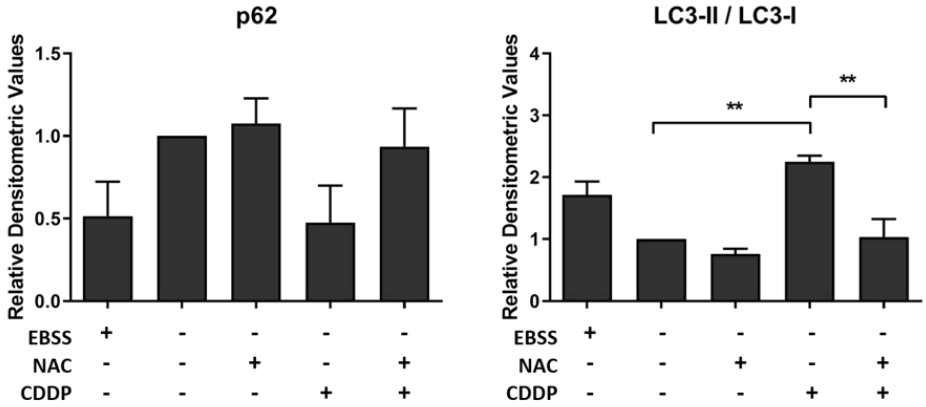

Figure 4.10 N-acetyl cysteine inhibits autophagy in the SCC4 cell line treated with cisplatin.

SCC4 cells were seeded at 300 x10^3 cells/flask. Cells were left for 24 h to adhere to the flask and then were treated with vehicle (0.009% (v/v) NaCl), 5mM NAC alone, 5 μM cisplatin (CDDP) alone or cisplatin in combination NAC for 48 h. EBSS for 4 h was used as a positive control for autophagy induction. After incubation, cells were lysed and 20 μg of protein was loaded and separated on a 15% SDS-PAGE gel and transferred to a PVDF membrane. **A**. Membranes were probed with p62 and LC3-I/II antibodies. GAPDH served as loading control. **B**. Densitometric analysis of p62 and LC3-I/II bands was performed using ImageLab software and values were normalised by the loading control and the vehicle. Values represent the mean ± S.E.M of three independent experiments. Statistical analysis was performed using one-way ANOVA with Tukey's Multiple Comparison Test (Graphpad Prism 5). ** $p<0.01$.

4.2.6. Cisplatin induces activation of JNK signalling through ROS generation in OSCC cell lines

JNK is a protein kinase belonging to the MAPK family. Activation of JNK occurs through its phosphorylation at residues Thr183/Tyr185 and it can be induced by several kind of stimuli, including DNA damage and oxidative stress, suggesting a central role of JNK in stress signalling pathways [428]. In the present study the role of JNK in response to cisplatin was examined in OSCC cells.

Firstly, JNK activation in response to cisplatin was investigated by western blot analysis in SCC4 cells treated with cisplatin (5 μM) for 4, 8, 16, 24 and 48 h. Lysates were prepared and run on a 12% SDS-PAGE gel before being probed with an anti-phospho-JNK antibody. Cisplatin induced JNK activation in a time-dependent manner in SCC4 cells, with a first appearance of phospho-JNK observed as early as 8 h, followed by a peak at 16 h and then a progressive disappearance (Figure 4.11).

Additionally, in order to determine whether JNK activation occurred in a ROS-dependent manner, SCC4 cells were treated with cisplatin 5 μM alone, NAC (5mM) alone or pre-treated with NAC for 1 h before adding cisplatin for 24 h. Evaluation of phospho-JNK and total JNK was performed by western blot and densitometry analysis was employed to determine the ratio of phospho-JNK/JNK for an accurate measurement of JNK activation. As shown in Figure 4.12, increased levels of phospho-JNK/JNK ratio were observed in cisplatin treated cells compared to vehicle treated cells, confirming that treatment with cisplatin induced JNK activation in OSCC cells. Moreover, decreased levels of phospho-JNK/JNK ratio were found in cells treatment with NAC in combination with cisplatin compared to cells treated with cisplatin alone, suggesting that NAC abrogates cisplatin-induced JNK activation in OSCC cells.

Taken together, these results indicate that cisplatin induces JNK activation through ROS generation in OSCC cells.

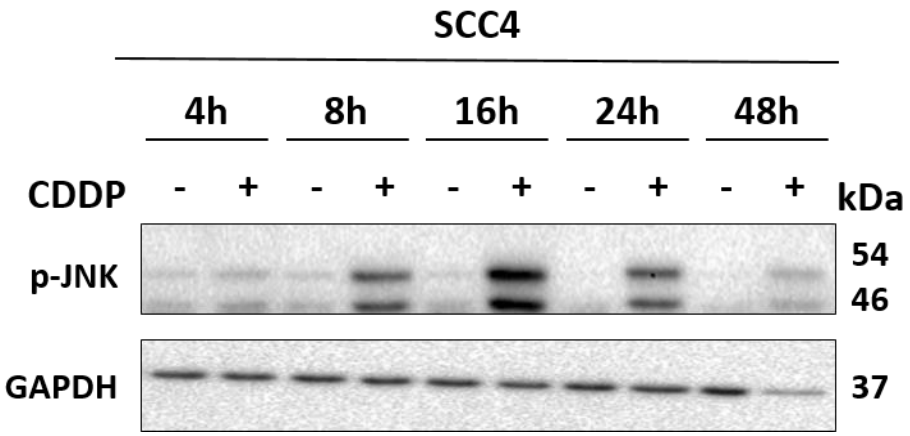

Figure 4.11 Cisplatin induces transient phosphorylation of JNK in SCC4 cells.

SCC4 cells were seeded at $300x10^3$ cells/flask in T25 flasks. Cells were left for 24 h to adhere to the flask and then were treated with vehicle (0.009% (v/v) NaCl) or with 5 μM cisplatin (CDDP). After the indicated times, cells were lysed and 20 μg of protein was loaded and separated on a 12% SDS-PAGE gel, transferred to a PVDF membrane and probed with anti-p-JNK antibody. GAPDH served as loading control. Results are representative of three independent experiments.

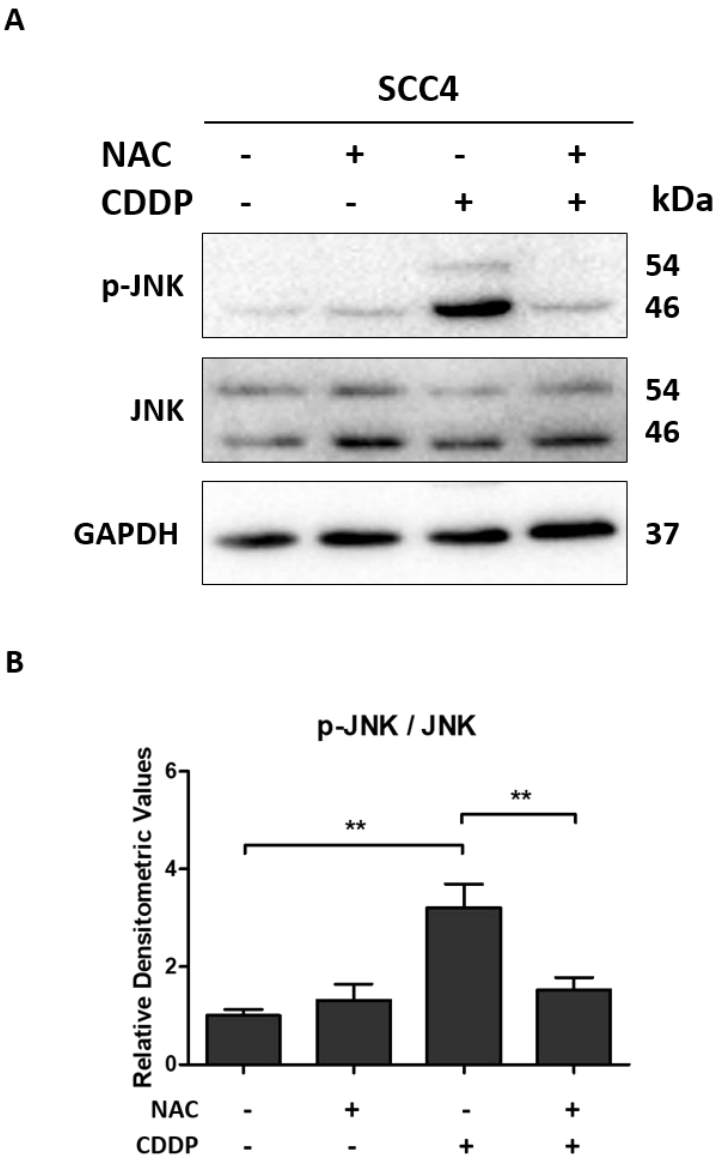

Figure 4.12 N-acetyl cysteine inhibits JNK activation in SCC4 cells treated with cisplatin.

SCC4 cells were seeded at $300x10^3$ cells/flask. Cells were left for 24 h to adhere to the flask and then were treated with vehicle (0.009% (v/v) NaCl), 5mM NAC alone, 5 μM cisplatin (CDDP) alone or cisplatin in combination NAC for 24 h. After incubation, cells were lysed and 20 μg of protein was loaded and separated on a 12% SDS-PAGE gel and transferred to a PVDF membrane. **A**. Membranes were probed with anti-p-JNK and anti-JNK antibodies. GAPDH served as loading control. **B**. Densitometric analysis of p-JNK and JNK bands was performed using ImageLab software and values were normalised by the loading control and the vehicle. Values represent the mean ±S.E.M of three independent experiments. Statistical analysis was performed using one-way ANOVA with Tukey's Multiple Comparison Test (Graphpad Prism 5). ** $p<0.01$.

4.2.7. Cisplatin-induced JNK activation may partially mediate caspase 3 activation and autophagy in OSCC cell lines

The role of JNK in cisplatin-induced apoptosis and autophagy was next investigated in OSCC cells. In order to determine whether induction of apoptosis and autophagy in response to cisplatin occurred in a JNK-dependent manner, the JNK inhibitor SP600125 was employed. SP600125 is a novel and selective JNK inhibitor which acts by competing with ATP for the phosphorylation of c-Jun [438].

The activity of SP600125 was firstly evaluated by western blot analysis of phospho-JNK and total JNK protein expression. SCC4 cells were treated with cisplatin (5 μM) alone, SP600125 (20 μM) alone or pre-treated with SP600125 for 1 h before adding cisplatin for 24 h. Lysates were prepared and run on a 12% SDS-PAGE gel before being probed with the required antibodies. As expected, an increase in phospho-JNK expression was observed in cells treated with cisplatin compared to control cells (Figure 4.13). Also, cells treated with SP600125 in combination with cisplatin showed a substantial (although non-significant) reduction in the phospho-JNK/JNK ratio compared to cells treated with cisplatin alone, suggesting that pre-treatment of cells with SP600125 may inhibit cisplatin-induced JNK activation in SCC4 cells. This result validates the activity of SP600125 as a JNK inhibitor.

Moreover, expression analysis of cleaved caspase 3 was also performed by western blot for the evaluation of cisplatin-induced apoptosis. SCC4 cells were treated with cisplatin 5 μM alone, SP600125 (20 μM) alone or pre-treated with SP600125 for 1 h before adding cisplatin for a further 48 h. As shown in Figure 4.14, a significant increase in cleaved caspase 3 levels was observed in cells treated with cisplatin. Interestingly, pre-treatment of cells with SP600125 reduced (although not significantly) cisplatin-induced cleaved caspase 3, suggesting a link between the JNK signalling pathway and apoptosis activation in response to cisplatin in SCC4 cells.

Finally, analysis of autophagy was performed by western blot through the evaluation of p62 and LC3-I/II protein levels. SCC4 cells were treated as described above and EBSS treated cells were used as positive control for autophagy induction. Higher levels of p62 were observed in cells treated with SP600125 alone or in combination with cisplatin compared to control cells or cisplatin treated cells (Figure 4.15). Moreover, a significant increase in the LC3-II/LC3-I ratio was found in cells treated with SP600125 in

combination with cisplatin compared to cells treated with cisplatin alone or SP600125 alone. This result suggests that suppression of JNK using SP600125 may result in the accumulation of autophagic vesicles, possibly due to late stage autophagy inhibition.

Taken together, these results suggest that JNK activation in response to cisplatin, which is in turn controlled by ROS generation, can partially affect both cisplatin-induced caspase 3 activation and autophagy in OSCC cells.

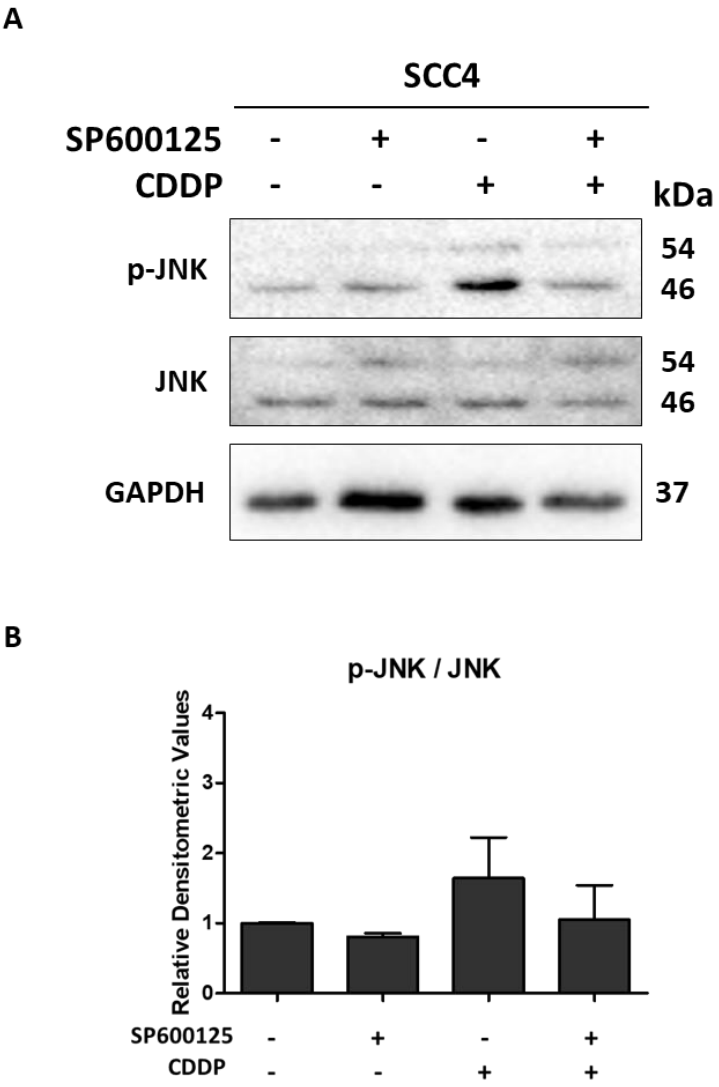

Figure 4.13 Effect of SP600125 on JNK activation in SCC4 cells treated with cisplatin.

SCC4 cells were seeded at $300x10^3$ cells/flask. Cells were left for 24 h to adhere to the flask and then were treated with vehicle (0.009% (v/v) NaCl), 20 μM SP600125 alone, 5 μM cisplatin (CDDP) alone or cisplatin in combination with SP600125 for 24 h. After incubation, cells were lysed and 20 μg of protein was loaded and separated on a 12% SDS-PAGE gel and transferred to a PVDF membrane. **A**. Membranes were probed with anti-p-JNK and anti-JNK antibodies. GAPDH served as loading control. **B**. Densitometric analysis of p-JNK and JNK bands was performed using ImageLab software and values were normalised by the loading control and the vehicle. Values represent the mean ± S.E.M of three independent experiments. Statistical analysis was performed using one-way ANOVA with Tukey's Multiple Comparison Test (Graphpad Prism 5).

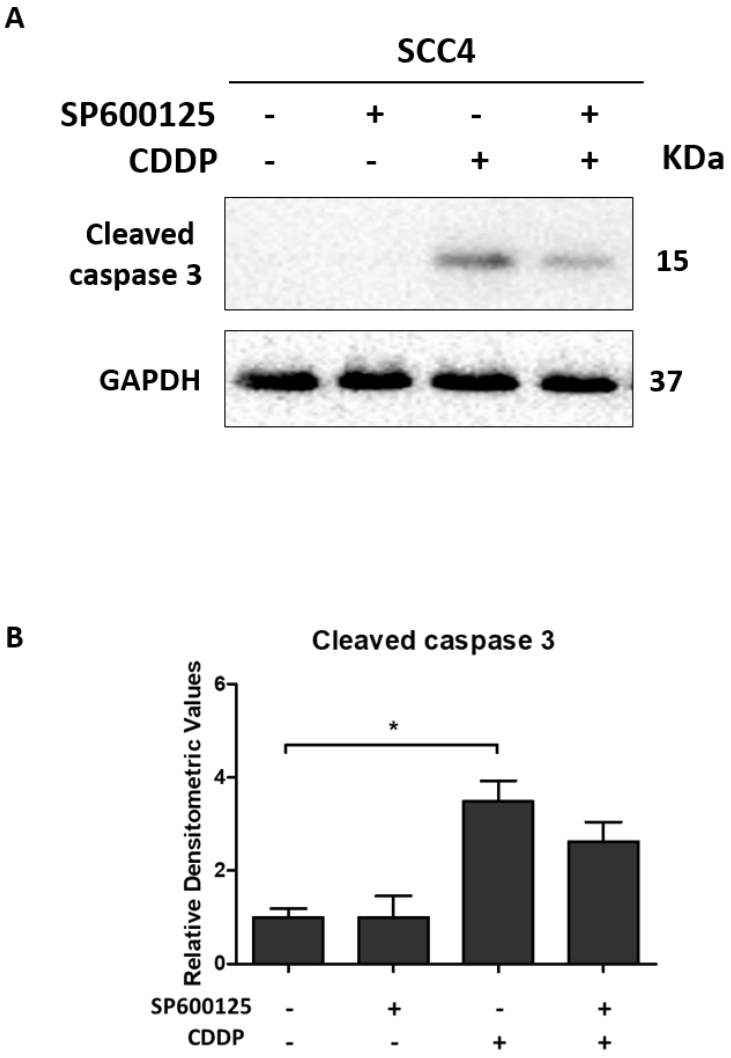

Figure 4.14 Effect of SP600125 on caspase 3 activation in SCC4 cells treated with cisplatin.

SCC4 cells were seeded at $300x10^3$ cells/flask. Cells were left for 24 h to adhere to the flask and then were treated with vehicle (0.009% (v/v) NaCl), 20 μM SP600125 alone, 5 μM cisplatin (CDDP) alone or cisplatin in combination with SP600125 for 48 h. After incubation, cells were lysed and 20 μg of protein was loaded and separated on a 12% SDS-PAGE gel and transferred to a PVDF membrane. **A**. Membranes were probed with an anti-cleaved caspase 3 antibody. GAPDH served as loading control. **B**. Densitometric analysis of cleaved caspase 3 bands was performed using ImageLab software and values were normalised by the loading control and the vehicle. Statistical analysis was performed using one-way ANOVA with Tukey's Multiple Comparison Test (Graphpad Prism 5). * $p<0.05$.

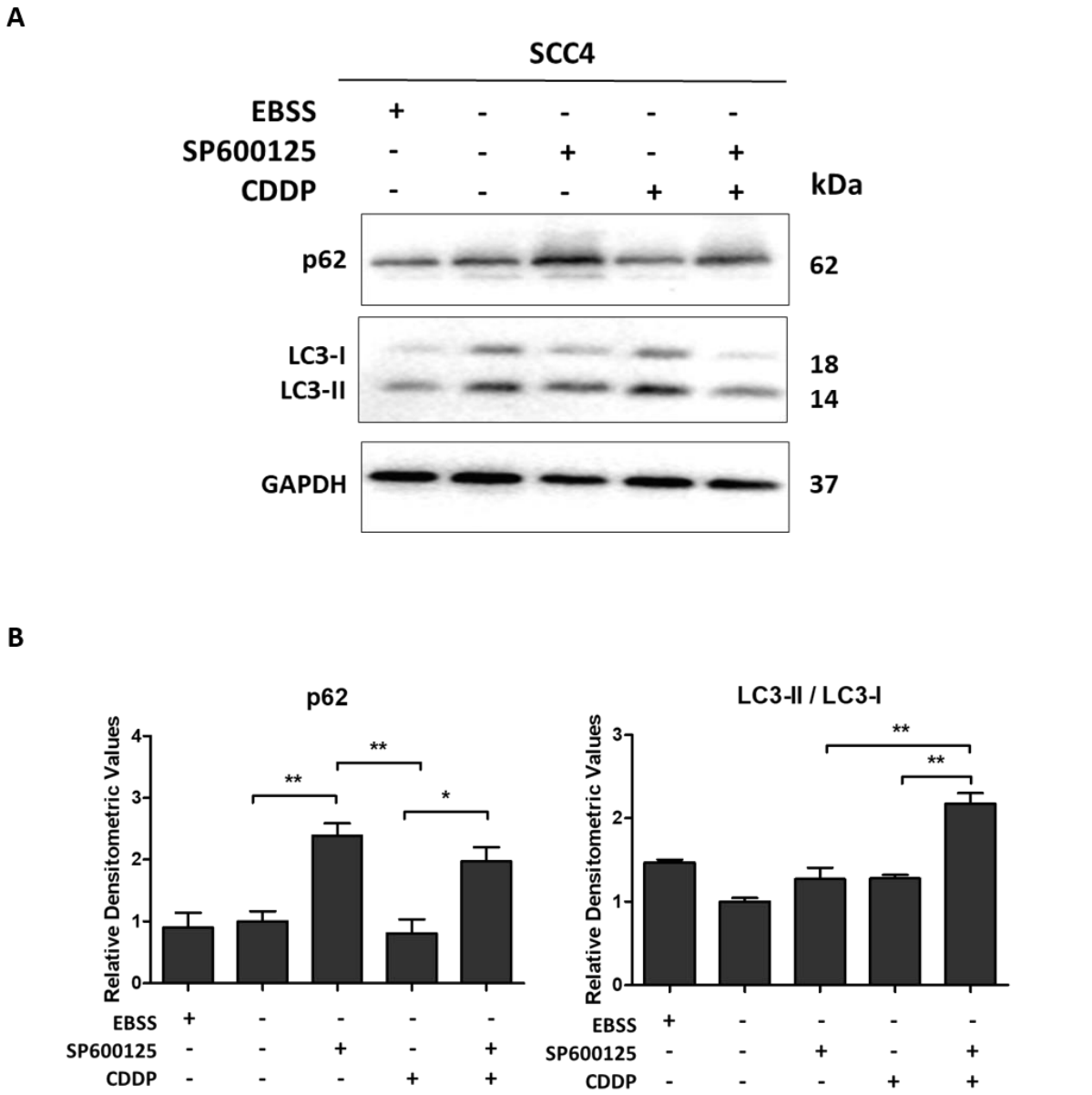

Figure 4.15 SP600125 inhibits autophagy in SCC4 cells treated with cisplatin.

SCC4 cells were seeded at $300x10^3$ cells/flask. Cells were left for 24 h to adhere to the flask and then were treated with vehicle (0.009% (v/v) NaCl), 20 μM SP600125 alone, 5 μM cisplatin (CDDP) alone or cisplatin in combination with SP600125 for 48 h. EBSS (4 h) was used as positive control for autophagy. After incubation, cells were lysed and 20 μg of protein was loaded and separated on a 12% SDS-PAGE gel and transferred to a PVDF membrane. **A**. Membranes were probed with anti-p62 and anti-LC3-I/II antibodies. GAPDH served as loading control. **B**. Densitometric analysis of p62, LC3-I and LC3-II bands was performed using ImageLab software and values were normalised by the loading control and the vehicle. Statistical analysis was performed using one-way ANOVA with Tukey's Multiple Comparison Test (Graphpad Prism 5). * $p<0.05$.

4.2.8. The pan-caspase inhibitor Z-VAD-fmk abrogates cisplatin-induced autophagy in OSCC cell lines

In the previous chapter, targeting autophagy with genetic and pharmacological autophagy inhibitors was shown to affect the apoptotic pathway, suggesting a potential crosstalk between apoptosis and autophagy in OSCC cells treated with cisplatin. In order to further investigate the relationship between autophagy and apoptosis, analysis of autophagy in OSCC cells treated with cisplatin in combination with the pan-caspase inhibitor Z-VAD-fmk was performed.

SCC4 cells were treated with cisplatin (5 μM) alone, Z-VAD-fmk (50 μM) alone or pre-treated with Z-VAD-fmk for 1 h before adding cisplatin for 48 h. Cells treated with EBSS for 4 h were used as a positive control for autophagy induction. Expression levels of p62 and LC3-I/II proteins were assessed by western blot analysis for the evaluation of autophagy. Lysates were prepared and run on a 15% SDS-PAGE gel before being probed with the required antibodies. Inhibition of caspases using Z-VAD-fmk induced accumulation of p62 in SCC4 cells treated with cisplatin compared to cells treated with cisplatin alone (Figure 4.16). Moreover, a significant decrease in LC3-II/LC3-I ratio was observed in cells treated with cisplatin in combination with Z-VAD--fmk compared to cells treated with cisplatin alone, suggesting that inhibition of cisplatin-induced apoptosis abrogates cisplatin-induced autophagy in OSCC cells.

This result suggests that cisplatin-induced apoptosis and autophagy may be interlinked in OSCC, thus inhibition of one of the two signalling pathways leads an alteration of the other one.

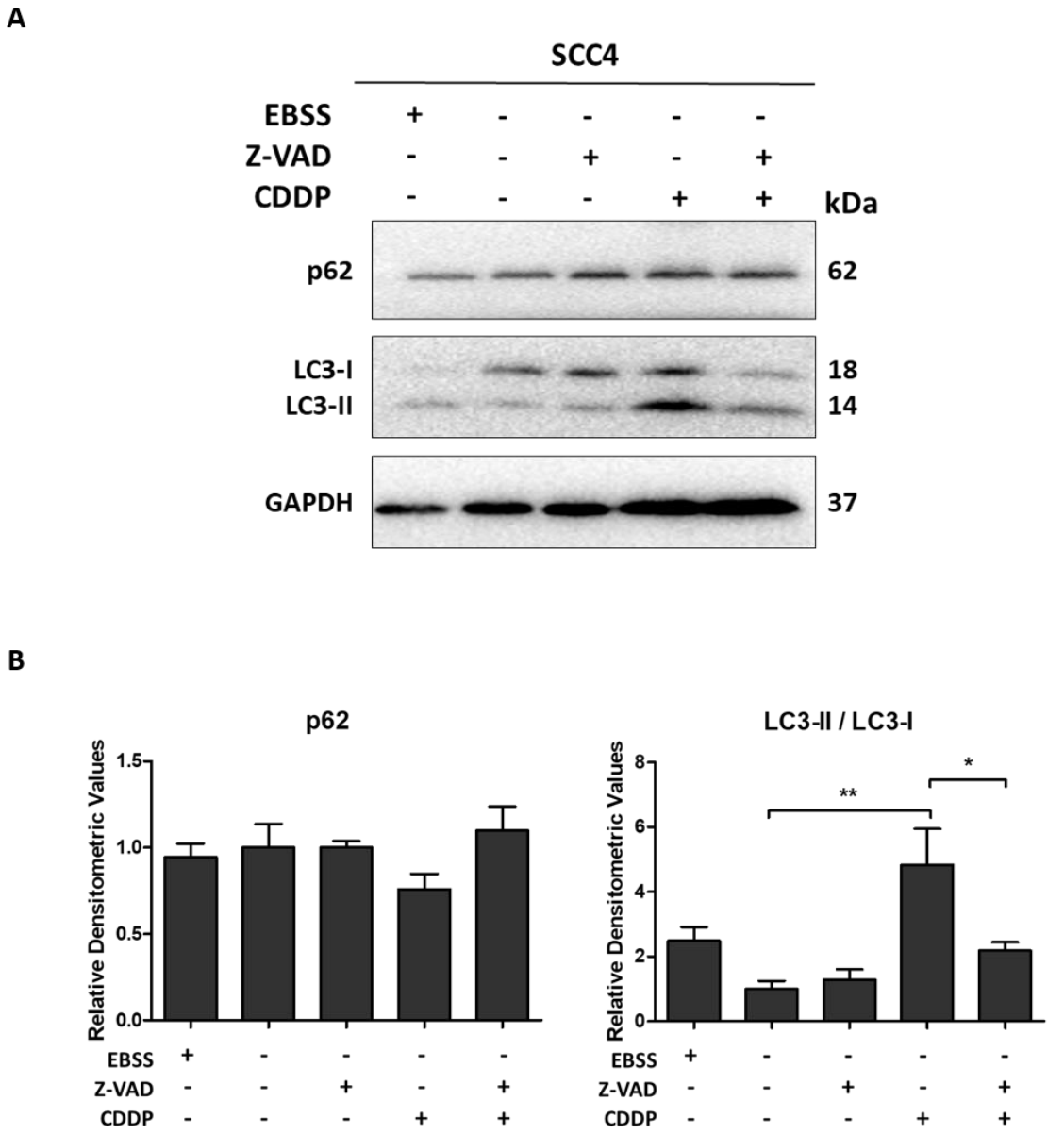

Figure 4.16 The pan-caspase inhibitor Z-VAD-fmk inhibits autophagy in SCC4 cells treated with cisplatin.

SCC4 cells were seeded at $300x10^3$ cells/flask. Cells were left for 24 h to adhere to the flask and then were treated with vehicle (0.009% (v/v) NaCl), 50 μM Z-VAD-fmk alone, 5 μM cisplatin (CDDP) alone or cisplatin in combination with Z-VAD-fmk for 48 h. EBSS (4 h) was used as positive control for autophagy. After incubation, cells were lysed and 20 μg of protein was loaded and separated on a 12% SDS-PAGE gel and transferred to a PVDF membrane. **A**. Membranes were probed with anti-p62 and anti-LC3-I/II antibodies. GAPDH served as loading control. **B**. Densitometric analysis of LC3-I and LC3-II bands was performed using ImageLab software and values were normalised by the loading control and the vehicle. Statistical analysis was performed using one-way ANOVA with Tukey's Multiple Comparison Test (Graphpad Prism 5). ** $p<0.01$, * $p<0.05$.

4.3. Discussion

Cisplatin is one of the most effective drugs for the treatment of solid tumours. It was firstly approved by the Food and Drug Administration (FDA) for the treatment of testicular cancer in 1978. Since then, the use of cisplatin as a chemotherapeutic drug has been extended to other types of cancers, including bladder, cervical, ovarian, lung, gastric and breast cancer [35]. The use of cisplatin has also been approved for the treatment of head and neck cancers, which comprise all the malignancies arising in the oral cavity, pharynx and larynx. Response to cisplatin in head and neck cancers has been observed in 13-40% of cases, confirming the strong but also limited efficacy of this drug [439]. Over the past 50 years, researchers have tried to identify the mechanisms underlying cisplatin cytotoxicity in order to improve its effectiveness as chemotherapeutic drug. The ability of cisplatin to induce DNA damage through the formation of covalent adducts between the drug and DNA has been considered the main mechanism of action of cisplatin [357]. Nevertheless, a significant body of evidence reported during the last few years has shown that the toxic effect of cisplatin may not only be due to DNA adducts but it may also be the consequence of other cellular mechanisms induced by the drug [440]. Therefore, a greater understanding of the signalling pathways implicated in cisplatin cytotoxicity is mandatory to develop new chemotherapeutic strategies and improve the response of patients to this drug. In the present study, the signalling pathways implicated in cisplatin cytotoxicity in OSCC were investigated. In the previous chapter it was demonstrated that cisplatin induced cell cycle arrest, apoptosis and autophagy in oral cancer cells. Moreover, crosstalk between apoptosis and autophagy in mediating cisplatin cytotoxicity has been proposed. Thus, the mechanisms underlying the activation of these two pathways in response to cisplatin were herein evaluated.

It has been recently reported that apart from DNA adducts, cisplatin can also induce the intracellular formation of ROS [441]. High levels of ROS within cells in response to cisplatin have been found in various types of cancer, such as bladder cancer, ovarian cancer and malignant mesothelioma [442–444]. Also, a recent study in 2020 conducted by Xue *et al*. showed that cisplatin can induce ROS generation in the tongue squamous carcinoma cell line CAL-27 [294]. In the present study, intracellular ROS levels were also investigated in tongue squamous cell carcinoma, in particular in the SCC4 and SCC9 cell lines. Results herein, obtained by flow cytometric analysis of H_2DCFDA stained cells, correlated with results reported in the literature, showing a significant enhancement

in ROS formation in response to cisplatin in both cell lines. Endogenous ROS production has been reported to be attributable to various cellular sources (e.g. mitochondria, cytosol, peroxisomes, endosomes and exosomes), whereas ROS produced in response to cisplatin originates mainly in the mitochondria from the electron transport chain [417]. This has been demonstrated by Marullo *et al.* using a respiratory incompetent prostate cancer cell line due to the lack of mitochondrial DNA (DU145ρ°) along with the corresponding control parental cell line (DU145). Evaluation of the endogenous intracellular ROS levels in these cell lines has shown basal levels of ROS in both DU145 and DU145ρ° cells, suggesting that a mitochondrial-independent source of ROS must have been activated in the respiratory incompetent cells. In contrast, after 24 h exposure to cisplatin, a significant increase in ROS generation was observed only in the DU145 cell line and no changes were found in the DU145ρ° cell line, suggesting that mitochondria were the main source of ROS in response to cisplatin. Moreover, according to the authors, exposure to cisplatin can induce both nuclear DNA damage and mitochondrial DNA damage. The former leads to a block in nuclear DNA transcription and replication, while the latter elicits a disruption of essential mitochondrial functions, including reduction of mitochondrial protein synthesis and impairment of the electron transport chain, which results in increased intracellular levels of ROS. Interestingly, a correlation between sensitivity to cisplatin and ROS generation has been observed in ovarian cancer, where higher levels of mitochondrial ROS were found in cisplatin-sensitive cell lines compared to cisplatin-resistant cell lines [443]. Accordingly, in the present study, even though cisplatin was used with a lower concentration in the SCC4 cell line, a higher rate of ROS generation was observed in this cell line compared to the SCC9 cell line. Considering the higher sensitivity of SCC4 cells to cisplatin compared to SCC9 cells, this result supports the idea of a potential correlation between ROS generation and sensitivity to cisplatin in OSCC.

Accumulation of ROS within cells has been strongly linked to oxidative stress. Oxidative stress represents an imbalance in the cellular redox state which is usually due to the reduced ability of antioxidant systems to eliminate the excess of ROS within cells [248]. It has been reported that oxidative stress can induce oxidative damage, including damage to several cellular components such as proteins, DNA and lipids, resulting in cytotoxicity [423]. In order to establish whether increased intracellular levels of ROS lead to oxidative stress and cytotoxicity, it is important to determine the efficiency of cellular antioxidant defence systems. As mentioned previously, glutathione is considered the major

antioxidant system within cells [420]. Under oxidising conditions, glutathione is converted from its reduced form (GSH) to its oxidised form (GSSG) through a two-electron oxidation, which results in ROS reduction and neutralisation. Accordingly, conversion of GSH to GSSG is indicative of the redox state of cells, hence the ratio of GSH/GSSG is considered a good marker for oxidative stress [255]. In the present study, the GSH/GSSG ratio was determined in OSCC cells in response to cisplatin using the GSH/GSSG kit. Results obtained showed a significant drop in the GSH/GSSG ratio in SCC4 cells treated with cisplatin compared to control cells, while a considerable but not significant decrease in the GSH/GSSG ratio was observed in SCC9 cells treated with cisplatin compared to control cells. Overall, the reduction in the GSH/GSSG ratio along with the intracellular accumulation of ROS indicated that treatment with cisplatin induced oxidative stress in OSCC cells.

Interestingly, several studies have suggested that a reduction in the GSH/GSSG ratio may not be the consequence of the conversion of GSH to GSSG, but it may depend on the depletion of glutathione caused by the drug itself [323, 445]. A reduction in glutathione levels in response to cisplatin has been demonstrated in several tissues of tumour-bearing mice, including kidney, liver and spleen [445]. Moreover, it has been suggested that reduced levels of glutathione may be implicated in cisplatin mediated cytotoxicity through various mechanisms. Firstly, depletion of glutathione may result in the failure of ROS elimination due to a decrease in the antioxidant defence system. According to this, cisplatin may induce oxidative stress not only by enhancement of ROS generation due to the disruption of the electron transport chain, but also by depletion of glutathione, which in turn further promotes ROS accumulation [418, 419]. Secondly, depletion of glutathione in response to cisplatin may result in the intracellular accumulation of cisplatin and enhancement of its toxicity [446]. Several studies have reported that glutathione plays an important role in cisplatin metabolism through the modulation of its uptake and elimination [418], and it has been demonstrated that once cisplatin enters the cytosol, it can be bound by glutathione through S-conjugation links between the thiol group of GSH and the electrophilic moiety of cisplatin [447]. This binding is catalysed by the glutathione S-transferase (GST) enzyme and results in the formation of GSH-cisplatin adducts. These complexes can be ejected from the cells by specific export pumps in an ATP-dependent manner in order to reduce the intake of the drug and prevent the consequent DNA damage [418]. Given this, it is clear that reduced levels of glutathione

results in reduced elimination of the drug and in its intracellular accumulation, thus in an enhancement of cytotoxicity. In support of these findings, reduced levels of glutathione along with reduced GST activity have been demonstrated in Dalton's lymphoma cells after treatment with cisplatin, suggesting that depletion of glutathione results in reduced conjugation of glutathione to cisplatin [445]. Accordingly, treatment of cells with the glutathione inhibitor buthionine sulfoximine (BSO) was shown to decrease the expression of the GST enzyme in malignant melanoma cells [448]. Moreover, inhibition of GST activity using the GST inhibitor sulphasalazine has been demonstrated to enhance cisplatin toxicity in small cell lung carcinoma, whilst activation of GST activity with prolactin has led to the acquisition of a cisplatin resistant phenotype in breast cancer cells [449, 450]. Interestingly, depletion of glutathione has also been associated with an increase in inter-strand DNA crosslink formation and cytotoxicity [285, 446, 451]. In this regard, an increase in DNA damage has been found in cisplatin-resistant rat ovarian tumours after treatment with BSO [452]. Also, inhibition of DNA repair after treatment with cisplatin has been observed in an ovarian carcinoma cell line treated with BSO [453]. All these findings support the involvement of cisplatin-mediated depletion of GSH and inhibition of GST in cisplatin anticancer activity. Given this strong link between cisplatin cytotoxicity and glutathione, a further evaluation of the role of glutathione in cisplatin activity and resistance will be described in the next chapter.

In the present study, the role of oxidative stress in cisplatin cytotoxicity in OSCC has been investigated using the antioxidant N-acetyl cysteine (NAC). The antioxidant activity of NAC has been ascribed to various mechanisms. It has been reported that NAC can act both as a direct antioxidant, through its scavenging activity for some oxidant species, and as an indirect antioxidant through its ability to replenish GSH and breaking thiol modified proteins [454]. In this regard, it has been demonstrated that NAC can act as a precursor of GSH, hence treatment of cells with NAC has been shown to reduce oxidative stress by protecting cells from GSH depletion [455]. Moreover, it has been shown that NAC disulphide breaking activity can lead to the release of free thiols, which in turn can regulate the redox state of cells by acting as scavengers for free radicals and by boosting the synthesis of GSH [454]. In the present study, the antioxidant activity of NAC has been examined through determination of the GSH/GSSG ratio along with evaluation of the intracellular levels of ROS in OSCC cells treated with cisplatin. From the luminometric analysis of glutathione levels using a GSH/GSSG kit, it was observed that NAC partially

prevented the drop in the GSH/GSSG ratio induced by cisplatin in SCC4 cells. Moreover, from the flow cytometric analysis of H_2DCFDA stained cells, it was found that NAC significantly abrogated cisplatin-induced ROS in both SCC4 and SCC9 cell lines. Overall, the increase of the GSH/GSSG ratio in cells treated with NAC in combination with cisplatin compared to cells treated with cisplatin alone suggested that NAC protected cells from oxidative stress induced by cisplatin in OSCC cells. Additionally, the results presented herein suggested that in these cell models of OSCC the antioxidant activity of NAC may be attributable to its ROS scavenger activity.

NAC has been extensively used for its antioxidant properties as a tool to elucidate the role of oxidative stress in response to chemotherapeutics. In the present study, viability analysis of OSCC cells treated with NAC and/or cisplatin showed that pre-treatment with NAC protected cells from cisplatin-induced reduction of viability, indicating that oxidative stress is implicated in cisplatin cytotoxicity in OSCC cells. Moreover, only a partial but significant reduction in cisplatin cytotoxicity was observed when SCC4 cells were pre-treated with NAC, whilst an almost total protection from cisplatin cytotoxicity was observed in the SCC9 cell line pre-treated with NAC. This result may suggest that cisplatin cytotoxicity occurs mainly through induction of oxidative stress in the SCC9 cell line, while multiple mechanisms may be implicated in the SCC4 cell line. Interestingly, it has been proposed that cytotoxicity induced by oxidative stress may represent the major cause of side effects associated with cisplatin treatment [417]. In fact, the formation of nuclear DNA adducts induced by cisplatin and the consequent arrest of DNA replication and/or transcription explains the cytotoxic effect of the drug in dividing cells such as cancer cells. However, a high toxicity of cisplatin has also been observed in post-mitotic cells such as cells in kidney, ears and sensory nerves, resulting in side effects such as nephrotoxicity, ototoxicity and neurotoxicity. In this context, oxidative stress induced by cisplatin has been considered as the mechanism responsible for cisplatin toxicity in normal cells [417]. Given this, the lack of a non-cancerous cell line as negative control represents a limitation of this study. In fact, comparison of the cellular response to cisplatin in OSCC cells and in normal cells of the oral mucosa would be of interest to determine whether oxidative stress is induced in both cell lines following treatment with cisplatin. This would shed light on the implication of oxidative stress in cisplatin-induced side effects and on the potential therapeutic strategies to reduce them during OSCC. Moreover, Marullo *et al.* have also compared the toxic effect of cisplatin with the

analogue carboplatin, which is often used as alternative to cisplatin because of the reduced side effects. From this comparison, it has been demonstrated that carboplatin was less toxic than cisplatin. Concurrently, carboplatin was shown to be less efficient at inducing mitochondrial impairment and ROS production, suggesting that carboplatin cytotoxicity may be mainly attributable to genotoxic stress rather than oxidative stress [417]. Given this, combining cisplatin with antioxidants may represent a valuable strategy to improve cisplatin treatment and reduce side effects caused by the drug. Accordingly, several studies *in vivo* have shown that NAC can reduce ototoxicity, nephrotoxicity and neurotoxicity associated with cisplatin treatment [456–460]. Currently, clinical trials are still underway to determine the beneficial effects of NAC on cancer patients during chemotherapy. In oral squamous cell carcinoma, the use of NAC has led to an increase in survival rate of patients and in the preservation of organ function [35].

As oxidative stress had been implicated in cisplatin cytotoxicity of SCC4 and SCC9 cells, the signalling pathways involved in this process were next investigated. It has been reported that cisplatin-induced ROS can trigger cell death through apoptosis [265]. The tight relationship between apoptosis and oxidative stress in response to cisplatin has been widely investigated in the literature by using the antioxidant NAC. In this regard, a protective effect of NAC in cisplatin-induced apoptosis has been demonstrated in several types of cancer, such as prostate and hepatocarcinoma [277, 461]. Similarly, in the present study, it was found that pre-treatment with NAC protected SCC4 and SCC9 cells from cisplatin-induced apoptosis, suggesting that cisplatin-induced ROS generation mediated apoptotic cell death in OSCC cell lines. This finding is consistent with a report by Yang *et al.* showing that apoptosis induced by cisplatin in squamous cell carcinoma of head and neck may result from the effect of the drug on mitochondria and not necessarily from its binding to nuclear DNA [462]. Moreover, in the present study, a partial decrease in the apoptotic rate was observed in SCC4 cells pre-treated with NAC compared to cells treated with cisplatin alone, whilst total inhibition of cisplatin-induced apoptosis was found in SCC9 cells pre-treated with NAC. This result aligns with the results obtained from the viability assay, indicating that cisplatin cytotoxicity may be mainly attributable to ROS-induced apoptosis in the SCC9 cell line, whilst additional pathways may be implicated in the SCC4 cell line. In addition, in the present study, NAC partially reduced cisplatin-induced caspase 3 activation in SCC4 cells, indicating that NAC inhibition of apoptosis occurred in a caspase-dependent manner. This result is in agreement with a report by Wu

et al., where abrogation of caspase 3 and 9 activation in small-cell lung carcinoma cells treated with cisplatin was observed following pre-treatment with NAC [463].

A correlation between oxidative stress and autophagy has also been reported in the literature. In fact, ROS has been shown to play an important role in autophagy by regulating its induction [464]. Accumulation of H_2O_2 has been found to activate autophagy both directly through ATG4 oxidation, resulting in the increased formation of autophagosomes, and indirectly through regulation of AMP-activated protein kinase (AMPK), resulting in the inhibition of mTOR and the phosphorylation of ULK1/2 complex [465–467]. Moreover, ROS can also regulate autophagy through the modulation of the transcription factor NF-κB, which leads to the activation of Beclin-1 and p62 [468]. It has also been proposed that not only can ROS regulate autophagy, but also autophagy can regulate ROS. Accordingly, induction of autophagy by ROS results in the elimination of damaged mitochondria which represents the main source of free radicals [143]. Thus, prevention of ROS accumulation by autophagy represents a cell survival mechanism to maintain cell homeostasis. Nevertheless, even though autophagy is generally recognised as a protective mechanism, it may also represent an anti-tumour mechanism associated with apoptosis. Interestingly, in some reports ROS generation in response to physiological insults, such as starvation, has been linked to protective autophagy, whereas ROS production in response to non-physiological insults, such as chemotherapeutics and radiation, has been correlated to cell death [469]. In support of this hypothesis, it has been observed that autophagy induced by ROS after treatment with selenite promoted cell death in malignant glioma cells [470]. Also, suppression of autophagy induced by H_2O_2 treatment was shown to inhibit cell death in HeLa cells [471]. In the present study, pre-treatment of cells with NAC reduced not only cisplatin-induced apoptosis but also cisplatin-induced autophagy in OSCC cells. Indeed, western blot analysis of SCC4 cells showed a significant decrease in the LC3-II/LC3-I ratio and a marked increase in p62 protein expression in cells treated with cisplatin in combination with NAC compared to cells treated with cisplatin alone. This result suggested that cisplatin-induced autophagy occurred as a consequence of ROS generation in OSCC cells. Also, results from the previous chapter suggested that autophagy induced by cisplatin in OSCC cells may not represent a cell survival mechanism. Together, these findings corroborate the hypothesis that autophagy induced by a non-physiological insult such as cisplatin may be linked to cell death. Nevertheless, it should be noted that the interplay between ROS and autophagy

may be more complicated than this. Several studies have indeed demonstrated that treatment of cells with chemotherapeutic agents can activate ROS-induced autophagy which in turn can lead to drug resistance, suggesting a cell survival role of autophagy [464]. According to Poillet-Perez *et al.*, the complex relationship between ROS, autophagy and cell death in response to chemotherapeutics can be explained with 4 models, which summarises the findings reported in the literature [464]. In the first model, anticancer drugs can induce ROS accumulation which in turn leads to cell death and concurrently autophagy induction to reduce ROS levels and escape from stress. In the second model, induction of ROS generation by chemotherapeutic agents leads to autophagy activation as a protective mechanism to block cell death induced by the drug. In the third model, ROS accumulation in response to anticancer drugs is not the cause of autophagy, but it may be the consequence of autophagy inhibition. Thus, combining autophagy inhibitors with chemotherapeutics would enhance cell death through ROS accumulation. Finally, in the fourth model, anticancer drugs induce ROS generation, which in turn activates cytotoxic autophagy.

Interestingly, activation of JNK by both endogenous and exogenous ROS has been widely reported in the literature [472, 473]. Moreover, a consistent body of evidence has also reported that both apoptosis and autophagy induced by oxidative stress may occur through activation of JNK. Given that, in the present study, JNK activation in response to cisplatin along with its implication in cisplatin-induced ROS generation, apoptosis and autophagy was investigated. Western blot analysis of phospho-JNK protein expression showed that cisplatin induced phosphorylation of JNK in a time-dependent manner, with a first appearance of phospho-JNK observed as early as 8 h, followed by a peak at 16 h and then a progressive disappearance. Moreover, pre-treatment of SCC4 cells with NAC suppressed JNK activation induced by cisplatin, suggesting that cisplatin-induced JNK activation occurred in a ROS-dependent manner in OSCC cells. Additionally, the role of JNK in cisplatin-induced apoptosis and autophagy was investigated in OSCC cells using the JNK inhibitor SP600125. Pre-treatment of SCC4 cells with SP600125 partially reduced the levels of cleaved caspase 3 induced by cisplatin, suggesting that JNK activation may play a part in cisplatin-induced apoptosis in OSCC cells. Moreover, alteration in the protein expression of the autophagic markers p62 and LC3-I/II observed after treatment of cells with SP600125 and/or cisplatin also suggested a potential role of JNK in autophagy induction in OSCC cells. As mentioned previously, accumulation of

p62 protein and increase in the LC3-II/LC3-I ratio are indicative of a build-up of autophagic vesicles likely due to the block of the autophagic flux at late stages. Consistently, increased levels of p62 and LC3-II/LC3-I ratio in cells treated with SP600125 in combination with cisplatin compared to cells treated with cisplatin alone were found in SCC4 cells, suggesting that suppression of JNK activation may lead to inhibition of cisplatin-induced autophagy. However, it is worth noting that high levels of p62 were also detected in cells treated with SP600125 alone compared to vehicle and cisplatin treated cells suggesting that SP600125 may inhibit basal levels of autophagy. Furthermore, one cannot rule out the possibility that this pharmacological JNK inhibitor may elicit off-target effects. Thus, autophagy inhibition following treatment of cells with SP600125 may occur in a JNK-independent manner. Accordingly, further experiments using a knockdown approach for targeting the JNK pathway may be required to confirm the role of JNK in cisplatin-induced autophagy.

Overall, preliminary results obtained through this study may indicate that ROS-induced JNK activation plays a role in apoptosis and possibly autophagy induced by cisplatin in OSCC cells. However, it is important to note that further studies on a greater number of OSCC cell lines may be required to confirm these findings. This proposed mechanism of action of cisplatin is consistent with similar data recently published by Xue *et al.*, who demonstrated that up-regulation of intracellular ROS can chemosensitise a cisplatin resistant CAL-27 tongue carcinoma cell line, by inducing apoptosis and autophagy through the MAPK pathway [294]. Moreover, JNK activation in response to ROS induced by various chemotherapeutic drugs and its implication in apoptosis and autophagy has been reported in other studies. For example, Wang *et al.* demonstrated that rasfonin (a fungal metabolite with anti-tumour properties) activated both autophagy and apoptosis in human renal cancer cells concomitant with a dramatic increase in ROS production [474]. Also, suppression of ROS using NAC inhibited both autophagic flux and caspase-dependent apoptosis induced by rasfonin. In the same study, it has been reported that rasfonin increased the phosphorylation of JNK, which in turn was inhibited by NAC. Moreover, SP600125, an inhibitor of JNK, reduced rasfonin-dependent autophagic flux and apoptosis. The authors concluded that rasfonin activated autophagy and apoptosis through upregulation of the ROS/JNK signalling pathway. Similar to rasfonin, treatment of osteosarcoma cells with metformin was shown to induce both apoptosis and autophagy through the ROS/JNK signalling pathway [475]. Likewise, it has been demonstrated that

the KIOM-C, a novel herbal medicine, induced apoptotic and autophagic cell death through activation of ROS-induced JNK in fibrosarcoma cells [476]. Additionally, it was found that propofol, an anaesthetic agent with well-known antioxidant properties, reduced hypoxia-induced apoptosis and autophagy through JNK inhibition in kidney cells [477].

Finally, results obtained in the present study indicated that oxidative stress in response to cisplatin concurrently led to apoptosis and autophagy induction through the activation of the same ROS/JNK signalling pathway. This suggests a close relationship between autophagy and apoptosis. The interplay between the two processes is not well understood, although it has been extensively discussed in the literature. Several studies have demonstrated that the two processes can mutually influence each other, thus targeting autophagy may result in apoptosis dysregulation and vice versa [205]. However, an inconsistent relationship between apoptosis and autophagy has also been reported in different studies, suggesting that the relationship may be context-dependent based on the cellular model, the apoptotic/autophagic stimuli and the experimental conditions [206].

In the previous chapter, the effect of genetic and pharmacological autophagy inhibition on cisplatin-induced apoptosis was evaluated in OSCC cells. Results obtained demonstrated that targeting different stages of the autophagic flux elicited differential effects on cisplatin-induced apoptosis, suggesting a complex interplay between the two pathways at several levels. The relationship between apoptosis and autophagy in response to cisplatin in OSCC cells was herein further investigated through the evaluation of cisplatin-induced autophagy following inhibition of apoptosis. For this analysis, SCC4 cells were treated with cisplatin alone or in combination with the pan-caspase inhibitor Z-VAD-fmk and expression levels of p62 and LC3-I/II proteins were assessed by western blotting. In the previous chapter it was demonstrated that pre-treatment of SCC4 cells with Z-VAD-fmk completely protected against apoptosis, indicating that cisplatin-induced apoptosis occurs in a caspase-dependent manner (Figure 3.12). In this chapter, results obtained showed that treatment of cells with Z-VAD-fmk in combination with cisplatin also induced accumulation of p62 and decreased the LC3-II/LC3-I ratio in SCC4 cells compared to cells treated with cisplatin alone, suggesting that inhibition of cisplatin-induced apoptosis abrogated cisplatin-induced autophagy in OSCC cells. Similarly, a recent study has demonstrated that Z-VAD-fmk reduced autophagy activation induced by pristimerin, a natural quininemethide triterpenoid extracted from plants, in human breast cancer *in vitro* and *in vivo* [478]. Interestingly, in the same study it was also found that

pristimerin triggered both autophagy and apoptosis through the ROS/ASK1/JNK pathway. In contrast with these findings, other studies have reported that inhibition of caspases with Z-VAD-fmk can result in autophagy activation. For instance, it has been reported that Z-VAD-fmk enhanced autophagy induced by the HDAC inhibitor apicidin in salivary mucoepidermoid carcinoma cells [479]. This further demonstrates the complex relationship between apoptosis and autophagy which may be dependent on cell-type and stimulus. Collectively these findings suggest that caspases play a role in both apoptotic and autophagic signalling pathways, representing a key node in the crosstalk between these two biological processes.

In conclusion, in the present chapter, evaluation of the signalling pathways involved in cisplatin-mediated cytotoxicity in OSCC was undertaken. Oxidative stress was implicated in cisplatin-induced cytotoxicity in OSCC cells and cisplatin was shown to induce oxidative stress by increasing the generation of ROS. Additionally, cisplatin-induced oxidative stress induced both apoptosis and autophagy partly through activation of the JNK signalling pathway in OSCC cells. Finally, a coordinated relationship between cisplatin-induced apoptosis and autophagy was demonstrated, suggesting that the two pathways interact with one another to induce cell death in OSCC cells.

5. Evaluation of the mechanisms implicated in cisplatin resistance in OSCC

5.1. Introduction

Chemotherapy represents the main therapeutic strategy for the treatment of advanced and unresectable OSCCs [480]. However, many OSCC patients either poorly respond to chemotherapy or become refractory after a few chemotherapy cycles [108]. This usually results in tumour relapse and disease progression, leading ultimately to death. The lack of response to chemotherapy is defined as chemoresistance. In cancer biology, chemoresistance (or drug resistance) refers to the ability of cancer cells to escape from the effect of drugs. Currently, chemoresistance represents a major challenge for OSCC patients undergoing chemotherapy [481].

To date, several studies have tried to identify the mechanisms underlying drug resistance in order to develop new improved strategies for the treatment of OSCC patients. The main mechanisms associated with chemoresistance in OSCC have already been discussed in this thesis in the general introduction (see chapter 1). It is worth noting that all these mechanisms can act independently or in combination, making chemoresistance a complex multifactorial-mediated process. Additionally, it has been reported that the involvement of a certain mechanism may depend on the cell type and on the type of drug which cells are resistant to [482]. Thus, chemoresistance develops as an incredibly complex process which can vary among cell models even within the same type of cancer. This complexity helps to explain why, despite the constant efforts, no single therapeutic strategy has been found to bypass drug resistance to date. Therefore, there is a need to more fully understand these complex processes in OSCC.

Platinum-based chemotherapy represents the golden standard treatment for advanced stage OSCC [108]. It has been widely reported that although many patients initially respond well to platinum-based treatments, they can become resistant to therapy in a short time [108]. This suggests a high correlation between platinum-based chemotherapy and acquired chemoresistance. Overall, several mechanisms have been linked to platinum-based resistance in a variety of cancers, including reduced cellular drug accumulation, increased detoxification systems, increased DNA repair processes, decreased apoptosis and enhancement of autophagy [483]. In particular, among the platinum-based agents, cisplatin is the most intensively studied to date. Cisplatin resistance has been strongly correlated to altered localisation, activity or expression level of several platinum-transporters which mediate drug uptake and efflux. Amongst them, it is worth mentioning the organic cation transporters (OCT1-3), the copper transporters (CTR1-2), some P-type

ATPases (ATP7A/7B) and the multidrug resistance proteins (MRP) [483, 484] In addition, several cisplatin-resistant cells have shown increased levels of glutathione, which can form cisplatin-conjugates that are easily expelled by cells in order to reduce cellular cisplatin accumulation [483]. Besides the mechanisms involved in cisplatin accumulation, a strong correlation between cisplatin resistance and dysregulation of signalling pathways involved in the cellular response to cisplatin has also been proposed [485]. In fact, it is generally accepted that cisplatin can generate genotoxic and oxidative stress within cells, which eventually leads to apoptosis. Accordingly, increased DNA repair pathways, increased antioxidant systems and overexpression of anti-apoptotic proteins have been found in various cisplatin-resistant cell models [485]. Furthermore, a strong link between cisplatin resistance and general stress response pathways such as autophagy has also been suggested [485]. Consistently, elevated basal levels of autophagy and cisplatin-induced autophagy has been observed in numerous cisplatin-resistant cells such as human lung adenocarcinoma cells, resulting in an adaptive response of cells to overcome stress [486, 487] Finally, recent studies have reported that cisplatin resistance may also be linked to enrichment of cancer stem cells (CSCs), which are multipotent highly tumorigenic and resistant cells capable of self-renewal [101, 488].

The molecular mechanisms underlying acquired resistance to cisplatin in OSCC remain unclear. Given the importance of cisplatin-based chemotherapy for the treatment of OSCC, the aim of this chapter was to generate and characterise a cisplatin-resistant OSCC cell line in order to better understand the mechanisms implicated in cisplatin resistance in OSCC and to identify new potential strategies to improve the clinical outcome of OSCC patients. In the previous chapter, treatment of OSCC cells with cisplatin was shown to induce autophagy and oxidative stress. Following on from this, an additional aim of this chapter, was to further investigate the role of both oxidative stress and autophagy in acquired resistance to cisplatin in OSCC.

5.2. Results

5.2.1. Generation of a cisplatin-resistant OSCC cell line

To aid in the study of the mechanisms involved in drug resistance in oral cancer, a cisplatin-resistant OSCC cell line was generated. The development of drug-resistant cells from drug-sensitive parental cells allows one to better investigate the mechanisms implicated in acquired drug resistance through comparison of drug-sensitive and drug-resistant cell populations within the same cell line. Results obtained in chapter 3, showed that the SCC4 cell line was highly sensitive to cisplatin, thus it was selected in this study as the parental cell line from which a cisplatin-resistant population was generated.

As described in the Materials and Methods section, induction of resistance was obtained by pulsed stepwise exposure of cells to cisplatin over a period of 12 months. As shown in Table 3.1 (see chapter 3), after 72 h of treatment, the concentration of cisplatin required to inhibit 50% of cell viability (IC_{50}) was 1.1±0.4 μM. Given that, the IC_{25} value was calculated and used as an initial concentration of cisplatin to apply to cells. After a 72 h treatment with cisplatin, viable cells were maintained in fresh media and, once recovered, were considered a new generation of cells. This procedure was repeated 9 times and increasing concentrations of cisplatin were used for each generation of cells, as reported in Table 5.1. Importantly, an untreated control set of parental SCC4 cells was grown alongside cisplatin treated cells in order to compare each generation of cisplatin-sensitive (SCC4) and -resistant (SCC4cisR) cells.

From the 4^{th} generation of cells (G4), the difference in sensitivity between SCC4 and SCC4cisR cells was examined using the alamar blue assay. For this viability assay, parental and cisplatin-resistant cells were treated with several concentrations of cisplatin (0-25 μM) for 72 h and the IC_{50} values were calculated (Table 5.2). The induction of a resistant phenotype was determined by considering the variation in the IC_{50} values after each treatment with cisplatin. A progressive increase in the IC_{50} values was observed across the generations of cells in the SCC4cisR cell line treated with cisplatin, while minimal changes were observed in the paired parental cell line (Figure 5.1A). This result suggested that acquired resistance to cisplatin was progressively obtained after each exposure to the drug. Moreover, the first significant difference in the IC_{50} values between the two cell populations was observed at G8.

To quantify the difference in sensitivity, the resistance index (RI) of the SCC4cisR cell line was calculated for each generation of cells (Table 5.2). The RI was determined as the ratio of the IC_{50} of SCC4cisR cells/IC_{50} of SCC4 cells. In the present study, an RI ≥5 was considered significant and clinically relevant to determine the acquisition of a resistant phenotype. In Figure 5.1B, a progressive increase in the RI of the SCC4cisR cell line across the generations of cells is shown. Also, RI values above 5 were found as early as G8 and increased up to G10, confirming that the first relevant difference in the susceptibility to the drug between the two cell populations was obtained after the 7^{th} treatment with cisplatin and reached a peak after the last treatment.

In Figure 5.2, viability curves obtained from the last generation (G10) of SCC4 and SCC4cisR cells treated with cisplatin are reported. As expected, cisplatin reduced the viability of both SCC4 and SCC4cisR cells in a dose-dependent manner. However, a notable shift to the right was observed in the viability curve of the SCC4cisR cells compared to the viability curve of the parental cells, suggesting a difference in the susceptibility to the drug in the two populations of cells. Accordingly, the IC_{50} value obtained in the SCC4 cells was 1.1 ± 0.2 µM, whilst the IC_{50} value obtained in the SCC4cisR cells was 16.2 ± 4.8 µM. Therefore, SCC4cisR cells exhibited a RI of 13.7, suggesting that pulsed exposure of cells to the drug resulted in the acquisition of a resistant phenotype. This RI was considered relevant to define the SCC4cisR cells as an independent cell line derived from the sensitive parental SCC4 cell line.

To summarise, these data demonstrate that induction of cisplatin resistance in OSCC can be accomplished through pulsed stepwise exposure of cells to the drug. Accordingly, in the present study, a novel cisplatin-resistant cell line was generated from the parental cisplatin-sensitive SCC4 cell line.

Cell generation	Cisplatin treatment (72 h)
G0	0.6 µM
G1	0.7 µM
G2	0.8 µM
G3	0.9 µM
G4	1.0 µM
G5	1.5 µM
G6	2.0 µM
G7	2.5 µM
G8	4.0 µM
G9	8.0 µM
G10	-

Table 5.1 Cisplatin treatments used for the generation of the cisplatin-resistant OSCC cell line (SCC4cisR) from the parental sensitive cell line (SCC4).

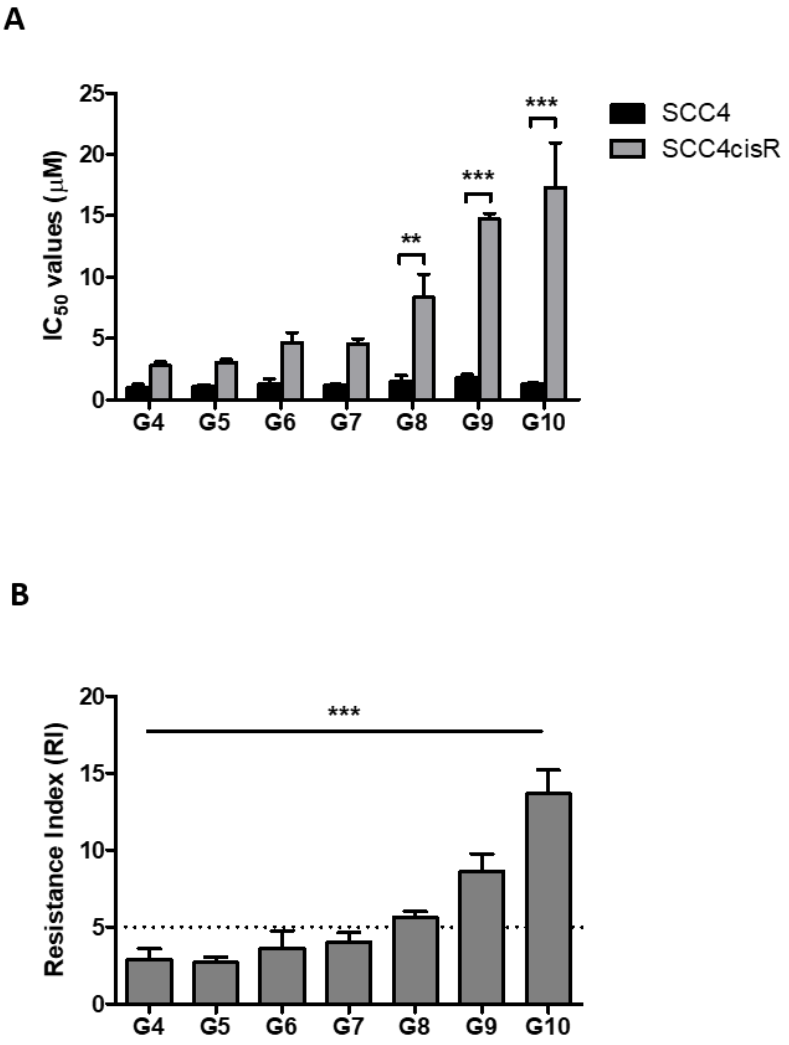

Figure 5.1 Variation in the sensitivity to cisplatin in the SCC4cisR cell line across generations of cells. **A.** IC_{50} values obtained from cell viability analysis of SCC4 and SCC4cisR cells treated with cisplatin were plotted using Graphpad Prism 8. Values represent the mean ±S.E.M. of three independent experiments. Statistical analysis was performed using two-way ANOVA with Tukey's Multiple Comparison Test to compare mean values between the two cell lines (Graphpad Prism 8). *** $p<0.001$, ** $p<0.01$. **B.** Resistant Index (RI) variation of SCC4cisR cells in relation to cisplatin. RI values were calculated by dividing the IC_{50} values of SCC4cisR by the IC50 values of the generation-matched SCC4 cells. Data were plotted using Graphpad Prism 5. Values represent the mean ±S.E.M. of three independent experiments. Statistical analysis was performed using one-way ANOVA (Graphpad Prism 8). *** $p<0.001$.

Cell generation	SCC4 IC_{50} values (µM)	SCC4cisR IC_{50} values (µM)	Resistance Index (RI)
G4	0.9 ± 0.3	2.7 ± 0.4	2.9 ± 1.0
G5	1.1 ± 0.1	3.0 ± 0.3	2.7 ± 0.5
G6	1.2 ± 0.6	3.6 ± 1.2	3.6 ± 1.7
G7	1.0 ± 0.1	4.5 ± 0.5	4.0 ± 0.9
G8	1.5 ± 0.6	9.3 ± 2.6	5.6 ± 0.6
G9	1.7 ± 0.4	14.7 ± 0.6	8.6 ± 1.7
G10	1.1 ± 0.2	16.2 ± 4.8	13.7 ± 2.7

Table 5.2 IC50 and RI values of SCC4 and SCC4cisR cells treated with cisplatin.

Values represent the mean ± S.E.M. of three independent experiments.

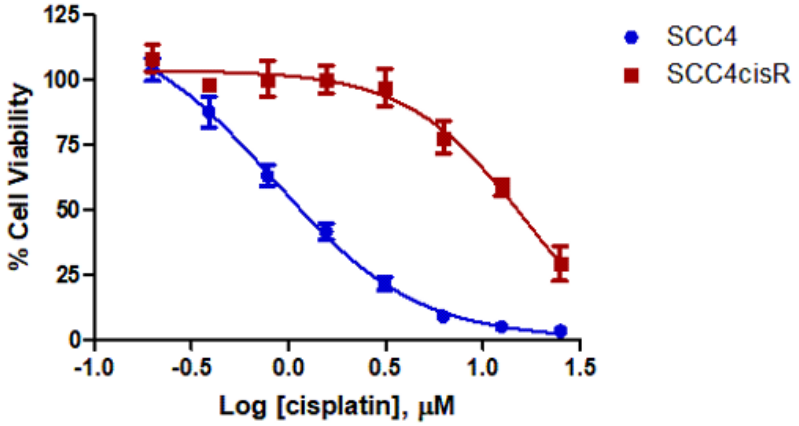

Figure 5.2 Differences in cisplatin susceptibility of SCC4 and SCC4cisR cell lines.

SCC4 and SCC4cisR cell lines (G10) were seeded at $5x10^3$ cells/well in 96 well plates. Cells were left for 24 h to adhere to the plate and then were treated with vehicle (0.009% (v/v) NaCl) or a range of concentrations of cisplatin (0.1-25 µM) for 72 h. Alamar blue (10% (v/v)) was added to each well 6 h before the end of the treatment and plates were kept in the dark at 37°C. Fluorescence was measured on the SpectraMax Gemini EM Microplate Reader at an excitation wavelength of 544 nm and an emission wavelength of 590 nm. Values obtained from cells treated with cisplatin were normalised against vehicle treated cells and results were plotted using Graphpad Prism 8. Values represent the mean ± S.E.M. of three independent experiments.

5.2.2. Cisplatin induces reduced activation of apoptosis in the cisplatin-resistant SCC4cisR cell line

Evaluation of apoptosis was undertaken in SCC4 and in SCC4cisR cells treated with cisplatin in order to compare the activation of this process in drug-sensitive and resistant cell populations. To study apoptosis, flow cytometric analysis of annexin V/PI stained cells was performed. Cells were treated with vehicle or with increasing concentrations of cisplatin (1-15 μM) for 48 h, and then were double stained with annexin V-FITC and PI. The percentage of cells in early and late apoptosis was acquired on the BD Accuri flow cytometer using the BD Accuri software. Cisplatin induced apoptotic cell death in both SCC4 and SCC4cisR cells in a dose-dependent manner (Figure 5.3). As expected, a significant increase in the apoptotic rate in the SCC4 cell line was observed when concentrations of cisplatin increased from 5 μM to 15 μM. Conversely, a significant induction of apoptosis in SCC4cisR cells was observed only when cells were treated with 15 μM cisplatin. From the comparison of the two cell lines, a statistically significant variation in the apoptotic rate between SCC4 and SCC4cisR cells was detected at 5 μM, 10 and 15 μM cisplatin. These results suggest that cisplatin induced reduced activation of apoptosis in the SCC4cisR cell line compared to the SCC4 cell line.

These findings correlate with the results obtained from the viability assay, confirming the change in cisplatin susceptibility of the resistant SCC4cisR cell line compared to the age-matched parental SCC4 cell line.

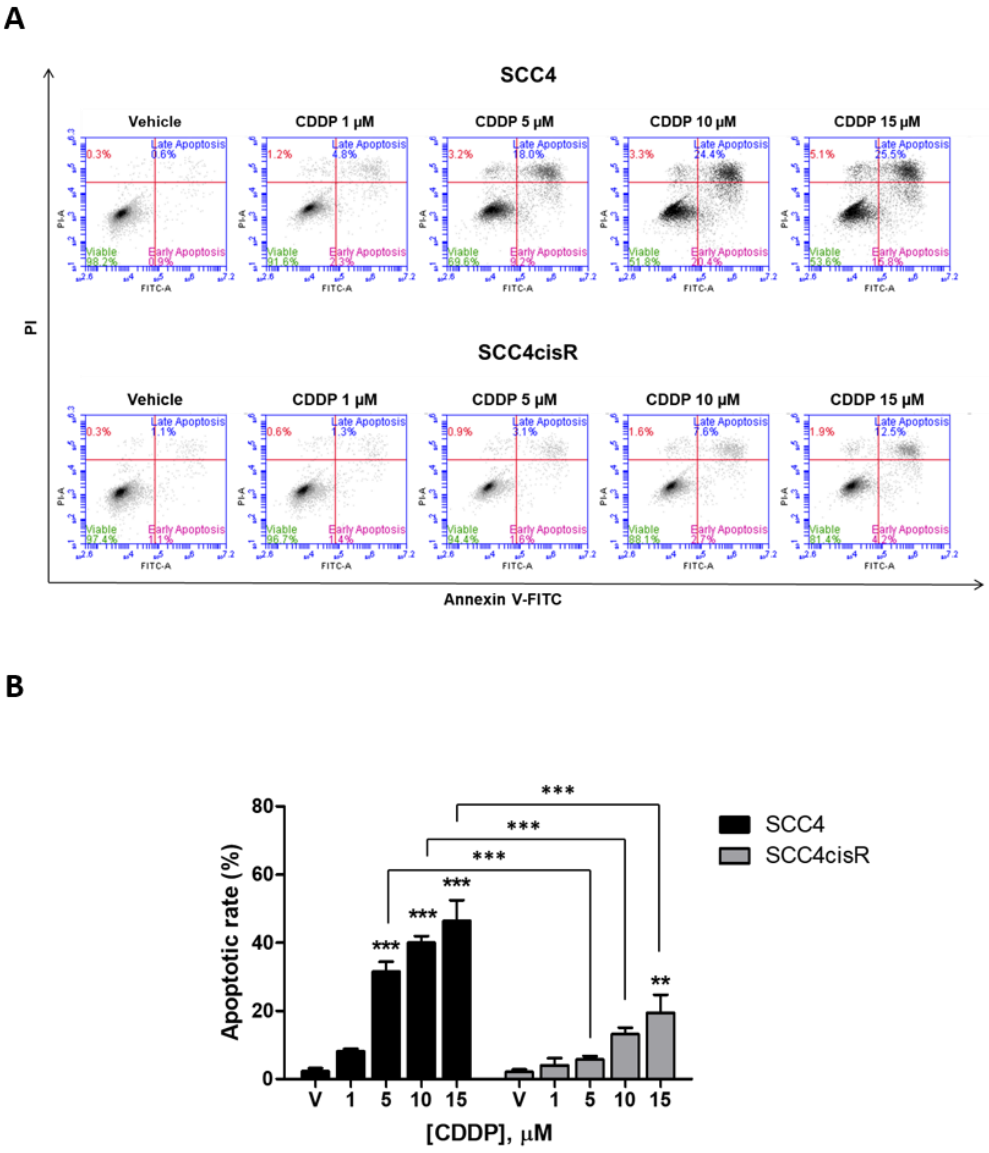

Figure 5.3 Cisplatin induces reduced activation of apoptosis in the SCC4cisR cell line compared to the parental SCC4 cell line.

SCC4 and SCC4cisR cells were seeded at 150x10^3 cells/well in 6 well plates. Cells were left for 24 h to adhere to the plate and then were treated with vehicle (0.009% (v/v) NaCl) or with increasing concentrations of cisplatin (CDDP) (1-15 µM). After 48 h, cells were harvested, and double stained with annexin V/PI. Cells were then analysed by flow cytometry using BD Accuri software. 10,000 single cells were gated on vehicle treated cells and the percentage of cells undergoing early and late apoptosis was acquired. **A.** Representative dot plot of treated cells. **B.** Apoptotic rate values were obtained by summing early and late apoptotic cell percentages. Data represent the mean ±S.E.M of three independent experiments. Statistical analysis was performed using one-way ANOVA with Dunnett's Multiple Comparison Test to compare mean values within the same cell line and two-way ANOVA with Tukey's Multiple Comparison Test to compare mean values between the two cell lines (Graphpad Prism 8). *** $p<0.001$, ** $p<0.01$.

5.2.3. Analysis of the colony forming ability in cisplatin-sensitive and resistant OSCC cell lines

The colony forming assay (CFA) was employed to evaluate the survival potential of SCC4 and SCC4cisR cells following treatment with cisplatin. The CFA is an *in vitro* assay based on the capacity of single cells to grow into colonies [308]. This assay involves the detection of colonies formed after exposure of cells to cytotoxic agents such as drugs or irradiation. Assuming that each colony derives from a single surviving cell, determination of the number of colonies formed after cytotoxic treatments is indicative of the ability of cells to recover and survive. Moreover, exposure of cells to several doses of cytotoxic agents allows one to determine a cell survival curve, which is representative of the relationship between treatment dose and fraction of cells retaining the ability to reproduce (survival fraction). In the present study, survival curves of SCC4 and SCC4cisR cells treated with cisplatin were generated.

Before commencing the experiments, optimisation of seeding density was required in order to determine the optical cell density for colony counting. In fact, a too low cell density does not allow the formation of a relevant number of colonies, while a too high cell density leads to overlapping colonies resulting in inaccurate colony counting [308]. Optimisation of the seeding density was assessed in both SCC4 and SCC4cisR cell lines. Cells were seeded at a cell density range of 250-1500 cells/well in 6 well plates and were left growing for 12 days to mimic the treatment times. After the incubation, colonies obtained were fixed and stained with crystal violet, and images of the plates were acquired using the GelCount image scanner. As shown in Figure 5.4, a correlation between cell density and number of colonies was observed in the SCC4 and SCC4cisR cell lines. A cell density of 500 cells/well was selected as optical seeding density for subsequent experiments in both cell lines.

In order to determine the cell survival potential, SCC4 and SCC4cisR cells were seeded as mentioned above and treated with vehicle or with increasing concentrations of cisplatin (0.2-2 μM) for 48 h. After the treatment, cells that had survived were incubated in drug-free media for 9 days to allow cell recovery, and colonies obtained were fixed and stained with crystal violet. From a visual analysis, a decrease in the number of colonies was observed at increasing concentrations of cisplatin in both SCC4 and SCC4cisR cells, suggesting a dose-dependent correlation between the treatment and the survival potential of the two cell lines (Figure 5.5A). Moreover, a notable difference in the number of

colonies was displayed in the SCC4cisR cells treated with cisplatin compared to the parental SCC4 cells. In fact, colonies were extremely rare in SCC4 cells treated with cisplatin from concentrations as low as 0.5 μM, whilst a sizeable number of colonies were still visible at 1 μM cisplatin in the SCC4cisR cells, clearly demonstrating a higher ability to survive and recover from cytotoxic drug treatments. To estimate the survival potential of the two cell lines, colonies were manually counted and the survival fractions were determined. As shown in Figure 5.5B, a shift to the right was observed in the survival curve of SCC4cisR cells compared to SCC4 cells, indicating a substantial difference in the survival potential between the two cell lines. Accordingly, a significantly higher survival fraction was found in SCC4cisR cells treated with 0.2, 0.5 and 1 μM cisplatin compared to the parental cells.

Taken together, these data showed a higher recovery and survival ability of the SCC4cisR cells compared to the SCC4 cells following exposure to cisplatin, confirming the induction of a cisplatin-resistant phenotype.

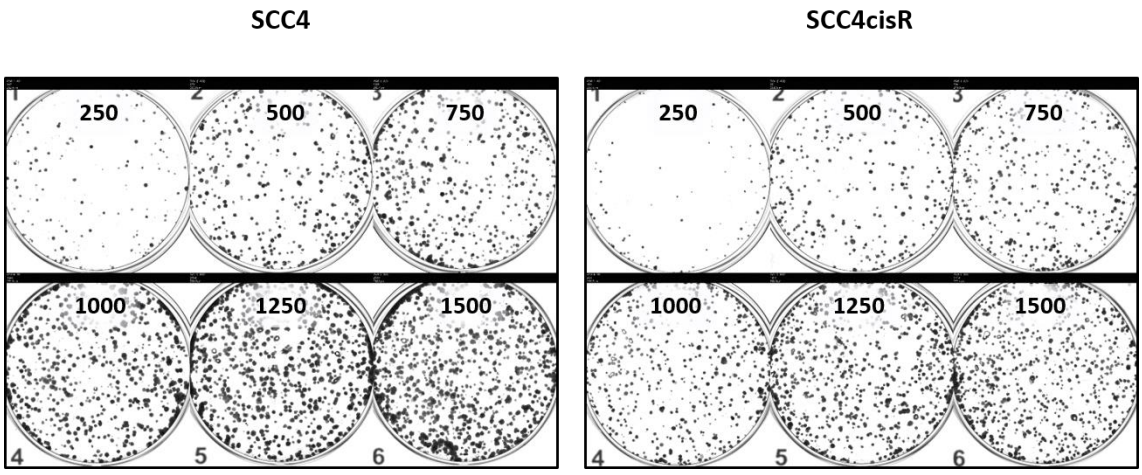

Figure 5.4 Optimisation of the seeding density for the colony forming assay in SCC4 and SCC4cisR cell lines.

SCC4 and SCC4cisR cells were seeded at various densities (250-1500 cells/well) in 6 well plates with a total volume of 2 mL in each well. After 12 days, cells were fixed and stained with crystal violet for 1 h. Images of the plates were acquired with the GelCount image scanner.

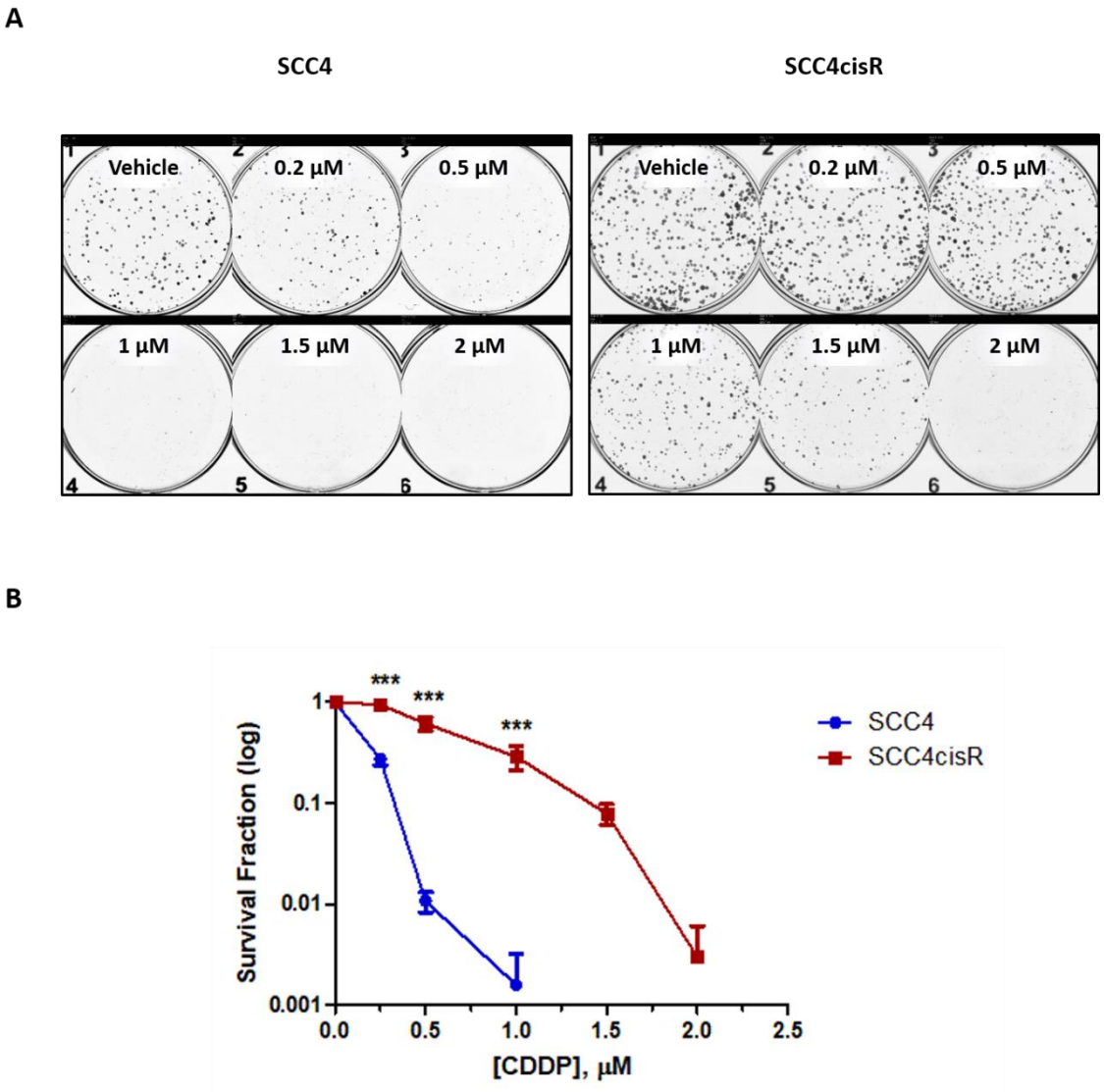

Figure 5.5 Analysis of the survival fractions in SCC4 and SCC4cisR cells treated with cisplatin.
SCC4 and SCC4cisR cells were seeded at 500 cells/well in 6 well plates. Cells were left for 24 h to adhere to the plate and then were treated with vehicle (0.009% (v/v) NaCl) or with increasing concentrations of cisplatin (CDDP) (0.2-2 µM). After 48 h, cells were incubated in drug-free media for 9 days before being fixed and stained with crystal violet. **A.** Images of the plates were acquired with the GelCount image scanner. **B.** The survival fraction was calculated as the number of colonies counted divided by the number of colonies plated with a correction for the plating efficiency (number of colonies formed in control cells/number of cells plated x 100). Values represent the mean ±S.E.M of three independent experiments. Statistical analysis was performed using two-way ANOVA with Tukey's Multiple Comparison Test to compare mean values between the two cell lines (Graphpad Prism 8). *** $p<0.001$.

5.2.4. Analysis of the $CD44^+/CD24^-$ fraction in cisplatin-sensitive and resistant OSCC cell lines

Resistance to chemotherapy has been associated to a subpopulation of cells named cancer stem cells (CSCs). CSCs have been defined as multipotent and highly tumorigenic cells capable of self-renewal [101]. The evaluation of cell surface markers such as CD44 and CD24 represents a widely used method for the identification of CSCs [489]. Recently, some studies have proposed that the presence of CD44 along with the lack of CD24 ($CD44^+/CD24^-$) on the cell surface may be used as marker of CSC phenotype in various cancers, including breast cancer, colon cancer as well as OSCC [314, 489]. In the present study, the presence of a $CD44^+/CD24^-$ cell population was investigated in the SCC4 cell line and in the derived cisplatin-resistant SCC4cisR cell line in order to evaluate whether resistance to cisplatin in OSCC may be correlated to this population of cells.

Flow cytometric analysis of CD44-FITC/CD24-APC stained cells was performed to identify the $CD44^+/CD24^-$ cell population in SCC4 and SCC4cisR cell lines. Two breast cancer cell lines, MCF-7 and MDA-MB-231, were used as negative and positive controls respectively for the $CD44^+/CD24^-$ profile. Cells were seeded at a density of $150x10^3$ cells/well in a 6-well plate and left adhere to the plate overnight. The next day, cells were double stained with CD44-FITC and CD24-APC, and the percentage of cells positive to one or both stains was determined using the BD Accuri flow cytometer. A dot plot showed the different cell populations: $CD44^-/CD24^-$ in the lower left quadrant, $CD44^-/CD24^+$ in the lower right quadrant, $CD44^+/CD24^+$ in the upper right quadrant and $CD44^{+/}CD24^-$ in the upper left quadrant. As shown in Figure 5.6, a low percentage of $CD44^+/CD24^-$ cells (~3%) was observed in the MCF-7 cell line (negative control), whilst a high percentage of $CD44^+/CD24^-$ cells (~98%) was observed in the MDA-MB-231 cell line (positive control). Interestingly, high expression of the two surface markers CD44 and CD24 was found in both SCC4 and SCC4cisR cells. Accordingly, a low percentage of $CD44^+/CD24^-$ cells was detected in the two cell lines due to the high expression of CD24. Furthermore, no differences in the expression of the two markers were detected between the SCC4 and the SCC4cisR cell line, implying no changes in the abundance of the $CD44^+/CD24^-$ cell population during the acquisition of the resistant phenotype.

This result indicates a scarce $CD44^+/CD24^-$ cell population in the SCC4 cell line as well as in the derived cisplatin-resistant SCC4cisR cell line, suggesting that this population of cells may not be implicated in chemoresistance in the cell model herein examined.

A

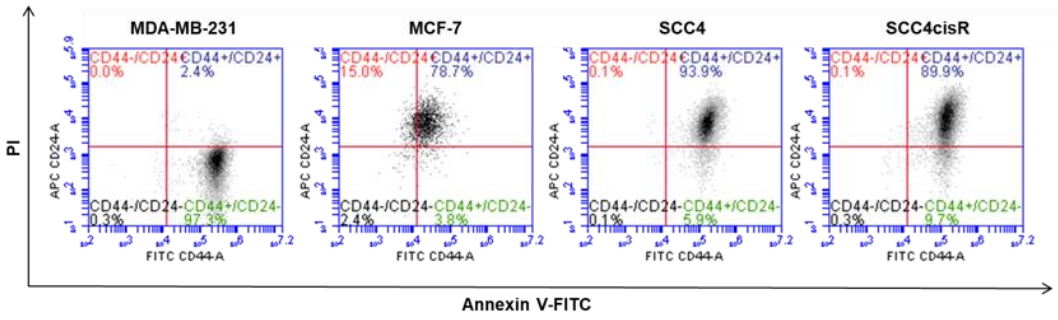

B

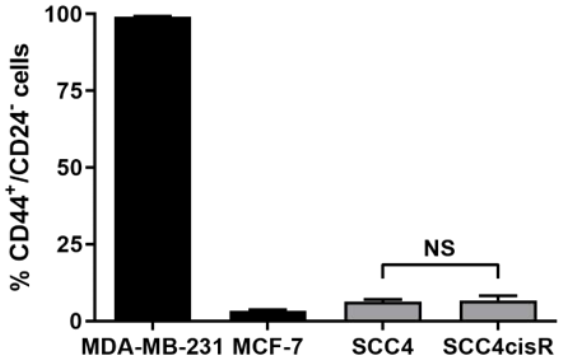

Figure 5.6 Analysis of the CD44+/CD24- fraction in SCC4 and SCC4cisR cells.

SCC4 and SCC4cisR cells were seeded at 150x10^3 cells/well in 6 well plates along with MDA-MB-231 cells (positive control) and MCF-7 cells (negative control). The next day cells were harvested and double stained with CD44-FITC and CD24-APC antibodies. Cells were then analysed by flow cytometry using BD Accuri software. 10,000 single cells were gated on control cells and the percentage of $CD44^+/CD24^-$ cells was acquired. **A.** Representative dot plot. **B.** Data represent the mean ±S.E.M of three independent experiments. Statistical analysis was performed using two-tailed t-test to compare mean values between the two SCC4 cell lines (Graphpad Prism 8). NS = no significance.

5.2.5. Analysis of cross-resistance in the cisplatin-resistant SCC4cisR cell line

The induction of resistance to a specific drug can lead to the development of multidrug resistance, which results in cross-resistance to diverse chemotherapeutic agents [490]. In the present study, the effect of various anticancer drugs on the viability of SCC4 and SCC4cisR cells was examined in order to determine whether the induction of a cisplatin-resistant phenotype led to a multidrug resistance phenotype. For this analysis, cell viability in response to the platinum-based compound carboplatin, the tubulin-targeting agent docetaxel and multi-kinase inhibitor sorafenib was assessed in both SCC4 and SCC4cisR cells using the alamar blue assay.

SCC4 and SCC4cisR cells were treated with several concentrations of carboplatin (3.9-100 μM), docetaxel (0.04-10 nM) and sorafenib (3.1-200 μM) for 72 h. From the viability curves obtained, it was observed that all the three drugs reduced the viability of both cell lines in a dose-dependent manner, with a micromolar range obtained for the cell sensitivity to carboplatin and sorafenib and a low nanomolar range for the cell sensitivity to docetaxel (Figure 5.7). Interestingly, a shift to the right was observed in the viability curve of the SCC4cisR cell line treated with carboplatin compared to viability curve of the SCC4 cell line, suggesting that a reduced sensitivity to carboplatin was acquired in the SCC4cisR cells compared to the parental cell line. By contrast, no notable changes were observed in the viability curves of SCC4cisR cells treated with docetaxel and sorafenib compared to the parental cells, indicating that the two cell lines had almost the same susceptibility to these drugs.

To estimate the sensitivity of the SCC4 and SCC4cisR cells to carboplatin, docetaxel and sorafenib, the IC_{50} values and the RI values were calculated (Table 5.3 and Figure 5.8). In the present study, a RI $\geq$5 was considered significant and relevant to determine the acquisition of a resistant phenotype. Interestingly, IC_{50} values of 65.2±6.5 μM and 551±100.1 μM were found in SCC4 and SCC4cisR cells, respectively, after 72 h treatment with carboplatin. Given that the RI of SCC4cisR cells in relation to carboplatin was 8.4, this suggested that pulsed exposure of cells to cisplatin may lead also to acquired cross-resistance to carboplatin. Moreover, IC_{50} values of 0.7±0.38 nM and 0.5±0.1 nM were obtained for docetaxel in SCC4 and SCC4cisR cells respectively, whilst IC_{50} values of 18.6±3.2 μM and 12.1±1.1 μM were obtained for sorafenib in SCC4 and SCC4cisR cells respectively. Since the RI of SCC4cisR cells in relation to docetaxel and sorafenib

were lower than 5, it was concluded that no resistance to these two drugs was acquired during the induction of the cisplatin-resistant phenotype.

Given that cisplatin and carboplatin belong to the same group of compounds, namely platinum-based agents, these results indicate that pulsed exposure of cells to cisplatin may lead to an acquired resistance not only to cisplatin, but also to similar compounds like carboplatin. However, no resistance to other types of drugs (such as docetaxel or sorafenib) was observed in the SCC4cisR cell line, suggesting the development of cross-resistance only to structurally similar compounds.

.

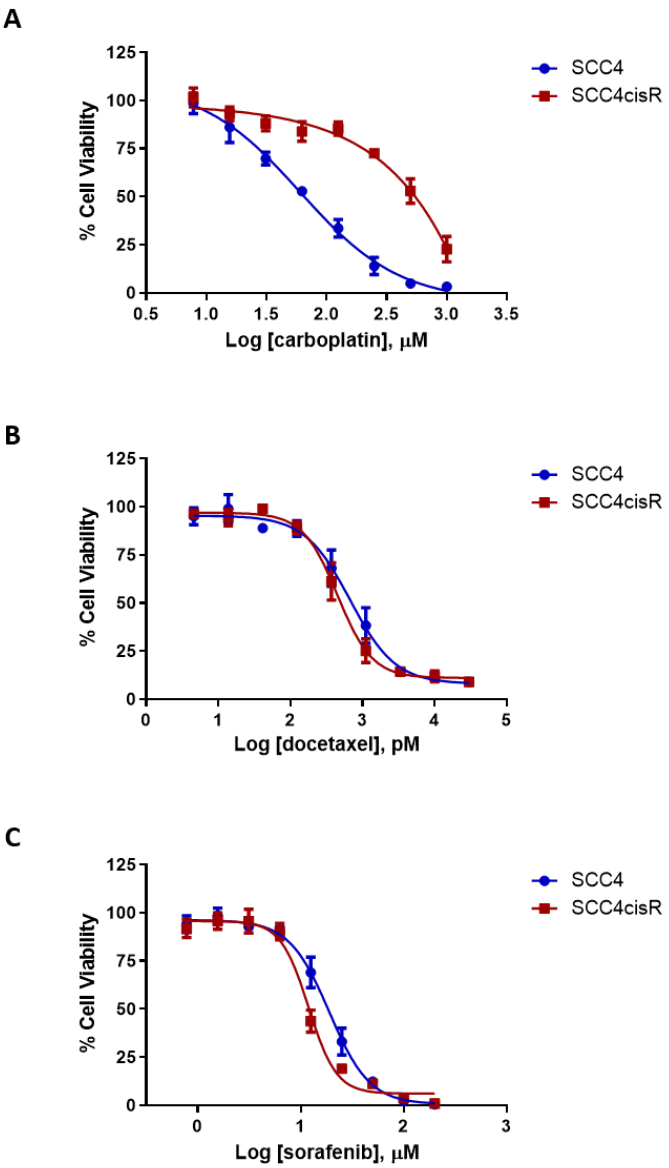

Figure 5.7 Differences in the sensitivity of SCC4 and SCC4cisR cell lines to carboplatin, docetaxel and sorafenib.

SCC4 and SCC4cisR cells were seeded at $5x10^3$ cells/well in 96 well plates and were left for 24 h to adhere to the plate before being treated. **A.** Cells were treated with a vehicle (1% (v/v) H_2O) or a range of concentrations of carboplatin (3.9-100 µM) for 72 h. **B.** Cells were treated with a vehicle (1% (v/v) ethanol) or a range of concentrations of docetaxel (0.04-10 nM) for 72 h. **C.** Cells were treated with a vehicle (0.1% (v/v) DMSO) or a range of concentrations of sorafenib (3.1-200 µM) for 72 h. Alamar blue (10% (v/v)) was added to each well 6 h before the end of the treatment and plates were kept in the dark at 37°C. Fluorescence was measured on the SpectraMax Gemini EM Microplate Reader at an excitation wavelength of 544 nm and an emission wavelength of 590 nm. Values obtained from cells treated with the drugs were normalised against vehicle treated cells and results were plotted using Graphpad Prism 8. Values represent the mean ± S.E.M. of three independent experiments.

Drug	SCC4 IC_{50} values	SCC4cisR IC_{50} values	Resistance Index (RI)
Carboplatin	65.2±6.5 µM	551.2±100 µM	8.4 ± 1.6
Docetaxel	0.7±0.3 nM	0.5±0.1 nM	0.7 ± 0.1
Sorafenib	18.6±3.2 µM	12.1±1.1 µM	0.6 ± 0.0

Table 5.3 IC50 and RI values of SCC4 and SCC4cisR cells treated with carboplatin, docetaxel and sorafenib.

Values represent the mean ± S.E.M. of three independent experiments.

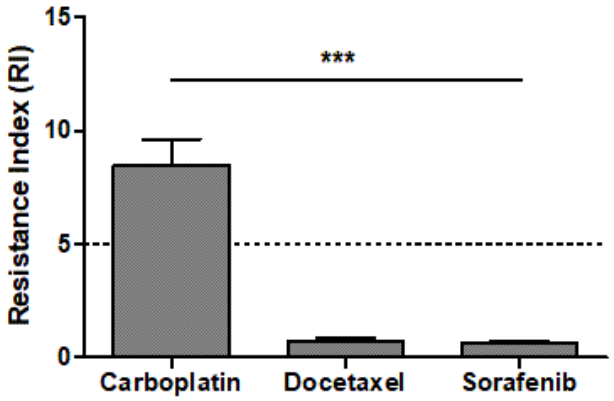

Figure 5.8 RI variation of SCC4cisR cells in relation to carboplatin, docetaxel and sorafenib.

RI values were calculated by dividing the IC_{50} values of SCC4cisR by the IC_{50} values of the SCC4 cells. Data were plotted using Graphpad Prism 8. Values represent the mean ±S.E.M. of three independent experiments. Statistical analysis was performed using one-way ANOVA (Graphpad Prism 8). *** $p<0.001$.

5.2.6. Role of autophagy in cisplatin resistance in OSCC cells

Autophagy activation in response to chemotherapeutics has been proposed as a potential mechanism implicated in chemoresistance [491]. In the present study, the enhancement of autophagy in OSCC cells treated with cisplatin was demonstrated in chapter 3, and the implication of autophagy in chemoresistance in OSCC cells was examined by targeting the autophagic flux with pharmacological and genetic autophagy inhibitors. Analysis of autophagy in cisplatin-sensitive and resistant OSCC cells derived from the same cell line was herein undertaken in order to further evaluate the role of autophagy in chemoresistance in OSCC.

5.2.6.1. Evaluation of endogenous and starvation-induced autophagy in cisplatin-sensitive and resistant OSCC cell lines

Endogenous levels of autophagy along with autophagy activation in response to external stimuli was assessed in cisplatin-sensitive SCC4 cells and in cisplatin-resistant SCC4cisR cells under normal and starvation conditions. Western Blot analysis of p62 and LC3-I/II protein expression was employed to study autophagy. Activation of autophagy was determined by monitoring the autophagic flux using the late stage autophagy inhibitor bafilomycin-A1.

SCC4 and SCC4cisR cells were left untreated or treated with EBSS for 2 or 4 h in the presence/absence of bafilomycin-A1 (100 μM) added 1 h before the end of the incubation period. Lysates were prepared and run on a 15% SDS-PAGE gel before being probed with anti-p62 and anti-LC3-I/II antibodies. Accumulation of LC3-II and p62 proteins in cells treated with bafilomycin-A1 compared to control cells was observed in both SCC4 and SCC4cisR cell lines, indicating that basal levels of autophagy were constitutively activated in both cell lines under normal conditions (Figure 5.9). Interestingly, a slight difference in basal autophagy levels was detected from the initial comparison of the two cell lines. In fact, increased p62 expression levels and reduced LC3-II/LC3-I ratio in control and bafilomycin-A1 treated cells was observed in the SCC4cisR cell line compared to the SCC4 cell line, implying lowered levels of endogenous autophagy in the cisplatin-resistant cells compared to the parental cells. However, following statistical analysis across three separate experiments no significant differences in basal autophagy levels were determined between the sensitive and resistant cells. Interestingly, conversion

of LC3-I to LC3-II along with p62 degradation was found in SCC4 and SCC4cisR cells treated with EBSS for 2 and 4 h, indicating the induction of the autophagic flux under starvation conditions in both cell lines.

Taken together, these results suggest that there was no significant difference in basal autophagy levels between the SCC4cisR cells and the parental SCC4 cells and that both cell lines showed a similar ability to undergo autophagy in response to external stimuli such as starvation.

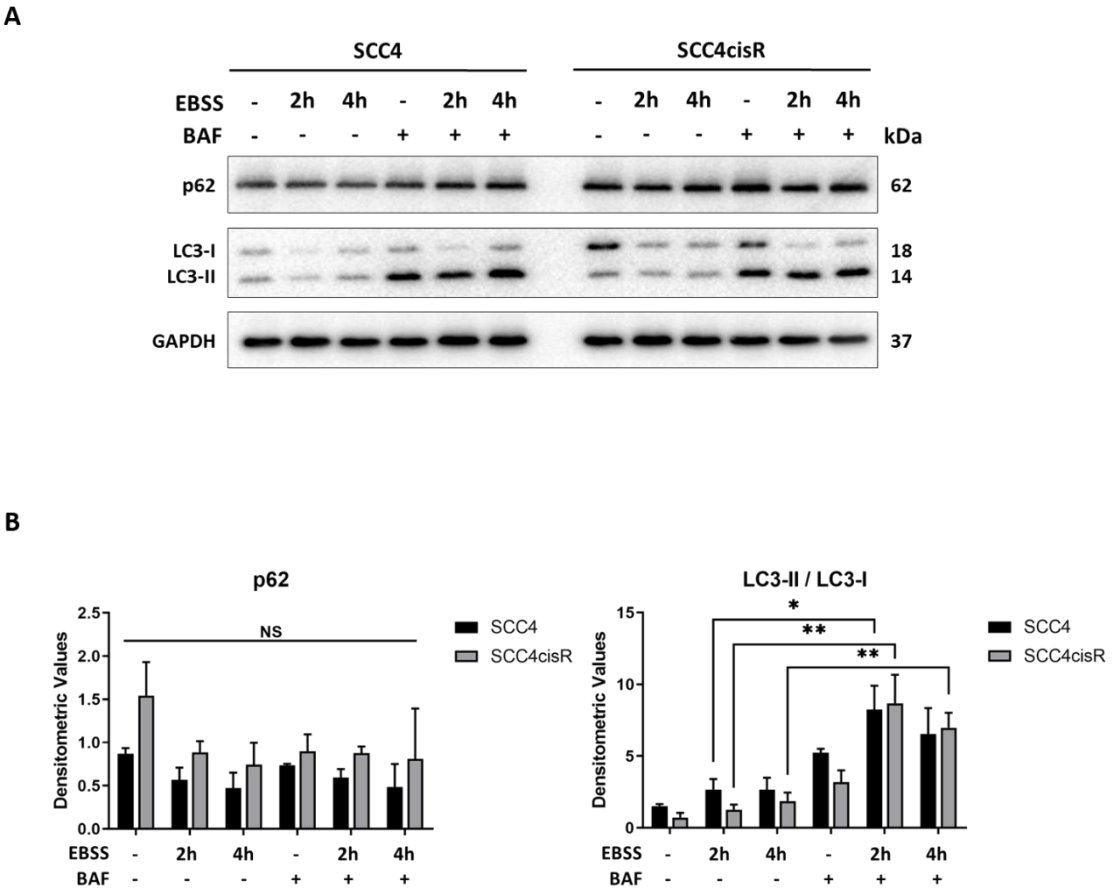

Figure 5.9 Evaluation of basal levels of autophagy in SCC4 and SCC4cisR cell lines.

SCC4 and SCC4cisR cells were seeded at $300x10^3$ cells/well in 6 well plates. Cells were left for 24 h to adhere to the plate and then were treated with EBSS for 2 or 4 h in presence/absence of bafilomycin-A1 (100 μM) added 1 h before the end of the treatment. Cells were lysed and 20 μg of protein was loaded and separated in a 15% SDS-PAGE gel, transferred to a PVDF membrane and probed with anti-p62 and anti-LC3-I/II antibodies. GAPDH served as loading control. **A**. Results are representative of three independent experiments. **B**. Densitometric analysis of p62, LC3-I and LC3-II bands was performed using ImageLab software and values were normalised to the loading control. Data represent the mean ± S.E.M. of three independent experiments. Statistical analysis was performed using one-way ANOVA with Tukey's Multiple Comparison Test to compare mean values within the same cell line and two-way ANOVA with Tukey's Multiple Comparison Test to compare mean values between the two cell lines (Graphpad Prism 8). ** $p<0.01$, * $p<0.05$.

5.2.6.2. SCC4 and SCC4cisR cells display a differential autophagic response to cisplatin

In order to determine whether autophagy plays a role in chemoresistance, autophagy activation in response to cisplatin was examined in cisplatin-resistant SCC4cisR cells and in the age-matched parental sensitive cells.

SCC4 and SCC4cisR cells were treated with vehicle or 5 μM cisplatin for 48 h and LC3-I/II protein expression levels were determined by Western Blot analysis. Lysates were prepared and run on a 15% SDS-PAGE gel before being probed with an anti-LC3-I/II antibody. As expected, a significant conversion of LC3-I to LC3-II was observed in parental SCC4 cells treated with cisplatin compared to vehicle treated cells, indicating autophagy activation in response to the drug (Figure 5.10). However, under the same treatment, no changes were observed in the LC3-II/LC3-I ratio between vehicle treated cells and cisplatin treated cells in the SCC4cisR cell line, suggesting that at this concentration of cisplatin (5 μM) activation of autophagy was induced only in the cisplatin-sensitive OSCC cell line but not in the cisplatin-resistant OSCC cell line. This result suggests a differential autophagic response to cisplatin following acquisition of chemoresistance.

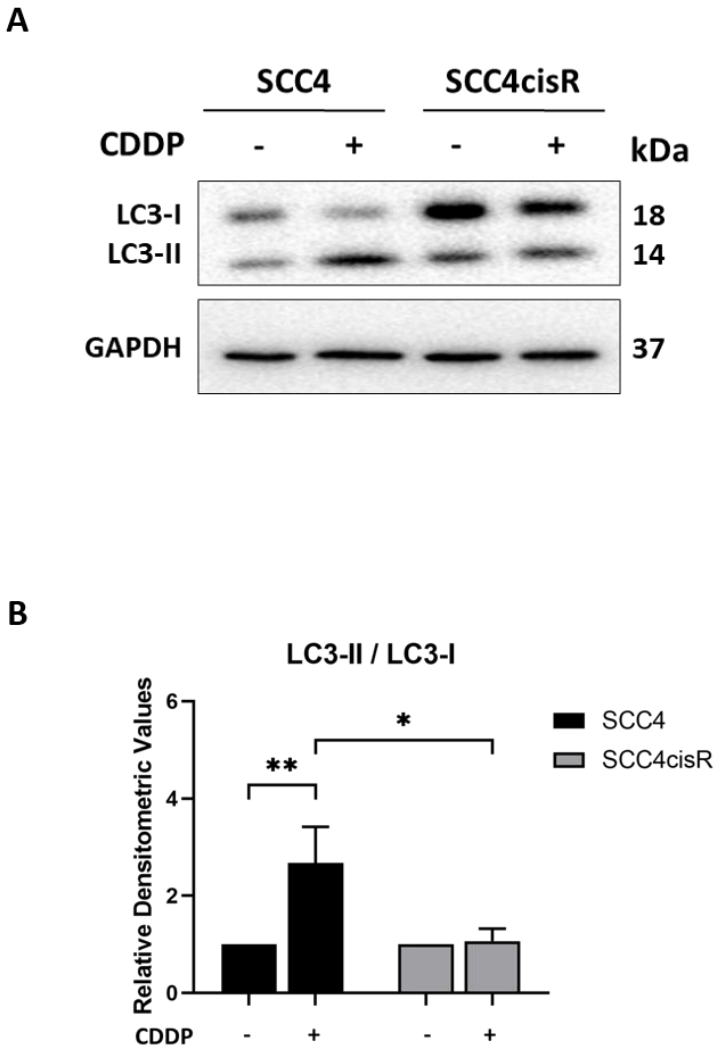

Figure 5.10 SCC4 and SCC4cisR cells display a differential autophagic response to cisplatin.

SCC4 and SCC4cisR cells were seeded at $300x10^3$ cells/flask. Cells were left for 24 h to adhere to the flask and then were treated vehicle (0.009% (v/v) NaCl) or with 5 μM cisplatin (CDDP) for 48 h. After incubation, cells were lysed and 20 μg of protein was loaded and separated on a 12% SDS-PAGE gel and transferred to a PVDF membrane. **A**. Membranes were probed with an anti-LC3-I/II antibody. GAPDH served as loading control. **B**. Densitometric analysis of LC3-I and LC3-II bands was performed using ImageLab software and values were normalised by the loading control. Values obtained from treated cells were normalised by control cells. Statistical analysis was performed using two-way ANOVA with Multiple Comparison Test to compare mean values within the same cell line and between the two cell lines (Graphpad Prism 8). ** $p<0.01$, * $p<0.05$.

5.2.7. Chloroquine sensitises cisplatin-resistant OSCC cells to cisplatin

Enhancement of cisplatin-induced apoptosis in OSCC cells treated with chloroquine was demonstrated in chapter 3 (Figures 3.22-23). The effect of chloroquine on cisplatin-resistant SCC4cisR cells was herein examined in order to confirm whether targeting autophagy with chloroquine may represent a strategy to sensitise OSCC cells to cisplatin.

Apoptosis induction was investigated in SCC4cisR cells and in the aged-matched parental SCC4 cells through flow cytometric analysis of annexin V/PI stained cells. SCC4 and SCC4cisR cells were treated with cisplatin 5 μM alone, chloroquine 10 μM alone and cisplatin in combination with chloroquine for 48 h. Cells were then double stained with annexin V-FITC and PI, and the percentage of cells in early and late apoptosis was acquired using the BD Accuri flow cytometer. As shown in Figure 5.11, SCC4 and SCC4cisR cells treated with chloroquine alone exhibited no increase in the apoptotic rate when compared to vehicle treated cells. As expected, parental SCC4 cells treated with cisplatin alone showed a significant increase in the apoptotic rate compared to control cells, while no induction of apoptosis was observed in SCC4cisR cells treated with cisplatin alone compared to control cells. Interestingly, in both cell lines, treatment of chloroquine in combination with cisplatin displayed a significant increase in the rate of apoptosis compared to vehicle treated cells and to cisplatin treated cells, suggesting that chloroquine enhanced cisplatin-induced apoptosis in both cisplatin-sensitive and resistant OSCC cell lines.

The significant enhancement of cisplatin-induced apoptosis in both cisplatin-sensitive and resistant OSCC cell lines treated with chloroquine may suggest a beneficial effect of this compound to sensitise OSCC cells to cisplatin. Moreover, since no activation of autophagy was observed in SCC4cisR cells treated with cisplatin, this result may imply that chloroquine can enhance cisplatin-induced apoptosis through an autophagy-independent mechanism.

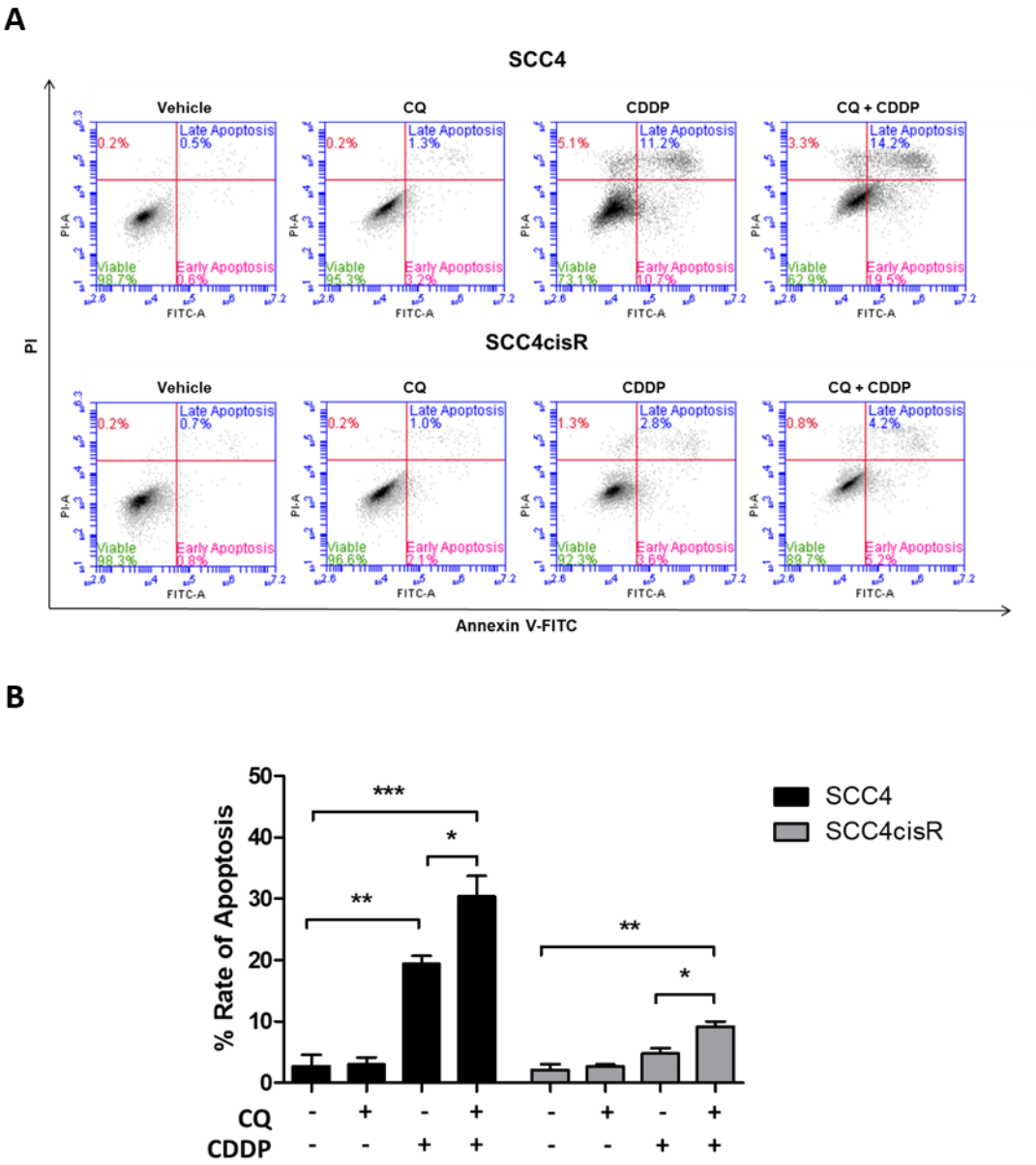

Figure 5.11 Chloroquine enhances cisplatin-induced apoptosis in SCC4 and SCC4cisR cell lines. SCC4 and SCC4cisR cells were seeded at 150x10^3 cells/well in 6 well plates. Cells were left for 24 h to adhere to the plate and then were treated with vehicle (0.009% (v/v) NaCl), 10 µM chloroquine (CQ) alone, 5 µM cisplatin (CDDP) alone, or cisplatin in combination with chloroquine for 48 h. Cells were then analysed by flow cytometry using BD FACS Accuri software. 10,000 single cells were gated on vehicle treated cells and the percentage of cells undergoing early and late apoptosis was acquired. **A**. Representative dot plot of treated cells. **B**. Values represent the mean ± S.E.M. of three independent experiments. Statistical analysis was performed using one-way ANOVA with Tukey's Multiple Comparison Test to compare treatments within the same cell line (Graphpad Prism 8). *** $p<0.001$, ** $p<0.01$, * $p<0.05$.

5.2.8. Role of oxidative stress in cisplatin resistance in OSCC cells

In chapter 4, treatment of OSCC cells with cisplatin was shown to induce oxidative stress (Figures 4.2-3). To evaluate whether oxidative stress was involved in cisplatin resistance in oral cancer, evaluation of intracellular levels of ROS along with the analysis of antioxidant defence systems such as glutathione, nuclear factor erythroid 2–related factor 2 (Nrf2) and heme oxygenase-1 (HO-1) was herein undertaken in cisplatin-sensitive and -resistant OSCC cells.

5.2.8.1. Determination of intracellular ROS levels in cisplatin-sensitive and resistant OSCC cells

To determine whether ROS are involved in cisplatin susceptibility, intracellular ROS levels were evaluated in both drug-sensitive and -resistant OSCC cells in response to cisplatin. For this analysis, SCC4 and SCC4cisR cells were left untreated or treated with cisplatin for 48 h. Cells were then stained with H_2DCFDA for 30 min and fluorescence was measured using the BD Accuri flow cytometer. As expected, a statistically significant increase in ROS levels was observed in SCC4 cells treated with cisplatin compared to untreated cells, confirming that cisplatin enhanced ROS generation in OSCC cells (Figure 5.12A, Figure A.7). Similarly, a notable increase in ROS levels was found in cisplatin treated SCC4cisR cells compared to untreated cells. Interestingly, a significant difference in ROS levels was displayed between the two cell lines in response to cisplatin, with a two-fold increase in cisplatin-induced ROS levels detected in the SCC4cisR cells compared to the SCC4 cells. This result indicates an enhancement in ROS generation in the cisplatin-resistant cell line compared to the paired parental cell line following treatment with cisplatin. Furthermore, to aid in evaluating the role of ROS in mediating cisplatin resistance, ROS levels obtained from untreated SCC4 and SCC4cisR cells were independently compared to assess the difference in endogenous ROS between the two cell lines (Figure 5.12B). An unpaired two-tailed student t-test was applied for this analysis, and interestingly showed a significant increase in the endogenous levels of ROS in the SCC4cisR cells compared to the SCC4 cells. Taken together, these data indicate a significant increase in both endogenous and cisplatin-induced ROS levels in the cisplatin-resistant OSCC cell line compared to the paired parental cell line, suggesting a possible role for ROS in mediating cisplatin resistance.

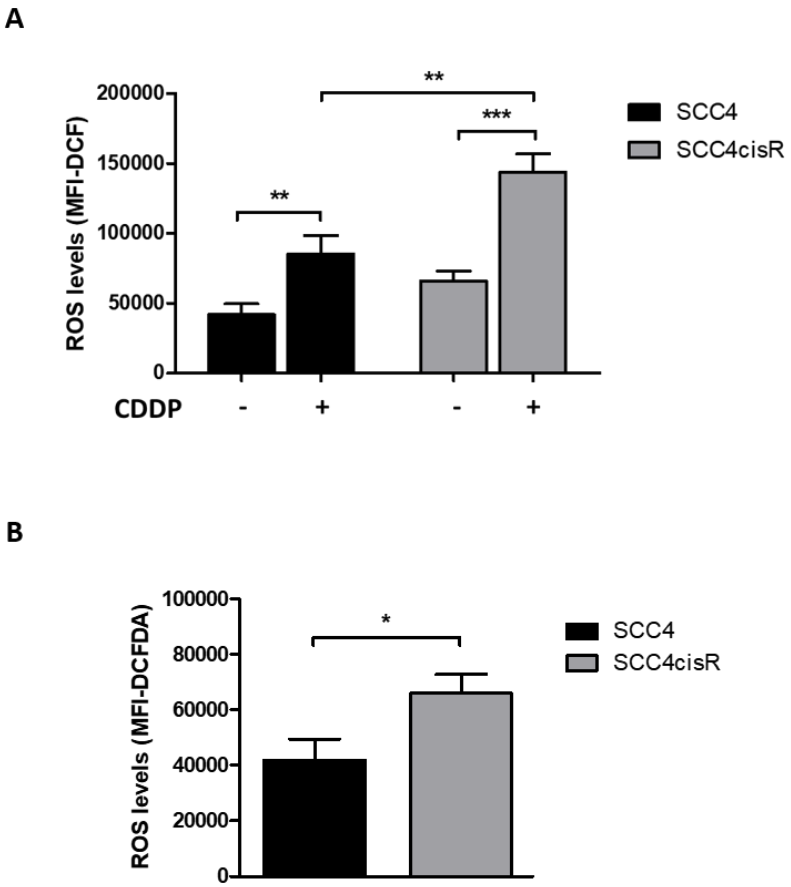

Figure 5.12 Intracellular ROS levels in cisplatin-sensitive and -resistant OSCC cell lines.

A. SCC4 and SCC4cisR cells were seeded at $150x10^3$ cells/well in 6 well plates. Cells were left for 24 h to adhere to the plate and then were left untreated or treated with 5 μM cisplatin. After 48 h, 10 μM H_2DCFDA dye was added to each well for 30 min. Cells were then harvested and analysed on the flow BD FACS Accuri cytometer. 10,000 single cells were gated on control cells and median fluorescence intensity (MFI) was acquired**.** Values represent the mean ±S.E.M. of three independent experiments. Statistical analysis was performed using two-way ANOVA with Tukey's Multiple Comparison Test (Graphpad Prism 8). ** $p<0.01$, * $p<0.05$. **B.** Endogenous ROS levels in SCC4 and SCC4cisR cells. Statistical analysis was performed using an unpaired two-tailed student t-test (Graphpad Prism 8). * $p<0.05$.

5.2.8.2. Glutathione analysis in cisplatin-sensitive and resistant OSCC cell lines

Glutathione analysis was next performed to compare the antioxidant capacity of cisplatin-sensitive and -resistant OSCC cell lines in the presence/absence of cisplatin. SCC4 and SCC4cisR cells were left untreated or treated with 5 μM cisplatin for 48 h. Cells were then analysed with the GSH/GSSG-Glo kit and luminescence intensity was detected using the SpectraMax Gemini EM Microplate Reader. Evaluation of the GSH/GSSG ratio was assessed in order to determine the conversion of GSH (reduced glutathione) to GSSG (oxidised glutathione). Oxidation of GSH to GSSG results in a decrease in the GSH/GSSG ratio, which is a widely used marker of oxidative stress [255]. As expected, a drop in the GSH/GSSG ratio was observed in cisplatin treated cells compared to untreated treated cells in the SCC4 cell line, indicating that treatment with cisplatin induced oxidative stress in OSCC cells (Figure 5.13A). Conversely, no difference in the GSH/GSSG ratio was observed in the SCC4cisR cell line treated with cisplatin compared to control cells, suggesting that no oxidative stress was induced in this cell line after exposure to cisplatin. Additionally, endogenous GSH levels were examined in the cisplatin-sensitive and resistant-cell lines. GSH levels obtained from untreated SCC4 and SCC4cisR cells were compared using an unpaired t-student test (Figure 5.13B). Interestingly, no difference in the endogenous levels of glutathione were found between the two cell lines, suggesting that basal levels of glutathione were maintained during the acquisition of the resistance phenotype.

Taken together, these results indicate that the increase in ROS levels observed in the SCC4cisR cell line treated with cisplatin did not result in a decrease in the GSH/GSSG ratio, suggesting that cisplatin-induced ROS production may be counteracted by antioxidant systems in the cisplatin-resistant OSCC cell line. Although no differences in the endogenous levels of glutathione were found between the two cell lines, the high GSH/GSSG ratio observed in the drug-resistant cell line compared to the drug-sensitive cell line following treatment with cisplatin may suggest a role of glutathione in mediating cisplatin resistance.

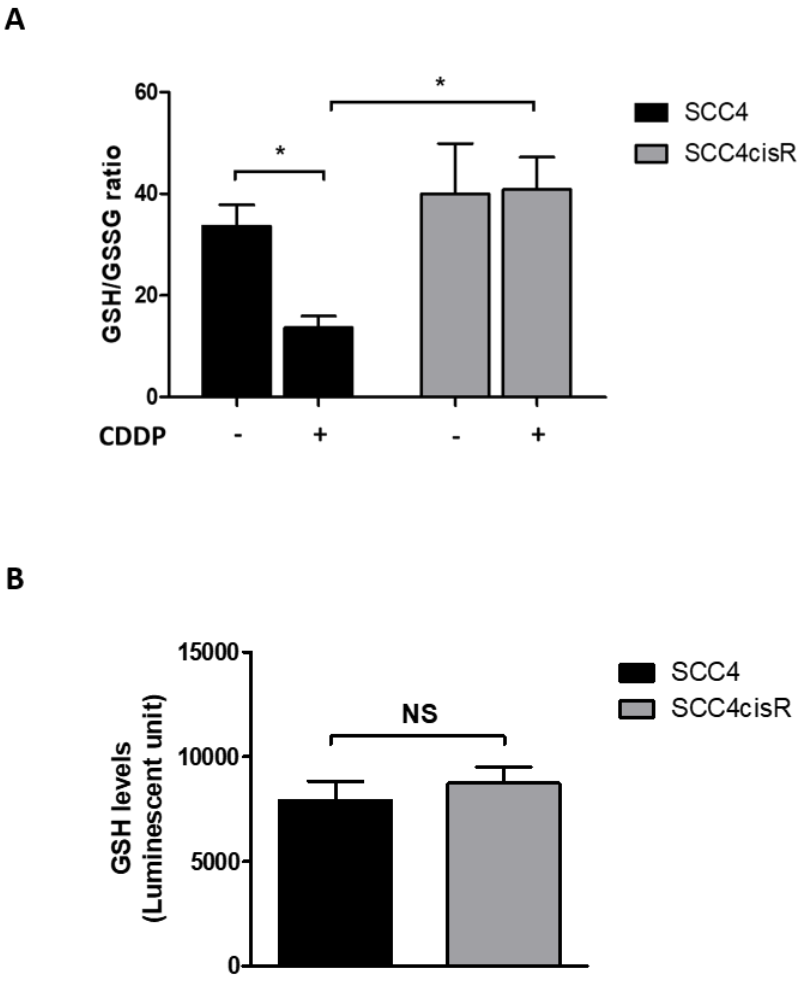

Figure 5.13 Glutathione analysis in cisplatin-sensitive and -resistant OSCC cell lines.

SCC4 and SCC4cisR cells were seeded at $5x10^3$ cells/well in 96 well plates. Cells were left for 24 h to adhere to the plate and then were left untreated or treated with 5 μM cisplatin. After 48 h, cells were analysed using the GSH/GSSG-Glo kit and luminescence was measured on the SpectraMax Gemini EM Microplate Reader. **A**. GSH/GSSG ratio. Values represent the mean ± S.E.M. of three independent experiments. Statistical analysis was performed using two-way ANOVA with Tukey's Multiple Comparison Test (Graphpad Prism 8). * $p<0.05$. **B**. Endogenous GSH levels in SCC4 and SCC4cisR cells. Statistical analysis was performed using unpaired two-tailed student t-test (Graphpad Prism 8). NS=not significant.

5.2.8.3. Protein expression analysis of Nrf2 and HO-1 in cisplatin-sensitive and resistant OSCC cell lines

In the present study, to aid in the evaluation of the antioxidant defence systems, the Nrf2/HO-1 pathway was next investigated. Nrf2 is a transcription factor involved in the antioxidant response [492]. Under normal conditions, Nrf2 is inhibited by Keap1 (kelch-like ECH-associated protein 1) and degraded through the proteasomal pathway. In the presence of ROS, the release of Nrf2 from Keap1 results in its translocation to the nucleus and in the regulation of several antioxidant genes, including HO-1 and glutathione [492]. In the present study, protein expression levels of Nrf2 and HO-1 were assessed in presence/absence of cisplatin through western blot analysis.

SCC4 and SCC4cisR cells were left untreated or treated with cisplatin for 48 h. Lysates were prepared and run on a 12% SDS-PAGE gel before being probed with anti-Nrf2 and anti-HO-1 antibodies. A decrease in Nrf2 and HO-1 protein expression was observed in both cell lines treated with cisplatin compared to control cells, with a more marked effect seen in sensitive cells (Figure 5.14). Interestingly, a difference in the expression levels of Nrf2 and HO-1 was observed from the comparison of the two cell lines. In fact, a significant increase in Nrf2 protein expression along with a notable and significant increase in HO-1 protein expression was found in untreated SCC4cisR cells compared to untreated SCC4 cells, suggesting increased endogenous levels of these proteins in the drug-resistant cell line. Similarly, increased levels of Nrf2 and HO-1 in cisplatin treated SCC4cisR cells compared to cisplatin treated SCC4 cells indicated a greater antioxidant response after exposure of cells to cisplatin in the drug-resistant cell line compared to the drug-sensitive cell line.

This result indicates an enhancement of the antioxidant Nrf2/HO-1 system in the cisplatin-resistant OSCC cell line compared to the parental cell line. Also, it suggests a greater antioxidant response following treatment with cisplatin in drug-resistant cells to counteract the intracellular accumulation of ROS and to overcome oxidative stress.

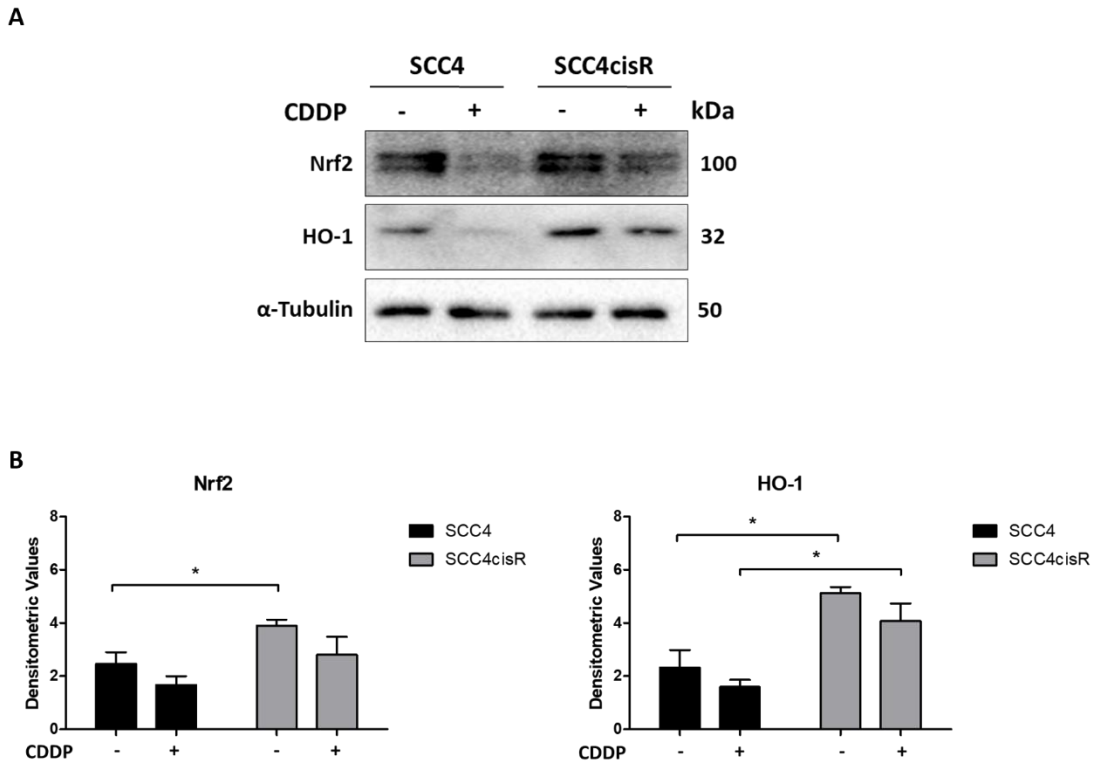

Figure 5.14 Analysis of endogenous and cisplatin-induced Nrf2 and HO-1 expression levels in SCC4 and SCC4cisR cells.

SCC4 and SCC4cisR cells were seeded at $300x10^3$ cells/flask. Cells were left for 24 h to adhere to the flask and then were left untreated or treated with 5 μM cisplatin for 48 h. After incubation, cells were lysed and 20 μg of protein was loaded and separated on a 12% SDS-PAGE gel and transferred to a PVDF membrane. **A**. Membranes were probed with anti-Nrf2 and anti-HO-1 antibodies. α-Tubulin served as loading control. **B**. Densitometric analysis of Nrf-2 and HO-1 bands was performed using ImageLab software and values were normalised by the loading control. Statistical analysis was performed using two-way ANOVA with Tukey's Multiple Comparison Test (Graphpad Prism 8). * $p<0.05$.

5.2.9. Evaluation of targeting the antioxidant systems to reduce cisplatin resistance in OSCC

Given the potential implication of the antioxidant systems in cisplatin resistance, the effects of glutathione depletion and Nrf2 inhibition were investigated in cisplatin-sensitive and -resistant OSCC cells in the presence/absence of cisplatin. Flow cytometric analysis of Annexin V/PI stained cells was performed to determine whether targeting the antioxidant systems may represent a valuable strategy to improve chemotherapy.

5.2.9.1. Glutathione depletion enhances cisplatin-induced apoptosis in cisplatin-sensitive and resistant OSCC cell lines

In the results presented above, the high GSH/GSSG ratio in cisplatin treated SCC4cisR cells compared to cisplatin-treated SCC4 cells was associated with an enhanced ability of the cisplatin-resistant cells to counteract cisplatin-induced ROS as protection from oxidative stress. In order to further investigate the importance of glutathione in cisplatin-induced cytotoxicity and resistance in OSCC, the effect of glutathione depletion was examined in both drug-sensitive and -resistant OSCC cells treated with cisplatin. Depletion of glutathione was accomplished using buthionine sulfoximine (BSO), a potent inhibitor of glutathione synthesis [283, 493]. GSH levels and the GSH/GSSG ratio were firstly assessed in SCC4 cells following treatment with BSO to validate its inhibitory activity. Cells were left untreated or treated with 200 or 400 µM BSO for 48 h before being analysed with the GSH/GSSG-Glo kit. The significant decrease in GSH levels and in the GSH/GSSG ratio observed in both SCC4 cells treated with BSO compared to control cells confirmed the inhibitory activity of BSO on glutathione (Figure 5.15).

Additionally, flow cytometric analysis of annexin V/PI stained cells was performed to evaluate the effect of BSO on cisplatin-induced apoptosis in both SCC4 and SCC4cisR cell lines. Cells were treated with vehicle, cisplatin 5 µM alone, BSO 200 µM alone or cisplatin in combination with BSO, for 48 h. Cells were then double stained with annexin V-FITC and PI, and the percentage of cells in early and late apoptosis was acquired using the BD Accuri flow cytometer. As expected, parental SCC4 cells treated with cisplatin alone showed a significant increase in the apoptotic rate compared to vehicle treated cells, while no induction of apoptosis was observed in SCC4cisR cells treated with cisplatin alone (Figure 5.16). Moreover, SCC4 and SCC4cisR cells treated with BSO alone

exhibited no increase in the apoptotic rate when compared to vehicle treated cells, suggesting that depletion of glutathione alone does not induce apoptosis activation. Furthermore, a limited and non significant increase in the apoptotic rate was found in the SCC4 cells treated with cisplatin in combination with BSO compared to cells treated with cisplatin alone. Interestingly, a notable and significant increase in the percentage of apoptotic cells was observed in the SCC4cisR cells treated with cisplatin in combination with BSO compared to cells treated with cisplatin alone, suggesting that BSO sensitised the cisplatin-resistant cells to cisplatin. However, it should be noted that BSO did not fully restore cisplatin sensitivity in the SCC4cisR cells. This would indicate that glutathione may contribute to chemoresistance only in part and other mechanisms may also play a role.

Taken together, these results may suggest the potential involvement of glutathione in chemoresistance. Accordingly, depletion of glutathione with BSO may represent a valuable strategy to sensitise OSCC cells to cisplatin.

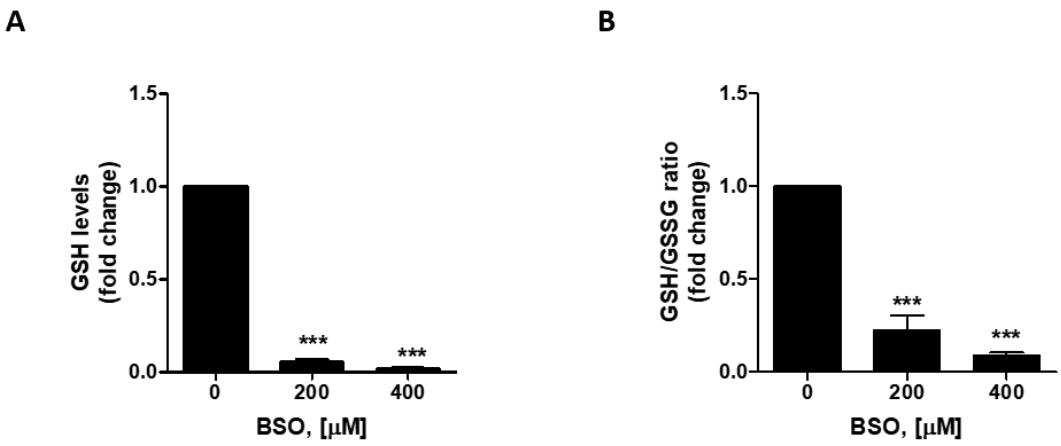

Figure 5.15 BSO induced glutathione depletion and oxidative stress in SCC4 cells.

SCC4 cells were seeded at $5x10^3$ cells/well in 96 well plates. Cells were left for 24 h to adhere to the plate, and then were left untreated or treated with 200 or 400 μM BSO. After 48 h, cells were analysed using the GSH/GSSG-Glo kit and luminescence was measured on the SpectraMax Gemini EM Microplate Reader. A. GSH levels. **B** GSH/GSSG ratio. Fold change values were obtained by normalising data obtained from treated cells to data obtained from control cells. Values represent the mean ± S.E.M. of three independent experiments. Statistical analysis was performed using one-way ANOVA with Dunnett's Multiple Comparison Test to compare mean values between treated and control cells (Graphpad Prism 8). ***$p<0.0001$.

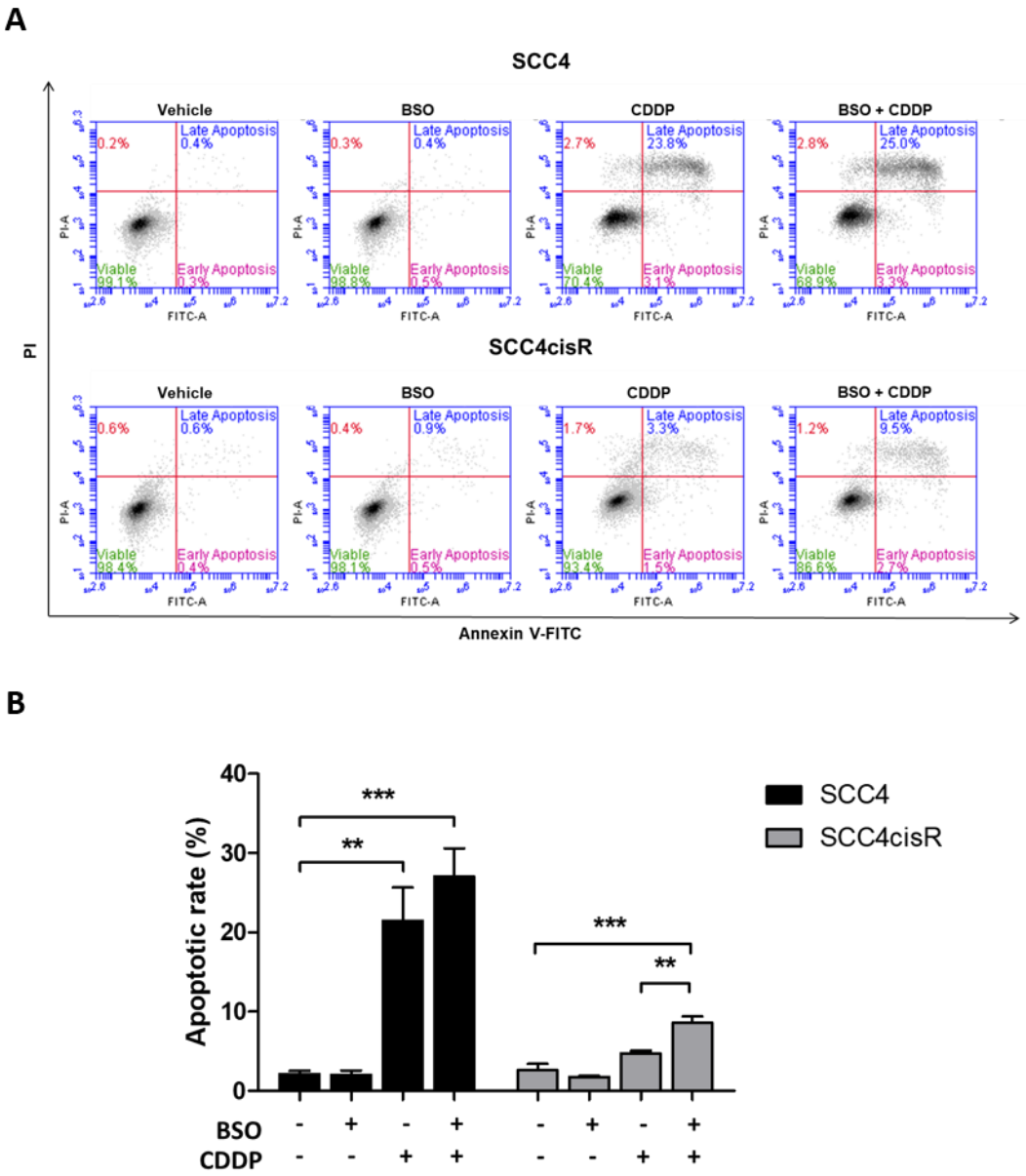

Figure 5.16 BSO significantly enhances cisplatin-induced apoptosis in SCC4cisR cells.

SCC4 and SCC4cisR cells were seeded at 150x10^3 cells/well in 6 well plates. Cells were left for 24 h to adhere to the plate and then were treated vehicle (0.009% (v/v) NaCl), with 200 µM BSO alone, 5 µM cisplatin (CDDP) alone, or cisplatin in combination with BSO for 48 h. Cells were then analysed by flow cytometry using BD FACS Accuri software. 10,000 single cells were gated on vehicle treated cells and the percentage of cells undergoing early and late apoptosis was acquired. **A**. Representative dot plot of treated cells. **B**. Values represent the mean and S.E.M. of three independent experiments. Statistical analysis was performed using one-way ANOVA with Tukey's Multiple Comparison Test to compare treatments within the same cell line (Graphpad Prism 8) . *** $p<0.001$, ** $p<0.01$, * $p<0.05$.

5.2.9.2. Targeting Nrf2 partially restores cisplatin sensitivity in cisplatin-resistant OSCC cells

Given the activation of the Nrf2/HO-1 axis in the SCC4cisR cell line in presence/absence of cisplatin, a potential role for this signalling pathway in mediating chemoresistance was evaluated. Thus, the effect of targeting Nrf2 was examined in both drug-sensitive and -resistant OSCC cells treated with cisplatin. For this purpose, the Nrf2 inhibitor ML385 was employed. Firstly, the inhibitory activity of ML385 on the Nrf2/HO-1 axis was validated on the SCC4 cell line. Cells were left untreated or treated with 20 or 40 µM ML385 for 48 h before being harvested and lysed. Lysates were then run on a 12% SDS-PAGE gel and membranes were probed with an anti- Nrf2 and anti-HO-1 antibodies. A progressive decrease in the Nrf2 and HO-1 levels was found at increased concentrations of ML385, with a significant decrease in both of these proteins observed at 40 µM ML385 (Figure 5.17).

Next, flow cytometric analysis of annexin V/PI stained cells was performed to evaluate the effect of ML385 on cisplatin-induced apoptosis in both SCC4 and SCC4cisR cell lines. Cells were treated with vehicle, cisplatin 5 µM alone, ML385 40 µM alone or cisplatin in combination with ML385, for 48 h. Cells were then double stained with annexin V-FITC and PI, and the percentage of cells in early and late apoptosis was acquired using the BD Accuri flow cytometer. A slight but non significant increase in apoptosis was observed in both cell lines treated with ML385 alone compared to vehicle treated cells (Figure 5.18). Moreover, a limited and again non significant increase in the apoptotic rate was found in the SCC4 cells treated with cisplatin in combination with ML385 compared to cells treated with cisplatin alone. Interestingly, a notable and significant increase in the percentage of apoptotic cells was observed in the SCC4cisR cells treated with cisplatin in combination with ML385 compared to cells treated with cisplatin alone and ML385 alone.

Taken together, these results indicate that inhibition of Nrf2 with ML385 can partially restore cisplatin sensitivity in the SCC4cisR cells, confirming the involvement of the Nrf2/HO-1 signalling pathway in cisplatin resistance. Moreover, these data suggest the beneficial effect of targeting Nrf2 to overcome chemoresistance in OSCC patients and suggest a potential application of ML385 in clinic.

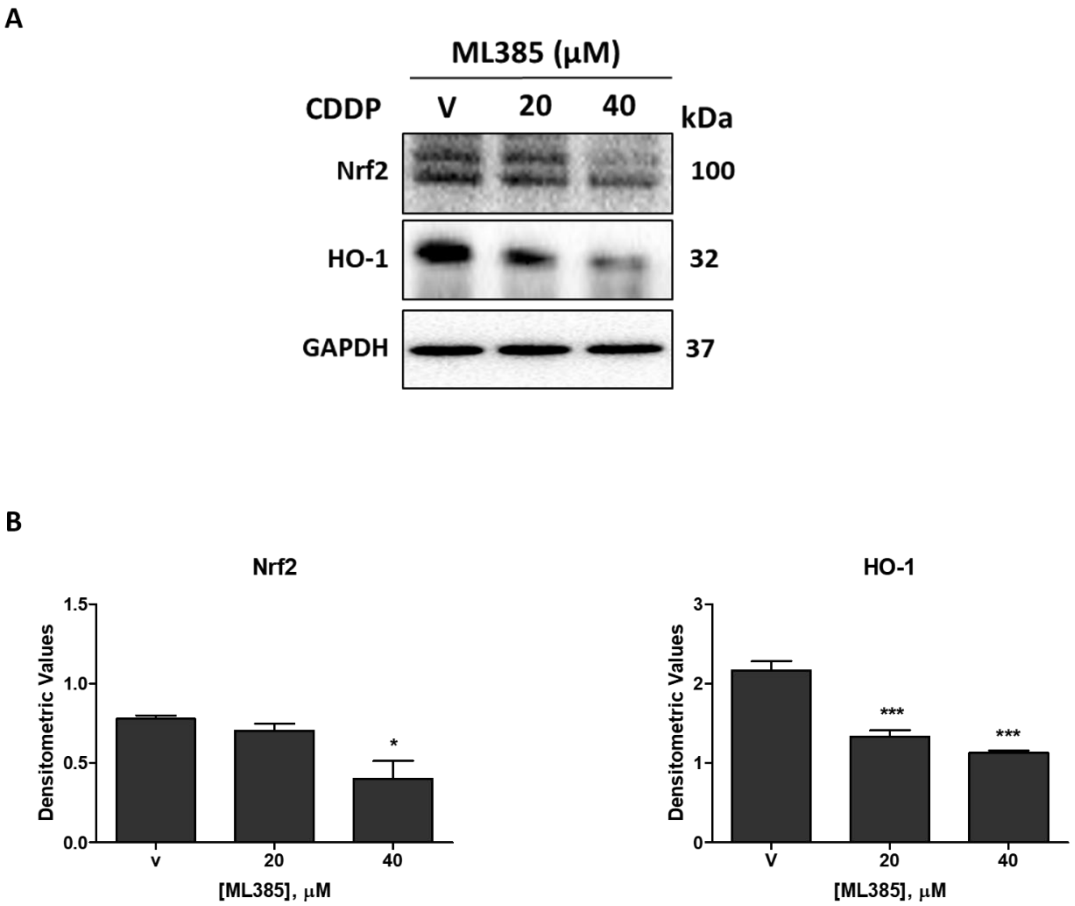

Figure 5.17 The Nrf2 inhibitor ML385 reduces the levels of Nrf2 and HO-1 proteins in SCC4 cells. SCC4 cells were seeded at $300x10^3$ cells/flask. Cells were left for 24 h to adhere to the flask and then were left untreated or treated with 20 or 40 μM ML385. After incubation, cells were lysed and 20 μg of protein was loaded and separated on a 12% SDS-PAGE gel and transferred to a PVDF membrane. **A**. Membranes were probed with anti-Nrf2 and anti-HO-1 antibodies. GAPDH served as loading control. **B**. Densitometric analysis of Nrf-2 and HO-1 bands was performed using ImageLab software and values were normalised by the loading control. Statistical analysis was performed using one-way ANOVA with Dunnett's Multiple Comparison Test to compare mean values between treated and control cells (Graphpad Prism 8). ***$p<0.0001$, * $p<0.05$.

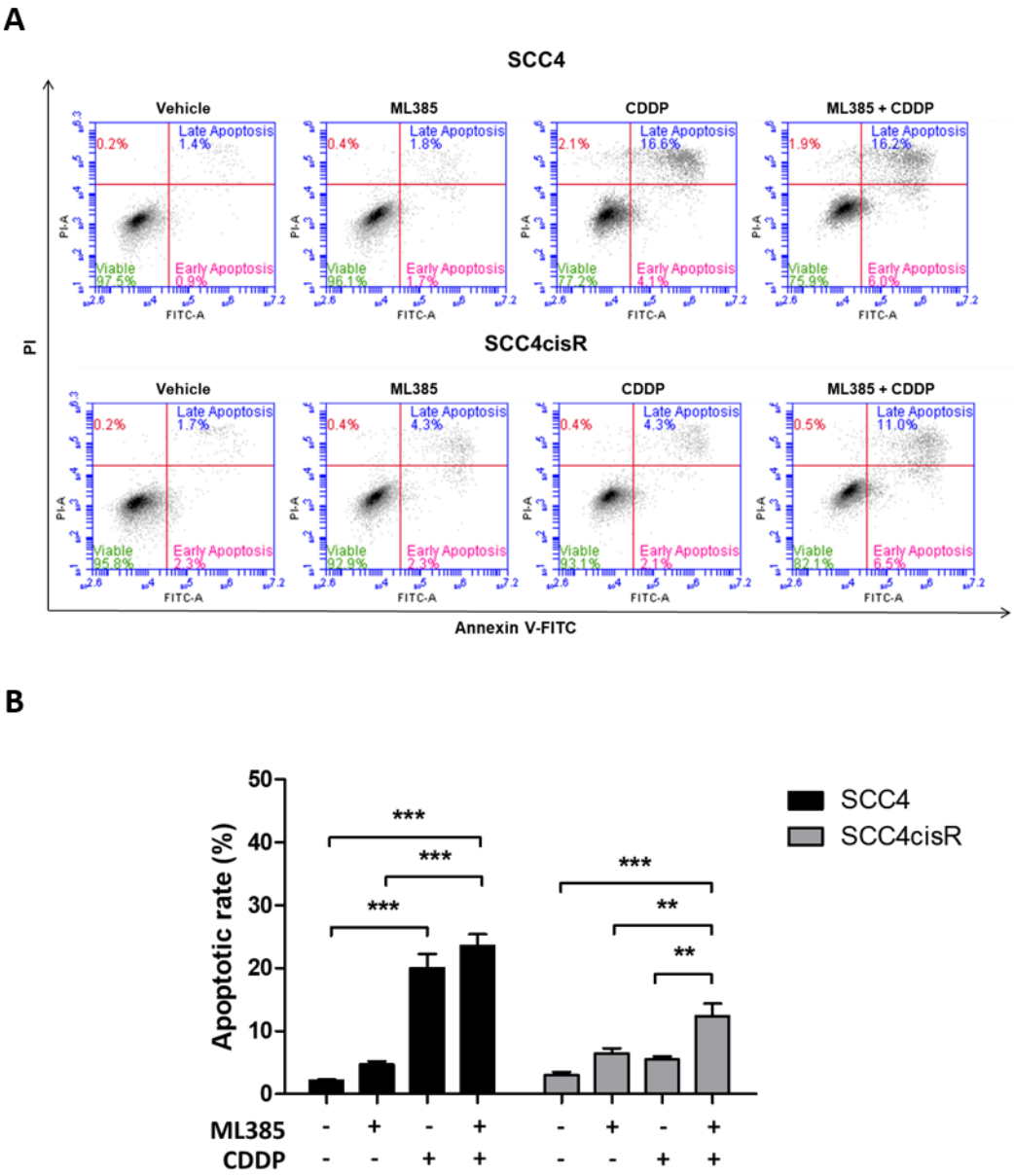

Figure 5.18 ML385 partially restores cisplatin sensitivity in SCC4cisR cells.

SCC4 and SCC4cisR cells were seeded at 150x10^3 cells/well in 6 well plates. Cells were left for 24 h to adhere to the plate and then were treated with vehicle (0.009% (v/v) NaCl), 40 μM ML35 alone, 5 μM cisplatin (CDDP) alone, or cisplatin in combination with ML385 for 48 h. Cells were then analysed by flow cytometry using BD FACS Accuri software. 10,000 single cells were gated on vehicle treated cells and the percentage of cells undergoing early and late apoptosis was acquired. **A**. Representative dot plot of treated cells. **B**. Values represent the mean and S.E.M. of three independent experiments. Statistical analysis was performed using one-way ANOVA with Tukey's Multiple Comparison Test to compare treatments within the same cell line (Graphpad Prism 8). *** $p<0.001$, ** $p<0.01$.

5.2.10. Analysis of the Ras/ERK signalling pathway in cisplatin-sensitive and resistant OSCC cells

A correlation between drug resistance and dysregulation of the Ras/ERK signalling pathway has been reported in various cancerous [494]. Moreover, recent findings have also demonstrated a link between the Ras/ERK pathway and Nrf2, suggesting a potential activation of Nrf2 by Ras through ERK activation [495]. In the present study, given the increased levels of Nrf2 and HO-1 observed in the SCC4cisR cell line compared to the SCC4 cell line, a preliminary analysis of the Ras/ERK signalling pathway was undertaken in order to determine whether it is implicated in cisplatin chemoresistance by regulating the Nrf2/HO-1 axis. In the present study, Ras expression levels and ERK activation were examined by western blot analysis in SCC4 and SCC4cisR cells in the presence/absence of cisplatin. Since activation of ERK occurs through its phosphorylation at residues Thr202/Tyr204, both the total ERK and phospho-ERK were evaluated, and the ratio of phospho-ERK/total ERK was considered as a measure of its activation.

SCC4 and SCC4cisR cells were left untreated or treated with cisplatin for 48 h. Lysates were prepared and run on a 12% SDS-PAGE gel before being probed with anti-Ras, anti-phospho-ERK and anti-ERK antibodies. A significant increase in Ras levels were observed in the SCC4cisR cells compared to the SCC4 cells both in the absence and presence of cisplatin, suggesting an activation of Ras during the acquisition of the cisplatin resistant phenotype (Figure 5.19). Moreover, phosphorylation of ERK was observed in both untreated SCC4 and SCC4cisR cells, indicating activation of ERK in both cell lines under normal conditions. No differences were observed in the phospho-ERK/ERK ratio between the two cell lines. Additionally, a drop in the phospho-ERK/ERK ratio was found only in the SCC4 cells treated with cisplatin compared to control cells, whilst no difference in the phospho-ERK/ERK ratio was found in the SCC4cisR cells treated with cisplatin compared to control cells. This may indicate a failure in the activation of the pro-survival ERK pathway only in the cisplatin-sensitive cells treated with cisplatin, but not in the cisplatin-resistant cell line treated with the same concentration of cisplatin. Taken together, these preliminary results demonstrate the greater activation of the Ras/ERK pathway in the cisplatin-resistant OSCC cell line compared to the parental cisplatin-sensitive cell line, suggesting a role for this pathway in cisplatin resistance in OSCC. Further analyses are required in order to determine a correlation between the Ras/ERK pathway and the Nrf2/HO-1 axis.

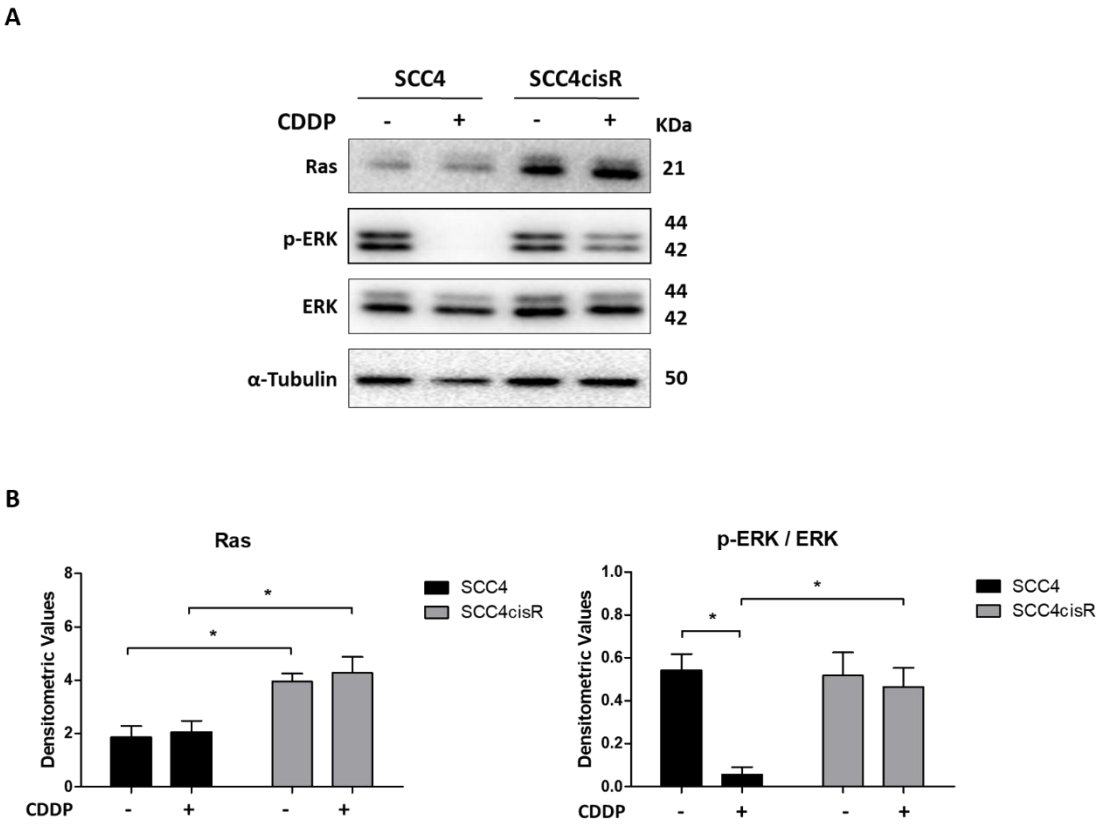

Figure 5.19 Analysis of RAS expression and ERK activation in SCC4 and SCC4cisR cells.

SCC4 and SCC4cisR cells were seeded at $300x10^3$ cells/flask. Cells were left for 24 h to adhere to the flask and then were left untreated or treated with 5 μM cisplatin for 48 h. After incubation, cells were lysed and 20 μg of protein was loaded and separated on a 12% SDS-PAGE gel and transferred to a PVDF membrane. **A**. Membranes were probed with anti-Ras, anti-phospho-ERK and anti-ERK antibodies. α-Tubulin served as loading control. **B**. Densitometric analysis of Ras, phospho-ERK and ERK bands was performed using ImageLab software and values were normalised by the loading control. Statistical analysis was performed using two-way ANOVA with Tukey's Multiple Comparison Test (Graphpad Prism 8). * $p<0.05$.

5.3. Discussion

Chemotherapy represents one of the main therapeutic strategies for unresectable or advanced cancers [480]. Despite the high efficiency of chemotherapeutic drugs in reducing viability and inducing programmed cell death in tumour cells, various limitations have been linked to the use of these drugs in cancer therapy. Among them, drug resistance is considered the main impediment during chemotherapy and the major cause of treatment failure [44]. Therefore, chemoresistance has become a compelling challenge in medical oncology as well an emerging area of research. Indeed, the innate or acquired ability of some cells to not respond to certain treatments has been widely investigated over the past few years. However, the current knowledge in this field is insufficient to date to develop an efficient strategy to overcome drug resistance during chemotherapy. Therefore, a further understanding of the molecular and biochemical mechanisms implicated in chemoresistance is required to improve the clinical outcome of cancer patients.

To date, many relevant findings about drug resistance come from studies on tumour cells made resistant *in vitro* [496, 497]. This method consists of the induction of a resistant phenotype in cultured cells which are initially sensitive to a specific treatment. This results in the generation of a resistant population of cells which is identical in all properties to the parental one, except for the resistance. Thus, the comparison of the resistant and parental sensitive cell populations allows one to identify the mechanisms implicated in the acquisition of the resistant phenotype. In this regard, various studies in the literature have reported that induction of resistance can be accomplished through repeated exposure of cells to particular drugs [498, 499]. Accordingly, one of the first publications describing the development of a drug-resistant *in vitro* model dates back to 1970, when actinomycin D-resistant cells were obtained from parental Chinese hamster cells through stepwise exposure of cells to the drug [500]. Since then, several papers have described the generation and the establishment of drug-resistant cell lines and numerous protocols have been proposed. Moreover, given the wide use of cisplatin in chemotherapy and its strong correlation to chemoresistance, it is not surprising that a huge body of studies have focused on the generation of cisplatin-resistant cell lines. In fact, induction of cisplatin resistance in cultured cells has been reported in various cancer cell lines, including ovarian cancer, cervical cancer, non-small lung cell carcinoma as well as oral

cancer [109, 498, 501–504]. In the present study, a cisplatin-resistant OSCC cell line has been generated to aid in the study of chemoresistance in oral cancer.

According to McDermott *et al.*, two types of drug-resistant cell models can be developed to investigate chemoresistance: clinically relevant models and high-level laboratory models [505]. The former can be obtained through pulsed stepwise exposure of cells to low doses of drugs, while the latter can be developed by continuous exposure of cells to high and escalating doses of drugs. Overall, the main difference between these two groups is that the clinically relevant models tend to mimic the cycles of chemotherapy a patient receives in the clinic, while the high-level laboratory models aim to reproduce an ideal *in vitro* system to study the mechanisms responsible for chemoresistance [505]. Consistently, mutagenesis and/or selection of resistant clones can also be used as additional strategies to facilitate the generation and the isolation of drug-resistant high-level laboratory cell lines for a better investigation of the resistant phenotype. Importantly, based on the research objectives, advantages and disadvantages need to be considered in the choice of the drug-resistant model. In fact, if on one hand the drug-resistant clinically relevant cell lines are representative of the real clinical conditions, they are usually characterised by low levels of resistance and a modest stability. Conversely, the drug-resistant high-dose laboratory cell lines are not clinically relevant but they usually are stable and highly resistant. In the present study, a clinically relevant model of cisplatin-resistant OSCC cells has been developed in order to mimic the clinical scenario and identify a valuable strategy to overcome chemoresistance in oral cancer patients.

The selection of the parental cell line represents an important step for the success of resistant cell generation. According to the guidelines proposed by McDermott *et al.*, it is crucial to opt for a parental cell line easy to culture, as derived resistant variants usually become more difficult to maintain [505]. Moreover, it is important to choose a parental cell line highly sensitive to the drug of interest in order to detect the increase in acquired resistance during the procedure. Basing on these criteria, the SCC4 cell line was selected for this study as the parental cell line from which the cisplatin-resistant cells were generated. The treatment strategy herein employed was planned by considering the sensitivity of the parental cells to the drug. In fact, from the viability curve of SCC4 cells treated with cisplatin for 72 h, the concentration of cisplatin required to inhibit 25% of cell viability (IC_{25}) was calculated and used as the first treatment concentration. Minimal escalations of cisplatin doses were applied to cells for initial treatments in order to not

over-stress the cells, while marked escalations were used for the last treatments when cells were already acquiring a certain degree of resistance. Importantly, cisplatin doses were chosen in order to not exceed the IC_{50} obtained from the viability assay performed on the surviving daughter cells after each treatment. Overall, nine cisplatin treatments of 72 h each were performed over a period of 12 months, and cells were allowed to recovery in drug-free media after each exposure to the drug in order to mimic the clinical scenario. Viable surviving cells following cisplatin treatments represented a new cisplatin-resistant SCC4 cell population, herein named SCC4cisR. A progressive increase in the IC_{50} values of the SCC4cisR cells was observed after each exposure of cells to cisplatin and the first significant difference in the IC_{50} between SCC4cisR and parental SCC4 cells was detected after the 7^{th} treatment with cisplatin and reached a peak after the last treatment when IC_{50} values of 1.1 ± 0.2 µM and 16.2 ± 4.8 µM were obtained in SCC4 and SCC4cisR cells respectively.

Induction of drug resistance in cultured cells can be quantified through the evaluation of the resistance index (RI). The RI is defined as the ratio of the IC_{50} of resistant cells/IC_{50} of paired parental cells and indicates the extent of chemoresistance compared to its parental cell line [497, 501, 506]. RI values of drug-resistant cells generated *in vitro* can be highly variable, depending on the methodology employed, the *in vitro* model developed and the parental cell line selected. Thus, it is difficult to set an RI value threshold for a significant resistance level. According to Michalak *et al.*, RI values between 0 and 2 indicate no induction of resistance; RI values between 2 to 10 indicate a moderate acquisition of resistance to the drug; finally, RI values above 10 indicates strong drug resistance [507]. On the other hand, it has been reported that several cell lines derived from cancer patients before and after chemotherapy displayed RI values between 2 to 8, suggesting that RI values within this range may be clinically relevant [505]. Given this, in the present study, it was arbitrarily decided to consider RI values above 5 significant and clinically relevant. Accordingly, from the analysis of the RI of SCC4cisR cells after each cisplatin treatment, the first significant and clinically relevant difference in resistance between the SCC4cisR cells and the parental SCC4 cells was observed after the 7^{th} treatment with cisplatin (RI=5.6), reaching a peak after the last treatment (RI=13.7).

Generation of oral cancer cells resistant to cisplatin have been reported in other studies in the literature. For example, Nakamura *et al.* have reported the generation of a cisplatin-

resistant cell line (H-1R) obtained from an OSCC cell line (H-1) established from an oral specimen biopsy in the lower gingiva [109]. In this study, the H-1R cell line was obtained through continues stepwise dose escalation of cisplatin and a 10-fold change in resistance was obtained. Similarly, Ghosh *et al.* generated two OSCC cisplatin-resistant cell lines, SCC084/R and SCC131/R, from the parental SCC084 and SCC131 cell lines respectively by gradual incremental doses of cisplatin over a period of 6-8 months, reaching RIs of 1.5 and 3.5, respectively [508]. In both these studies, resistant cells were maintained in cisplatin enriched medium. Additionally, generation of a tongue squamous cell carcinoma cell line resistant to cisplatin (CAL-27/CDDP) was reported by Gosepath *et al.*, who obtained a 10-fold increase in resistance using a clonal selection approach [509]. Although all these models resulted in a significant induction of resistance, they may not be considered as clinically relevant models. In the present study, pulsed stepwise treatment of cells with cisplatin resulted in a ~14-fold increase in cisplatin resistance, highlighting the establishment of a highly resistant and clinically relevant *in vitro* model of tongue squamous cell carcinoma, which represents a very useful resource to investigate cisplatin resistance in OSCC.

Once generated and established, the SCC4cisR cell line was characterised in terms of apoptotic and survival potential. As already mentioned in previous chapters, cisplatin treatment mainly results in apoptotic cell death. Given this, it was likely that the induction of a cisplatin-resistant phenotype would correlate with a reduced ability of cells to undergo apoptosis in response to cisplatin. In the present study, a dose-dependent activation of apoptosis was observed in the SCC4cisR cells and in the age-matched parental SCC4 cells treated with cisplatin, confirming the ability of both cell lines to undergo apoptosis. However, a significant decrease in the apoptotic rate was detected in the SCC4cisR cells compared to the parental cells following treatment with cisplatin, indicating the reduced ability of the cisplatin-resistant cell line to undergo apoptosis in response to this drug. Additionally, a considerable difference in the survival potential between the SCC4 and the SCC4cisR cells was also displayed. In fact, a significant increase in the survival fraction was found in the SCC4cisR cells treated with cisplatin compared to the parental cells, indicating the higher ability of the cisplatin-resistant cells to survive and recover after the exposure to the drug. Taken together, the reduced apoptotic activity along with the increased survival potential observed in the SCC4cisR cells treated with cisplatin confirmed the acquisition of a cisplatin-resistant phenotype.

Several studies have reported that resistance to chemotherapy may be driven by a subpopulation of cells named CSCs [510]. CSCs are defined as multipotent and highly tumorigenic cells capable of self-renewal [101]. According to the cancer stem cell hypothesis, CSCs are cancer progenitor cells responsible for tumour initiation, development, maintenance and spread [511]. The presence of CSCs has been demonstrated in various types of solid tumours, including brain, ovarian, prostate as well as oral cancer [314, 512–514]. Along with migration and invasive properties, a high ability to escape chemotherapeutic treatments has been linked to CSCs, suggesting their potential role in acquired drug resistance [515]. Accordingly, increased CSC populations have been detected in drug-resistant cell lines compared to the parental cell lines in various cancer types, such as gastric cancer and non-small cell lung carcinoma [498, 514]. Although several cell surface proteins have been proposed as markers for CSCs, the identification of this cell population is still controversial due to the frequent phenotypic transitions and the high variability in cell composition among cell types [489]. To date, the expression of the hyaluronan receptor protein CD44 on the cell surface represents a widely recognised marker for CSCs in various cancers [313]. Nevertheless, recent studies have reported that the expression of CD44 alone may not specifically identify CSCs [516]. Accordingly, in some cancers such as breast or colon cancer, it has been demonstrated that the presence of CD44 along with the lack of the glycoprotein CD24 may be considered a reliable marker for CSCs [515, 517]. Even though the expression of CD24 is still controversial, CSC properties have previously been demonstrated in $CD44^+/CD24^-$ populations of several OSCC cells [489]. Given that, in the present study, the presence of $CD44^+/CD24^-$ cells in the SCC4 cell line and in the derived cisplatin-resistant SCC4cisR cell line was investigated through flow cytometric analysis to determine whether acquired resistance to cisplatin may be correlated to this population of cells. Results obtained showed a high expression of both CD44 and CD24 proteins on the surface of the two cell lines, resulting in a scarce $CD44^+/CD24^-$ pool of cells (~7%). Interestingly, from the comparison of the cisplatin-resistant and the parental cell lines, no differences in the expression of the two markers were detected, suggesting no changes in the abundance of the $CD44^+/CD24^-$ cell population during the acquisition of the resistant phenotype. This result indicates that the $CD44^+/CD24^-$ cell population may not be involved in chemoresistance in the cell model herein examined. Nevertheless, analysis of additional markers may be required for future experiment to further examine the stem-like properties of the SCC4cisR cell line.

Furthermore, preliminary analysis of multidrug resistance (MDR) was undertaken in the newly established SCC4cisR cell line. MDR consists of innate or acquired cross-resistance of cells to various chemotherapeutic agents [490]. Acquired MDR has been widely reported in cancer patients treated with chemotherapy. In fact, treatment of patients with a specific chemotherapeutic drug can result in the ability of tumours to become refractory not only to the drug used for primary chemotherapy, but also to similar or diverse drugs [518]. This results in limited efficacy of second line chemotherapy and consequently in treatment failure and tumour relapse. Accordingly, development of acquired cross-resistance has also been reported *in vitro* in several cancer models. For example, in liver cancer, exposure of HepG2 cells to adriamycin resulted in cross-resistance to vincristine [519]. Similarly, in a breast cancer model, doxorubicin-resistant MCF-7 cells showed a strong cross-resistance to paclitaxel [520, 521]. Basing on these findings, acquired cross-resistance was investigated in the present study in order to determine whether the induction of cisplatin resistance can result in the development of MDR phenotype. Thus, cell sensitivity in response to three chemotherapeutic agents (carboplatin, docetaxel and sorafenib) was evaluated in the cisplatin-resistant SCC4cisR cells and in the parental SCC4 cells using the alamar blue assay. Results obtained showed the ability of all three drugs to reduce viability in both cell lines. Interestingly, a substantial increase in the IC_{50} values was observed in SCC4cisR cells treated with carboplatin compared to SCC4 cells, suggesting a reduced sensitivity to carboplatin in the cisplatin-resistant cell line compared to the parental one. Conversely, no differences in susceptibility were detected between the two cell lines in response to docetaxel and sorafenib. Accordingly, RI values of 8.4, 0.7 and 0.6 were obtained in the SCC4cisR cell line for carboplatin, docetaxel and sorafenib respectively. As already mentioned, in the present study, an RI value above 5 was considered significant and clinically relevant to assume the development of chemoresistance. Given this, it is suggested that pulsed exposure of cells to cisplatin may result in acquired resistance not only to cisplatin, but also to carboplatin. Cross-resistance to cisplatin and carboplatin has been reported in several clinical and *in vitro* models [518, 522, 523]. Considering that both cisplatin and carboplatin belong to the same class of compounds, namely platinum-based compounds, it is accepted that they have a similar mechanism of action [524]. This may imply that the development of the resistant phenotype in the cell model herein examined may be attributable to mechanisms implicated in the response to platinum-based compounds. In the present study, induction of oxidative stress and autophagy has been demonstrated in

OSCC cells in response to cisplatin. Accordingly, the role of these two mechanisms in acquired cisplatin-resistance was further investigated in the SCC4cisR cell line in order to identify valuable therapeutic options to improve chemotherapy in OSCC.

As already mentioned, the implication of autophagy in chemoresistance has been widely reported in the literature. In this regard, activation of autophagy in response to chemotherapy and reduction in cell viability following inhibition of drug-induced autophagy have been demonstrated in various cancers [189]. These findings have led to the hypothesis that autophagy activation following chemotherapy may represent a protective mechanism that allows cancer cells to survive and escape from stress, resulting in the development of a resistant phenotype. However, the role of autophagy in chemoresistance in OSCC remains controversial. In the present study, levels of basal autophagy and starvation-induced autophagy were compared in SCC4 and SCC4cisR cells. Data obtained from western blot analysis of p62 and LC3-I/II protein expression showed a basal activation of autophagy in both cell lines and a further induction of autophagic flux following treatment of cells with EBSS. This result confirmed the ability of the two cell lines to undergo autophagy under normal conditions and in response to external stimuli such as starvation. Interestingly, from a comparison of the two cell lines, no significant change to the basal levels of autophagy was detected in the SCC4cisR cell line compared to the parental cell line. This is in contrast with several reports in the literature which showed an increase in basal levels of autophagy in drug-resistant cells compared to drug-sensitive cells. For example, an increase in the LC3-II-puncta has been found in the cisplatin-resistant A549 cells (A549/CDDP) compared to the parental cells in non-small cell lung carcinoma and, similarly, in the cisplatin-resistant HeLa/CDDP cells compared to the parental HeLa cells in cervical cancer [525, 526]. Enhanced autophagy activation in these cell lines has been linked to an implication of autophagy in acquired drug resistance. In the present study, the lack of a significant change in the basal levels of autophagy in the SCC4cisR cell line compared to the SCC4 cell line may imply that autophagy is not involved in acquired drug resistance in OSCC. In support of these findings, one should consider that autophagy activation represents only one of the numerous mechanisms that has been linked to chemoresistance. Thus, it is plausible that other mechanisms may be implicated in drug resistance in the cell model herein examined. Furthermore, autophagy activation in the presence/absence of cisplatin was also investigated in the SCC4cisR cell line and in the parental cell line to better understand

the role of autophagy in mediating chemoresistance in OSCC. Interestingly, a significant increase in the LC3-II/LC3I ratio was observed only in the cisplatin-sensitive SCC4 cell line treated with cisplatin. No activation of autophagy was detected in the derived resistant SCC4cisR cell line treated with the same concentration of cisplatin. The lack of cisplatin-induced autophagy in the SCC4cisR cell line corroborates the hypothesis that autophagy is not implicated in chemoresistance in these cells. In fact, the concomitant suppression of cisplatin-induced autophagy and apoptosis in cisplatin-resistant cells may suggest a role for autophagy as a pro-death mechanism in association with apoptosis rather than a survival mechanism. These findings are in line with results previously shown in chapter 4 indicating a simultaneous induction of autophagy and apoptosis in OSCC cells treated with cisplatin through the activation of a common pathway(s).

Additionally, in chapter 3, inhibition of autophagy using late stage autophagy inhibitors, such as chloroquine, were shown to enhance cisplatin-induced apoptosis in OSCC cells. This result suggested the potential application of this compound in the clinic to improve cisplatin efficacy during chemotherapy. In the present study, the effect of chloroquine in combination with cisplatin was examined in the cisplatin-resistant SCC4cisR cell line in order to confirm the beneficial effect of chloroquine in cisplatin-based therapy. Results obtained showed a significant increase in the apoptotic rate in SCC4cisR cells treated with cisplatin in combination with chloroquine compared to cells treated with cisplatin alone, suggesting that chloroquine may enhance cisplatin cytotoxicity in drug-resistant cells. The ability of chloroquine to sensitise both cisplatin-sensitive and resistant OSCC cells to the treatment confirms that a combinatory therapy using chloroquine and cisplatin may represent a valuable strategy to improve chemotherapy in OSCC. Interestingly, since a lack of autophagy was observed in SCC4cisR cells treated with cisplatin, results obtained herein corroborate the suggestion that chloroquine may enhance cell death through an autophagy-independent mechanism, as already discussed in chapter 3.

The role of oxidative stress in acquired drug resistance was next examined. In the previous chapter, increased ROS levels and a reduced GSH/GSSG ratio were demonstrated in OSCC cells treated with cisplatin, indicating the induction of oxidative stress in response to cisplatin. Moreover, treatment of cells with the antioxidant NAC was shown to increase cell viability following cisplatin treatment, suggesting a role for oxidative stress in mediating cisplatin cytotoxicity. So, on one hand a pro-death role for oxidative stress has been reported here and in other studies; however, a correlation between oxidative stress

and chemoresistance has also been proposed. In this regard, it has been suggested that exposure of cells to chemotherapeutic drugs can lead to the development of a cellular adaptive response that allows cells to escape from the dangerous effect of drug-induced oxidative stress [86, 527]. Accordingly, acquired chemoresistance may result from the ability of cells to adapt to oxidative stress.

In the present study, evaluation of intracellular ROS levels and analysis of antioxidant defence systems were undertaken in the cisplatin-resistant SCC4cisR cell line and in the parental SCC4 cell line in order to understand whether oxidative stress may be involved in cisplatin resistance. From the flow cytometric analysis of H_2DCFDA stained cells, a difference in the ROS levels between the two cell lines in the presence/absence of cisplatin was detected. In fact, a significant increase in ROS levels was observed in the untreated SCC4cisR cells compared to the SCC4 cells, and a marked and significant increment of ROS was detected in the SCC4cisR cells treated with cisplatin compared to the parental cells treated with the same concentration of cisplatin. This result suggested higher endogenous and cisplatin-induced ROS levels in the cisplatin-resistant OSCC cell line compared to the parental cell line. Similar findings have also been reported in the literature. In fact, increased levels of ROS have been found in rat glioblastoma cells resistant to 3-bis (2-chloroethyl)-1-nitrosourea (BCNU) compared to the parental cells [528]. Also, high ROS levels have been detected in gemcitabine-resistant human pancreatic ductal adenocarcinoma cells and in cisplatin-resistant human lung carcinoma cells compared to the respective sensitive parental cells [529, 530]. In these studies, high levels of ROS have been correlated to an enhanced capacity of resistant cells to generate ROS due to their continuous exposure to ROS-inducing drugs. In this regard, Wangpaichitr *et al.* reported that enhanced ROS generation in cisplatin-resistant lung carcinoma cells may occur as a consequence of cellular metabolic reprogramming [531]. Accordingly, the authors found that cisplatin-resistant cells were no longer addicted to the glycolytic pathway, but rather they relied on oxidative metabolism which promotes ROS generation. Moreover, in the same study, increased glutamine uptake was observed in the cisplatin-resistant cells compared to the parental cells, suggesting enhanced glutathione synthesis. Given the ROS-scavenger activity of glutathione, this finding suggested that activation of antioxidant systems may occur in drug resistant cells in order to counteract the high levels of ROS. Accordingly, several studies have reported the enhancement of the antioxidant defences in drug-resistant cells [532]. Among the main

antioxidant systems associated with chemoresistance, it is worth considering glutathione, Nrf2 and HO-1.

As reported in chapter 4, glutathione is considered the major antioxidant system within cells [13]. A potential implication of glutathione in drug resistance has been proposed in recent years. Accordingly, increased basal levels of glutathione have been demonstrated in various drug-resistant cell lines compared to the corresponding parental cell lines [529, 531, 533]. According to Traverso *et al.*, the role of glutathione in cisplatin resistance may be attributable to the glutathione ability of regulating the cellular redox balance following ROS accumulation, but also to its activity as a copper chelator and as a cofactor in MRP2-mediated cisplatin efflux [534]. For example, mouse doxorubicin-resistant leukaemia cells as well as human cisplatin-resistant lung carcinoma cells were shown to have higher glutathione levels compared to their respective sensitive cells [529, 531, 533]. Given this, in the present study, the role of glutathione in acquired cisplatin resistance was investigated in the SCC4 and SCC4cisR cells. Interestingly, results obtained herein showed no differences in the endogenous levels of glutathione between the cisplatin-sensitive and cisplatin-resistant OSCC cell lines. However, a substantial and significant difference was found in the GSH/GSSG ratio in the two cell lines following treatment with cisplatin. In fact, on the one hand a drop in the GSH/GSSG ratio was found in SCC4 cells treated with cisplatin compared to control cells, whilst on the other hand, no differences in the GSH/GSSG ratio were observed in the SCC4cisR cells treated with the same concentration of cisplatin compared to control cells. Since the decrease in the GSH/GSSG ratio is a widely recognised marker for oxidative stress, results obtained suggested that cisplatin may induce oxidative stress only in cisplatin-sensitive cells but not in cisplatin-resistant cells. Taken together, although no differences in the endogenous levels of glutathione between the two cell lines were detected, the higher GSH/GSSG ratio observed in the SCC4cisR cell line compared to the SCC4 cell line following treatment with cisplatin suggest a role for glutathione in cisplatin susceptibility. In line with this finding, a recent paper of Silva *et al.* have shown an increase in the GSH/GSSG ratio in cells resistant to cisplatin compared to cells sensitive to cisplatin in lung cancer cells, demonstrating also an inverse correlation between the GSH/GSSG ratio and the amount of DNA damage induced by cisplatin [535].

Similar to glutathione, Nrf2 has also been linked to chemoresistance. Nrf2 is a transcription factor involved in the regulation of several antioxidant pathways. Under

normal conditions, Nrf2 is inhibited by Keap1 and degraded through the proteasomal pathway. In the presence of ROS, the release of Nrf2 from Keap1 results in its translocation to the nucleus and in the regulation of several antioxidant genes, including HO-1 and glutathione [492]. In the present study, Nrf2/HO-1 protein levels were investigated in the parental and SCC4cisR cell lines in the absence/presence of cisplatin in order to determine whether increased levels of ROS resulted in enhanced antioxidant systems in cisplatin-resistant cells. Western blot analysis of Nrf2 and HO-1 protein levels showed a significantly heightened expression of these two proteins in untreated SCC4cisR cells compared to untreated SCC4 cells, suggesting a greater expression of the Nrf2/HO-1 axis in the cisplatin-resistant cell line compared to the parental cell line. Moreover, higher levels of HO-1 in cisplatin treated SCC4cisR cells compared to cisplatin treated SCC4 cells indicated a greater antioxidant response after exposure of cells to cisplatin in the drug-resistant cell line compared to the drug-sensitive cell line. Collectively, this result indicates an enhancement of the antioxidant Nrf2/HO-1 system in the cisplatin-resistant OSCC cell line compared to the parental cell line. Moreover, it suggests a greater antioxidant response following treatment with cisplatin in drug-resistant cells to counteract the intracellular accumulation of ROS and to overcome oxidative stress. In line with these findings, induction of the Nrf2/HO-1 pathway has been associated with chemoresistance in various types of cancer [536]. For example, high levels of Nrf2 has been found in ovarian and mammary cells resistant to doxorubicin compared to the respective sensitive cells [537, 538]. Similarly, increased levels of HO-1 have been found in drug-resistant cells compared to parental cells in acute myeloid leukaemia [539]. Moreover, induced overexpression of Nrf2 through genetic approaches was shown to induce resistance to cisplatin in non-small cell lung carcinoma, while its silencing resulted in an increase in susceptibility [535]. Taken together all the results herein obtained are in accordance with other studies in the literature, indicating that the activation of antioxidant systems in drug-resistant cells represents an adaptive response to counteract high levels of ROS. Moreover, it may be presumed that the increase in ROS levels and the concurrent increase of antioxidant systems in cisplatin-resistant cells may result in a new cellular redox balance which occurs as a consequence of adaptation to oxidative stress induced by repeated exposure of cells to the drug.

Given the link between oxidative stress and chemoresistance, modulating the ROS signalling pathway has been proposed as a potential approach for use in the clinic in order

to reduce chemoresistance. Targeting the antioxidant systems has thus been proposed as a valuable strategy to improve chemotherapy [283]. Accordingly, many researchers are currently investigating the beneficial effects of combining chemotherapeutic agents with antioxidant defence inhibitors. BSO is an inhibitor of glutamylcysteine synthetase (g-GCS) which induces depletion of glutathione by blocking its synthesis [283, 493]. Targeting glutathione with BSO has been shown to enhance the cytotoxic effect of various drugs in several cancer cell models, including biliary tract cancer, glioma and neuroblastoma [284–286]. Interestingly, several of these preclinical studies have demonstrated the beneficial effect of BSO in increasing cisplatin efficacy, suggesting a potential application of this pro-oxidant agent during cisplatin treatment. However, the effect of BSO and cisplatin in combination in OSCC cells remains poorly understood. Therefore, in the present study, the effect of BSO in combination with cisplatin was examined in cisplatin-sensitive and -resistant OSCC cell lines. Treatment of both SCC4 and SCC4cisR cells with BSO for 48 h strongly depleted glutathione levels in a dose-dependent manner. Moreover, from flow cytometric analysis of annexin V/PI stained cells, treatment of cells with BSO in combination with cisplatin displayed a significant increase in the rate of apoptosis compared to control cells and to cisplatin treated cells only in the SCC4cisR cells, suggesting that BSO enhanced cisplatin-induced apoptosis in the cisplatin-resistant OSCC cell line. This result supported a role for glutathione in cisplatin resistance in OSCC. Moreover, even though treatment of SCC4cisR cells with BSO did not fully restore the cisplatin-sensitive phenotype, a beneficial effect of BSO on cisplatin treatment was observed. Accordingly, depletion of glutathione with BSO may represent a valuable strategy to sensitise OSCC cells to the treatment and to reduce drug resistance. To the best of our knowledge, only one other study in the literature has investigated the effect of BSO in combination with cisplatin in OSCC cells. Nevertheless, in this study, only a small and non significant effect on cisplatin-induced apoptosis was observed in OSCC cells treated with BSO [293]. According to the authors, the somewhat limited efficacy of BSO in enhancing cisplatin cytotoxicity may be due to the inability of BSO to penetrate mitochondria, resulting in continued mitochondrial synthesis of glutathione which can protect cells from glutathione depletion. Thus, according to the authors, the use of different glutathione inhibitors (i.e. diethyl maleate) may be more effective in overcoming cisplatin resistance in OSCC.

Additionally, given the potential role of the Nrf2/HO-1 axis in mediating drug resistance, modulation of this signalling pathway has also been proposed as an alternative strategy to improve cancer therapy. Accordingly, a recent study has reported that genetic inhibition of Nrf2 resulted in a decrease in the cell growth and an increase in radiosensitivity in lung carcinoma cells [540]. Similarly, knockdown of Nrf2 by shRNA was shown to sensitise cervical cancer cells to various drugs such as cisplatin, doxorubicin, 5-fluorouracil and paclitaxel [287]. Also, in the same study, Nrf2 knockdown in combination with cisplatin resulted in the inhibition of tumour growth in an *in vivo* model. Given this, Nrf2 has been proposed as a novel regulator of therapeutic resistance [541]. Currently, despite numerous data suggesting the promising application of Nrf2 inhibition in the clinic, no pharmacological Nrf2 inhibitors are currently clinically available or under clinical trials [542]. Recently, a study published by Singh *et al.* has identified a new Nrf2 specific compound named ML385 through a quantitative high-throughput screen (qHTS) of the Molecular Libraries Small Molecule Repository (MLSMR) in a model of non-small cell lung carcinoma [541]. According to the authors, ML385 was shown to directly bind Nrf2, resulting also in reduced GSH levels and cellular antioxidant capacity. Given this, in the present study, Nrf2 inhibition using the Nrf2 inhibitor ML385 was performed in both cisplatin-sensitive and -resistant OSCC cells in the presence/absence of cisplatin in order to determine whether targeting the Nrf2/HO-1 signalling pathway with ML385 may result in an enhancement of cisplatin cytotoxicity in OSCC. From flow cytometric analysis of annexin V/PI stained cells, a notable and significant increase in the percentage of apoptotic cells was observed in the SCC4cisR cells treated with cisplatin in combination with ML385 compared to cells treated with cisplatin alone and ML385 alone whereas no significant enhancement was observed in the parental cells. Taken together, these results indicate that inhibition of Nrf2 with ML385 can partially restore cisplatin sensitivity in the SCC4cisR cells, confirming the involvement of the Nrf2/HO-1 signalling pathway in cisplatin resistance. This finding is in agreement with the previously mentioned study of Singh *et al*. where, treatment of lung cancer cells with ML385 was shown to potentiate the toxicity of various chemotherapeutic drugs such as paclitaxel, docetaxel and carboplatin [541]. Moreover, ML385 in combination with carboplatin was also shown to further reduce tumour weight and size in a xenograph model of lung cancer. However, it should be noted that an anti-tumour activity of ML385 alone was also detected in this study. In this regard, the authors demonstrated a selective toxicity of ML385 in cancer cells with gain of Nrf2 function,

implying the specificity of this compound for Nrf2. Collectively, the anticancer activity of ML385 either alone or in combination with drugs confirmed the importance of Nrf2 in chemoresistance and suggests the application of ML385 in cancer therapy. In line with this data, results herein obtained corroborate the beneficial effect of targeting Nrf2 with ML385 to improve chemotherapy in OSCC.

Moreover, it is worth noting that although results obtained showed that targeting the antioxidant systems results in a significant increase in cisplatin-induced cell death in the drug-resistant cell model generated herein, the increase did not exceed ~10%. This may rely on the nature of the cells itself. Indeed, as already mentioned, if on the one hand the clinically relevant drug-resistant cell lines are more representative of a clinical scenario, on the other hand they may not be an ideal *in vitro* model [505]. In fact, the limited fold change in drug resistance along with the high cell heterogeneity (due to the pool of resistant clones following treatment of cells with cisplatin) may represent a limitation for the identification of the mechanisms implicated in chemoresistance. Given this, it cannot be excluded that the slight effect of the antioxidant inhibitors on cisplatin-induced apoptosis in SCC4cisR cells may be attributable to the fact that only a subpopulation of cells has developed resistance to cisplatin through enhancement of the antioxidant response. Accordingly, highly resistant cell lines obtained through a clonal selection approach may be useful to confirm the involvement of the antioxidant systems in acquired resistance to cisplatin in OSCC. Nevertheless, it should be highlighted that results obtained herein in the clinically relevant SCC4cisR cells may be promising for clinical applications and require confirmation in a greater number of cisplatin-sensitive/resistant OSCC cell lines to corroborate the beneficial effect of this combinatorial therapeutic strategy to reduce chemoresistance in OSCC.

Finally, a large body of evidence has recently demonstrated that some oncogenic signalling pathways can influence the activity of Nrf2 increasing its mRNA levels [542]. In particularly, a link between the Ras/ERK pathway and Nrf2 have been demonstrated in recent years. The Ras/ERK pathway is a survival pathway involved in the regulation of many important cellular processes such as differentiation, proliferation and stress response [494]. Disruption of the Ras/ERK pathway has been widely reported in the literature and it has been associated with tumour progression and chemoresistance [543]. Recent studies have shown that dysregulation of Ras can result in an increase in Nrf2 levels in various studies *in vitro* [544]. For example, Ras overexpression was shown to

increase Nrf2 mRNA levels and reduce oxidative stress in pancreatic cancer cells [545]. Given the link between the Ras/ERK pathway and the Nrf2/HO-1 axis and their potential implication in chemoresistance, evaluation of the Ras/ERK signalling pathway was undertaken in the present study. Results obtained herein showed Ras overexpression in the SCC4cisR cells compared to the SCC4 cells both in the absence and presence of the drug, suggesting an upregulation of Ras during the acquisition of the cisplatin resistant phenotype. Moreover, phosphorylation of ERK was observed in both untreated SCC4 and SCC4cisR cells, indicating that ERK was activated in both cell lines under normal conditions, Additionally, treatment of cells with cisplatin resulted in a decrease in ERK activation in the SCC4 cell line only, but not in the SCC4cisR cell line. Given the role of ERK as a pro-survival pathway the significant difference in ERK activation between the two cell lines following treatment with cisplatin may be linked to the chemoresistant properties of the SCC4cisR cell line. Similar to the results obtained herein, activation of the Ras/ERK pathway was shown to mediate cisplatin resistance in ovarian cancer cells [73]. Moreover, a greater activation of the Ras/ERK pathway was found in doxorubicin-resistant hematopoietic cells compared to the sensitive cells after treatment with doxorubicin [546]. Additionally, a ROS-dependent activation of the Ras/ERK pathway was linked to the development of acquired drug resistance in leukaemia [543]. A large body of evidence in the literature has also demonstrated that K-Ras mutations may result in resistance to chemotherapy in various cancers [547, 548]. Interestingly, a recent paper published by Tao *et al.* demonstrated that overexpression of K-Ras enhanced the resistance of cells to cisplatin through a Nrf2-dependent mechanism [495]. Consistently, in this study, knockdown of Nrf2 resulted in the loss of cisplatin resistance, confirming the Nrf2 dependency of K-Ras-mediated chemoresistance. Moreover, in the same study, the authors demonstrated that oncogenic K-Ras enhanced Nrf2 through activation of ERK. In the present study, upregulation of both the Ras/ERK pathway and the Nrf2/HO-1 pathway were demonstrated. Thus, a link between these two pathways may be suggested and may be associated with the development of the cisplatin resistance phenotype. Accordingly, further analysis on the role of Ras/ERK pathway in cisplatin resistance and in Nrf2 regulation may be required for a better understanding of the regulatory pathways implicated in cisplatin resistance.

In conclusion, in the present chapter, evaluation of the mechanisms involved in acquired cisplatin resistance in OSCC was undertaken. Analysis of chemoresistance was carried

out through the generation and characterisation of a cisplatin-resistant OSCC cell line obtained by pulsed stepwise exposure of drug-sensitive cells to cisplatin. Autophagy does not appear to play a role in acquired cisplatin resistance in the model examined herein. Conversely, a role for oxidative stress may be implicated in the development of a cisplatin-resistant phenotype in OSCC. A greater antioxidant response was initiated in resistant cells following treatment with cisplatin to counteract the intracellular accumulation of ROS and to overcome oxidative stress. Accordingly, impairment of redox signalling by depleting glutathione levels with BSO (an inhibitor of glutathione synthesis) and by targeting the Nrf2/HO-1 pathway with the specific Nrf2 inhibitor ML385 was shown to enhance cisplatin cytotoxicity in SCC4cisR cells. Finally, preliminary results obtained herein may also suggest a potential role for the Ras/ERK pathway in mediating cisplatin resistance in OSCC and further analysis of the role that the Ras/ERK pathway plays in Nrf2 regulation is warranted.

6. Analysis of key autophagic proteins in OSCC patient samples

6.1. Introduction

A correlation between autophagy and cancer has become well-established over the past number of years. However, the role of autophagy in cancer and its implication in carcinogenesis remains controversial [549]. As previously mentioned in the general introduction, autophagy has been defined as a double-edged sword in cancer biology, acting both as a tumour suppressor and tumour promoter mechanism [143]. Interestingly, a stage-dependent role of autophagy has been demonstrated during cancer development [168]. In fact, during the early stages of tumour progression, autophagy can prevent oxidative stress and reduce the accumulation of damaged proteins, exerting a tumour suppressor role. This is followed by a tumour promoter role of autophagy in advanced stages of carcinogenesis, resulting in a cellular adaptation to hypoxia, nutrient deprivation and other adverse microenvironment conditions through autophagy. Given this, tumour initiation has been associated with transient reduced levels of autophagy, which results in a failure of its tumour suppressor function, resulting in genome damage and instability [168]. Conversely, tumour progression and maintenance has been linked to enhanced activation of autophagy. Although this model may be applied to many types of cancer, a tumour-specific role of autophagy has also been proposed [550]. On the one hand overexpression of some autophagic proteins such as ATG5 or LC3 have been found in various cancers, suggesting a tumour promoter role of autophagy in these tumour models. On the other hand the loss of the autophagic marker Beclin-1 has been found in some other cancers and it has been linked to a potential role of autophagy as a tumour suppressor mechanism [167]. Furthermore, it has been proposed that some cancers may be autophagy-addicted, whilst some others may be autophagy-independent [550]. In the latter case, either a lack of autophagy or the presence of dysfunctional autophagy has been reported.

Despite the research efforts in this field to date, the role of autophagy in oral cancer has not been clearly defined [551]. Several studies have recently reported an alteration in the levels of autophagic proteins in OSCC tissues, suggesting a role for autophagy in oral cancer development [182, 183, 551]. However, whether autophagy may be enhanced or inhibited in OSCC is not totally understood. Thus, further studies are required to better understand the role of autophagy in OSCC and to determine its role during the various phases of oral carcinogenesis. In fact, OSCC development is a multistep process resulting from genetic mutations, which lead to the selection of transformed epithelial cells [552].

The progressive accumulation of these transformed cells usually results in an alteration of the structural organisation of the oral epithelium, leading to a condition known as dysplasia, which may represent the initial step of oral carcinogenesis. From a clinical point of view, OSCC lesions are usually preceded by precancerous lesions, which may potentially develop into a primary tumour [3]. These precancerous lesions can be either associated with a normal or dysplastic epithelium and they can be classified, depending on their appearance, into three main groups; homogeneous leukoplakia (white plaques), non-homogeneous leukoplakia (white irregular plaques) or erythroleukoplakia (white and red irregular plaques) [552]. Given this, whether dysregulation of autophagy may occur as early as in the precancerous lesions and whether a dysfunctional autophagy may be maintained during OSCC progression remains unclear.

To better elucidate the role of autophagy in cancer, several studies have tried to evaluate the levels of autophagy-related proteins in various tumour models. LC3, p62 and Beclin-1 are the most commonly studied autophagic proteins in cancer. Together these three markers reflect the whole autophagy process from the nucleation, elongation and degradation stages of autophagosomes, respectively [553]. Moreover, Beclin-1 has recently been shown to be of particular interest in cancer biology, because of its interaction with the anti-apoptotic Bcl-2 family proteins (such as Bcl-2 and Bcl-xL). Thus, Beclin-1 and Bcl-2 proteins represent a key node in the interplay between autophagy and apoptosis, which is another pathway notoriously dysregulated during cancer progression [130].

In the previous chapters, activation of proficient autophagy in OSCC cell lines was demonstrated, and the role of autophagy in response to chemotherapy along with its involvement in chemoresistance in OSCC was investigated. In the present chapter, in order to further elucidate the involvement of autophagy in oral cancer its role in OSCC development was examined. To this end, endogenous levels of the autophagic markers LC3, p62 and Beclin-1, along with the levels of the anti-apoptotic protein Bcl-xL, were investigated in OSCC patient tissue samples. Interestingly, in this study the whole histopathological spectrum of oral cancer development, consisting of normal, precancerous and cancerous stages, was evaluated in two OSCC cohorts of patients, consisting of suitably identified cases from a Spanish and an Irish hospital. Proteins of interest were examined through western blot and immunohistochemistry analysis respectively.

6.2. Results

6.2.1. Expression analysis of p62 and LC3 proteins in fresh oral biopsies from a Spanish cohort

The expression of key autophagic markers during OSCC development was firstly investigated in a Spanish patient cohort. This analysis was carried out at the University of Valencia, in the Molecular Oncology Laboratory of the General University Hospital Research Foundation. p62 and LC3 proteins were selected as autophagy markers for this study and their expression was evaluated in fresh/frozen tissue samples by western blot analysis. Following ethical approval for the study, 59 oral biopsy samples over a period of 12 months were collected from patients by Prof Jose Bagan after informed consent and immediately snap frozen and stored at -80°C. Autophagy protein expression levels were compared among three different groups of patients: Control (N=20), Precancerous (N=19) and OSCC (N=21) samples. Frozen tissues were thawed and lysed, and samples were run on a 15% SDS-PAGE gel before being probed with LC3-I/II and p62 antibodies. SCC4 cells under normal and starvation conditions (EBSS for 4 h) were used as a negative and positive control for autophagy activation, respectively. Densitometric analysis of p62, LC3-I and LC3-II bands was performed using ImageJ software and data were normalised to the loading control (β-actin). To estimate the LC3 protein expression in oral tissue samples, the total LC3 levels (LC3-I + LC3-II) were assessed. Moreover, to examine autophagy activation, the conversion rate of LC3-I to LC3-II was examined through calculation of the LC3-II/LC3-I ratio.

In Figure 6.1, a representative blot of Control (N=4), Precancerous (N=4) and OSCC (N=4) patient samples along with SCC4 cells used as positive/negative control is shown. As expected, a decrease in p62 protein expression levels and an increase in the conversion of LC3-I to LC3-II were found in EBSS-treated SCC4 cells compared to untreated cells, indicating autophagy induction and validity of the assay. A basic descriptive study of patient sample data was firstly performed using JMP software. Various statistical parameters, including mean, median, minimum and maximum values, first and third quartiles, standard deviation (SD), variance and coefficient of variation (CV), were calculated for p62 and LC3 expression and for the LC3-II/LC3I ratio in each group of

patients, as reported in Tables 6.1-3. Few samples were excluded from this analysis due to technical reasons.

Expression levels of p62 and LC3 proteins along with the LC3-II/LC3-I ratio of Control, Precancerous and OSCC samples were then compared. Interestingly, a slight trend appears to be emerging among the three groups of patients. Overall, p62 decreased in Precancerous and OSCC samples compared to Control samples (Figure 6.2A). In contrast, an increase in the LC3 levels and the LC3-II/LC3-I ratio was found in OSCC samples compared to Precancerous and Control samples (Figure 6.2B-C). Taken together, these results suggest an opposing trend in the expression levels of p62 and LC3 during OSCC progression, with a decrease in p62 levels and a progressive increase in LC3 levels observed during oral tumorigenesis. Moreover, decreased levels of p62 along with an increase in the LC3-II/LC3-I ratio in cancerous patients may suggest autophagy activation during cancer progression in OSCC. Nevertheless, a non-parametric statistical test (Kruskal-Wallis H test) did not show any statistically significant difference in the levels of these autophagy markers among the three groups of patients, likely because of the limited number of patients in the two cohorts and the high heterogeneity between samples within each category.

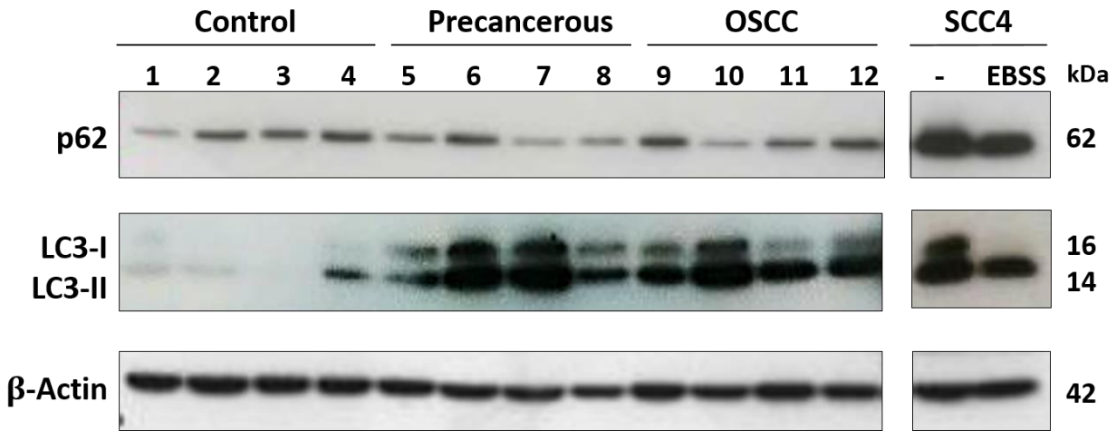

Figure 6.1 Expression analyses of p62 and LC3-I/II in oral tissue samples.

Representative Western Blot of Control (N=4), Precancerous (N=4) and OSCC (N=4) patient samples. Frozen patient biopsies were thawed, lysed and 60 µg of protein was loaded and separated on a 15% SDS-PAGE gel, transferred to a PVDF membrane and probed with an anti-LC3-I/II and anti-p62 antibodies. SCC4 cells treated with EBSS for 4 h or left untreated were used as positive and negative controls of autophagic induction (see right hand panel). β-actin served as loading control.

	Control	Precancerous	OSCC
N	19	17	18
N excluded	1	2	3
Mean	0.67	0.52	0.51
Median	0.52	0.40	0.48
Minimum	0.02	0.10	0.02
Maximum	2.04	1.91	1.38
Upper 95% Mean	0.92	0.73	0.68
Lower 95% Mean	0.42	0.30	0.35
Std. Deviation (SD)	0.18	0.42	0.33
Coefficient of Variation (CV)	76.13	81.69	64.65

Table 6.1 Descriptive statistics for p62 protein expression levels in Control, Precancerous and OSCC patient samples.

	Control	Precancerous	OSCC
N	19	17	20
N excluded	1	2	1
Mean	3.20	4.48	5.53
Median	1.78	2.50	3.25
Minimum	0.06	0.66	1.48
Maximum	14.89	28.32	33.79
Upper 95% Mean	5.08	7.82	9.95
Lower 95% Mean	0.89	1.15	2.12
Std. Deviation (SD)	3.90	6.49	7.29
Coefficient of Variation (CV)	121.87	144.80	131.76

Table 6.2 Descriptive statistics for total LC3 protein expression in Control, Precancerous and OSCC patient samples.

	Control	Precancerous	OSCC
N	19	17	20
N excluded	1	2	1
Mean	0.83	0.76	0.99
Median	0.74	0.63	0.89
Minimum	0.07	0.06	0.29
Maximum	1.86	2.76	2.82
Upper 95% Mean	1.12	1.09	1.13
Lower 95% Mean	0.54	0.44	0.67
Std. Deviation (SD)	0.60	0.63	0.69
Coefficient of Variation (CV)	71.49	81.79	69.79

Table 6.3 Descriptive statistics for LC3-II/LC3-I ratio in Control, Precancerous and OSCC patient samples.

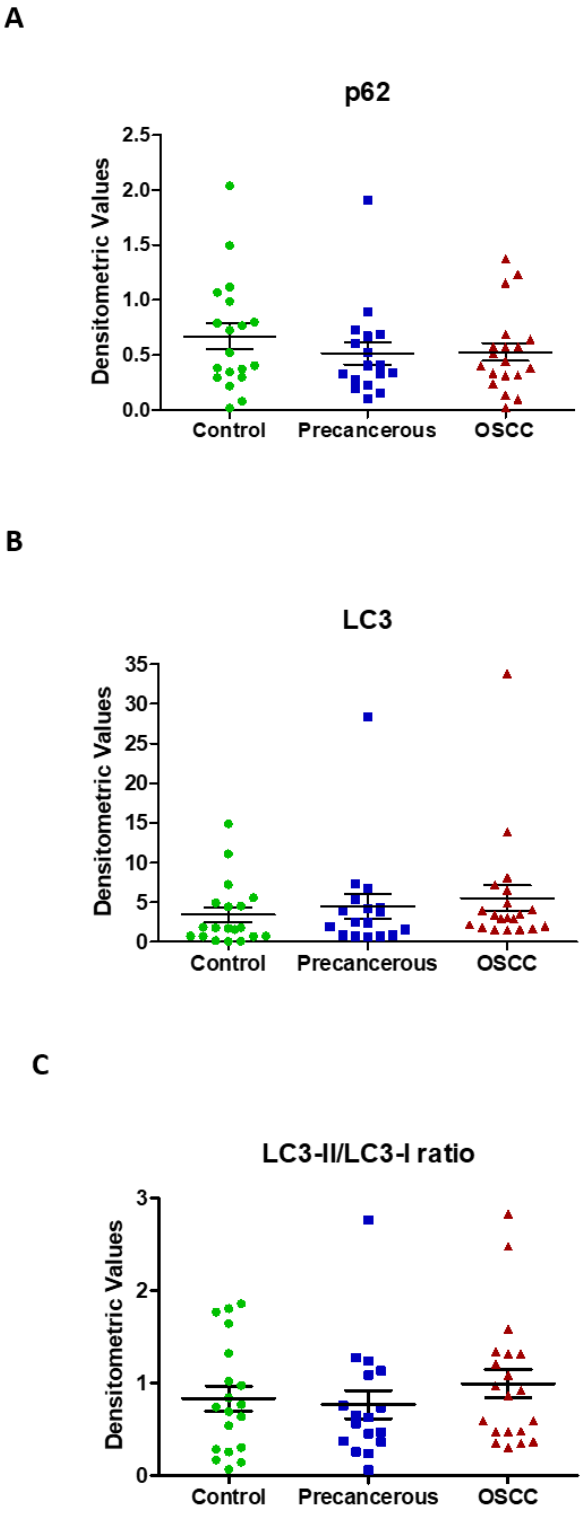

Figure 6.2 Analysis of p62 and LC3 protein expression levels and LC3-II/LC3-I ratio in oral tissue samples.

Scatter plots of p62 (**A**) and LC3 (**B**) protein expression levels along with the LC3-II/LC3-I ratio (**B**) in Control, Precancerous and OSCC patient samples. Data represent the mean ±S.E.M. Statistical analysis was performed using Kruskal-Wallis H Test with Dunn's Multiple Comparison to compare the three groups of samples (Graphpad Prism 8). $p>0.05$.

6.2.2. Correlation analysis of autophagy markers with clinical-pathological factors in Spanish cohort of OSCC patients

6.2.2.1. Patient characteristics

Demographic and clinical-pathological characteristics of the patient cohort herein examined were reported in Table 6.4. Among the 20 patients belonging to the Control group, the median age was 26.5 years old, 50% were females and 50% were males. In the Precancerous group of patients, the median age was 61 years old, 63.13% of the patients were females and 36.84% were males. Within this group, the lesion site with the highest incidence was the tongue (42.11%), followed by the gingiva (38.84%), the palate (15.79%) and the floor of the mouth (5.26%). Moreover, 57.89% of the precancerous lesions examined were verrucous leukoplakia, 21.05% were erythroleukoplakia and the remaining 21.05% were homogeneous leukoplakia. Additionally, histological analysis was carried out for all the Precancerous samples, revealing a dysplastic phenotype in 52.63% of patients. In regard to the OSCC group, the median age was 72.5 years old, 42.85% of patients were females and 57.15% were males. Gingiva (38.84%) and tongue (33.33%) were the most relevant tumour sites, followed by buccal mucosa, floor of the mouth and palate (9.52%, 9.52% and 4.76% respectively). With the exception of one sample where the information on tumour size was not provided, half of these tumours were equal to or smaller than 2.5 cm, while the remaining half were bigger than 2.5 cm. Ultimately, only 14.28% of tumours showed neck metastasis.

Control	N	% of Total
Total	20	100%
Median age	26.5	
Gender		
Female	10	50.00%
Male	10	50.00%

Precancerous	N	% of Total
Total	19	100%
Median age	61	
Gender		
Female	12	63.13%
Male	7	36.84%
Lesion site		
Floor of the mouth	1	5.26%
Gingiva	7	38.84%
Palate	3	15.79%
Tongue	8	42.11%
Clinical appearance		
Erythroleukoplakia	4	21.05%
Homogeneous leukoplakia	4	21.05%
Verrucous leukoplakia	11	57.89%
Dysplasia		
No	9	47.37%
Yes	10	52.63%

OSCC	N	% of Total
Total	21	100%
Median age	72.5	
Gender		
Female	9	42.85%
Male	12	57.15%
Tumour site		
Buccal Mucosa	2	9.52%
Floor of the mouth	2	9.52%
Gingiva	9	42.85%
Palate	1	4.76%
Tongue	7	33.33%
Tumour size (cm)		
≤2.5	10	47.61%
>2.5	10	47.61%
Neck metastasis		
No	18	85.71%
Yes	3	14.28%

Table 6.4 Demographic and clinical-pathological characteristics of Control, Precancerous and OSCC patients.

6.2.2.2. Autophagic markers do not correlate with the clinical appearance of lesions and the dysplasia phenotype in Precancerous patient samples

In the present study, the precancerous cohort of patients was divided into various sub-cohorts based on two clinical-pathological features: clinical appearance of the lesions and presence of a dysplastic phenotype. Correlation analysis of autophagic markers with respect to these two features was undertaken, and a non-parametric test (Kruskal-Wallis H Test) was applied to determine any significant difference among groups of samples.

Three different types of precancerous lesion were considered based on clinical appearance: homogeneous leukoplakia (HL), verrucous leukoplakia (VL) and erythroleukoplakia (EL). No significant differences in the p62 and LC3 expression levels were detected among the three clinical types, suggesting no correlation between these markers and the clinical appearance of precancerous lesions in the oral cavity (Figure 6.3). Additionally, correlation analysis between autophagic markers and the presence of a dysplastic phenotype did not show any significant correlation either in respect of p62 or LC3 proteins (Figure 6.4).

Overall, in the present study, no differences in the levels of p62 and LC3 were detected among sub-groups of precancerous patients.

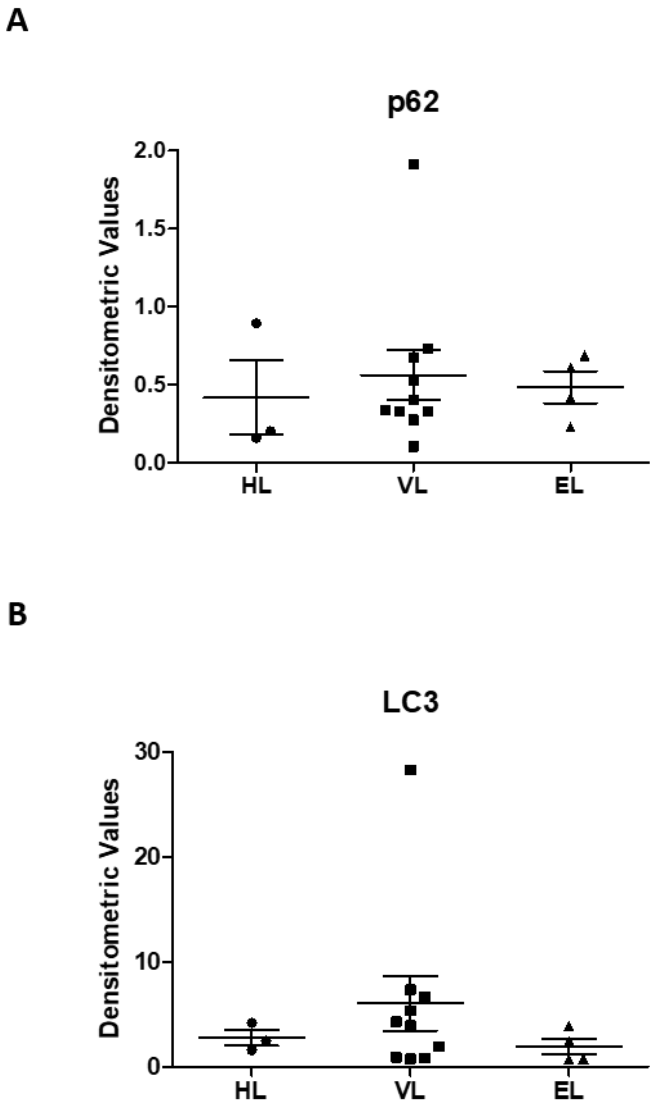

Figure 6.3 Expression levels of p62 and LC3 proteins did not correlate with the clinical appearance of lesions in Precancerous samples.

Scatter plots of p62 (**A**) and LC3 (**B**) protein expression levels in N=3 homogeneous leukoplakia (HL), N=10 verrucous leukoplakia (VL) and N=4 erythroleukoplakia (EL). Data represent the mean ±S.E.M. Statistical analysis was performed using Kruskal-Wallis H Test with Dunn's Multiple Comparison to compare the three groups of patients (Graphpad Prism 8). $p>0.05$.

.

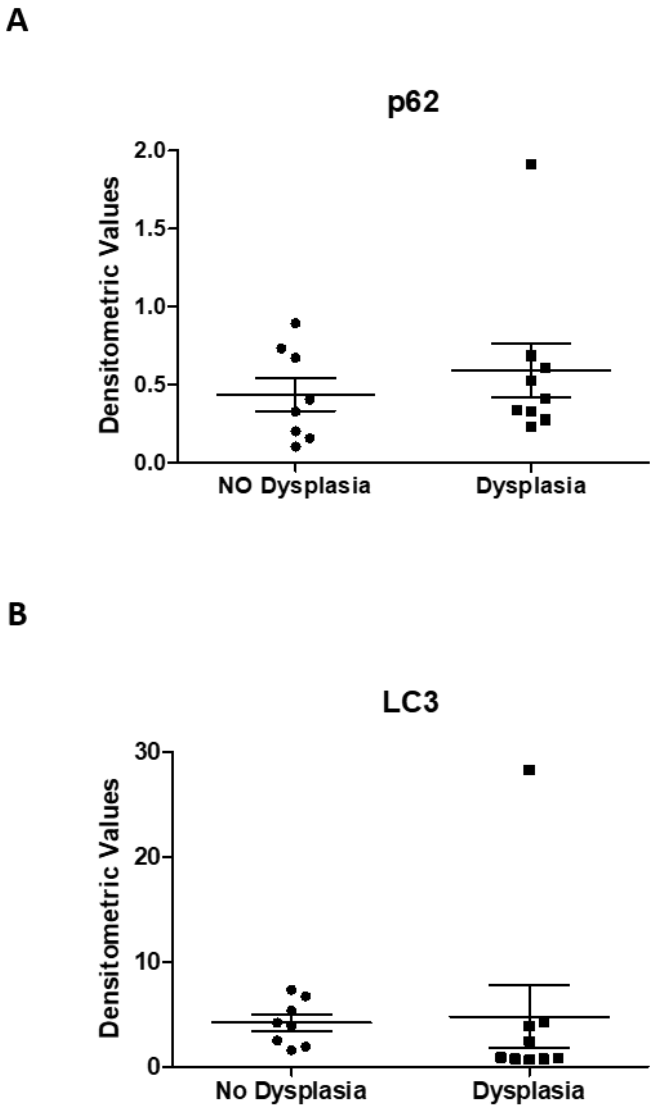

Figure 6.4 Expression levels of p62 and LC3 proteins did not correlate with the presence of a dysplasia phenotype in Precancerous samples.

Scatter plots of p62 (**A**) and LC3 (**B**) protein expression levels in N=8 patients with No Dysplasia and N=9 patients with Dysplasia. Data represent the mean ±S.E.M. Statistical analysis was performed using Mann-Whitney Test to compare the two groups of patients (Graphpad Prism 8). $p>0.05$.

6.2.2.3. p62 protein expression correlates with tumour size in OSCC patients

Correlation analysis of autophagic markers and the clinical-pathological parameter of "tumour size" was next undertaken in the OSCC samples. The tumour size in the OSCC cohort herein examined varied within the range of 1.5 cm to 5 cm, with a median value of 2.7 cm. Given this, OSCC patients were divided in two sub-groups: OSCC ≤2.5 cm and OSCC >2.5 cm. The two categories were compared in respect of the expression levels of p62 and LC3, and the Mann-Whitney Test was applied to determine any significant difference between categories.

Interestingly, a significant decrease in p62 expression levels was observed in OSCC >2.5 cm compared to OSCC ≤2.5 cm, suggesting a negative correlation between p62 protein expression and the size of tumours in OSCC (Figure 6.5). Moreover, a slight (although not significant) decrease in the LC3 levels was also found in OSCC >2.5 cm compared to OSCC ≤2.5 cm. However, due to the high variability observed in the OSCC >2.5 cm category with respect to the LC3 expression, no firm conclusion can be drawn regarding a potential correlation between tumour size and LC3 expression in OSCC.

Taken together, these results may indicate a correlation between p62 expression and tumour size, supporting a potential role for p62 in OSCC progression. However, due to the high variability amongst patients, further analysis with a bigger sample size may be required to determine whether there may also be a correlation between LC3 expression and tumour size.

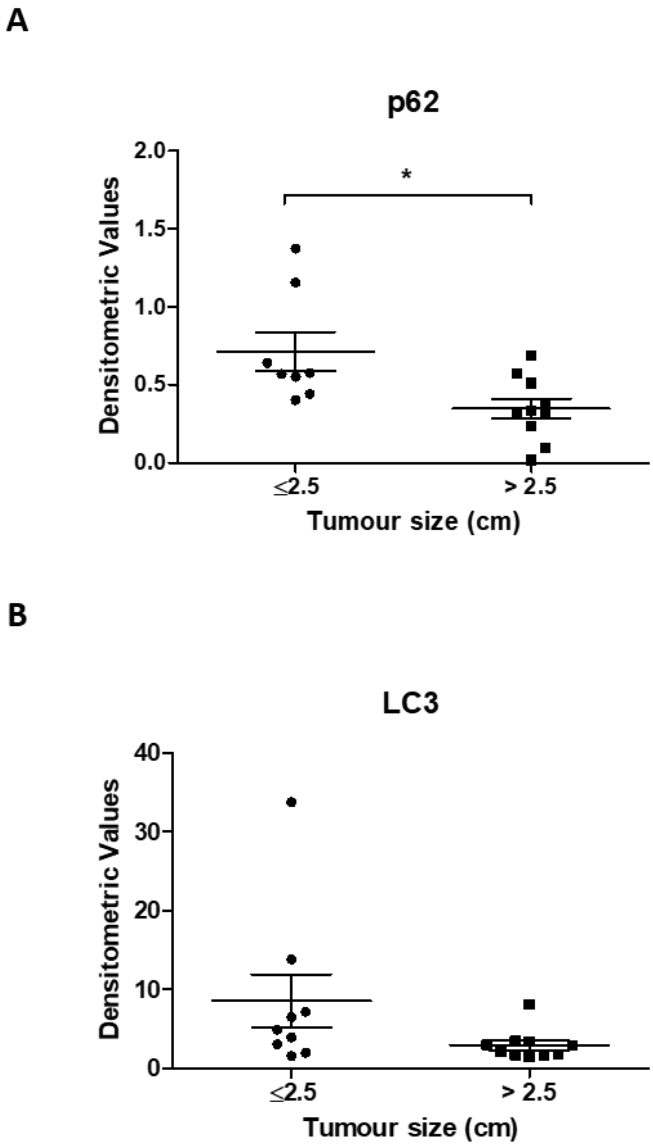

Figure 6.5 Expression levels of p62 correlated with tumour size in OSCC samples.

Scatter plots of p62 (**A**) and LC3 (**B**) protein expression levels in N=8 OSCC≤2.5 cm and N=10 OSCC>2.5 cm. Data represent the mean ±S.E.M. Statistical analysis was performed using Mann-Whitney Test to compare the two groups of patients (Graphpad Prism 8). *p<0.05.

6.2.3. Optimisation of antibody concentrations for immunohistochemical staining

To further investigate the role of autophagy during OSCC progression, the expression of autophagic markers in oral tissue samples was also investigated by immunohistochemistry (IHC). IHC is the most commonly used microscopy-based technique for visualising cellular components, such as proteins, in tissue samples [554]. In the present study, three autophagic proteins were examined for this analysis: LC3, Beclin-1 and Bcl-xL. Prior to commencing the experiments, optimisation of primary antibodies was undertaken. Firstly, different staining protocols were examined for each antibody of interest, as described in the Materials and Methods section. Once the best staining protocol was determined, the optimal primary antibody concentration was assessed in control tissues. Paraffin-embedded control tissue blocks were cut and sections were mounted on slides before being stained on a Ventana BenchMark XT immunostainer.

The control tissue utilised for LC3 was lung adenocarcinoma tissue, as it has been previously shown to stain positive for LC3 [555, 556]. A negative control (secondary antibody only) along with three LC3 antibody dilutions (1:300, 1:100 and 1:50) were tested to determine the non-specific binding of the secondary antibody and the optimal primary antibody concentration for subsequent experiments. No staining was obtained in the representative negative control slide, indicating that the secondary antibody did not non-specifically bind other cellular targets (Figure 6.6A). Moreover, positive LC3 staining was observed in the cytoplasm of lung adenocarcinoma cells when the primary antibody was applied, with a progressive increase in staining intensity at more concentrated dilutions of primary antibody (Figure 6.6B-D). An antibody dilution of 1:50 was herein chosen for subsequent experiments, as it gave the strongest and clearest staining in the control tissue.

The control tissues utilised for Beclin-1 were normal colon tissue and kidney tissue, as both have been previously shown to stain positive for Beclin-1 [557–560] Similar to LC3, a negative control (secondary antibody only) and two Beclin-1 antibody dilutions (1:400 and 1:300) were assessed. Negative staining was observed in the secondary antibody only controls (Figure 6.7 A, D), whilst strong Beclin-1 staining was obtained in both tissues stained with the two antibody dilutions (Figure 6.7 B-C, E-F). Since the lowest antibody

dilutions showed some non-specific binding in the kidney tissue, a dilution of 1:400 was used for subsequent experiments.

Finally, the positive control tissues utilised for Bcl-xL were prostate tissue and gastric cancer tissue, as positive staining for Bcl-xL has been reported in the literature in benign prostatic hyperplasia (BPH) and in the normal adjacent area as well as in gastric cancer [561, 562]. In Figure 6.8 a representative image of secondary antibody only controls along with three concentrations of Bcl-xL antibody (1:600, 1:300, 1:100) in the two control tissues is displayed. Positive cytoplasmic staining for Bcl-xL was observed in both prostate and gastric cancer tissues and a concentration of 1:300 was chosen for subsequent experiments, as it gave the clearest staining.

In conclusion, results obtained from these optimisation experiments correlate with results reported in the literature in regard to LC3, Beclin-1 and Bcl-xL expression in control tissues, suggesting antibody specificity at the aforementioned dilutions. Additionally, no cross-reactivity between secondary antibody and non-specific cellular components was demonstrated.

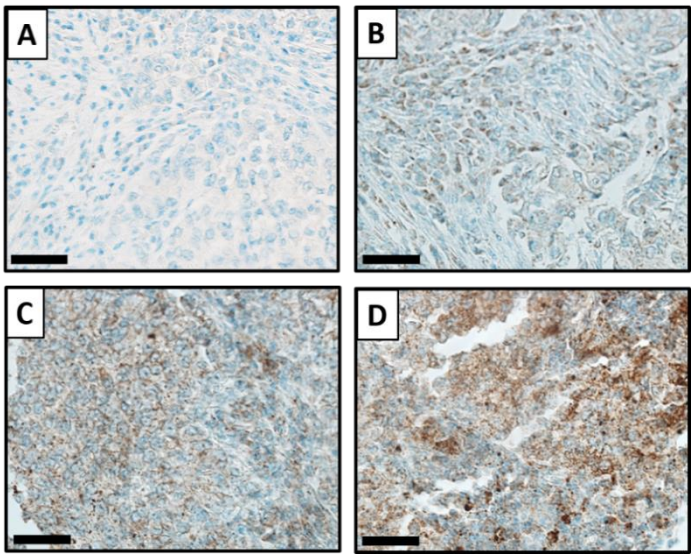

Figure 6.6 Optimisation of LC3 antibody concentration in lung adenocarcinoma tissue.

Representative images of paraffin-embedded lung adenocarcinoma tissue. Tissue was cut and sections were mounted on slides before being stained with an anti-LC3 antibody on the Ventana BanchMark XT immunostainer. A negative control (secondary antibody only) was assessed (**A**) along with various LC3 antibody dilutions: 1:300 (**B**), 1:100 (**C**) and 1:50 (**D**). Images were taken using an Olympus BX51 microscope at 20X magnification. Scale bar: 50 µm.

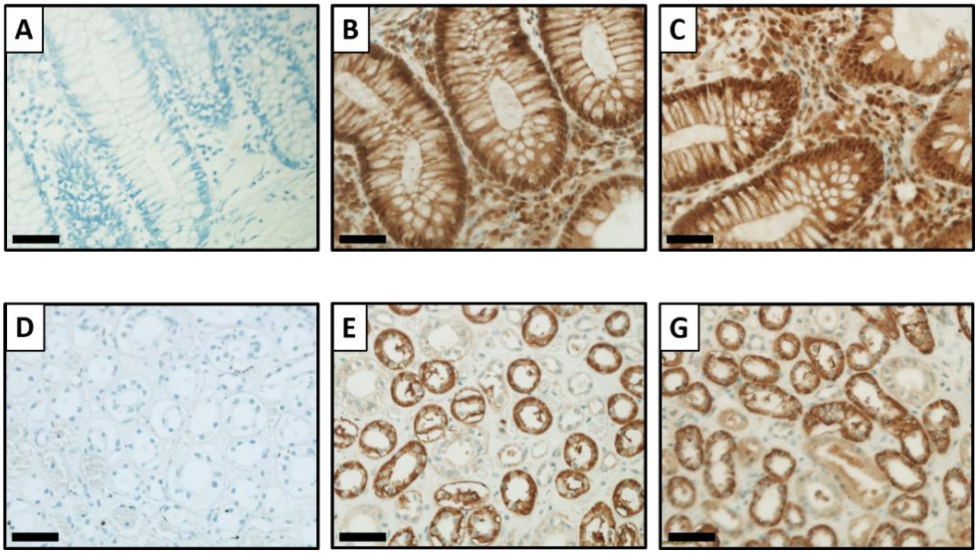

Figure 6.7 Optimisation of Beclin-1 antibody concentration in colon tissue and kidney tissue.
Representative images of paraffin-embedded colon tissue (**A-C**) and kidney tissue (**D-G**). Tissues were cut and sections were mounted on slides before being stained with an anti-Beclin-1 antibody on the Ventana BanchMark XT immunostainer. Negative controls (secondary antibody only) were assessed (**A**, **D**) along with two Beclin-1 antibody dilutions: 1:400 (**B**, **E**), 1:300 (**C**, **G**). Images were taken using an Olympus BX51 microscope at 20X magnification. Scale bar: 50 µm.

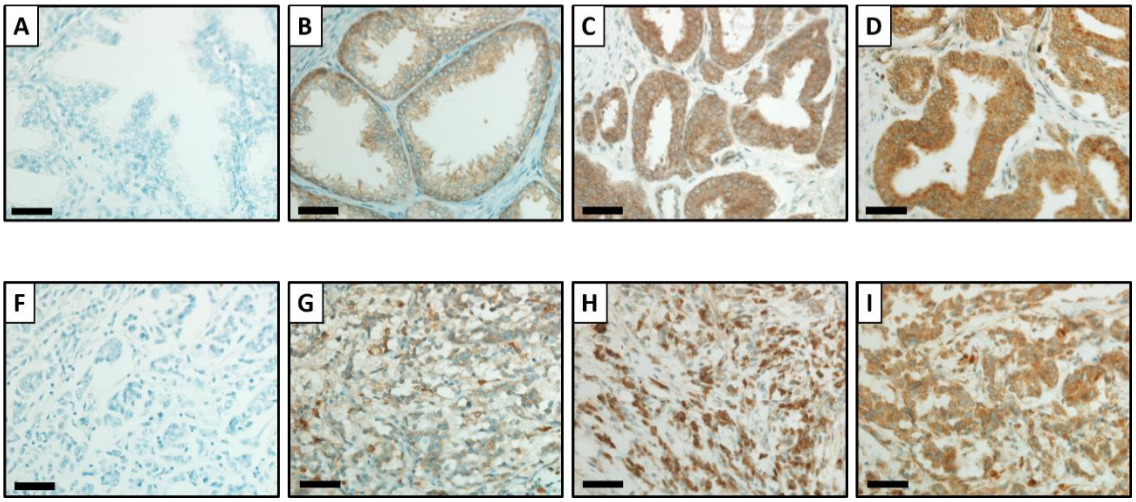

Figure 6.8 Optimisation of Bcl-xL antibody concentration in prostate tissue and gastric cancer tissue. Representative images of paraffin-embedded prostate tissue (**A**-**D**) and gastric cancer tissue (**F**-**I**). Tissues were cut and sections were mounted on slides before being stained with an anti-Bcl-xL antibody on the Ventana BanchMark XT immunostainer. Negative controls (secondary antibody only) were assessed (**A**, **F**) along with three Bcl-xL antibody dilutions: 1:600 (**B**, **G**), 1:300 (**C**, **H**), 1:100 (**D**, **I**). Images were taken using an Olympus BX51 microscope at 20X magnification. Scale bar: 50 µm.

6.2.4. IHC analysis of LC3, Beclin-1 and Bcl-xL proteins in paraffin-embedded oral biopsies from an Irish patient cohort

IHC analysis of LC3, Beclin-1 and Bcl-xL was undertaken in paraffin-embedded oral biopsies from an Irish cohort of patients. Following receipt of ethical approval, this analysis was performed at the Central Pathology Laboratory in St. James's Hospital (Dublin) and patient samples (N=29) were provided by Dr Mary Toner, lead pathologist of the Oral Maxillofacial & Pathology Unit in St. James's Hospital. Firstly, samples were coded, sectioned and stained with haematoxylin & eosin (H&E) for histological assessment. H&E slides were reviewed by Dr Mary Toner and the presence of Normal, Dysplasia and OSCC tissue was assessed for each slide (Figure 6.9). Overall, N=20 Normal, N=23 Dysplasia and N=17 OSCC tissue samples were analysed in this study and the protein expression of LC3, Beclin-1 and Bcl-xL were compared amongst the three types of tissues. Sample blocks were cut and sections were stained with relevant antibodies using a Ventana BenchMark XT immunostainer. Immunostaining was double scored blindly (S. Magnano & E. Flis) based on the observed staining intensity of squamous epithelial cells. For each protein of interest four scores were assigned to the samples: +1 (weak staining), +2 (medium staining), +3 (strong staining) and +4 (very strong staining), as shown in Figure 6.10. The IHC scores obtained were then averaged and plotted using GraphPad Prism software.

All of the samples exhibited cytoplasmic LC3 staining in squamous epithelial cells (Figure 6.11). A mean IHC score of 2.3±0.9 was obtained in the normal oral mucosa, whilst mean IHC scores of 2.6±0.7 and 3.3±0.9 were obtained in the dysplastic and cancerous oral tissues respectively. Consistently, statistical analysis showed a significant increase in LC3 IHC score in OSCC samples compared to both Normal and Dysplasia samples. Similarly, positive Beclin-1 staining was observed in squamous epithelial cells of all samples, with a statistically significant increase in the IHC score in OSCC samples (mean IHC score 3.8±0.2) compared to Dysplasia samples (mean IHC score 3.0±0.8) and Normal samples (mean IHC score 2.7±0.7), indicating a positive regulation of Beclin-1 expression during cancer progression (Figure 6.12). Additionally, all of the samples exhibited cytoplasmic Bcl-xL staining in squamous epithelial cells (Figure 6.13). A statistically significant increase in the Bcl-xL IHC score was found in OSCC samples (mean IHC score 3.4±0.6) compared to Normal samples (mean IHC score 2.5±0.9), whilst

no significant differences were observed between OSCC samples and Dysplasia samples (mean IHC score 2.9±0.6).

Additionally, in order to show the distribution pattern of LC3, Beclin-1 and Bcl-xL protein expression in relation to the histological stages in OSCC progression, data obtained herein were further analysed and summarised in a frequency distribution table (Table 6.5). For this purpose, the weak (+1) and medium staining (+2) were regarded as low expression, whilst the strong (+3) and the very strong (+4) staining were regarded as high expression. Among the 60 samples examined, 53.4% of samples showed high LC3 expression in squamous epithelial cells. In the Normal and in the Dysplasia groups, 8 out of 20 and 9 out of 23 samples displayed a high expression of LC3 respectively, whilst 15 out of 17 OSCC samples exhibited high LC3 expression. Additionally, 70% of all samples displayed high Beclin-1 expression in squamous epithelial cells. Interestingly, none of the 17 OSCC samples showed a low Beclin-1 expression, which in contrast was observed in 11 out of 20 Normal samples and in 7 out of 23 Dysplasia samples. Interestingly, a Pearson's chi-squared test showed a significant association between the LC3 and Beclin-1 protein expression and the histological stages of OSCC progression. Finally, 63.3% of the total samples exhibited high expression Bcl-xL in squamous epithelial cells. A high expression of Bcl-xL was found in only 9 out of 20 Normal samples, in 15 out of 23 Dysplasia samples and in 14 out of 17 OSCC samples.

Taken together, these results demonstrated a significant increase in the expression levels of LC3, Beclin-1 and Bcl-xL during oral cancer progression, suggesting a role for these proteins in OSCC development. Moreover, results herein obtained by IHC in regard to LC3 expression in OSCC patient samples from an Irish cohort align with the results obtained by western blot analysis in OSCC patients from a Spanish cohort. The consistency between these two results strongly support a role for LC3 in OSCC progression.

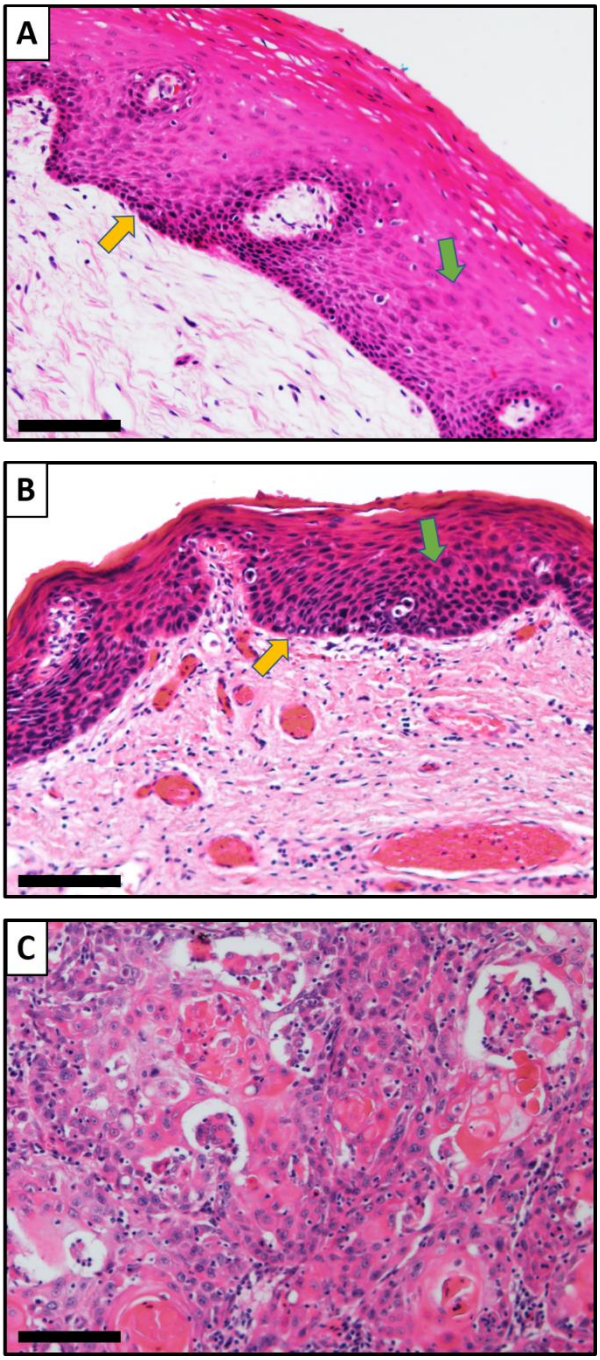

Figure 6.9 H&E staining of paraffin-embedded oral patient tissue biopsies.

Representative images of Normal (**A**), Dysplasia (**B**) and OSCC (**C**) tissues. Tissues were cut and sections were mounted on slides before beeing stained with hematoxylin & eosin on the Tissue-Tek Prisma Plus Automated Slide Stainer. Green arrows: stratified squamous epithelium; yellow arrows: basal cell layer. Images were taken using an Olympus BX51 microscope at 10X magnification. Scale bar: 100 µm.

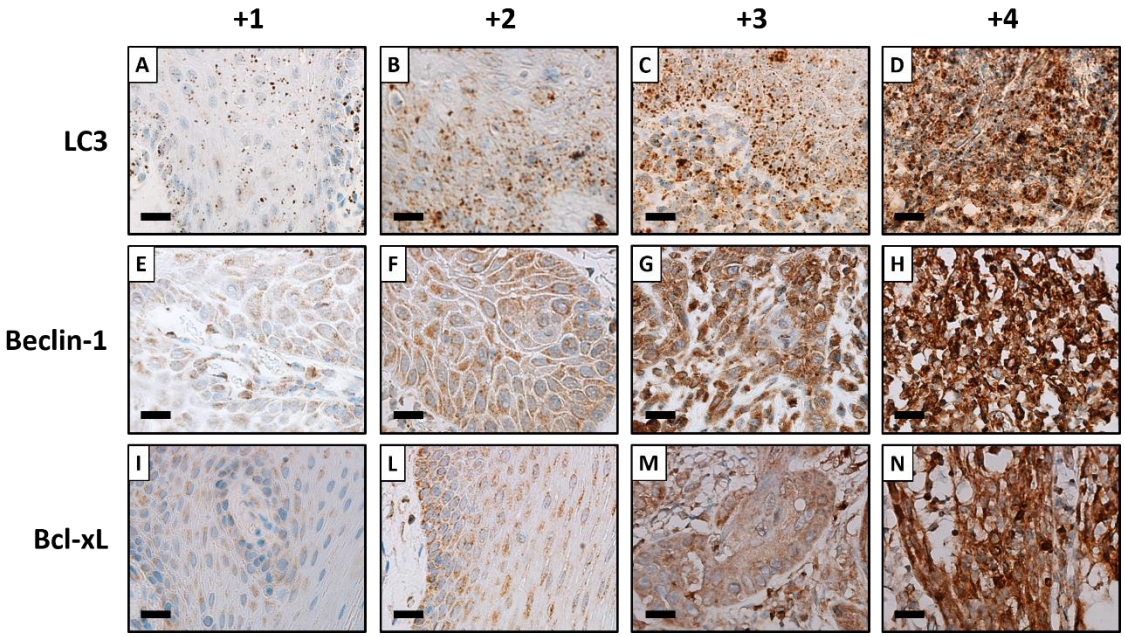

Figure 6.10 IHC scoring for LC3, Beclin-1 and Bcl-xL staining.

Representative images of the immunostained oral patient tissue samples. Tissues were cut and sections were mounted on slides before being stained with anti-LC3, anti-Beclin-1 and anti-Bcl-xL antibodies on the Ventana BanchMark XT immunostainer. Four IHC scores were assigned for each protein based on the staining intensity of squamous epithelial cells: weak staining +1 (**A**, **E**, **I**), medium staining +2 (**B**, **F**, **L**), strong staining +3 (**C**, **G**, **M**) and very strong staining +4 (**D**, **H**, **N**). Images were taken using an Olympus BX51 microscope at 40X magnification. Scale bar: 20 µm.

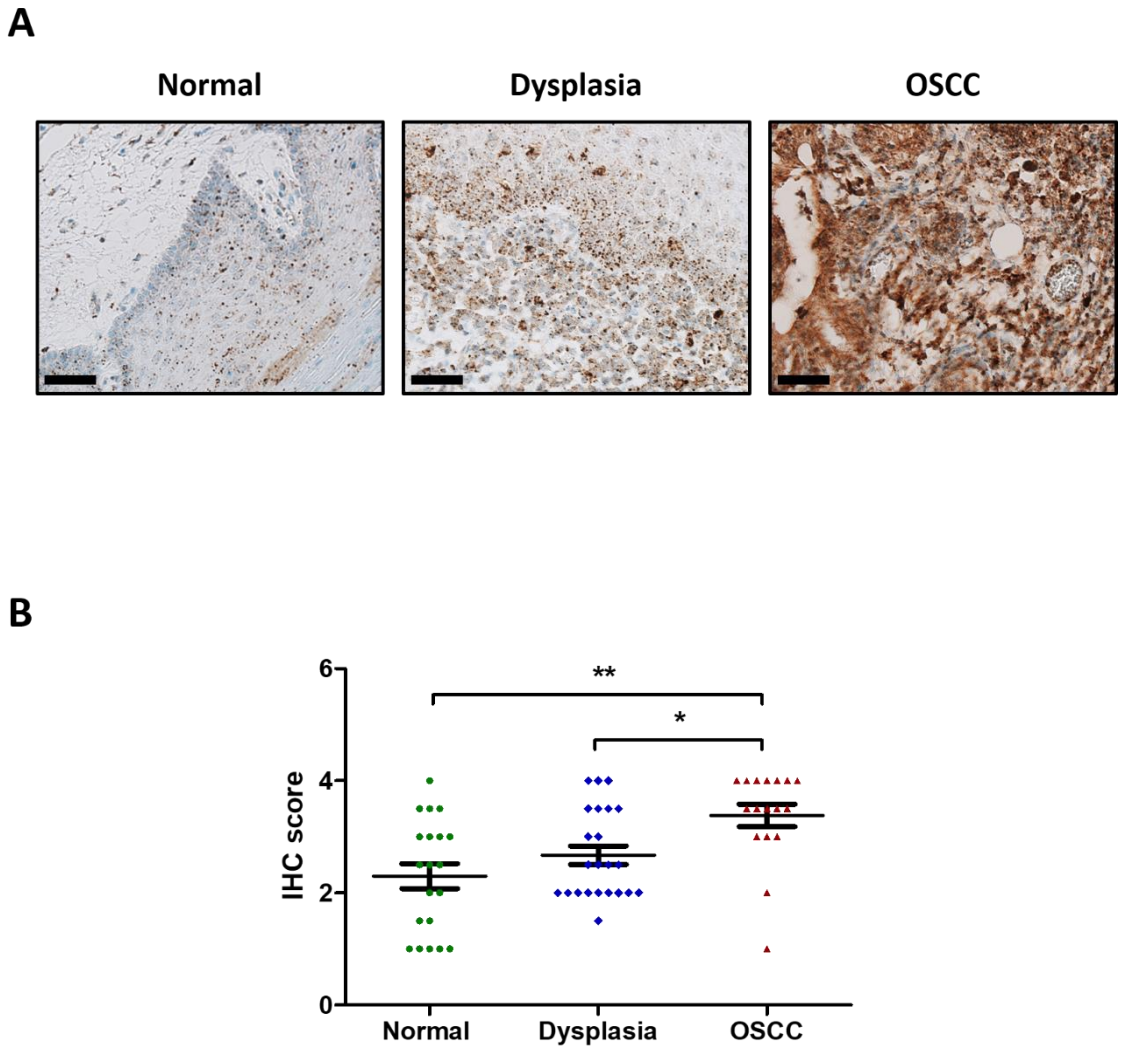

Figure 6.11 Increased LC3 levels in OSCC tissue samples from an Irish cohort of patients.

Oral patient tissues were cut and sections were mounted on slides before being stained with an anti-LC3 antibody on the Ventana BanchMark XT immunostainer. **A.** Representative images of Normal, Dysplasia and OSCC tissue samples. Images were taken using an Olympus BX51 microscope at 20X magnification. Scale bar: 50 µm. **B.** Scatter plot of LC3 IHC score in Normal (N=20), Dysplasia (N=23) and OSCC (N=17) epithelial tissue samples. Data represent the mean ±S.E.M. Statistical analysis was performed using Kruskal-Wallis H Test with Dunn's Multiple Comparison to compare the three groups of patients (Graphpad Prism 8). p**<0.01, p*<0.05.

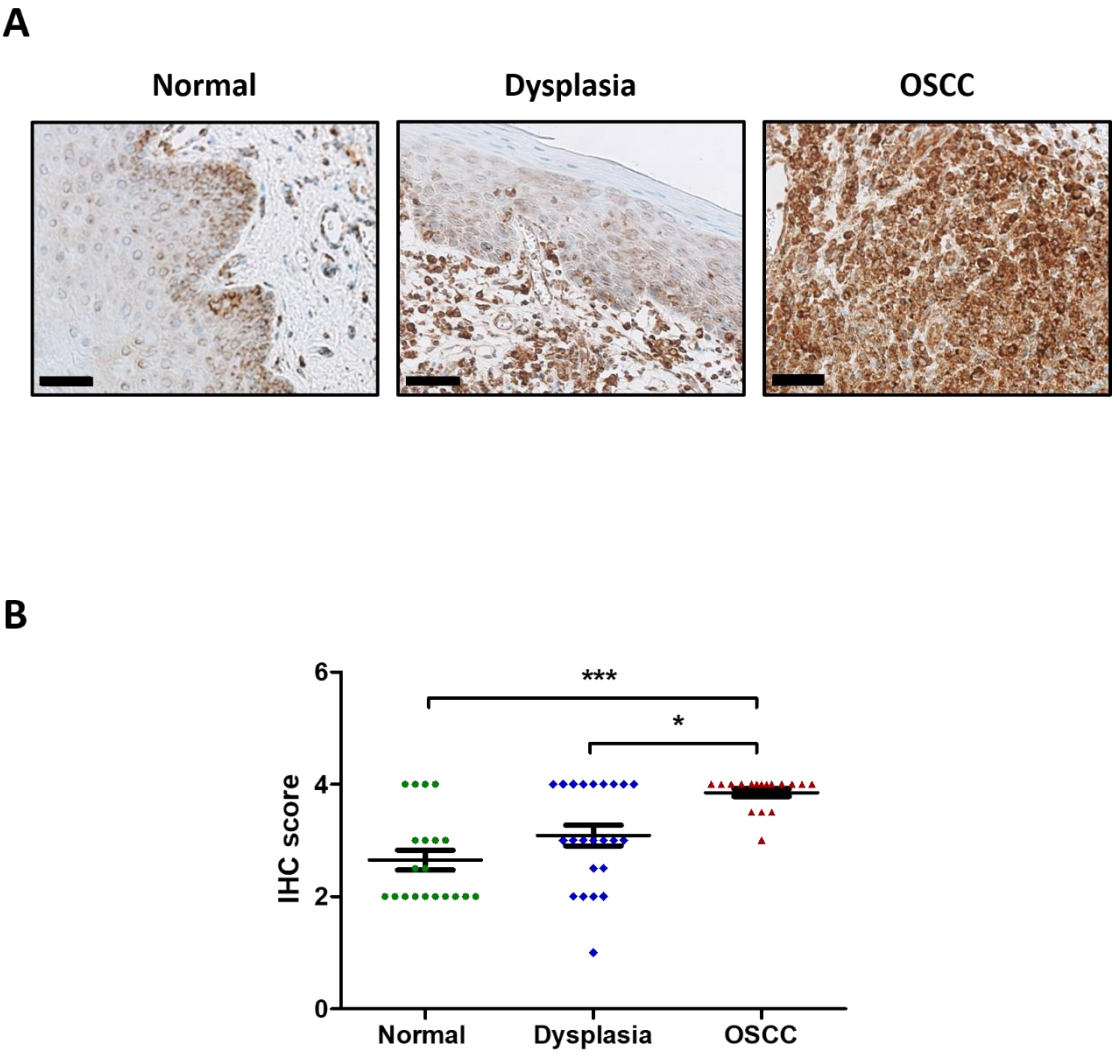

Figure 6.12 Increased Beclin-1 levels in OSCC tissue samples from an Irish cohort of patients.
Oral patient tissue samples were cut and sections were mounted on slides before being stained with an anti-Beclin-1 antibody on the Ventana BanchMark XT immunostainer. **A.** Representative images of Normal, Dysplasia and OSCC tissue samples. Images were taken using an Olympus BX51 microscope at 20X magnification. Scale bar: 50 µm. **B.** Scatter plot of Beclin-1 IHC score in Normal (N=20), Dysplasia (N=23) and OSCC (N=17) epithelial tissue samples. Data represent the mean ±S.E.M. Statistical analysis was performed using Kruskal-Wallis H Test with Dunn's Multiple Comparison to compare the three groups of patients (Graphpad Prism 8). p***<0.001, p*<0.05.

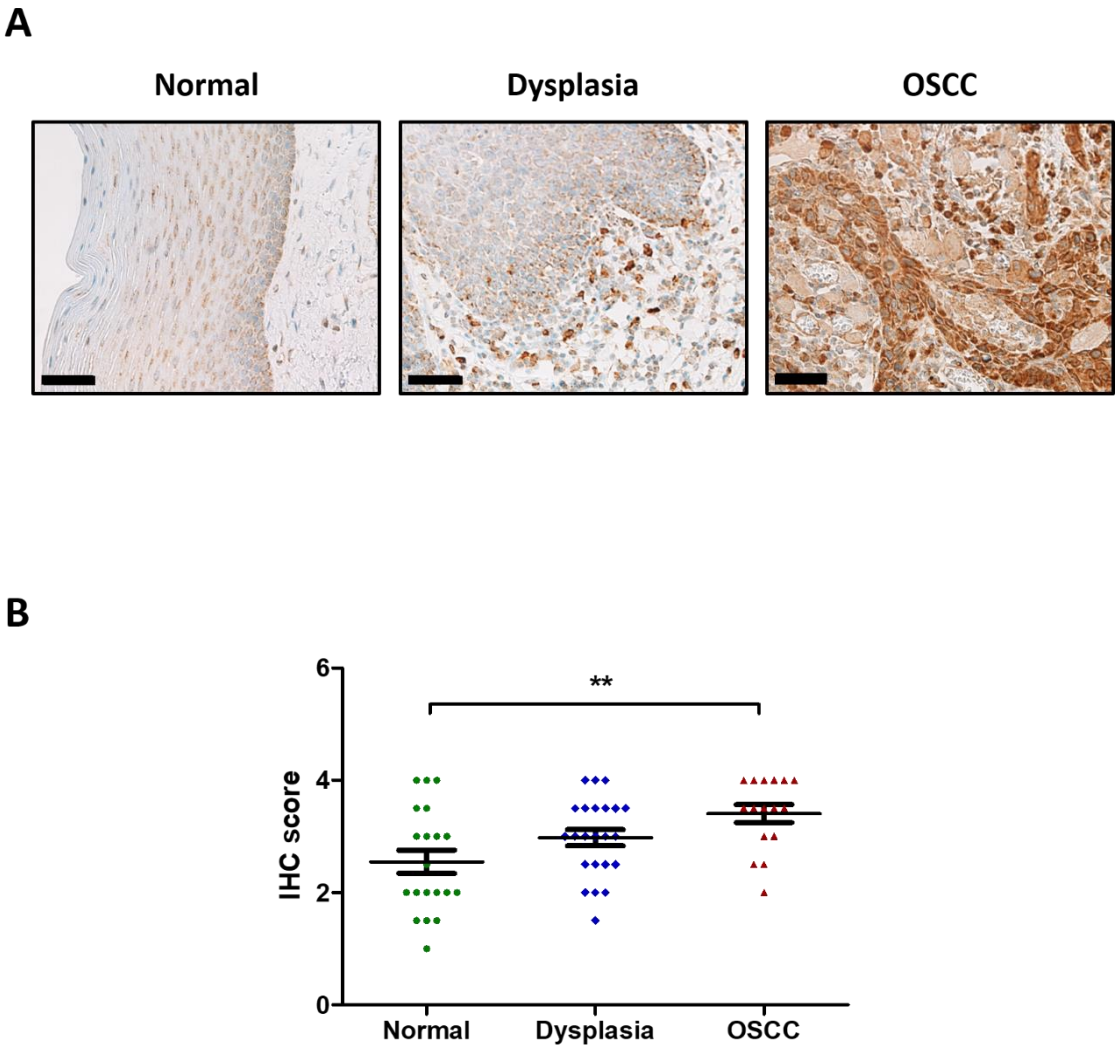

Figure 6.13 Increased Bcl-xL levels in OSCC tissue samples from an Irish cohort of patients.
Oral patient tissue samples were cut and sections were mounted on slides before being stained with an anti-Bcl-xL antibody on the Ventana BanchMark XT immunostainer. **A.** Representative images of Normal, Dysplasia and OSCC tissue samples. Images were taken using an Olympus BX51 microscope at 20X magnification. Scale bar: 50 µm. **B.** Scatter plot of Bcl-xL IHC score in Normal (N=20), Dysplasia (N=23) and OSCC (N=17) epithelial tissue samples. Data represent the mean ±S.E.M. Statistical analysis was performed using Kruskal-Wallis H Test with Dunn's Multiple Comparison to compare the three groups of patients (Graphpad Prism 8). p**<0.01.

		LC3			Beclin-1			Bcl-xL		
	N	Low	High	p-value	Low	High	p-value	Low	High	p-value
Normal	20 (33.3%)	12 (20.0%)	8 (13.3%)	0.003**	11 (18.3%)	9 (15.0%)	0.001**	11 (18.3%)	9 (15.0%)	0.061
Dysplasia	23 (38.3%)	14 (23.3%)	9 (15.0%)		7 (11.7%)	16 (26.6%)		8 (13.3%)	15 (25.0%)	
OSCC	17 (28.3%)	2 (3.3%)	15 (25.5%)		0 (0.0%)	17 (28.3%)		3 (5.0%)	14 (23.3%)	
Total	60 (100%)	28 (46.6%)	32 (53.4%)		18 (30.0%)	42 (70.0%)		22 (36.7%)	38 (63.3%)	

Table 6.5 Frequency distribution table of LC3, Beclin-1 and Bcl-xL protein expression in Normal, Dysplasia and OSCC tissue samples.

Statistical analysis was performed using a Pearson's chi squared test to compare determine the association between protein expression and the histological stage of OSCC progression (Graphpad Prism 8). p**<0.01.

6.2.5. LC3 and Beclin-1 expression can partially predict the OSCC phenotype

Given the significant association between LC3 and Beclin-1 expression and the histological stages of OSCC progression, the predictive power of these two markers for OSCC identification was next examined. To evaluate whether LC3 and Beclin-1 may represent a potential tool to discriminate the OSCC phenotype, the ROC (Receiver Operating Characteristic) curves were calculated using MedCalc software.

ROC analysis is a commonly used tool for evaluating the performance of diagnostic tests [317]. The ROC curve consists of a graphical representation of the true positive rate (sensitivity) in function of the false positive rate (100-specificity) of a certain parameter calculated for different cut-off values [317]. The ROC curve allows the calculation of the Area Under the Curve (AUC) which represents a measure of the predictive power of a certain parameter to discriminate between two diagnostic groups (e.g. normal/disease) [316]. When the parameter cannot distinguish between the two groups examined the AUC will be 0.5. Conversely, when the parameter discriminates the two groups perfectly without any overlapping of the distributions, the AUC will be 1 and the ROC curve will reach the upper left corner of the plot [317].

In the present study, to calculate the ROC curves, the IHC score values obtained for LC3 and Beclin-1 were used. Moreover, for this analysis, the Control samples and the Dysplasia samples were pooled together as non-cancerous tissue samples and were compared to the cancerous OSCC tissue samples. An AUC value of 0.797 with 85.7% sensitivity and 65.5% specificity was obtained for LC3 protein (95% CI 0.646-0.904, cut-off values>2.49) (Figure 6.14A). Moreover, an AUC value of 0.811 with 92.9 % sensitivity and 66.7% specificity was obtained for Beclin-1 (95% CI 0.680-0.906; cut-off values>2.79) (Figure 6.14B). Both these curves showed a significant p-value<0.001, suggesting a discrete predictive power of these two proteins for the identification of OSCC.

Taken together, this preliminary analysis may indicate a potential diagnostic power of LC3 and Beclin-1 for OSCC detection, suggesting the use of these autophagic proteins as OSCC biomarkers. However, due to the limited samples size, no firm conclusions can be drawn at this stage and further analysis may be required with a bigger cohort of patients to better evaluate the relevance of LC3 and Beclin-1 as OSCC biomarkers.

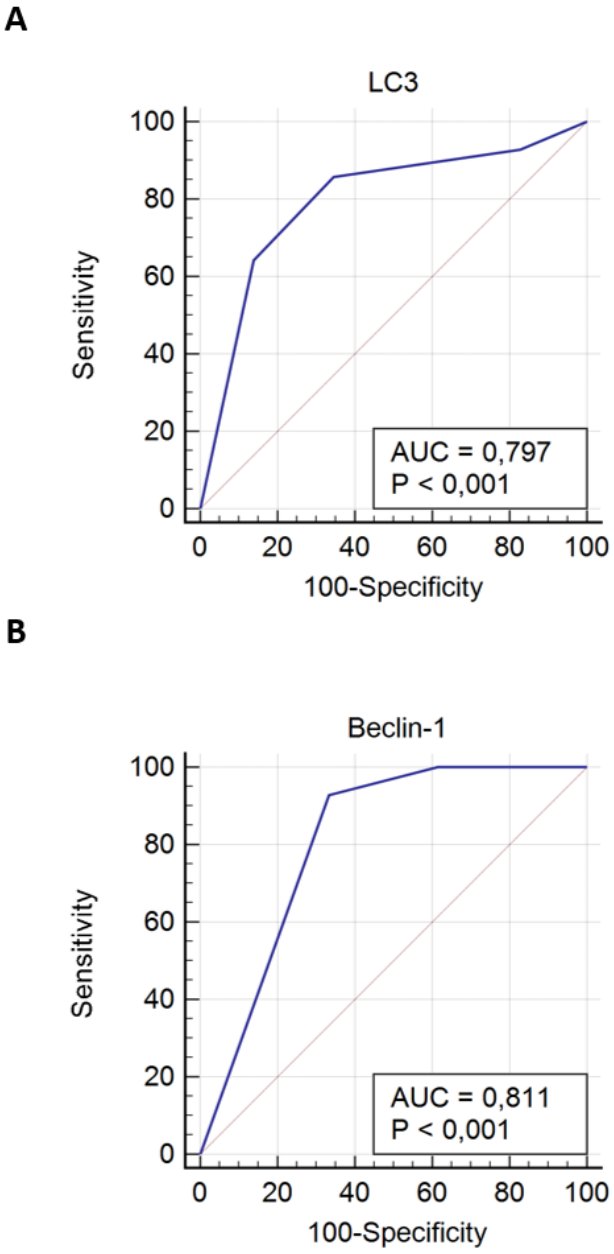

Figure 6.14 LC3 and Beclin-1 can partially predict the OSCC phenotype.

LC3 and Beclin-1 IHC scores of non-cancerous (Normal and Dysplasia) and cancerous (OSCC) tissue samples were used to calculate the ROC curves by using the MedCalc software. **A.** ROC curve of LC3. AUC=0.797, sensitivity=85.7%, specificity=65.5% (95% CI 0.646-0.904; cut-off values>2.49). **p<0.001. **B**. ROC curve of Beclin-1. AUC=0.811, sensitivity=92.9%, specificity=66.7% (95% CI 0.680-0.906, cut-off values>2.79). **p<0.001.

6.3. Discussion

A role for autophagy in cancer development has been strongly suggested over the past few years. To date, numerous studies have tried to determine whether an impairment of autophagy may occur during cancer progression and whether dysregulation of autophagy can actively take part in tumour promotion. Although much progress has been made in this field, a role for autophagy in cancer still remains controversial [563]. This may be attributable to the tumour complexity and heterogeneity, which is manifested not only amongst varying cancer types but also amongst different individuals as well as in the singular cells within an individual [167]. Accordingly, depending on the tumour/cell-type, autophagy can either play a role in tumour promotion or as a tumour suppressor mechanism [169]. Also, autophagy can be either activated or inhibited during cancer development, contributing differently to tumorigenesis [167]. To further add to this complex scenario, a differing role of autophagy during cancer developmental stages has also been proposed, suggesting a stage-dependent involvement of autophagy in cancer [143]. Therefore to date the role of autophagy in OSCC tumorigenesis is not totally understood [551]. A better understanding of the role of autophagy during OSCC progression can be exploited to establish whether, depending on the cancer developmental stage of OSCC patients, autophagy inhibition or induction may be applied to cancer therapy.

In the present study, investigation of autophagic markers in OSCC patient samples was undertaken. To better evaluate the role of autophagy in OSCC progression, two parallel analyses were carried out. Firstly, the expression of autophagic markers was investigated by western blotting in fresh/frozen oral biopsies from a Spanish cohort of patients. For this analysis, a collaboration was initiated with Prof Jose Bagan, head of the Department of Stomatology and Maxillofacial Surgery at the General University Hospital of Valencia and patient samples were analysed at the Molecular Oncology Laboratory of the General University Hospital Research Foundation (Valencia). Additionally, a further analysis of autophagic markers in oral archival tissue samples from an Irish cohort of OSCC patients was also performed by IHC. This latter analysis was carried out at Central Pathology Laboratory in St. James Hospital (Dublin) in collaboration with Dr Mary Toner, lead pathologist of the Oral and Maxillofacial Unit. Given the high tumour heterogeneity among patients and the complexity of studying autophagy in tissue samples, an

investigation of autophagy in two separate cohorts of patients using two different techniques confers an additional value to this study.

Western blot analysis of the two autophagic proteins LC3 and p62 was firstly performed in a Spanish cohort of patients (N=60). Oral biopsies were collected by Prof Jose Bagan, and samples were divided in three groups based on the clinical diagnosis: Control (N=20), Precancerous (N=19) and OSCC (N=21) patient samples. Densitometric analysis of p62 bands showed an emerging negative trend in the protein expression of p62 during OSCC progression, with a decrease in p62 levels observed in OSCC samples compared to Precancerous and Control samples. Moreover, evaluation of the total LC3 levels (LC3-I+LC3-II) showed a trend towards a positive correlation of LC3 protein expression to tumour progression in OSCC patients. In fact, OSCC samples showed the highest LC3 levels compared to Precancerous and Control samples. To further investigate the role of autophagy in OSCC progression, the conversion of LC3-I to LC3-II was also evaluated through the determination of the LC3-II/LC3-I ratio. Interestingly, an increase in the LC3-II/LC3-I ratio was observed in OSCC samples compared to Precancerous and Control samples, suggesting enhanced autophagosome formation during OSCC progression. Taken together, a decrease in p62 levels along with an increase in LC3 levels and in the LC3-II/LC3-I ratio in OSCC samples may suggest autophagy activation during OSCC progression. It should however be noted that statistical analysis of the three groups of samples did not show any significant difference in the levels of these autophagic markers, likely because of the inherent high variability in protein expression between patients within each category and the overall low patient number.

Additionally, to better evaluate the involvement of p62 and LC3 in tumour progression, correlation analysis of protein expression levels and clinical-pathological features of patients was also performed. In the precancerous group of samples, both LC3 and p62 expression did not show any significant correlation with respect to the clinical appearance of the lesion (homogeneous leukoplakia, verrucous leukoplakia and erythroleukoplakia) or the histological phenotype (non-dysplastic/dysplastic). Moreover, in the OSCC group of patients, no association was found between LC3 expression and tumour size. Conversely, a significant negative correlation between p62 expression and tumour size was demonstrated. Indeed, significantly decreased levels of p62 protein were found in tumours >2.5 cm compared to tumours ≤2.5 cm. This last finding supports the potential implication of p62 downregulation in OSCC development. However, the limited sample

size in each subgroup of patient samples is acknowledged as a limitation in this analysis, suggesting that no firm conclusion can be drawn.

Reduced p62 protein levels herein observed in OSCC patient samples compared to Control samples agree with a recent study published by Groulx *et al.*, where p62 expression was examined in 12 colon cancer specimens by immunofluorescence microscopy [564]. In this study, a weaker p62 fluorescent signal was observed in the tumour tissues compared to the corresponding normal resected margin tissues. Also, the same analysis showed an inverse expression pattern for Beclin-1, which was overexpressed in cancer tissues compared to the corresponding normal mucosa. A co-localisation of p62 with Beclin-1-positive autophagosomes also suggested regulation of p62 by autophagy. In contrast with these findings, it is worth noting that high p62 expression has been reported by many other studies in the literature conducted in various cancers, including breast, lung, gastric, oesophageal and hepatocellular carcinomas [565–568]. Moreover, p62 overexpression was associated with poor prognosis in glioma and colon cancer [569, 570]. Given the inconsistency in results among studies and the potential involvement of p62 in tumorigenesis, the role of p62 in cancer progression warrants further analysis.

In a recently published paper by Liu *et al.* the role of p62 was investigated in OSCC progression [182]. In this study, p62 levels were studied in oral mucosa, verrucous hyperplasia and OSCC samples by IHC. According to the authors, both cytoplasmic and nuclear p62 positive staining were observed in oral tissues, displaying a differential pattern of expression in the three groups of samples. In fact, on the one hand a loss of nuclear p62 was observed in OSCC samples compared to normal and verrucous hyperplasia samples, on the other hand an increase in the cytoplasmic p62 was also found during OSCC progression. Moreover, the loss in correlation between the cytoplasmic and nuclear p62 levels observed in OSCC patients suggested an altered p62 subcellular localisation in cancerous tissues, which was correlated with OSCC progression and poor prognosis. In the present study, evaluation of p62 by western blotting did not allow its subcellular localisation to be determined. Given the potential relevance of p62 localisation within cells, the technique herein employed may represent a limitation for an extensive analysis of the role of p62 in OSCC.

The increased LC3 levels herein observed in OSCC tissues compared to normal mucosa are in agreement with other studies in the literature. In fact, high LC3 levels have been

previously demonstrated in various types of cancers, such as gastric cancer, colon cancer and pancreatic adenocarcinoma [570–572]. Moreover, an overexpression of LC3 has been linked to high tumour grade in lung cancer and glioma [555, 569]. According to Tang *et al.*, high expression of LC3 has also been detected in OSCC, and it was highly correlated with the stage of the disease, tumour size and regional lymph node involvement [573]. In the Tang study, increased LC3 levels were determined in 57 OSCC samples out of 90 (63.3%) by IHC and the correlation with clinical-pathological factors showed a significant association with poor overall survival. Likewise, LC3 overexpression was linked to poor prognosis in colon cancer, glioma and breast cancer, whilst it was associated with good prognosis in hepatocellular carcinoma [569, 570, 572, 574]. Recently, an interesting paper published by Hayaki *et al.* reported the expression levels of LC3 during head and neck cancer progression [553]. Premalignant and malignant lesions along with the normal tissues were investigated in this study and showed a progressive increase in LC3 levels across the various stages of cancer progression. Similarly, in the previously mentioned paper of Liu *et al.*, a correlation between LC3 expression and OSCC development was also shown [182]. In this study, the levels of LC3 were assessed by IHC in 37 normal oral mucosa, 47 verrucous hyperplasia (precancerous condition) and 195 OSCC. Interestingly, the authors reported a significant increase in LC3 levels in OSCC tissues compared to verrucous hyperplasia and normal mucosa, suggesting a progressive accumulation of LC3 during OSCC progression. Consistently, increased expression of LC3 was also detected in oral premalignant and in OSCC lesions in mice treated with the tumorigenic compound 4-nitroquinoline-1-oxide (4NQO), suggesting a role for LC3 in OSCC development [551]. All these findings aligned with the emerging positive trend in LC3 expression toward OSCC progression obtained in the present study.

To better investigate the role of autophagy in OSCC progression, an additional study on the expression of autophagic markers in an independent cohort of OSCC patients (Irish cohort) was undertaken. For this analysis, paraffin-embedded oral biopsies were analysed by IHC, which is a commonly used technique to study autophagy in human tissue samples. According to Martinet *et al.*, analysis of the autophagic marker LC3 by IHC represents a recognised and reliable method to monitor autophagy *in situ* [575]. Thus, in the present study, LC3 levels were investigated by IHC using a highly specific and strongly recommended LC3 monoclonal antibody from NanoTools (clone 5F10) [576,

577]. In addition, levels of Beclin-1, another well-recognised autophagy marker, along with its direct interactor Bcl-xL were also herein assessed by IHC. Bcl-xL is an anti-apoptotic protein belonging to the Bcl-2 protein family. The binding of Bcl-xL to Beclin-1 results in the inhibition of Beclin-1-induced autophagy; conversely, the release of Beclin-1 from Bcl-xL results in the formation of the Beclin-1:Vps34:UVRAG complex which positively regulates autophagosome formation and maturation [211]. Given this, an indirect autophagy regulatory role of Bcl-xL, along with its well-established anti-apoptotic role, has been proposed [210]. In the present study, endogenous levels of LC3, Beclin-1 and Bcl-xL in squamous epithelial cells were compared among three groups of oral patient tissue samples: Normal, Dysplasia and OSCC. These three categories summarise the three main histological types observed during oral tumorigenesis, with the dysplastic tissue representing a precancerous stage. Results herein obtained showed significantly increased levels of LC3, Beclin-1 and Bcl-xL in OSCC tissue samples compared to Dysplasia and Normal tissue samples, suggesting a progressive increase in the levels of these three markers during OSCC development. Unfortunately, due to ethical issues, patient details were unavailable. hence in this study it was not possible to associate the expression of these proteins with positive or negative prognostic factors.

Interestingly, the increased levels of LC3 protein observed in OSCC tissue samples from an Irish patient cohort correlate with the increased LC3 levels previously shown in OSCC samples from a Spanish cohort of patients. These results also align with the aforementioned studies relating to LC3 expression in OSCC. Taken together, the consistency between the two analyses performed herein and their agreement with other studies in the literature strongly suggest a role for LC3 in OSCC progression, implying also a role for autophagy in cancer development. It is worth noting that, in the present study, a significant variation in LC3 protein expression was only observed by IHC analysis, whilst no statistical significance was obtained by western blotting. This discrepancy may be as a result of the methodologies employed. Western blot analysis allows one to quantify proteins in tissue extracts obtained from the whole biopsy sample, whilst IHC allows one to determine protein levels in a sectioned biopsy sample. The evaluation of intact tissues represents an advantage of the IHC technique, allowing a distinction between different cell types within the same sample (e.g. stromal fibroblasts from squamous epithelial cells). Accordingly, the analysis of a pool of cells/tissues

through western blotting may result in a higher heterogeneity amongst samples, thus it may be less accurate when compared to the IHC analysis.

Similar to LC3, increased Beclin-1 levels were also observed during OSCC progression in the present study. In this regard, it is important to note that, although high levels of Beclin-1 have been demonstrated in some types of cancers, reduced Beclin-1 levels have also been reported in some other cancer types. Therefore, Beclin-1 expression and its role in tumour progression still remains controversial. Deletion of Beclin-1 has been reported in 40-70% of breast, ovarian and prostate cancers [578, 579]. In this regard, Liang *et al.* have demonstrated that the Beclin-1 gene was monoallelic deleted in the MCF7 breast cancer cell line and its re-expression resulted in autophagy activation and tumorigenesis suppression [580]. Moreover, in a mouse model, Beclin-1 deletion was correlated to spontaneous formation of liver and lung cancer, leukaemia and lymphomas [581]. Decreased levels of Beclin-1 protein were found in various human cancer models, including gastric cancer, hepatocellular cancer and melanoma [582–584]. Additionally, in several studies conducted in ovarian, hypopharyngeal and lung cancer, reduced levels of Beclin-1 were also linked to decreased levels of LC3, confirming suppression of autophagy in these tumours. Altogether these studies support the hypothesis of a tumour suppressor role of autophagy, suggesting also that reduced or inhibited autophagy may result in tumour progression [585–587]. In contrast with these findings, in a study by Wu *et al.,* an increase in Beclin-1 and LC3 protein expression was observed in colon cancer tissues compared to counterpart normal colon tissues in 40 fresh/frozen samples analysed by western blotting [570]. Similarly, elevated levels of Beclin-1, LC3 and p62 were also reported in gastric cancer [588]. Moreover, other studies conducted in lung cancer and glioma showed that high levels of Beclin-1 and LC3 were positively correlated with high tumour grade [555, 589]. Together these studies support the tumour promoter role of Beclin-1 and autophagy in cancer progression. Consistently with the dual role of Beclin-1 in cancer, some studies have also shown that high expression of Beclin-1 may result in unfavourable clinic-pathological parameters, whilst other studies have shown that reduced Beclin-1 levels may be associated with poor prognosis [589–592]. In regard to the expression of Beclin-1 in oral cancer, Kapoor *et al.* have reported an 8-fold lower expression of Beclin-1 mRNA in tumour tissues compared to normal tissues obtained from 10 oral cancer patients, suggesting that reduced levels of Beclin-1 may be implicated in oral cancer progression [183]. In contrast, Tang *et al.* have reported that increased

levels of Beclin-1 were found in 55 out of 90 OSCC biopsies [186]. In this study, the presence of Beclin-1 was correlated with tumour grade and lymph node metastasis. Moreover, in another study, IHC analysis of 52 OSCC patients showed a positive expression of Beclin-1 in 78.4 % of cases [551]. Furthermore, Liu *et al.* reported a positive correlation between Beclin-1 expression and poor prognosis in OSCC [593]. These latter studies are in line with the results obtained herein showing increased expression of Beclin-1 in OSCC.

The role of Bcl-xL, and in more general Bcl-2 family members, in cancer development has drawn attention over the past few years. The emerging interest in this group of proteins is mainly attributable to their anti-apoptotic properties, although an apoptosis-independent role for these proteins has also been proposed [594, 595]. Several papers have reported an overexpression of Bcl-xL in some types of cancer such as melanoma and glioblastoma [594]. In particular, in melanoma, higher levels of Bcl-xL have been observed in metastatic tumours compared to the counterpart primary tumours, suggesting also a correlation between Bcl-xL expression and metastasis development [596]. Moreover, Song *et al*. have demonstrated that colorectal cancer patients with high Bcl-xL expression showed poorer overall survival compared to those with low Bcl-xL expression, implying a prognostic significance of Bcl-xL in this cancer model [597]. Similarly, Bcl-xL mRNA overexpression was associated with poor prognosis in non-squamous cell lung carcinoma [598]. In support of these studies, increased expression of Bcl-2, another Bcl-2 family member, has also been reported in numerous cancers, such as nasopharynx, lung, colorectum, prostate, stomach and oesophagus [599, 600]. Interestingly, an overexpression of Bcl-2 has also been found in pre-cancerous lesions of the colorectum, stomach, and oesophagus, suggesting a role for Bcl-2 during tumour initiation in these organs [599, 600]. Similarly, Singh *et al.* have demonstrated increased levels of Bcl-2 in oral severe dysplasia tissues compared to mild dysplasia tissues and as well in poorly differentiated OSCC tissues compared to well differentiated OSCC tissues, implying a role for Bcl-2 in OSCC progression [600]. Consistent with these findings, in the present study, a progressive increase in the levels of Bcl-xL were detected in oral Dysplasia and in OSCC tissue samples compared to Normal oral mucosa samples, corroborating the hypothesis that anti-apoptotic Bcl-2 proteins may play a role in OSCC progression.

Furthermore, in the present study, a significant association between LC3 and Beclin-1 protein expression and the histological stages of OSCC progression was determined using the Pearson's chi-squared test. Given this, a potential use of these two autophagic proteins as OSCC biomarkers may be suggested. Accordingly, a preliminary analysis of the predictive diagnostic power of LC3 and Beclin-1 in OSCC was herein undertaken through calculation of the ROC curves. Results obtained showed an AUC of 0.797 with 85.7% sensitivity and 65.5% specificity (cut-off values>2.49) for LC3. Moreover, an AUC of 0.811 with 92.9 % sensitivity and 66.7% specificity (cut-off values>2.79) was determined for Beclin-1. These preliminary results may suggest that increased levels of both LC3 and Beclin-1 can discriminate the OSCC phenotype with a discrete predictive power. However, it is important to note that the sample size examined herein is too small to draw firm conclusions with regards to the potential use of these proteins as OSCC biomarkers. Therefore, further analysis may be required with a bigger cohort of patients.

In conclusion, in this chapter, analysis of key autophagic proteins was undertaken to evaluate the role of autophagy in oral cancer development. Decreased p62 levels along with an increase in LC3 expression and LC3-II/LC3-I ratio was demonstrated by western blotting in OSCC patient samples compared to precancerous and control samples. Additionally, from the same analysis, a significant negative correlation between p62 expression and tumour size was observed. Moreover, increased LC3, Beclin-1 and Bcl-xL levels in squamous epithelial cells were demonstrated by IHC in oral cancerous tissues compared to dysplastic and normal tissues. Taken together, all these findings suggest an activation of autophagy during OSCC progression, implying a potential tumour promoter role of autophagy in this cancer type. Finally, despite the limited sample size, preliminary analysis showed a discrete predictive power of LC3 and Beclin-1 to discriminate the OSCC phenotype. Accordingly, further analysis on a bigger sample size may be warranted to better investigate the potential use of these proteins as OSCC biomarkers.

7. Concluding Remarks

Oral Squamous Cell Carcinoma (OSCC) accounts for 5% of all cancers worldwide [5]. The highest incidence of this malignancy has been found in people between 45-70 years old, although an increasing incidence has been recently observed in young people due to their early exposure to high-risk habits, such as alcohol consumption and tobacco smoking [19][7]. Moreover, the commonly used practice of tobacco, betel quid and areca-nut chewing has been considered to be a determining factor for the high prevalence of OSCC in countries like Pakistan and India, where oral cancer represents 10% and 45% of all the cancers, respectively [3, 4, 8]. OSCC can arise from genetic and epigenetic mutations of oncogenes (i.e. EGFR, c-Myc and Stat3) and tumour suppressor genes (i.e. p53, p16 and RB1) [22, 601] Accumulation of genetic mutations results in the selection of transformed epithelial cells, which leads to a loss of tissue organisation and ultimately OSCC progression [552]. It has been reported that the 5-year survival rate of patients with OSCC is lower than 50% [602]. Therefore, given the high mortality rate associated with this malignancy, there is a compelling need to find more efficient strategies to improve the clinical outcome of OSCC patients. Currently, surgery along with chemotherapy and radiotherapy represent the main therapeutic strategies for the treatment of OSCC. In particular, chemotherapy is a first line therapy for the treatment of unresectable and advanced OSCC [480]. Despite the high efficacy of chemotherapy in counteracting tumour growth, various limitations have been linked to its use, including the fact that cancer cells can become resistant to drugs after a few cycles of chemotherapy. Accordingly, a better understanding of the cellular response to chemotherapeutics may be helpful to develop new strategies to improve the treatment of OSCC patients.

Autophagy is a physiological mechanism which takes part in numerous biological processes such as development, ageing and cell differentiation [143]. In healthy cells, autophagy plays a crucial role in maintaining tissue and cell homeostasis. Thus, it is not surprising that a dysregulation of autophagy has been implicated in the pathogenesis of various diseases including cancer. In the past few years, the importance of autophagy in cancer has exponentially developed, especially since Yoshinori Ohsumi was awarded the Nobel Prize in Medicine in 2016 for his discoveries on the molecular mechanisms of autophagy. In particular, an emerging role of autophagy in cancer has been proposed in regard to (i) the response of cancer cells to chemotherapeutics, (ii) chemoresistance and (iii) tumour initiation and development. In the present study, the role of autophagy in these three aspects of cancer biology was investigated in oral cancer cell lines and in oral

patient tissues, with the overall objective of better elucidating the role of autophagy in OSCC and determining whether manipulation of autophagy may represent an additional therapeutic strategy for the treatment of this cancer.

In the first part of this study, the role of autophagy in response to chemotherapeutics was investigated. Activation of autophagy following treatment with various drugs has been widely reported in the literature [189, 370, 371]. Also, it has been demonstrated that drug-induced autophagy can act both as a cell survival mechanism associated with a reduced drug cytotoxicity or as a pro-death mechanism which can occur in association with apoptosis [189]. This paradoxical role of drug-induced autophagy may depend on various factors, such as the type of cells and drugs and the levels of cellular stress induced by the drugs [549, 603]. In this regard, it has been proposed that modest cellular stresses may result in a cell survival response, while persistent stresses may lead to cell death for limiting the proliferation of abnormal cells [189]. In the present study, the role of autophagy in the cellular response to chemotherapy was investigated in two tongue carcinoma cell lines, SCC4 and SCC9. Cisplatin was chosen as the representative OSCC chemotherapeutic agent as it represents one of the most commonly used drugs for the treatment of OSCC [35]. A concurrent induction of both apoptosis and autophagy in response to cisplatin was herein demonstrated, for the first time, in the SCC4 and SCC9 cell lines, suggesting a role for autophagy in the cellular response to cisplatin in OSCC cells and a potential link between the apoptotic and autophagic pathways.

Autophagy activation in response to cisplatin has been reported in various studies in the literature [290, 372–374], however its role in OSCC is still not clearly defined. In fact, although some studies have suggested that cisplatin-induced autophagy may represent a protective mechanism which can ultimately lead to chemoresistance in OSCC [290, 291], further research is required to confirm or challenge this hypothesis. In the present study, the role of cisplatin-induced autophagy was investigated by using various pharmacological autophagy inhibitors. However, inconsistent results were obtained from this analysis. The early stage autophagy inhibitors, 3-methyladenine and SAR405, did not sensitise OSCC cells to cisplatin, whilst treatment of cells with cisplatin in combination with late stages autophagy inhibitors, chloroquine and bafilomycin-A1, resulted in an enhancement of cisplatin-induced cell death. The opposing effects herein observed using various autophagy inhibitors may suggest that targeting different phases of the autophagic flux can result in a different cellular response. However, it is worth considering that this

discrepancy may also rely on the specificity of the drugs and on their ability of targeting exclusively the autophagic process. Given this, genetic inhibition of autophagy using an siRNA approach against a key autophagy protein ATG5 was also undertaken, but ATG5 knockdown did not significantly modulate sensitivity to cisplatin. This result may suggest that cisplatin-induced autophagy does not represent a protective mechanism in OSCC cell lines. However, due to the numerous protein interactions between autophagy and apoptosis and the multilayer inter-regulation of these two pathways, it cannot be excluded that opposing effects on cell viability may be obtained depending on the stage of autophagy and/or the protein targeted.

Interestingly, in the present study, a significant enhancement of cisplatin-induced apoptosis was observed when chloroquine and bafilomycin-A1 were applied to OSCC cells in combination with cisplatin. Although an autophagic-independent effect of these inhibitors could not be ruled out, their application in combination with chemotherapeutics may be exploited in the clinic to improve chemotherapy in OSCC patients. Chloroquine is already a widely used clinically approved drug for the treatment of malaria [604]. The antimalarial effect of chloroquine may be attributable to its ability to prevent the formation of hemozoin (polymerised heme) during proteolysis of haemoglobin in the digestive vacuoles of the malaria parasite *Plasmodium*, resulting in the accumulation of free heme within vesicles, which ultimately leads to oxidative damage and death of the parasite [605]. Moreover, the use of chloroquine has also been considered in the clinic for other pathologies such as acute and chronic rheumatoid arthritis and lupus erythematosus [604, 606]. Additionally, in the last few months, the Food and Drug Administration (FDA) has also temporarily approved an emergency use of chloroquine for the treatment of Covid-19, although the beneficial effect of this drug for the treatment of this new disease is currently under review [607]. The importance of chloroquine alone or in combination with chemotherapeutics for the treatment of cancer has also been evaluated in numerous clinical trials in various tumours (ClinicalTrials.gov Identifier: NCT01575782, NCT02333890, NCT00969306, NCT01446016, NCT02071537, NCT01777477, NCT01023477, NCT02496741, NCT01894633, NCT01438177, NCT00224978) , however its efficacy in cancer therapy may require further study. Also, its potential application for the treatment of OSCC still needs to be defined. The pre-clinical data herein obtained may suggest a new avenue for the clinical application of chloroquine in the treatment of OSCC. Conversely, to the best of our knowledge, no

clinical trials are currently investigating the potential use of bafilomycin-A1 for the treatment of cancer. However, several studies *in vitro* and *in vivo* have shown the beneficial effect of this drug in various cancers, such as colorectal cancer, gastric cancer cells, breast cancer, leukaemia, nasopharyngeal carcinoma and osteosarcoma [371, 401, 402, 608–611]. In line with these studies, data obtained herein also support the beneficial effect of bafilomycin-A1 for the treatment of OSCC.

In the second part of this study, the complex crosstalk between autophagy and apoptosis was investigated in OSCC cells by evaluating the molecular mechanisms underlying the activation of these two pathways in response to cisplatin. An important role of oxidative stress in the cellular response to cisplatin has been reported in several studies [416]. Cisplatin-induced oxidative stress is mainly attributable to an enhancement in intracellular ROS generation. Excessive ROS production within cells may ultimately lead to the activation of the MAPK signalling pathways, involved in the cellular response to stress [612]. In the present study, it was demonstrated that cisplatin induced accumulation of ROS in OSCC cells, which in turn initiated both autophagy and apoptosis. Moreover, activation of the stress-related JNK signalling pathway in response to cisplatin-induced ROS was demonstrated using the ROS scavenger N-acetyl cysteine. Finally, targeting JNK with the pharmacological inhibitor SP600125 was shown to partially inhibit both the autophagic flux and caspase 3 activation. Overall, these findings may suggest that cisplatin-induced oxidative stress induces both apoptosis and autophagy partially through activation of the JNK signalling pathway in OSCC cells. Moreover, the activation of both cisplatin-induced autophagy and apoptosis through the same signalling pathway corroborates the tight relationship between these two biological processes in response to chemotherapeutics.

In the third part of this study, the mechanisms implicated in acquired resistance to cisplatin in OSCC were investigated. In particular, among the numerous mechanisms to date associated with chemoresistance, it was decided to focus attention on the role that the stress-adaptative mechanisms play in chemoresistance. In fact, given the ability of chemotherapeutics to induce stress within cells, it is not surprising that cells have developed new strategies to adapt to the stress induced by drugs [79]. In this regard, a crucial role for autophagy in reducing ROS and misfolded protein accumulation has been proposed [80, 84, 85]. Accordingly, increased levels of autophagy have been found in various cisplatin resistant cells such as lung adenocarcinoma cells and ovarian cancer

cells [486, 613]. Similarly, an enhancement of intracellular antioxidant systems to reduce drug-induced oxidative stress has also been implicated in chemoresistance [86]. In this regard, an enhancement of antioxidant systems such as glutathione or Nrf2 has been reported in drug resistant cells in various cancers [529, 531, 533, 537, 538].

In the present study, analysis of chemoresistance in OSCC was carried out through the generation and characterisation of a cisplatin resistant OSSC cell line, the SCC4cisR cell line, obtained by pulsed stepwise exposure of drug-sensitive SCC4 cells to cisplatin. The new independent cell line obtained was shown to be ~14-times more resistant to cisplatin compared to the parental cell line, demonstrating to be a highly interesting and clinically relevant model for the study of chemoresistance. Interestingly, autophagy did not appear to play a role in cisplatin resistance in the SCC4cisR cell line. In fact, no significant differences were found in the autophagy levels in the presence/absence of the drug between the SCC4cisR and the SCC4 cells. However, it must be highlighted that this result cannot exclude a role for autophagy in chemoresistance in general. Indeed, chemoresistance occurs as a result of various mechanisms which can be activated depending on the context, thus the involvement of a certain mechanism may depend on the cell type and on the type of drug which cells are resistant to [482]. Conversely, an interesting link between oxidative stress and chemoresistance was demonstrated in the present study. An increase in the endogenous and cisplatin-induced ROS levels were found in the cisplatin-resistant SCC4cisR cell line compared to the parental sensitive SCC4 cell line. Interestingly, the increased ROS levels observed did not correlate with an increase in oxidative stress and consequent cell death. Accordingly, a greater antioxidant response through enhancement of the Nrf2/HO-1 signalling axis was demonstrated in the cisplatin-resistant cell line, suggesting that cellular adaptation to ROS-induced oxidative stress may represent a potential mechanism involved in chemoresistance in the OSCC cisplatin resistant model examined herein.

Chemoresistance represents a major challenge for OSCC patients undergoing chemotherapy [481]. Indeed, a strong association between platinum-based chemotherapy and development of drug resistance has been reported [108]. Given this, there is a compelling need to identify the mechanisms involved in cisplatin resistance in order to develop new therapeutic strategies to overcome chemoresistance in OSCC patients. In the present study, the enhancement of antioxidant systems in cisplatin-resistant OSCC cells suggested that targeting the cellular response to ROS-induced oxidative stress may reduce

chemoresistance. Accordingly, depletion of glutathione using buthionine sulfoximine (BSO) and inhibition of Nrf2 using the new specific Nrf2 inhibitor ML385 was shown to partially restore the cisplatin-sensitive phenotype in the SCC4cisR cell line, corroborating the importance of oxidant stress-adaptation in chemoresistance. All these findings strongly imply that targeting the cellular antioxidant systems may be exploited in the clinic to bypass drug resistance. Nevertheless, although many studies have shown promising effects of redox anticancer drugs for the treatment of cancer, not many of these drugs have shown clinical efficacy [614]. This low success has been linked to a limited understanding of the redox targets in normal and cancer cells, resulting either in a low effect of the drug or in off-target drug cytotoxicity [614]. Accordingly, although it has been shown that BSO enhanced the cytotoxic effect of various drugs both *in vitro* and *in vivo*, a relevant effect in the various clinical trials was not demonstrated [614]. Also, its short-half life has been considered a limitation in its application in clinic, leading researchers to focus on alternative approaches for targeting GSH within cells [615]. Conversely, not many studies have been yet investigated the beneficial effects of targeting Nrf2 with ML385 for the treatment of cancer. Thus, given the promising preclinical results obtained herein, the use of ML385 in combination with chemotherapeutics may warrant further studies. Also, given the clear implication of oxidative stress in cancer and chemoresistance, a better understanding of redox signalling may be required to develop new improved therapeutic strategies.

In the last part of this study, the role of autophagy in OSCC development was investigated. A controversial role of autophagy in tumour initiation and progression has been proposed, with autophagy acting either as a tumour suppressor or tumour promoter mechanism during cancer development [169, 563]. Moreover, both activation and inhibition of autophagy have been reported in tumorigenesis depending on the cancer type [167]. Currently, the role of autophagy in OSCC development is still not clearly defined [551]. Accordingly, the expression of autophagic markers in OSCC tissue samples from two independent cohorts of patients (Spanish and Irish) were herein investigated by western blotting and immunohistochemistry respectively. Results obtained from these two analyses showed an increase in the expression of the autophagic markers LC3 and Beclin-1 in OSCC samples compared to precancerous and control samples. Moreover, an increase (although not significant) in the LC3-II/LC3-I ratio and a decrease in p62 expression were also found in OSCC samples compared to precancerous and control

samples. Taken together these results suggest the progressive activation of autophagy during OSCC progression, implying a pro-tumour role of autophagy in OSCC development. Also, a significant negative correlation between p62 expression and tumour size was demonstrated in OSCC patients, suggesting a role for this protein in OSCC tumour progression. Additionally, increased levels of the antiapoptotic marker Bcl-xL were also observed in OSCC samples compared to precancerous and control samples, suggesting that inhibition of the apoptotic pathway may also occur during OSCC development.

Finally, in the present study, the potential application of autophagic markers for the diagnosis of OSCC was examined. In fact, it has been estimated that the high mortality rate associated with OSCC is mainly due to late diagnosis, which can partially be attributable to an initial misdiagnosis of this malignancy [13]. Given this, there is a compelling need to define new specific biomarkers to help dentists and pathologists in the diagnosis of OSCC [616]. Currently, a considerable number of biomarkers have been investigated for OSCC detection. In particular, salivary cytokines and circulating microRNAs from plasma, serum and saliva have shown an interesting potential as non-invasive tools for the early detection of OSCC [144]. Dysregulated proteins in tumour tissues but not in normal tissues also possess the potential of being used as biomarkers for the diagnosis of cancer [617]. In the present study, a role for LC3 and Beclin-1 as OSCC biomarkers was considered. Interestingly, a discrete discriminatory power of these autophagic markers was determined through ROC (Receiver Operating Characteristic) analysis in cancerous and non-cancerous patient samples, showing an Area Under the Curve (AUC) of 0.797 with 85.7% sensitivity and 65.5% specificity for LC3 protein ($p<0.001$) and an AUC of 0.811 with 92.9 % sensitivity and 66.7% specificity for Beclin-1 ($p<0.001$). These preliminary results suggest a potential application of these markers for OSCC detection, however no firm conclusions can be drawn because of the limited cohort of patients herein analysed. Thus, further analysis on a greater number of samples is warranted. Also, it should be highlighted, that the early detection of the autophagic state in patient samples may be useful to develop new therapeutic strategies using appropriate autophagy modulators to improve the treatment of OSCC patients.

In summary, this project has demonstrated autophagy activation as a cellular response to cisplatin in OSCC cells and has also indicated a tight relationship between cisplatin-induced autophagy and apoptosis through a coordinated regulation of these processes by

the ROS/JNK signalling pathway. Moreover, targeting autophagy with the lysosomal inhibitors chloroquine and bafilomycin-A1 in combination with cisplatin was demonstrated to sensitise OSCC cells to cisplatin, suggesting their application in the clinic to improve chemotherapy in OSCC patients. Additionally, analysis of autophagy in a cisplatin-resistant OSCC cell line generated herein did not indicate a role for autophagy in chemoresistance. In contrast, an increased cellular response to cisplatin-induced ROS was implicated. Accordingly, targeting the ROS signalling pathway was shown to partially restore the cisplatin-sensitive phenotype in the resistant OSCC cells. Finally, analysis of oral tissue samples showed an increase of autophagy activation in OSCC samples compared to precancerous and normal samples, indicating a role for autophagy in tumour development and suggesting a potential application of LC3 and Beclin-1 as biomarkers for OSCC detection.

8. Future Work

In the present study, cisplatin, a representative OSCC chemotherapeutic agent, was shown to concurrently induce both apoptosis and autophagy in two OSCC cell lines, SCC4 and SCC9. Moreover, analysis of the signalling pathways underlying cisplatin-induced apoptosis and autophagy showed a critical role for cisplatin-induced oxidative stress in the activation of both processes. Furthermore, results obtained suggested a role for the JNK signalling pathway in mediating both apoptosis and autophagy in response to cisplatin-induced oxidative stress. In fact, treatment of cells with the JNK inhibitor SP600125 resulted in the inhibition of autophagic flux and caspase 3 cleavage. However, due to the ability of SP600125 to also modulate endogenous autophagy, the possibility that this pharmacological JNK inhibitor may elicit off-target effects cannot be ruled out. Therefore, further experiments using a knockdown approach for targeting the JNK pathway may be required to confirm the role of JNK in cisplatin-induced autophagy.

In addition to oxidative stress, many studies have also reported a role for endoplasmic reticulum stress (ER stress) in the cellular response to cisplatin. The endoplasmic reticulum (ER) plays a crucial role within cells in protein folding, assembly, and secretion [618]. Accumulation of unfolded or incompletely folded proteins in the ER after treatment with cisplatin has been correlated to ER stress [619, 620]. Excessive and persistent ER stress has been linked to cell death and apoptosis through the activation of effector molecules such as CHOP (C/EBP homologous protein**)** and caspase 4 [621]. Moreover, some studies have reported that autophagy may be induced to alleviate ER stress in order to clear the accumulated misfolded proteins from the ER lumen [84, 85]. Also, inhibition of autophagy has been shown to trigger cisplatin-induced apoptosis by increasing ER stress in glioma cell lines [199]. Given this, evaluation of key ER stress related proteins, such as BIP (immunoglobulin heavy chain-binding protein)**,** PERK (protein kinase R (PKR)-like endoplasmic reticulum kinase), IRE1 (Inositol-requiring enzyme 1) and CHOP in OSCC cells treated with cisplatin may be of interest to determine whether ER stress is implicated in the cellular response to cisplatin in OSCC. Moreover, analysis of both cisplatin-induced autophagy and apoptosis in the presence/absence of ER stress inhibitors such as 4-phenylbutyric acid (4-PBA) could also be conducted to clarify the relationship between ER stress, autophagy and apoptosis in response to cisplatin.

Additionally, in the present study, a cisplatin-resistant OSCC cell line (SCC4cisR) was generated by pulsed stepwise exposure of cells to cisplatin. This cell line represents a clinically relevant model for the study of chemoresistance in OSCC. Even though

autophagy did not appear to play a role in acquired resistance to cisplatin in the SCC4cisR cells, a role for stress-response pathways was demonstrated. However, given the complexity of chemoresistance, the involvement of multiple mechanisms cannot be excluded. Thus, to further progress this study, additional analysis of other mechanisms implicated in chemoresistance in the cell model generated herein may be warranted.

As reported in chapter 5, the Ras/Raf/MEK/ERK pathway is a survival pathway involved in the regulation of many important cellular processes such as differentiation, proliferation and stress response [494]. An interesting link between dysregulation of this signalling pathway and chemoresistance has been proposed in numerous studies [622]. For example, ectopic mutation of Ras has been shown to induce doxorubicin and paclitaxel-resistance in breast cancer cells [622, 623]. In the present study, preliminary results displayed increased endogenous and cisplatin-induced levels of Ras in the SCC4cisR cells compared to the parental cells. Moreover, increased activation of ERK was also demonstrated in the SCC4cisR cells treated with cisplatin compared to the SCC4 cells. These results suggest a potential role for the Ras/Raf/MEK/ERK signalling pathway in mediating cisplatin resistance in the cell model examined herein. However, to confirm a role for this pathway in chemoresistance in OSCC, evaluation of the effect of Ras, Raf, MEK and/or ERK inhibition on cisplatin-induced apoptosis in SCC4cisR cells may be required. Inhibition of the Ras/ERK pathway has been shown to sensitise cells to the effect of chemotherapeutics in various studies. For example, inhibition of ERK using the specific ERK signalling pathway inhibitor PD98059 was shown to reduce cell viability following treatment with 5-fluorouracil in a drug-resistant pancreatic cancer cell line [624]. Given this, evaluation of the effect of ERK inhibition using pharmacological inhibitors, such as PD98059 or UO126, on cisplatin-induced apoptosis in the SCC4cisR cell line may be of interest to determine whether targeting the Ras/Raf/MEK/ERK pathway may be exploited as a therapeutic option to reduce chemoresistance in OSCC patients.

Moreover, in the present study, activation of the antioxidant Nrf2/HO-1 pathway has been demonstrated in the SCC4cisR cell line. Along with HO-1, other Nrf2 targets have been reported in the literature, suggesting that Nrf2 can control the activation of other pathways. In particular, Nrf2 was shown to promote proliferation and migration in breast cancer cells by activating the glucose-6-phosphate dehydrogenase (G6PD)/hypoxia-inducible factor 1-alpha (HIF-1α)/Notch1 signalling axis, which controls the expression

of proteins such as Jagged1 and Hes1 involved in the epithelial-mesenchymal transition (EMT) [625]. Also, Nrf2 was shown to mediate the constitutive and inducible expression of multidrug resistance proteins (MRP) in small-cell lung cancer [626]. The involvement of Nrf2 in these pathways corroborate its role in chemoresistance and also suggest a redox-independent role of Nrf2 in chemoresistance. Western blotting analysis of some of the Nrf2 targets mentioned above in the SCC4cisR cells may be of interest to better understand the role of Nrf2 in chemoresistance. Furthermore, a link between the Ras/ERK signalling pathway and Nrf2 activation has also been proposed, suggesting that Ras can control Nrf2 through activation of ERK [495]. Given this, evaluation of the relationship between Ras, ERK and Nrf2 may also be of interest to better elucidate the role of this signalling pathway in mediating cisplatin resistance in OSCC. Finally, analysis of Nrf2 expression in paraffin-embedded oral tissue samples from control and OSCC patients and correlation of Nrf2 levels with chemotherapeutic regimens of patients and overall survival represents a further avenue of exploration in order to provide a comprehensive overview of the role of Nrf2 in tumour development and chemoresistance in OSCC patients.

A recent study published by Kim *et al.* showed that treatment of cells with cisplatin in combination with wogonin, a natural anticancer drug with Nrf2 inhibitory activity, enhanced cisplatin sensitivity both *in vitro* and in an *in vivo* xenograft model of head and neck cancer [627]. In line with these findings, in the present study, promising results showed that inhibiting Nrf2 with the specific inhibitor ML385 resulted in a partial restoration of the cisplatin-sensitive phenotype in the SCC4cisR cells. Given this, it would be of interest to evaluate the translational efficacy of inhibiting Nrf2 with ML385 in combination with cisplatin in an *in vivo* xenograft model of OSCC. Such preclinical studies would further clarify whether inhibiting Nrf2 with ML385 may represent a possible therapeutic option to bypass resistance in OSCC patients.

Furthermore, a link between Cancer Stem Cells (CSCs) and chemoresistance has also been reported in the literature [515]. In the present study, preliminary experiments were performed to investigate whether acquired resistance to cisplatin was driven by a CSC or CSC-like population in the cell model herein examined. Evaluation of the two cell surface markers CD44 and CD24 in both SCC4 and SCC4cisR cells demonstrated only a small population of cells (equal in both cell lines) with a $CD44^{+}/CD24^{-}$ expression pattern, which has been reported as indicative of the CSC phenotype in OSCC [314, 489]. Although, this result may suggest that CSCs are not involved in acquired resistance to

cisplatin in this model, it should be noted that many other proteins have been proposed as markers for the CSC phenotype. Also, the identification of CSCs is still controversial due to the frequent phenotypic transitions and the high variability in cell composition among cell types [489]. In this regard, it has been reported that in addition $CD133^+$ and aldehyde dehydrogenase $(ADH)^+$ cells showed stem-like and EMT properties in head and neck cancer [628]. Accordingly, evaluation of these additional two markers may be required to better examine the stem-like properties of the SCC4cisR cell line.

Additionally, to aid in the study of cisplatin resistance in OSCC, evaluation of other mechanisms correlated to the development of the resistant phenotype may be warranted. In particular, one of the main features of cisplatin resistance consists of the reduced accumulation of cisplatin within cells [484]. This is mainly due to a decrease in uptake or an increase in efflux of the drug, and it may be attributable to alteration of various membrane transporters, such as organic cation transporters (OCT1-3), copper transporters (CTR1-2), P-type ATPases (ATP7A/7B) and MRP [484][483]. Moreover, given the well-known ability of cisplatin to induce DNA adducts, enhancement of the DNA repair systems has been linked to the acquisition of resistant phenotypes [484]. Accordingly, high levels of ERCC1 (excision repair cross-complementing protein) were reported in various cisplatin-resistant cells compared with cisplatin-sensitive cells [49][75]. Expression analysis of the above-mentioned proteins in the SCC4cisR cell line by western blotting may provide a comprehensive overview of the mechanisms implicated in cisplatin resistance in the OSCC cell model herein examined. In addition, altered mitochondrial functions and metabolic reprogramming have also been linked to drug resistance [629]. In this regard, increased glucose uptake and enhanced aerobic glycolysis were shown to induce cisplatin resistance in gastric cancer cells [630]. Also, a high glycolytic rate and a reduced mitochondrial activity were reported in ovarian and cervical cisplatin-resistant cells compared to the parental sensitive cells, while a low glycolytic rate was found in cisplatin-resistant lung carcinoma cells [629]. Based on these studies, investigation of the association between cisplatin resistance and metabolism in the OSCC cisplatin-resistant model generated herein may be of interest to better elucidate the correlation between cisplatin resistance and metabolism in OSCC. For such experiments, a Seahorse XFe24 analyser to determine the oxygen consumption rate (OCR) and extracellular acidification rate (ECAR) in both SCC4 and SCC4cisR under normoxic and hypoxic conditions could be utilised.

Finally, the present study has presented promising results demonstrating an increase in expression of two autophagic markers, LC3 and Beclin-1, in an Irish cohort of OSCC patients, suggesting a role for autophagy in OSCC development. Moreover, preliminary analyses showed a discrete predictive power of LC3 and Beclin-1 for OSCC detection. However, the small sample size represented the main limitation of this study. Thus, further analysis on a bigger sample size is required to confirm the preliminary data obtained herein. Moreover, the lack of information about the clinical-pathological characteristics of the Irish patient cohort represented a second limitation of this study. Accordingly, if further ethical approval could be obtained with regards to accessing patient details, it would be of interest to investigate the correlation of LC3 and Beclin-1 expression with clinical-pathological variables such as tumour size, presence of metastasis and overall survival of patients, with the final aim of determining whether these two markers may also have potential for use as prognostic markers in OSCC.

In summary, this project shows promising results on the mechanisms underlying cisplatin cytotoxicity and resistance in OSCC as well as providing a comprehensive overview of the role of autophagy in response to cisplatin in chemoresistance and OSCC development. Further expansion of the work is warranted for a better understanding of the mechanisms involved in cisplatin cytotoxicity and resistance in OSCC and to determine the potential application of the autophagic markers LC3 and Beclin-1 as OSCC biomarkers.

References

1. Montero PH, Patel SG. *Cancer of the oral cavity.* Surg Oncol Clin N Am 2015; 24: 491–508.
2. Russo D, Merolla F, Mascolo M, et al. *FKBP51 immunohistochemical expression: A new prognostic biomarker for OSCC?* Int J Mol Sci 2017; 18(2): 443.
3. Malik UU, Zarina S, Pennington SR. *Oral squamous cell carcinoma: Key clinical questions, biomarker discovery, and the role of proteomics*. Arch Oral Biol 2016; 63: 53–65.
4. Markopoulos AK. *Current Aspects on Oral Squamous Cell Carcinoma*. Open Dent J 2012; 6: 126–130.
5. Jiang X, Wu J, Wang J, Huang R. *Tobacco and oral squamous cell carcinoma: A review of carcinogenic pathways*. Tob Induc Dis 2019; 17:29.
6. Lawal AO, Adisa AO, Effiom OA. *A review of 640 Oral squamous cell carcinoma cases in Nigeria*. J Clin Exp Dent 2017; 9: e767–e771.
7. Feller L, Lemmer J. *Oral Squamous Cell Carcinoma: Epidemiology, Clinical Presentation and Treatment*. J Cancer Ther 2012; 03: 263–268.
8. Attar E, Dey S, Hablas A, Seifeldin IA, Ramadan M, Rozek LS, Soliman AS. *Head and neck cancer in a developing country: A population-based perspective across 8 years*. Oral Oncol 2010; 46: 591–596.
9. Mehrotra R, Yadav S. *Oral squamous cell carcinoma: etiology, pathogenesis and prognostic value of genomic alterations.* Indian J Cancer 2006; 43: 60–66.
10. Shiboski CH, Schmidt BL, Jordan RCK. *Racial disparity in stage at diagnosis and survival among adults with oral cancer in the US*. Community Dent Oral Epidemiol 2007; 35: 233–240.
11. Gandini S, Botteri E, Iodice S, Boniol M, Lowenfels AB, Maisonneuve P, Boyle P. *Tobacco smoking and cancer: A meta-analysis*. Int J Cancer 2008; 122: 155–164.
12. Neville BW, Day T a. *Oral cancer and precancerous lesions*. Ca-A Cancer J Clin 2002; 52: 195–215.
13. Rivera C. *Essentials of oral cancer*. Int J Clin Exp Pathol 2015; 8: 11884–11894.
14. Petti S. *Lifestyle risk factors for oral cancer*. Oral Oncol 2009; 45: 340–350.
15. Hashibe M, Brennan P, Chuang SC, et al. *Interaction between tobacco and alcohol use and the risk of head and neck cancer: Pooled analysis in the international head and neck cancer Epidemiology consortium*. Cancer Epidemiol Biomarkers Prev 2009; 8(2)541-550.
16. Pelucchi C, Tramacere I, Boffetta P, Negri E, Vecchia C La. *Alcohol consumption and cancer risk*. Nutr Cancer 2011; 63(7)983-990.
17. Manjari M, Popli R, Paul S, Gupta VP, Kaholon SK. *Prevalence of oral cavity, pharynx, larynx and nasal cavity malignancies in Amritsar, Punjab*. Indian J Otolaryngol Head Neck Surg; 48: 191–195.
18. Lin BM, Wang H, D'Souza G, Zhang Z, Fakhry C, Joseph AW, Drake VE, Sanguineti G, Westra WH, Pai SI. *Long-term prognosis and risk factors among patients with HPV-associated oropharyngeal squamous cell carcinoma*. Cancer 2013; 119: 3462–3471.
19. Warnakulasuriya S. *Global epidemiology of oral and oropharyngeal cancer*. Oral Oncol 2009; 45: 309–316.
20. Williams HK. *Molecular pathogenesis of oral squamous carcinoma.* Mol Pathol 2000; 53: 165–72.

21. John LS St. *Effects of exogeneous p53 on growth suppression, apoptosis, and differentiation in oral cancer cell lines*. Texas Med Cent Diss (via ProQuest).
22. Sidransky D. *Molecular genetics of head and neck cancer.* Curr Opin Oncol 1995; 7: 229–33.
23. Van Houten VM, Tabor MP, van den Brekel MW, Alain Kummer J, Denkers F, Dijkstra J, Leemans R, van der Waal I, Snow GB, Brakenhoff RH. *Mutated p53 as a molecular marker for the diagnosis of head and neck cancer*. J Pathol 2002; 198: 476–486.
24. Rothenberg SM, Ellisen LW. *The molecular pathogenesis of head and neck squamous cell carcinoma*. J Clin Invest 2012; 122: 1951–1957.
25. Ram H, Sarkar J, Kumar H, Konwar R, Bhatt MLB, Mohammad S. *Oral cancer: risk factors and molecular pathogenesis.* J Maxillofac Oral Surg 2011; 10: 132–7.
26. Weijers M, Ten Hove I, Allard RHB, Bezemer DPD, Van Der Waal I. *Patients with oral cancer developing from pre-existing oral leukoplakia: Do they do better than those with de novo oral cancer?* J Oral Pathol Med 2008; 37: 134–136.
27. Bagan J, Sarrion G, Jimenez Y. *Oral cancer: Clinical features*. Oral Oncol 2010; 46: 414–417.
28. Shah JP, Gil Z. *Current concepts in management of oral cancer – Surgery*. Oral Oncol 2009; 45: 394–401.
29. Chi AC, Day TA, Neville BW. *Oral cavity and oropharyngeal squamous cell carcinoma-an update*. CA Cancer J Clin 2015; 65: 401–421.
30. Ord RA, Blanchaert RH. *Current management of oral cancer. A multidisciplinary approach.* J Am Dent Assoc 2001; 132 Suppl: 19S-23S.
31. Chin D, Boyle GM, Porceddu S, Theile DR, Parsons PG, Coman WB. *Head and neck cancer: past, present and future*. Expert Rev Anticancer Ther 2006; 6: 1111–1118.
32. Zakrzewska JM. *Fortnightly review: oral cancer.* BMJ 1999; 318: 1051–4.
33. Del Corso G, Villa A, Tarsitano A, Gohel A. *Current trends in oral cancer: a systematic review*. Cancer Cell Microenviron 2016; 3: e1332.
34. Omura K. *Current status of oral cancer treatment strategies: surgical treatments for oral squamous cell carcinoma*. Int J Clin Oncol 2014; 19: 423–430.
35. Madhulaxmi M, Iyer K, Periasamy R, Gajendran P, Lakshmi T. *Role of cisplatin in oral squamous cell carcinoma – A review*. J Adv Pharm Educ Res 2017; 7: 39–42.
36. Eastman A. *The formation, isolation and characterization of DNA adducts produced by anticancer platinum complexes.* Pharmacol Ther 1987; 34: 155–66.
37. Siddik ZH. *Cisplatin: mode of cytotoxic action and molecular basis of resistance*. Oncogene 2003; 22: 7265–7279.
38. Zhang N, Yin Y, Xu S-J, Chen W-S, Zhang N, Yin Y, Xu S-J, Chen W-S. *5-Fluorouracil: Mechanisms of Resistance and Reversal Strategies*. Molecules 2008; 13: 1551–1569.
39. Parker WB, Cheng YC. *Metabolism and mechanism of action of 5-fluorouracil*. Pharmacol Ther 1990; 48: 381–395.
40. Abal M, Andreu JM, Barasoain I. *Taxanes: microtubule and centrosome targets, and cell cycle dependent mechanisms of action.* Curr Cancer Drug Targets 2003; 3: 193–203.
41. Gligorov J, Lotz JP. *Preclinical pharmacology of the taxanes: implications of the differences.* Oncologist 2004; 9 Suppl 2: 3–8.
42. Housman G, Byler S, Heerboth S, Lapinska K, Longacre M, Snyder N, Sarkar S. *Drug resistance in cancer: An overview*. Cancers (Basel) 2014; 6: 1769–1792.

43. Zheng H-C. *The molecular mechanisms of chemoresistance in cancers.* Oncotarget 2017; 8: 59950–59964.
44. Wang X, Zhang H, Chen X. *Drug resistance and combating drug resistance in cancer*. Cancer Drug Resist 2019; 2:141-160.
45. Li X, Lewis MT, Huang J, Gutierrez C, Osborne CK, Wu MF, Hilsenbeck SG, Pavlick A, Zhang X, Chamness GC, Wong H, Rosen J, Chang JC. *Intrinsic resistance of tumorigenic breast cancer cells to chemotherapy*. J Natl Cancer Inst 2008; 100(9):672–9.
46. Greaves M, Maley CC. *Clonal evolution in cancer*. Nature 2012; 481(7381): 306–313.
47. Kuczynski EA, Sargent DJ, Grothey A, Kerbel RS. *Drug rechallenge and treatment beyond progression-implications for drug resistance*. Nat Rev Clin Oncol 2013; 10(10):571-87.
48. Frank NY, Schatton T, Frank MH. *The therapeutic promise of the cancer stem cell concept*. J Clin Invest 2010; 120(1): 41–50.
49. Luqmani YA. *Mechanisms of drug resistance in cancer chemotherapy*. Med Princ Pract 2005; 14: 35–48.
50. Dumontet C, Fabianowska-Majewska K, Mantincic D, et al. *Common resistance mechanisms to deoxynucleoside analogues in variants of the human erythroleukaemic line K562*. Br J Haematol 1999; 106: 78–85.
51. Gamcsik MP, Dubay GR, Cox BR. *Increased rate of glutathione synthesis from cystine in drug-resistant MCF-7 cells.* Biochem Pharmacol 2002; 63: 843–51.
52. Zahreddine H, Borden KLB. *Mechanisms and insights into drug resistance in cancer*. Front Pharmacol 2013; 4: 28.
53. Kelley SL, Basu A, Teicher BA, Hacker MP, Hamer DH, Lazo JS. *Overexpression of metallothionein confers resistance to anticancer drugs*. Science (80-) 1988; 241(4874):1813–5.
54. Komiya K, Matsuda T, Nishio K, Ohmori T, Sugimoto Y, Saijo N. *Metallothionein Content Correlates with the Sensitivity of Human Small Cell Lung Cancer Cell Lines to Cisplatin*. Cancer Res 1991; 51(12):3237–42.
55. Quintás-Cardama A, Kantarjian HM, Cortes JE. *Mechanisms of primary and secondary resistance to imatinib in chronic myeloid leukemia*. Cancer Control 2009; 16(2):122-31.
56. Jabbour EJ, Cortes JE, Kantarjian HM. *Resistance to tyrosine kinase inhibition therapy for chronic myelogenous leukemia: A clinical perspective and emerging treatment options*. Clin Lymphoma, Myeloma Leuk 2013; 3(5):515-29.
57. Shaffer BC, Gillet JP, Patel C, Baer MR, Bates SE, Gottesman MM. *Drug resistance: Still a daunting challenge to the successful treatment of AML*. Drug Resist Updat 2012; 15(1-2):62-9.
58. Baudis M, Prima V, Yoon HT, Hunger SP. *ABCB1 over-expression and drug-efflux in acute lymphoblastic leukemia cell lines with t(17;19) and E2A-HLF expression*. Pediatr Blood Cancer 2006; 47(6):757-64.
59. Peng XX, Tiwari AK, Wu HC, Chen ZS. *Overexpression of P-glycoprotein induces acquired resistance to imatinib in chronic myelogenous leukemia cells*. Chin J Cancer 2012; 31(2): 110–118.
60. Abolhoda A, Wilson AE, Ross H, Danenberg P V., Burt M, Scotto KW. *Rapid activation of MDR1 gene expression in human metastatic sarcoma after in vivo exposure to doxorubicin*. Clin Cancer Res 1999; 5(11):3352-6.
61. Fojo AT, Ueda K, Slamon DJ, Poplack DG, Gottesman MM, Pastan I. *Expression of a multidrug-resistance gene in human tumors and tissues*. Proc Natl Acad Sci

U S A 1987; 84(1):265–9.
62. Yin J, Zhang J. *Multidrug resistance-associated protein 1 (MRP1/ABCC1) polymorphism: From discovery to clinical application*. J Cent South Univ Medical Sci 2011; 36: 927–938.
63. Cole SPC, Bhardwaj G, Gerlach JH, Mackie JE, Grant CE, Almquist KC, Stewart AJ, Kurz EU, Duncan AMV, Deeley RG. *Overexpression of a transporter gene in a multidrug-resistant human lung cancer cell line*. Science (80-) 1992; 258(5088):1650–4.
64. Hart SM, Ganeshaguru K, Hoffbrand A V., Prentice HG, Mehta AB. *Expression of the multidrug resistance-associated protein (MRP) in acute leukaemia*. Leukemia 1994; 8(6):990–7.
65. Norris MD, Bordow SB, Marshall GM, Haber PS, Cohn SL, Haber M. *Expression of the gene for multidrug-resistance-associated protein and outcome in patients with neuroblastoma*. N Engl J Med 1996; 334(4):231–8.
66. Cho S, Lu M, He X, Ee PLR, Bhat U, Schneider E, Miele L, Beck WT. *Notch1 regulates the expression of the multidrug resistance gene ABCC1/MRP1 in cultured cancer cells*. Proc Natl Acad Sci U S A 2011; 108(51):20778–83.
67. Mao Q, Unadkat JD. *Role of the Breast Cancer Resistance Protein (BCRP/ABCG2) in Drug Transport—an Update*. AAPS J 2015; 17(1):65-82.
68. Horsey AJ, Cox MH, Sarwat S, Kerr ID. *The multidrug transporter ABCG2: Still more questions than answers*. Biochem Soc Trans 2016; 44(3): 824–830.
69. Stacy AE, Jansson PJ, Richardson DR. *Molecular Pharmacology of ABCG2 and its role in chemoresistance*. Mol Pharmacol 2013; 84(5):655–69.
70. Yanase K, Tsukahara S, Asada S, Ishikawa E, Imai Y, Sugimoto Y. *Gefinitib reverses breast cancer resistance protein-mediated drug resistance*. Mol Cancer Ther 2004; 3(9):1119-25.
71. Kuroda H, Takeno M, Murakami S, Miyazawa N, Kaneko T, Ishigatsubo Y. *Inhibition of heme oxygenase-1 with an epidermal growth factor receptor inhibitor and cisplatin decreases proliferation of lung cancer A549 cells*. Lung Cancer 2010; 67(1):31–6.
72. Lakshmanan I, Salfity S, Seshacharyulu P, Rachagani S, Thomas A, Das S, Majhi PD, Nimmakayala RK, Vengoji R, Lele SM, Ponnusamy MP, Batra SK, Ganti AK. *MUC16 regulates TSPYL5 for lung cancer cell growth and chemoresistance by suppressing p53*. Clin Cancer Res 2017; 23(14):3906-3917.
73. Zhang P, Zhang P, Shi B, Zhou M, Jiang H, Zhang H, Pan X, Gao H, Sun H, Li Z. *Galectin-1 overexpression promotes progression and chemoresistance to cisplatin in epithelial ovarian cancer*. Cell Death Dis 2014; 5(1):e991.
74. McNeil EM, Melton DW. *DNA repair endonuclease ERCC1-XPF as a novel therapeutic target to overcome chemoresistance in cancer therapy*. Nucleic Acids Res 2012; 40(20):9990-10004.
75. Chu G. *Cellular responses to cisplatin. The roles of DNA-binding proteins and DNA repair*. J Biol Chem 1994; 269(2):787–90.
76. Passagne I, Evrard A, Depeille P, Cuq P, Cupissol D, Vian L. *O6-methylguanine DNA-methyltransferase (MGMT) overexpression in melanoma cells induces resistance to nitrosoureas and temozolomide but sensitizes to mitomycin C*. Toxicol Appl Pharmacol 2006; 211(2):97–105.
77. de Angelis PM, Fjell B, Kravik KL, Haug T, Tunheim SH, Reichelt W, Beigi M, Clausen OP, Galteland E, Stokke T. *Molecular characterizations of derivatives of HCT116 colorectal cancer cells that are resistant to the chemotherapeutic agent 5-fluorouracil.* Int J Oncol 2004; 24(5):1279-88.

78. De Angelis PM, Svendsrud DH, Kravik KL, Stokke T. *Cellular response to 5-fluorouracil (5-FU) in 5-FU-resistant colon cancer cell lines during treatment and recovery*. Mol Cancer 2006; 5: 20.
79. Tiligada E. *Chemotherapy: Induction of stress responses*. In: *Endocrine-Related Cancer*. 2006, pp. 13 Suppl 1:S115-24. doi: 10.1677/erc.1.01272.
80. Huang Z, Zhou L, Chen Z, Nice EC, Huang C. *Stress management by autophagy: Implications for chemoresistance*. Int J Cancer 2016; 139(1):23–32.
81. Malhi H, Kaufman RJ. *Endoplasmic reticulum stress in liver disease*. J Hepatol 2011; 795–809.
82. Deavall DG, Martin EA, Horner JM, Roberts R. *Drug-induced oxidative stress and toxicity*. J Toxicol 2012; 2012:645460.
83. Wojtkowiak JW, Verduzco D, Schramm KJ, Gillies RJ. *Drug resistance and cellular adaptation to tumor acidic pH microenvironment*. Mol Pharm 2011; 8(6):2032-8.
84. Shi S, Tan P, Yan B, Gao R, Zhao J, Wang J, Guo J, Li N, Ma Z. *ER stress and autophagy are involved in the apoptosis induced by cisplatin in human lung cancer cells*. Oncol Rep 2016; 35: 2606–2614.
85. Kouroku Y, Fujita E, Tanida I, Ueno T, Isoai A, Kumagai H, Ogawa S, Kaufman RJ, Kominami E, Momoi T. *ER stress (PERK/eIF2α phosphorylation) mediates the polyglutamine-induced LC3 conversion, an essential step for autophagy formation*. Cell Death Differ 2007; 14(2):230–9.
86. Landriscina M, Maddalena F, Laudiero G, Esposito F. *Adaptation to oxidative stress, chemoresistance, and cell survival*. Antioxidants Redox Signal 2009; 11: 2701–2716.
87. Garofalo M, Croce CM. *MicroRNAs as therapeutic targets in chemoresistance*. Drug Resist Updat 2013; 16(3-5):47-59.
88. Magee P, Shi L, Garofalo M. *Role of microRNAs in chemoresistance*. Ann Transl Med 2015; 3(21):332.
89. Valeri N, Gasparini P, Braconi C, Paone A, Lovat F, Fabbri M, Sumani KM, Alder H, Amadori D, Patel T, Nuovo GJ, Fishel R, Croce CM. *MicroRNA-21 induces resistance to 5-fluorouracil by down-regulating human DNA MutS homolog 2 (hMSH2)*. Proc Natl Acad Sci U S A 2010; 107(49): 21098–21103.
90. Feng B, Wang R, Song HZ, Chen LB. *MicroRNA-200b reverses chemoresistance of docetaxel-resistant human lung adenocarcinoma cells by targeting E2F3*. Cancer 2012; 118(13):3365–76.
91. Xia L, Zhang D, Du R, Pan Y, Zhao L, Sun S, Hong L, Liu J, Fan D. *miR-15b and miR-16 modulate multidrug resistance by targeting BCL2 in human gastric cancer cells*. Int J Cancer 2008; 123(2):372-379.
92. Xie Y, Tobin LA, Camps J, Wangsa D, Yang J, Rao M, Witasp E, Awad KS, Yoo N, Ried T, Kwong KF. *MicroRNA-24 regulates XIAP to reduce the apoptosis threshold in cancer cells*. Oncogene 2013; 32(19): 2442–2451.
93. Sharma M, Astekar M, Soi S, Manjunatha B, Shetty D, Radhakrishnan R. *pH Gradient Reversal: An Emerging Hallmark of Cancers*. Recent Pat Anticancer Drug Discov 2015; 10(3):244-58.
94. Bindra RS, Glazer PM. *Genetic instability and the tumor microenvironment: Towards the concept of microenvironment-induced mutagenesis*. Mutat Res - Fundam Mol Mech Mutagen 2005; 569(1-2):75-85.
95. Quail DF, Bowman RL, Akkari L, Quick ML, Schuhmacher AJ, Huse JT, Holland EC, Sutton JC, Joyce JA. *The tumor microenvironment underlies acquired resistance to CSF-1R inhibition in gliomas*. Science (80-) 2016;

352(6288):aad3018.
96. De Palma M, Lewis CE. *Macrophage regulation of tumor responses to anticancer therapies*. Cancer Cell 2013; 23(3):277-86.
97. Kreger BT, Johansen ER, Cerione RA, Antonyak MA. *The enrichment of survivin in exosomes from breast cancer cells treated with paclitaxel promotes cell survival and chemoresistance*. Cancers (Basel) 2016; 8(12): 111.
98. Chen W xian, Cai Y qin, Lv M meng, Chen L, Zhong S liang, Ma T fei, Zhao J hua, Tang J hai. *Exosomes from docetaxel-resistant breast cancer cells alter chemosensitivity by delivering microRNAs*. Tumor Biol 2014; 35(10):9649-59.
99. Bhatnagar N, Li X, Padi SKR, Zhang Q, Tang MS, Guo B. *Downregulation of miR-205 and miR-31 confers resistance to chemotherapy-induced apoptosis in prostate cancer cells*. Cell Death Dis 2010; 1(12): e105.
100. Abell AN, Johnson GL. *Implications of Mesenchymal Cells in Cancer Stem Cell Populations: Relevance to EMT*. Curr Pathobiol Rep 2014; 2(1): 21–26.
101. Nör C, Zhang Z, Warner KA, Bernardi L, Visioli F, Helman JI, Roesler R, Nör JE. *Cisplatin induces Bmi-1 and enhances the stem cell fraction in head and neck cancer*. Neoplasia (United States) 2014; 16(2): 137–146.
102. Shibue T, Weinberg RA. *EMT, CSCs, and drug resistance: The mechanistic link and clinical implications*. Nat Rev Clin Oncol 2017; 14(10):611-629.
103. Graham SM, Jørgensen HG, Allan E, Pearson C, Alcorn MJ, Richmond L, Holyoake TL. *Primitive, quiescent, Philadelphia-positive stem cells from patients with chronic myeloid leukemia are insensitive to STI571 in vitro*. Blood 2002; 99(1):319–25.
104. Zheng X, Carstens JL, Kim J, Scheible M, Kaye J, Sugimoto H, Wu CC, Lebleu VS, Kalluri R. *Epithelial-to-mesenchymal transition is dispensable for metastasis but induces chemoresistance in pancreatic cancer*. Nature 2015; 527(7579):525-530.
105. Saxena M, Stephens MA, Pathak H, Rangarajan A. *Transcription factors that mediate epithelial-mesenchymal transition lead to multidrug resistance by upregulating ABC transporters*. Cell Death Dis 2011; 2(7):e179.
106. Li J, Liu H, Yu J, Yu H. *Chemoresistance to doxorubicin induces epithelial-mesenchymal transition via upregulation of transforming growth factor β signaling in HCT116 colon cancer cells*. Mol Med Rep 2015; 12(1):192–8.
107. Lee JW, Guan W, Han S, Hong DK, Kim LS, Kim H. *MicroRNA-708-3p mediates metastasis and chemoresistance through inhibition of epithelial-to-mesenchymal transition in breast cancer*. Cancer Sci 2018; 109(5):1404-1413.
108. Wang C, Liu XQ ian., Hou JS on., Wang JN in., Huang HZ han. *Molecular Mechanisms of Chemoresistance in Oral Cancer*. Chin J Dent Res 2016; 19: 25–33.
109. Nakamura M, Nakatani K, Uzawa K, Ono K, Uesugi H, Ogawara K, Shiiba M, Bukawa H, Yokoe H, Wada T, Fujita S, Tanzawa H. *Establishment and characterization of a cisplatin-resistant oral squamous cell carcinoma cell line, H-1R*. Oncol Rep 2005; 14(5):1281–6.
110. Naramoto H, Uematsu T, Uchihashi T, Doto R, Matsuura T, Usui Y, Uematsu S, Li X, Takahashi M, Yamaoka M, Furusawa K. *Multidrug resistance-associated protein 7 expression is involved in cross-resistance to docetaxel in salivary gland adenocarcinoma cell lines*. Int J Oncol 2007; 30(2):393-401.
111. Yanamoto S, Kawasaki G, Yamada SI, Yoshitomi I, Kawano T, Yonezawa H, Rokutanda S, Naruse T, Umeda M. *Isolation and characterization of cancer stem-like side population cells in human oral cancer cells*. Oral Oncol 2011; 47(9):855-

60.
112. Zhang P, Zhang Z, Zhou X, Qiu W, Chen F, Chen W. *Identification of genes associated with cisplatin resistance in human oral squamous cell carcinoma cell line*. BMC Cancer 2006; 6:224.
113. Song J, Chang I, Chen Z, Kang M, Wang CY. *Characterization of side populations in HNSCC: Highly invasive, chemoresistant and abnormal Wnt signaling*. PLoS One 2010; 5(7):e11456.
114. Li X, Li Y, Qiu L hua, Tong X, Wang Q ming, Li T. *Expression of excision repair cross-complementation gene in drug-resistant process of carboplatin administration in tongue squamous cell cancer (Tca8113)*. Zhonghua Kou Qiang Yi Xue Za Zhi 2011; 46(7):437–41.
115. Harada K, Ferdous T, Ueyama Y. *Establishment of 5-fluorouracil-resistant oral squamous cell carcinoma cell lines with epithelial to mesenchymal transition changes*. Int J Oncol 2014; 44(4):1302–8.
116. Sun L, Yao Y, Liu B, Lin Z, Lin L, Yang M, Zhang W, Chen W, Pan C, Liu Q, Song E, Li J. *MiR-200b and miR-15b regulate chemotherapy-induced epithelial-mesenchymal transition in human tongue cancer cells by targeting BMI1*. Oncogene 2012; 432–45.
117. Dennis M, Wang G, Luo J, Lin Y, Dohadwala M, Abemayor E, Elashoff DA, Sharma S, Dubinett SM, St. John MA. *Snail controls the mesenchymal phenotype and drives erlotinib resistance in oral epithelial and head and neck squamous cell carcinoma cells*. Otolaryngol - Head Neck Surg (United States) 2012; 47(4):726–32.
118. Masui T, Ota I, Yook JI, Mikami S, Yane K, Yamanaka T, Hosoi H. *Snail-induced epithelial-mesenchymal transition promotes cancer stem cell-like phenotype in head and neck cancer cells*. Int J Oncol 2014; 147(4):726–32.
119. Yu Z wei, Zhong L ping, Ji T, Zhang P, Chen W tao, Zhang C ping. *MicroRNAs contribute to the chemoresistance of cisplatin in tongue squamous cell carcinoma lines*. Oral Oncol 2010; 46(4):317–22.
120. Elmore S. *Apoptosis: a review of programmed cell death.* Toxicol Pathol 2007; 35: 495–516.
121. Norbury CJ, Hickson ID. *Cellular responce to DNA damage*. Annu Rev Pharmacol Toxicol 2001; 41: 367–401.
122. Bratton SB, MacFarlane M, Cain K, Cohen GM. *Protein Complexes Activate Distinct Caspase Cascades in Death Receptor and Stress-Induced Apoptosis*. Exp Cell Res 2000; 256: 27–33.
123. Igney FH, Krammer PH. *Death and anti-death: tumour resistance to apoptosis*. Nat Rev Cancer 2002; 2: 277–288.
124. Deming P, Kurokawa M. *Dismantling the Apoptotic Cell by Caspases*. In: *eLS*. Chichester, UK: John Wiley & Sons, Ltd, pp. 1–10.
125. Saelens X, Festjens N, Walle L Vande, Gurp M van, Loo G van, Vandenabeele P. *Toxic proteins released from mitochondria in cell death*. Oncogene 2004; 23: 2861–2874.
126. Ashkenazi A, Dixit VM. *Death receptors: signaling and modulation.* Science 1998; 281: 1305–8. doi: 10.1126/science.281.5381.1305.
127. Roy S, Nicholson DW. *Cross-talk in cell death signaling.* J Exp Med 2000; 192: F21-5.
128. Marzban H, Del Bigio MR, Alizadeh J, Ghavami S, Zachariah RM, Rastegar M. *Cellular commitment in the developing cerebellum.* Front Cell Neurosci 2014; 8: 450.

129. Letai A. *Apoptosis and Cancer*. Annu Rev Cancer Biol 2017; 1: 275–294.
130. Wong RSY. *Apoptosis in cancer: from pathogenesis to treatment.* J Exp Clin Cancer Res 2011; 30: 87.
131. Bai L, Zhu W. *p53 : Structure , Function and Therapeutic Applications*. Cancer mol 2006; 2: 141–153.
132. Suni Ann Thomas and Sethupathy. S. *Expression of apoptotic markers in patients with oral squamous cell carcinoma (OSCC)\n*. IOSR J Dent Med Sci 2014; 13: 78–81.
133. Shen X-G, Wang C, Li Y, Wang L, Zhou B, Xu B, Jiang X, Zhou Z-G, Sun X-F. *Downregulation of caspase-9 is a frequent event in patients with stage II colorectal cancer and correlates with poor clinical outcome*. Color Dis 2010; 12: 1213–1218.
134. Itoh M, Noutomi T, Chiba H, Mizuguchi J. *Bcl-xL antisense treatment sensitizes Bcl-xL-overexpressing squamous cell carcinoma cells to carboplatin*. Oral Oncol 2002; 38(8):752–6.
135. Wang H, Zhang Z, Wei X, Dai R. *Small-molecule inhibitor of Bcl-2 (TW-37) suppresses growth and enhances cisplatin-induced apoptosis in ovarian cancer cells*. J Ovarian Res 2015; 8:3.
136. Virrey JJ, Guan S, Li W, Schönthal AH, Chen TC, Hofman FM. *Increased survivin expression confers chemoresistance to tumor-associated endothelial cells*. Am J Pathol 2008; 173(2):575–85.
137. Xu JH, Wang AX, Huang HZ, Wang JG, Pan C Bin, Zhang B. *Survivin shRNA induces caspase-3-dependent apoptosis and enhances cisplatin sensitivity in squamous cell carcinoma of the tongue*. Oncol Res 2010; 18(8):377-85.
138. Kumar B, Yadav A, Lang JC, Cipolla MJ, Schmitt AC, Arradaza N, Teknos TN, Kumar P. *YM155 reverses cisplatin resistance in head and neck cancer by decreasing cytoplasmic survivin levels*. Mol Cancer Ther 2012; 11(9): 1988–1998.
139. Hassan M, Watari H, Abualmaaty A, Ohba Y, Sakuragi N. *Apoptosis and molecular targeting therapy in cancer*. Biomed Res Int 2014; 150845.
140. Adhauliya N, Kalappanavar AN, Ali IM, Annigeri RG. *Autophagy : A boon or bane in oral cancer*. Oral Oncol 2016; 61: 120–126.
141. Pasquier B. *Autophagy inhibitors*. Cell Mol Life Sci 2016; 73(5):985-1001.
142. Galluzzi L, Pietrocola F, Bravo-San Pedro JM, et al. *Autophagy in malignant transformation and cancer progression*. EMBO J 2015; 34(7):856-80.
143. Boya P, Codogno P. *Autophagy: Molecular Mechanisms, Physiology & Pathology*. Tocris Biosci Sci Rev Ser 2015; 1–12.
144. Khan T, Relitti N, Brindisi M, Magnano S, Zisterer D, Gemma S, Butini S, Campiani G. *Autophagy modulators for the treatment of oral and esophageal squamous cell carcinomas*. Med Res Rev 2019; 40(3):1002-1060.
145. Nakamura S, Yoshimori T. *New insights into autophagosome-lysosome fusion*. J Cell Sci 2017; 130: 1209–1216.
146. Klionsky MJ and DJ. *Regulation of autophagy: Modulation of the size and number of autophagosomes*. FEBS Lett 2015; 588: 2457–2463.
147. Feng Y, He D, Yao Z, Klionsky DJ. *The machinery of macroautophagy*. Nat Publ Gr 2013; 24: 24–41.
148. Yang Z, Klionsky DJ. *Mammalian autophagy: core molecular machinery and signaling regulation.* Curr Opin Cell Biol 2010; 22: 124–31.
149. Kuang E, Qi J, Ronai Z. *Emerging roles of E3 ubiquitin ligases in autophagy*. Trends Biochem Sci 2013; 38(9):453-60.
150. Liu WJ, Ye L, Huang WF, Guo LJ, Xu ZG, Wu HL, Yang C, Liu HF. *p62 links the autophagy pathway and the ubiqutin-proteasome system upon ubiquitinated*

protein degradation. Cell Mol Biol Lett 2016; 21: 29.
151. Orhon I, Reggiori F. *Assays to Monitor Autophagy Progression in Cell Cultures*. Cells 2017; 6: 20.
152. Codogno P, Mehrpour M, Proikas-Cezanne T. *Canonical and non-canonical autophagy: Variations on a common theme of self-eating?* Nat Rev Mol Cell Biol 2012; 13: 7–12.
153. Meijer AJ, Codogno P. *Autophagy: Regulation and role in disease*. Crit Rev Clin Lab Sci 2009; 46: 210–240.
154. Kim YC, Guan KL. *MTOR: A pharmacologic target for autophagy regulation*. J Clin Invest 2015; 125: 25–32.
155. Lorin S, Hamaï A, Mehrpour M, Codogno P. *Autophagy regulation and its role in cancer*. Semin Cancer Biol 2013; 23: 361–379.
156. Garcia D, Shaw RJ. *AMPK: Mechanisms of Cellular Energy Sensing and Restoration of Metabolic Balance*. Mol Cell 2017; 66(6):789-800.
157. Schmukler E, Kloog Y, Pinkas-Kramarski R. *Ras and autophagy in cancer development and therapy.* Oncotarget 2014; 5: 577–86.
158. Furuta S, Hidaka E, Ogata A, Yokota S, Kamata T. *Ras is involved in the negative control of autophagy through the class I PI3-kinase*. Oncogene 2004; 23(22):3898-904.
159. Mendoza MC, Er EE, Blenis J. *The Ras-ERK and PI3K-mTOR pathways: Cross-talk and compensation*. Trends Biochem Sci 2011; 36(6):320–8.
160. Liu B, Bao J-K, Yang J-M, Cheng Y. *Targeting autophagic pathways for cancer drug discovery.* Chin J Cancer 2013; 32: 113–20.
161. Mrakovcic M, Fröhlich LF. *p53-Mediated Molecular Control of Autophagy in Tumor Cells.* Biomolecules 2018; 36(6):320–8.
162. Wei JL, Fang M, Fu ZX, Zhang SR, Guo JB, Wang R, Lv ZB, Xiong YF. *Sestrin 2 suppresses cells proliferation through AMPK/mTORC1 pathway activation in colorectal cancer*. Oncotarget 2017; 8(30): 49318–49328.
163. Tasdemir E, Maiuri MC, Galluzzi L, et al. *Regulation of autophagy by cytoplasmic p53*. Nat Cell Biol 2008; 10: 676–687.
164. Rébé C, Végran F, Berger H, Ghiringhelli F. *STAT3 activation: A key factor in tumor immunoescape*. JAK-STAT 2013; 2(1):e23010.
165. You L, Wang Z, Li H, Shou J, Jing Z, Xie J, Sui X, Pan H, Han W. *The role of STAT3 in autophagy.* Autophagy 2015; 11: 729–39.
166. Li M, Gao P, Zhang J. *Crosstalk between autophagy and apoptosis: Potential and emerging therapeutic targets for cardiac diseases*. Int J Mol Sci 2016; 17: 1-19. doi: 10.3390/ijms17030332.
167. Marinković M, Šprung M, Buljubašić M, Novak I. *Autophagy Modulation in Cancer: Current Knowledge on Action and Therapy*. Oxid Med Cell Longev 2018; 2018: 1–18.
168. Eileen White and Robert S. DiPaola. *The Double-edged Sword of Autophagy Modulation in Cancer Eileen*. 2010; 15: 5308–5316.
169. Kubisch J, Türei D, Földvári-Nagy L, Dunai ZA, Zsákai L, Varga M, Vellai T, Csermely P, Korcsmáros T. *Complex regulation of autophagy in cancer - Integrated approaches to discover the networks that hold a double-edged sword*. Semin Cancer Biol 2013; 23: 252–261.
170. Rosenfeldt MT, Ryan KM. *The multiple roles of autophagy in cancer.* Carcinogenesis 2011; 32: 955–63.
171. Qu X, Yu J, Bhagat G, Furuya N, Hibshoosh H, Troxel A, Rosen J, Eskelinen E-L, Mizushima N, Ohsumi Y, Cattoretti G, Levine B. *Promotion of tumorigenesis*

by heterozygous disruption of the beclin 1 autophagy gene. J Clin Invest 2003; 112: 1809–1820.
172. Kang MR, Kim MS, Oh JE, Kim YR, Song SY, Kim SS, Ahn CH, Yoo NJ, Lee SH. *Frameshift mutations of autophagy-related genes ATG2B, ATG5, ATG9B and ATGI2 in gastric and colorectal cancers with microsatellite instability*. J Pathol 2009; 217(5):702–6.
173. He S, Zhao Z, Yang Y, et al. *Truncating mutation in the autophagy gene UVRAG confers oncogenic properties and chemosensitivity in colorectal cancers*. Nat Commun 2015; 3;6:7839.
174. Barakat DJ, Friedman AD. *Autophagy is required for PTEN-loss driven prostate cancer*. Transl Cancer Res 2016; 5: S725–S729.
175. Scherz-Shouval R, Weidberg H, Gonen C, Wilder S, Elazar Z, Oren M. *p53-dependent regulation of autophagy protein LC3 supports cancer cell survival under prolonged starvation.* Proc Natl Acad Sci U S A 2010; 107: 18511–6.
176. Levy JMM, Foreman NK, Thorburn A. *Using BRAFV600E as a marker of autophagy dependence in pediatric brain tumors*. Autophagy 2014; 10(11): 2077–2078.
177. Levy JMM, Towers CG, Thorburn A. *Targeting autophagy in cancer*. Nat Rev Cancer 2017; 17: 528–542.
178. Guo JY, Chen H-Y, Mathew R, et al. *Activated Ras requires autophagy to maintain oxidative metabolism and tumorigenesis.* Genes Dev 2011; 25: 460–70.
179. Yun CW, Lee SH. *The Roles of Autophagy in Cancer*. Int J Mol Sci 2018; 19(11):3466.
180. Liu C, Sun L, Yang J, Liu T, Yang Y, Kim S-M, Ou X, Wang Y, Sun L, Zaidi M, New MI, Yuen T, Guo Q. *FSIP1 regulates autophagy in breast cancer.* Proc Natl Acad Sci U S A 2018; 115: 13075–13080.
181. Cosway B, Lovat P. *The role of autophagy in squamous cell carcinoma of the head and neck.* Oral Oncol 2016; 54: 1–6.
182. Liu J-L, Chen F-F, Lung J, Lo C-H, Lee F-H, Lu Y-C, Hung C-H. *Prognostic significance of p62/SQSTM1 subcellular localization and LC3B in oral squamous cell carcinoma*. Br J Cancer 2014; 111: 944–954.
183. Kapoor V, Paliwal D, Baskar Singh S, Mohanti BK, Das SN. *Deregulation of Beclin 1 in patients with tobacco-related oral squamous cell carcinoma*. Biochem Biophys Res Commun 2012; 422(4):764–9.
184. Tang JY, Hsi E, Huang YC, Hsu NCH, Yang WC, Chang HW, Chai CY, Chu PY. *Overexpression of Autophagy-Related 16-Like 1 in Patients with Oral Squamous Cell Carcinoma*. Pathol Oncol Res 2015; 21(2):301–5.
185. Weng J, Wang C, Wang Y, Tang H, Liang J, Liu X, Huang H, Hou J. *Beclin1 inhibits proliferation, migration and invasion in tongue squamous cell carcinoma cell lines*. Oral Oncol 2014; 50(10):983-90.
186. Tang JY, Fang YY, Edward H, Huang YC, Hsu NCH, Yang WC, Chang HW, Chai CY, Chu PY. *Immunopositivity of Beclin-1 and ATG5 as indicators of survival and disease recurrence in oral squamous cell carcinoma*. Anticancer Res 2013; 33(12):5611–6.
187. Tan YQ, Zhang J, Zhou G. *Autophagy and its implication in human oral diseases*. Autophagy 2017; 13(2): 225–236.
188. Tang JY, Hsi E, Huang YC, Hsu NCH, Chen YK, Chu PY, Chai CY. *ATG9A overexpression is associated with disease recurrence and poor survival in patients with oral squamous cell carcinoma*. Virchows Arch 2013; 463: 737–742.
189. Sui X, Chen R, Wang Z, Huang Z, Kong N, Zhang M, Han W, Lou F, Yang J,

Zhang Q, Wang X, He C, Pan H. *Autophagy and chemotherapy resistance: A promising therapeutic target for cancer treatment*. Cell Death Dis 2013; 4: 1–12.
190. Debnath J, Baehrecke EH, Kroemer G. *Does autophagy contribute to cell death?* Autophagy 2005; 1: 66–74.
191. Quan HY, Zhou LJ, Li A di, Zhang ZB. *Mechanism of chloroquine in promoting sensitivity of chemotherapeutics in oral squamous cell carcinoma CAL-27 cell line to cisplatin*. Shanghai Kou Qiang Yi Xue 2015; 24(1):30–6.
192. Liu D, Yang Y, Liu Q, Wang J. *Inhibition of autophagy by 3-MA potentiates cisplatin-induced apoptosis in esophageal squamous cell carcinoma cells*. Med Oncol 2011; 28(1):105–11.
193. Zhao XG, Sun RJ, Yang XY, Liu DY, Lei DP, Jin T, Pan XL. *Chloroquine-enhanced efficacy of cisplatin in the treatment of hypopharyngeal carcinoma in xenograft mice*. PLoS One 2015; 10(4): e0126147.
194. Jiang L, Huang S, Zhang D, Zhang B, Li K, Li W, Zhang S, Zhang W, Zheng P. *Inhibition of autophagy augments chemotherapy in human salivary adenoid cystic carcinoma*. J Oral Pathol Med 2014; 43(4):265-72.
195. Tsai CW, Lai FJ, Sheu HM, et al. *WWOX suppresses autophagy for inducing apoptosis in methotrexate-treated human squamous cell carcinoma*. Cell Death Dis 2013; 4(9):e792.
196. Han HY, Kim H, Jeong SH, Lim DS, Ryu MH. *Sulfasalazine induces autophagic cell death in oral cancer cells via Akt and ERK pathways*. Asian Pacific J Cancer Prev 2014; 15(16):6939-44.
197. Chu SC, Hsieh YS, Yu CC, Lai YY, Chen PN. *Thymoquinone induces cell death in human squamous carcinoma cells via caspase activation-dependent apoptosis and LC3-II activation-dependent autophagy*. PLoS One 2014; 9(7):e101579.
198. Huang AC, Lien JC, Lin MW, Yang JS, Wu PP, Chang SJ, Lai TY. *Tetrandrine induces cell death in SAS human oral cancer cells through caspase activation-dependent apoptosis and LC3-I and LC3-II activation-dependent autophagy*. Int J Oncol 2013; 43(2):485-94.
199. Zhang R, Wang R, Chen Q, Chang H. *Inhibition of autophagy using 3-methyladenine increases cisplatin-induced apoptosis by increasing endoplasmic reticulum stress in U251 human glioma cells.* Mol Med Rep 2015; 12: 1727–32.
200. Li L, Xie W, Pan D, Chen H, Zhang L. *Inhibition of autophagy by bafilomycin A1 promotes chemosensitivity of gastric cancer cells*. Tumor Biol 2016; 37: 653–659.
201. Li J, Hou N, Faried A, Tsutsumi S, Kuwano H. *Inhibition of autophagy augments 5-fluorouracil chemotherapy in human colon cancer in vitro and in vivo model*. Eur J Cancer 2010; 46(10):1900–9.
202. Chude CI, Amaravadi RK. *Targeting Autophagy in Cancer: Update on Clinical Trials and Novel Inhibitors.* Int J Mol Sci 2017; 18(6): 1279.
203. Goldberg SB, Supko JG, Neal JW, Muzikansky A, Digumarthy S, Fidias P, Temel JS, Heist RS, Shaw AT, McCarthy PO, Lynch TJ, Sharma S, Settleman JE, Sequist L V. *A phase I study of erlotinib and hydroxychloroquine in advanced non-small-cell lung cancer.* J Thorac Oncol 2012; 7: 1602–8.
204. Wolpin BM, Rubinson DA, Wang X, et al. *Phase II and Pharmacodynamic Study of Autophagy Inhibition Using Hydroxychloroquine in Patients With Metastatic Pancreatic Adenocarcinoma*. Oncologist 2014; 19: 637–638.
205. Rubinstein AD, Kimchi A. *Life in the balance - A mechanistic view of the crosstalk between autophagy and apoptosis*. J Cell Sci 2012; 125: 5259–5268.
206. Eisenberg-Lerner A, Bialik S, Simon HU, Kimchi A. *Life and death partners: Apoptosis, autophagy and the cross-talk between them*. Cell Death Differ 2009;

16: 966–975.
207. Zhao GX, Pan H, Ouyang DY, He XH. *The critical molecular interconnections in regulating apoptosis and autophagy*. Ann Med 2015; 47: 305–315.
208. Menon MB, Dhamija S. *Beclin 1 phosphorylation - at the center of autophagy regulation*. Front Cell Dev Biol 2018; 6: 137.
209. Pattingre S, Tassa A, Qu X, Garuti R, Xiao HL, Mizushima N, Packer M, Schneider MD, Levine B. *Bcl-2 antiapoptotic proteins inhibit Beclin 1-dependent autophagy*. Cell 2005; 122: 927–939.
210. Marquez RT, Xu L. *Bcl-2:Beclin 1 complex: multiple, mechanisms regulating autophagy/apoptosis toggle switch.* Am J Cancer Res 2012; 2: 214–21.
211. Maiuri MC, Le Toumelin G, Criollo A, Rain JC, Gautier F, Juin P, Tasdemir E, Pierron G, Troulinaki K, Tavernarakis N, Hickman JA, Geneste O, Kroemer G. *Functional and physical interaction between Bcl-XL and a BH3-like domain in Beclin-1*. EMBO J 2007; 26(10):2527-39.
212. Elgendy M, Sheridan C, Brumatti G, Martin SJ. *Oncogenic Ras-Induced Expression of Noxa and Beclin-1 Promotes Autophagic Cell Death and Limits Clonogenic Survival*. Mol Cell 2011; 42: 23–35.
213. Tang D, Kang R, Livesey KM, Cheh CW, Farkas A, Loughran P, Hoppe G, Bianchi ME, Tracey KJ, Zeh HJ, Lotze MT. *Endogenous HMGB1 regulates autophagy*. J Cell Biol 2010; 190(5):881–92.
214. Bellot G, Garcia-Medina R, Gounon P, Chiche J, Roux D, Pouyssegur J, Mazure NM. *Hypoxia-Induced Autophagy Is Mediated through Hypoxia-Inducible Factor Induction of BNIP3 and BNIP3L via Their BH3 Domains*. Mol Cell Biol 2009; 29(10):2570-81.
215. Sui X, Kong N, Ye L, Han W, Zhou J, Zhang Q, He C, Pan H. *p38 and JNK MAPK pathways control the balance of apoptosis and autophagy in response to chemotherapeutic agents*. Cancer Lett 2014; 344: 174–179.
216. Zalckvar E, Berissi H, Mizrachy L, Idelchuk Y, Koren I, Eisenstein M, Sabanay H, Pinkas-Kramarski R, Kimchi A. *DAP-kinase-mediated phosphorylation on the BH3 domain of beclin 1 promotes dissociation of beclin 1 from Bcl-XL and induction of autophagy*. EMBO Rep 2009; 10: 285–292.
217. Shiloh R, Gilad Y, Ber Y, Eisenstein M, Aweida D, Bialik S, Cohen S, Kimchi A. *Non-canonical activation of DAPK2 by AMPK constitutes a new pathway linking metabolic stress to autophagy*. Nat Commun 2018; 9(1):1759.
218. Gurkar AU, Chu K, Raj L, Bouley R, Lee SH, Kim YB, Dunn SE, Mandinova A, Lee SW. *Identification of ROCK1 kinase as a critical regulator of Beclin1-mediated autophagy during metabolic stress*. Nat Commun; 4.
219. Maejima Y, Kyoi S, Zhai P, Liu T, Li H, Ivessa A, Sciarretta S, Del Re DP, Zablocki DK, Hsu CP, Lim DS, Isobe M, Sadoshima J. *Mst1 inhibits autophagy by promoting the interaction between beclin1 and Bcl-2*. Nat Med 2013; 19: 1478–1488.
220. Chang NC, Nguyen M, Germain M, Shore GC. *Antagonism of Beclin 1-dependent autophagy by BCL-2 at the endoplasmic reticulum requires NAF-1*. EMBO J 2010; 29(3):606–18.
221. Wei Y, Sinha S, Levine B. *Dual role of JNK1-mediated phosphorylation of Bcl-2 in autophagy and apoptosis regulation*. Autophagy 2008; 4(7): 949–951.
222. Adams JM, Cory S. *Bcl-2-regulated apoptosis: mechanism and therapeutic potential*. Curr Opin Immunol 2007; 19: 488–496.
223. Martinou JC, Youle RJ. *Mitochondria in Apoptosis: Bcl-2 Family Members and Mitochondrial Dynamics*. Dev Cell 2011; 21: 92–101.

224. Wu H, Che X, Zheng Q, Wu A, Pan K, Shao A, Wu Q, Zhang J, Hong Y. *Caspases: A molecular switch node in the crosstalk between autophagy and apoptosis*. Int J Biol Sci 2014; 10: 1072–1083.
225. Maiuri MC, Zalckvar E, Kimchi A, Kroemer G. *Self-eating and self-killing: Crosstalk between autophagy and apoptosis*. Nat Rev Mol Cell Biol 2007; 8: 741–752.
226. Sadasivan S, Waghray A, Larner SF, Dunn WA, Hayes RL, Wang KKW. *Amino acid starvation induced autophagic cell death in PC-12 cells: Evidence for activation of caspase-3 but not calpain-1*. Apoptosis 2006; 1573–82.
227. Zhu Y, Zhao L, Liu L, Gao P, Tian W, Wang X, Jin H, Xu H, Chen Q. *Beclin 1 cleavage by caspase-3 inactivates autophagy and promotes apoptosis*. Protein Cell 2010; 1(5):468-77.
228. Gordy C, He YW. *The crosstalk between autophagy and apoptosis: Where does this lead?* Protein Cell 2012; 3: 17–27.
229. Wirawan E, Vande Walle L, Kersse K, Cornelis S, Claerhout S, Vanoverberghe I, Roelandt R, De Rycke R, Verspurten J, Declercq W, Agostinis P, Vanden Berghe T, Lippens S, Vandenabeele P. *Caspase-mediated cleavage of Beclin-1 inactivates Beclin-1-induced autophagy and enhances apoptosis by promoting the release of proapoptotic factors from mitochondria*. Cell Death Dis 2010; 1: e18-10.
230. Betin VMS, Lane JD. *Caspase cleavage of Atg4D stimulates GABARAP-L1 processing and triggers mitochondrial targeting and apoptosis*. J Cell Sci 2009; 2554–66.
231. You M, Savaraj N, Kuo MT, Wangpaichitr M, Varona-Santos J, Wu C, Nguyen DM, Feun L. *TRAIL induces autophagic protein cleavage through caspase activation in melanoma cell lines under arginine deprivation*. Mol Cell Biochem 2013; 374(1-2):181-90.
232. Norman JM, Cohen GM, Bampton ETW. *The in vitro cleavage of the hAtg proteins by cell death proteases*. Autophagy 2010; 6(8):1042-56.
233. Oral O, Oz-Arslan D, Itah Z, Naghavi A, Deveci R, Karacali S, Gozuacik D. *Cleavage of Atg3 protein by caspase-8 regulates autophagy during receptor-activated cell death*. Apoptosis 2012; 17(8):810-20.
234. Han J, Hou W, Goldstein LA, Stolz DB, Watkins SC, Rabinowich H. *A complex between Atg7 and caspase-9: A novel mechanism of cross-regulation between autophagy and apoptosis*. J Biol Chem 2014; 289: 6485–6497.
235. Fan YJ, Zong WX. *The cellular decision between apoptosis and autophagy*. Chin J Cancer 2013; 32: 121–129.
236. Radoshevich L, Debnath J. *ATG12-ATG3 and mitochondria*. Autophagy 2011; 7(1): 109–111.
237. Yousefi S, Perozzo R, Schmid I, Ziemiecki A, Schaffner T, Scapozza L, Brunner T, Simon HU. *Calpain-mediated cleavage of Atg5 switches autophagy to apoptosis*. Nat Cell Biol 2006; 8(10):1124-32.
238. Rubinstein AD, Eisenstein M, Ber Y, Bialik S, Kimchi A. *The autophagy protein atg12 associates with antiapoptotic Bcl-2 family members to promote mitochondrial apoptosis*. Mol Cell 2011; 44(5):698-709.
239. Liu K, Lou J, Wen T, Yin J, Xu B, Ding W, Wang A, Liu D, Zhang C, Chen D, Li N. *Depending on the stage of hepatosteatosis, p53 causes apoptosis primarily through either DRAM-induced autophagy or BAX*. Liver Int 2013; 33(10):1566-74.
240. Lee JS, Li Q, Lee JY, Lee SH, Jeong JH, Lee HR, Chang H, Zhou FC, Gao SJ, Liang C, Jung JU. *FLIP-mediated autophagy regulation in cell death control*. Nat

Cell Biol 2009; 11: 1355–1362.
241. Su M, Mei Y, Sinha S. *Role of the crosstalk between autophagy and apoptosis in cancer*. J Oncol 2013; 2013:102735.
242. Yin X, Cao L, Peng Y, Tan Y, Xie M, Kang R, Livesey KM, Tang D. *A critical role for UVRAG in apoptosis*. Autophagy 2011; 7(10): 1242–1244.
243. Takahashi Y, Coppola D, Matsushita N, Cualing HD, Sun M, Sato Y, Liang C, Jung JU, Cheng JQ, Mulé JJ, Pledger WJ, Wang HG. *Bif-1 interacts with Beclin 1 through UVRAG and regulates autophagy and tumorigenesis*. Nat Cell Biol 2007; 9(10):1142-51.
244. Ruppert SM, Li W, Zhang G, Carlson AL, Limaye A, Durum SK, Khaled AR. *The major isoforms of Bim contribute to distinct biological activities that govern the processes of autophagy and apoptosis in interleukin-7 dependent lymphocytes*. Biochim Biophys Acta - Mol Cell Res 2012; 1823(10):1877–93.
245. Rahmani M, Aust MM, Attkisson E, Williams DC, Ferreira-Gonzalez A, Grant S. *Inhibition of Bcl-2 antiapoptotic members by obatoclax potently enhances sorafenib-induced apoptosis in human myeloid leukemia cells through a Bim-dependent process*. Blood 2012; 119(25): 6089–6098.
246. Luo S, Garcia-Arencibia M, Zhao R, Puri C, Toh PPC, Sadiq O, Rubinsztein DC. *Bim Inhibits Autophagy by Recruiting Beclin 1 to Microtubules*. Mol Cell 2012; 47(3):359-70.
247. Sosa V, Moliné T, Somoza R, Paciucci R, Kondoh H, LLeonart ME. *Oxidative stress and cancer: An overview*. Ageing Res Rev 2013; 12: 376–390.
248. Burton GJ, Jauniaux E. *Oxidative stress*. Best Pract Res Clin Obstet Gynaecol 2011; 25(3): 287–299.
249. El-Bahr SM. *Biochemistry of Free Radicals and Oxidative Stress*. Sci Int 2013; 1: 111–117.
250. Leone A, Roca MS, Ciardiello C, Costantini S, Budillon A. *Oxidative Stress Gene Expression Profile Correlates with Cancer Patient Poor Prognosis: Identification of Crucial Pathways Might Select Novel Therapeutic Approaches*. Oxid Med Cell Longev 2017; 2017:2597581.
251. Snezhkina A V., Kudryavtseva A V., Kardymon OL, Savvateeva M V., Melnikova N V., Krasnov GS, Dmitriev AA. *ROS Generation and Antioxidant Defense Systems in Normal and Malignant Cells*. Oxid Med Cell Longev 2019; 2019: 6175804.
252. Vásquez-Vivar J, Kalyanaraman B, Kennedy MC. *Mitochondrial aconitase is a source of hydroxyl radical. An electron spin resonance investigation*. J Biol Chem 2000; 275(19):14064–9.
253. Marengo B, Nitti M, Furfaro AL, Colla R, Ciucis C De, Marinari UM, Pronzato MA, Traverso N, Domenicotti C. *Redox homeostasis and cellular antioxidant systems: Crucial players in cancer growth and therapy*. Oxid Med Cell Longev 2016; 2016: 6235641.
254. Bigarella CL, Liang R, Ghaffari S. *Stem cells and the impact of ROS signaling*. Dev 2014; 141(22):4206–18.
255. Birben E, Sahiner UM, Sackesen C, Erzurum S, Kalayci O. *Oxidative stress and antioxidant defense*. World Allergy Organ J 2012; 5(1):9-19.
256. Kumari S, Badana AK, Murali Mohan G, Shailender G, Malla RR. *Reactive Oxygen Species: A Key Constituent in Cancer Survival*. Biomark Insights 2018; 13: 1177271918755391.
257. Griffith OW. *Biologic and pharmacologic regulation of mammalian glutathione synthesis*. Free Radic Biol Med 1999; 27(9-10):922-35.

258. Habtemariam S. *The Nrf2/HO-1 Axis as Targets for Flavanones: Neuroprotection by Pinocembrin, Naringenin, and Eriodictyol*. Oxid Med Cell Longev 2019; 2019:4724920.
259. Liou GY, Storz P. *Reactive oxygen species in cancer*. Free Radic Res 2010; 44(5): 10.3109/10715761003667554.
260. Kesarwala A, Krishna M, Mitchell J. *Oxidative Stress in Oral Diseases*. Physiol Behav 2017; 176: 139–148.
261. Singh A, Misra V, Thimmulappa RK, Lee H, Ames S, Hoque MO, Herman JG, Baylin SB, Sidransky D, Gabrielson E, Brock M V., Biswal S. *Dysfunctional KEAP1-NRF2 interaction in non-small-cell lung cancer*. PLoS Med 2006; 3(10):e420.
262. Chen Z, Seimiya H, Naito M, Mashima T, Kizaki A, Dan S, Imaizumi M, Ichijo H, Miyazono K, Tsuruo T. *ASK1 mediates apoptotic cell death induced by genotoxic stress*. Oncogene 1999; 18(1):173-80.
263. Ishikawa K, Takenaga K, Akimoto M, Koshikawa N, Yamaguchi A, Imanishi H, Nakada K, Honma Y, Hayashi JI. *ROS-generating mitochondrial DNA mutations can regulate tumor cell metastasis*. Science (80-) 2008; 320(5876):661–4.
264. Simon HU, Haj-Yehia A, Levi-Schaffer F. *Role of reactive oxygen species (ROS) in apoptosis induction*. Apoptosis 2000; 5(5):415-8.
265. Redza-Dutordoir M, Averill-Bates DA. *Activation of apoptosis signalling pathways by reactive oxygen species*. Biochim Biophys Acta - Mol Cell Res 2016; 1863: 2977–2992.
266. Abdalla MY. *Glutathione as Potential Target for Cancer Therapy ; More or Less is Good?* Jordan J Biol Sci 2011; 4(3)119-124.
267. Goodwin G. *Relationships Between Neuroendocrine Differentiation and Sensitivity to γ-Radiation in Culture Line OH-1 of Human Small Cell Lung Carcinoma*. Cancer Res 1982; 42(4):1361–7.
268. Carney DN, Mitchell JB, Kinsella TJ. *In vitro radiation and chemotherapy sensitivity of established cell lines of human small cell lung cancer and its large cell morphological variants*. Cancer Res 1983; 43(6):2806–11.
269. Chio IIC, Jafarnejad SM, Ponz-Sarvise M, et al. *NRF2 Promotes Tumor Maintenance by Modulating mRNA Translation in Pancreatic Cancer*. Cell 2016; 166: 963–976.
270. Warburg O. *On the origin of cancer cells*. Science (80-) 1956; 123(3191):309–14.
271. Kim JW, Dang C V. *Cancer's molecular sweet tooth and the warburg effect*. Cancer Res 2006; 66(18):8927–30.
272. Liu Y, Zha L, Li B, Zhang L, Yu T, Li L. *Correlation between superoxide dismutase 1 and 2 polymorphisms and susceptibility to oral squamous cell carcinoma*. Exp Ther Med 2013; 7(1): 171–178.
273. Chen CL, Chi CW, Liu TY. *Hydroxyl radical formation and oxidative dna damage induced by areca quid in vivo*. J Toxicol Environ Heal - Part A 2002; 65(3-4):327-36.
274. Cao JY, Mansouri S, Frappier L. *Changes in the Nasopharyngeal Carcinoma Nuclear Proteome Induced by the EBNA1 Protein of Epstein-Barr Virus Reveal Potential Roles for EBNA1 in Metastasis and Oxidative Stress Responses*. J Virol 2012; 86(1):382-94.
275. Kuo MT, Chen HHW. *Role of glutathione in the regulation of cisplatin resistance in cancer chemotherapy*. Met Based Drugs 2010; 2010: 430939.
276. Li PD, Liu Z, Cheng TT, Luo WG, Yao J, Chen J, Zou ZW, Chen LL, Ma C, Dai XF. *Redox-dependent modulation of metformin contributes to enhanced sensitivity*

of esophageal squamous cell carcinoma to cisplatin. Oncotarget 2017; 8(37): 62057–62068.
277. Wang F, Liu S, Shen Y, Zhuang R, Xi J, Fang H, Pan X, Sun J, Cai Z. *Protective effects of N-acetylcysteine on cisplatin-induced oxidative stress and DNA damage in HepG2 cells.* Exp Ther Med 2014; 8: 1939–1945.
278. Spagnuolo G, D'Antò V, Cosentino C, Schmalz G, Schweikl H, Rengo S. *Effect of N-acetyl-l-cysteine on ROS production and cell death caused by HEMA in human primary gingival fibroblasts*. Biomaterials 2006; 27: 1803–1809.
279. Calvert P, Yao KS, Hamilton TC, O'Dwyer PJ. *Clinical studies of reversal of drug resistance based on glutathione*. Chem Biol Interact 1998; 111-112:213–24.
280. Jiang T, Chen N, Zhao F, Wang XJ, Kong B, Zheng W, Zhang DD. *High levels of Nrf2 determine chemoresistance in type II endometrial cancer*. Cancer Res 2010; 70(13):5486-96.
281. Marinello PC, Panis C, Silva TNX, Binato R, Abdelhay E, Rodrigues JA, Mencalha AL, Lopes NMD, Luiz RC, Cecchini R, Cecchini AL. *Metformin prevention of doxorubicin resistance in MCF-7 and MDA-MB-231 involves oxidative stress generation and modulation of cell adaptation genes*. Sci Rep 2019; 9: 2045–2322.
282. Hayes JD, McLellan LI. *Glutathione and glutathione-dependent enzymes represent a co-ordinately regulated defence against oxidative stress*. Free Radic Res 1999; 31(4):273-300.
283. Glasauer A, Chandel NS. *Targeting antioxidants for cancer therapy*. Biochem Pharmacol 2014; 92(1):90-101.
284. Li Q, Yin X, Wang W, Zhan M, Zhao B, Hou Z, Wang J. *The effects of buthionine sulfoximine on the proliferation and apoptosis of biliary tract cancer cells induced by cisplatin and gemcitabine*. Oncol Lett 2016; 11(1): 474-480.
285. Rocha CRR, Garcia CCM, Vieira DB, Quinet A, De Andrade-Lima LC, Munford V, Belizário JE, Menck CFM. *Glutathione depletion sensitizes cisplatin- and temozolomide-resistant glioma cells in vitro and in vivo*. Cell Death Dis 2014; 5(10):e1505.
286. Marengo B, De Ciucis C, Verzola D, Pistoia V, Raffaghello L, Patriarca S, Balbis E, Traverso N, Cottalasso D, Pronzato MA, Marinari UM, Domenicotti C. *Mechanisms of BSO (L-buthionine-S,R-sulfoximine)-induced cytotoxic effects in neuroblastoma*. Free Radic Biol Med 2008; 44(3):474-82.
287. Ma X, Zhang J, Liu S, Huang Y, Chen B, Wang D. *Nrf2 knockdown by shRNA inhibits tumor growth and increases efficacy of chemotherapy in cervical cancer*. Cancer Chemother Pharmacol 2012; 69(2):485-94.
288. Xu Z, Huang CM, Shao Z, Zhao XP, Wang M, Yan TL, Zhou XC, Jiang EH, Liu K, Shang ZJ. *Autophagy induced by areca nut extract contributes to decreasing cisplatin toxicity in oral squamous cell carcinoma cells: Roles of reactive oxygen species/AMPK signaling*. Int J Mol Sci 2017; 18(3):524.
289. Li B, Lu M, Jiang XX, Pan MX, Mao JW, Chen M. *Inhibiting reactive oxygen species-dependent autophagy enhanced baicalein-induced apoptosis in oral squamous cell carcinoma*. J Nat Med 2017; 71(2):433-441.
290. Zhao L, Jiang L, Meng Z, Liu J, Chen H, Li K, Zhang B. *3-MA sensitize oral squamous carcinoma cells to cisplatin by antagonizing cisplatin-initiated autophagy*. Int J Clin Exp Pathol 2016; 9: 11599–11606.
291. Lin F, Gao L, Su Z, Cao X, Zhan Y, Li Y, Zhang B. *Knockdown of KPNA2 inhibits autophagy in oral squamous cell carcinoma cell lines by blocking p53 nuclear translocation*. Oncol Rep 2018; 40(1):179-194.

292. Fang L, Wang H, Zhou L, Yu D. *FOXO3a reactivation mediates the synergistic cytotoxic effects of rapamycin and cisplatin in oral squamous cell carcinoma cells*. Toxicol Appl Pharmacol 2011; 251(1):8–15.
293. Rikiishi H, Shinohara F, Sato T, Sato Y, Suzuki M, Echigo S. *Chemosensitization of oral squamous cell carcinoma cells to cisplatin by histone deacetylase inhibitor, suberoylanilide hydroxamic acid*. Int J Oncol 2007; 30: 1181–1188.
294. Xue DF, Pan ST, Huang G, Qiu JX. *ROS enhances the cytotoxicity of cisplatin by inducing apoptosis and autophagy in tongue squamous cell carcinoma cells*. Int J Biochem Cell Biol 2020; 122:105732.
295. Kim JY, Cho TJ, Woo BH, Choi KU, Lee CH, Ryu MH, Park HR. *Curcumin-induced autophagy contributes to the decreased survival of oral cancer cells*. Arch Oral Biol 2012; 57(8):1018–25.
296. Chen YT, Hsieh MJ, Chen PN, Weng CJ, Yang SF, Lin CW. *Erianin Induces Apoptosis and Autophagy in Oral Squamous Cell Carcinoma Cells*. Am J Chin Med 2020; 48(1):183-200.
297. Park B-S, Choi N-E, Lee JH, Kang H-M, Yu S-B, Kim H-J, Kang H-K, Kim I-R. *Crosstalk between Fisetin-induced Apoptosis and Autophagy in Human Oral Squamous Cell Carcinoma*. J Cancer 2019; 10: 138–146.
298. Cheng MF, Lin SR, Tseng FJ, Huang YC, Tsai MJ, Fu YS, Weng CF. *The autophagic inhibition oral squamous cell carcinoma cancer growth of 16-hydroxy-cleroda-3,14-dine-15,16-olide*. Oncotarget 2017; 8(45): 78379–78396.
299. Sulkshane P, Teni T. *BH3 mimetic Obatoclax (GX15-070) mediates mitochondrial stress predominantly via MCL-1 inhibition and induces autophagy-dependent necroptosis in human oral cancer cells*. Oncotarget 2017; 8(36): 60060–60079.
300. Pan ST, Qin Y, Zhou ZW, He ZX, Zhang X, Yang T, Yang YX, Wang D, Zhou SF, Qiu JX. *Plumbagin suppresses epithelial to mesenchymal transition and stemness via inhibiting Nrf2-mediated signaling pathway in human tongue squamous cell carcinoma cells*. Drug Des Devel Ther 2015; 9:5511-51.
301. Yu S Bin, Kang HM, Park DB, Park BS, Kim IR. *Cudraxanthone D Regulates Epithelial-Mesenchymal Transition by Autophagy Inhibition in Oral Squamous Cell Carcinoma Cell Lines*. Evidence-based Complement Altern Med 2019; 2019:5213028.
302. Masui A, Hamada M, Kameyama H, Wakabayashi K, Takasu A, Imai T, Iwai S, Yura Y. *Autophagy as a Survival Mechanism for Squamous Cell Carcinoma Cells in Endonuclease G-Mediated Apoptosis*. PLoS One 2016; 11: e0162786.
303. Yu CI, Chen CY, Liu W, Chang PC, Huang CW, Han KF, Lin IP, Lin MY, Lee CH. *Sandensolide induces oxidative stress-mediated apoptosis in oral cancer cells and in zebrafish xenograft model*. Mar Drugs 2018; 16(10):387.
304. Zhang L, Zhang W, Wang YF, Liu B, Zhang WF, Zhao YF, Kulkarni AB, Sun ZJ. *Dual induction of apoptotic and autophagic cell death by targeting survivin in head neck squamous cell carcinoma*. Cell Death Dis 2015; 6(5):e1771.
305. Li KL, Wang YF, Qin JR, Wang F, Yang YT, Zheng LW, Li MH, Kong J, Zhang W, Yang HY. *Rapamycin enhances the antiangiogenesis and anti-proliferation ability of YM155 in oral squamous cell carcinoma*. Tumor Biol 2017; 39(6):1010428317706213.
306. Rheinwald JG, Beckett M a. *Tumorigenic Keratinocyte Lines Requiring Anchorage and Fibroblast Support Cultured from Human Squamous Cell Carcinomas Tumorigenic Keratinocyte Lines Requiring Anchorage and Fibroblast Support Cultured from Human Squamous Cell Carcinomas*. Cancer Res 1981; 1657–1663.

307. Barretina J, Caponigro G, Stransky N, et al. *The Cancer Cell Line Encyclopedia enables predictive modelling of anticancer drug sensitivity*. Nature 2012; 483(7391): 603–607.
308. Franken NAP, Rodermond HM, Stap J, Haveman J, van Bree C. *Clonogenic assay of cells in vitro*. Nat Protoc 2006; 1, 2315–2319.
309. Bleloch J. *CytoSMART | clonogenic assays: what, why and how*. 2020; https://www.cytosmart.com/resources/clonogenic-ass.
310. Demchenko AP. *Beyond annexin V: Fluorescence response of cellular membranes to apoptosis*. Cytotechnology 2013; 65(2): 157–172.
311. Guo S, Liang Y, Murphy SF, Huang A, Shen H, Kelly DF, Sobrado P, Sheng Z. *A rapid and high content assay that measures cyto-ID-stained autophagic compartments and estimates autophagy flux with potential clinical applications*. Autophagy 2015; 11: 560.
312. Yoon D, Lee M-H, Cha D. *Measurement of Intracellular ROS in Caenorhabditis elegans Using 2',7'-Dichlorodihydrofluorescein Diacetate*. Bio-Protocol 2018; 8(6): e2774.
313. Tahmasebi E, Alikhani M, Yazdanian A, Yazdanian M, Tebyanian H, Seifalian A. *The current markers of cancer stem cell in oral cancers*. Life Sci 2020; 249: 117483.
314. Todoroki K, Ogasawara S, Akiba J, Nakayama M, Naito Y, Seki N, Kusukawa J, Yano H. *CD44v3+/CD24- cells possess cancer stem cell-like properties in human oral squamous cell carcinoma*. Int J Oncol 2016; 48(1): 99–109.
315. Almeida R, Allshire RC. *RNA silencing and genome regulation*. Trends Cell Biol 2005; 15(5):251–8.
316. Hajian-Tilaki K. *Receiver operating characteristic (ROC) curve analysis for medical diagnostic test evaluation*. Casp J Intern Med 2013; 4(2): 627–635.
317. Zou KH, O'Malley AJ, Mauri L. *Receiver-operating characteristic analysis for evaluating diagnostic tests and predictive models*. Circulation 2007; 115(5):654–7.
318. McGurk M, Chan C, Jones J, O'Regan E, Sherriff M. *Delay in diagnosis and its effect on outcome in head and neck cancer*. Br J Oral Maxillofac Surg 2005; 43(4):281–4.
319. Robert BM, Dakshinamoorthy M, Brindha GR, Dhandapani M, Thangaiyan R, Muthusamy G, Nirmal RM, Prasad NR. *Predicting Tumor Sensitivity to Chemotherapeutic Drugs in Oral Squamous Cell Carcinoma Patients*. Sci Rep 2018; 8, 15545.
320. Carmen A, Menéndez JC. *Medicinal Chemistry of Anticancer Drugs (Second Edition)*. In: *Medicinal Chemistry of Anticancer Drugs*. 2015, pp. 197–241.
321. Wang D, Lippard SJ. *Cellular processing of platinum anticancer drugs*. Nat Rev Drug Discov 2005; 4: 307–320.
322. Macciò A, Madeddu C. *Cisplatin: An old drug with a newfound efficacy-from mechanisms of action to cytotoxicity*. Expert Opin Pharmacother 2013; 14(13):1839-57.
323. Shaloam D, Tchounwou PB. *Cisplatin in cancer therapy: Molecular mechanisms of action*. Eur J Pharmacol 2014; 740: 364–378.
324. Delou, Souza, Souza, Borges. *Highlights in Resistance Mechanism Pathways for Combination Therapy*. Cells 2019; 8: 1013.
325. Huang GC, Liu SY, Lin MH, Kuo YY, Liu YC. *The synergistic cytotoxicity of cisplatin and Taxol in killing oral squamous cell carcinoma*. Jpn J Clin Oncol 2004; 34(9):499-504.

326. Rao R, Suhas SS, Shenoy V, Hegde MC, Prasad V, Prasad K. *Induction chemotherapy with cisplatin and 5-fluorouracil in advanced head and neck cancers: A short term response evaluation*. J Clin Diagnostic Res 2015; 9(10): XC08–XC12.
327. Klionsky DJ. *Autophagy: From phenomenology to molecular understanding in less than a decade*. Nat Rev Mol Cell Biol 2007; 8(11):931–7.
328. Zhao Y, Butler EB, Tan M. *Targeting cellular metabolism to improve cancer therapeutics*. Cell Death Dis 2013; 4(3):e532.
329. Wu WKK, Coffelt SB, Cho CH, Wang XJ, Lee CW, Chan FKL, Yu J, Sung JJY. *The autophagic paradox in cancer therapy*. Oncogene 2012; 31(8):939-53.
330. Czekanska EM. *Assessment of cell proliferation with resazurin-based fluorescent dye.* Methods Mol Biol 2011; 740:27–32.
331. Hartner L. *Chemotherapy for Oral Cancer*. Dent Clin North Am 2018; 62: 87–97.
332. Mazumder S, Plesea D, Almasan A. *Caspase-3 activation is a critical determinant of genotoxic stress-induced apoptosis*. Methods Mol Biol 2007; 414:13–21.
333. Klionsky DJ, Abdelmohsen K, Abe A, Abedin J, Abeliovich H, Bartolom A, Beckham JD, Bertolotti A, Bess AS, Bozhkov P V. *Guidelines for the use and interpretation of assays for monitoring autophagy (3rd edition)*. Autophagy 2016; 12: 1–222.
334. Yu L, Gu C, Zhong D, Shi L, Kong Y, Zhou Z, Liu S. *Induction of autophagy counteracts the anticancer effect of cisplatin in human esophageal cancer cells with acquired drug resistance*. Cancer Lett 2014; 355: 34–45.
335. Mizushima N, Yoshimori T, Levine B. *Methods in mammalian autophagy research.* Cell 2010; 140: 313–26.
336. Zhang X, Chen S, Huang K, Le W. *Why should autophagic flux be assessed?* Acta Pharmacol Sin 2013; 34: 595–9.
337. Zhu J, Zheng Y, Zhang H, Zhu J, Sun H. *Low concentration of chloroquine enhanced efficacy of cisplatin in the treatment of human ovarian cancer dependent on autophagy.* Am J Transl Res 2017; 9: 4046–4058.
338. Circu M, Cardelli J, Barr M, Byrne KO, Mills G. *Modulating lysosomal function through lysosome membrane permeabilization or autophagy suppression restores sensitivity to cisplatin in refractory non-small-cell lung cancer cells*. PLoS One 2017; 12(9):e0184922.
339. Liao Y, Guo Z, Xia X, Liu Y, Huang C, Jiang L, Wang X, Liu J, Huang H. *Inhibition of EGFR signaling with Spautin-1 represents a novel therapeutics for prostate cancer*. J Exp Clin Cancer Res 2019; 38: 157.
340. Pasquier B. *SAR405, a PIK3C3/VPS34 inhibitor that prevents autophagy and synergizes with MTOR inhibition in tumor cells*. Autophagy 2015; 11(4):725–6.
341. Steinman RM, Mellman IS, Muller WA, Cohn ZA. *Endocytosis and the recycling of plasma membrane*. J Cell Biol 1983; 96(1): 1–27.
342. Yamamoto A, Tagawa Y, Yoshimori T, Moriyama Y, Masaki R, Tashiro Y. *Bafilomycin A1 Prevents Maturation of Autophagic Vacuoles by Inhibiting Fusion between Autophagosomes and Lysosomes in Rat Hepatoma Cell Line, H-4-II-E Cells.* Cell Struct Funct 1998; 23(1):33-42.
343. Rubinsztein DC, Codogno P, Levine B. *Autophagy modulation as a potential therapeutic target for diverse diseases*. Nat Rev Drug Discov 2012; 11(9):709-30.
344. Martins WK, Baptista MS. *Autophagy Modulation for Organelle-Targeting Therapy*. In: *Autophagy in Current Trends in Cellular Physiology and Pathology*. InTech, 2016. 2016.
345. Fahmy AM, Labonté P. *The autophagy elongation complex (ATG5-12/16L1)*

positively regulates HCV replication and is required for wild-type membranous web formation. Sci Rep 2017; 7:40351.
346. Ye X, Zhou XJ, Zhang H. *Exploring the role of autophagy-related gene 5 (ATG5ATG5) yields important insights into autophagy in autoimmune/autoinflammatory diseases*. Front Immunol 2018; 9: 2334.
347. Xiong X, Wu M, Zhang H, et al. *Atg5 siRNA inhibits autophagy and enhances norcantharidin-induced apoptosis in hepatocellular carcinoma*. Int J Oncol 2015; 47: 1321–1328.
348. Wang Y, Xiong H, Liu D, Hill C, Ertay A, Li J, Zou Y, Miller P, White E, Downward J, Goldin RD, Yuan X, Lu X. *Autophagy inhibition specifically promotes epithelial-mesenchymal transition and invasion in RAS-mutated cancer cells*. Autophagy 2019; 15(5):886-899.
349. Jung S, Sielker S, Purcz N, Sproll C, Acil Y, Kleinheinz J. *Analysis of angiogenic markers in oral squamous cell carcinoma-gene and protein expression*. Head Face Med 2015; 11: 19.
350. Geng M, Wang L, Li P. *Correlation between chemosensitivity to anticancer drugs and Bcl-2 expression in gastric cancer.* Int J Clin Exp Pathol 2013; 6: 2554–9.
351. De Roock W, Claes B, Bernasconi D, et al. *Effects of KRAS, BRAF, NRAS, and PIK3CA mutations on the efficacy of cetuximab plus chemotherapy in chemotherapy-refractory metastatic colorectal cancer: A retrospective consortium analysis*. Lancet Oncol 2010; 11(8):753-62.
352. Lièvre A, Bachet JB, Le Corre D, Boige V, Landi B, Emile JF, Côté JF, Tomasic G, Penna C, Ducreux M, Rougier P, Penault-Llorca F, Laurent-Puig P. *KRAS mutation status is predictive of response to cetuximab therapy in colorectal cancer*. Cancer Res 2006; 66(8):3992–5.
353. Van Cutsem E, Köhne CH, Hitre E, et al. *Cetuximab and chemotherapy as initial treatment for metastatic colorectal cancer*. N Engl J Med 2009; 360(14):1408–17.
354. Mise Y, Zimmitti G, Shindoh J, Kopetz S, Loyer EM, Andreou A, Cooper AB, Kaur H, Aloia TA, Maru DM, Vauthey JN. *RAS Mutations Predict Radiologic and Pathologic Response in Patients Treated with Chemotherapy Before Resection of Colorectal Liver Metastases*. Ann Surg Oncol 2015; 22(3):834-842.
355. Perego P, Giarola M, Righetti SC, Supino R, Caserini C, Delia D, Pierotti MA, Miyashita T, Reed JC, Zunino F. *Association between cisplatin resistance and mutation of p53 gene and reduced bax expression in ovarian carcinoma cell systems.* Cancer Res 1996; 56: 556–62.
356. Liu C, Zhu Y, Lou W, Nadiminty N, Chen X, Zhou Q, Shi XB, deVere White RW, Gao AC. *Functional p53 determines docetaxel sensitivity in prostate cancer cells.* Prostate 2013; 73: 418–27.
357. Basu A, Soumya K. *Cellular Responses to Cisplatin-Induced DNA Damage*. Jounal of Nucleic Acids 2010; 10: 240–247.
358. Yang W, Soares J, Greninger P, et al. *Genomics of Drug Sensitivity in Cancer (GDSC): a resource for therapeutic biomarker discovery in cancer cells*. Nucleic Acids Res 2012; 41: D955–D961.
359. Aminuddin A, Ng PY, Leong CO, Chua EW. *Mitochondrial DNA alterations may influence the cisplatin responsiveness of oral squamous cell carcinoma*. Sci Rep 2020; 10(1):7885.
360. Wagner JM, Karnitz LM. *Cisplatin-induced DNA damage activates replication checkpoint signaling components that differentially affect tumor cell survival.* Mol Pharmacol 2009; 76: 208–14.
361. Velma V, Dasari SR, Tchounwou PB. *Low Doses of Cisplatin Induce Gene*

Alterations, Cell Cycle Arrest, and Apoptosis in Human Promyelocytic Leukemia Cells. Biomark Insights 2016; 11: 113–21.
362. Cummings BS, Schnellmann RG. *Cisplatin-Induced Renal Cell Apoptosis : Caspase 3-Dependent and -Independent Pathways*. J Pharmacol Exp Ther 2002; 302: 8–17.
363. Siddik ZH, Mims B, Lozano G, Thai G. *Independent pathways of p53 induction by cisplatin and X-rays in a cisplatin-resistant ovarian tumor cell line.* Cancer Res 1998; 58: 698–703.
364. Mizushima N. *The pleiotropic role of autophagy: From protein metabolism to bactericide*. Cell Death Differ 2005; 12 Suppl 2:1535-41.
365. Mizushima N. *Autophagy: Process and function*. Genes Dev 2007; 21(22):2861-73.
366. Barth S, Glick D, Macleod KF. *Autophagy: Assays and artifacts*. J Pathol 2010; 221: 117–124.
367. Samdal H, Sandmoe MA, Olsen LC, Jarallah EAH, Høiem TS, Schønberg SA, Pettersen CHH. *Basal level of autophagy and MAP1LC3B-II as potential biomarkers for DHA-induced cytotoxicity in colorectal cancer cells*. FEBS J 2018; 285(13):2446-2467.
368. Wiersma VR, de Bruyn M, Wei Y, van Ginkel RJ, Hirashima M, Niki T, Nishi N, Zhou J, Pouwels SD, Samplonius DF, Nijman HW, Eggleton P, Helfrich W, Bremer E. *The epithelial polarity regulator LGALS9/galectin- 9 induces fatal frustrated autophagy in KRAS mutant colon carcinoma that depends on elevated basal autophagic flux*. Autophagy 2015; 11(8):1373-88.
369. Mokarram P, Albokashy M, Zarghooni M, et al. *New frontiers in the treatment of colorectal cancer: Autophagy and the unfolded protein response as promising targets*. Autophagy 2017; 13(5):781-819.
370. Kondo Y, Kanzawa T, Sawaya R, Kondo S. *The role of autophagy in cancer development and response to therapy*. Nat Rev Cancer 2005; 5(9):726-34.
371. Greene LM, Nolan DP, Regan-Komito D, Campiani G, Williams DC, Zisterer DM. *Inhibition of late-stage autophagy synergistically enhances pyrrolo-1,5-benzoxazepine-6-induced apoptotic cell death in human colon cancer cells*. Int J Oncol 2013; 43: 927–935.
372. Wang J, Wu GS. *Role of autophagy in cisplatin resistance in ovarian cancer cells.* J Biol Chem 2014; 289: 17163–73.
373. Lin J-F, Lin Y-C, Tsai T-F, Chen H-E, Chou K-Y, Hwang TI-S. *Cisplatin induces protective autophagy through activation of BECN1 in human bladder cancer cells.* Drug Des Devel Ther 2017; 11: 1517–1533.
374. Wu T, Wang MC, Jing L, Liu ZY, Guo H, Liu Y, Bai YY, Cheng YZ, Nan KJ, Liang X. *Autophagy facilitates lung adenocarcinoma resistance to cisplatin treatment by activation of AMPK/mTOR signaling pathway*. Drug Des Devel Ther 2015; 9: 6421–6431.
375. Eisenberg-Lerner A, Kimchi A. *The paradox of autophagy and its implication in cancer etiology and therapy*. Apoptosis 2009; 14: 376–391.
376. Shi YH, Ding Z Bin, Zhou J, Hui B, Shi GM, Ke AW, Wang XY, Dai Z, Peng YF, Gu CY, Qiu SJ, Fan J. *Targeting autophagy enhances sorafenib lethality for hepatocellular carcinoma via ER stress-related apoptosis*. Autophagy 2011; 7(10):1159-72.
377. Sun WL, Chen J, Wang YP, Zheng H. *Autophagy protects breast cancer cells from epirubicin-induced apoptosis and facilitates epirubicin-resistance development*. Autophagy 2011; 7(9):1035-44.

378. Shimgu T, Fujiwara K, Bogler O, Akiyama Y, Meritake K, Shinojima N, Tamacla Y, Yokoyama T, Kondo S. *Inhibition of autophagy at a late stage enhances imatinib-induced cytotoxicity In human malignant glioma cells*. Int J Cancer 2009; 124(5):1060–71.
379. Salazar M, Carracedo A, Salanueva ÍJ, et al. *Cannabinoid action induces autophagy-mediated cell death through stimulation of ER stress in human glioma cells*. J Clin Invest 2009; 119(5): 1359–1372.
380. Jiang Y, Ji F, Liu Y, He M, Zhang Z, Yang J, Wang N, Zhong C, Jin Q, Ye X, Chen T. *Cisplatin-induced autophagy protects breast cancer cells from apoptosis by regulating yes-associated protein*. Oncol Rep 2017; 38: 3668–3676.
381. Leisching G, Loos B, Botha M, Engelbrecht A-M. *A Nontoxic Concentration of Cisplatin Induces Autophagy in Cervical Cancer*. Int J Gynecol Cancer 2015; 25: 380–388.
382. Ballestreri É, Simon D, de Souza AP, Grott CS, Nabinger DD, Dihl RR, Grivicich I. *Resistance mechanism to cisplatin in NCI-H460 non-small cell lung cancer cell line: investigating apoptosis, autophagy, and cytogenetic damage*. Cancer Drug Resist 2018; 1: 72–81.
383. Piya S, Andreeff M, Borthakur G. *Targeting autophagy to overcome chemoresistance in acute myleogenous leukemia*. Autophagy 2017; 13(1): 214–215.
384. Garcia-Cano J, Ambroise G, Pascual-Serra R, Carrion MC, Serrano-Oviedo L, Ortega-Muelas M, Cimas FJ, Sabater S, Ruiz-Hidalgo MJ, Sanchez Perez I, Mas A, Jalon FA, Vazquez A, Sanchez-Prieto R. *Exploiting the potential of autophagy in cisplatin therapy: A new strategy to overcome resistance.* Oncotarget 2015; 6: 15551–15565.
385. Wu YT, Tan HL, Shui G, Bauvy C, Huang Q, Wenk MR, Ong CN, Codogno P, Shen HM. *Dual role of 3-methyladenine in modulation of autophagy via different temporal patterns of inhibition on class I and III phosphoinositide 3-kinase*. J Biol Chem 2010; 285(14):10850–61.
386. Pérez-Hernández M, Arias A, Martínez-García D, Pérez-Tomás R, Quesada R, Soto-Cerrato V. *Targeting autophagy for cancer treatment and tumor chemosensitization*. Cancers (Basel) 2019; 11(10): 1599.
387. Liu J, Xia H, Kim M, et al. *Beclin1 Controls the Levels of p53 by Regulating the Deubiquitination Activity of USP10 and USP13*. Cell 2011; 147: 223–234.
388. Tolkovsky AM, Xue L, Fletcher GC, Borutaite V. *Mitochondrial disappearance from cells: A clue to the role of autophagy in programmed cell death and disease?* Biochimie 2002; 84(2-3):233-40.
389. O'Donovan TR, O'Sullivan GC, McKenna SL. *Induction of autophagy by drug-resistant esophageal cancer cells promotes their survival and recovery following treatment with chemotherapeutics.* Autophagy 2011; 7: 509–24.
390. Ronan B, Flamand O, Vescovi L, et al. *A highly potent and selective Vps34 inhibitor alters vesicle trafficking and autophagy*. Nat Chem Biol 2014; 10: 1013–9.
391. Young CD, Arteaga CL, Cook RS. *Dual inhibition of Type I and Type III PI3 kinases increases tumor cell apoptosis in HER2+ breast cancers*. Breast Cancer Res 2015; 17: 148.
392. Schlütermann D, Skowron MA, Berleth N, Böhler P, Deitersen J, Stuhldreier F, Wallot-Hieke N, Wu W, Peter C, Hoffmann MJ, Niegisch G, Stork B. *Targeting urothelial carcinoma cells by combining cisplatin with a specific inhibitor of the autophagy-inducing class III PtdIns3K complex*. Urol Oncol Semin Orig Investig

2018; 36(4):160.e1-160.e13.
393. Liang X, Tang J, Liang Y, Jin R, Cai X. *Suppression of autophagy by chloroquine sensitizes 5-fluorouracil-mediated cell death in gallbladder carcinoma cells*. Cell Biosci 2014; 4: 1–11.
394. Liang B, Kong D, Liu Y, Liang N, He M, Ma S, Liu X. *Autophagy inhibition plays the synergetic killing roles with radiation in the multi-drug resistant SKVCR ovarian cancer cells*. Radiat Oncol 2012; 7: 213.
395. Han MW, Lee JC, Choi J-Y, Kim GC, Chang HW, Nam HY, Kim SW, Kim SY. *Autophagy inhibition can overcome radioresistance in breast cancer cells through suppression of TAK1 activation.* Anticancer Res 2014; 34: 1449–55.
396. Li C, Liu Y, Zhang W, Shen C, Cho K, Chen X, Bi Y, Yang Z, Zheng Z, Wang K, Wang X, Zhang J, Zhong C, Zhao S. *Impact of Autophagy Inhibition at Different Stages on Cytotoxic Effect of Autophagy Inducer in Glioblastoma Cells*. Cell Physiol Biochem 2015; 35: 1303–1316.
397. Young MM, Takahashi Y, Khan O, Park S, Hori T, Yun J, Sharma AK, Amin S, Hu CD, Zhang J, Kester M, Wang HG. *Autophagosomal membrane serves as platform for intracellular death-inducing signaling complex (iDISC)-mediated caspase-8 activation and apoptosis*. J Biol Chem 2012; 287: 12455–12468.
398. Ma X, Liu H, Foyil SR, Godar RJ, Weinheimer CJ, Hill JA, Diwan A. *Impaired autophagosome clearance contributes to cardiomyocyte death in ischemia/reperfusion injury*. Circulation 2012; 125(25): 3170–3181.
399. Maycotte P, Aryal S, Cummings CT, Thorburn J, Morgan MJ, Thorburn A. *Chloroquine sensitizes breast cancer cells to chemotherapy independent of autophagy*. Autophagy 2012; 8: 200–212.
400. Chu HY, Wang W, Chen X, Jiang YE, Cheng R, Qi X, Zhong ZM, Zeng MS, Zhu XF, Sun CZ. *Bafilomycin A1 increases the sensitivity of tongue squamous cell carcinoma cells to cisplatin by inhibiting the lysosomal uptake of platinum ions but not autophagy*. Cancer Lett 2018; 423: 105–112.
401. Li L, Xie W, Pan D, Chen H, Zhang L. *Inhibition of autophagy by bafilomycin A1 promotes chemosensitivity of gastric cancer cells*. Tumor Biol; 37.
402. Han MW, Lee JC, Choi J-Y, Kim GC, Chang HW, Nam HY, Kim SW, Kim SY. *Autophagy inhibition can overcome radioresistance in breast cancer cells through suppression of TAK1 activation.* Anticancer Res 2014; 34: 1449–55.
403. Rojas-Puentes LL, Gonzalez-Pinedo M, Crismatt A, Ortega-Gomez A, Gamboa-Vignolle C, Nuñez-Gomez R, Dorantes-Gallareta Y, Arce-Salinas C, Arrieta O. *Phase II randomized, double-blind, placebo-controlled study of whole-brain irradiation with concomitant chloroquine for brain metastases*. Radiat Oncol 2013; 8:209.
404. Molenaar RJ, Coelen RJS, Khurshed M, et al. *Study protocol of a phase IB/II clinical trial of metformin and chloroquine in patients with IDH1-mutated or IDH2-mutated solid tumours.* BMJ Open 2017; 7: e014961.
405. Sotelo J, Briceño E, López-González MA. *Adding Chloroquine to Conventional Treatment for Glioblastoma Multiforme*. Ann Intern Med 2006; 144: 337.
406. Manic G, Obrist F, Kroemer G, Vitale I, Galluzzi L. *Chloroquine and hydroxychloroquine for cancer therapy*. Mol Cell Oncol 2014; 1(1): e29911.
407. Pyo J-O, Jang M-H, Kwon Y-K, Lee H-J, Jun J-I, Woo H-N, Cho D-H, Choi B, Lee H, Kim J-H, Mizushima N, Oshumi Y, Jung Y-K. *Essential Roles of Atg5 and FADD in Autophagic Cell Death*. J Biol Chem 2005; 280(21):20722–9.
408. Chen J, Zhang L, Zhou H, Wang W, Luo Y, Yang H, Yi H. *Inhibition of autophagy promotes cisplatin-induced apoptotic cell death through Atg5 and Beclin 1 in A549*

human lung cancer cells. Mol Med Rep 2018; 17(5):6859-6865.
409. Zhao H, Li Q, Pang J, Jin H, Li H, Yang X. *Blocking autophagy enhances the pro-apoptotic effect of bufalin on human gastric cancer cells through endoplasmic reticulum stress*. Biol Open 2017; 6: 1416–1422.
410. Hollomon MG, Gordon N, Santiago-O'Farrill JM, Kleinerman ES. *Knockdown of autophagy-related protein 5, ATG5, decreases oxidative stress and has an opposing effect on camptothecin-induced cytotoxicity in osteosarcoma cells*. BMC Cancer 2013; 13:500.
411. Jamal-Hanjani M, Quezada SA, Larkin J, Swanton C. *Translational implications of tumor heterogeneity*. Clin Cancer Res 2015; 21: 1258–1266.
412. Ramón y Cajal S, Sesé M, Capdevila C, Aasen T, De Mattos-Arruda L, Diaz-Cano SJ, Hernández-Losa J, Castellví J. *Clinical implications of intratumor heterogeneity: challenges and opportunities*. J Mol Med 2020; 98: 161–177.
413. Beck DJ, Brubaker RR. *Effect of cis platinum (II) diamminodichloride on wild type and deoxyribonucleic acid repair deficient mutants of Escherichia coli*. J Bacteriol 1973; 116(3): 1247–1252.
414. Fraval HNA, Rawlings CJ, Roberts JJ. *Increased sensitivity of UV-repair-deficient human cells to DNA bound platinum products which unlike thymine dimers are not recognized by an endonuclease extracted from Micrococcus luteus*. Mutat Res - Fundam Mol Mech Mutagen 1978; 51(1):121–32.
415. Tanida S, Mizoshita T, Ozeki K, Tsukamoto H, Kamiya T, Kataoka H, Sakamuro D, Joh T. *Mechanisms of cisplatin-induced apoptosis and of cisplatin sensitivity: Potential of BIN1 to act as a potent predictor of cisplatin sensitivity in gastric cancer treatment*. Int J Surg Oncol 2012; 2012:862879.
416. Choi Y-M, Kim H-K, Shim W, Anwar MA, Kwon J-W, Kwon H-K, Kim HJ, Jeong H, Kim HM, Hwang D, Kim HS, Choi S. *Mechanism of Cisplatin-Induced Cytotoxicity Is Correlated to Impaired Metabolism Due to Mitochondrial ROS Generation*. PLoS One 2015; 10: e0135083.
417. Marullo R, Werner E, Degtyareva N, Moore B, Altavilla G, Ramalingam SS, Doetsch PW. *Cisplatin Induces a Mitochondrial-ROS Response That Contributes to Cytotoxicity Depending on Mitochondrial Redox Status and Bioenergetic Functions*. PLoS One 2013; 8: e81162.
418. Ishikawa T, Ali-Osman F. *Glutathione-associated cis-diamminedichloroplatinum(II) metabolism and ATP-dependent efflux from leukemia cells. Molecular characterization of glutathione-platinum complex and its biological significance*. J Biol Chem 1993; 268(27):20116–25.
419. DeLeve LD, Kaplowitz N. *Glutathione metabolism and its role in hepatotoxicity*. Pharmacol Ther 1991; 52(3):287-305.
420. Aguilar TAF, Navarro BCH, Pérez JAM. *Endogenous Antioxidants: A Review of their Role in Oxidative Stress*. In: *A Master Regulator of Oxidative Stress - The Transcription Factor Nrf2*. IntechOpen, 2016.
421. Lu Y, Cederbaum A. *The mode of cisplatin-induced cell death in CYP2E1-overexpressing HepG2 cells: Modulation by ERK, ROS, glutathione, and thioredoxin*. Free Radic Biol Med 2007; 43: 1061–1075.
422. Murphy ME, Scholich H, Sies H. *Protection by glutathione and other thiol compounds against the loss of protein thiols and tocopherol homologs during microsomal lipid peroxidation*. Eur J Biochem 1992; 210: 139–146.
423. Schieber M, Chandel NS. *ROS function in redox signaling and oxidative stress*. Curr Biol 2014; 24(10): 453–462.
424. Guégan JP, Ezan F, Théret N, Langoüt S, Baffet G. *MAPK signaling in cisplatin-*

induced death: Predominant role of ERK1 over ERK2 in human hepatocellular carcinoma cells. Carcinogenesis 2013; 34(1):38-47.
425. Achkar IW, Abdulrahman N, Al-Sulaiti H, Joseph JM, Uddin S, Mraiche F. *Cisplatin based therapy: The role of the mitogen activated protein kinase signaling pathway*. J Transl Med 2018; 16, 96.
426. Liu J, Lin A. *Role of JNK activation in apoptosis: A double-edged sword*. Cell Res 2005; 15(1):36-42.
427. Brozovic A, Osmak M. *Activation of mitogen-activated protein kinases by cisplatin and their role in cisplatin-resistance*. Cancer Lett 2007; 251(1):1–16.
428. Davis RJ. *Signal transduction by the JNK group of MAP kinases*. Cell 2000; 103(2):239–52.
429. Corcelle E, Djerbi N, Mari M, Nebout M, Fiorini C, Fénichel P, Hofman P, Poujeol P, Mograbi B. *Control of the autophagy maturation step by the MAPK ERK and p38: Lessons from environmental carcinogens*. Autophagy 2007; 3(1):57-9.
430. Zhou YY, Li Y, Jiang WQ, Zhou LF. *MAPK/JNK signalling: A potential autophagy regulation pathway*. Biosci Rep 2015; 35(3): e00199.
431. Wu D, Yotnda P. *Production and detection of reactive oxygen species (ROS) in cancers*. J Vis Exp 2011; (57):3357.
432. Caricchio R, Kovalenko D, Kaufmann WK, Cohen PL. *Apoptosis provoked by the oxidative stress inducer menadione (vitamin K3) is mediated by the Fas/Fas ligand system*. Clin Immunol 1999; 93: 65–74.
433. Loor G, Kondapalli J, Schriewer JM, Chandel NS, Vanden Hoek TL, Schumacker PT. *Menadione triggers cell death through ROS-dependent mechanisms involving PARP activation without requiring apoptosis*. Free Radic Biol Med 2010; 49(12): 1925–1936.
434. Ivanova D, Zhelev Z, Getsov P, Nikolova B, Aoki I, Higashi T, Bakalova R. *Vitamin K: Redox-modulation, prevention of mitochondrial dysfunction and anticancer effect*. Redox Biol 2018; 16: 352–358.
435. Zitka O, Skalickova S, Gumulec J, Masarik M, Adam V, Hubalek J, Trnkova L, Kruseova J, Eckschlager T, Kizek R. *Redox status expressed as GSH:GSSG ratio as a marker for oxidative stress in paediatric tumour patients*. Oncol Lett 2012; 4: 1247–1253.
436. Sun SY. *N-acetylcysteine, reactive oxygen species and beyond*. Cancer Biol Ther 2010; 9(2): 109–110.
437. Azad MB, Chen Y, Gibson SB. *Regulation of autophagy by reactive oxygen species (ROS): Implications for cancer progression and treatment*. Antioxidants Redox Signal 2009; 11: 777–790.
438. Zhang T, Inesta-Vaquera F, Niepel M, et al. *Discovery of potent and selective covalent inhibitors of JNK*. Chem Biol 2012; 19(1): 140–154.
439. Wen Y, Grandis JR. *Emerging drugs for head and neck cancer*. Expert Opin Emerg Drugs 2015; 20(2): 313–329.
440. Makovec T. *Cisplatin and beyond: Molecular mechanisms of action and drug resistance development in cancer chemotherapy*. Radiol Oncol 2019; 53: 148–158.
441. Brozovic A, Ambriović-Ristov A, Osmak M. *The relationship between cisplatin-Induced reactive oxygen species, glutathione, and BCL-2 and resistance to cisplatin*. Crit Rev Toxicol 2010; 40(4):347-59.
442. Park BH, Lim JE, Jeon HG, Seo S Il, Lee HM, Choi HY, Jeon SS, Jeong BC. *Curcumin potentiates antitumor activity of cisplatin in bladder cancer cell lines via ROS-mediated activation of ERK1/2*. Oncotarget 2016; 7(39): 63870–63886.
443. Kleih M, Böpple K, Dong M, Gaißler A, Heine S, Olayioye MA, Aulitzky WE,

Essmann F. *Direct impact of cisplatin on mitochondria induces ROS production that dictates cell fate of ovarian cancer cells*. Cell Death Dis 2019; 10, 851.
444. Lee Y-J, Lee S-H. *Pro-oxidant activity of sulforaphane and cisplatin potentiates apoptosis and simultaneously promotes autophagy in malignant mesothelioma cells*. Mol Med Rep 2017; 16: 2133–2141.
445. Khynriam D, Prasad SB. *Changes in endogenous tissue glutathione level in relation to murine ascites tumor growth and the anticancer activity of cisplatin*. Brazilian J Med Biol Res 2003; 36(1):53-63.
446. Pendyala L, Perez R, Weinstein A, Zdanowicz J, Creaven PJ. *Effect of glutathione depletion on the cytotoxicity of cisplatin and iproplatin in a human melanoma cell line*. Cancer Chemother Pharmacol 1997; 40: 38–44.
447. Welters MJP, Fichtinger-Schepman AMJ, Baan RA, Flens MJ, Scheper RJ, Braakhuis BJM. *Role of glutathione, glutathione S-transferases and multidrug resistance-related proteins in cisplatin sensitivity of head and neck cancer cell lines*. Br J Cancer 1998; 77(4): 556–561.
448. Fruehauf JP, Zonis S, Al-Bassam M, Kyshtoobayeva A, Dasgupta C, Milovanovic T, Parker RJ, Buzaid AC. *Selective and Synergistic Activity of L-S,R-Buthionine Sulfoximine on Malignant Melanoma Is Accompanied by Decreased Expression of Glutathione-S-Transferase*. Pigment Cell Res 1997; 10(4):236-49.
449. Awasthi S, Sharma R, Singhal SS, Herzog NK, Chaubey M, Awasthi YC. *Modulation of cisplatin cytotoxicity by sulphasalazine*. Br J Cancer 1994; 70: 190–194.
450. Lapensee EW, Schwemberger SJ, Lapensee CR, Bahassi EM, Afton SE, Ben-Jonathan N. *Prolactin confers resistance against cisplatin in breast cancer cells by activating glutathione-S-transferase*. Carcinogenesis 2009; 30(8): 1298–1304.
451. Robichaud NJ, Fram RJ. *Schedule dependence of buthionine sulfoximine in reversing resistance to cisplatin*. Chem Biol Interact 1990; 76(3):333–42.
452. Chen G, Zeller WJ. *Augmentation of cisplatin (DDP) cytotoxicity in vivo by DL-buthionine sulfoximine (BSO) in DDP - sensitive and - resistant rat ovarian tumors and its relation to DNA interstrand cross links*. Anticancer Res 1991; 11(6):2231–7.
453. Lai GM, Ozols RF, Young RC, Hamilton TC. *Effect of glutathione on DNA repair in cisplatin-resistant human ovarian cancer cell lines*. J Natl Cancer Inst 1989; 81: 535–539.
454. Aldini G, Altomare A, Baron G, Vistoli G, Carini M, Borsani L, Sergio F. *N-Acetylcysteine as an antioxidant and disulphide breaking agent: the reasons why*. Free Radic Res 2018; 52: 751–762.
455. Schimel AM, Abraham L, Cox D, Sene A, Kraus C, Dace DS, Ercal N, Apte RS. *N-acetylcysteine amide (NACA) prevents retinal degeneration by up-regulating reduced glutathione production and reversing lipid peroxidation*. Am J Pathol 2011; 178(5): 2032–2043.
456. Dickey DT, Muldoon LL, Doolittle ND, Peterson DR, Kraemer DF, Neuwelt EA. *Effect of N-acetylcysteine route of administration on chemoprotection against cisplatin-induced toxicity in rat models*. Cancer Chemother Pharmacol 2008; 62(2):235–41.
457. Muldoon LL, Wu YJ, Pagel MA, Neuwelt EA. *N-acetylcysteine chemoprotection without decreased cisplatin antitumor efficacy in pediatric tumor models*. J Neurooncol 2015; 121(3):433–40.
458. Dickey DT, Wu YJ, Muldoon LL, Neuwelt EA. *Protection against cisplatin-induced toxicities by N-acetylcysteine and sodium thiosulfate as assessed at the*

molecular, cellular, and in vivo levels. J Pharmacol Exp Ther 2005; 314(3):1052–8.
459. Huang S, You J, Wang K, Li Y, Zhang Y, Wei H, Liang X, Liu Y. *N - Acetylcysteine Attenuates Cisplatin-Induced Acute Kidney Injury by Inhibiting the C5a Receptor*. Biomed Res Int 2019; 2019: 2019: 4805853.
460. Abdel-Wahab WM, Moussa FI. *Neuroprotective effect of N-acetylcysteine against cisplatin-induced toxicity in rat brain by modulation of oxidative stress and inflammation*. Drug Des Devel Ther 2019; 13:1155-1162.
461. Itoh T, Terazawa R, Kojima K, Nakane K, Deguchi T, Ando M, Tsukamasa Y, Ito M, Nozawa Y. *Cisplatin induces production of reactive oxygen species via NADPH oxidase activation in human prostate cancer cells*. Free Radic Res 2011; 45: 1033–1039.
462. Yang Z, Schumaker LM, Egorin MJ, Zuhowski EG, Quo Z, Cullen KJ. *Cisplatin preferentially binds mitochondrial DNA and voltage-dependent anion channel protein in the mitochondrial membrane of head and neck squamous cell carcinoma: Possible role in apoptosis*. Clin Cancer Res 2006; 12(19):5817-25.
463. Wu YJ, Muldoon LL, Neuwelt EA. *The Chemoprotective Agent N-Acetylcysteine Blocks Cisplatin-Induced Apoptosis through Caspase Signaling Pathway*. J Pharmacol Exp Ther 2005; 312: 424–431.
464. Poillet-Perez L, Despouy G, Delage-Mourroux R, Boyer-Guittaut M. *Interplay between ROS and autophagy in cancer cells, from tumor initiation to cancer therapy*. Redox Biol 2015; 4: 184–192.
465. Scherz-Shouval R, Shvets E, Fass E, Shorer H, Gil L, Elazar Z. *Reactive oxygen species are essential for autophagy and specifically regulate the activity of Atg4*. EMBO J 2007; 26(7): 1749–1760.
466. Gwinn DM, Shackelford DB, Egan DF, Mihaylova MM, Mery A, Vasquez DS, Turk BE, Shaw RJ. *AMPK Phosphorylation of Raptor Mediates a Metabolic Checkpoint*. Mol Cell 2008; 30(2): 214–226.
467. Kim J, Kundu M, Viollet B, Guan KL. *AMPK and mTOR regulate autophagy through direct phosphorylation of Ulk1*. Nat Cell Biol 2011; 13(2):132-41.
468. Djavaheri-Mergny M, Amelotti M, Mathieu J, Besançon F, Bauvy C, Souquère S, Pierron G, Codogno P. *NF-κB activation represses tumor necrosis factor-α-induced autophagy*. J Biol Chem 2006; 281(41):30373–82.
469. Walsh CM, Edinger AL. *The complex interplay between autophagy, apoptosis, and necrotic signals promotes T-cell homeostasis*. Immunol Rev 2010; 236: 95–109.
470. Kim EH, Sohn S, Kwon HJ, Kim SU, Kim MJ, Lee SJ, Choi kyeong S. *Sodium selenite induces superoxide-mediated mitochondrial damage and subsequent autophagic cell death in malignant glioma cells*. Cancer Res 2007; 67(13):6314–24.
471. Chen Y, McMillan-Ward E, Kong J, Israels SJ, Gibson SB. *Oxidative stress induces autophagic cell death independent of apoptosis in transformed and cancer cells*. Cell Death Differ 2008; 15(1):171-82.
472. Ichijo H, Nishida E, Irie K, Ten Dijke P, Saitoh M, Moriguchi T, Takagi M, Matsumoto K, Miyazono K, Gotoh Y. *Induction of apoptosis by ASK1, a mammalian MAPKKK that activates SAPK/JNK and p38 signaling pathways*. Science (80-) 1997; 275(5296):90–4.
473. Shen HM, Liu ZG. *JNK signaling pathway is a key modulator in cell death mediated by reactive oxygen and nitrogen species*. Free Radic Biol Med 2006; 40: 928–939.
474. Wang W, Sun H, Che Y, Jiang X. *Rasfonin promotes autophagy and apoptosis via*

upregulation of reactive oxygen species (ROS)/JNK pathway. Mycology 2016; 7: 64–73.
475. Li B, Zhou P, Xu K, Chen T, Jiao J, Wei H, Yang X, Xu W, Wan W, Xiao J. *Metformin induces cell cycle arrest, apoptosis and autophagy through ROS/JNK signaling pathway in human osteosarcoma*. Int J Biol Sci 2020; 16(1): 74–84.
476. Kim A, Im M, Yim NH, Kim T, Ma JY. *A novel herbal medicine, KIOM-C, induces autophagic and apoptotic cell death mediated by activation of JNK and reactive oxygen species in HT1080 human fibrosarcoma cells*. PLoS One 2014; 9(5):e98703.
477. Wang H, Peng X, Huang Y, Xiao Y, Wang Z, Zhan L. *Propofol attenuates hypoxia/reoxygenation-induced apoptosis and autophagy in HK-2 cells by inhibiting JNK activation*. Yonsei Med J 2019; 60(12): 1195–1202.
478. Zhao Q, Liu Y, Zhong J, Bi Y, Liu Y, Ren Z, Li X, Jia J, Yu M, Yu X. *Pristimerin induces apoptosis and autophagy via activation of ROS/ASK1/JNK pathway in human breast cancer in vitro and in vivo*. Cell Death Discov 2019; 5,125.
479. Ahn MY, Ahn JW, Kim HS, Lee J, Yoon JH. *Apicidin inhibits cell growth by downregulating IGF-1R in salivary mucoepidermoid carcinoma cells*. Oncol Rep 2015; 33: 1899–1907.
480. Rajagopal PS, Nipp RD, Selvaggi KJ. *Chemotherapy for advanced cancers.* Ann Palliat Med 2014; 3: 203–20328.
481. Khoo XH, Paterson IC, Goh BH, Lee WL. *Cisplatin-resistance in oral squamous cell carcinoma: Regulation by tumor cell-derived extracellular vesicles*. Cancers (Basel) 2019; 11(8): 1166.
482. Gottesman MM. *Mechanisms of Cancer Drug Resistance*. Annu Rev Med 2002; 53:615–27.
483. Zhou J, Kang Y, Chen L, Wang H, Liu J, Zeng S, Yu L. *The Drug-Resistance Mechanisms of Five Platinum-Based Antitumor Agents*. Front Pharmacol 2020; 11: 1–17.
484. Shen DW, Pouliot LM, Hall MD, Gottesman MM. *Cisplatin resistance: A cellular self-defense mechanism resulting from multiple epigenetic and genetic changes*. Pharmacol Rev 2012; 64: 706–721.
485. Galluzzi L, Senovilla L, Vitale I, Michels J, Martins I, Kepp O, Castedo M, Kroemer G. *Molecular mechanisms of cisplatin resistance*. Oncogene 2012; 31: 1869–1883.
486. Ren JH, He WS, Nong L, Zhu QY, Hu K, Zhang RG, Huang LL, Zhu F, Wu G. *Acquired cisplatin resistance in human lung adenocarcinoma cells is associated with enhanced autophagy*. Cancer Biother Radiopharm 2010; 25(1):75-80.
487. Kroemer G, Mariño G, Levine B. *Autophagy and the Integrated Stress Response*. Mol Cell 2010; 40(2): 280–293.
488. Thakur B, Ray P. *Cisplatin triggers cancer stem cell enrichment in platinum-resistant cells through NF-κB-TNFα-PIK3CA loop*. J Exp Clin Cancer Res 2017; 36,174.
489. Ghuwalewala S, Ghatak D, Das P, Dey S, Sarkar S, Alam N, Panda CK, Roychoudhury S. *CD44 high CD24 low molecular signature determines the Cancer Stem Cell and EMT phenotype in Oral Squamous Cell Carcinoma*. Stem Cell Res 2016; 16: 405–417.
490. Wang J, Seebacher N, Shi H, Kan Q, Duan Z. *Novel strategies to prevent the development of multidrug resistance (MDR) in cancer*. Oncotarget 2017; 8(48): 84559–84571.
491. Li X, Zhou Y, Li Y, Yang L, Ma Y, Peng X, Yang S, Liu J, Li H. *Autophagy: A*

novel mechanism of chemoresistance in cancers. Biomed Pharmacother 2019; 119:109415.
492. Ma Q. *Role of Nrf2 in Oxidative Stress and Toxicity*. Annu Rev Pharmacol Toxicol 2013; 2013; 53: 401–426.
493. Weber JS, Samlowski WE, Gonzalez R, Ribas A, Stephenson J, O'Day S, Sato T, Dorr R, Grenier K, Hersh E. *A phase 1-2 study of imexon plus dacarbazine in patients with unresectable metastatic melanoma*. Cancer 2010; 116(15):3683–91.
494. Guo Y, Pan W, Liu S, Shen Z, Xu Y, Hu L. *ERK/MAPK signalling pathway and tumorigenesis (Review)*. Exp Ther Med; 19(3):1997.
495. Tao S, Wang S, Moghaddam SJ, Ooi A, Chapman E, Wong PK, Zhang DD. *Oncogenic KRAS confers chemoresistance by upregulating NRF2*. Cancer Res; 74(24):743.
496. Sales Amaral MV, De Sousa Portilho AJ, Da Silva EL, Sales LDO, Da Silva Maués JH, Amaral De Moraes ME, Moreira-Nunes CA. *Establishment of drug-resistant cell lines as a model in experimental oncology: A review*. Anticancer Res 2019; 39: 6443–6455.
497. Zuo Q, Liu J, Zhang J, Wu M, Guo L, Liao W. *Development of trastuzumab-resistant human gastric carcinoma cell lines and mechanisms of drug resistance*. Sci Rep 2015; 5: 11634.
498. Barr MP, Gray SG, Hoffmann AC, Hilger RA, Thomale J, O'Flaherty JD, Fennell DA, Richard D, O'Leary JJ, O'Byrne KJ. *Generation and characterisation of cisplatin-resistant non-small cell lung cancer cell lines displaying a stem-like signature.* PLoS One 2013; 8: e54193.
499. Zhang X, Yashiro M, Qiu H, Nishii T, Matsuzaki T, Hirakawa K. *Establishment and characterization of multidrug-resistant gastric cancer cell lines.* Anticancer Res 2010; 30: 915–21.
500. Biedler JL, Riehm H. *Cellular resistance to actinomycin D in Chinese hamster cells in vitro: cross-resistance, radioautographic, and cytogenetic studies.* Cancer Res 1970; 30(4):1174-84.
501. Nikounezhad N, Nakhjavani M, Shirazi FH. *Generation of Cisplatin-resistant ovarian cancer cell lines*. Iran J Pharm Sci 2016; 8(1): e54193.
502. Sherman-Baust CA, Becker KG, Wood WH, Zhang Y, Morin PJ. *Gene expression and pathway analysis of ovarian cancer cells selected for resistance to cisplatin, paclitaxel, or doxorubicin*. J Ovarian Res 2011; 4: 21.
503. Liang XJ, Shen DW, Garfield S, Gottesman MM. *Mislocalization of membrane proteins associated with multidrug resistance in cisplatin-resistant cancer cell lines*. Cancer Res 2003; 63(18):5909–16.
504. Shen DW, Akiyama SI, Akiyama SI, Schoenlein P, Pastan I. *Characterisation of high-level cisplatin-resistant cell lines established from a human hepatoma cell line and human KB adenocarcinoma cells: Cross-resistance and protein changes*. Br J Cancer 1995; 71(4): 676–683.
505. McDermott M, Eustace AJ, Busschots S, Breen L, Crown J, Clynes M, O'Donovan N, Stordal B. *In vitro development of chemotherapy and targeted therapy drug-resistant cancer cell lines: A practical guide with case studies*. Front Oncol 2014; 4: 40.
506. Battista AR, Resnati M, Facchi C, Ruggieri E, Cremasco F, Paradiso F, Orfanelli U, Giordano L, Bussi M, Cenci S, Milan E. *Autophagy mediates epithelial cancer chemoresistance by reducing p62/SQSTM1 accumulation*. PLoS One 2018; 13(8):e0201621.
507. Michalak M, Lach MS, Antoszczak M, Huczynski A, Suchorska WM. *Overcoming*

resistance to platinum-based drugs in ovarian cancer by salinomycin and its derivatives—an in vitro study. Molecules 2020; 25: 1–16.
508. Ghosh RD, Ghuwalewala S, Das P, Mandloi S, Alam SK, Chakraborty J, Sarkar S, Chakrabarti S, Panda CK, Roychoudhury S. *MicroRNA profiling of cisplatin-resistant oral squamous cell carcinoma cell lines enriched with cancer-stem-cell-like and epithelial-mesenchymal transition-type features*. Sci Rep 2016; 6: 23932.
509. Gosepath EM, Eckstein N, Hamacher A, Servan K, Von Jonquieres G, Lage H, Györffy B, Royer HD, Kassack MU. *Acquired cisplatin resistance in the head-neck cancer cell line Cal27 is associated with decreased DKK1 expression and can partially be reversed by overexpression of DKK1*. Int J Cancer 2008; 123(9):2013–9.
510. Yu SS, Cirillo N. *The molecular markers of cancer stem cells in head and neck tumors*. J Cell Physiol 2020; 235: 65–73.
511. Clarke MF, Dick JE, Dirks PB, Eaves CJ, Jamieson CHM, Jones DL, Visvader J, Weissman IL, Wahl GM. *Cancer stem cells - Perspectives on current status and future directions: AACR workshop on cancer stem cells*. Cancer Res 2006; 66(19):9339–44.
512. Singh SK, Clarke ID, Terasaki M, Bonn VE, Hawkins C, Squire J, Dirks PB. *Identification of a cancer stem cell in human brain tumors*. Cancer Res 2003; 63(18):5821–8.
513. Zhang S, Balch C, Chan MW, Lai HC, Matei D, Schilder JM, Yan PS, Huang THM, Nephew KP. *Identification and characterization of ovarian cancer-initiating cells from primary human tumors*. Cancer Res 2008; 68(11):4311–20.
514. Li C, Heidt DG, Dalerba P, Burant CF, Zhang L, Adsay V, Wicha M, Clarke MF, Simeone DM. *Identification of pancreatic cancer stem cells*. Cancer Res 2007; 67(3):1030–7.
515. Phi LTH, Sari IN, Yang YG, Lee SH, Jun N, Kim KS, Lee YK, Kwon HY. *Cancer stem cells (CSCs) in drug resistance and their therapeutic implications in cancer treatment*. Stem Cells Int 2018; 2018:5416923.
516. Jaggupilli A, Elkord E. *Significance of CD44 and CD24 as cancer stem cell markers: An enduring ambiguity*. Clin Dev Immunol 2012; 2012:708036.
517. Shao J, Fan W, Ma B, Wu Y. *Breast cancer stem cells expressing different stem cell markers exhibit distinct biological characteristics*. Mol Med Rep 2016; 14(6): 4991–4998.
518. Hamaguchi K, Godwin AK, Yakushyi M, O'Dwyer PJ, Ozols RF, Hamilton TC. *Cross-Resistance to Diverse Drugs Is Associated with Primary Cisplatin Resistance in Ovarian Cancer Cell Lines*. Cancer Res 1993; 53: 5225–5232.
519. Zhai BJ, Shao ZY, Zhao CL, Hu K, Wu F. *Development and characterization of multidrug resistant human hepatocarcinoma cell line in nude mice*. World J Gastroenterol 2006; 12(41): 6614–6619.
520. Guo B, Villeneuve DJ, Hembruff SL, Kirwan AF, Blais DE, Bonin M, Parissenti AM. *Cross-resistance studies of isogenic drug-resistant breast tumor cell lines support recent clinical evidence suggesting that sensitivity to paclita*. Breast Cancer Res Treat 2004; 85: 31–51.
521. Iseri ÖD, Kars MD, Eroğlu S, Gündüz U. *Drug resistant MCF-7 cell lines also developed cross-resistance to structurally unrelated anticancer agents*. UHOD - Uluslararasi Hematol Derg 2009; 19: 1–8.
522. Gore ME, Fryatt I, Wiltshaw E, Dawson T, Robinson BA, Calvert AH. *Cisplatin/carboplatin cross-resistance in ovarian cancer*. Br J Cancer 1989; 60(5): 767–769.

523. Rixe O, Ortuzar W, Alvarez M, Parker R, Reed E, Paull K, Fojo T. *Oxaliplatin, tetraplatin, cisplatin, and carboplatin: Spectrum of activity in drug-resistant cell lines and in the cell lines of the National Cancer Institute's Anticancer Drug Screen panel*. Biochem Pharmacol 1996; 52(12): 1855-1865.
524. de Sousa GF, Wlodarczyk SR, Monteiro G. *Carboplatin: Molecular mechanisms of action associated with chemoresistance*. Brazilian J Pharm Sci 2014; 50(4): 693-701.
525. Pan X, Chen Y, Shen Y, Tantai J. *Knockdown of TRIM65 inhibits autophagy and cisplatin resistance in A549/DDP cells by regulating miR-138-5p/ATG7*. Cell Death Dis 2019; 10, 429.
526. Duan G, Song Z, Qi M, Bai X, Wang J, Zhang Y, Zou X, Guo Q, Wan P. *Increased Autophagy Levels Mediate Cisplatin Resistance in Cisplatin-Resistant Cells while Also Rendering Them Vulnerable to Autophagy Induction*. Biomed Res Int 2018; 2018: 1736738.
527. Kim EK, Jang M, Song MJ, Kim D, Kim Y, Jang HH. *Redox-mediated mechanism of chemoresistance in cancer cells*. Antioxidants 2019; 8(10): 471.
528. Stojković S, Podolski-Renić A, Dinić J, Stanković T, Banković J, Hadžić S, Paunović V, Isaković A, Tanić N, Pešić M. *Development of resistance to antiglioma agents in rat C6 cells caused collateral sensitivity to doxorubicin*. Exp Cell Res 2015; 335: 248–257.
529. Wangpaichitr M, Wu C, You M, Maher J, Dinh V, Feun L, Savaraj N. *N'1,N'3-Dimethyl-N'1,N'3-bis(phenylcarbonothioyl) Propanedihydrazide (Elesclomol) Selectively Kills Cisplatin Resistant Lung Cancer Cells through Reactive Oxygen Species (ROS)*. Cancers (Basel) 2009; 1(1): 23–28.
530. Ju HQ, Gocho T, Aguilar M, Wu M, Zhuang ZN, Fu J, Yanaga K, Huang P, Chiao PJ. *Mechanisms of overcoming intrinsic resistance to gemcitabine in pancreatic ductal adenocarcinoma through the redox modulation*. Mol Cancer Ther 2015; 14(3):788-98.
531. Wangpaichitr M, Wu C, Li YY, Nguyen DJM, Kandemir H, Shah S, Chen S, Feun LG, Prince JS, Kuo MT, Savaraj N. *Exploiting ROS and metabolic differences to kill cisplatin resistant lung cancer*. Oncotarget 2017; 8: 49275–49292.
532. Qian Q, Chen W, Cao Y, Cao Q, Cui Y, Li Y, Wu J. *Targeting Reactive Oxygen Species in Cancer via Chinese Herbal Medicine*. Oxid Med Cell Longev 2019; 2019:9240426.
533. Furusawaa S, Kimura E, Kisara S, Nakano S, Murata R, Tanaka Y, Sakaguchi S, Takayanagi M, Takayanagi Y, Sasaki KI. *Mechanism of resistance to oxidative stress in doxorubicin resistant cells*. Biol Pharm Bull 2001; 24(5):474–9.
534. Traverso N, Ricciarelli R, Nitti M, Marengo B, Furfaro AL, Pronzato MA, Marinari UM, Domenicotti C. *Role of glutathione in cancer progression and chemoresistance*. Oxid Med Cell Longev 2013; 2013:972913.
535. Silva MM, Rocha CRR, Kinker GS, Pelegrini AL, Menck CFM. *The balance between NRF2/GSH antioxidant mediated pathway and DNA repair modulates cisplatin resistance in lung cancer cells*. Sci Rep 2019; 9: 17639.
536. Furfaro AL, Traverso N, Domenicotti C, Piras S, Moretta L, Marinari UM, Pronzato MA, Nitti M. *The Nrf2/HO-1 Axis in Cancer Cell Growth and Chemoresistance*. Oxid Med Cell Longev 2016; 2016:1958174.
537. Shim G seong, Manandhar S, Shin D ha, Kim TH, Kwak MK. *Acquisition of doxorubicin resistance in ovarian carcinoma cells accompanies activation of the NRF2 pathway*. Free Radic Biol Med 2009; 47(11):1619–31.
538. Zhong Y, Zhang F, Sun Z, Zhou W, Li ZY, You QD, Guo QL, Hu R. *Drug*

resistance associates with activation of Nrf2 in MCF-7/DOX cells, and wogonin reverses it by down-regulating Nrf2-mediated cellular defense response. Mol Carcinog 2013; 52(10):824–34.
539. Zhe N, Wang J, Chen S, Lin X, Chai Q, Zhang Y, Zhao J, Fang Q. *Heme oxygenase-1 plays a crucial role in chemoresistance in acute myeloid leukemia*. Hematology 2015; 20(7):384-91.
540. Yoshino H, Murakami K, Nawamaki M, Kashiwakura I. *Effects of Nrf2 knockdown on the properties of irradiated cell conditioned medium from A549 human lung cancer cells*. Biomed Reports 2018; 8(5): 461–465.
541. Singh A, Venkannagari S, Oh KH, et al. *Small molecule inhibitor of NRF2 selectively intervenes therapeutic resistance in KEAP1-deficient NSCLC tumors*. ACS Chem Biol 2016; 11(11):3214-3225.
542. Panieri E, Saso L. *Potential applications of NRF2 inhibitors in cancer therapy*. Oxid Med Cell Longev 2019; 2019:8592348.
543. McCubrey JA, Steelman LS, Chappell WH, et al. *Roles of the Raf/MEK/ERK pathway in cell growth, malignant transformation and drug resistance*. Biochim Biophys Acta - Mol Cell Res 2007; 1773(8): 1263–1284.
544. Shao J, Glorieux C, Liao J, Chen P, Lu W, Liang Z, Wen S, Hu Y, Huang P. *Impact of Nrf2 on tumour growth and drug sensitivity in oncogenic K-ras-transformed cells in vitro and in vivo*. Free Radic Res 2018; 52(6):661-671.
545. Denicola GM, Karreth FA, Humpton TJ, et al. *Oncogene-induced Nrf2 transcription promotes ROS detoxification and tumorigenesis*. Nature 2011; 75(7354):106–9.
546. McCubrey JA, Abrams SL, Ligresti G, Misaghian N, Wong EWT, Steelman LS, Bäsecke J, Troppmair J, Libra M, Nicoletti F, Molton S, McMahon M, Evangelisti C, Martelli AM. *Involvement of p53 and Raf/MEK/ERK pathways in hematopoietic drug resistance*. Leukemia 2008; 2080–90.
547. Saki M, Toulany M, Rodemann HP. *Acquired resistance to cetuximab is associated with the overexpression of Ras family members and the loss of radiosensitization in head and neck cancer cells*. Radiother Oncol 2013; 108(3):473–8.
548. Pao W, Wang TY, Riely GJ, Miller VA, Pan Q, Ladanyi M, Zakowski MF, Heelan RT, Kris MG, Varmus HE. *KRAS mutations and primary resistance of lung adenocarcinomas to gefitinib or erlotinib*. PLoS Med 2005; 2(1): e17.
549. Choi KS. *Autophagy and cancer*. Exp Mol Med 2012; 44(2):109–20.
550. White E. *The role for autophagy in cancer*. J Clin Invest 2015; 125(1): 42–46.
551. Wu JS, Li L, Wang SS, Pang X, Wu JB, Sheng SR, Tang YJ, Tang YL, Zheng M, Liang XH. *Autophagy is positively associated with the accumulation of myeloid-derived suppressor cells in 4-nitroquinoline-1-oxide-induced oral cancer*. Oncol Rep 2018; 40(6):3381-3391.
552. Celetti A, Merolla F, Luise C, Siano M, Staibano S. *Novel Markers for Diagnosis and Prognosis of Oral Intraepithelial Neoplasia*. In: *Intraepithelial Neoplasia*. IntechOpen, 2012. 2012.
553. Havaki S, Vlachou V, Zampetidis CP, Selemenakis P, Kotsinas A, Mavrogonatou E, Rizou S V., Kyrodimos E, Evangelou K, Kletsas D, Giatromanolaki A, Gorgoulis VG. *Monitoring autophagy immunohistochemically and ultrastructurally during human head and neck carcinogenesis. Relationship with the DNA damage response pathway*. Int J Mol Sci 2017; 18(9): 1920.
554. Ramos-Vara JA. *Principles and methods of immunohistochemistry*. Methods Mol Biol 2017; 691:83–96.

555. Chen Y, Schnitzler KL, Ma Y, Nenkov M, Theis B, Petersen I. *The Clinical Influence of Autophagy-Associated Proteins on Human Lung Cancer*. Dis Markers 2018; 2018:8314963.
556. Schläfli AM, Berezowska S, Adams O, Langer R, Tschan MP. *Reliable LC3 and p62 autophagy marker detection in formalin fixed paraffin embedded human tissue by immunohistochemistry*. Eur J Histochem 2015; 59: 2481.
557. Hao X, Yang B, Liu X, Yang H, Liu X. *Expression of Beclin1 in the colonic mucosa tissues of patients with ulcerative colitis.* Int J Clin Exp Med 2015; 8: 21098–105.
558. Koukourakis MI, Giatromanolaki A, Sivridis E, Pitiakoudis M, Gatter KC, Harris AL. *Beclin 1 over- and underexpression in colorectal cancer: Distinct patterns relate to prognosis and tumour hypoxia*. Br J Cancer 2010; 103(8): 1209–1214.
559. Liu XD, Yao J, Tripathi DN, et al. *Autophagy mediates HIF2α degradation and suppresses renal tumorigenesis*. Oncogene 2015; 34(19): 2450–2460.
560. Deng Q, Wang Z, Wang L, Zhang L, Xiang X, Wang Z, Chong T. *Lower mRNA and protein expression levels of LC3 and beclin1, markers of autophagy, were correlated with progression of renal clear cell carcinoma*. Jpn J Clin Oncol 2013; 43(12):1261–8.
561. Li F, Pascal LE, Zhou J, Zhou Y, Wang K, Parwani A V, Dhir R, Guo P, He D, Nelson JB, Wang Z. *BCL-2 and BCL-XL expression are down-regulated in benign prostate hyperplasia nodules and not affected by finasteride and/or celecoxib.* Am J Clin Exp Urol 2018; 6(1): 1–10.
562. Zhou WH, Tang F, Xu J, Wu X, Yang SB, Feng ZY, Ding YG, Wan XB, Guan Z, Li HG, Lin DJ, Shao CK, Liu Q. *Low expression of Beclin 1, associated with high Bcl-xL, predicts a malignant phenotype and poor prognosis of gastric cancer*. Autophagy 2012; 8(3):389-400.
563. Bhutia SK, Mukhopadhyay S, Sinha N, Das DN, Panda PK, Patra SK, Maiti TK, Mandal M, Dent P, Wang XY, Das SK, Sarkar D, Fisher PB. *Autophagy: Cancer's friend or foe?* Adv Cancer Res 2013; 118: 61–95.
564. Groulx JF, Khalfaoui T, Benoit YD, Bernatchez G, Carrier JC, Basora N, Beaulieu JF. *Autophagy is active in normal colon mucosa*. Autophagy 2012; 8(6): 893–902.
565. Thompson HGR, Harris JW, Wold BJ, Lin F, Brody JP. *p62 overexpression in breast tumors and regulation by prostate-derived Ets factor in breast cancer cells*. Oncogene 2003; 22(15):2322-33.
566. Inoue D, Suzuki T, Mitsuishi Y, et al. *Accumulation of p62/SQSTM1 is associated with poor prognosis in patients with lung adenocarcinoma*. Cancer Sci 2012; 103: 760–766.
567. Qian HL, Peng XX, Chen SH, Ye HM, Qui JH. *p62 expression in primary carcinomas of the digestive system*. World J Gastroenterol 2005; 11(12): 1788–1792.
568. Lu M, Nakamura RM, Dent EDB, Zhang JY, Nielsen FC, Christiansen J, Chan EKL, Tan EM. *Aberrant expression of fetal RNA-binding protein p62 in liver cancer and liver cirrhosis*. Am J Pathol 2001; 159(3):945–53.
569. Jiang T, Wu Z. *Immunohistochemical assessment of autophagic protein LC3B and p62 levels in glioma patients*. Int J Clin Exp Pathol 2018; 11: 862–868.
570. Niklaus M, Adams O, Berezowska S, Zlobec I, Graber F, Slotta-Huspenina J, Nitsche U, Rosenberg R, Tschan MP, Langer R. *Expression analysis of LC3B and p62 indicates intact activated autophagy is associated with an unfavorable prognosis in colon cancer.* Oncotarget 2017; 8: 54604–54615.
571. Wang JY, Wu T, Ma W, Li S, Jing WJ, Ma J, Chen DM, Guo XJ, Nan KJ.

Expression and clinical significance of autophagic protein LC3B and EMT markers in gastric cancer. Cancer Manag Res 2018; 10: 1479–1486.
572. Lee YJ, Ha YJ, Na Kang Y, Kang KJ, Hwang JS, Chung WJ, Cho KB, Park KS, Kim ES, Seo H-Y, Kim M-K, Park K-G, Jang BK. *The Autophagy-Related Marker LC3 Can Predict Prognosis in Human Hepatocellular Carcinoma*. PLoS One 2013; 8: e81540.
573. Tang J-Y, Hsi E, Huang Y-C, Hsu NC-H, Chu P-Y, Chai C-Y. *High LC3 expression correlates with poor survival in patients with oral squamous cell carcinoma*. Hum Pathol 2013; 44: 2558–2562.
574. He Y, Zhao X, Subahan NR, Fan L, Gao J, Chen H. *The prognostic value of autophagy-related markers beclin-1 and microtubule-associated protein light chain 3B in cancers: a systematic review and meta-analysis*. Tumor Biol 2014; 35(8):7317–26.
575. Martinet W, Roth L, Meyer GRY De. *Standard Immunohistochemical Assays to Assess Autophagy in Mammalian Tissue*. 2017; 1–12.
576. Martinet W, Schrijvers DM, Timmermans JP, Bult H, De Meyer GRY. *Immunohistochemical analysis of macroautophagy: Recommendations and limitations*. Autophagy 2013; 9(3):386-402.
577. Ladoire S, Chaba K, Martins I, Sukkurwala AQ, Adjemian S, Michaud M, Poirier-Colame V, Andreiuolo F, Galluzzi L, White E, Rosenfeldt M, Ryan KM, Zitvogel L, Kroemer G. *Immunohistochemical detection of cytoplasmic LC3 puncta in human cancer specimens.* Autophagy 2012; 8: 1175–84.
578. Cheng Z, Xin H, Han T. *BECN1 promotes the migration of NSCLC cells through regulating the ubiquitination of Vimentin*. Cell Adhes Migr 2019; 13(1): 249–259.
579. Aita VM, Liang XH, Murty VVVS, Pincus DL, Yu W, Cayanis E, Kalachikov S, Gilliam TC, Levine B. *Cloning and genomic organization of beclin 1, a candidate tumor suppressor gene on chromosome 17q21*. Genomics 1999; 59(1):59-65.
580. Liang XH, Jackson S, Seaman M, Brown K, Kempkes B, Hibshoosh H, Levine B. *Induction of autophagy and inhibition of tumorigenesis by beclin 1*. Nature 1999; 402: 672–676.
581. Turcotte S, Giaccia AJ. *Targeting cancer cells through autophagy for anticancer therapy*. Curr Opin Cell Biol 2010; 22(2): 246–251.
582. Wang Y, Xie J, Wang H, Huang H, Xie P. *Beclin-1 suppresses gastric cancer progression by promoting apoptosis and reducing cell migration.* Oncol Lett 2017; 14: 6857–6862.
583. Qiu D-M, Wang G-L, Chen L, Xu Y-Y, He S, Cao X-L, Qin J, Zhou J-M, Zhang Y-X, E Q. *The expression of beclin-1, an autophagic gene, in hepatocellular carcinoma associated with clinical pathological and prognostic significance*. BMC Cancer 2014; 14: 327.
584. Miracco C, Cevenini G, Franchi A, Luzi P, Cosci E, Mourmouras V, Monciatti I, Mannucci S, Biagioli M, Toscano M, Moretti D, Lio R, Massi D. *Beclin 1 and LC3 autophagic gene expression in cutaneous melanocytic lesions*. Hum Pathol 2010; 41(4):503–12.
585. Valente G, Morani F, Nicotra G, Fusco N, Peracchio C, Titone R, Alabiso O, Arisio R, Katsaros D, Benedetto C, Isidoro C. *Expression and clinical significance of the autophagy proteins BECLIN 1 and LC3 in ovarian cancer*. Biomed Res Int 2014; 2014:462658.
586. Wang J, Pan X-L, Ding L-J, Liu D-Y, Da-Peng Lei D-P, Jin T. *Aberrant Expression of Beclin-1 and LC3 Correlates with Poor Prognosis of Human Hypopharyngeal Squamous Cell Carcinoma*. PLoS One 2013; 8: e69038.

587. Jiang ZF, Shao LJ, Wang WM, Yan XB, Liu RY. *Decreased expression of Beclin-1 and LC3 in human lung cancer*. Mol Biol Rep 2012; 39(1):259-67.
588. Masuda GO, Yashiro M, Kitayama K, et al. *Clinicopathological Correlations of Autophagy-related Proteins LC3, Beclin 1 and p62 in Gastric Cancer.* Anticancer Res 2016; 36: 129–36.
589. Padmakrishnan C, Easwer H, Vinod V, Girish RM, Suresh N, Srinivas G. *High LC3/Beclin Expression Correlates with Poor Survival in Glioma: a Definitive Role for Autophagy as Evidenced by In Vitro Autophagic Flux*. Pathol Oncol Res 2019; 25(1):137-148.
590. Giatromanolaki A, Koukourakis MI, Koutsopoulos A, Chloropoulou P, Liberis V, Sivridis E. *High Beclin 1 expression defines a poor prognosis in endometrial adenocarcinomas*. Gynecol Oncol 2011; 123(1): 147-151.
591. Cai M, Hu Z, Liu J, Gao J, Liu C, Liu D, Tan M, Zhang D, Lin B. *Beclin 1 expression in ovarian tissues and its effects on ovarian cancer prognosis*. Int J Mol Sci 2014; 15(4): 5292–5303.
592. Chen Y, Lu Y, Lu C, Zhang L. *Beclin-1 expression is a predictor of clinical outcome in patients with esophageal squamous cell carcinoma and correlated to hypoxia-inducible factor (HIF)-1α expression*. Pathol Oncol Res 2009; 15(3): 487–493.
593. Liu JL, Chen FF, Chang SF, Chen CN, Lung J, Lo CH, Lee FH, Lu YC, Hung CH. *Expression of beclin family proteins is associated with tumor progression in oral cancer*. PLoS One 2015; 10(10): e0141308.
594. Trisciuoglio D, Tupone MG, Desideri M, Di Martile M, Gabellini C, Buglioni S, Pallocca M, Alessandrini G, D'aguanno S, Del Bufalo D. *BCL-XL overexpression promotes tumor progression-associated properties article*. Cell Death Dis 2017; 8(12):3216.
595. Choi S, Chen Z, Tang LH, Fang Y, Shin SJ, Panarelli NC, Chen YT, Li Y, Jiang X, Du YCN. *Bcl-xL promotes metastasis independent of its anti-apoptotic activity*. Nat Commun 2016; 7:10384.
596. Zhang H, Rosdahl I. *Bcl-xL and bcl-2 proteins in melanoma progression and UVB-induced apoptosis*. Int J Oncol 2006; 28(3):661–6.
597. Jin-Song Y, Zhao-Xia W, Cheng-Yu L, Xiao-Di L, Ming S, Yuan-Yuan G, Wei D. *Prognostic significance of Bcl-xL gene expression in human colorectal cancer*. Acta Histochem 2011; 113(8):810–4.
598. Karczmarek-Borowska B, Filip A, Wojcierowski J, Smoleń A, Korobowicz E, Korszen-Pilecka I, Zdunek M. *Estimation of prognostic value of Bcl-xL gene expression in non-small cell lung cancer*. Lung Cancer 2006; 51(1):61–9.
599. Chen Y, Kayano T, Takagi M. *Dysregulated expression of bcl-2 and bax in oral carcinomas: Evidence of post-transcriptional control*. J Oral Pathol Med 2000; 29(2):63–9.
600. Singh BB, Chandler FW, Whitaker SB, Forbes-Nelson AE. *Immunohistochemical evaluation of bcl-2 oncoprotein in oral dysplasia and carcinoma*. Oral Surg Oral Med Oral Pathol Oral Radiol Endod 1998; 85(6):692–8.
601. Kim SY, Han YK, Song JM, Lee CH, Kang K, Yi JM, Park HR. *Aberrantly hypermethylated tumor suppressor genes were identified in oral squamous cell carcinoma (OSCC)*. Clin Epigenetics 2019; 11(1):116.
602. Le Campion ACOV, Ribeiro CMB, Luiz RR, Da Silva Júnior FF, Barros HCS, Dos Santos KDCB, Ferreira SJ, Gonçalves LS, Ferreira SMS. *Low Survival Rates of Oral and Oropharyngeal Squamous Cell Carcinoma*. Int J Dent 2017; 2017:5815493.

603. Amaravadi RK, Lippincott-Schwartz J, Yin XM, Weiss WA, Takebe N, Timmer W, DiPaola RS, Lotze MT, White E. *Principles and current strategies for targeting autophagy for cancer treatment*. Clin Cancer Res 2011; 17(4): 654–666.
604. Goel P, Gerriets V. *Chloroquine*. In: *StatPearls*. StatPearls Publishing, Treasure Island (FL). 2019.
605. Slater AFG. *Chloroquine: Mechanism of drug action and resistance in plasmodium falciparum*. Pharmacol Ther 1993; 57(2-3):203-35.
606. Al-Bari AA. *Chloroquine analogues in drug discovery: New directions of uses, mechanisms of actions and toxic manifestations from malaria to multifarious diseases*. J Antimicrob Chemother 2014; 70(6):1608–21.
607. Rome BN, Avorn J. *Drug evaluation during the Covid-19 pandemic*. N Engl J Med 2020; 382:2282-2284.
608. Fitzwalter BE, Towers CG, Sullivan KD, Andrysik Z, Hoh M, Ludwig M, O'Prey J, Ryan KM, Espinosa JM, Morgan MJ, Thorburn A. *Autophagy Inhibition Mediates Apoptosis Sensitization in Cancer Therapy by Relieving FOXO3a Turnover*. Dev Cell 2018; 44: 555-565.e3.
609. Yuan N, Song L, Zhang S, et al. *Bafilomycin A1 targets both autophagy and apoptosis pathways in pediatric B-cell acute lymphoblastic leukemia*. Haematologica 2015; 100: 345.
610. Liu Z, Liu J, Li L, Nie D, Tao Q, Wu J, Fan J, Lin C, Zhao S, Ju D. *Inhibition of Autophagy Potentiated the Antitumor Effect of Nedaplatin in Cisplatin-Resistant Nasopharyngeal Carcinoma Cells*. PLoS One 2015; 10: e0135236.
611. Xie Z, Xie Y, Xu Y, Zhou H, Xu W, Dong Q. *Bafilomycin A1 inhibits autophagy and induces apoptosis in MG63 osteosarcoma cells*. Mol Med Rep 2014; 10: 1103–1107.
612. Zhang J, Wang X, Vikash V, Ye Q, Wu D, Liu Y, Dong W. *ROS and ROS-Mediated Cellular Signaling*. Oxid Med Cell Longev 2016; 2016:4350965.
613. Bao L, Jaramillo MC, Zhang Z, Zheng Y, Yao M, Zhang DD, Yi X. *Induction of autophagy contributes to cisplatin resistance in human ovarian cancer cells*. Mol Med Rep 2015; 11: 91–98.
614. Kirkpatrick DL, Powis G. *Clinically Evaluated Cancer Drugs Inhibiting Redox Signaling*. Antioxidants Redox Signal 2017; 26(6): 262–273.
615. Smith AC, Grieshaber CK, Liao JTF, Page JG, Wientjes MG. *Pharmacokinetics of Buthionine Sulfoximine (NSC 326231) and Its Effect on Melphalan-induced Toxicity in Mice*. Cancer Res 1989; 49:5385-5391.
616. Zhong L, Liu Y, Wang K, He Z, Gong Z, Zhao Z, Yang Y, Gao X, Li F, Wu H, Zhang S, Chen L. *Biomarkers: paving stones on the road towards the personalized precision medicine for oral squamous cell carcinoma*. BMC Cancer 2018; 18: 911.
617. Wang M, Smith JS, Wei WQ. *Tissue protein biomarker candidates to predict progression of esophageal squamous cell carcinoma and precancerous lesions*. Ann N Y Acad Sci 2018; 1434(1):59–69.
618. Basseri S, Austin RC. *Endoplasmic reticulum stress and lipid metabolism: Mechanisms and therapeutic potential*. Biochem Res Int 2012; 2012:841362.
619. Mandic A, Hansson J, Linder S, Shoshan MC. *Cisplatin Induces Endoplasmic Reticulum Stress and Nucleus-independent Apoptotic Signaling*. J Biol Chem 2003; 278: 9100–9106.
620. Schröder M, Kaufman RJ. *ER stress and the unfolded protein response*. Mutat Res - Fundam Mol Mech Mutagen 2005; 569(1-2):29-63.
621. Xu Y, Wang C, Su J, Xie Q, Ma L, Zeng L, Yu Y, Liu S, Li S, Li Z, Sun L. *Tolerance to endoplasmic reticulum stress mediates cisplatin resistance in human*

ovarian cancer cells by maintaining endoplasmic reticulum and mitochondrial homeostasis. Oncol Rep; 34(6):3051.
622. I. Elshimali Y, Wu Y, Khaddour H, Wu Y, Gradinaru D, Sukhija H, S. Chung S, V. Vadgama J. *Optimization Of Cancer Treatment Through Overcoming Drug Resistance*. J Cancer Res Oncobiology; 1(2):107.
623. Garnett MJ, Marais R. *Guilty as charged: B-RAF is a human oncogene*. Cancer Cell 2004; 6:313-319.
624. Zhao Y, Shen S, Guo J, Chen H, Yu Greenblatt D, Kleeff J, Liao Q, Chen G, Friess H, Sing Leung P. *Mitogen-Activated Protein Kinases and Chemoresistance in Pancreatic Cancer Cells*. J Surg Res 2006; 136(2):325–35.
625. Zhang HS, Zhang ZG, Du GY, Sun HL, Liu HY, Zhou Z, Gou XM, Wu XH, Yu XY, Huang YH. *Nrf2 promotes breast cancer cell migration via up-regulation of G6PD/HIF-1α/Notch1 axis*. J Cell Mol Med; 23(5):3451.
626. Ji L, Li H, Gao P, Shang G, Zhang DD, Zhang N, Jiang T. *Nrf2 Pathway Regulates Multidrug-Resistance-Associated Protein 1 in Small Cell Lung Cancer*. PLoS One; 8(5):e6340.
627. Kim EH, Jang H, Shin D, Baek SH, Roh JL. *Targeting Nrf2 with wogonin overcomes cisplatin resistance in head and neck cancer*. Apoptosis 2016; 21(11):1265-1278.
628. Major AG, Pitty LP, Farah CS. *Cancer stem cell markers in head and neck squamous cell carcinoma*. Stem Cells Int 2013; 2013:319489.
629. Zaal EA, Berkers CR. *The influence of metabolism on drug response in cancer*. Front Oncol 2018; 8:500.
630. Xu W, Wang S, Chen Q, Zhang Y, Ni P, Wu X, Zhang J, Qiang F, Li A, Re OD, Xu S, Wang M, Zhang R, Zhou J. *TXNL1-XRCC1 pathway regulates cisplatin-induced cell death and contributes to resistance in human gastric cancer*. Cell Death Dis 2014; 5(2): e1055.

Appendix

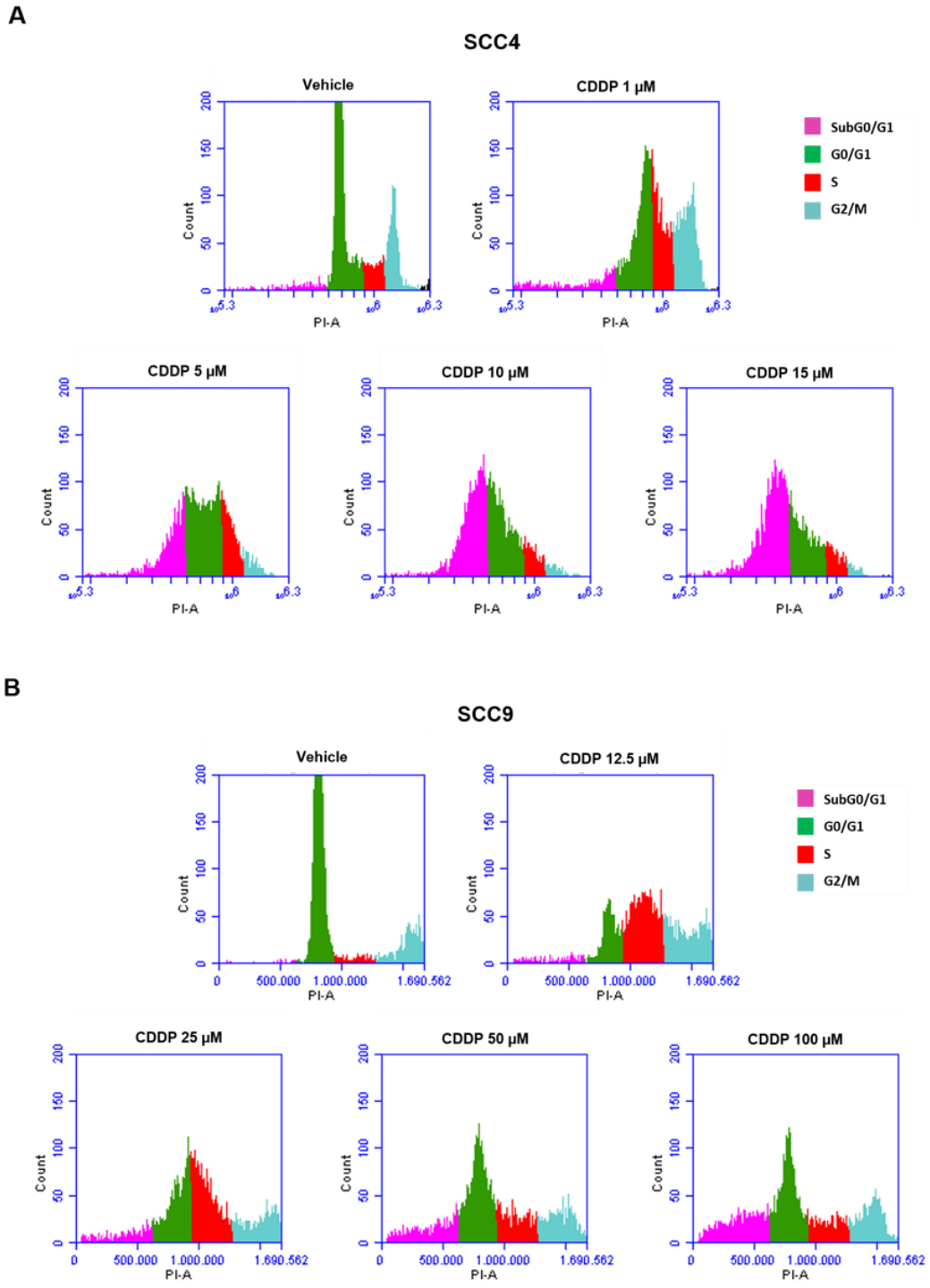

Figure A.1 Cell cycle analysis in OSCC cells treated with cisplatin.

Representative flow cytometric histograms of cell cycle stages in OSCC cells treated with vehicle (0.009% (v/v) NaCl) or varying concentrations of cisplatin (CDDP): 1-15 µM and 12.5-100 µM for SCC4 (**A**) and SCC9 (**B**) cell lines, respectively. Cells were fixed with 70% ice cold ethanol and stained with PI, before being analysed on the flow BD FACS Accuri cytometer. The subG0/G1 peak along with the G0/G1, S and G2/M phases of the cell cycle were determined on the basis of the level of PI intensity. Plots were created using the BD Accuri Software. Analysis of N=3 is reported in Figure 3.5 and Table 3.4.

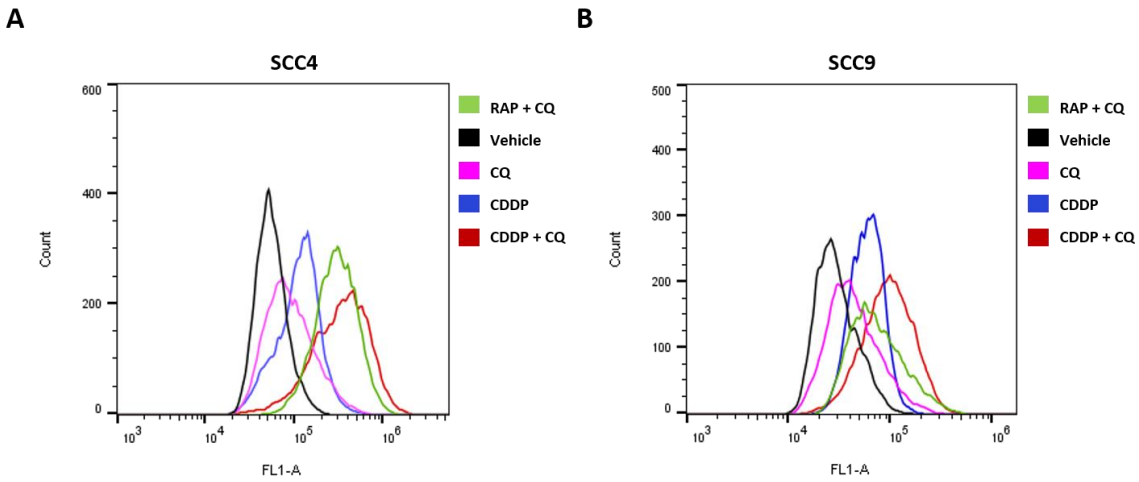

Figure A.2 Cyto-ID analysis of autophagic flux in OSCC cells treated with cisplatin.

Representative flow cytometric histograms of OSCC cells treated with the vehicle (0.009% (v/v) NaCl), chloroquine (CQ) 10 µM alone, cisplatin (CDDP) alone (5 µM and 25 µM in SCC4 (**A**) and SCC9 (**B**) cells respectively) or cisplatin in combination with chloroquine. Rapamycin (RAP) 0.5 µM in combination with chloroquine 10 µM was used as positive control. Cells were stained with Cyto-ID green autophagy dye and then analysed on the flow BD FACS Accuri cytometer. Plots were created using FlowJo v10 and alive cells were gated on vehicle treated cells. Analysis of N=3 is reported in Figure 3.16.

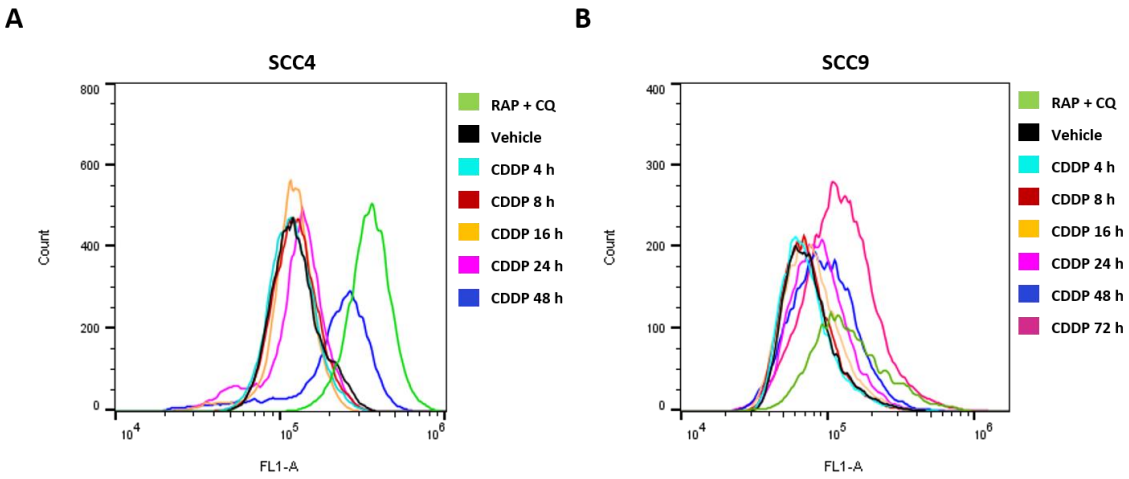

Figure A.3 Time course analysis of autophagy in OSCC cells treated with cisplatin.

Representative flow cytometric histograms of OSCC cells of treated with the vehicle (0.009% (v/v) NaCl) or with cisplatin (CDDP) 5 or 25 µM in SCC4 (**A**) and SCC9 (**B**) respectively for the indicated times. Rapamycin (RAP) 0.5 µM in combination with chloroquine (CQ) 10 µM was used as positive control. Cells were stained with Cyto-ID green autophagy dye and then analysed on the flow BD FACS Accuri cytometer. Plots were created using FlowJo v10 and alive cells were gated on vehicle treated cells. Analysis of N=3 is reported in Figure 3.17.

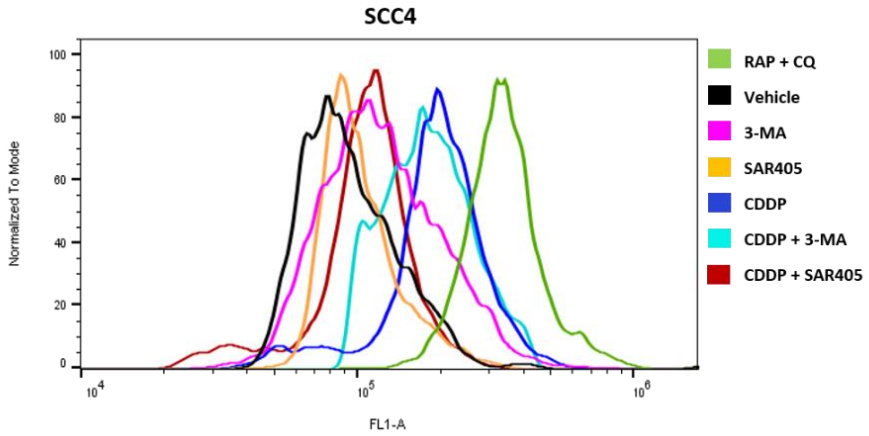

Figure A.4 Cyto-ID analysis of SCC4 cells treated with cisplatin in combination with early stage autophagy inhibitors.

Representative flow cytometric histograms of SCC4 cells pre-treated with either 3-MA (5 mM) or SAR405 (1 µM) for 1 h before adding cisplatin (5 µM) for a further 48 h. Rapamycin (RAP) 0.5 µM in combination with chloroquine 10 µM was used as positive control. Cells were stained with Cyto-ID green autophagy dye and then analysed on the flow BD FACS Accuri cytometer. Plots were created using FlowJo v10 and alive cells were gated on vehicle treated cells. Plots show the cell count normalised to the mode. Analysis of N=3 is reported in Figure 3.19.

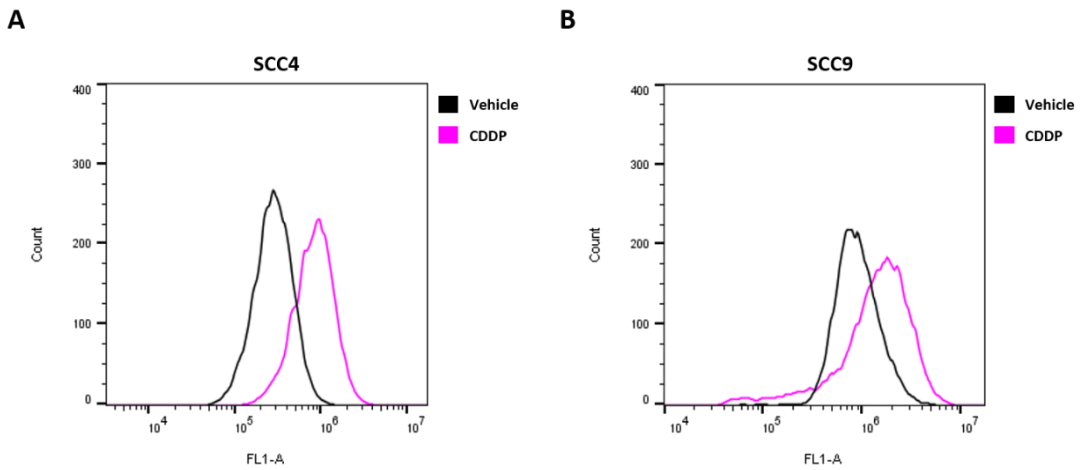

Figure A.5 Flow cytometric analysis of intracellular levels of ROS in OSCC cells treated with cisplatin.

Representative flow cytometric histograms of OSCC cells treated with the vehicle (0.009% (v/v) NaCl) or with cisplatin (CDDP) (5 μM and 25 μM in SCC4 (**A**) and SCC9 (**B**) cells respectively). Cells were stained with H_2DCFDA dye and then analysed on the flow BD FACS Accuri cytometer. Plots were created using Analysis of N=3 is reported in Figure 4.2.

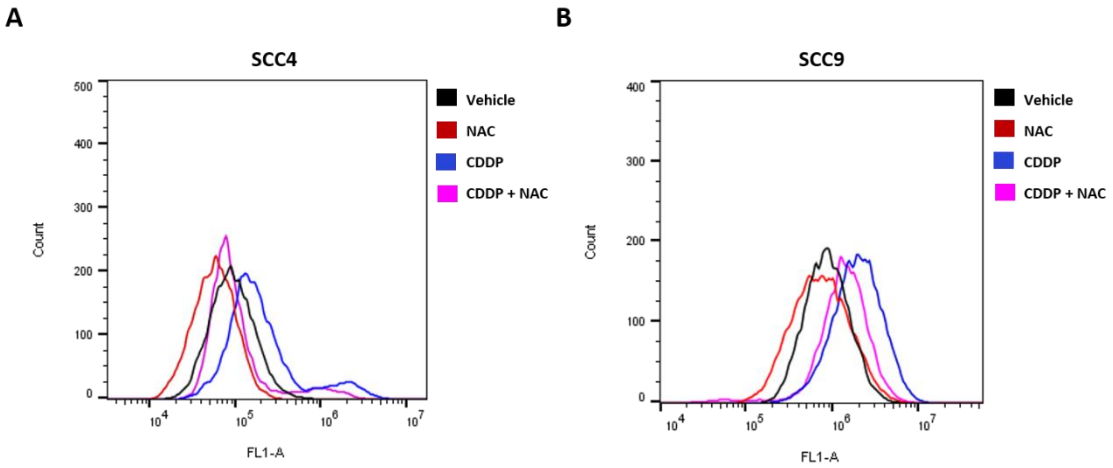

Figure A.6 Flow cytometric analysis of intracellular levels of ROS in OSCC cells treated with cisplatin in combination with NAC.

Representative flow cytometric histograms of OSCC cells treated with vehicle (0.009% (v/v) NaCl), NAC alone (5mM), cisplatin (CDDP) (5 μM or 25 μM in SCC4 (**A**) and SCC9 (**B**) cells respectively) or cisplatin in combination with NAC. Cells were stained with H_2DCFDA dye and then analysed on the flow BD FACS Accuri cytometer. Plots were created using FlowJo v10 and alive cells were gated on vehicle treated cells. Analysis of N=3 is reported in Figure 4.5.

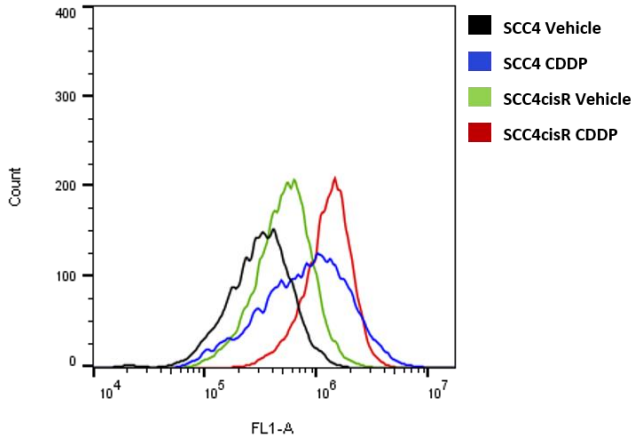

Figure A.7 Flow cytometric analysis of endogenous and cisplatin-induced ROS in SCC4 and SCC4cisR cells.

Representative flow cytometric histograms of SCC4 and SCC4cisR cells untreated or treated with 5 μM cisplatin. Cells were stained with H_2DCFDA dye and then analysed on the flow BD FACS Accuri cytometer. Plots were created using FlowJo v10 and alive cells were gated on vehicle treated cells. Analysis of N=3 is reported in Figure 5.12